ANNUAL REVIEW

INSTITUTE FOR MOLECULAR SCIENCE

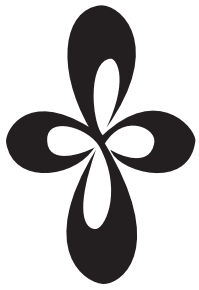

2003

(Sep. 2002 ~ Aug. 2003)

Published by
Institute for Molecular Science
Okazaki National Research Institutes
Myodaiji, Okazaki 444-8585, Japan
Phone: +81-564-55-7418 (Secretary Room)
Facsimile: +81-564-54-2254 (Secretary Room)
URL: http://www.ims.ac.jp/

Editorial Committee 2003

IMS 2003

From coming April, 2004, five national institutes including the Institute for Molecular Science unify together to establish a new research organization. This organization is aimed at the establishment of new research areas of science by the collaboration among different regimes.

As seen in this annual review, researches at IMS extend widely from chemistry, physics to biology focusing our attention upon molecules and ensembles of molecules. In the other word, IMS has been already challenging for the collaboration between different areas of science in order to create unique and novel research areas based on molecular science.

Finally, I wish to announce that Emeritus Professor Hiizu Iwamura received Japan Academy Prize this year for his great contribution to the Study of Molecular Magnet.

October, 2003

KAYA, Koji
Director General, Institute for Molecular Science

CONTENTS

Equipment Development Center

Ultraviolet Synchrotron Orbital Radiation Facility

Computer Center

RESEARCH ACTIVITIES IX

Center for Integrative Bioscience

Abbreviations

IMS: Institute for Molecular Science
GUAS: The Graduate University for Advanced Studies

ORGANIZATION AND STAFF

Organization

The Institute for Molecular Science comprises twenty research laboratories, each staffed by a professor, an associate professor, two research associates and several technical associates, and two research laboratories with foreign visiting professors and five research facilities.

The laboratories are grouped into six departments and one facility for coordination chemistry:

Department of Theoretical Studies	Theoretical Studies I
	Theoretical Studies II
	Theoretical Studies III[1)]
	Theoretical Studies IV
Department of Molecular Structure	Molecular Structure I
	Molecular Structure II[1)]
	Molecular Dynamics
Department of Electronic Structure	Excited State Chemistry
	Excited State Dynamics
	Electronic Structure[1)]
	Molecular Energy Conversion[2)]
Department of Molecular Assemblies	Solid State Chemistry
	Molecular Dynamics Assemblies
	Molecular Assemblies[1)]
Department of Applied Molecular Science	Applied Molecular Science I
	Applied Molecular Science II[1)]
Department of Vacuum UV Photoscience	Photochemistry
	Chemical Dynamics
	Synchrotron Radiation Research[2)]
Coordination Chemistry Laboratories	Complex Catalysis
	Functional Coordination Chemistry
	Coordination Bond[1)]

The research facilities are:

• Laser Research Center for Molecular Science	Advanced Lasers for Chemical Reaction Studies
	Advanced Lasers for Synchrotron Radiation Applications
	Advanced UV and IR Tunable Lasers
• Research Center for Molecular-scale Nanoscience	Molecular-scale Electronics
	Nanocatalysis and Biomolecular Devices
	Nano-scale Photoscience
	Interface Molecular Science[3)]
	Molecular Clusters[3)]

- Equipment Development Center
- UVSOR (Ultraviolet Synchrotron Orbital Radiation) Facility
- Computer Center

The research facilities of ONRI (related to IMS) are:

- Center for Integrative Bioscience
- Research Center for Computational Science

1) Professors and associate professors are visiting professors from other universities.
2) Research laboratories with foreign visiting professors.
3) Professors, associate professors, and research associates, along with their positions, are transferred from other universities.

Scientific Staff

KAYA, Koji — **Professor, Director-General**

Emeritus Professors

NAGAKURA, Saburo	The Japan Academy
HIROTA, Eizi	Professor Emeritus, The Graduate University for Advanced Studies
KIMURA, Katsumi	Senior Researcher, Molecular Photonics & Photoelectron Group, Communications Research Laboratory
MOROKUMA, Keiji	Professor, Emory University, U. S. A.
INOKUCHI, Hiroo	Chief Scientist of Space Utilization Research Program, National Space Development Agency of Japan
MARUYAMA, Yusei	Professor, Hosei University
YOSHIHARA, Keitaro	Professor, Japan Advanced Institute of Science and Technology
HANAZAKI, Ichiro	Professor Emeritus, The Graduate University for Advanced Studies
IWAMURA, Hiizu	Professor, University of the Air
SAITO, Shuji	Professor, Fukui University
IWATA, Suehiro	Professor, National Institution for Academic Degree
ITO, Mitsuo	Professor Emeritus, The Graduate University for Advanced Studies, Tohoku University

Department of Theoretical Studies

Theoretical Studies I

NAGASE, Shigeru	Professor
OKAMOTO, Yuko	Associate Professor
KOBAYASHI, Kaoru	Research Associate
OKUMURA, Hisashi	Research Associate (October ’02–)
ISHIMURA, Kazuya	Technical Associate
CHOE, Yoong-Kee	IMS Fellow (–March ’03); Post-Doctoral Fellow (April ’03–)
NISHINO, Masamichi	IMS Fellow (April ’03–)
YODA, Takao	Research Associate of Research for the Future Program (–March ’03)[1)]
YAMAZAKI, Takeshi	Research Associate of Research for the Future Program (–March ’03)
SLANINA, Zdenek	Visiting Scientist; JSPS Invited Fellow (November ’02–)
LU, Jing	Visiting Scientist; JSPS Post-Doctoral Fellow
TAKAGI, Nozomi	JSPS Post-Doctoral Fellow
NOGUCHI, Hiroshi	JSPS Post-Doctoral Fellow (–March ’03)[2)]
RE, Suyong	JSPS Post-Doctoral Fellow (–March ’03); Post-Doctoral Fellow (April ’03–)
KAWASHIMA, Yukio	Post-Doctoral Fellow
KATOUDA, Michio	Research Fellow (April ’03–)
KOKUBO, Hironori	Graduate Student
MURATA, Katsumi	Graduate Student
SAKAE, Yoshitake	Graduate Student
ITO, Satoru	Graduate Student
NAGAYOSHI, Kanade	Graduate Student (from Osaka Prefecture University)* (–March ’03)[3)]
ONO, Yuriko	Graduate Student (from Tokyo Institute of Technology)* (August ’03–)

Theoretical Studies II

NAKAMURA, Hiroki	Professor
TANIMURA, Yoshitaka	Associate Professor (–May ’03)[4)]
TAKAMI, Toshiya	Research Associate
SUZUKI, Yoko	Research Associate
ZHU, Chaoyuan	Research Associate (–October ’02)[5)]
MIL’NIKOV, Gennady	Research Fellow (–October ’02), Research Associate

	(November ’02–)
KATO, Tsuyoshi	IMS Fellow (–September ’02)[6]
FUJISAKI, Hiroshi	IMS Fellow (–March ’03)[7]
ZOU, Shiyang	IMS Fellow (April ’03–)
CHIKAZUMI, Shinpei	IMS Fellow (April ’03–)
KAMISAKA, Hideyuki	Research Fellow (December ’02), IMS Fellow (January–March ’03)[8]
ISHKHANYAN, Artur	Visiting Scientist; MONBUSHO Invited Fellow (June ’03–)
SOLOVJIEV, Evgeni	Visiting Scientist; MONBUSHO Invited Fellow (August ’02–June ’03)
KUHN, Oliver	Visiting Scientist; MONBUSHO Invited Fellow (November ’02–March ’03)
KONDORSKY,Alexey	Visiting Scientist; JSPS Post-Doctoral Fellow
OLOYEDE, Oluwaponmile	Graduate Student (October ’02–)
SUZUKI, Youichi	Graduate Student (from Kyoto University)* (April–May ’03)

Theoretical Studies III

HIRAO, Kimihiko	Visiting Professor (from the University of Tokyo) (–March ’03)
NAGAOKA, Masataka	Visiting Professor (from Nagoya University) (August ’03–)
TAKAYANAGI, Toshiyuki	Visiting Associate Professor (from Japan Atomic Energy Research Institute) (–March ’03)
TORII, Hajime	Visiting Associate Professor (from Shizuoka University) (April ’03–)
KOVALENKO, Andriy F.	Research Associate (–July ’03)[9]

Theoretical Studies IV

HIRATA, Fumio	Professor
YONEMITSU, Kenji	Associate Professor
KISHINE, Jun-ichiro	Research Associate (–August ’03)[10]
OTSUKA, Yuichi	IMS Fellow
KOBRYN, Oleksandr	IMS Fellow (April ’03–)
YAMAZAKI, Takeshi	Post-Doctoral Fellow (April ’03–)
MARUYAMA, Yutaka	Post-Doctoral Fellow (April ’03–)
INOUE, Hitoshi	Post-Doctoral Fellow (July ’03–)
OMELYAN, Ihor P.	Visiting Scientist (November ’02–March ’03)
TANIMURA, Ayumi	Graduate Student
MATSUGAMI, Masaru	Graduate Student (April ’03–)
MIYASHITA, Naoyuki	Graduate Student (–March ’03)[11]

Department of Molecular Structure

Molecular Structure I

OKAMOTO, Hiromi	Professor
MORITA, Norio	Associate Professor
IMURA, Kouhei	Research Associate
NAGAHARA, Tetsuhiko	IMS Fellow

Molecular Structure II

AKUTSU, Hideo	Visiting Professor (from Osaka University) (–March ’03)
OHTA, Toshiaki	Visiting Professor (from The University of Tokyo) (April ’03–)
WADA, Akihide	Visiting Associate Professor (from Tokyo Institute of Technology)

Molecular Dynamics

KITAGAWA, Teizo	Professor (Center for Integrative Bioscience)
YOKOYAMA, Toshihiko	Prtofessor
DINSE, Klaus Peter	Visiting Professor (from Technische Universitat Darmstadt, Germany) (–October ’02)
KATO, Tatsuhisa	Associate Professor
UCHIDA, Takeshi	Research Associate
NAKAGAWA, Takeshi	Research Associate

FURUKAWA, Ko	Research Associate
NAGATOMO, Shigenori	Technical Associate
HAYASHI, Naoki	Technical Associate
WATANABE, Hirokazu	Technical Associate (April ’03–)
MARUYAMA, Koichi	IMS Fellow (April ’03–)
TOYAMA, Namiki	IMS Fellow (–March ’03)[12)]
PAL, Biswajit	Visiting Scientist; JSPS Invited Fellow
MATSUOKA, Hideto	JSPS Post-Doctral Fellow
OKUNO, Daichi	Graduate Student
SATO, Akira	Graduate Student
OKUBO, Shingo	Graduate Student (–September ’02)[13)]

Department of Electronic Structure

Excited State Chemistry

NISHI, Nobuyuki	Professor
NEGISHI, Yuichi	Research Associate
IMAI, Hiroyuki	Research Associate of Research for the Future Program
POKOP, Penta V	Research Associate of Research for the Future Program
KOSUGI, Kentaroh	Research Associate of Research for the Future Program
BUSHIRI, M. Junaid	Research Associate of Research for the Future Program (April ’03–)
LIU, Guang	Research Associate of Research for the Future Program (April –June ‘03)
OHSHIMO, Keijiro	JSPS Post-Doctoral Fellow (– June ‘03)[14)]
IKEDA, Shingo	Post-Doctoral Fellow (–March ’03)
MORI, Michiyasu	Post-Doctoral Fellow (–March ’03)
FUKAYA, Atsuko	Post-Doctoral Fellow (–March ’03)
OIKAWA, Kenichi	Post-Doctoral Fellow (–March ’03)
HINO, Kazuyuki	Graduate Student (from Kyushu University)* (–March ’03)[15)]
IWASE, Hiroki	Graduate Student (from Gunma University)* (–March ’03)
MIKAMI, Taiji	Graduate Student (from Tokyo Institute of Technology)* (December ’02–March ’03)*
KIMURA, Masahiro	Graduate Student (December ’02–March ’03)
OKABE, Chie	Graduate Student (from Kyushu University)* (December ’02 –)
NARUSHIMA, Takashi	Graduate Student (December ’02–)
UECHI, Ichiro	Graduate Student (from Hiroshima University)* (January ’03–March ’03)

Excited State Dynamics

FUJII, Masaaki	Professor (–March ’03)[16)]
SUZUKI, Toshinori	Associate Professor (–March ’03)[14)]
KOHGUCHI, Hiroshi	Research Associate (–January ’03)[14)]
SAKAI, Makoto	Research Associate (–May ’03)[16)]
MATSUMOTO, Yoshiteru	JSPS Post-Doctoral Fellow (–September ’02)[17)]
TSUBOUCHI, Masaaki	Graduate Student (–March ’03)[14)]

Electronic Structure

IIJIMA, Sumio	Visiting Professor (from Meijo University)
MISAWA, Kazuhiko	Visiting Associate Professor (from Tokyo University of Agriculture and Technology)
INOKUCHI, Yoshiya	Research Associate

Molecular Energy Conversion

SOLOVJEV, Evgeni	Visiting Professor (from Department of Theoretical Studies, Macedonian) (September ’02–June ‘03)
VAROTSIS, Constantinos	Visiting Professor (from Center for Integrative Bioscience, Greece) (July ’03–September ‘03)
KOZLOWSKI, Pawel M.	Visiting Associate Professor (from Center for Integrative Bioscience, USA) (July ’02–June ’03)
KUMAR, Kurishna, Subbarao, Venkata	Visiting Associate Professor (from Department of Vacuum UV Photoscience/Reaction Dynamics, India) (September ’02–June ‘03)

DAS, Puspendu, Kumar	Visiting Associate Professor (from Department of Electronic Structure, India) (June ’03–September ’03)

Department of Molecular Assemblies

Solid State Chemistry

YAKUSHI, Kyuya	Professor
NAKAMURA, Toshikazu	Associate Professor
YAMAMOTO, Kaoru	Research Associate
FUJIYAMA, Shigeki	Research Associate
YAMAMOTO, Takashi	IMS Fellow
NAKANO, Chikako	Research Fellow
DROZDOVA, Olga	Research Fellow (–July’03)
MAEDA, Keisuke	Graduate Student
SUZUKI, Kenji	Graduate Student

Molecular Assemblies Dynamics

KOBAYASHI, Hayao	Professor
FUJIWARA, Hideki	Research Associate
YAMADA, Ryo	Research Associate
WANG, Zhe-Ming	Visiting Scientist; MONBUSHO Invited Fellow (–July ’03)
ZHANG, Bin	Research Fellow (–January ’03), JST; Post-Doctoral Fellow (February ’03–May ’03); Research Fellow (June ’03–July ’03)
OTSUKA, Takeo	JSPS Post-Doctoral Fellow
LEE, Ha-Jin	Visiting Scientist; JSPS Post-Doctoral Fellow
TAKAHASHI, Kazuyuki	JST Post-Doctoral Fellow (April ’03–)
CUI, Heng-Bo	JST Post-Doctoral Fellow (April ’03–)
OTSUBO, Saika	Graduate Student (April ’03–)

Molecular Assemblies

ENOKI, Toshiaki	Visiting Professor (from Tokyo Institute of Technology)
NAITO, Toshio	Visiting Associate Professor (from Hokkaido University)

Department of Applied Molecular Science

Applied Molecular Science I

KINOSITA, Kazuhiko, Jr.	Professor (Center for Integrative Bioscience)
AONO, Shigetoshi	Professor (Center for Integrative Bioscience)
INOUE, Katsuya	Associate Professor
ADACHI, Kengo	Research Associate (January ’03–)
NAKAJIMA, Hiroshi	Research Associate (January ’03–April ’03)
HOSOKOSHI, Yuko	Research Associate (–September ’02)[18]
AKITA, Motoko	Research Associate (April ’03–)
SURESH, Eringathodi	Visiting Scientist; JSPS Post-Doctoral Fellow (November ’02–)
SUZUKI, Kentaro	Graduate Student (–March ’03)[19]
KATOH, Keiichi	Graduate Student (–March ’03)[20]
OKA, Yoshimi	Graduate Student
OKUDA, Kazuki	Graduate Student (April ’03–)

Applied Molecular Science II

AWAZU, Koichi	Visiting Professor (from National Institute of Advanced Science and Technology)
KIKUCHI, Koichi	Visiting Associate Professor (from Tokyo Metropolitan University)

Department of Vacuum UV Photoscience

Photochemistry

KOSUGI, Nobuhiro	Professor
HISHIKAWA, Akiyoshi	Associate Professor (April ’03–)
HATSUI, Takaki	Research Associate
OJI, Hiroshi	IMS Fellow (–March ’03)[21]
SETOYAMA, Hiroyuki	IMS Fellow (April ’03–)
MASUDA, Suomi	Graduate Student

Chemical Dynamics

URISU, Tsuneo	Professor
MITSUKE, Koichiro	Associate Professor
MIZUTANI, Masakazu	Research Associate
NONOGAKI, Youichi	Research Associate
TERO, Ryugo	Technical Associate (November ’02–)
KOU, Junkei	IMS Fellow
MORÉ, SAM D.	IMS Fellow (–October ‘02)
MORI, Takanori	Post-Doctoral Fellow
LI, Yanjun	Post-Doctoral Fellow (April ‘03–)
WANG, Zhihong	Post-Doctoral Fellow (May ‘03–)
WANG, Changshun	Research Fellow (–March ‘03)
SUGA, Yasuhiro	Visiting Scientist (from AISIN COSMOS R&D CO., LTD.) (August ’03–)
YAMAMURA, Shusaku	Graduate Student
TAKIZAWA, Morio	Graduate Student
FUJIKI, Satoshi	Graduate Student
RAHMAN, Mashiur	Graduate Student
KIM, Yong-Hoon	Graduate Student (October ’02–)
MISAWA, Nobuo	Graduate Student (April ’03–)

Synchrotron Radiation Research

DINSE, Klaus Peter	Visiting Professor (–October ’02)
MYROSLAV, F. Holovko	Visiting Professor (April–June ’03)
MORGUNOV, Roman	Visiting Professor (July ’03–)
GANGAVARAPU, Ranga Rao	Visiting Associate Professor (–July ’03)
DROZDOVA, Olga	Visiting Associate Professor (August ’03–)

Coordination Chemistry Laboratories

TANAKA, Koji	Director

Complex Catalysis

UOZUMI, Yasuhiro	Professor (Research Center for Molecular-scale Nanoscience: concurrently)
YAMASHITA, Masahiro	Visiting Professor (from Tokyo Metropolitan University)
CHATANI, Naoto	Visiting Associate Professor (from Osaka University) (–March ’03), Visiting Professor (from Osaka University) (April ’03–)
TAKENAKA, Kazuhiro	IMS Fellow
NAKAI, Yasushi	Graduate Student
KIMURA, Masahiro	Graduate Student
TAMAKI, Hirotaka	Graduate Student
SAKAMAKI, Jun-ichiro	Graduate Student (April ’03–)
MINAGAWA, Maki	Graduate Student (April ’03–)

Functional Coordination Chemistry

TANAKA, Koji	Professor
KAWAGUCHI, Hiroyuki	Associate Professor
WADA, Tohru	Research Associate
MATSUO, Tsukasa	Research Associate
MIZUKAWA, Tetsunori	Technical Associate
YUKI, Masahiro	IMS Fellow
SHIREN, Kazushi	Post-Doctoral Fellow
KOIZUMI, Takeaki	Post-Doctoral Fellow
FUJIHARA, Tetsuaki	Post-Doctoral Fellow
OHTSU, Hideki	Post-Doctoral Fellow
AIHARA, Hidenori	Post-Doctoral Fellow (–April ’03)[22)]
YASUE, Takahiro	Post-Doctoral Fellow
OKAMURA, Rei	Post-Doctoral Fellow
TSUTSUI, Kanako	Research Fellow
KOBAYASHI, Katsuaki	Research Fellow (–March ’03)
TOMON, Takashi	Post-Doctoral Fellow (April ’03–), Research Fellow (April

	’03–)
KOMURO, Takashi	Graduate Student (from Nagoya University)*
HINO, Takami	Graduate Student

Coordination Bond

MATSUSAKA, Hiroyuki	Visiting Professor (from Osaka Prefecture University) (April ’03–)
TOKITOH, Norihiro	Visiting Professor (from Kyoto University) (–March ’03)
UENO, Keiji	Visiting Associate Professor (from Gunma University) (April ’03–)
ONITSUKA, Kiyotaka	Visiting Associate Professor (from Osaka University) (–March ’03)

Research Facilities

Laser Research Center for Molecular Science

FUJII, Masaaki	Director (–March ‘03)
OKAMOTO, Hiromi	Director (April ’03–)

Advanced Lasers for Chemical Reaction Studies

Advanced Lasers for Synchrotron Radiation Applications

SARUKURA, Nobuhiko	Associate Professor
ONO, Shingo	Research Associate (March ’03–)
GOTO, Masahiro	IMS Fellow (April ’03–)
QUEMA, Alex	Research Fellow
TAKAHASHI, Hiroshi	Graduate Student

Advanced UV and IR Tunable Lasers

TAIRA, Takunori	Associate Professor
SHOJI, Ichiro	Research Associate
LUPEI, Voicu	Visiting Professor (from Institute of Atomic Physics, Romania) (–August ’03)
YI, Jong-Hoon	Visiting Associate Professor; MONBUSHO Invited Fellow (from Yeungnam University, Korea)
ISHIZUKI, Hideki	Research Fellow (–March ’03), IMS Fellow (April ’03–)
TSUNEKANE, Masaki	Research Fellow (May ’03–)
DASCALU, Traian	Research Fellow
SATO, Yoichi	Research Fellow
SAIKAWA, Jiro	Research Fellow
PAVEL, Nicolaie	Visiting Scientist (from Institute of Atomic Physics, Romania) (–August ’03)

Research Center for Molecular-scale Nanoscience

KAYA, Koji	Director (–April ’03)
OGAWA, Takuji	Director (May ’03–)

Molecular-scale Electronics

OGAWA, Takuji	Professor (February ’03–)
SUZUKI, Toshiyasu	Associate Professor
TADA, Hirokazu	Associate Professor
TANAKA, Shoji	Research Associate
SAKAMOTO, Youichi	Research Associate
TOMURA, Masaaki	Technical Associate
SHIRASAWA, Nobuhiko	IMS Fellow
FUJIWARA, Eiichi	IMS Fellow
ARAKI, Koiti	Post-Doctoral Fellow (March ’03–)
NAKAO, Satoru	Post-Doctoral Fellow (April ’03–)
ITO, Kaname	Graduate Student (–March ’03), Post-Doctoral Fellow (April ’03–)
ARA, Masato	Graduate Student
TAKADA, Masaki	Graduate Student
SAKANOUE, Tomo	Graduate Student (April ’03–)
ENDO, Hiroaki	Graduate Student (from Ehime University)* (April ’03–)
KAWAO, Masahiro	Graduate Student (from Ehime University)* (April ’03–)

MIZUGUCHI, Eisuke	Graduate Student (from Ehime University)* (April ’03–)
OZAWA, Hiroaki	Graduate Student (from Ehime University)* (April ’03–)
SATOU, Hirokazu	Graduate Student (from Ehime University)* (April ’03–)

Nanocatalysis and Biomolecular Devices

UOZUMI, Yasuhiro	Professor (Coordination Chemistry Laboratories, concurrently)
FUJII, Hiroshi	Associate Professor (Center for Integrative Bioscience)
NAGATA, Toshi	Associate Professor
KURAHASHI, Takuya	Research Associate
NAGASAWA, Takayuki	Research Associate (November ’02–)
HOSOKAWA, Youichi	IMS Fellow
TAKENAKA, Kazuhiro	IMS Fellow
HOCKE, Heiko	JST Post-Doctoral Fellow
KIKUCHI, Makoto	Post-Doctoral Fellow (–March ’03)
KOBAYASHI, Yukinari	Visiting Scientist (from Daiichi Parmaceutical Co. Ltd.) (–March ’03)
KIKUZAWA, Yoshihiro	Graduate Student
NAKAI, Yasushi	Graduate Student
KIMURA, Masahiro	Graduate Student
TAMAKI, Hirotaka	Graduate Student
SAKAMAKI, Junichiro	Graduate Student (April ’03–)
MINAKAWA, Maki	Graduate Student (April ’03–)

Nano-scale Photoscience

MATSUMOTO, Yoshiyasu	Professor (from the Graduate University for Advanced Studies) (April ’03–)
TSUKUDA, Tatsuya	Associate Professor
NARUSHIMA, Takashi	Graduate Student (October ’02–)

Interface Molecular Science

KOMIYAMA, Masaharu	Professor (from Yamanashi University) (–March ’03)
MIZUNO, Akira	Professor (from Toyohashi University of Technology) (April ’03–)
OKUDAIRA, Koji	Associate Professor (from Chiba University) (–March ’03)
TAKAHASHI, Masahiko	Associate Professor (from Tohoku University) (April ’03–)
TAKASHIMA, Yoshifumi	Research Associate (from Nagoya University) (–March ’03)
KUBOZONO, Yoshihiro	Research Associate (from Okayama University) (–March ’03)
KERA, Satoshi	Research Associate (from Chiba University) (April ’03–)
WATANABE, Noboru	Research Associate (from Tohoku Univerisity) (April ’03–)
MATSUMOTO, Taki	IMS Fellow (–October ’02)
KSHIRSAGAR RAJENDRA, Balwant	IMS Fellow (November ’02–March ’03)
YOSHIMURA, Daisuke	Research Fellow (–March ’03)
LI, Yan Jun	Research Fellow (–February ’03)
YANG, Hanpei	Research Fellow (December ’02–March ’03)
TAKABAYASHI, Yasuhiro	Graduate Student (from Okayama University) (–March ’03)
YAMANE, Hiroyuki	Graduate Student (from Chiba University) (–March ’03)
YOKOYAMA, Takahiro	Graduate Student (from Nagoya University) (–March ’03)
KIYOHARA, Kohei	Graduate Student (from Shimane University) (–March ’03)
OKAMOTO, Masayuki	Graduate Student (from Toyohashi University of Technology)* (June’03–)
TUN, Lwin	Graduate Student (from Toyohashi University of Technology)* (June ’03–)
KOMATU, Jun	Graduate Student (from Toyohashi University of Technology)* (June ’03–)
KINOSHITA, Youhei	Graduate Student (from Toyohashi University of Technology)* (June ’03–)
SUNG, Bongjo	Graduate Student (from Toyohashi University of Technology)* (June ’03–)
YOGI, Osamu	Graduate Student (from Toyohashi University of Technology)* (June ’03–)
SUZUKI, Masanori	Graduate Student (from Toyohashi University of

	Technology)* (June ’03–)

Molecular Clusters

TANIMOTO, Yoshifumi	Professor (from Hiroshima University)
ISHIDA, Toshimasa	Associate Professor (from Shizuoka University)
FUJIWARA, Masao	Research Associate (from Hiroshima University)
OBA, Toru	Research Associate (from Utsunomiya University)
DUNIN-BARKOVSKIY, Lev	IMS Fellow (December ’02–)
UECHI, Ichiro	Graduate Student (from Hiroshima University)*
HANASAKI, Mitsuru	Graduate Student (from Utsunomiya University)* (–March ’03)
FUJIWARA, Umihito	Graduate Student (from Utsunomiya University)* (–March ’03)
TAKATOYA, Haruki	Graduate Student (from Utsunomiya University)* (April ’03–)
TOBITA, Hiromi	Graduate Student (from Utsunomiya University)* (April ’03–)

Equipment Development Center

YAKUSHI, Kyuya	Director
WATANABE, Michio	Associate Professor

Ultraviolet Synchrotron Orbital Radiation Facility

KOSUGI, Nobuhiro	Director
KATOH, Masahiro	Associate Professor
SHIGEMASA, Eiji	Associate Prorfessor
KIMURA, Shin-ichi	Associate Professor
HORI, Yoichiro	Visiting Associate Professor (from Photon Factory) (–March ’03)
ITO, Kenji	Visiting Associate Professor (from Photon Factory) (April ’03–)
HOSAKA, Masahito	Research Associate
GEJO, Tatsuo	Research Associate (–March ’03)[23)]
TAKAHASHI, Kazutoshi	Research Associate (–March ’03)[24)]
MOCHIHASHI, Akira	Research Associate
ITO,Takahiro	Research Associate (April ’03)
AZUMA, Junpei	JSPS Post-Doctral Fellow (–March ’03)[24)]
TANAKA, Senku	Graduate Student (–March ’03)[25)]
NISHI, Tatsuhiko	Graduate Student

Computer Center

HIRATA, Fumio	Director (–March ’03)
NAGASE, Shigeru	Director (April ’03–)
OKAZAKI, Susumu	Professor
AOYAGI, Mutsumi	Professor (from Kyushu University) (–March ’03)
NANBU, Shinkoh	Research Associate
OONO, Hitoshi	Research Associate
MIURA, Shinichi	Research Associate
MINAMINO, Satoshi	Technical Associate
MAKI, Jun	IMS Fellow (–April ’03)
IWAHASHI, Kensuke	IMS Fellow
KINOSHITA, Tomoko	Graduate Student
MIKAMI, Taiji	Graduate Student (from Tokyo Institute of Technology)*
SATO, Masahiro	Graduate Student (from Tokyo Institute of Technology)*
KOMATSU, Takahiro	Graduate Student (from Tokyo Institute of Technology)*
TANAKA, Junji	Graduate Student (from Tokyo Institute of Technology)* (–March ’03), Research Fellow (April ’03–)

Research Facility of Okazaki National Research Institutes

Center for Integrative Bioscience

Department of Strategic Methodology

KINOSITA, Kazuhiko, Jr.	Professor
AONO, Shigetoshi	Professor
FUJII, Hiroshi	Associate Professor

NAKAJIMA, Hiroshi	Research Associate (January ’03–April ’03)
ADACHI, Kengo	Research Associate (January ’03–)
KOBAYASHI, Katsuaki	IMS Fellow (April ’03–)
KUJIME, Masato	IMS Fellow (April ’03–)
BERTINI, Ivano	Visiting Scientist; JSPS Invited Fellow (July ’03–August ’03)
FUJIWARA, Ikuko	JSPS Post-Doctoral Fellow (April ’03–)
ALI, Md. Yusuf	Post-Doctoral Fellow
MAKI, Yasushi	Post-Doctoral Fellow
KON, Rieko	Post-Doctoral Fellow
FURUIKE, Shou	Post-Doctoral Fellow
SHIROGUCHI, Katsuyuki	Post-Doctoral Fellow
KANDA, Ritsuko	Research Fellow
YOGO, Katsunori	Graduate Student (from Waseda University)
SAKAKI, Naoyoshi	Graduate Student
ONOUE, Yasuhiro	Graduate Student
INAGAKI, Sayaka	Graduate Student
YOSHIMURA, Hideaki	Graduate Student

Department of Bio-environmental Science

KITAGAWA, Teizo	Professor
YAMATO, Takehisa	Visiting Associate Professor
UCHIDA, Takeshi	Research Associate
NAGATOMO, Shigenori	Technical Associate
KIM, Younkyoo	Visiting Scientist; MONBUSHO Invited Fellow (June ’03–August ’03)
WALKER, Gilbert Creighton	Visiting Scientist; JSPS Invited Fellow (April ’03–)
MAHINAY, Myrna Sillero	Visiting Scientist; JSPS Post-Doctoral Fellow (June ’03–)
HIRAMATSU, Hirotsugu	IMS Fellow (–March ’03), JSPS Post-Doctoral Fellow (April ’03–)
TOSHA, Takehiko	IMS Fellow (August ’03–)
OHTA, Takehiro	JSPS Post-Doctoral Fellow
NAGANO, Yasutomo	JSPS Post-Doctoral Fellow
OKUNO, Daichi	Graduate Student
SATO, Akira	Graduate Student

* Carries out graduate research of IMS on Cooperative Education Program of IMS with other graduate schools.

Technical Staff

SAKAI, Kusuo	Technical Division Head
MATSUDO, Osamu	Technical Section Chief
KATO, Kiyonori	Technical Section Chief
YAMANAKA, Takaya	Technical Section Chief
HORIGOME, Toshio	Technical Section Chief (October '02–)
SUZUI, Mitsukazu	Equipment Development Center (Unit Chief) (–September '02); Technical Section Chief (October '02–)
NAKAMURA, Eiken	Electronic Structure (Unit Chief)
YOSHIDA, Hisashi	Molecular Assemblies (Unit Chief)
YAMAZAKI, Jun-ichiro	Laser Research Center for Molecular Science (Unit Chief)
UEDA, Tadashi	Laser Research Center for Molecular Science
NAGATA, Masaaki	Research Center for Molecular-scale Nanoscience (Unit Chief)
TAKAYAMA, Takashi	Research Center for Molecular-scale Nanoscience (Unit Chief)
SAKAI, Masahiro	Research Center for Molecular-scale Nanoscience
MAKITA, Seiji	Research Center for Molecular-scale Nanoscience
MIZUTANI, Nobuo	Equipment Development Center (Unit Chief)
UCHIYAMA, Kouichi	Equipment Development Center
TOYODA, Tomonori	Equipment Development Center
YANO, Takayuki	Equipment Development Center
MATSUSHITA, Koji	Equipment Development Center
HASUMOTO, Masami	UVSOR facility (Unit Chief)
KONDOU, Naonori	UVSOR facility
HAYASHI, Kenji	UVSOR facility
MIZUTANI, Fumiyasu	Computer Center (Unit Chief)
TESHIMA, Fumitsuna	Computer Center
NAITOU, Shigeki	Computer Center
SAWA, Masataka	Computer Center (April '03–)

List of Present Addresses

1) Nagahama Institute of Bio-Science and Technology, Tamuracho, Nagahama, 526-0826
2) Institute fuer Festkoerperforshung, Forschungszentrum Juelich, D-52425 Juelich, Germany
3) TOYOTA TECHNO SERVICE CORP. 1-21 Imae Hanamotocho Toyota 470-0334
4) Department of Chemistry, Graduate School of Science, Kyoto University, Kitashirakawa-Oiwakecho, Sakyo-ku, Kyoto 606-8502
5) Department of Chemistry, University of Minnesota, 207 Pleasant St. SE, Minneapolis, MN55455-0431, USA
6) Department of Chemistry, Faculty of Science, Tohoku University, Aramaki-Aoba, Aoba-ku, Sendai, 980-8578
7) Chemistry Department, Boston University, 590 Commonwealth Ave., Boston, MA 02215, USA
8) Department of Chemical System Engineering, School of Engineering, the University of Tokyo, Hongo, Bunkyo-ku, Tokyo 113-8656
9) National Institute of Nanotechnology, National Research Council Canada, University of Alberta, 9107-116 Street, Edmonton, AB T6G 2V4, Canada
10) Department of Mathematics, Physics and Computer Aided Science, Faculty of Engineering, Kyushu Institute of Technology, Senshuicho, Tobata-ku, Kitakyushu, 804-8550
11) Institute of Molecular and Cellular Biosciences, the University of Tokyo, Yayoi, Bunkyo-ku, Tokyo, 113-0032
12) Genesis Research Institute, Inc., 717-86 Futamata, Ichikawa, Chiba 272-0001, Japan
13) RIKEN, 2-1 Hirosawa, Wako, Saitama 351-0198, Japan
14) Chemical Dynamics Laboratory, The Institute of Physical and Chemical Research (RIKEN), Wako, Saitama 351-01
15) Department of Chemistry, Faculty of Education, Aichi University of Education, Hirosawa 1, Igaya, Kariya 448-5842
16) Chemical Spectroscopy Division, Chemical Resources laboratory, Tokyo Institute of Technology, 4259 Nagatsuta, Midori-ku, yokohama, Kanagawa 226-8503
17) Department of Material Science, Graduate School of Science, Himeji Institute of technology, 3-2-1 Kohto, Kamigori, Hyogo 678-1297
18) College of Integrated Arts and Sciences, Osaka Prefecture University, 1-1 Gakuen-cho, Sakai, Osaka 599-8531, JAPAN
19) Department of Basic Science, the Graduate School of Arts and Sciences, the University of Tokyo, 3-8-1 Komaba, Meguro-ku, Tokyo 153-8902, JAPAN

20) Research Institute for Electronic Science, Hokkaido University, Kita 12, Nishi 6, Sapporo 060-0812, JAPAN
21) Nanotechnology Comprehensive Support Project, Ritsumeikan University, Noji higashi 1-1-1, Kusatsu, Shiga 525-8577
22) Sagami Chemical Research Center
23) Department of Material Science, Himeji Institute of Technology, 3-2-1 Kouto, Kamigori, 679-1200
24) Synchrotron Light Application Center, Saga University, 1 Honjyo, Saga, 840-8502
25) Department of Chemistry, Division of Material Science, Graduate School of Science, Nagoya University, Furo-cho, Chikusa-ku, Nagoya 464-8602

COUNCIL

KAYA, Koji **Director-General**

Councillors

Chairperson	HOSOYA, Haruo	Professor Emeritus, Ochanomizu University
Vice-Chairperson	HIROTA, Noboru	Professor Emeritus, Kyoto University
	ARIKAWA, Yoshiko	Professor, Japan Women's University
	IIYOSHI, Atsuo	President, Chubu University
	ISHITANI, Akira	Executive Director, Kanagawa Academy of Science and Technology
	OHTSUKA, Eiko	Fellow, National Institute of Advanced Industrial Science & Technology
	OGINO, Hiroshi	Director, Miyagi Study Center of the University of the Air
	KAIFU, Norio	Director General, National Astronomical Observatory of Japan
	KITAGAWA, Genshiro	Director, The Institute of Statistical Mathematics
	KINOSHITA, Minoru	Professor Emeritus, Tokyo University
	GOTO, Keishi	Vice President, Science Create Inc.
	KONDOW, Tamotsu	Visiting Professor, Toyota Technological Institute, Cluster Research Laboratory
	KOMA, Atsushi	Director, Institute of Materials Structure Science
	TAKAHASHI, Riichi	President and Chief Operating Officer, Toyota Central Research & Development Laboratories,Inc.
	TSUCHIYA, Soji	Invited Professor, Josai University
	FUKUYAMA, Hidetoshi	Professor, The Institute for Solid State Physics, University of Tokyo
	YAMAZAKI, Toshimitsu	Professor Emeritus, Tokyo University
	YAMAMURA, Shosuke	Professor Emeritus, Keio University
	FLEMING, Graham R.*	Professor, University of California, Berkeley
	JORTNER, Joshua*	Professor, Tel Aviv University

The Council is the advisory board for the Director-General.
* Two of the councillors are selected among distinguished foreign scientists.

Distinguished Research Consultants

NAGAKURA, Saburo	The Japan Academy
INOKUCHI, Hiroo	Chief Scientist of Space Utilization Research Program, National Space Development Agency of Japan
TSUCHIYA, Soji	Invited Professor, Josai University
ITO, Mitsuo	Professor Emeritus, Insitute for Molecular Science, The Graduate University for Advanced Studies, Tohoku University
HIROTA, Noboru	Professor Emeritus, Kyoto University
KONDOW, Tamotsu	Visiting Professor, Toyota Technological Institute

Administration Bureau

MORISHIGE, Kazuko	Director-General, Administration Bureau
SUNADA, Hitoshi	Director, General Affairs Department (–March ’03)
KUBO, Tetsuo	Director, General Affairs Department (April ’03–)
YUKI, Yoshihisa	Director, Finance and Facilities Department (–Oct ’02)
HARAGUCHI, Masaaki	Director, Finance and Facilities Department (Nov ’02–)
FURUKAWA, Masato	Head, General Affairs Division
UCHIDA, Yoshio	Head, Personnel Division
NAGINO, Tomoe	Head, Research Cooperation Division
KITAGAWA, Hiroshi	Head, International Affairs Division
HIRAI, Tokio	Head, Budget Division (–March ’03)
OGOSHI, Kazuhiro	Head, Budget Division (April ’03–)
KUBOKAWA, Tomoyuki	Head, Accounts Division
KATOH, Masayoshi	Head, Construction Division
FUJIMOTO, Shigeo	Head, Equipment Division

BUILDINGS AND CAMPUS

The IMS campus covering 62,343 m^2 is located on a low hill in the middle of Okazaki city. The inequality in the surface of the hill and growing trees are preserved as much as possible, and low-storied buildings are adopted for conservation of the environment. The buildings of IMS are separated according to their functions as shown in the map. The Research Office Building and all Research Facilities except for the Computer Center are linked organically to the Main Laboratory Buildings by corridors. Computer Center, Library and Administration Buildings are situated between IMS and neighboring National Institute for Basic Biology and National Institute for Physiological Sciences, because the latter two facilities are common to these three institutes.

The lodging facility of IMS called Yamate Lodge, located within ten minutes' walk, has sleeping accommodations for 15 guests and two families. Mishima Lodge, located within four minutes' walk east of IMS can accommodate 74 guests and 20 families. Scientists who visit IMS as well as the two other institutes can make use of these facilities. Foreign visiting scientists can also live at these lodgings with their families during their stays. The Okazaki Conference Center, which has four conference rooms capable of between 50 and 250 attendance, was built in April, 1997 in Mishima area. Two buildings for Center for Integrative Bioscience, Research Center for Computational Science, and research facilities of ONRI were built in February, 2002 in Area E.

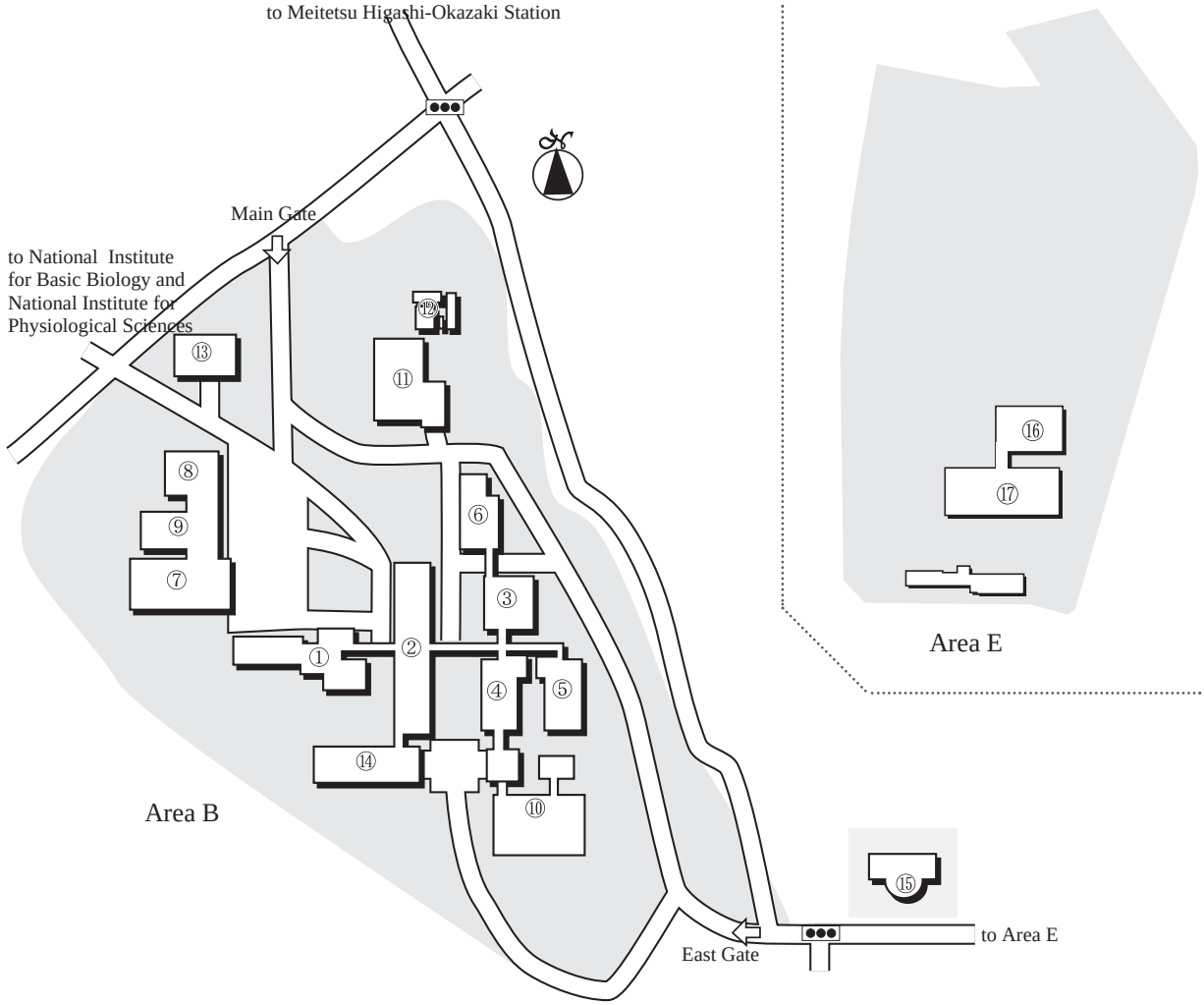

1. Research Office Building
2 Main Laboratory Building
3. Equipment Development Center
4. Laser Research Center for Molecular Science
5. Research Center for Molecular-scale Nanoscience
6. Low-Temperature Facilities Building
7. Computer Center
8. Library
9. Central Administration
10. UVSOR Facility
11. Power Station
12. Waste-Water Disposition Facilities
13. Faculty Club
14. South Laboratory Building
15. Okazaki Conference Center
16. Center for Integrative Bioscience and Research Center for Computational Science
17. Research Facilities of ONRI

Okazaki (population 348,000) is 260 km west of Tokyo, and can be reached by train in about 3 hours from Tokyo via Shinkansen and Meitetsu Line.

The nearest large city is Nagoya, about 40 km northwest of Okazaki.

RESEARCH ACTIVITIES I
Department of Theoretical Studies

I-A Theoretical Study and Design of New Bonding, Structures, and Reactions

It is an important subject to develop molecules with novel bonding and structures. Thus, new bonds containing heavier atoms are investigated, which are the focus of interest as new building block for molecular design. In addition, cage-like molecules and clusters are investigated to characterize guest-host interactions, which serve as molecular containers and recognition. Efficient computational methods are also investigated to perform calculations of large molecular systems.

I-A-1 Theoretical Investigation of Triple Bonding between Transition Metal and Main Group Elements in (η^5-C_5H_5)$(CO)_2$M≡ER (M = Cr, Mo, W; E = Si, Ge, Sn, Pb; R = Terphenyl Groups)

TAKAGI, Nozomi; YAMAZAKI, Kentaro[1]; NAGASE, Shigeru
([1]Univ. Tokyo)

[*Bull. Korean Chem. Soc. (a special issue)* **24**, 832–836 (2003)]

To extend the knowledge of triple bonding between group 6 transition metal and heavier group 14 elements, the structural and bonding aspects of (η^5-C_5H_5)$(CO)_2$-M≡ER (M = Cr, Mo, W; E = Si, Ge, Sn, Pb) are investigated by hybrid density functional calculations at the B3PW91 level. Substituent effects are also investigated with R = H, Me, SiH_3, Ph, C_6H_3-2,6-Ph_2, C_6H_3-2,6-(C_6H_2-2,4,6-Me_3)$_2$, and C_6H_3-2,6-(C_6H_2-2,4,6-*i*Pr_3)$_2$.

I-A-2 Synthesis and Characterization of Cyclic Silicon Compounds of Fullerenes

WAKAHARA, Takatsugu[1]; KAKO, Masahiro[2]; MAEDA, Yutaka[3]; AKASAKA, Takeshi[1]; KOBAYASHI, Kaoru; NAGASE, Shigeru
([1]Univ. Tsukuba; [2]Univ. Electron-Communication; [3]Tokyo Gakugei Univ.)

[*Curr. Org. Chem.* **7**, 927–943 (2003)]

Organosilicon compounds are among the most important inter-element compounds, as exemplified by disilanes and polysilanes. Since the availability of C_{60} in preparatively useful quantities, the chemical functionalization has attracted considerable interest, which leads to new cyclic silicon compounds. It is experimentally and theoretically investigated how silylenes, which are derived from a variety of disilanes under thermal and photochemical conditions, react with fullerenes and endohedral metallofullerenes. Mono-, bis-, and even multi-silylation of fullerenes lead to a new class of silicon compounds that are useful in material applications.

I-A-3 Calculation of Packing Structure of Methanol Solid using Ab Initio Latice Energy at the MP2 Level

NAGAYOSHI, Kanade[1]; KITAURA, Kazuo[2]; KOSEKI, Shiro[3]; RE, Suyong; KOBAYASHI, Kaoru; CHOE, Yoong-Kee; NAGASE, Shigeru
([1]IMS and Osaka Prefecture Univ.; [2]AIST; [3]Osaka Prefecture Univ.)

[*Chem. Phys. Lett.* **369**, 597–604 (2003)]

An ab initio MO based lattice energy minimization method is applied to the calculation of packing structures of methanol crystal, α- and β-phases. The second order Møller-Plesset perturbation theory (MP2) is employed to calculate lattice energies. The lattice parameters optimized at the MP2/6-31G++G(*d*,*p*) level for α- and β-phases are in good and moderate agreement with the experimental values, respectively. The average relative errors of calculated cell lengths are 0.9 and 6.2% for α- and β-phases, respectively.

I-A-4 Computational Procedure of Lattice Energy using the Ab Initio MO Method

NAGAYOSHI, Kanade[1]; IKEDA, Tohru[2]; KITAURA, Kazuo[3]; NAGASE, Shigeru
([1]IMS and Osaka Prefecture Univ.; [2]Osaka Prefecture Univ.; [3]AIST)

[*J. Theor. Comput. Chem.* **2**, 233–244 (2003)]

Recently, we have proposed a computational procedure for calculations of lattice energies of molecular crystals using the *ab initio* MO method. This procedure does not use potential functions and is applicable to a variety of molecular crystals. The procedure has been successfully applied to calculation of packing structure of electron donor-acceptor complex, H_3N-BF_3, and hydrogen bonding crystal, CH_3OH. In this work, we present a full account of the computational procedure. This method is applied to the packing structure calculations of hydrocarbon crystals, C_2H_2, C_2H_4 and C_6H_6. The lattice parameters optimized at the MP2/6-311++G** level are in good agreement with the experimental values. The basis set dependence of the lattice constants

is also discussed for several crystals.

I-A-5 $La_2@C_{80}$: Is the Circular Motion of Two La Atoms Controllable by Exohedral Addition?

KOBAYASHI, Kaoru; NAGASE, Shigeru; MAEDA, Yutaka[1]; WAKAHARA, Takatsugu[2]; AKASAKA, Takeshi[2]
([1]Tokyo Gakugei Univ.; [2]Univ. Tsukuba)

[*Chem. Phys. Lett.* **374**, 562–566 (2003)]

Density functional calculations are carried out for the $La_2@C_{80}$ derivatives to investigate whether the motion of metals encapsulated inside fullerenes is controlled by exohedral addition. It is shown that the three-dimensional random motion of two La atoms in $La_2@C_{80}$ can be restricted to the circular motion in a plane by attaching electron-donating molecules on the outer surface of the C_{80} cage. It is expected that the two-dimensional circular motion will help to induce a unique electronic or magnetic field.

I-A-6 A Theoretical Study of Spin Density Distributions and Isotropic Hyperfine Couplings of N and P atoms in $N@C_{60}$, $P@C_{60}$, $N@C_{70}$, $N@C_{60}(CH_2)_6$, and $N@C_{60}(SiH_2)_6$

KOBAYASHI, Kaoru; NAGASE, Shigeru; DINSE, Klaus-Peter[1]
([1]IMS and TU-Darmstadt)

[*Chem. Phys. Lett.* **377**, 93–98 (2003)]

Spin density distributions and isotropic hyperfine coupling constants of $N@C_{60}$, $P@C_{60}$, $N@C_{70}$, $N@C_{60}(CH_2)_6$, and $N@C_{60}(SiH_2)_6$ are theoretically investigated by testing B3LYP and MP2 methods for the free N and P atoms. When N is encapsulated inside C_{60}, the calculated spin density at nucleus N increases. In $P@C_{60}$, the corresponding increase is much larger. $N@C_{60}$ has a slightly larger spin density at N than $N@C_{70}$. These agree well with the observed isotropic hyperfine coupling constants. Upon addition of CH_2 groups on the $N@C_{60}$ cage, the spin density at N is slightly decreased. However, addition of SiH_2 groups increases significantly the spin density at the nitrogen nucleus.

I-A-7 Theoretical Identification of C_{20} Carbon Clusters

LU, Jing[1]; RE, Suyong; CHOE, Yoong-Kee; NAGASE, Shigeru; ZHOU, Yunsong[2]; HAN, Rushan[2]; PENG, Lianmao[2]; ZHANG, Xinwei[2]; ZHAO, Xiangeng[2]
([1]IMS and Peking Univ.; [2]Peking Univ.)

[*Phys. Rev. B* **67**, 125415 (7 pages) (2003)]

Free energies, electron affinities and vibrational modes are theoretically investigated for several C_{20} isomers. The dominant C_{20} species generated by vaporizing graphite is first clarified. It turns out to be the monocyclic ring, followed by a tadpole (a short chain attached to a monocyclic ring), linear chain, and a bicyclic ring. On this basis, the two recently synthesized C_{20} isomers [*Nature* **407**, 60 (2000)] may be exclusively attributed to fullerene and bowl structures. Therefore, the existence of the smallest fullerene and C_{20} bowl isomer appear to be fully confirmed.

I-A-8 Structural and Electronic Properties of Metal-Encapsulated Silicon Clusters in a Large Size Range

LU, Jing[1]; NAGASE, Shigeru
([1]IMS and Peking Univ.)

[*Phys. Rev. Lett.* **90**, 115506 (4 pages) (2003)]

Structural and electronic properties of metal-doped silicon clusters MSi_n (M = W, Zr, Os, Pt, *etc.*) in a large size range $8 \le n \le 20$ are theoretically investigated. In contrast to a recent experiment suggesting that a metal atom is encapsulated inside the Si_n cluster, we reveal that the formation of endohedral structures depends strongly on the size of silicon clusters. Two novel structures of chemically stable endohedral species are manifested. The suitable $M@Si_n$ building blocks of self-assembly materials vary in the range $10 \le n \le 16$. The thermodynamical magic numbers are found to coincide with the chemical magic numbers for five clusters.

I-A-9 Metal-Doped Germanium Clusters MGe_n at the Sizes of n = 12 and 10: Divergence of Growth Patterns from the MSi_n Clusters

LU, Jing[1]; NAGASE, Shigeru
([1]IMS and Peking Univ.)

[*Chem. Phys. Lett.* **372**, 394–398 (2003)]

Structural and electronic properties of metal-doped germanium clusters MGe_n (M = Hf, W, Os, Ni, and Zn) in the sizes of n = 12 and 10 are investigated using hybrid density functional theory calculations. It is found that the growth patters are different from those of $M@Si_n$ clusters, though the pure Ge_n and Si_n clusters have identical geometries in the two sizes. The MGe_{12} (M = W and Os) and $ZnGe_{12}$ clusters have endohedral distorted hexagonal prismatic and endohedral perfect icosahedral structures, respectively, and show higher chemical stability among these checked MGe_n clusters. This makes them attractive for cluster-assembled materials.

I-A-10 $Ca@C_{72}$ IPR and Non-IPR Structures; Computed Temperature Development of their Relative Concentrations

SLANINA, Zdenek[1]; KOBAYASHI, Kaoru; NAGASE, Shigeru
([1]IMS and Academia Sinica)

[*Chem. Phys. Lett.* **372**, 810–814 (2003)]

Relative concentrations of four isomers of $Ca@C_{72}$

(one species with isolated pentagons, two isomers with a pentagon-pentagon junction, one structure with a heptagon) are computed using the Gibbs energy in a broad temperature interval. It is shown that both isomers with pentagon-pentagon junction are relatively close in concentrations at higher temperatures while the structure with isolated pentagons comes as a minor isomer (though it is the highest in potential energy) and the structure with heptagon is always negligible.

I-A-11 Photochemical Bissilylation of C_{70} with Disilane

RAHMAN, G. M. Aminur[1]; MAEDA, Yutaka[2]; WAKAHARA, Takatsugu[2]; KAKO, Masahiro[3]; SATO, Soichi[2]; OKAMURA, Mutsuo[1]; AKASAKA, Takeshi[2]; KOBAYASHI, Kaoru; NAGASE, Shigeru
([1]Niigata Univ; [2]Univ. Tsukuba; [3]Univ. Electro-Communications)

[*ITE Lett. Batt. New Tech. Med.* **4**, 60–66 (2003)]

The photochemical reaction of C_{70} with disilane affords bisadducts and monoadducts as major and minor products, respectively, which are successfully isolated. Theoretical calculations are carried out to disclose the structural features. The reaction patterns are characterized by calculating spin density distributions. It is expected that the silicon derivatives will play an important role in material and catalytic applications.

I-A-12 Redox Properties of Carbosilylated and Hydrosilylated Fullerene Derivatives

WAKAHARA, Takatsugu[1]; RAHMAN, G. M. Aminur[2]; MAEDA, Yutaka[1]; KAKO, Masahiro[3]; SATO, Soichi[2]; OKAMURA, Mutsuo[2]; AKASAKA, Takeshi[1]; KOBAYASHI, Kaoru; NAGASE, Shigeru
([1]Univ. Tsukuba; [2]Niigata Univ; [3]Univ. Electro-Communications)

[*ITE Lett. Batt. New Tech. Med.* **4**, 67–73 (2003)]

Experimental results and theoretical calculations suggest that the electrochemical properties of fullerenes, such as reduction and oxidation potentials, are significantly modified by attaching exohedrally silicon atoms on carbon cages. Among these, hydrosilylation and carbosilylation of C_{60} are useful to produce electronegative fullerene derivatives. It is expected that the derivatives with highly low oxidation potentials will open up a new application of C_{60} as a unique electron-donor.

I-A-13 B3LYP/6-31G* Computations of $C_{60}F_{36}$ (*g*) Isomers

SLANINA, Zdenek[1]; BOLTALINA, Olga V.[2]; KOBAYASHI, Kaoru; NAGASE, Shigeru
([1]IMS and Academia Sinica; [2]Moscow State Univ.)

Three isomers of $C_{60}F_{36}$ have been known from experiment. Previous computations however suggested five low-energy isomers though different methods do not always agree on the separation energetics. The present B3LYP/6-31G* computations support the observation of just three species. However, the computed energetics must still be adjusted in order to reproduce the observed concentration ratios.

I-B Prediction of Protein Tertiary Structures and Protein Folding Problem

Prediction of the three-dimensional structures of protein molecules by computer simulations is a very challenging problem in theoretical molecular science. The difficulty of the problem lies in two facts: (1) the inclusion of accurate solvent effects is non-trivial and time-consuming (2) there exist a huge number of local minima in the energy function, forcing conventional simulations to get trapped in states of energy local minima. We have been exploring the strategies that allow us to overcome these difficulties and to study the protein folding mechanism by directly folding proteins.

I-B-1 Molecular Dynamics of C-Peptide of Ribonuclease A Studied by Replica-Exchange Monte Carlo Method and Diffusion Theory

LA PENNA, Giovanni[1]; MITSUTAKE, Ayori[2]; MASUYA, Masato[3]; OKAMOTO, Yuko
([1]Natl. Res. Council, Inst. Macromol. Studies, Italy; [2]Keio Univ.; [3]Kagoshima Univ.)

[*Chem. Phys. Lett.* in press]

Generalized-ensemble algorithm and diffusion theory have been combined in order to compute the dynamical properties monitored by nuclear magnetic resonance experiments from efficient and reliable evaluation of statistical averages. Replica-exchange Monte Carlo simulations have been performed with a C-peptide analogue of ribonuclease A, and Smoluchowski diffusion equations have been applied. A fairly good agreement between the calculated and measured ^{1}H-NOESY NMR cross peaks has been obtained. The combination of these advanced and continuously improving statistical tools allows the calculation of a wide variety of dynamical properties routinely obtained by experiments.

I-B-2 Multi-Overlap Simulations for Transitions between Reference Configurations

BERG, Bernd A.[1]; NOGUCHI, Hiroshi; OKAMOTO, Yuko
([1]Florida State Univ.)

[*Phys. Rev. E* in press]

We introduce a new procedure to construct weight factors, which flatten the probability density of the overlap with respect to some pre-defined reference configuration. This allows one to overcome free energy barriers in the overlap variable. Subsequently, we generalize the approach to deal with the overlaps with respect to two reference configurations so that transitions between them are induced. We illustrate our approach by simulations of the brainpeptide Met-enkephalin with the ECEPP/2 energy function using the global-energy-minimum and the second lowest-energy states as reference configurations. The free energy is obtained as functions of the dihedral and the root-mean-square distances from these two configurations. The latter allows one to identify the transition state and to estimate its associated free energy barrier.

I-C Development of Simulation Algorithms for Complex Systems

Developing a powerful simulation algorithm that can alleviate the multiple-minima problem is important in many complex systems. We have been advocating the uses of the so-called generalized-ensemble algorithms such as multicanonical algorithm and replica-exchange method.

I-C-1 Monte Carlo Simulations in Multibaric-Multithermal Ensemble

OKUMURA, Hisashi; OKAMOTO, Yuko

[*Chem. Phys. Lett.* in press]

We propose a new generalized-ensemble algorithm, which we refer to as the multibaric-multithermal Monte Carlo method. The multibaric-multithermal Monte Carlo simulations perform random walks widely both in volume space and in potential energy space. From only one simulation run, one can calculate isobaric-isothermal-ensemble averages at any pressure and any temperature. We test the effectiveness of this algorithm by applying it to the Lennard-Jones 12-6 potential system with 500 particles. It is found that a single simulation of the new method indeed gives accurate average quantities in isobaric-isothermal ensemble for a wide range of pressure and temperature.

I-D Applications of the Zhu-Nakamura Theory to Electronically Nonadiabatic Chemical Dynamics

I-D-1 Trajectory Surface Hopping Approach to Conical Intersection System

MIL'NIKOV, Gennady V.; OLOYEDE, Ponmile[1]; NAKAMURA, Hiroki
([1]GUAS)

The Zhu-Nakamura theory was proved to work well within the TSH (trajectory surface hopping) scheme in the case of DH_2^+ which presents a typical example of crossing seam type chemical reactions. It was found that the classically forbidden nonadiabatic transitions which cannot be treated by the Landau-Zener theory play important roles. In the present work the similar kind of analysis is carried out for a triatomic model reaction system of conical intersection. By doing this we would like to establish a general TSH method applicable to high dimensional systems.

I-D-2 Incorporation of the Zhu-Nakamura Theory into the Frozen Gaussian Propagation Method

KONDORSKIY, Alexey[1]; NAKAMURA, Hiroki
([1]IMS and Lebedev Physical Inst., Russia)

A new semiclassical theory is developed by combining the Herman-Kluk semicalassical theory for adiabatic propagation on single potential energy surface and the semiclassical Zhu-Nakamura theory for nonadiabatic transition. The formulation with use of natural mathematical principles leads to a quite simple expression for the propagator based on classical trajectories and simple formulas are derived for overall adiabatic and nonadiabatic processes. The theory is applied to electronically nonadiabatic photodissociation processes: one-dimensional problem of H_2^+ in a cw laser field and two-dimensional model problem of H_2O in a cw laser field. The theory is found to work well for the propagation duration of several molecular vibrational periods and wide wave packet energy range. Although the formulation is made for the case of laser induced nonadiabatic process, it is straghtforwardly applicable to ordinary electronically nonadiabatic chemical dynamics.

I-E Theory of Nonadiabatic Transitions

I-E-1 Semiclassical Theory of Nonadiabatic Transitions between Asymptotically Degenerate States

OSHEROV, Vladimir I.[1]; USHAKOV, Vladimir G.[1]; NAKAMURA, Hiroki
([1]Inst. Chemical Physics, Russia)

[*Russ. Chem. Phys.* in press]

The semiclassical analysis is carried out for a two-state model potential system, in which two asymptotically degenerate Morse type potentials are coupled by an exponential diabatic coupling. Both crossing and non-crossing cases are treated and explicit analytical expressions for the full scattering matrix are obtained. A numerical test demonstrates the accuracy of the theory. The result for non-crossing case provides the analytical expression of nonadiabatic transition matrix and can be used in a more general multichannel problem involving the present type of asymptotic transitions.

I-E-2 Analytical Treatment of S-P Type Collisional Resonant Excitation Transfer

OSHEROV, Vladimir I.[1]; USHAKOV, Vladimir G.[1]; NAKAMURA, Hiroki
([1]Inst. Chemical Physics, Russia)

[*Russ. Chem. Phys.* in press]

The analytical solution developed in the previous paper is applied to the S-P type collisional resonant excitation transfer between atoms. The corresponding cross-sections are calculated in the high energy approximation. Good agreement is obtained with the results calculated previously by Watanabe with use of the fully numerical integration of the time-dependent coupled differential equations. This indicates usefulness of the present analytical theory developed in our previous papers.

I-E-3 Analytic Solution to Wave Packet Dynamics in a Laser Field: The Case of Linear Chirp

NAKAMURA, Hiroki

[*Chem. Phys.* in press]

An analytical expression for the nonadiabatic transition probability is derived for the case that two linear potentials in coordinate space are coupled by a linearly chirped time-dependent laser field. This constitutes a solution to the wave packet dynamics in the high energy approximation. Numerical calculations are carried out to demonstrate the applicability of the formula.

I-E-4 Nonadiabatic Transition—An Origin of Mutability of This World

NAKAMURA, Hiroki

(In "Nonadiabatic Transitions in Quantum Systems," Russian Academic Publishing House, to be published)

A brief review of the Zhu-Nakamura theory and a brief explanation how to use the theory are presented together with some numerical applications. Recent theoretical developments on the other types of nonadiabatic transitions such as non-crossing case, exponential potential model and transitions among asymptotically degenerate states are also briefly described. Further discussions are made on laser control of molecular processes, intriguing phenomenon of complete reflection, and its applications such as molecular switching and bound states in the continuum.

I-E-5 Semiclassical Theory for Quantum Defect Function of Diatomic Molecules

SOLOVEV, Evgeni A.[1]; NAKAMURA, Hiroki
([1]IMS and Macedonian Acad. Sci. and Arts, Macedonia)

[*J. Phys. B* **36**, 3697 (2003)]

The simple analytical expression for the quantum defect function $\Delta_{lm}(R)$ of diatomic molecule is derived with use of the uniform semiclassical approach including the effects of hidden-crossing. $\Delta_{lm}(R)$ is a function of the internuclear distance R and the effective charge at each nucleus which is again a function of R. Thus, in the case of homonuclear molecule this expression gives universal dependence on R. The derived expression is applied to H_2 molecule. The quantum defects are found to be in good agreement with the *ab initio* numerical data by Wolniewicz and Dressler (*J.Chem.Phys.* **100**, 444).

I-E-6 Non-Linear Landau-Zener Model for Photoassociation of Cold Atoms

ISHKANYAN, Artur[1]; NAKAMURA, Hiroki
([1]IMS and Engineering Cent. Armenian Natl. Acad. Sci., Armenia)

A basic nonlinear model of the two state problem generic in classical and bosonic field theories with a cubic nonlinearity is considered taking the photoassociation of an atomic Bose-Einstein condensate as a specific example. For the class of models with constant external field amplitude a general strategy for attacking the problem is developed based on the reduction of the initial system of equations for the semi-classical atom-molecule amplitudes to a nonlinear Volterra integral equation for the molecular probability. The first approximation term of a uniformly convergent series solution to the Landau-Zener problem is derived and an asymptotic expression for the nonlinear transition probability to the molecular state is established for the weak interaction regime.

I-E-7 Nonadiabatic Transitions Induced by a Laser Field

OSHEROV, Vladimir I.[1]; USHAKOV, Vladimir G.[1]; NAKAMURA, Hiroki
([1]Inst. Chemical Physic, Russia)

The analytical study is carried out for a basic nonadiabatic atomic collision problem of two quantum states coupled by a laser field. The exact semiclassical solution has been found for the resonant type transitions and in the low frequency laser field limit. The high frequency field limit has also been considered in pseudoenergy ridge approach by a matching method.

I-F Quantum Dynamics of Chemical Reactions

I-F-1 Chemical Reactions in the O(^1D) + HCl System I. Ab Initio Global Potential Energy Surfaces for the 1^1A', 2^1A', and 1^1A'' States

NANBU, Shinkoh; AOYAGI, Mutsumi; KAMISAKA, Hideyuki[1]; NAKAMURA, Hiroki; BIAN, Wensheng[2]; TANAKA, Kiyoshi[3]
([1]GUAS; [2]IMS and Shandong Univ., China; [3]Hokkaido Univ.)

[*J. Theor. Comput. Chem.* **1**, 263 (2002)]

New global *ab initio* potential energy surfaces (PES) are presented for the low-lying 1^1A', 1^1A'' and 2^1A' electronic states which are correlated to O(^1D) + HCl. These potential energy surfaces are computed by using the multi-reference configuration interaction method with the Davidson correction (MRCI + Q). The reference functions are constructed by the complete active space self-consistent field (CASSCF) calculations using the quadruple zeta + polarization basis set augmented with diffuse functions. The computations are carried out at about 5000 molecular conformations on each three-dimensional potential energy surface. The high accuracy of the computations is confirmed by a comparison with the available most accurate data for the ground state 1^1A'; thus the present work is the first report of the accurate potential energy surfaces for the two excited states. Three low-lying transition states on the excited surfaces, two (TS2 and TS4) on 1^1A'' and one (TS3) on 2^1A', are found. Since TS2 and TS3 are as low as 0.07 eV and 0.28 eV, respectively, and correlate to the OH($^2\Pi$) + Cl(^2P) product, these excited surfaces are expected to play quite important roles in the reaction

dynamics. Possible effects of nonadiabatic couplings among the three PESs are also briefly discussed, although the nonadiabatic couplings have not yet been estimated. The quantum reaction dynamics in these three PESs are discussed in the second accompanying paper, Paper II.

I-F-2 Chemical Reactions in the O(^1D) + HCl System II. Dynamics on the Ground 1^1A' State and Contributions of the Excited (1^1A'' and 2^1A') States

KAMISAKA, Hideyuki[1]; NAKAMURA, Hiroki; NANBU, Shinkoh; AOYAGI, Mutsumi; BIAN, Wensheng[2]; TANAKA, Kiyoshi[3]
([1]GUAS; [2]IMS and Shandong Univ., China; [3]Hokkaido Univ.)

[*J. Theor. Comput. Chem.* **1**, 275 (2002)]

Using the accurate global potential energy surfaces for the 1^1A', 1^1A'', and 2^1A' states reported in the previous sister Paper I, detailed quantum dynamics calculations are performed for these three adiabatic surfaces separately for $J = 0$ (J: total angular momentum quantum number). Overall reaction probabilities for O + HCl → OH + Cl and H + ClO, the branching ratio between the two reactions, effects of the initial rovibrational excitation, and product rovibrational distributions are evaluated in the total energy region $E_{tot} \leq 0.9$ eV. Significant contributions to the overall reaction dynamics are found from the two excited 1^1A'' and 2^1A' potential energy surfaces, clearly indicating the insufficiency of the dynamics only on the ground 1^1A' surface. The detailed dynamics on the excited surfaces are reported in the third paper of this series.

I-F-3 Chemical Reactions in the O(^1D) + HCl System III. Quantum Dynamics on the Excited (1^1A'' and 2^1A') Potential Energy Surfaces

KAMISAKA, Hideyuki[1]; NAKAMURA, Hiroki; NANBU, Shinkoh; AOYAGI, Mutsumi; BIAN, Wensheng[2]; TANAKA, Kiyoshi[3]
([1]GUAS; [2]IMS and Shangdong Univ., China; [3]Hokkaido Univ.)

[*J. Theor. Comput. Chem.* **1**, 285 (2002)]

Using the accurate global potential energy surfaces for the 1^1A'' and 2^1A' states reported in the previous sister Paper I, detailed quantum dynamics calculations are performed for these adiabatic surfaces separately for $J = 0$ (J: total angular momentum quantum number). In addition to the significant overall contributions of these states to the title reactions reported in the second Paper II of this series, quantum dynamics on these excited potential energy surfaces (PES) are clarified in terms of the PES topographies, which are quite different from that of the ground PES. The reaction mechanisms are found to be strongly selective and nicely explained as vibrationally nonadiabatic transitions in the vicinity of potential ridge.

I-F-4 Quantum Reaction Dynamics of Triatomic Systems in the Hyperspherical Elliptic Coordinates

KAMISAKA, Hideyuki[1]; NAKAMURA, Hiroki
([1]GUAS)

The Hamiltonian expression for the case of general nonzero total angular momentum J is derived in the hyperspherical *elliptic* coordinates which present a powerful tool for analyzing heavy-light-heavy reactions. Implementation of scattering calculations is also discussed. Numerical demonstrations are made by taking the Cl + HD reaction as an example.

I-G Theory of Multi-Dimensional Tunneling

I-G-1 Practical Implementation of the Instanton Theory. II. Decay of Metastable State Through Tunneling

MIL'NIKOV, Gennady V.; NAKAMURA, Hiroki

[*J. Chem. Phys.* **117**, 10081 (2002)]

A new instanton theory for decay rate problem at zero temperature is presented. The canonically invariant expression for the lifetime of metastable state is derived. The theory is fully implemented by an effective numerical recipe to find the instanton trajectory and is applicable to any high dimensional systems.

I-G-2 Tunneling Splitting in Polyatomic Molecules: Application to Malonaldehyde

MIL'NIKOV, Gennady V.; YAGI, Kiyoshi[1]; TAKETSUGU, Tetsuya[2]; NAKAMURA, Hiroki; HIRAO, Kimihiko[1]
([1]Univ. Tokyo; [2]Ochanomizu Univ.)

[*J. Chem. Phys.* **119**, 10 (2003)]

We report an accurate and efficient full dimensional semiclassical *ab initio* method for calculation of energy level splitting due to tunneling in polyatomic system. The method is applied to 21-dimensional 9-atomic malonaldehyde molecule. The tunneling splittings obtained are ΔE(H) = 21.2 cm^{-1} for hydrogen atom transfer and ΔE(D) = 3.0 cm^{-1} for deuterium atom transfer, which are in excellent agreement with the experimental values of 21.6 cm^{-1} and, 2.9 cm^{-1} respectively. We believe that the present analysis gives the

final solution to the longstanding problem.

I-G-3 Semiclassical Theory of Tunneling Splitting for Vibrationally Excited States

MIL'NIKOV, Gennady V.; NAKAMURA, Hiroki

The theory developed before for ground state tunneling splitting is extended to excited state. Both longitudinal and transverse excitation are considered and canonically in variant formulas of energy splitting are derived for the low-lying excited states. The multi-dimensional effect of oscillation of tunneling splitting against vibrational excitation can be nicely interpreted in terms of the local frequency.

I-G-4 A Novel Method to Determine Caustics on a Family of Classical Trajectories

OLOYEDE, Ponmile[1]; MIL'NIKOV, Gennady V.; NAKAMURA, Hiroki
([1]GUAS)

A new method to find caustics in multi-dimensional space is proposed. This is composed of the solution of the first order differential equations satisfied by $A_{ij} = \delta p_i/\delta q_j$ and the canonical transformation to avoid the divergence of this quantity. The repetitive use of this transformation enables us to detect closely-lying caustics. This method is useful in semiclassical treatment of chemical dynamics, since we can take into account the tunneling effects by restarting tunneling trajectories from caustics.

I-H Laser Control of Molecular Processes

I-H-1 Control of Molecular Processes by a Sequence of Linearly Chirped Pulses

NAGAYA, Kuninobu[1]; TERANISHI, Yoshiaki[2]; NAKAMURA, Hiroki
([1]GUAS; [2]Adv. Photon Res. Cent.)

[*J. Chem. Phys.* **117**, 9588 (2002)]

A new scheme of controlling molecular processes by a sequence of linearly chirped pulses is proposed and is applied to selective excitation of an energy level among closely lying ones and to complete electronic excitation of a diatomic molecule. The basic idea is quite different from the conventional ones utilizing chirped pulses in the sense that the present one does not rely on the idea of adiabatic rapid passage at all, but tries to control basic nonadiabatic transitions explicitly. Control of molecular processes can be achieved by controlling nonadiabatic transitions among Floquet (or dressed) states with use of the interference effects. The scheme can be formulated with use of the analytical theories of nonadiabatic transitions, and the proper control parameters can be estimated theoretically. Numerical demonstrations are provided to confirm the robustness of the method in comparison with the other conventional ones. Namely, the present scheme is shown to be stable against the variation of pulse area, complete and selective in population transfer, and fast to accomplish the transition. It is expected that the method can be applied to general multilevel systems and various types of wave packet dynamics. Its experimental realizability can also be expected, since linear chirping can now be relatively easily realized and manipulated.

I-H-2 Control of Photodissociation Branching Using the Complete Reflection Phenomenon: Application to HI Molecule

FUJISAKI, Hiroshi; TERANISHI, Yoshiaki[1]; NAKAMURA, Hiroki
([1]Adv. Photon Res. Cent.)

[*J. Theor. Comput. Chem.* **1**, 245 (2002)]

The laser control of photodissociation branching in a diatomic molecules is demonstrated to be effectively achieved with use of the complete reflection phenomenon. The phenomenon and the control condition can be nicely formulated by the semiclassical (Zhu-Nakamura) theory. The method is applied to the branching between $I(^2P_{3/2})(HI \rightarrow H + I)$ and $I^*(^2P_{1/2})$-$(HI \rightarrow H + I^*)$ formation, and nearly complete control is shown to be possible by appropriately choosing an initial vibrational state and laser frequency in spite of the fact that there are three electronically excited states involved. Numerical calculations of the corresponding wavepacket dynamics confirm the results.

I-H-3 Photodissociation of H_2^+ and HD^+ in an Intense Laser Field

KONDORSKIY, Alexey[1]; NAKAMURA, Hiroki
([1]IMS and Lebedev Physical Inst., Russia)

[*Phys. Rev. A* **66**, 05412 (2002)]

The photodissociation of H_2^+ and HD^+ by an intense laser pulse is investigated by solving the close-coupling equations without discretization. For the case of H_2^+ the photodissociation spectra are calculated under the condition mimicking the experimental one, and a fairly good agreement with the experiment is obtained. The uncertainty in the relative phases of initial states is found to lead to somewhat smoothing of the spectra, depending on the pulse length. It is also found that Raman-type transitions via intermediate dissociation continuum play an important role in determining the photodissociation spectra. This leads to a population increase of lower vibrational states and deforms the

spectral profile. Dissociation from the lower vibrational states due to the bond softening is not strong enough. Photodissociation spectra and angular distribution are calculated also for HD^+ under the same conditions as in the H_2^+ case. The dipole transitions lead to additional structures in the energy spectra and angular distribution. There is a noticeable difference in the peak positions of dissociation spectrum for particles dissociated by the direct electronic-dipole transition and by the transitions via intermediate bound states. The photodissociation dynamics is further clarified by using the three-dimensional plots of the spectra as a function of the field intensity and frequency.

I-H-4 Control of Photodissociation by Using a Sequence of Chirped Pulses and Nonadiabatic Transitions

ZOU, Shiyang; KONDORSKIY, Alexey[1]; NAKAMURA, Hiroki
([1]IMS and Levedev Physical Inst., Russia)

Laser control of photodissociation is decomposed into two processes: (1) to shift an initial wave packet to an appropriate position on the ground potential curve, and (2) to let that packet transit to upper dissociative potential curve. The first step can be realized by using a sequence of chirped pulses and the second step is made possible by controlling the nonadiabatic transition between the dressed states.

I-I New Method of Scattering Calculation

I-I-1 Calculation of Resonances in a $dt\mu$ Molecule by the R-Matrix Method

MIL'NIKOV, Gennady V.; NAKAMURA, Hiroki

[*Phys. Rev. A* **67**, 034501 (2003)]

Using the spectral representation of Green's function, we calculate the density of states and extract parameters of resonances in the scattering system. The method is implemented for the resonances in the $dt\mu$ molecule below the $t\mu$ ($n = 2$) threshold.

I-J Theoretical Studies of Ultrafast Nonlinear Optical Spectroscopy of Molecules in Condensed Phases

Nonlinear optical interactions of laser fields with matter provide powerful spectroscopic tools for the understanding of microscopic interactions and dynamic processes. We attempt to provide theoretical basis for a wide class of nonlinear spectroscopic techniques, focusing on the underlying physical processes in the condensed phases.

I-J-1 Energy-Level Diagrams and Their Contribution to Two-Dimensional Spectroscopic Signal: Distinction between Relaxation Mechanisms by Two-Dimensional Spectroscopy

OKUMURA, Ko[1]; TANIMURA, Yoshitaka
([1]Ochanomizu Univ.)

[*J. Phys. Chem. B* (2003) in press]

We develop a Feynman rule for energy-level diagrams emphasizing their connections to the double-sided Feynman diagrams and physical processes in the Liouville space. Thereby, we completely identify such diagrams and processes contributing to the 2D response function in the Brownian oscillator model. We classify such diagrams or processes in quartets and numerically present signals separately from each quartet of diagrams or Liouville-space processes. We find that the signal from each quartet is distinctly different from the others; we can identify each peak in the frequency domain with a certain quartet. This provides the basis for analyzing and assigning actual 2D peaks and suggests the possibility of Liouville-space path-selective spectroscopy. As an application, we demonstrate an example in which two familiar homogeneous models of relaxation are distinguished by the existence or nonexistence of certain peaks on the 2D map; the appearance or disappearance of certain peaks is sensitive to the choice of coupling models. We also point out some confusion in the literature with regard to the inclusion of relaxation effects.

I-J-2 Two-Dimensional Spectroscopy for a Two-Dimensional Rotator Coupled to a Gaussian-Markoffian Noise Bath

SUZUKI, Yoko; TANIMURA, Yoshitaka

[*J. Chem. Phys.* **119**, 1650–1660 (2003)]

The dynamics of a system in the condensed phase are more clearly characterized by the multi-time correlation functions of physical observables than two-time ones. We investigate a two-dimensional motion of a rigid rotator coupled to a Gaussian-Markovian harmonic oscillator bath. The analytical expression of a four-time correlation function of a dipole that is the observable of the two-dimensional microwave or infrared spectroscopy is obtained from a generating functional approach. The spectra in the absence of damping are discrete and reveal transitions between eigenstates of the angular momentum quantized due to the cyclic boundary condition. For the weakly damped case, the result predicts an echo-like signal that can be explained by the Liouville space path ways. The two-dimensional spectra are more sensitive to the noise effects than the one-dimensional (linear-absorption) spectra, which mean two-time correlation functions of dipole. It is because the effects of the initial thermal distribution are cancelled through the higher-order optical transition process in the two-dimensional spectroscopy, while such thermal effects determine the profile of the line shape in the one-dimensional spectroscopy. The two-dimensional spectrum reveals three peaks corresponding to transition processes between the rotational energy levels even in the damped case, which cannot be observed in the one-dimensional spectroscopy. For the strongly damped case, the two-dimensional spectra reveal peaks that arise from the strongly damped motion and librational motion caused by the strong coupling between the system and the heat bath oscillators with narrow band spectral distribution. Whereas the effects of these motions are shown in the bimodal line of the one-dimensional spectroscopy, the profile of the two-dimensional spectrum clearly implies the origin of these two peaks.

I-J-3 Two-Dimensional Vibrational Spectroscopy of a Double Minimum System in a Dissipative Environment

KHÜN, Oliver; TANIMURA, Yoshitaka

[*J. Chem. Phys.* **119**, 2155–2164 (2003)]

A dissipative bistable system presents the simplest model to describe condensed phase reaction dynamics. Using a quantum master equation approach to calculate multitime dipole correlation functions we demonstrate how the dissipative dynamics can be characterized by time-resolved third-order infrared spectroscopy. Thereby we incorporate bilinear and linear–quadratic system–bath interaction into the Redfield relaxation tensor. Investigating equilibrium and nonequilibrium initial conditions for a symmetric system it is shown that bath-induced coherence transfer can have a dramatic influence on the two-dimensional signals. This occurs when the inverse of the ground state tunneling splitting is of the order of the coherence transfer time.

I-K Simulation and Dynamics of Real Molecular Systems

Accurate quantum computational chemistry has evolved dramatically. The size of molecular systems, which can be studied accurately using molecular theory is increasing very rapidly. Theoretical chemistry has opened up a world of new possibilities. It can treat real systems with predictable accuracy. Computational chemistry is becoming an integral part of chemistry research. Theory can now make very significant contribution to chemistry. The project focuses on the theoretical development in methodologies for the study of molecular electronic structures. We are aiming at developing accurate molecular theory on systems containing hundreds of atoms. We have continued our research in the following three directions: (i) development of new *ab initio* theory, particularly multireference based perturbation theory, (ii) development of exchange and correlation functionals in density functional theory, and (iii) development of molecular theory including relativistic effects.

I-K-1 UTChem—A Program for *Ab Initio* Quantum Chemistry

YANAI, Takeshi[1]; NAKANO, Haruyuki[2]; NAKAJIMA, Takahito[2,3]; TSUNEDA, Takao[2]; HIRATA, So[4]; KAWASHIMA, Yukio; NAKAO, Yoshihide[2]; KAMIYA, Muneaki[2]; SEKINO, Hideo[5]; HIRAO, Kimihiko[6]
([1]Oak Ridge Natl. Laboratory, USA; [2]Univ. Tokyo, [3]PREST; [4]William R Wiley Environmental Molecular Sci. Laboratory Battelle, USA; [5]Toyahashi Univ. Tech.; [6]IMS and Univ. Tokyo)

[*Computational Science—ICCS 2003, Lecture Notes in Computer Science*, Springer, 84–95 (2003)]

Present molecular quantum theory is highly sophisticated, and has evolved dramatically. Software forms a basis for computational chemistry. However, it is not an easy task for an individual/group to develop a comprehensive new program package in *ab initio* quantum chemistry from scratch. Several years ago, we decided to accept this challenge. In view of the availability of such good programs as Gaussian, Gamess, Molcas, NWChem, *etc.*, one may question the relevance of a new program package. We have three arguments for our project. (1) First, we believe that healthy competition is very important in science. (2) Second, we can have a good harvest by doing research using other programs, but it is an abortive flower. We could not make a true breakthrough if we were circumscribed by current software limitations. (3) Third, in spite of the excellent performance of other programs, there are important and powerful methods that others cannot yet handle. We have developed new methodologies in quantum chemistry, particularly the multireference-based perturbation theory for describing chemical reactions and excited states, relativistic molecular theory to treat heavy elements, parameter-free (less) exchange and correlation functionals in DFT, highly efficient algorithms for calculating molecular integrals over generally contracted Gaussians, *etc*. UTChem is a research product of our work to develop new and better theoretical methods in quantum chemistry. Most of the codes have been developed recently by Hirao's group at the University of Tokyo. The basic philosophy behind UTChem is to develop methods that allow an accurate and efficient computational chemistry of electronic structure problems for molecular systems in both the ground and excited states. UTChem also contains codes for well-developed methods such as MPn, CI, CC, *etc*., which are standard in most quantum chemistry programs. We are aiming ultimately at better performance than other programs. UTChem will soon be ready for distribution. Here you will be able to see the features of UTChem. UTChem contains a large number of improvements and some interesting new features, which others cannot match.

I-K-2 Douglas-Kroll Transformation to the Relativistic Many-Electron Hamiltonian

NAKAJIMA, Takahito[1,2]; HIRAO, Kimihiko[3]
([1]Univ. Tokyo; [2]PREST; [3]IMS and Univ. Tokyo)

[*J. Chem. Phys.* **119**, 4105–4111 (2003)]

A new generalized Douglas-Kroll (DK) approach has been proposed for the relativistic many-electron Hamiltonian including the electron-electron interaction. In order to consider the higher-order DK transformation to the two-electron interaction, the present approach adopts the effective one-electron potential in the Dirac-Hartree-Fock (DHF)/Dirac-Kohn-Sham (DKS) operator as an expansion parameter in the DK transformation. Its numerical performance is tested for the atomic Hg and molecular HAt and At_2 systems. The third-order DK transformation to both one-electron and two-electron Hamiltonians, which is the highest level of theory treated in this study, gives excellent agreement with the four-component relativistic approach. The first-order DK correction to the two-electron interaction is proved to be satisfactory for both atomic and molecular systems.

I-K-3 A Four-Index Transformation in Dirac's Four-Component Relativistic Theory

ABE, Minori[1]; YANAI, Takeshi[2]; NAKAJIMA, Takahito[1,3]; HIRAO, Kimihiko[4]
([1]Univ. Tokyo; [2]Oak Ridge Natl. Laboratory, USA; [3]PREST; [4]IMS and Univ. Tokyo)

[*J. Chem. Phys.* submitted]

A four-index transformation from atomic orbitals to molecular orbitals is an essential first step in any calculation that aims to account for correlation effects. An efficient integral transformation program based on the four-component spinors resulting from the Dirac-

Hartree-Fock method is implemented in our program package, *UTChem*. By adopting generally contracted spherical harmonic Gaussian-type spinors, the number of small-component basis functions is reduced to about one half compared with commonly used kinetically balanced basis sets. The decrease in basis functions permits an efficient integral transformation. The present integral transformation program is four to eight times faster than the pioneering programs of MOLFDIR and DIRAC. As illustrative examples, the singles and doubles coupled-cluster methods with and without perturbative triples [CCSD, CCSD(T)] are applied to the ground state of thallium hydride. The computed spectroscopic constants are in good agreement with experiment.

I-K-4 Recent Advances in Multireference-Based Perturbation Theory

NAKANO, Haruyuki[1]; HIRAO, Kimihiko[2]
([1]Univ. Tokyo; [2]IMS and Univ. Tokyo)

[*Bull. Korean Chem. Soc.* **24**, 812–816 (2003)]

Accurate *ab initio* computational chemistry has evolved dramatically. In particular, the development of multireference-based approaches has opened up a completely new area, and has had a profound impact on the potential of theoretical chemistry. Multireference-based perturbation theory (MRPT) is an extension of the closed-shell single reference Møller-Plesset method, and has been successfully applied to many chemical and spectroscopic problems. MRPT has established itself as an efficient technique for treating nondynamical and dynamical correlations. Usually, a complete active space self-consistent field (CASSCF) wave function is chosen as a reference function of MRPT. However, CASSCF often generates too many configurations, and the size of the active space can outgrow the capacity of the present technology. Many attempts have been proposed to reduce the dimension of CASSCF and to widen the range of applications of MRPT. This review focuses on our recent development in MRPT.

I-L Theoretical Studies of Quantum Effects in Chemical Reactions

Although the study of quantum mechanical effects in chemical reactions has its long standing history, quantitative understandings of the importance of quantum effects in reactions have not been achieved. We investigate quantum effects, tunneling, resonances, interference, and electronically nonadiabatic transitions, in simple reaction systems by means of various theoretical approaches, including quantum reactive scattering methods, semiclassical dynamical methods, and classical trajectory methods.

I-L-1 Ab Initio Calculations of Low-Lying Potential Energy Surfaces of the HHeF System

TAKAYANAGI, Toshiyuki
(IMS and JAERI)

[*Chem. Phys. Lett.* **371**, 675 (2003)]

The low-lying singlet potential energy surfaces for the HHeF system have been calculated using the ab initio electronic structure method at the multireference configuration interaction level of theory. It is found that the interaction of helium with HF($B^1\Sigma^+$) in the ion-pair electronically excited state is attractive in a wide rage of the orientation angle and that the helium atom strongly stabilize the ion-pair HHe^+F^- complex on the $3^1A'$ surface, which is asymptotically correlating to the HF($B^1\Sigma^+$) state. We also found that the electronically nonadiabatic coupling between the $1^1A'$ ground state and $3^1A'$ state plays an essential role in the topographical features of these two surfaces.

I-L-2 Photodissociation of Cl_2 in Helium Clusters: An Application of Hybrid Method of Quantum Wavepacket Dynamics and Path Integral Centroid Molecular Dynamics

TAKAYANAGI, Toshiyuki[1]; SHIGA, Motoyuki[2]
([1]IMS and JAERI; [2]JAERI)

[*Chem. Phys. Lett.* **372**, 90 (2003)]

The photodissociation dynamics of Cl_2 embedded in helium clusters is studied by numerical simulation with an emphasis on the effect of quantum character of helium motions. The simulation is based on the hybrid model in which Cl–Cl internuclear dynamics is treated in a wavepacket technique, while the helium motions are described by a path integral centroid molecular dynamics approach. It is found that the cage effect largely decreases when the helium motion is treated quantum mechanically. The mechanism is affected not only by the zero-point vibration in the helium solvation structure, but also by the quantum dynamics of helium.

I-L-3 Theoretical Simulations on Photoexcitation Dynamics of the Silver Atom Embedded in Helium Clusters

WADA, Akira[1]; TAKAYANAGI, Toshiyuki[2]; SHIGA, Motoyuki[1]
([1]JAERI; [2]IMS and JAERI)

[*J. Chem. Phys.* **119**, 5478 (2003)]

Quantum molecular dynamics simulations have been performed to study the photoexcitation $Ag(5p^2P_J) \leftarrow Ag(5s^2S_{1/2})$ in size-selected helium clusters considering electronically nonadiabatic transitions. We employed the hybrid method in which the electronic degree of freedom of $Ag(^2P)$ was treated quantum mechanically while the motions of helium atoms were described by the semiclassical path integral centroid molecular dynamics method in order to take the quantum fluctuation effect into account. It has been found that the dynamics after photoexcitation is dominantly nonadiabatic in all cluster sizes studied, and that nonadiabatic transitions are enhanced by quantum fluctuation of helium motions. Most of the photoexcited AgHen clusters decompose into an isolated Ag atom and free helium atoms within several picoseconds. However, Ag^*He_n ($n = 1 \sim 5$) exciplex formation was also found to occur for all helium cluster sizes studied, although this process is found to be minor.

I-M Molecular Vibrations and Intermolecular Interactions in Condensed Phases

In this project, intermolecular interactions and their effects on molecular vibrations in condensed phases are analyzed theoretically to clarify the relation between the structures and dynamics of the systems and the frequency- and time-domain spectroscopic features. Specifically, (1) the resonant transfer of vibrational excitations, vibrational dephasing, and their competition in liquids and biomolecules and (2) the relation between electronic structural features of molecules and intermolecular interactions are analyzed with great emphasis.

I-M-1 The Role of Atomic Quadrupoles in Intermolecular Electrostatic Interactions of Polar and Nonpolar Molecules

TORII, Hajime
(IMS and Shizuoka Univ.)

[*J. Chem. Phys.* **119**, 2192–2198 (2003)]

For the purpose of getting insight into the reason for the anomalous vibrational frequency shifts observed in some usually used solvents for a mode that has a large dipole derivative, the role of atomic quadrupoles in intermolecular electrostatic interactions is studied for some halogen-containing molecules (CX_4, HX, and X_2 with X = F, Cl, and Br), CH_4, CO_2, and CS_2. From the fitting to the electrostatic potentials around the molecules, large atomic quadrupoles are obtained for the chlorine, bromine, and sulfur atoms, suggesting that the atomic quadrupolar effect is important for electrostatic interactions around covalently bonded atoms on the third and higher rows in the periodic table. Taking the case of the chlorine atoms as an example, the electron densities inside the atoms in CCl_4, HCl, and Cl_2 are examined. It is found that these electron densities are highly anisotropic. This anisotropy in electron densities is reasonably explained by the forms of the occupied molecular orbitals, and is considered to be the electronic structural origin of the large atomic quadrupoles.

I-M-2 Pressure Dependence of the Liquid Structure and the Raman Noncoincidence Effect of Liquid Methanol

TORII, Hajime
(IMS and Shizuoka Univ.)

[*Pure Appl. Chem.* in press]

Pressure dependence of the liquid structure and the Raman noncoincidence effect of liquid methanol is examined with the combination of molecular dynamics (MD) simulations and the intermolecular resonant vibrational interactions determined by the transition dipole coupling (TDC) mechanism (MD/TDC method). It is shown that the observed decrease of the Raman noncoincidence ν_{NCE} of the CO stretching band with increasing density reported in the literature is quantitatively reproduced by the present calculation. As the density increases, the hydrogen bonds get slightly shorter, but molecules belonging to different hydrogen-bond chains get closer to each other to a greater extent. This anisotropic change in the liquid structure is the reason for the behavior of ν_{NCE}. It is also shown that the concentration dependence of ν_{NCE} in the methanol/CCl_4 binary mixtures reported in a previous study and the pressure dependence of ν_{NCE} in methanol may be described in a consistent way as a function of the number density of methanol in the liquid systems.

I-M-3 Extent of Delocalization of Vibrational Modes in Liquids as a Result of Competition between Diagonal Disorder and Off-Diagonal Coupling

TORII, Hajime
(IMS and Shizuoka Univ.)

The changes in the extent of delocalization of vibrational modes in liquids arising from the competition between diagonal disorder and off-diagonal coupling in the vibrational exciton picture are examined theoretically. Calculations of vibrational modes and polarized Raman spectra are carried out on a model liquid system, in which spherical particles interact with each other by the Lennard-Jones and dipole-dipole interactions, and a one-dimensional oscillator (representing a vibrational degree of freedom) with a transition dipole and a Raman tensor is buried in each particle. The diagonal disorder is assumed to be in a Gaussian form, and the transition dipole coupling is introduced as the off-diagonal coupling in the vibrational Hamiltonian. The magnitude of the Raman noncoincidence effect (NCE), which is the phenomenon that the vibrational frequency positions of the isotropic and anisotropic components of a Raman band do not coincide and is often used as an experimental measure of the delocalization of vibrational modes, is calculated. In addition, two theoretical measures of the delocalization of vibrational modes are introduced, and their changes with the thermodynamic state of the liquid, the diagonal disorder, and the strength of the off-diagonal coupling are examined. It is shown that the extent of delocalization of vibrational modes is correlated with the "NCE detectability," defined as the ratio of the magnitude of the NCE and the isotropic or anisotropic Raman band width. This result indicates that the extent of delocalization of vibrational modes in a vibrational band that shows the NCE may be estimated from the observed spectral profile of the band. The size of the space in which vibrational spectra can probe structural formation is also discussed.

I-N Electronic Structure of a Molecule in Solution

Chemical reaction is undoubtedly the most important issue in the theoretical chemistry, and the electronic structure is a key to solve the problem. As long as molecules in the gas phase are concerned, the theory for the electronic structure has been enjoying its great success. However, when it comes to molecules in solution, the stage of theory is still an infant. We have recently proposed a new method refereed to as RISM-SCF based on the integral equation theory of molecular liquids (RISM) and the ab initio electronic structure theory (SCF).[1)] The integral equation approach replaces the reaction field in the continuum models by a microscopic expression in terms of the site-site radial distribution functions between solute and solvent.

$$V_\lambda = \sum_j \int 4\pi\rho \frac{q_j}{r} g_{j\lambda}(r)\, dr$$

where j and λ specify solvent and solute sites, respectively, and r denotes the solvent density. The site-site radial distribution functions $g_{\lambda j}(r)$ can be calculated from the extended RISM equation. Using V_λ the solvated Fock operator is defined as,

$$F^s = F^g - \sum_\lambda V_\lambda b_\lambda$$

where b_λ is a population operator of solute atoms. The statistical solvent distribution around solute is determined by the electronic structure or the partial charges of solute, while the electronic structure of solute is influenced by the solvent distribution. Therefore, the Hartree-Fock equation and the RISM equation should be solved in a self-consistent manner. It is this self-consistent determination of the solute electronic structure and the solvent distribution around the solute that features the RISM-SCF procedure.

The same Fock operator can be derived from a variation principle.[2)] Defining the Helmholtz free energy A as following;

$$A = E_{solute} + \Delta\mu$$

where E_{solute} is the energy of solute under solvent influence, and $\Delta\mu$ is the solvation free energy represented in terms of the Singer-Chandler formula. The Fock operator for a solute molecule in solvent as well as the RISM-HNC equations can be obtained as the first order variations with respect to the wave functions and the pair correlation functions under the constraint of the orthonormality to the molecular orbitals. The latest development along this line are reported below.

References

1) S. Ten-no, F. Hirata and S. Kato, *Chem. Phys. Lett.* **214**, 391 (1993); *J. Chem. Phys.* **100**, 7443 (1994).
2) H. Sato, F. Hirata and S. Kato, *J. Chem. Phys.* **105**, 1546 (1996).

I-N-1 Enthalpy and Entropy Decomposition of Free-Energy Changes for Side-Chain Conformations of Asparatic Acid and Asparagine in Acidic, Neutral, and Basic Aqueous Solutions

KIMURA, Tomohiro[1]; MATSUBAYASHI, Nobuyuki[1]; SATO, Hirofumi; HIRATA, Fumio; NAKAHARA, Masaru[1]
([1]Kyoto Univ.)

[*J. Phys. Chem. B* **106**, 12336 (2002)]

Trans and gauche conformational equilibria in the side chains of aspartic acid (Asp) and asparagine (Asn) were investigated by measuring the vicinal spin-spin coupling constants of ^{1}H NMR in acidic, neutral, and basic aqueous solutions over a wide range of temperature (5–90 ˚C). The standard free-energy changes ΔG^0 were obtained for the trans to gauche conformational variations on the C_α–C_β bond with respect to the α-carboxyl group and the β-carboxyl group in Asp (β-amide in Asn) and were decomposed into enthalpic ΔH^0 and entropic-$T\Delta S^0$ components. The hydration of ionic and polar groups in Asp competes against the large intramolecular electrostatic repulsion energy and stabilizes the gauche more than the trans conformer in correspondence to a larger degree of separation of positive and negative partial charges. In the neutral solutions, where both the carboxyl groups are negatively ionized, the hydration part even overwhelms the intramolecular repulsion and leads to a negative ΔH^0. The fact that the hydration almost cancels the intramolecular electrostatic repulsion contradicts the widely accepted view that the trans preference in the conformational equilibrium is due to the intramolecular repulsion between α-CO_2- and β-CO_2- (or β-$CONH_2$).

I-N-2 Theoretical Study on Electronic and Solvent Reorganization Processes Associated with a Charging Process of Organic Compounds: I. Molecular and Atomic Level Description of Solvent Reorganization

SATO, Hirofumi; KOBORI, Yasuhiro[2]; TERO-KUBOTA, Shozo[2]; HIRATA, Fumio
([1]Kyoto Univ.; [2]Tohoku Univ.)

[*J. Chem. Phys.* **119**, 2753 (2003)]

Electronic and solvation structures of *N*,*N*-dimethylaniline (DMA) in acetonitrile are examined by means of the ab initio reference interaction site model—self-consistent field (RISM-SCF) theory coupled with the method to evaluate nonequilibrium solvation free energy developed by Chong *et al*. [*J. Phys. Chem.* **99**, 10526 (1995)]. The key quantities characterizing the solvation process, free energy profile governing the solvent fluctuations and solvent reorganization, are evaluated from the first principle. A new scheme, which enables us to partition solvent reorganization into atomic contributions in the solute molecule, is proposed and used to analyze the process in atomic level. We found that the linear response approximation holds well and the overall observable, λs is not much affected by solute geometry, while the individual atomic contribution is significantly changed, especially, by the wagging motion of the amino group.

I-N-3 A Quantum Solute-Solvent Interaction Using Spectral Representation Technique Applied to the Electronic Structure Theory in Solution

YAMAZAKI, Takeshi; SATO, Hirofumi[1]; HIRATA, Fumio
([1]Kyoto Univ.)

[*J. Chem. Phys.* **119**, 6663 (2003)]

In this paper, we present a new approach to treat the electronic structure of a molecule in solution. Unlike the hybrid-type method such as the reference interaction site model self-consistent-field(RISM-SCF) theory, the new approach describes not only the electronic structure of solute but also solute-solvent interactions in terms of the quantum chemistry based on the Hartree-Fock frozen density formulation. In the treatment, the quantum effect due to solvent, including exchange repulsion, is projected on to the solute Hamiltonian using the spectral representation method. The solvent distribution around the solute is handled by the integral equation theory of liquids. As illustrative applications of the approach, the electronic and solvation structure of noble atoms, neon and argon, in liquid neon are studied. We also investigate the electronic structure of an excess electron in liquid helium. The preliminary results demonstrate that the quantum mechanical effect on the electronic and solvation structure of the solute due to solvent molecules is successfully represented by the new method.

I-N-4 Interplay between the Repulsive and Attractive Interaction and the Spacial Dimensionality of an Excess Electron in a Simple Fluid

SETHIA, Ashok[1]; BITTNER, Eric R.[1]; HIRATA, Fumio
([1]Univ. Houston, USA)

[*J. Theor. Comput. Chem*. **2**, 129 (2003)]

The behavior of an excess electron in a one, two and three dimensional classical liquid has been studied with the aid of Chandler, Singh and Richardson (CSR) theory [*J. Chem. Phys.* **81**, 1975 (1984)]. The size or dispersion of the wavepacket associated with the solvated electron is very sensitive to the interaction between the electron and fluid atoms, and exhibits complicated behavior in its density dependence. The behavior is interpreted in terms of an interplay among four causes: the excluded volume effect due to solvent, the pair attractive interaction between the electron and a solvent atom, the thermal wavelength of the electron (λ_e), a balance of the attractive interactions from different solvent atoms and the range of repulsive interaction between electron and solvent atom. Electron self-trapping behavior in all the dimensions has been studied for the same solvent-solvent and electron-solvent interaction potential and the results are presented for the same parameter in every dimension to show the comparison between the various dimensions.

I-O Solvation Thermodynamics of Protein and Related Molecules

Concerning biomolecules such as protein, it is a final goal for the biochemistry and biophysics to explore the relation between conformations and biological functions. The first important step toward the goal would be to explain the conformational stability of biomolecules in terms of the microscopic structure of the molecules in solvent. It is an extremely difficult problem by any means due to the overwhelmingly large degrees of freedom to be handled, including protein and solvent. As long as the small and/or short-time fluctuations of protein around the native structure is concerned, a variety of molecular simulation techniques provides a quite powerful tool to explore the microscopic structure of protein and solvent. However, the techniques are not so effective to characterize stability of the macromolecules in solution, to which the thermodynamic limit ($V \to \infty$, $N \to \infty$, with V/N = const.) is concerned. In such a case, methods based on the statistical mechanics of liquids should be natural choice for sampling configurations of solvent interacting biomolecules. The extended RISM theory is the most promising

candidate of such methods, which provides not only solvation thermodynamics but also microscopic description at the level of the pair correlation functions.[1)] Obvious technical difficulties which one may face in applying the theory to such a large system are not only the computation time but also the stability of the numerical solution.[2)]

Here, we present our recent effort to tackle the problem using the two theoretical tools based on the statistical mechanics of liquids: the extended RISM and the scaled particle theories (SPT).[3)] The studies for the solvation thermodynamics of small molecules such as ions are also included because it is regarded as elementary processes for the solvation of biomolecules, and because it is prerequisite for studying the more complicated molecules.

References

1) M. Kinoshita, Y. Okamoto and F. Hirata, *J. Am. Chem. Soc.* **120**, 1855 (1998).
2) A. Kitao, F. Hirata and N. Go, *J. Phys. Chem.* **97**, 10231 (1993).
3) M. Irisa, K. Nagayama and F. Hirata, *Chem. Phys. Lett.* **207**, 430 (1993).

1-O-1 Partial Molar Volume and Compressibility of a Molecule with Internal Degrees of Freedom

IMAI, Takashi[1]; HIRATA, Fumio
([1]Ritsumeikan Univ.)

[*J. Chem. Phys.* **119**, 5623 (2003)]

Statistical mechanical expressions for the partial molar volume (PMV) and the partial molar compressibility (PMC) of a solute molecule with internal degrees of freedom are derived. The equilibrium PMV is expressed simply by the conformational ensemble average of PMV. The equilibrium PMC consists of two terms: the conformational ensemble average of PMC and the mean square fluctuation of PMV along conformational axis. As an illustrative application of the theory, the equilibrium PMV and PMC of butane in aqueous solution are calculated from the relations, in which the thermodynamic quantities of each conformer appearing in the relations are obtained by the RISM theory. The conformational ensemble average of PMC is the predominant contribution to the equilibrium PMC in this particular example. Possibility of shedding light on the protein conformation in terms of PMV and PMC is discussed.

1-O-2 A Density-Functional Theory for Polymer Liquids Based on Interaction Site Model

SUMI, Tomonari; HIRATA, Fumio

[*J. Chem. Phys*. **118**, 2431 (2003)]

The density-functional theory (DFT) for molecular fluids [*J. Chem. Phys.* **115**, 6653 (2001)] is extended to the case of polymer liquids. A system consisting of the ideal chains is employed as a reference system for the DFT, where many-body effects are considered as an effective field that acts on each site of the ideal chains. We derived a relation between the site-site pair distribution functions and the site-density distribution functions under a mean field arising from a single polymer molecule. An integral equation for the site-site pair distribution functions is obtained by the DFT, where the external field is taken to be the mean field. We propose an approximate expression of the intramolecular correlation functions for isolated single-polymer chains to take account for the excluded volume effects inside a polymer chain. The intramolecular correlation function considering the excluded volume effects was in qualitative agreement with those obtained from a simulation for liquid consisting of freely jointed tangent-soft-core chains. The site-density integral equation under the mean field, using the intramolecular correlation function, reproduces the simulation results for site-site pair distribution functions of the system of freely jointed tangent-soft-core chains.

I-P Collective Density Fluctuations in Polar Liquids and Their Response to Ion Dynamics

As to the model for molecular diffusion in polar liquids, there are two quite different points of view. One is the conventional rot-translation model, and the other the interaction-site description which sees the diffusion of a molecule as a correlated motion of each atom (site).[1)] It is clearly advantageous to use the interaction-site description compared to the rot-translation model to account for chemical characteristics of solvent as well as solute dynamics. However, the interaction-site description has its own disadvantage in interpreting physical meaning of the results, since it does not give an explicit picture for the rotational relaxation of molecules, which can be directly probed by many experimental means including the dielectric and NMR relaxation. We have solved the problem by extracting collective modes of the density fluctuation from the site-site density correlation functions. In our recent study for dynamics of molecular liquids based on the interaction-site model, we have succeeded to abstract the collective excitations in liquids, which can be identified as optical and acoustic modes, by diagonalizing the collective frequency matrix appearing in the generalized Langevin equation. The two modes arise essentially from

the rotational and translational motions of molecules. [2] We applied the method to the ion dynamics in a dipolar liquid, and could have explained successfully the peculiar size dependence of friction of alkali and halide ions in terms of response of the collective excitations in solvent to the solute displacement.[3]

In the past year, we have elaborated the memory kernel in our generalized Langevin equation base on the mode coupling theory. We have also extended our treatment to dynamics of water and hydrated ions. Those studies as well as other related topics are reviewed below.

References

1) F. Hirata, *J. Chem. Phys.* **96**, 4619 (1992).
2) S. Chong and F. Hirata, *Phys. Rev. E* **57**, 1691 (1998).
3) S. Chong and F. Hirata, *J. Chem. Phys.* **108**, 7339 (1998).

I-P-1 Solute-Structure Dependence of Solvation Dynamics Studied by Reference Interaction-Site Model Theory

NISHIYAMA,Katsura[1]; HIRATA, Fumio; OKADA, Tadashi[1]
([1]Osaka Univ.)

[*J. Chem. Phys.* **118**, 2279 (2003)]

A combination of the reference interaction-site model theory and site-site Smoluchowski-Vlasov equation is applied to estimate the dynamic response function of the average-energy relaxation of the solute-solvent system, $S_S(t)$. We calculate $S_S(t)$ for 13 model solutes with different structure, from a simple ion to an octopole, in a polar solvent. The partial charges of the ions and multipoles are changed to investigate nonlinear character of $S_S(t)$. The ''nonlinear character'' we study here corresponds to the response of the solvent fluctuation after the sudden change of the solute charge-distribution. Our present results reveal that $S_S(t)$ depends on the molecular structure and charge distribution of the solute. $S_S(t)$ is decomposed into two parts: one corresponding to the optical mode of solvent, the other to the acoustic mode. We show that for multipoles the optical mode is responsible for the fast part of $S_S(t)$, while the acoustic mode plays an important role in the slower dynamics. The dual nature of $S_S(t)$ is essential for the nonlinearity of solvation dynamics.

I-P-2 Dielectric Relaxation Spectrum of Water Studied by the Site-Site Generalized Langevin/Modified Mode-Coupling Theory

YAMAGUCHI, Tsuyoshi[1]; CHONG, Song-Ho[2]; HIRATA, Fumio
([1]Nagoya Univ.; [2]Univ. Roma, Italy)

[*Mol. Phys.* **101**, 1211 (2003)]

The dielectric relaxation spectrum of water is calculated from the site-site generalized Langevin/modified mode-coupling theory. The main part of the relaxation follows the Debye-type function, and a small deviation from the Debye relaxation is found on the high-frequency side. This tendency is consistent with recent experiments, although the absolute relaxation time does not agree with the experimental value quantitatively. The time-development of the longitudinal polarization function resembles the dielectric part of the memory function, and we consider that this is because the dielectric friction dominates the collective reorientation of the dipole moment of water. We performed calculations with different dielectric constants using the reference interaction-site model integral equation, and found that the large gap between the time-scales of the dielectric relaxation and the longitudinal polarization relaxation causes the Debye-type dielectric relaxation when the dielectric friction is dominant in the friction on the collective reorientation of the dipole moment. Namely, the longitudinal polarization relaxation is fast enough to be considered as a white noise to the dielectric relaxation process, so that the relaxation becomes a Markov process. The large gap between the two relaxation times originates from a large local field correction due to the large dielectric constant of water. It is also suggested that the deviation from the Debye relaxation at the high-frequency side is the manifestation of the slow memory caused by the long-time part of the longitudinal polarization relaxation in the low-wavenumber region.

I-P-3 Theoretical Study on the Molecular Motion of Liquid Water under High Pressure

YAMAGUCHI, Tsuyoshi; CHONG, Song-Ho[1]; HIRATA, Fumio
([1]Univ. Roma, Italy)

[*J. Chem. Phys.* **119**, 1021 (2003)]

The pressure effects on the molecular dynamics of liquid water are investigated using the site-site generalized Langevin/modified mode-coupling theory. The calculations are performed for temperatures from 273 to 373 K and densities from 0.9 to 1.2 g/cm^3. The static structure factor required as input is obtained from the reference interaction-site model/hypernetted chain integral equation. The shear viscosity, the dielectric relaxation time, the translational diffusion coefficient, and the first-rank reorientational relaxation times are evaluated. All these quantities show unusual pressure dependence in the low-density, low-temperature region in that the molecular mobility is enhanced by applying the pressure. The magnitude of the enhancement is larger on the reorientational motions than on the translational ones. These tendencies are consistent with experimental observations, although the quantitative agreement is not so good. An analysis of the theory indicates that the decrease in the dielectric friction on the collective polarization at small wavenumbers upon

increasing pressure is the principal reason for the pressure-induced enhancement of the dielectric relaxation, and the decrease in the dielectric relaxation time affects other motions. The decrease in the dielectric friction is caused by the decrease in the number-density fluctuation around the low-wavenumber edge of the first-peak of the structure factor by compression. The comparison between the results for water and acetonitrile extracts two characteristic features of water that are important for the anomalous pressure effect on its molecular motion. The first one is the small collisional friction on the reorientation due to the spherical repulsive core, and the second one is the strong short-range Coulombic interaction caused by the formation of the hydrogen-bonding. A theoretical calculation on a model diatomic liquid consisting of oxygen and hydrogen atoms proposes that the above two characteristic properties of water are sufficient for the emergence of the anomalous pressure dependence. This conclusion is also supported by the molecular dynamics simulation performed on the same model diatomic liquid.

I-Q Developing Theories of Liquids and Liquid Mixtures

In the past few years, we have been concentrating our effort on building theories for chemical processes in solution. Our main concern in such study was to develop new theories which can describe "solvation" or "solvent effect" on chemical processes of interest by means of the statistical mechanics of liquids. A key to such development is the "RISM theory," and many intriguing chemistry as well as physics have been investigated in our group using the theory at least in qualitative level. On the hand, we are also experiencing serious break down of the theory sometime as we try to explore new problems such as the gas-liquid phase transition, protein solution, and liquid-liquid mixtures.

In what follows, we describe our challenges to explore new problems related to liquids and liquid mixtures. The challenge inevitably includes methodological development in the statistical mechanics of liquids.

I-Q-1 Compressibility of Tert-Butyl Alcohol-Water Mixture: The RISM Theory

OMELYAN, Ihor[1]; KOVALENKO, Andriy F.; HIRATA, Fumio
([1]Inst. Cond. Matt. Phys., Ukraine)

[*J. Theor. Comput. Chem.* **2**, 193 (2003)]

The isothermal compressibility χ_T of binary mixtures of water and *tert*-butyl alcohol (TBA) is calculated using the reference interaction site model (RISM) integral equation theory. The calculations are performed over the whole concentration from $x = 0$ to 1 and a wide temperature from $T = 283$ to 313 K ranges employing an extended point charge model for water and optimized site-site potentials for TBA molecules. The results obtained are compared versus available experimental data. It is demonstrated that, despite an approximate character of the model potentials and closure relation applied, the theory is able to reproduce qualitatively all main features of the x- and T-dependencies of χ_T inherent in real experiment. Such features include the decrease of compressibility with increasing T in the low TBA concentration limit x to 0 (pure water), and the increase of χ_T with rising T in the opposite regime x to 1 (pure alcohol); the presence of a concentration region where the function $\chi_T(x,T)$ does not depend much on T; as well as the existence of a minimum in χ_T with respect to x at each given T. The question of how to achieve a quantitative agreement between the theoretical and experimental values by correcting the closure relation is also discussed.

I-Q-2 Molecular Theory of an Electrochemical Double Layer in a Nanoporous Carbon Supercapacitor

TANIMURA, Ayumi[1]; KOVALENKO, Andriy F.; HIRATA, Fumio
([1]GUAS)

[*Chem. Phys. Lett.* **378**, 638 (2003)]

We develop the replica RISM theory of electrolyte solution sorbed in a nanoporous carbon electrode. The model comprises carbon nanospheres forming a disordered network with the porosity, pores sizes and surface area fitted to carbonized polyvinylidene chloride (PVDC) material, and to activated carbon. We obtained the huge capacitance comparable to that achieved in supercapacitors, and found the higher capacitance per pores surface for carbonized PVDC material with uniform nanoporous texture than for activated carbon with micro-as well as nanopores. Unlike a planar electrochemical double layer with the voltage dominated by the inner layer, the nanoporous supercapacitor voltage is driven by the solvation chemical potentials of the sorbed ions.

I-R Multicritical Behavior of Charge-Transfer Complexes

In the mixed-stack organic charge-transfer complex, TTF-CA, neutral-ionic and dimerization-induced ferroelectric phase transitions are observed. At ambient pressure, they occur simultaneously and discontinuously. Under high pressure, these transitions take place at different temperatures, that is, its phase diagram contains a paraelectric ionic phase in addition to the ferroelectric ionic and neutral phases. To treat both the ionicity (*i.e.*, degree of charge transfer from the donor to acceptor molecules) and the dimerization, which causes a finite polarization, we employ a classical spin-1 model called Blume-Emery-Griffiths model. However, this model itself cannot reproduce the proper solid-liquid-gas phase diagram due to hidden symmetries, so that an additional interaction is necessary.

I-R-1 Ferroelectric Phase Transition, Ionicity Condensation, and Multicriticality in Charge-Transfer Organic Complexes

KISHINE, Jun-ichiro[1]; LUTY, Tadeusz[2]; YONEMITSU, Kenji
([1]Kyushu Inst. Tech.; [2]Tech. Univ. Wroclaw)

[*Phys. Rev. B* submitted]

To elucidate a novel pressure-temperature phase diagram of the quasi-one-dimensional mixed-stack charge-transfer (CT) complex TTF-CA, we study the quasi-one-dimensional spin-1 Blume-Emery-Griffiths (BEG) model. In addition to the local charge transfer energy and the inter-stack polar (dipole-dipole) interaction, we take account of the inter-stack electrostriction effect. Using the self-consistent chain-mean-field theory, where the intra-stack degrees of freedom are exactly treated by the transfer-matrix method, we reproduce the gas-liquid-solid like phase diagram corresponding to the neutral (N), paraelectric ionic (I_{para}), and ferroelectric ionic (I_{ferro}) phases, respectively. We also give an explanation on the experimentally observed multicritical behavior and concomitant discontinuous inter-stack lattice contraction in TTF-CA.

I-S Photoinduced Phase Transitions in Charge-Transfer, Spin-Crossover, and Binuclear Metal Complexes

Now a variety of materials show photoinduced phase transitions. Their characters depend much on the magnitude of the hysteresis loop. The TTF-CA complex has small hysteresis and the transition is described by a deterministic approach. Especially, macroscopic coherent oscillations of neutral-ionic domain walls need to be described by a model that consists of interacting electrons and lattice displacements. The evolution of the system is described by the time-dependent Schrödinger equation. On the other hand, organometal spin-crossover complexes generally have large hysteresis and the transition is described by a stochastic approach. Ising-like models are sufficient to describe the slow transition between high- and low-spin phases. The evolution of the system is governed by thermal processes and described by the master equation. Even in a case with large hysteresis, a deterministic approach can be useful. In the iodine-bridged binuclear platinum complexes with ligand pop, a photoinduced transition takes place mainly from the charge-density-wave to charge-polarization phases within a large hysteresis loop. Its explanation needs off-diagonal elements of the Hamiltonian, so that a deterministic approach is necessary.

I-S-1 Electronic and Lattice Dynamics in the Photoinduced Ionic-to-Neutral Phase Transition in a One-Dimensional Extended Peierls-Hubbard Model

MIYASHITA, Naoyuki[1]; KUWABARA, Makoto[2]; YONEMITSU, Kenji
([1]Univ. Tokyo; [2]Inst. Pure Appl. Phys.)

[*J. Phys. Soc. Jpn.* **72** (2003) in press]

Real-time dynamics of charge density and lattice displacements is studied during photoinduced ionic-to-neutral phase transitions by using a one-dimensional extended Peierls-Hubbard model with alternating potentials for the one-dimensional mixed-stack charge-transfer complex, TTF-CA. The time-dependent Schrödinger equation and the classical equation of motion are solved for the electronic and lattice parts, respectively. We show how neutral domains grow in the ionic background. As the photoexcitation becomes intense, more neutral domains are created. Above threshold intensity, the neutral phase is finally achieved. After the photoexcitation, ionic domains with wrong polarization also appear. They quickly reduce the averaged staggered lattice displacement, compared with the averaged ionicity. As the degree of initial lattice disorder increases, more solitons appear between these ionic domains with different polarizations, which obstruct the growth of neutral domains and slow down

the transition.

I-S-2 Coherence Recovery and Photoinduced Phase Transitions in One-Dimensional Halogen-Bridged Binuclear Platinum Complexes

YONEMITSU, Kenji; MIYASHITA, Naoyuki[1]
([1]Univ. Tokyo)

[*Phys. Rev. B* **68**, 075113 (9 pages) (2003)]

A photoinduced transition from a charge-density-wave (CDW) phase to a charge-polarization (CP) phase has been recently found in a one-dimensional halogen-bridged binuclear platinum complex $R_4[Pt_2(pop)_4I]$-$n$$H_2O$ (pop = $P_2O_5H_2^{2-}$, R = $(C_2H_5)_2NH_2$). Its mechanism is theoretically studied by solving the time-dependent Hartree-Fock equation for a one-dimensional two-band three-quarter-filled Peierls-Hubbard model. Above a threshold in the photoexcitation intensity, a transition takes place from the CDW to CP phases. The threshold intensity depends on the relative stability of these phases, which can be explained qualitatively by their diabatic potentials. However, the transition from the CP to CDW phases is hardly realized for two reasons: (i) low-energy charge-transfer processes occur only within a binuclear unit in the CP phase; (ii) it is difficult for the CDW order to become long-ranged owing to its weak coherence. The effective transfer integrals required for the coherence are evaluated.

I-S-3 Two-Step Photo-Induced Phase Transitions in a Two-Sublattice Model

OTSUKA, Yuichi; YONEMITSU, Kenji

Photo-induced phase transition (PIPT) phenomena in organometal spin-crossover complexes have been widely investigated. As an effective model for a two-step spin transition, we study a two-sublattice spin model that takes into account an intra-site antiferromagnetic coupling and inter-site ferromagnetic couplings. Since each site takes low-spin (L) or high-spin (H) state, the model has four (LL, LH, HL, and HH) possible phases. First, we discuss the temperature dependence of the high spin fraction by using a mean-field approximation. The results indeed show a two-step spin transition due to the competition between the intra- and inter-site couplings. Next, we apply Monte Carlo (MC) simulations including a photoexcitation term. The MC dynamics of the high spin fraction shows non-linear characteristics such as step-like change, threshold-like behavior, and phase separation.

I-S-4 Quasiparticle Structure in the Vicinity of the Heisenberg Model: One and Higher Dimensions

MORITA, Yoshifumi[1]; OTSUKA, Yuichi; HATSUGAU, Yasuhiro[1]
([1]Univ. Tokyo)

We study quasiparticle structures in a class of quantum spin and half-filled Hubbard models where the antiferromagnetic correlation is suppressed. First, we focus on the one-dimensional case and study how the solitonic quasiparticles and their bound states appear. Then, we propose its analogue in higher dimensions and compare the results with those of the two-dimensional Hubbard model at half filling on a triangular-type lattice.

RESEARCH ACTIVITIES II
Department of Molecular Structure

II-A Development of Near-Field Dynamic Spectroscopy and Application to Mesophase Systems

There is much demand for the study of local optical properties of molecular assemblies and materials, to understand mesoscopic phenomena and/or to construct optoelectronic devices in nanometric scale. Near-field optical microscopy, which enables spatial resolution beyond the diffraction limit of light, shows remarkable progress in technology in these days. Combination of this advanced optical technology with ultrafast spectroscopic methods may offer a direct probe of molecular dynamical processes in mesoscopic systems. It may bring essential and basic knowledge for analyzing origins of characteristic features and functionalities of mesophase systems. We are constructing apparatus for near-field dynamic spectroscopy with femtosecond temporal resolution and nanometer spatial resolution. Outlines of the construction and some experimental results are summarized here.

II-A-1 Construction of a Scanning Near-Field Optical Microscope with Closed-Loop Operated Stage and an Apparatus for Fluorescence Life-Time Measurement

IMURA, Kohei; NAGAHARA, Tetsuhiko; OKAMOTO, Hiromi

Scanning near-field optical microscope (SNOM) is the only method that can measure local optical properties beyond the diffraction limit of light. Piezo-electric translator, which is used for sample scanning in SNOM, has a large hysteresis and creeping. Thus, reproducible positioning and stability, which are crucial for investigating local properties in detail, is quite poor. We have developed a SNOM apparatus equipped with closed-loop feedback controlled scanning stage, and achieved about 1 nm positioning accuracy.

The developed instrument consists of light source, sample stage, probe head, distance regulation feedback system, and detection systems. Schematic drawing is depicted in Figure 1. Major mechanical parts of the instrument were made of Super Invar steel to ensure thermal stability. Light source is either a laser or a discharge lamp, the latter is used for absorption spectral measurements. Distance between the probe tip and the sample surface is kept within 10 nm by the shear force feedback control. A polychromator equipped with a CCD array detector is used for spectral measurements while an avalanche photodiode or a photomultiplier tube is used for single photon counting measurements. With this apparatus, we have obtained the lateral resolution down to 50 nm, simultaneously measuring topographic image of the sample.

Time-correlated single photon counting system can be also combined with the SNOM apparatus. It consists of photon detectors, time-to-amplitude converter (TAC), and multi-channel buffer (MCB). From time-correlated photon histograms, fluorescence lifetime can be obtained. Temporal response of the system is determined by the response of the avalanche photodiode, ca. 350 ps.

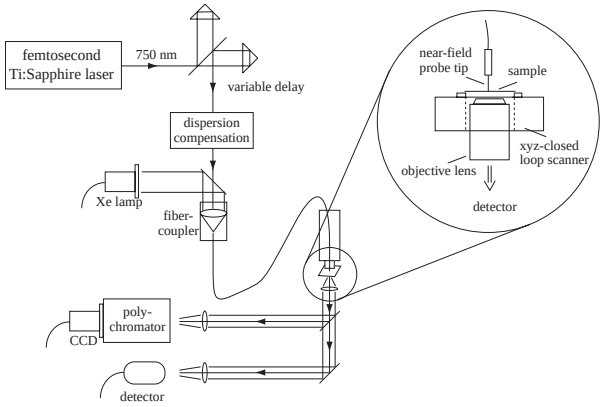

Figure 1. Schematic diagram of experimental set-up. Expansion near the probe is shown at right side.

II-A-2 Near-Field Optical Transmittance Microscopy on the Thin Film of Porphyrin J-Aggregate

NAGAHARA, Tetsuhiko; IMURA, Kohei; OKAMOTO, Hiromi

[*Chem. Phys. Lett.* **381**, 368 (2003)]

Mesoscopic structures and photophysical properties of water-insoluble tetrakis(4-methoxyphenyl)porphyrin (TMeOPP) J-aggregate in thin film have been investigated by illumination (transmission) mode SNOM. In the surface topography (Figure 1A), the TMeOPP J-aggregate sample has been found to be composed of planar microcrystalline structures. In the far-field, a broad strong absorption band centered at 760 nm is seen, whereas a narrower band in the 700–800 nm region and several small peaks are observed in the site-specific near-field spectra (Figure 1B). The differences between the far-field and near-field spectra can be ascribed to spatial inhomogeneities, which is related to the *broad* J-bands.

To analyze further the spatial inhomogeneity, we have assumed that there exists a sharp spectral component, and calculated the correlation between this spectral component and the observed spectra. The mapped

correlation images (Figures 1C and D) show structures that have some correlations with the topography. The finer structures (black arrows) seem to show a tendency to be oriented to the polarization directions, indicating a large transition moment parallel to their long crystalline axes. The results suggest that the assumed sharp spectral component is relevant to a substance that is buried in the inhomogeneously broadened spectrum.

Reference

1) S. Okada and H. Segawa, *J. Am. Chem. Soc.* **125**, 2792–2796 (2003).

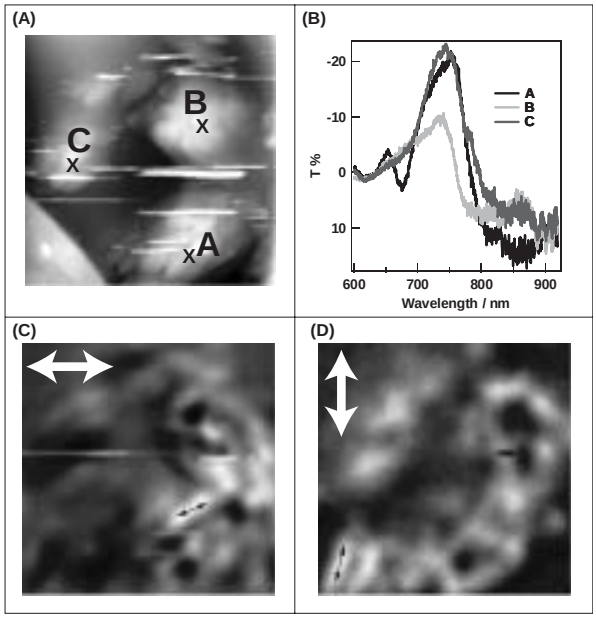

Figure 1. (A) Surface topography of the sample. (B) Transmittance difference spectra in the near-field at positions indicated in (A). (C),(D) Spatial distribution of an assumed spectral component of J-aggregate. Scan range: 5 μm × 5 μm. Arrows in (C) and (D) indicate the directions of the observing polarization.

II-A-3 Time-Resolved Near-Field Spectroscopy of Porphyrin J-Aggregates

NAGAHARA, Tetsuhiko; IMURA, Kohei; OKAMOTO, Hiromi

[*Chem. Phys. Lett.* **381**, 368 (2003)]

We have measured the time-resolved equal-pulse transmission correlation (EPC) of porphyrin (TMeOPP) J-aggregate in the near-field, and tried to elucidate site-specific optical features in mesoscopic scales. In Figure 1B, typical pump-probe EPC signal of TMeOPP observed at position "X" indicated in the topography (Figure 1A) is shown. Time and spatial resolutions, and wavelength of our femtosecond pump-probe SNOM apparatus were 100 fs, 100 nm, and 780 nm, respectively. The observed decay may be ascribed to population decrease in the excited-state. Similar exponential decays are also observed at various positions, but not at a bare glass surface. The lifetimes are raging from 10 to 50 ps, that are of the same order as the reported lifetime (50 ps) of J-aggregate of tetrakis(4-sulfonatophenyl)-porphyrin/H_2O in the far-field, and are distinct from that of monomer (3.87 ns).[1] The scatter of the obtained lifetimes may be ascribed either to site-specificity or experimental errors. Further detailed investigations, to clarify the origin of the variations of the excited-state lifetimes may be needed. More precise lifetime measurements by using moderately lower repetition-rate and higher peak power laser pulses are under way.

Reference

1) N. C. Maiti *et al.*, *J. Phys. Chem.* **99**, 17192–17197 (1995).

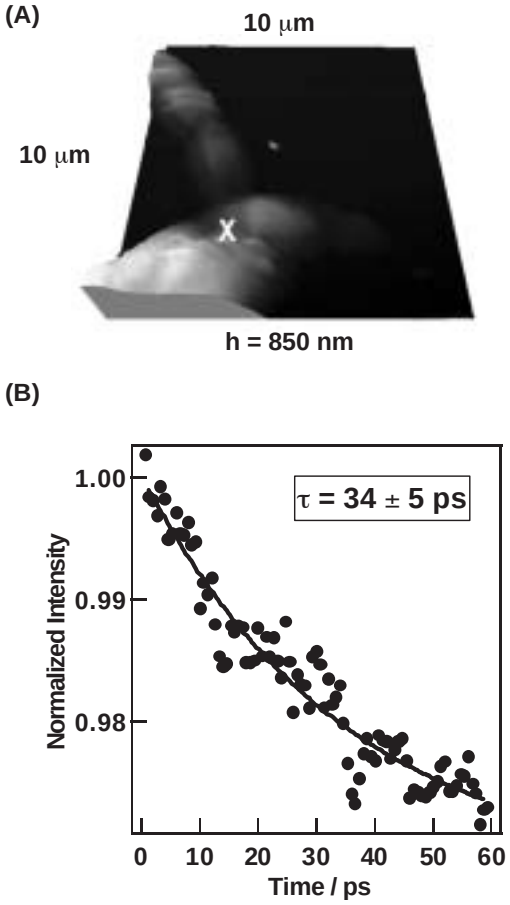

Figure 1. (A) Surface topography of the sample. (B) Equal-pulse transmission correlation signal intensity as a function of delay time, together with that of the least-squares fit.

II-A-4 Near-Field Optical Observation of Gold Nanoparticles

IMURA, Kohei; NAGAHARA, Tetsuhiko; OKAMOTO, Hiromi

For past decades, the surface plasmons (SP) due to collective oscillation of electrons have been widely investigated, for the purpose of understanding physical mechanism in surface enhanced Raman scattering (SERS), and for potential applications in industry as well. Local electric field enhancement near the particle has been recognized as one of the enhancement sources in SERS. Although evidence of local field enhancement has been easily observed after near-field effect translat-

ed into the far-field, little observation in near-field has been reported. In order to understand interaction of photons and the particle in near-field, we have measured near-field transmission spectrum of the particles by a scanning near-field optical microscope (SNOM).

Sample was prepared by spin-coating of 100 nm diameter gold spheres followed by spin-coating with polymer in order to attain flat surface of the sample. Figure 1 shows typical transmission spectrum of a gold particle measured in near-field. Positive and negative signs correspond to enhancement and reduction of the transmission, respectively. We ascribe the enhanced transmission to the antenna effect of the particle. The evanescent wave emerging from the aperture probe first couples into the surface mode of the particle, followed by re-radiation into the far-field. SNOM probe is a source not only of non-propagating evanescent wave but also of propagating wave. Thus, propagating wave also contributes to the observed signal. Absorptive part of the spectrum can be attributed to scattering and absorption, on the gold particle, of the propagating wave from the aperture probe. These considerations imply that spectral profile consists of two different contributions of evanescent and propagating waves.

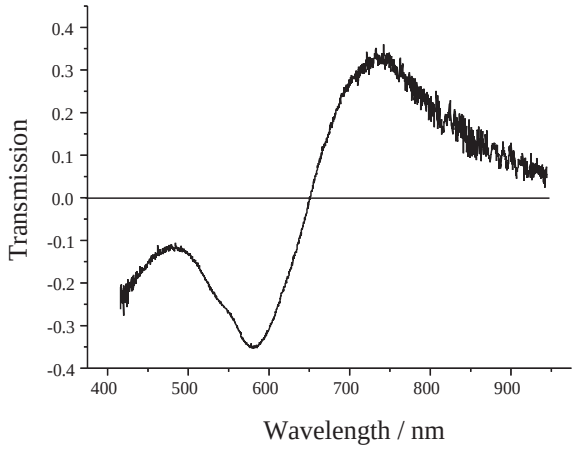

Figure 1. Transmission spectrum of gold sphere (100 nm diameter) measured in near-field.

II-B Laser Cooling and Trapping of Metastable Helium Atoms

In the past two decades, extensive developments have occurred in the laser cooling and trapping of neutral atoms, with many workers reporting the application of these techniques to such diverse atomic species as alkali atoms, alkali earth atoms, and rare gas atoms. Among these, the helium atom is unique on account of its small mass, simple energy level structure, and easy availability in two isotopic forms (^{3}He and ^{4}He) of differing quantum statistics. For this reason, we have been studying the laser cooling and trapping of helium atoms.

II-B-1 Liquid Helium Cooled Metastable Helium Beam Source for Laser Cooling/Trapping Experiments

MORITA, Norio

For laser cooling/trapping of atoms, it is preferable that the initial velocity of an atomic beam is as small as possible, because the higher velocity requires the longer length for stopping the atoms and, therefore, results in the more significant divergence of the beam. For the helium atom, this requirement is more difficult to satisfy, not only because of the small mass, but also because the atoms that can be decelerated and trapped by lasers are only metastable atoms; metastable atoms are, more or less, heated through the excitation procedure, such as discharge. For this reason, metastable helium atoms are, so far, usually produced by discharge in liquid nitrogen cooled circumstances. In the present study, however, we have developed a discharge cell cooled by liquid helium, and investigated the performance of this metastable atomic source. As a result, for ^{4}He, we have found that the metastable beam velocity can be as small as 250 m/s at the peak of the velocity distribution with a width of about 50 m/s, while it is as large as 750 m/s with a liquid nitrogen cooled discharge cell. For ^{3}He, the peak velocity and width are 290 m/s and about 60 m/s, respectively. These results mean that for both ^{4}He and ^{3}He the length enough to stop the atoms is only 15 cm, which is one ninth of the one necessary for stopping metastable atoms produced with a liquid nitrogen cooled source. We can expect that such dramatic shortening of the stopping length will much reduce the difficulty in the cooling/trapping experiments on metastable helium atoms.

II-C Spectroscopic Studies on Atoms and Ions in Liquid Helium

Atoms and ions in liquid helium are known to reside in bubble-like cavities due to the Pauli repulsive force between electrons. Physical properties of these exotic surroundings are determined by the potential energy of the impurity-He$_n$ system, the surface tension energy of the liquid helium, and the pressure-volume work. Spectroscopic studies of such impurity atoms and ions in liquid helium are expected not only to give information on the structure and dynamics of the bubbles but also to contribute to the study on physical properties of superfluid liquid helium.

II-C-1 Laser Spectroscopic Studies of Eu Atoms in Liquid and Solid Helium: Helium Pressure Dependences

MORIWAKI, Yoshiki[1]; MORITA, Norio
([1]Toyama Univ.)

Spectra of Inner shell transitions in Eu atoms distributed in liquid helium have relatively sharp peaks accompanied with long tails of phonon sidebands. The sharp peaks are zero-phonon lines (ZPL), and are largely shifted along with the sidebands, depending on the helium pressure. In this study, we have investigated this pressure shift for both ^{4}He and ^{3}He over a wide pressure range including the solidification region. The pressure shifts of ZPL's in excitation spectra of the inner shell transition $4f^6(^7\mathrm{F})5d6s^2\ ^8\mathrm{F}_{7/2} \leftarrow 4f^7 6s^2\ ^8\mathrm{S}_{7/2}$ at 1.1 K are plotted in Figure 1. As seen in Figure 1, for both ^{4}He and ^{3}He the ZPL is shifted toward longer wavelength at approximately the same rate, which is about 0.06 nm/MPa. For ^{4}He, the ZPL is slightly split above the solidification pressure (2.5 MPa), and two kinds of split pattern are seen, depending, for example, on the procedure of solidification. This might suggest the presence of two crystal structures in solid ^{4}He. Above the solidification pressure, the ZPL wavelength is almost constant and the overall spectral profile keeps unchanged. However, the spectral intensity abruptly increases when the pressure is increased across the solidification pressure. This may indicate that, in solid ^{4}He, Eu atoms are trapped in the solid and cannot freely diffuse. On the contrary, for ^{3}He, neither such abrupt increase of spectral intensity nor the split pattern of the ZPL is observed, while the ZPL wavelength and overall spectral profile keep unchanged above the solidification pressure, just like ^{4}He. This may suggest that, unlike ^{4}He, Eu atoms can move around and diffuse in ^{3}He even in the solid state.

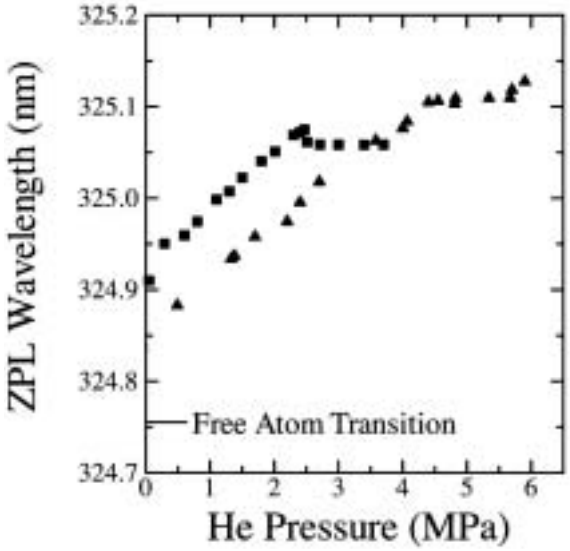

Figure 1. Helium pressure dependence of the wavelength of the zero-phonon line (ZPL) in the excitation spectrum of the $4f^6(^7\mathrm{F})5d6s^2\ ^8\mathrm{F}_{7/2} \leftarrow 4f^76s^2\ ^8\mathrm{S}_{7/2}$ transition of Eu atoms in liquid and solid helium at 1.1 K; ■ represents the ZPL for ^{4}He, and ▲ the one for ^{3}He. At 1.1 K, ^{4}He solidifies at 2.5 MPa, while ^{3}He at 4.3 MPa.

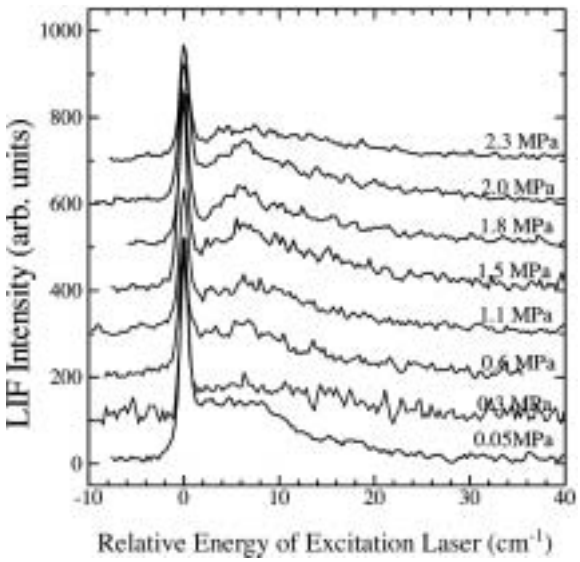

Figure 1. Excitation spectra of the $4f^6(^7\mathrm{F})5d6s^2\ ^8\mathrm{F}_{7/2} \leftarrow 4f^76s^2\ ^8\mathrm{S}_{7/2}$ transition of Eu atoms in liquid ^{4}He at several pressures; the peak shift of the zero-phonon line is ignored for all spectra.

II-C-2 Laser Spectroscopic Studies of Eu Atoms in Liquid ^{4}He: Roton Spectra

MORIWAKI, Yoshiki[1]; MORITA, Norio
([1]Toyama Univ.)

In our previous studies on spectra of the inner shell transition $4f^6(^7\mathrm{F})5d6s^2\ ^8\mathrm{F}_{7/2} \leftarrow 4f76s^2\ ^8\mathrm{S}_{7/2}$ of Eu atoms in liquid ^{4}He, we found some structure of the phonon sideband tail of this transition, and inferred that this structure may be roton spectra because the energy separation between the structure and zero-phonon line roughly agreed to the excitation energy (6 cm^{-1}) of the roton. In order to confirm this inference, in the present study, we have investigated the pressure dependence of the spectra: excitation spectra of this transition at 1.1 K have been measured at several pressures. The results are shown in Figure 1, in which peak shifts of the zero-phonon lines are ignored. In Figure 1, we can find that the peak on the long tail of the phonon sideband is gradually shifted toward lower energy with the increase of the liquid pressure. This characteristic behavior is the same as seen for roton peaks previously observed in two-roton Raman spectra.[1)] This fact strongly supports the inference that the peaks in our spectra are also due to the roton excitation.

Reference

1) K. Ohbayashi *et al.*, *Phys. Rev. B* **58**, 3351 (1998).

II-D Electron Transfer Regulation in Tetraheme Cytochromes *c*

Tetraheme cytochromes *c* are involved in the anaerobic energy metabolism. Cytochrome c_3 (cyt c_3) is an electron transport protein working in strictly anaerobic sulfate-reducing bacteria. This is a small (M.W. ≈ 14,000) soluble protein and shows very low redox potentials (typically, –240 ~ –357 mV *vs.* NHE). We have developed a new expression system using *Shewanella oneidensis*. Using this expression system, now we can examine the role of each amino acid by gene-engineering. At first, we have examined the role of tyrosine-43. We have also determined the complete *g* tensors of the four hemes. Small tetraheme cytochrome *c* (ST cyt *c*) is found in facultative anaerobes of *Shewanella* species and is the smallest tetraheme cytochrome (M.W. ≈ 12,000). The four hemes in ST cyt *c* is arranged in a chain-like manner in contrast to the cyclic heme architecture in cyt c_3. The major aims of this project is to elucidate the mechanism of the regulation of the electron transfer in tetraheme cytochromes *c* on the basis of tertiary structure and heme architecture. For this purpose, we are characterizing two different cytochromes mentioned above by NMR and electrochemistry. Since porphyrin is one of important elemental materials in nano-science, elucidation of the function of particular heme architectures would also contribute to this field.

II-D-1 Role of the Aromatic Ring of Tyr43 in Tetraheme Cytochrome c_3 from *Desulfovibrio vulgaris* Miyazaki F

OZAWA, Kiyoshi[3]; YASUKAWA, Fumiko[3]; TAKAYAMA, Yuki[2]; OHMURA, Tomoaki[4]; CUSANOVICH, Michael A.[5]; TOMIMOTO, Yusuke[6]; OGATA, Hideaki[6]; HIGUCHI, Yoshiki[6]; AKUTSU, Hideo[1]

([1]IMS and Osaka Univ.; [2]Osaka Univ.; [3]Yokohama Natl. Univ.; [4]Mitsubishi Heavy Industries; [5]Unv. Arizona; [6]Kyoto Univ.)

[*Biophys. J.* (2003) in press]

Tyrosine 43 is positioned parallel to the fifth heme axial ligand, His34, of heme 1 in the tetraheme cytochrome c_3. The macroscopic and microscopic formal redox potentials of Y43L and Y43F cytochromes c_3 were determined by differential pulse polarography and ^{1}H-NMR. Although the replacement of tyrosine with leucine increased all the redox potentials, the phenylalanine mutation generally did not change them. This strongly suggests that the aromatic ring at this position contributes to lower the redox potentials of cytochrome c_3. The effect of the leucine and phenylalanine mutations on the interacting potential between heme 1 and heme 2 shows that the aromatic ring is also involved in the cooperative reduction of these hemes. Furthermore, temperature dependent line-width broadening in partially reduced samples established that the aromatic ring at position 43 participates in the control of the kinetics of intramolecular electron exchange. The rate of reduction of Y43L cytochrome c_3 by 5-deazariboflavin semiquinone under partially reduced conditions was significantly different from that of the wild-type in the last stage of the reduction, supporting the involvement of Tyr43 in regulation of reduction kinetics. No significant change was found in the crystal structures of the wild-type and Y43L cytochrome c_3.

II-D-2 Correlation between the *g* Tensors and Nonplanarity of Porphyrin Rings in *Desulfovibrio vulgaris* Miyazaki F Cytochrome c_3 Studied by Single Crystal EPR

SAITOH, Takashi[1]; TACHIBANA, Yoshihiko[2]; HIGUCHI, Yoshiki[3]; HORI, Hiroshi[1]; AKUTSU, Hideo[4]

([1]Osaka Univ.; [2]Yokohama Natl. Univ.; [3]Himeji Inst. Tech.; [4]IMS and Osaka Univ.)

[*Bull. Chem. Soc. Jpn.* in press]

Single crystals of cytochrome c_3 from *Desulfovibrio vulgaris* Miyazaki F are examined by EPR at cryogenic temperature. The principal values and the eigenvectors are determined. The four sets of EPR signals are directly assigned to the specific four hemes in the three-dimensional structure. The relative energy levels of the three *d* orbitals (d_{xy}, d_{xz} and d_{yz}) of each heme iron calculated from the obtained principal *g* values have shown that the energy gap between d_{xy} and d_π is small for a heme with the S_4-ruffled distortion (heme 1 and heme 2) while the energy gap is large for a heme with the S_4-saddled distortion (heme 4). The determined *g* tensor orientations indicated that the principal *g* axes of heme 1, heme 2, heme 3 and heme 4 co-rotate with the imidazole planes of the sixth ligands.

II-D-3 A Directional Electron Transfer Regulator Based on Heme-Chain Architecture in The Small Tetraheme Cytochrome *c* from *Shewanella oneidensis*

HARADA, Erisa[2]; KUMAGAI, Jiro[3]; OZAWA, Kiyoshi[3]; IMABAYASHI, Shinichiro[3]; TSAPIN, Alexandre S.[4]; NEALSON, Kenneth H.[4]; MEYER, Terrance E.[5]; CUSANOVICH, Michael A.[5]; AKUTSU, Hideo[1]

([1]IMS and Osaka Univ.; [2]Osaka Univ.; [3]Yokohama Natl. Univ.; [4]Cal. Inst. Tech.; [5]Unv. Arizona)

[*FEBS. Lett.* **532**, 333–337 (2002)]

The macroscopic and microscopic redox potentials of the four hemes of the small tetraheme cytochrome *c* from *Shewanella oneidensis* were determined. The microscopic redox potentials show that the order of reduction is from hemes in the C-terminal domain (hemes 3 and 4) to the N-terminal domain (heme 1),

demonstrating the polarization of the tetraheme chain during reduction. This makes heme 4 the most efficient electron delivery site. Furthermore, multistep reduction of other redox centers through either heme 4 or heme 3 is shown to be possible. This has provided new insights into the two-electron reduction of the flavin in the homologous flavocytochrome *c*-fumarate reductase.

II-E Surface Chemical Reactions Studied by NEXAFS Spectroscopy

Near edge X-ray absorption fine structure (NEXAFS) is a very promising method to get the quantitative information of surface adsorbed species. Recently, we have developed an energy dispersive NEXAFS method, which is a technique to measure a NEXAFS spectrum in a certain energy range simultaneously. The Hettrick mount monochromator can be used as a polychromator by fully opening the exit slit. Energy dispersed X-rays from the polychromator irradiate the sample surface. Each position of the irradiated surface emits Auger electrons, of which number is proportional to the X-ray absorption coefficient at the corresponding photon energy. By using a position sensitive electron energy analyzer, we can obtain a NEXAFS spectrum from a monolayer-covered surface with a reasonably high signal-to-noise ratio in several tens seconds. This technique has been applied to the study of surface chemical reactions related to fundamental catalytic reactions.

II-E-1 Direct Spectroscopic Observations of the Water Formation Reaction on Pt(111) by NEXAFS and the Simulations with the Kinetic Monte Carlo and the Reaction Diffusion Methods

NAGASAKA, Masanari[1]; KONDOH Hiroshi[1]; AMEMIYA, Kenta[1]; NAMBU, Akira[1]; NAKAI, Ikuyo[1]; SHIMADA, Tohru[1]; OHTA, Toshiaki[2]
([1]Univ. Tokyo; [2]Univ. Tokyo and IMS)

[*J. Chem. Phys.* **119**, 9233 (2003)]

The catalytic water formation reaction was investigated by the energy dispersive NEXAFS spectroscopy. Oxygen covered Pt(111) surface with a (2×2) structure was exposed to gaseous hydrogen (5.0×10^{-9} Torr) at constant surface temperatures (120–140 K). O *K*-edge NEXAFS spectra were measured during the reaction with a time interval of 35 s. From quantitative analyses for the spectra, the coverage changes of the adsorbed species (O, OH, and H_2O) were obtained at 120, 130 and 140 K, as shown in Figure 1. The reaction is composed of three steps, which are characterized by the induction period (I), fast increase in coverage of OH and H_2O with consuming oxygen (II), and slow conversion of OH to H_2O after the consumption of oxygen (III). It was also found that the maximum OH coverage becomes smaller at a higher temperature. The kinetic Monte Carlo simulation has reproduced the three characteristic reaction steps, from which the steps are explained as follows; in the first step OH domains are created through two-dimensional aggregation of H_2O (I), after the nucleation process the second step sets in where the OH domains propagate by the auto-catalytic cycle until they contact with each other (II), and finally the merged OH domains convert to H_2O (III). The Reaction Diffusion simulation has revealed that the density of H_2O nuclei decreases due to its high diffusion rate at a high temperature, which results in reduction of the OH coverage.

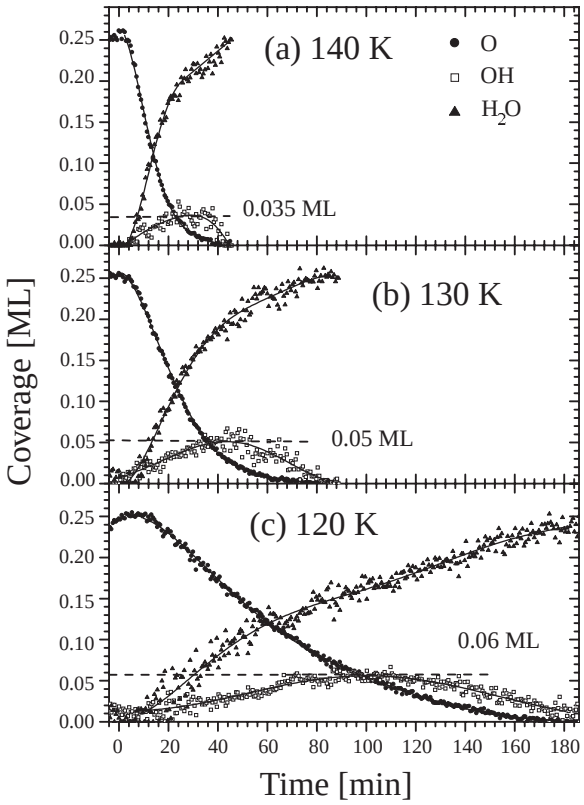

Figure 1. Coverages of O, OH, and H_2O as a function of time during dosing of gaseous H_2 (5.0×10^{-9} Torr) at a surface temperature of (a) 140 K, (b) 130 K, and (c) 120 K. The O-covered Pt(111) surface started exposing to gaseous H_2 at 0 min. The maximum OH coverage was 0.035 ML at 140 K, 0.05 ML at 130 K, and 0.06 ML at 120 K. The reaction finished in 45 minutes at 140 K, 80 minutes at 130 K, and 180 minutes at 120 K.

II-F Ultrafast Dynamics of Surface Adsorbed Species

Understanding of reaction dynamics at surfaces using ultra-short laser techniques is an important issue to clarify the mechanism of the reactions. Real-time observation of temporal change of surface species induced by UV, visible, and (Near-) infrared pump pulses is carried out using mid-IR pump-probe vibrational spectroscopy and Sum-frequency generation (SFG) spectroscopy which is one of the non-linear spectroscopies using ultra-short laser has high sensitivity for detection of molecular vibrations of adsorbed species on surface in the first layer. The aim of this study is the identification of molecular structures of the intermediates generated by electronic, vibrational, or thermal excitation and understanding of the reaction kinetics including potential energies, activation barriers, and entropies. Typical systems of our recent studies are formate (DCOO) adsorbed on Ni(111) surface, CO on OH group of zeolite, and C_6H_6 on Cu(111) surface.

II-F-1 Time-Resolved SFG Study of Formate on Ni(111) Surface under Irradiation of Picosecond Laser Pulses

NOGUCHI, Hidenori[1]; OKADA, Takuya[1]; ONDA, Ken[1]; KANO, Satoru S.[2]; WADA, Akihide[3]; DOMEN, Kazunari[1]
([1]Tokyo Inst. Tech.; [2]Hosei Univ.; [3]IMS and Tokyo Inst. Tech.)

[*Surf. Sci.* **528**, 183–188 (2003)]

Time-resolved sum-frequency generation (TR-SFG) spectroscopy was carried out on a deuterated formate (DCOO) adsorbed on Ni(111) surface to investigate the surface reaction dynamics under instantaneous surface temperature jump induced by the irradiation by pico-second laser pulses. The irradiation of pump pulse (800 nm) caused the rapid intensity decrease of both CD and OCO stretching modes of bridged formate on Ni(111). Different temporal behaviors of intensity recovery between these two vibrational modes were observed, *i.e.*, CD stretching mode recovered faster than OCO. This is the first result to show that the dynamics of adsorbates on metals strongly depends on the observed vibrational mode. From the results of temperature and pump fluence dependence, we concluded that the observed intensity change was not due to the decomposition or desorption, but was induced by a non-thermal process.

II-F-2 Vibrational Relaxation of Adsorbate and Adsorbent in the CO-adsorbed DM-20 Zeolite System

ONDA, Ken[1]; IWASAWA, Yasuhiro[2]; WADA, Akihide[3]
([1]Tokyo Inst. Tech.; [2]Univ. Tokyo; [3]IMS and Tokyo Inst. Tech.)

[*Chem. Phys. Lett.* **370**, 437–442 (2003)]

We made the first observation of transient vibrational spectra of both adsorbate and adsorbent at molecule-adsorbed surface using a two-color infrared picosecond laser system. The transient measurements were carried out on the CO-adsorbed surface hydroxyl group (OD) of DM-20 zeolite by pumping the CO stretching mode (2175 cm^{-1}) or OD stretching mode (2470 cm^{-1}) and probing over the CO and OD stretching region (2000–2700 cm^{-1}). The T_1 lifetime for OD was 5.8 ps and that for CO was 540 ps. By comparison with other CO-adsorbed systems, vibrational relaxation mechanisms of CO on various surfaces are discussed. We also found evidence of energy flows from the vibrational mode of the adsorbent (OD stretching) to that of the adsorbate (CO stretching) *via* van der Waals interaction.

II-F-3 Second Harmonic Observation of Cu(111) Surface: *In Situ* Measurements during Molecular Adsorption

ISHIDA, Hirokazu[1]; MIZOGUCHI, Ryuuichi[1]; ONDA, Ken[1]; HIROSE, Chiaki[1]; KANO, Satoru S.[2]; WADA, Akihide[3]
([1]Tokyo Inst. Tech.; [2]Hosei Univ.; [3]IMS and Tokyo Inst. Tech.)

[*Surf. Sci.* **526**, 201–207 (2003)]

Second harmonic generation (SHG) spectroscopy using a tunable femtosecond laser has been demonstrated as an effective and a practical *in situ* monitor of surface electronic states during adsorption processes. We have successfully shown this technique to be suitable for the study of surface electronic states, not only those induced by adsorbed molecules but also those associated with clean surfaces. By observing the change in the SH signals from a Cu(111) surface during exposure to benzene or CO molecules, we discovered new resonances of the clean Cu surface that could not be ascribed to the well-known surface state (SS)–image state (IS) transition. One of these was from a surface site that is less likely to adsorb benzene, where the SH signal intensity was kept constant until the Cu surface was covered by the sub-monolayer.

II-G Spin Reorientation Transitions of Ultrathin Magnetic Films Induced by Chemisorption

Magnetic anisotropy of ultrathin metal films is one of the most attractive subjects in magnetism. When one considers magnetic anisotropy of thin films within the framework of the classical electromagnetic theory, one finds that in-plane magnetization is always more stable than perpendicular magnetization. Perpendicular magnetic anisotropy (PMA) is, however, sometimes observed in real systems and the understanding of the origin of PMA is important from the viewpoints of both fundamental physics and technological applications to new-generation high-density recording media. We are investigating the microscopic mechanism of PMA that is stabilized by gaseous adsorption on magnetic film surfaces by means of the synchrotron radiation x-ray magnetic circular dichroism (XMCD) and the visible-light magneto-optical Kerr effect (MOKE) techniques. A goal of these works is spin engineering by which the magnetization of ultrathin metal films can be controlled artificially.

II-G-1 Perpendicular Magnetic Anisotropy in Ni/Cu(001) Stablized by Chemisorption of NO

NAKAGAWA, Takeshi; YOKOYAMA, Toshihiko

Spin reorientation transitions (SRT) of ultrathin Ni/Cu(001) films induced by adsorption of nitric oxide (NO) have been investigated by means of MOKE. A wedge-shaped Ni film (4–11 ML) was grown on a clean and ordered Cu(001) surface at room temperature, and was dosed with NO after cooling down to 90 K. The M-H curves were measured using both the polar and longitudinal MOKE geometries. Figure 1 show the observed coersivity (H_c) of the Ni film at 90 K as a function of Ni thickness. On the clean surface H_c abruptly increases at ~ 9 ML, implying that the SRT occurs at this coverage. On the other hand, the NO-adsorbed Ni film shows a clear shift of the SRT coverage at ~ 7 ML. It is concluded that the Ni/Cu(001) film with 7–9 ML thickness exhibits the SRT from in-plane magnetization to perpendicular after NO adsorption. This finding is consistent with the previous works on CO- and H-adsorbed Ni/Cu(001) films.

Let us here compare the coersivity between before and after NO adsorption at the Ni thickness where the SRT does not occur: less than 7 and more than 9 ML. Although the differences are not so large, it is found that in the in-plane magnetized films H_c is suppressed after NO adsorption while H_c is enhanced at the perpendicularly magnetized ones. These results again imply that NO adsorption stabilizes perpendicular magnetization. It is known that the surface magnetic anisotropy constant K_{2s} is negative and favors in-plane magnetization on clean Ni/Cu(001). After NO adsorption, $|K_{2s}|$ is reduced, this leading to the stabilization of perpendicular magnetization, the suppression of H_c for the in-plane magnetization, and the enhancement of H_c for the perpendicular magnetization.

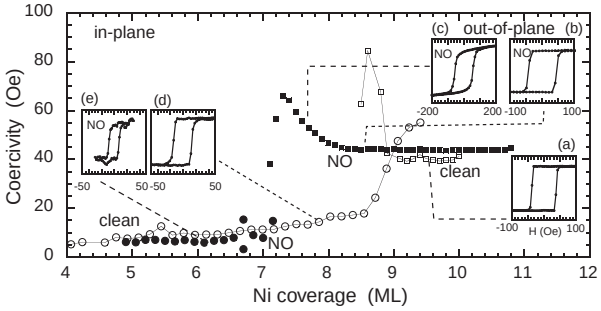

Figure 1. Coersivity of the Ni film at 90 K as a function of Ni thickness before (open circles and squares) and after (filled circles and squares) NO adsorption, obtained by the polar (open and filled squares) and longitudinal (open and filled circles) MOKE measurements. Typical M-H curves are inserted as (a)–(c) (polar) and (d)–(e) (longitudinal).

II-H Local Structures in Photoinduced States of Transition Metal Complexes

Photoinduced phase transition is closely related to bistability of the ground state in the material. Light irradiation stimulates the macroscopic phase transition between the ground state and the metastable state, although thermal fluctuation triggers the thermal phase transition. Although it has been believed that the photoinduced phase is the same state as the thermally induced phase, recent investigations have reported some differences in structure from the high-temperature phase. We have been studying local structures and electronic properties of photoinduced phases of several kinds of transition metal complexes by means of x-ray absorption fine structure (XAFS) spectroscopy. XAFS is one of the most suitable methods for these purposes since the technique does not require long-range order in the sample and provide element-specific information about each metal atom.

II-H-1 Metastable Photoinduced Phase of Cu(II) Ethylenediamine Complexes Studied by X-Ray-Absorption Fine-Structure Spectroscopy

YOKOYAMA, Toshihiko; TAKAHASHI, Kazuyuki[1]; SATO, Osamu[1]
([1]Kanagawa Acad. Sci. Tech.)

[*Phys. Rev. B* **67**, 172104 (4 pages) (2003)]

Recently, a new type of the photoinduced (PI) metastable phase was reported in $Cu(dieten)_2X_2$ (dieten = *N*,*N*-diethylethylenediamine, X = BF_4 and ClO_4) complexes. These materials are known to exhibit thermochromic phase transitions. From the color change the PI transition is expected to be similar to the thermally driven phase transition. The powder X-ray diffraction patterns of the PI phase were, however, found to be different from those of the HT phase, although no correspondence between the structure and diffraction patterns was deduced. In this work, Cu *K*-edge XAFS has been measured and analyzed in order to clarify the molecular structure in the PI phase.

The sample was irradiated by the UV lights (Hg lamp) at 30 K. The Cu *K*-edge near-edge structure indicates that the CuN_4 unit in the PI phase is distorted tetrahedrally, being similar to the HT phase. On the contrary, EXAFS shows a different finding in the second-nearest neighbor Cu–C shells], indicating that the configuration of the surrounding C atoms in the PI phase should be closer to the LT phase rather than to the HT phase.

We can conclude that the PI phase is a new metastable state, whose intramolecular structure is not equivalent to the one of either the HT or LT phase; the CuN_4 unit exhibits tetrahedral distortion, while the atomic configuration of ethylene and ethyl groups is similar to the LT one. One can thus propose a possible model structure shown in Figure 1. The $Cu(dieten)_2$ ion has an inversion center in the LT phase (point group C_i), while it has a C_2 axis in the HT phase (point group C_2). We can suppose that when the LT phase is transformed to the PI phase upon UV irradiation, the CuN_4 plane is distorted tetrahedrally with less reconstruction of the dieten ligand compared to the LT phase. This might be a reasonable hypothesis since the transformation of the configuration of the ethyl groups and also the anions would require too much activation energy to complete at low temperature like 30 K.

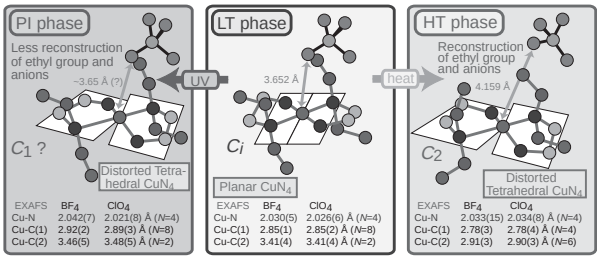

Figure 1. Proposed structure transformation in the PI phase transition.

II-I Molecular and Electronic Structures of Metallofullerenes

The continued interest in radical ions of fullerenes and metallofullerenes has resulted from the discovery of superconductivity in the CT complexes of alkali metals with fullerenes. Spectroscopic information concerning the electronic and spin states of the metallofullerenes has been obtained by ESR measurements.

II-I-1 A Multi-Frequency EPR Study of Endohedral Metallofullerenes Containing the Divalent Eu Ion

MATSUOKA, Hideto; FURUKAWA, Ko; KATO, Tatsuhisa; OZAWA, Norio[1]; KODAMA, Takeshi[1]; NISHIKAWA, Hiroyuki[1]; IKEMOTO, Isao[1]; KIKUCHI, Koichi[1]; SATO, Kazunobu[2]; SHIOMI, Daisuke[2]; TAKUI, Takeji[2]
([1]Tokyo Metropolitan Univ.; [2]Osaka City Univ.)

An endohedral fullerene containing a lanthanoid ion in C_{82} cage, M@C_{82} (M; a lanthanoid ion), has been widely investigated in the field of fullerene science. Our attention in this work has been paid to the metallofullerene containing the divalent Eu ion with the highest spin (S = 7/2) of lanthanoid ion, focusing on the surrounding symmetry of the ion. We isolated three isomers of Eu@C_{82} with the cage structures of C_S, C_2, and C_{2v} symmetry, and Eu@C_{74} with that of D_{3h} symmetry. Their formal electronic structures are represented by $Eu^{2+}@C_n^{2-}$ (n = 74 or 82), where two electrons of Eu atom transfer to the cages. In this work, multi-frequency Electron Paramagnetic Resonance (EPR) measurements were performed to determine their spin-Hamiltonian parameters related to the surrounding symmetry of Eu^{2+} ion. Figure (a) shows W-band EPR spectrum observed for Eu@C_{74} at 4 K. The spin-Hamiltonian parameters were precisely determined by spectral analysis including higher-order zero-field splitting (ZFS) terms. Figures (b) and (c) show the W-band CW-EPR spectra calculated for Eu@C_{74} by using positive and negative D values, respectively. Figure (b) was in good agreement with the observed spectrum, concluding that Eu@C_{74} has the positive D value. A non-zero rhombicity parameter E/D (= 0.11) was obtained for Eu@C_{74}, indicating that Eu(II) ion is not at the center of the C_{74} cage. The spin-Hamiltonian parameters including the signs of the D values for the other sample were also determined in this manner.

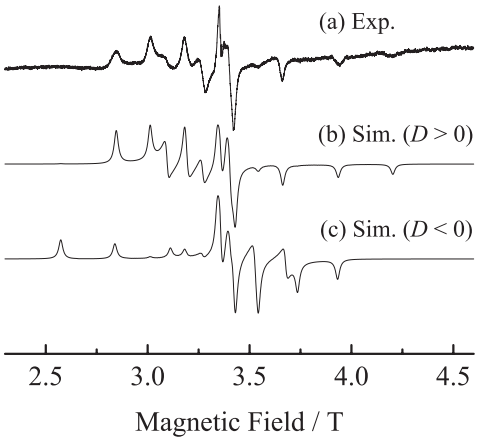

Figure 1. W-band EPR spectra of Eu@C_{74}; (a) experiment; (b) simulation (D > 0); and (c) simulation (D < 0). Experimental conditions: microwave frequency, 95 GHz; temperature, 4 K.

II-I-2 Study on the Electron Spin State of $La_2@C_{80}$ Anion

KATO, Tatsuhisa; MATSUOKA, Hideto; OKUBO, Shingo[1]; DINSE, Klaus-Peter[2]
([1]RIKEN; [2]Darmstadt Tech. Univ.)

An anion form of a lanthanum dimer with C_{80} cage ($La_2@C_{80}^-$) was obtained by chemical and electrochemical reduction. The $La_2@C_{80}^-$ anion exhibited the characteristic Electron Spin Resonance (ESR) pattern for the spin-doublet radical having very large hyper fine coupling (hfc) interaction with the identical two La nuclei, as seen in Figure. The exact values of hfc and g-tensor were determined by ESR measurements with two different frequencies, *i.e.* 9.5 GHz (X-band) and 95 GHz (W-band). The spectrum was completely simulated by parameters shown in Figure. Two La ions were identical, however, they formed a dimer and were fixed at the certain position within the $C_{80}(I_h)$ cage. The total symmetry of $La_2@C_{80}^-$ anion was D_{2h}. The picture of the electronic state was changed from those of a neutral form of $La_2@C_{80}$ by the injection of an excess electron.

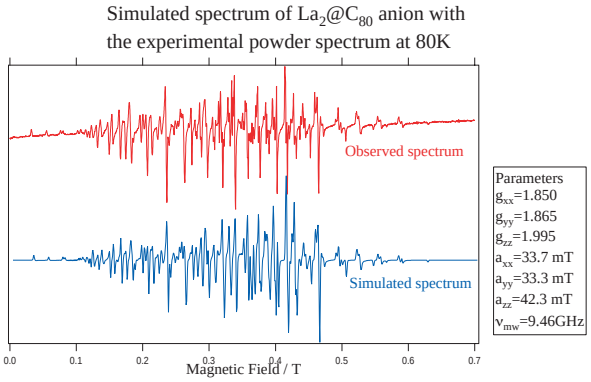

Figure 1. The ESR spectrum of $La_2@C_{80}^-$ anion. The upper spectrum was obtained by a 9.5 GHz (X-band) spectrometer, the lower one was obtained by the simulation using the parameters indicated in the right box.

II-I-3 Spin States of Water-Soluble C_{60} and Metallofullerenes

KATO, Tatsuhisa; MATSUOKA, Hideto; FURUKAWA, Ko; KATO, Haruhito[1]; SHINOHARA, Hisanori[1]; HUSEBO, Lars Olav[2]; WILSON, Lon J.[2]
([1]Nagoya Univ.; [2]Rice Univ.)

Nagoya group of author has shown an application of water-soluble metallofullerens to magnetic resonance imaging (MRI) contrast agents.[1)] It has been found *in vivo* and *in vitro* that water-soluble polyhydroxylated gadolinium metallofullerenols,[2)] $Gd@C_{82}(OH)_n$, exhibit a very strong ability of reducing water proton relaxation times, T_1 and T_2, which results a high MR signal enhancement. This property would be originated from the magnetization due to $4f^7$ radical electrons of Gd^{3+} ion. However, spin states of polyhydroxylated fullerenols have not been clarified in detail. We investigated spin states of $C_{60}(OH)_n$, $La@C_{82}(OH)_n$, $La_2@C_{80}(OH)_n$, and $Gd@C_{82}(OH)_n$ in aqueous solution by using cw-electron spin resonance (cw-ESR) and pulsed-ESR spectrometers. $Gd@C_{82}(OH)_n$ gave a broad cw-EPR spectrum which was characterized by the high spin state of $S = 7/2$, as shown in Figure 1. The other samples in frozen solution showed cw-ESR signal around $g = 4$ as well as $g = 2$. These spectra could be attributed to the spin state of higher spin than $S = 1/2$. Actually the nutation frequency corresponding not only to $S = 1/2$ but also to $S = 1$ was observed by 2D- nutation measurements. $C_{60}(OH)_n$, $La@C_{82}(OH)_n$, and $La_2@C_{80}(OH)_n$ exhibit ESR spectra due to the spin state of $S = 1$, and its magnetization gives the ability of reducing water proton relaxation times in MRI measurement.

References

1) M. Mikawa *et al.*, *Bioconjugate Chem.* **12**, 510–514 (2001).
2) H. Kato *et al.*, *Chem. Phys. Lett.* **324**, 255–259 (2000).

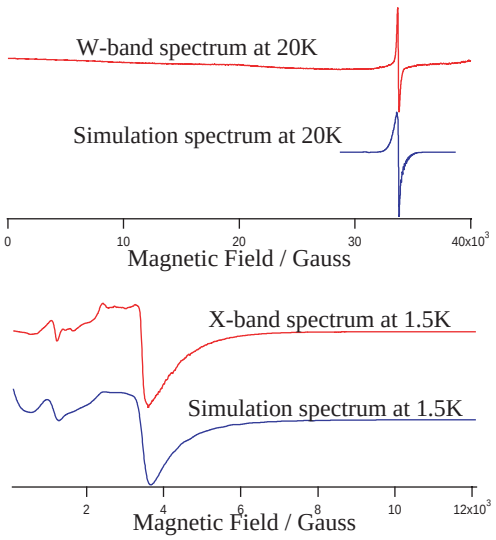

Figure 1. EPR spectra of $Gd@C_{82}(OH)_n$ obtained by a 9.5 GHz(X-band) spectrometer, the lower trace, and by a 95 GHz (W-band) one, the upper trace.

II-I-4 Chemical Reactivity and Redox Property of $Sc_3@C_{82}$

KATO, Tatsuhisa; KOBAYASHI, Kaoru; NAGASE, Shigeru; WAKAHARA, Takatsugu[1]; IIDUKA, Yuko[1]; SAKURABA, Akihiro[2]; OKAMURA, Mutsuo[2]; TSUCHIYA, Takahiro[1]; MAEDA, Yutaka[1]; ISHIZUKA, Midori O.[1]; AKASAKA, Takeshi[1]; KADISH, Karl M.[3]

([1]Univ. Tukuba; [2]Niigata Univ.; [3]Univ. Houston)

The photochemical and thermal reactions of $Sc_3@C_{82}$ with disilrane afforded an exohedral adduct indicating the high reactivity of $Sc_3@C_{82}$. The redox potentials of $Sc_3@C_{82}$ in *o*-dichlorobenzene show a high electron affinity and a small band gap. The $Sc_3@C_{82}$ anion was prepared by electrochemical reduction, which possesses a diamagnetic character. Recently, we have accomplished the chemical reduction of endohedral metallofullerenes as $La@C_{82}$ and $La_2@C_{80}$ in the pyridine and DMF solution. In this context, $Sc_3@C_{82}$ may exist as an anionic form in pyridine. No ESR signal was observed at room temperature in the ESR spectrum of $Sc_3@C_{82}$ in the presence of pyridine, indicating the formation of the diamagnetic $Sc_3@C_{82}$ anion (Figure 1). After removal of pyridine, the residue was resolved again in toluene. Interestingly, the ESR spectrum of $Sc_3@C_{82}$ was recovered, and it was accompanied by a triplet spectrum at $g = 2.0403$, as can be seen in Figure 1. The recovered spectrum was identical with the original $Sc_3@C_{82}$ one in terms of *g*-value, 1.9985, and isotropic hfs constant, 6.25 gauss. The accompanying triplet splitting would come from the hfs of ^{14}N nucleus, which would be due to a by-product of chemical reduction by pyridine. These observations surely reveal that $Sc_3@C_{82}$ can exist as an anionic form in pyridine.

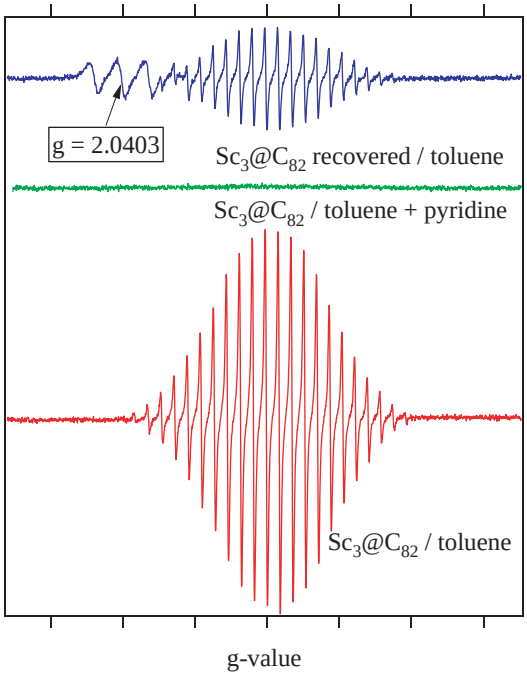

Figure 1. Twenty two lines of ESR spectrum of $Sc_3@C_{82}$ in toluene, the lower trace, disappeared in the presence of pyridine as shown in the middle trace, indicating the formation of the diamagnetic $Sc_3@C_{82}$ anion. After removal of pyridine, the residue was resolved again in toluene and exhibited the ESR spectrum of $Sc_3@C_{82}$. It was accompanied by a triplet spectrum at $g = 2.0403$. The recovered spectrum was identical with the original $Sc_3@C_{82}$ one in terms of *g*-value, 1.9985, and isotropic hfs constant, 6.25 gauss.

II-I-5 Hyperfine Interactions in La@C_{82} Studied by W-Band EPR and ENDOR

KATO, Tatsuhisa; WEIDEN, Norbert[1]; DINSE, Klaus-Peter[1]
([1]Darmstadt Tech. Univ.)

The analysis of dipolar and quadrupolar lanthanum hyperfine data measured with EPR and ENDOR reveals that at low temperatures no significant change occurs at the internal binding site of the endohedral complex. We interpret this result as indicative of freezing of the large-scale motion of the encased ion, which is observed at room temperature. Averaging of hyperfine interactions is fast on the time scale of the EPR experiment, prevening drastic changes of dipolar and quadrupolar hfi, providing that the equilibrium position is unchanged. The detection of hyperfine interaction in disordered samples was possible by invoking orientation selection in the 94 GHz EPR spectrum. Quadrupolar hfi could be directly measured for the first time in a metallo-endohedral fullerene complex.

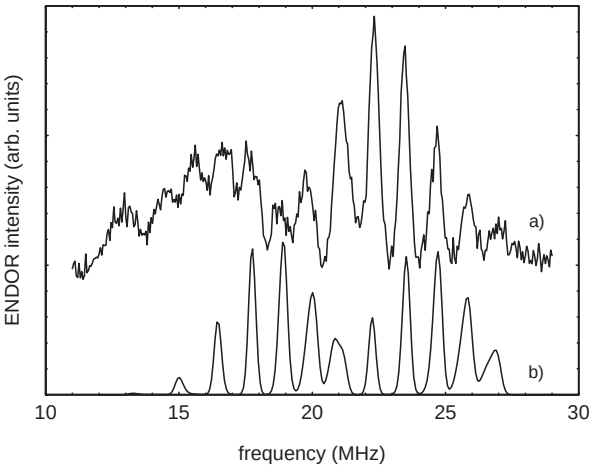

Figure 1. a) W-band pulsed ENDOR spectrum of La@C_{82}(I) measured at 10 K at B_0 = 3371.6 mT. The spectrum was accumulated when exciting the high-field edge of the EPR spectrum and by invoking a Davies pulse sequence. b) A simulated spectrum used to identify the individual line positions is also shown.

II-J High Field and Pulsed Electron Spin Resonance Spectroscopy

Electron paramagnetic resonance (EPR) spectroscopy has been a powerful technique for the characterization of radical species. The modern development of EPR spectroscopy enables us to investigate the heterogeneous and disordered system in detail. Especially the high frequency and pulsed EPR methods achieve the substantial resolution enhancement of spectrum. The advanced EPR spectroscopy is applied to study on the spin state in the heterogeneous system.

II-J-1 A Discrete Self-Assembled Metal Array in Artificial DNA

KATO, Tatsuhisa; TOYAMA, Namiki; TANAKA, Kentaro[1]; TENGEIJI, Atsushi[1]; SHIONOYA, Mitsuhiko[1]
([1]Univ. Tokyo)

[*Science* **299**, 1212–1213 (2003)]

DNA has a structural basis to array functionalized building blocks. Here we report the synthesis of a series of artificial oligonucleotides, d(5'-GH_nC-3') (n = 1 to 5), with hydroxypyridone nucleobases (H) as flat bidentate ligands. Righthanded double helices of the oligonucleotides, $n$$Cu^{2+}$ d(5'-GH_nC-3')$_2$ (n = 1 to 5), were quantitatively formed through copper ion (Cu^{2+}) –mediated alternative base pairing (H–Cu^{2+}–H), where the Cu^{2+} ions incorporated into each complex were aligned along the helix axes inside the duplexes with the Cu^{2+}–Cu^{2+} distance of 3.7 ± 0.1 angstroms. The Cu^{2+} ions were coupled ferromagnetically with one another through unpaired *d* electrons to form magnetic chains. Continuous-wave electron paramagnetic resonance (CW-EPR) spectra of the duplexes Cu-n (n = **1**–**5**) in a frozen aqueous solution were recorded at 1.5 K by a conventional X-band spectrometer (Figure 1). The spectrum of the mononuclear complex Cu-**1** was reproducible in a simulation as arising from a doublet (S = 1/2) radical of a Cu^{2+} center in the square-planar ligand field. However, spectra of Cu-**2**, Cu-**3**, Cu-**4**, and Cu-**5** exhibited quite different patterns from that of Cu-**1**. The spectrum of Cu-**2** could be attributed to the spin state of S = 1, that of Cu-**3** to S = 3/2, and those of Cu-**4** and Cu-**5** to S = 2 and S = 5/2, respectively. The results obtained by CW-ESR spectra were confirmed by the Transient Nutation measurement of a pulsed-ESR. With accumulating Cu^{2+} ions, the electron spins on adjacent Cu^{2+} centers are aligned parallel and couple in a ferromagnetic manner, with Cu-n (n = **1**–**5**) attaining the highest spin state, as expected from a lineup of n Cu^{2+} ions.

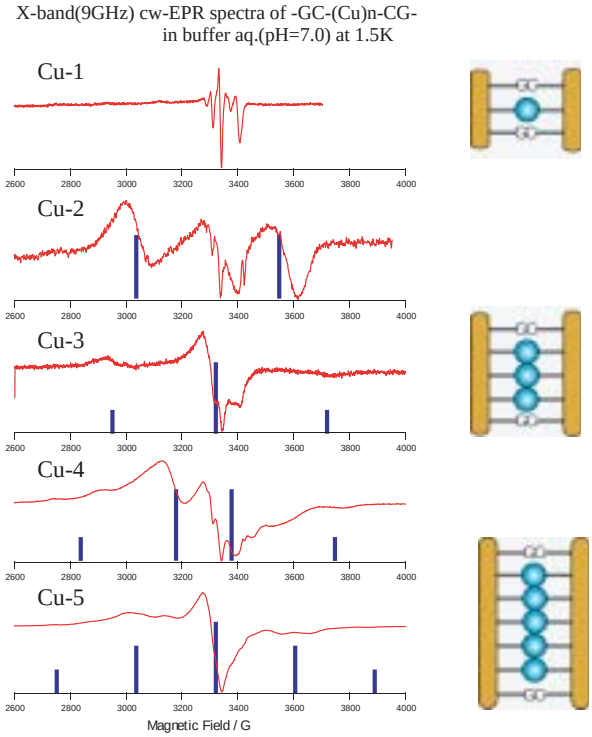

Figure 1. CW-EPR spectra of the duplexes Cu-*n* (*n* = **1**–**5**) in frozen aqueous solution at 1.5 K, recorded by an X-band spectrometer with a 9.5-GHz microwave.

II-J-2 Charge Transport in the Insulating State of (DMe-DCNQI)$_2$Li above T_{SP}: A Possible Fractional Charge Soliton Conduction with $\pm\frac{1}{2}e$

KATO, Tatsuhisa; HIRAOKA, Maki[1]; SAKAMOTO, Hirokazu[1]; MIZOKUCHI, Kenji[1]; KATO, Reizo[2]
([1]Tokyo Metropolitan Univ.; [2]RIKEN)

[*Phys. Rev. Lett.* **91**, 056604 (2003)]

A spin-Peierls system (DMe-DCNQI)$_2$Li is studied with *W*-band electron paramagnetic resonance (EPR) (94 GHz) to unveil a charge transport mechanism in the insulating $4k_F$ charge density wave state above T_{SP}. The electron hopping between the neighbor DCNQI columns provides an additional broadening of the EPR linewidth, since the neighbor columns are generally nonequivalent to each other with respect to *g* shift. The obtained intercolumn hopping rates lead us to the conclusion that the electron hopping to a hole soliton carrying a fractional charge of *e*/2 in the neighbor column dominates the intercolumn charge transport.

II-J-3 Magnetic Properties for Hexaphyrin

FURUKAWA, Ko; KATO, Tatsuhisa; VENKATARAMANARAO, G. Arnand[1]; SHIMIZU, Soji[1]; ARATANI, Naoki[1]; OSUKA, Atsuhiro[1]
([1]Kyoto Univ.)

Magnetic properties for the hexaphyrin **1** with the Cl and O bridging ligands, the hexaphyrin **2** without the bridging ligand, and the hexaphyrin **3** with the O bridging ligand (see Figure 1) were examined. In these hexaphyrins **1**–**3**, not the direct exchange coupling between the Cu ions but the superexchange coupling *via* the bridging ligands is expected due to the much long Cu–Cu distance. These systems are the attractive materials from the viewpoint of the superexchange interaction.

Figure 1 shows the temperature dependence of the χ_pT values for **1**–**3**. The observed values were reproduced by the typical spin hamiltonian $H = -2J\mathbf{S}_i\cdot\mathbf{S}_j$, where *J* denotes the exchange coupling parameters (J/k_B = –17.3 K for **1**, J/k_B = –230 K for **3**). The χ_pT values for **2** are independent of the temperature. The spin structures for both hexaphyrins **1** and **3** have the singlet ground states. The remarkable points are the following two; (1) the exchange coupling for both **1** and **3** is antiferromagnetic, although the superexchange interaction should be ferromagnetic according to the Goodenough-Kanamori-Anderson (GKA) rule[1)] and (2) the J/k_B value for **3** is much larger than that for **1**.

The GKA rule is assumed that the *d* orbital for the metal ions and the degenerated *p* orbitals for the bridging ligand take part in the superexchange interaction. The antiferromagnetic superexchange interaction is induced by the breakdown of the degeneracy of the *p* orbitals, which is caused by the chemical bond between the ligand O and the C atom on the hexaphyrin ring. In the hexaphyrin **1**, the superexchange interaction for the Cu–Cl–Cu pathway becomes ferromagnetic because of the equivalency between the *p* orbitals of the ligand Cl. Totally, the exchange coupling in **1** is weaker than that for **3**.

Reference

1) J. Goodenough, *Magnetism and the Chemical Bond*, John Wiley and Sons; New York (1963).

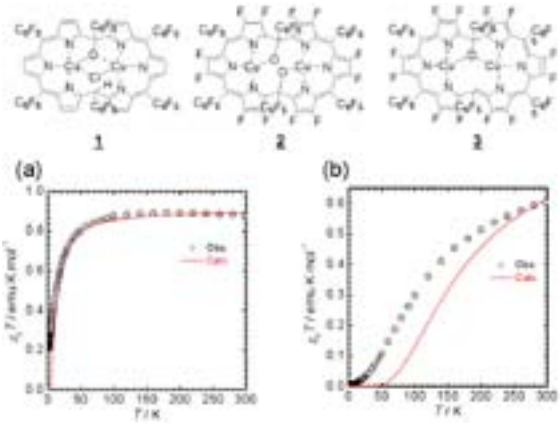

Figure 1. Temperature dependence of the χ_pT values for hexaphyrin (a)**1**, (b)**3**. The circles and lines stand for the observed and calculated values.

II-J-4 Determination of Spin State and Observation of ESEEM for Di- and Tri-Cation of Oligoanilines

KATO, Tatsuhisa; HIRAO, Yasukazu[1]; ITO, Akihiro[1]; TANAKA, Kazuyoshi[1]

([1]Kyoto Univ.)

The ESR spectroscopy showed that high-spin species were generated by chemical oxidation of N,N,N',N',N",N"-Hexakis[4-(di-4-anisylamino)-phenyl]-1,3,5- benzenetriamine in solution. The polycationic species formed by two equivalent of oxidant was assigned to be the triplet spin state, and that by three equivalent of oxidant to be the quartet spin state, respectively, on the basis of ESR spectroscopy. The assignment was confirmed by the 2 dimensional nutation (2D Nuation) measurement of pulsed ESR spectroscopy. Each polycation exhibited the specific ESEEM (Electron Spin Echo Envelope Modulation) frequency in 2-pulsed and 3-pulsed echo-decay measurement. And they gave the auto-correlation peak at the frequency associated with ESEEM in the two dimensional spectrum obtained by the HYSCORE (hyperfine sublevel correlation spectroscopy) sequence.

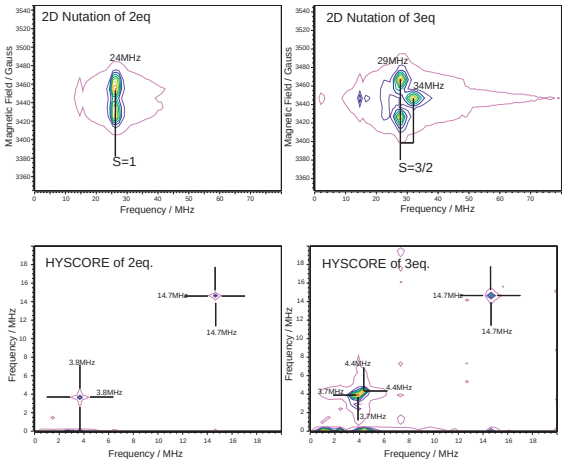

Figure. 1 The upper two contour maps are 2D Nutation spectra for the di-cation and the tri-cation. The lower two contour maps are HYSCORE spectra for the di-cation and the tri-cation.

II-K State Correlated Raman Spectroscopy

The vibrational Raman polarizability tensor responds to molecular reorientational relaxation process, and the structural environment in condensed media. The measurement of Raman scattering is a powerful technique for the investigations of molecular structure, molecular motion, and the mechanism of phase transition. We've built up the system of multichannel type detection of Raman scattering combined with the temperature controlled cell.

II-K-1 Intrinsic Aspect of V-Shaped Switching in Ferroelectric Liquid Crystals: Biaxial Anchoring Arising from Peculiar Short Axis Biasing in the Molecular Rotation around the Long Axis

HAYASHI, Naoki; KATO, Tatsuhisa; ANDO, Tomohiro[1]; FUKUDA, Atsuo[2]; KAWADA, Sachiko[3]; KONDOH, Shinya[3]
([1]Shinshu Univ.; [2]Univ. Dublin; [3]Citizen Watch Co., Ltd.)

[*Phys. Rev. E* **68**, 11702 (2003)]

To clarify the intrinsic aspect of practically usable thresholdless V-shaped switching in ferroelectric liquid crystals, we have observed textures and measured polarized Raman scattering as well as optical transmittance in a thin homogeneous cell of a single compound by applying an electric field. The results indicate that the so-called surface stabilized ferroelectric states are destabilized, and that there exist rather stable two domains [Figure 1(a)] with broad and narrow molecular orientational distributions, both of which show the almost ideal V-shaped switching with considerably low transmittance at the tip of the V [Figure 1(b)]. We have concluded that the main cause of the V-shaped switching is the biaxial anchoring on the substrates coated with polyimide, which makes the most polarizable short axis normal to the substrates. It is in a competition with the ordinary anchoring that favors the director parallel to the substrates, when the material has such a bulk intrinsic property that this short axis is parallel to the tilt plane. The competition makes the total anchoring energy almost independent of the azimuthal angle and gives rise to the V-shaped switching.

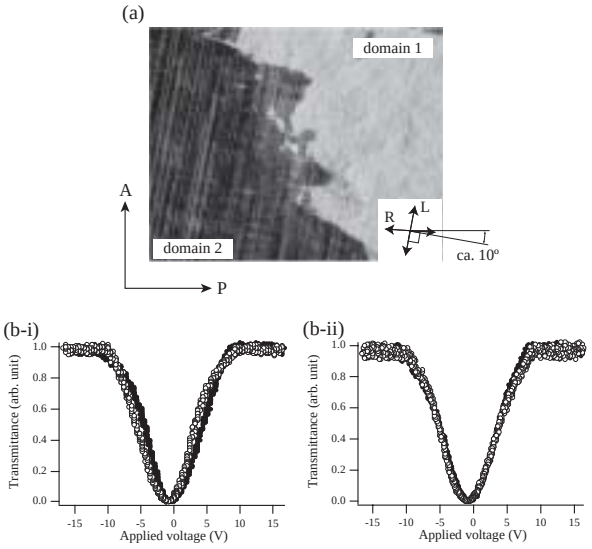

Figure 1. (a) Optical micrographs of textures taken after the long-term switching. The arrow "L" indicates the layer direction and the arrow "R" indicates the rubbing direction.

(b) Electro-optic responses observed in domains 1 [(b-i)] and 2 [(b-ii)]. Solid and open circles were obtained by increasing and decreasing the applied electric field, respectively.

II-K-2 A Large Tilt in the Core Relative to the Molecular Rotational Long Axis as Observed by Polarized Raman Scattering in a de Vries Smectic-*A* Liquid Crystal

HAYASHI, Naoki; KATO, Tatsuhisa; FUKUDA, Atsuo[1]; PANARIN, Yuri P.[1]; VIJ, Jagdish K.[1]; NACRI, J.[2]; SHASHIDHAR, R.[2]; KAWADA, Sachiko[3]; KONDOH, Shinya[3]
([1]Univ. Dublin; [2]Naval Research Laborator; [3]Citizen Watch Co., Ltd.)

The second- and fourth-order orientational order parameters of the core part of the molecule, $\langle P_2 \rangle$ and $\langle P_4 \rangle$, have been measured by polarized vibrational Raman spectroscopy for a homogeneously aligned ferroelectric smectic liquid crystal with three dimethyl siloxane groups in the achiral alkyl terminal chain, which shows the de Vries-type phenomena; very large electroclinic effect in the smectic-*A* (Sm-*A*) phase and a negligible layer contraction at the phase transition between the Sm-*A* and Sm-*C** phases. The orientational order parameters of the rigid core part of the molecule are extremely small both with and without the external electric field in Sm-*A*; $\langle P_4 \rangle$ is only approximately 0.1 while the apparent tilt angle reaches at 32º when a sufficiently high electric field is applied to the cell. This result indicates that the core part is tilted by 26–36º relative to the molecular rotational long axis (Figure 1).

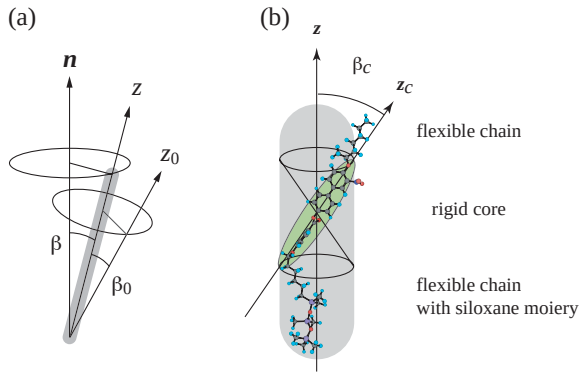

Figure 1. Schematic illustrations representing (a) the molecular rotational long axis (the *z* axis), the averaged direction of the molecular rotational long axes (the in-layer director, ***n***), and the longest principal axis of the Raman tensor (the z_0 axis), and (b) the molecular rotational long axis (the *z* axis) and the long axis of the core part (the z_c axis). Here β is the molecular tilt angle at an instant of time, β_0 the angle between the *z* and z_0 axes, and β_c the angle between the *z* and z_c axes. The molecules are rotating freely around their long axes, of which the distribution around the in-layer director is uniaxial. The z_c and z_0 axes are almost parallel each other and hence we assume $\beta_0 = \beta_c$. The conformation of the chemical structure illustrated is not a real one but is drawn just for the ease of understanding.

RESEARCH ACTIVITIES III
Department of Electronic Structure

III-A Synthesis and Characterization of Exotic Molecule Based Nano-Crystals with Transition Metal Cations : Toward Electron Beam Writing Yielding Metal Dot Arrays and Wires Encapsulated in Carbon Shells

Observation of photoelectron and vibrational spectra of gaseous M–C_2 molecules and clusters, where M = Fe, Co, Ni *etc.*, reminds us high potentiality of these salt-type clusters and nano-crystals for magnetic, catalytic and electronic functionalities. Due to the instability of the carbide compounds, the characterization of the MC_2 compounds has been left unknown. We have found that including MnC_2, all transition metal C_2 salt crystals are ferromagnetic, and that M^{2+}–C_2^{2-} ionic nano-crystals are the best materials for generating nano-metals encapsulated in carbon shells. Annealing or heating above 300 °C induces reduction of cations by anions and resulting segregation of metal atoms by locating C_2 radicals outer and connecting C_2 bi-radicals as graphite-like carbon shells. The relatively low segregation temperatures for FeC_2 and NiC_2 make it possible to draw metallic dots or wire circuits in MC_2 thin layers by scanning electron or laser beams. The small size matrix MC_2 crystals prevent the strong dipole-dipole interaction between the metallic dots, while one can also wash out the matrix salt crystals by acid solution leaving the carbon encapsulated nano-metals on the base plate.

III-A-1 Formation of Air-Stable Fe Nano-Particles in Polar Organic Solution: Fe Nano-Crystals with Graphitic Skin 3.5 nm Thick

KOSUGI, Kentaroh; BUSHIRI, Junaid M. ; NISHI, Nobuyuki

[*Appl. Phys. Lett.* in press]

In the process of investigating formation and characterization of FeC_2 nano-crystals, we found that $Fe^{2+}C_2^{2-}$ salt crystals are ferromagnetic and converted to neutral α-Fe nano-particles encapsulated in graphite-like carbon shells. The thickness of the carbon shells is almost constantly 3.5 nm without regard to size and shape, and corresponds to 10 layers of the graphite sheet, although the shells exhibit curvatures and straight lines bound to the metal core surfaces.

Fine particles of CaC_2 are suspended in acetonitrile solution of $FeCl_2$ and heated in a Pyrex tube situated in a pressure-resistant stainless steel vessel at 250 ºC for 48 hrs. The solution was stirred for the first 4 hrs. but the stirring was stopped the other 20 hrs. The solids obtained on the bottom of the tube contained organic compounds produced by the catalytic reacton of the intermediate product, FeC_2. The black magnetic particles are collected by magnets attached on the side wall of an Erlenmeyer flask and washed by methanol in a ultrasonic cleaning bath three times. Transmission electron microscope (TEM) images of the black deposit are shown in Figure 1. The powder was fixed in an epoxi-resin and sliced to a thickness of approximately 60 nm by a Leica Ultracut UCT microtome. X-ray diffraction pattern of the black deposit was displayed in Figure 2. From the width of α-carbon signals, the average size of the Fe cores is estimated to be 60 nm. At 2θ = 26.0°, a broad signal with asymmetric shape is seen. Bulk graphite shows a sharp peak at 2θ = 26.5°. It is reasonable that we see a peak slightly shifted to lower angle and a wide width correspondent with 3.5 nm thickness. TEM images in Figure 1 clearly show that the thickness of the carbon shells with various shapes and sizes are always 3.5 nm.

In principle, the thermal segregation of FeC_2 should produce Fe and carbon in 1:2 molar ratio. In the TEM observation, we saw amorphous carbon and the metallic Fe particles encapsulated in the carbon shells. The constant thickness of the graphite-like shells suggests the presence of attractive field on the metal core surface. This field must be produced by surface Fe atoms, and thus dependent only on the distance from each surface atom. The size of the particle is not concerned with the field generation. The surface Fe atoms are seen to be in good contact with the shell carbon atoms innermost. This contact may be due to ionic interaction remained only on the surface and the charge separation stabilized by occupation of an excess electron, originally in the carbon shell, in a Rydberg orbital of the cationic Fe atom. This hypothesis can be checked by examining other M(transition metal)C_2 compounds.

In the lower part, a TEM image of Fe-wire encapsulating carbon nano-tube (multi-wall) and an expanded image of its boader area are shown.

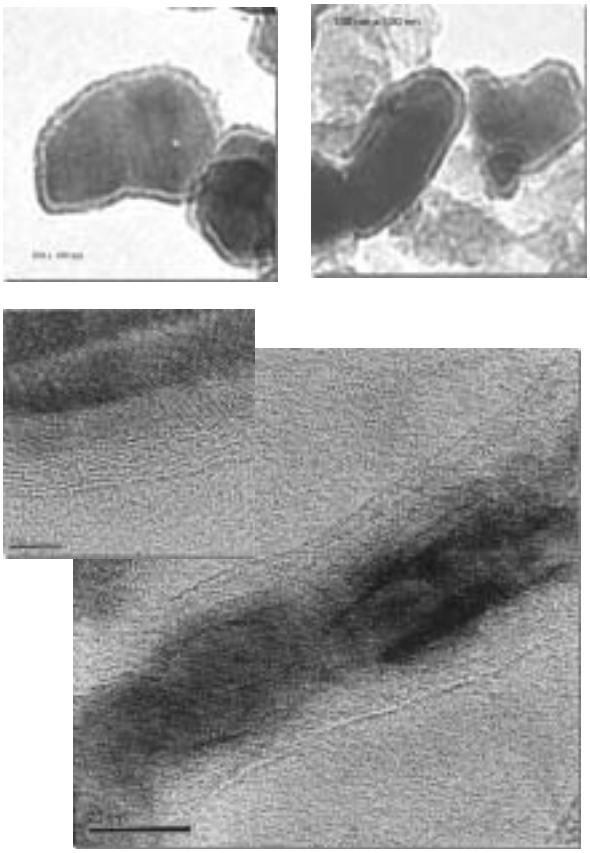

Figure 1. TEM images of α-Fe metallic nano-particles encapsulated in carbon-shell 3.5 nm thick (top) and Fe-wire encapsulating carbon nano-tube(lower).

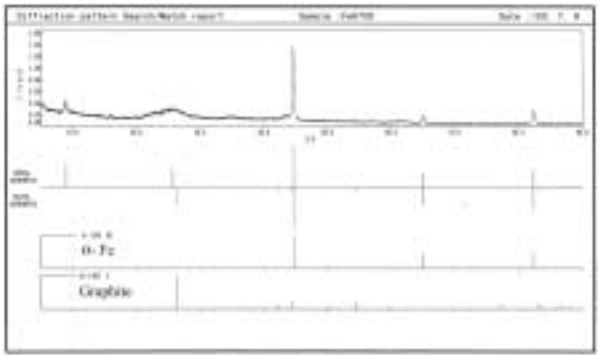

Figure 2. X-ray diffraction pattern of the Fe nano-metals encapsulated in graphite-like carbon shells 3.5 nm thick.

III-A-2 Infrared Absorption Studies of M(transition metal)$^{2+}C_2^{2-}$ Compounds: Bonding Nature and their Stabilities

BUSHIRI, Junaid M. ; KOSUGI, Kentaroh; HINO, Kazuyuki; NISHI, Nobuyuki

Transition metal C_2 compounds have been believed to be non-existent materials. In fact, as far as the metallic part is neutral, the presence of MC_2 is hardly possible due to the inequivalency of the bonding nature of M and C_2. Since C_2 is a di-valent anion, C_2^{2-}, on the other hand, a rock-salt type compound $M^{2+}C_2^{2-}$ can be stabilized by ionic interaction between cations and anions just like CaC_2 and MgC_2. For the synthesis, the simple ion exchange reaction is expected to produce MC_2 salts.

Since CaC_2 reacts with water producing acetylene (C_2H_2) and $Ca(OH)_2$, MCl_2 salt compounds are dissolved in dehydrated acetonitrile. In this solution, fine powders of CaC_2 are suspended and stirred gently. At the temperatures lower than 70 ºC, nothing happens in the solution. At above 75 ºC, the black precipitates are accumulated on the bottom of the reaction vessel.

Figure 1 displays the IR spectra of various ionic MC_2 compounds (M = Ca^{2+}, Mn^{2+}, Fe^{2+}, Co^{2+}, and Ni^{2+}. The doubly degenerated C=C stretching vibration bands of $Ca^{2+}C_2^{2-}$ are seen at 1418 and 1488 cm^{-1}. Among 6 coordinated C_2^{2-} ions, the four C_2^{2-} are located equivalently around the Ca^{2+} ion in a tetrahedral crystal of CaC_2. For one antisymmetric combination of the two C=C stretching oscillators, two sets of symmetric and anti-symmetric oscillators in other two axes split into low energy components and high energy components depending upon in-line (–C=C–Ca–C=C–) configuration or in-parallel configuration of the two C_2 oscillators. Thus the doublet appears around 1450 cm^{-1}. This splitting becomes much narrower in NiC_2.

The Fe–C stretching vibration in the gas phase FeC_2 molecule was found to be 550 cm^{-1} by ZEKE photo-electron spectroscopy (Drechsler *et al., J. Mol. Struct.* **348**, 337 (1995)). In the nano-crystals, a peak of a very broad band is seen at 456 cm^{-1}. The spectral feature of this band is similar to that of MnC_2, while those of CoC_2 and NiC_2 shift to much high frequencies around 600 cm^{-1}. Thus one can see that the M–C bonds in CoC_2 and NiC_2 is strong while those in MnC_2 and FeC_2 are rather weaker. This is in consistent with the reactivity of MC_2 compounds with water. CoC_2 and NiC_2 are stable against water, but MnC_2 and FeC_2 are reactive with water.

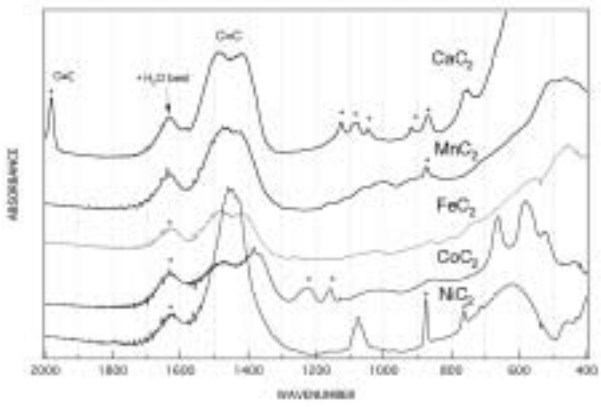

Figure 1. IR Spectra of MC_2 compounds.

III-A-3 Magnetic Behavior of MnC_2 and NiC_2

BUSHIRI, Junaid M.; KOSUGI, Kentaroh; NISHI, Nobuyuki

Most of manganese compounds, such as MnO, MnO_2, MnS, and $MnSO_4$, and pure Mn are antiferro-magnetic. Although pure Ni is ferromagnetic, most of nickel compounds are also antiferromagnetic. Since CoC_2 is ferromagnetic and the spin inversion blocking

temperature increases with increasing size of the nanocrystals, other transition metal acetylide compounds are expected to be ferromagnetic. Magnetic properties of the MnC_2 and NiC_2 nanoparticles synthesized at 78 ºC from their metal chloride compounds and CaC_2 were measured with a SQUID magnetometer (Quantum Design MPMS-7S). The synthesis at this temperature produces mostly several nm size crystals that normally limits the spin inversion blocking temperature lower than the room temperature. MnC_2 particles synthesized at 78 ºC are mostly superparamagnetic but only 10% of the products behaved as magnets at room temperature. MnC_2 particles synthesized at 200 ºC are mostly ferromagnetic exhibit the blocking temperature at 320 K.

Figure 1 displays the temperature change of the magnetic susceptibility of NiC_2 under the zero-field cooling (ZFC) condition and the field cooling (FC) at 50 Oe external field. Although the blocking temperature is seen at 10 K, the hysteresis curve at 1.85 K exhibits the cohesive force as large as 1,660 Oe. Annealing of this sample at 300 ºC for 2 hours changes the average size of 10–20 nm and the blocking temperature increases higher than room temperature.

NiC_2 particles are stable at the atmospheric condition, while MnC_2 is damaged by water in the atmosphere. On heating above 250 ºC, NiC_2 shows segregation into metallic nickel and carbon.

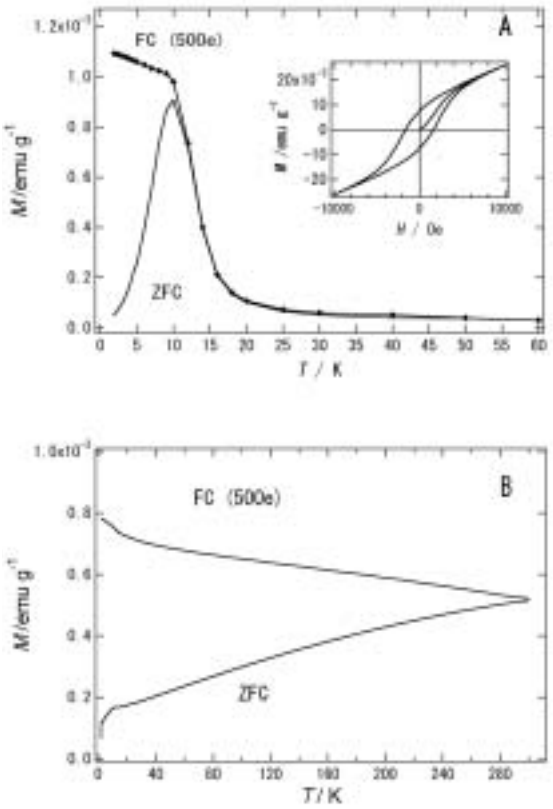

Figure 1. Temperature changes of magnetic susceptibility(*M*) of NiC_2 nanocrystals synthesized at 75 °C (**A**) and measured under the zero-field cooling condition (ZFC) and the field cooling (FC) condition. Inserted in **A** is a magnetic hysteresis curves at 1.8 K. Annealing at 300 °C for 2 hours produced 10 nm-size particles and the *M-T* curves change drastically as seen in B.

III-A-4 XAFS and XANES Studies of CoC_2

KOSUGI, Kentaroh; BUSHIRI, Junaid M.; HINO, Kazuyuki; YOKOYAMA, Toshihiko; NISHI, Nobuyuki

$Co^{2+}C_2^{2-}$ nano-clusters are ferromagnetic in contrast with antiferromagnetic electronic structure of $Co^{2+}O^{2-}$. CoC_2 nanoparticles are synthesized from acetonitrile solution of $CoCl_2$ with suspended CaC_2 fine powder. The products obtained from the solution at 340 K is called Sample LT (low temperature product). The CoC_2 nanoparticles are also synthesized from the thermal or photochemical reaction of $Co_4(CO)_{12}$ with solvent CH_2Cl_2. The particles are embedded in amorphous carbon. This sample is called Sample ME (matrix embedded).

XANES: The peak at 7724 eV seen for Sample LT coincides with that of hydrated Co^{2+} ion (as seen for $Co(NO_3)_2(6H_2O)$ suggesting that the Co is in a divalent cation state. The matrix embedded sample (Sample ME) also exhibits the peak at the same energy, while the width is expanded. This is in accord with the appearance of C_2^{2-} infrared absorption bands.

XAFS: The Fourier transform spectrum of XAFS signals of Sample ME exhibited a little difference from that of Sample LT, particularly in the region from 3.2 ~ 4.5 Å. As clearly seen from the appearance of water bands in IR spectra, the two samples contain coordinated water molecules. Therefore the peaks at 1.6 Å (2.08 Å after phase factor correction) are contributed from both Co–C and Co–O pairs. It is very difficult to analyze this peak. The peak at 2.80 Å (3.18 Å after phase factor correction) and other main peaks at much longer distances are attributed to Co–Co pairs. There is little contribution from the direct Co–Co bond at 2.05 Å (2.5 Å after phase factor correction). We have found, however, that the presence of oxygen gas in the solvent results in the appearance of the 2.05 Å peak. The de-oxygenation treatment in a globe box by Ar bubbling longer than 6 hours is necessary . On the basis of the assumption that the Co–C pairs hardly contribute to the peaks at distances longer than 3.5 Å, the Fourier transform spectra of Sample ME are analyzed with the models presented in Figure 1. Most of peaks are reproduced nicely, while the discrepancies in intensities between the calculated and observed spectra become serious at longer distances. This is thought due to the structural disorder in nano-particles. The observed spectra shows drastic intensity decrease at longer distances.

The structure of Sample ME is close to that of MgC_2. The structures derived from the analyses for Sample LT and Sample ME are shown on the top and the bottom of Figure 1.

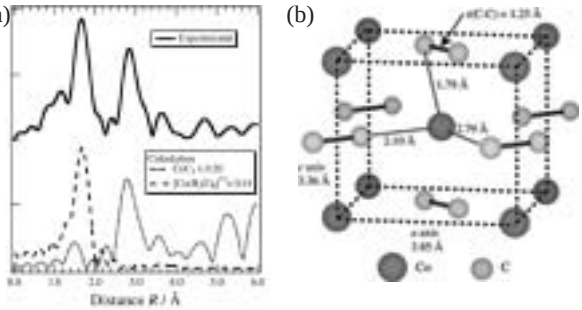

Figure 1. (a) Fourier transform of EXAFS signal. (b) Structure model of CoC_2.

III-A-5 Matrix Embedded Cobalt-Carbon Nano-Cluster Magnets: Behavior as Room Temperature Single Domain Magnets

NISHI, Nobuyuki ;KOSUGI, Kentaroh; HINO, Kazuyuki; YOKOYAMA, Toshihiko

[*Eur. J. Phys. D* **24**, 97 (2003)]

A new type of Co–C nanoparticles is synthesized from CH_2Cl_2 solution of $Co_4(CO)_{12}$ by heating up to 210 ºC in a closed vessel. Transmission electron microscope (TEM) as shown in Figure 1 and electron energy loss spectroscopy (EELS) observation show that the particles are embedded in amorphous carbon and their average size is 12 nm. The radial structure function obtained from the extended X-ray absorption fine structure (EXAFS) of the Co *K*-edge absorption of the Co–C nanoparticles provides a Co–C average distance of 2.08 Å, and the Co–Co distances of 3.18 Å , and 3.9 (±0.2) Å . The particles exhibit the magnetic hysteresis curve with a coercive force of 200 Oe at 20 K and 260 Oe at 300 K. The temperature dependence of the magnetic susceptibility measured under zero-field cooling and 10 Oe field cooling conditions exhibits the behavior characteristic of a set of single magnetic domain nanomagnets in an amorphous carbon matrix.

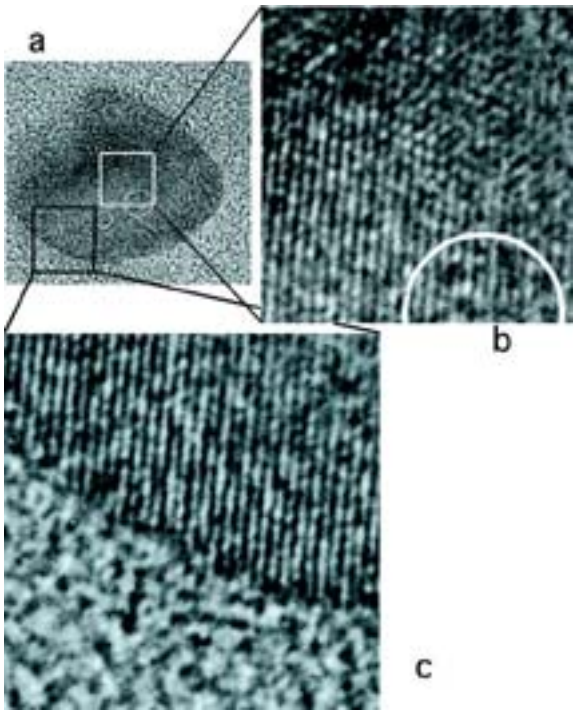

Figure 1. TEM image of a CoC_2 nano-crystal (a). Expanded images (b and c) show tetragonal lattice structure of the crystal.

III-B States of Neutral and Ionic Molecular Associates in Solutions

States of molecular associates particularly in aqueous solutions are of great importance in understanding the role of molecules in living organisms. We found that any ideally mixed state cannot be seen in protic-protic mixtures such as water-alcohol, water-acetic acid, and alcohol-acetic acid systems on the molecular level at solute molar fractions (χ_A) higher than 0.001. In such a system, solute-solute asociation is highly favored resulting in microscopic phase separation. In this year, we studied the aqueous mixture of *N*,*N*-dimethylacetamide (DMA), and have shown that hydrogen bonding between the C=O group and the water molecules and structural changes of predominant solvent clusters were taking place at these specific mole fractions of DMA in aqueous solution.

III-B-1 Structure of Aqueous Mixture of N,N-Dimethylacetamide Studied by Infrared Spectroscopy, X-Ray Diffraction, and Mass Spectrometry

TAKAMUKU, Toshiyuki; MATSUO, Daisuke; TABATA, Masaaki; YAMAGUCHI, Toshio; NISHI, Nobuyuki

[*J. Phys. Chem. B* **107**, 6070 (2003)]

Infrared (IR) spectroscopy and X-ray diffraction measurements have been performed at 298 K on mixtures of *N*,*N*-dimethylacetamide (DMA) and water over the entire range of DMA mole fractions (χ_{DMA}). Mass spectra have also been measured on the clusters that have been isolated by the adiabatic expansion of liquid droplets of the mixtures. The IR overtone band of the C=O stretching vibration for the DMA–D_2O mixtures and the O–D stretching band of HDO for the DMA–H_2O mixtures containing 5% D_2O both shifted to lower frequencies as the water content increased,

accompanied by two inflection points, at χ_{DMA} = 0.1 and 0.6. These results suggested that hydrogen bonding between the C=O group and the water molecules and structural changes of predominant solvent clusters were taking place at these specific mole fractions. The X-ray radial distribution functions have indicated that the structure of the predominant solvent clusters in the mixtures could be classified into four regimes: (1) $0 < \chi_{DMA} \leq 0.1$, where the water clusters predominate; (2) $0.1 < \chi_{DMA} \leq 0.3$, where more water clusters than DMA clusters are formed; (3) $0.3 < \chi_{DMA} \leq 0.6$, where the DMA structure becomes predominant but the water clusters still remain; and (4) $0.6 \leq \chi_{DMA} \leq 1$,where the DMA clusters are dominant in the mixtures. On the basis of the present results on the microscopic structure of the mixtures, the anomalies of thermodynamic parameters such as the enthalpy of mixing are discussed.

III-C Ultrafast Dynamics and Scanning Tunneling Microscopy

For the study of molecules on metallic or crystalline surface, very low temperature Scanning Tunneling Microscope (LT STM) system are now in use for collaboration with users in universities. Ultrafast laser systems with pico and femtosecond time resolutions are also available.

III-C-1 Low Temperature Scanning Tunneling Microscopy for Sub-Nanoscale Systems

WATANABE, Kazuo[3]; OHSHIMO, Keijiro[1]; INOKUCHI, Yoshiya; NAKABAYASHI, Takakazu[2]; NAGATA, Takashi[3]; NISHI, Nobuyuki
([1]RIKEN; [2]Hokkaido Univ.; [3]Univ. Tokyo)

Scanning tunneling microscopy/spectroscopy (STM/STS) is one of the most powerful tools for the real-space observation and the identification of sub-nanoscale materials on the surface. By combining with the ultrashort light pulses, it provides ultimate resolutions of both time and space. Figure 1 shows our STM apparatus which consists of two liquid helium cooled STM heads operating in the ultra-high-vacuum ($\sim 2 \times 10^{-11}$ Torr). The two heads are connected to a sample preparation chamber equipped with an argon ion sputter gun, a gas dosing system, a pulse injection system for the deposition of nanoparticles and bio-molecules, a quadrupole mass spectrometer, and a LEED/AES optics. The STM head (A) is cooled down to 10 K. It has a pair of UV compatible viewing ports from which the sample can be irradiated at ~ 20 K *in situ*. The output pulses (λ = 189 ~ 11200 nm, 4 ps) are introduced through the window from two independently tunable picosecond OPA systems with an optical delay stage. The STM head (B) is cooled below 4 K and used for STS studies. Figure 2 shows an STM image of an Au_{12} cluster (provided by Tsukuda's group) on a graphite surface at 10 K. The size of the cluster is measured ~ 0.8 Å, which is close to the TEM (Transmission Electron Microscope) results. STS investigation of the electronic structures of the nanoclusters is underway. We have also observed the adsorption structure of nitrous oxide molecules on a Pd(110) surface at 10 K (a joint project with Prof. Matsushima's Lab of Hokkaido University).

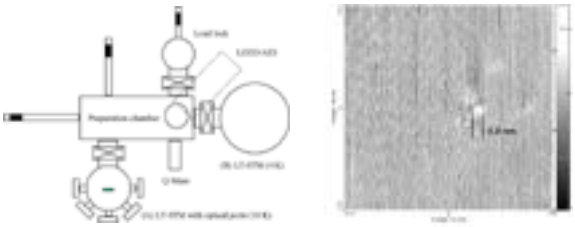

Figure 1. Schematic drawing of the experimental setup.

III-C-2 Ultrafast Time-Resolved Study of *N*-Salicilideneaniline in the Isolated State

OKABE, Chie[1]; NAKABAYASHI, Takakazu[2]; INOKUCHI, Yoshiya; SEKIYA, Hiroshi[1]; NISHI, Nobuyuki
([1]Kyushu Univ.; [2]Hokkaidou Univ.)

N-salicylideneaniline (SA) is a well-known photochromic aromatic anil. The photoexcitation of the $^1(\pi,\pi^*)$ state of the enol form produces the keto form *via* the excited state intramolecular proton transfer (ESIPT). To investigate ultrafast processes in the photoexcited SA, we have applied the femtosecond time-resolved resonance-enhanced multiphoton ionization technique under the isolated conditions. Figure 1 shows the decay profiles of the photoexcited SA measured by the excitation of the enol form with pump wavelength at 320 nm and probe wavelengths at 395 and 790 nm. The time profile in Figure 1 (a) is fitted with three decay components < 230 fs, 1.5 ps, and > 100 ps, while the time profile in Figure 1 (b) is reproduced by the convolution of < 230 fs and 3.5 ps decay components. The < 230 fs decay component is attributed to ultrafast ESIPT from the $^1(\pi,\pi^*)$ state of enol form to the cis-keto form. The 3.5 ps and 1.5 ps decay components are assigned to the ion signal from the $^1(n\pi^*)$ state of the enol form and that the $^1(\pi\pi^*)$ state of the *cis*-keto form produced *via* ESIPT, respectively. We have first to observe the $^1(n\pi^*)$ state of the enol form. The excitation wavelength dependence of ESIPT has been examined in the region from 360 to 373 nm. The rise time of the keto form is less than several hundreds fs even for the

excitation near the red-edge of the absorption of the enol form. In addition, the rise time of the keto form shows no significant OH/OD isotope effect. These results indicate that the ESIPT reaction occurs within several hundreds fs, and the barrier height to ESIPT from the $^1(\pi,\pi^*)$ state is low.

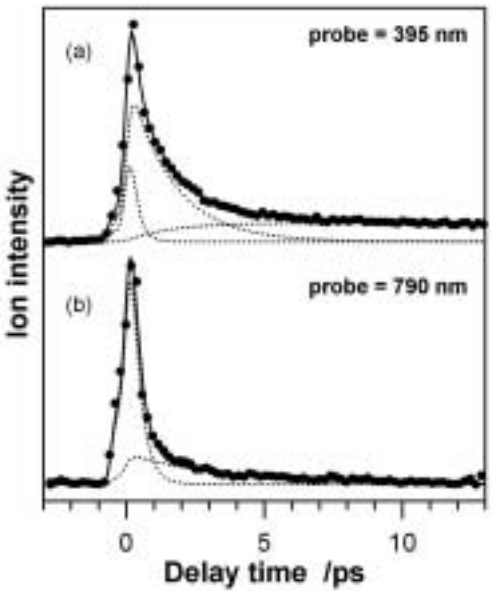

Figure 1. Time evolutions of ion signal of SA detected by femtosecond REMPI with pump wavelength at 320 nm and two different probe wavelengths at 395 nm.

III-C-3 Picosecond Time-Resolved Stokes and Anti-Stokes Raman Studies on the Photochromic Reactions of Diarylethene Derivatives

OKABE, Chie[1]; NAKABAYASHI, Takakazu[2]; FUKAMINATO, Tuyoshi[1]; KAWAI, Tsuyoshi[1]; IRIE, Masahiro[1]; SEKIYA, Hiroshi[1]; NISHI, Nobuyuki
([1]Kyushu Univ.; [2]Hokkaidou Univ.)

[*J. Phys. Chem. A* **107**, 5384 (2003)]

The cyclization and cycloreversion reactions of diarylethene derivatives have been studied with picosecond time-resolved Stokes and anti-Stokes Raman spectroscopies. The cyclization reaction of 1,2-bis(2,5-dimethyl-3-thienyl)perfluorocyclopentene (DMTF) is found to occur within 4 ps to produce the vibrationally excited closed forms in the ground electronic (S_0) state. The time constant of the vibrational relaxation toward a thermal equilibrium with solvent molecules is estimated to be about 10 ps. The cycloreversion reaction of 1,2-bis(3,4-dimethyl-5-phenyl-2-thienyl)perfluorocyclopentene (DMPTF) also generates the vibrationally excited open forms in the S_0 state within 4 ps, which decay on a picosecond time scale. The picosecond time-resolved anti-Stokes Raman spectra of DMPTF show two vibrational bands assignable to the C=C stretching modes of the cyclopentene and thiophene moieties of the generated open forms. The Raman intensity arising from the cyclopentene moiety relative to that from the thiophene moiety becomes smaller with the delay time, indicating that part of the excess energy generated *via* the cycloreversion reaction is localized on the C=C stretching mode of the cyclopentene moiety. This result suggests that the C=C stretching mode of the cyclopentene moiety is one of the promoting or the accepting modes in the cycloreversion reaction.

III-D Spectroscopic and Dynamical Studies of Molecular Cluster Ions

Electron defficiency of molecular cluster cations can attract electron rich groups or atoms exhibiting charge transfer or charge resonance interaction in the clusters. This causes dynamical structural change such as proton transfer or ion-core switching in hot cluster ions or clusters in solution.

III-D-1 Positive Charge Distribution in $(Benzene)_1(toluene)_2^+$ and $(Benzene)_2(toluene)_1^+$ Studied by Photodissociation Spectroscopy

INOKUCHI, Yoshiya; OHASHI, Kazuhiko[1]; SEKIYA, Hiroshi[1]; NISHI, Nobuyuki
([1]Kyushu Univ.)

[*J. Chem. Phys.* **117**, 10648 (2002)]

The positive charge distribution in benzene–toluene hetero-trimer ions is investigated by photodissociation spectroscopy in the near-infrared (6000–14000 cm^{-1}) and infrared (2800–3150 cm^{-1}) regions. The electronic spectra of $(benzene)_1(toluene)_2^+$ and $(benzene)_2(toluene)_1^+$ in the near-infrared region display the strong bands at 9430 and 8330 cm^{-1}, respectively. These bands are ascribed to the charge resonance band; the positive charge is not localized on a single molecule. The vibrational spectrum of $(benzene)_1(toluene\text{-}d_8)_2^+$ shows three distinct bands at 3054, 3084, and 3108 cm^{-1}; these bands are assigned to the CH stretching vibrations of the benzene moiety. The similarity of the spectral features to those of the neutral benzene monomer suggests that the benzene molecule in the $(benzene)_1(toluene)_2^+$ ion has a neutral character. The positive charge is localized on the toluene dimer unit with a structure written as

$(toluene)_2^+\cdots(benzene)_1$. The vibrational spectrum of $(benzene)_2(toluene)_1^+$ bears a resemblance to that of $(benzene)_2^+$. The vibrational spectrum of $(benzene\text{-}d_6)_2(toluene)_1^+$ shows dissimilar features to the spectrum of the neutral toluene monomer, suggesting that a certain amount of the positive charge is carried by the toluene moiety. These results are explained by the charge resonance interaction between $(benzene)_2$ and $(toluene)_1$. A simple perturbation theory is applied for determining the positive charge distribution in $(benzene)_2(toluene)_1^+$. The probability of finding the charge on the $(benzene)_2$ and $(toluene)_1$ moieties is analyzed to be 58 and 42%, respectively.

III-D-2 Infrared Photodissociation Spectroscopy of [Aniline–$(Water)_n$]$^+$ (n = 1–8)

INOKUCHI, Yoshiya; HONKAWA, Yoshiki[1]; OHASHI, Kazuhiko[1]; SEKIYA, Hiroshi[1]; NISHI, Nobuyuki
([1]Kyushu Univ.)

[*J. Phys. Chem. A* **107**, 4230 (2003)]

Infrared photodissociation spectra of [aniline–$(H_2O)_n$]$^+$ (n = 1–8) are measured in the 2700–3800 cm^{-1} region. The spectra are interpreted with the aid of density functional theory calculations. A substantially red-shifted and broadened transition is distinctly observed at 3105 cm^{-1} for the n = 1 ion, and assigned to the stretching vibration of the hydrogen-bonded NH oscillator of the aniline$^+$ moiety. The spectrum of the n = 2 ion demonstrates a large perturbation to both of the NH oscillators, indicating that each NH bond is bound to a water molecule in the most stable structure. For the n = 3 ion, three broad bands exist at 3070, 3230, and 3420 cm^{-1}, and there are two maxima and a weak hump at 3637, 3723, and 3696 cm^{-1}. The calculated spectrum of the 2-1 branch structure resembles the observed one very well. For the n = 4 ion, there exist three strong bands at 2960, 3100, and 3430 cm^{-1}, and a very weak one at 3550 cm^{-1}. The observed spectrum in the 3600–3800 cm^{-1} region is decomposed into four bands at 3640, 3698, 3710, and 3734 cm^{-1}. These bands are originated from the 2-2 branch isomer except for the 3550 and 3710 cm^{-1}bands. These two bands are due to the other isomer that has the five-membered ring. A characteristic transition in the observed spectrum of the n = 5 ion is the 3684 cm^{-1}band, which hardly emerges in the spectra of n = 1–4. This band is assigned to the free OH stretching vibration of the three-coordinated (double-acceptor–single-donor) H_2O, indicating the ring structure. The n = 5 ion has the five-membered ring structure with the fifth water molecule bound to the terminal (double-acceptor) H_2O. The observed spectra of the n = 6–8 ions show features quite different from those of n = 1–5; a very strong and broad band emerges around 3400 cm^{-1}. It is suggested that the n = 6–8 ions have the proton transfer form with some ring structure.

III-D-3 Infrared Spectra and Structures of $(CH_3NH_2)_nH^+$ (n = 1–4). Binding Features of an Excess Proton

MICHI, Takayuki[1]; OHASHI, Kazuhiko[1]; INOKUCHI, Yoshiya; NISHI, Nobuyuki; SEKIYA, Hiroshi[1]
([1]Kyushu Univ.)

[*Chem. Phys. Lett.* **371**, 111 (2003)]

Infrared photodissociation spectra of $CH_3NH_3^+$–**Ar** and $(CH_3NH_2)_nH^+$ with n = 2–4 are measured in the 2600–3500 cm^{-1} region and analyzed with the aid of ab initio calculations. The intensities of the CH-stretching transitions relative to the NH-stretching transitions increase with increasing n, suggesting the change of the binding features of an excess proton in the clusters. Two CH_3NH_2 molecules in $(CH_3NH_2)_2H^+$ equally share the proton. On the other hand, the proton is localized on the central molecule in $(CH_3NH_2)_4H^+$, forming the CH_3-NH_3^+ core solvated by three CH_3NH_2 molecules.

III-D-4 Fermi Resonance Interaction in Hetero-Dimer and Trimer Ions Containing Aniline$^+$

INOKUCHI, Yoshiya; OHSHIMO, Keijiro; OHASHI, Kazuhiko[1]; HONKAWA, Yoshiki[1]; SEKIYA, Hiroshi[1]; NISHI, Nobuyuki
([1]Kyushu Univ.)

[*Chem. Phys. Lett.* **373**, 568 (2003)]

Vibrational spectra of hetero-dimer and trimer ions containing aniline$^+$ are measured by infrared photodissociation spectroscopy. For the dimer ions, the NH_2 bending overtone band gains its intensity through Fermi resonance interaction with the hydrogen-bonded NH stretching fundamental. Unperturbed frequencies of the NH_2 bending overtone are calculated to be in the range of 3255–3276 cm^{-1}, suggesting that the frequency is almost intact upon cluster formation. For the trimer ions, Fermi resonance interaction occurs mainly between the NH_2 bending overtone and the stretching fundamental of the NH oscillator involved in the stronger hydrogen bond.

III-D-5 Infrared Spectra and Structures of Aniline$^+$–Furan and Aniline$^+$–Phenol: Preference between *p*-Type and *s*-Type Hydrogen-Bonded Structures

HONKAWA, Yoshiki[1]; INOKUCHI, Yoshiya; OHASHI, Kazuhiko[1]; NISHI, Nobuyuki; SEKIYA, Hiroshi[1]
([1]Kyushu Univ.)

[*Chem. Phys. Lett.* **376**, 244 (2003)]

Infrared photodissociation spectra of aniline$^+$–M (M = thiophene, furan and phenol) are measured in the 2700–3700 cm^{-1} region and analyzed by density functional theory calculations. Only a structure with a π-type hydrogen bond is found for aniline$^+$–thiophene. Two structural isomers are identified for aniline$^+$–furan and aniline$^+$–phenol, which have either a π-type or a σ-type hydrogen bond, where an amino proton of aniline$^+$ interacts with the π-electrons or the oxygen atom of the

neutral molecules, respectively. The isomer with a σ-type hydrogen bond is more stable for aniline$^+$–phenol, while less stable for aniline$^+$–furan.

III-D-6 Infrared Photodissociation Spectroscopy of Protonated Formic Acid and Acetic Acid Clusters

INOKUCHI, Yoshiya; NISHI, Nobuyuki

[*J. Phys. Chem. A* in press]

Infrared photodissociation spectra of protonated formic acid clusters, $H^+\cdot(HCOOH)_{2-5}$, are measured in the 3000–3700 cm^{-1} region. Density functional theory calculation is applied to $H^+\cdot(HCOOH)_{2-5}$. Geometry optimization of $H^+\cdot(HCOOH)_{2-5}$ indicates that stable forms of these clusters are open chain structures with free OH groups at both ends. In the infrared photodissociation spectra of the n = 2 and 3 species, there are two sharp bands in the range of 3400–3700 cm^{-1}. The lower- and higher-frequency bands of them are attributed to the free OH stretching vibrations of the peripheral COOH groups in the *E* and *Z* conformations, respectively. The intensity of the higher-frequency band relative to that of the lower-frequency one decreases from n = 2 to 3. The n = 4 and 5 ions show only one sharp band in the same region. This band is assigned to the free OH stretching vibrations of the end COOH groups in the *E* conformation; the n = 4 and 5 ions have the peripheral COOH groups only in the *E* conformation. We observe infrared photodissociation spectra of $H^+\cdot(HCOOH)_{6,7}$ in the 3500–3600 cm^{-1} region. The absence of any free OH band for n = 7 shows that both ends of chain structures of n = 7 are terminated by cyclic dimers. Infrared photodissociation spectra of $H^+\cdot(CH_3COOH)_{2-5}$ are also examined in the 3000–3700 cm^{-1} region. Resemblance of the spectra of $H^+\cdot(CH_3COOH)_n$ to those of $H^+\cdot(HCOOH)_n$ suggests that the acetic acid clusters have structures similar to those of the formic acid clusters; the intermolecular network is formed only by the COOH groups.

III-E Spectroscopy and Dynamics of Vibrationally Excited Molecules and Clusters

This research group is studying structure and dynamics of molecules and clusters by two-color double resonance spectroscopy. New spectroscopic methods will also be developed to observe the higher vibrational state under collision-free condition.

A molecular cluster is a microscopic system of solution and/or crystal, and is thought to provide detailed information on relaxation and reaction dynamics in condensed phase. However the previous studies are concentrated to stable clusters which has no reaction pathway after photo-excitation. Consequently, spectroscopic information which concerns the reaction mechanism has not been obtained sufficiently. In this research project started from 2000, we will apply various laser spectroscopies to the reactive clusters to reveal detailed mechanism of intracluster reaction.

For the study of the ground state, the structure of the cluster can be determined by the combination of the IR dip spectroscopy and *ab initio* MO calculations.[1)] The IR dip spectroscopy is a kind of IR-UV double resonance spectroscopy which provides the spectrum which corresponds to the infrared absorption spectrum of the cluster (see Figure 1). A tunable IR laser is introduced to the clusters and is scanned its frequency over the fundamental vibrational region (typically 2400 ~ 4000 cm^{-1}). Then a tunable UV laser, of which the frequency is fixed to the S_1 origin of a specific cluster, is introduced and resonant enhanced multiphoton ionization signal *via* S_1 is monitored. When the IR laser is resonant to a vibrational level of the cluster, the ion signal decreases much because of loss of the population in the vibrational ground state. Thus, the IR absorption spectrum of the cluster can be measured by this depletion spectroscopy. The same spectrum can be obtained when the fluorescence intensity from S_1 is monitored instead of the ion current.

The IR spectrum in the excited state S_1 can also be measured by the depletion spectroscopy, when the UV laser is introduced before the IR laser (the UV-IR fluorescence dip spectroscopy; see Figure 2). The molecule is excited to S_1 by the UV laser, and the fluorescence intensity is monitored as well as the IR dip spectroscopy for S_0. Then the S_1 molecules are further excited to the vibrationally excited level in S_1 by the IR laser. In general, the fluorescence quantum yield decreases in the higher vibronic level. Thus, the total fluorescence intensity decreases when the IR laser frequency is resonant to the vibrational level in S_1.

Similarly, the IR spectrum of the ionic cluster can be measured by the depletion spectroscopy (mass-selected ion dip spectroscopy; see Figure 3). The ionic cluster can be prepared by the multiphoton ionization *via* S_1, and the ion current due to the cation cluster of the specific size can be measured through a mass-filter. When the ionic cluster is vibrationally excited by the IR laser, the cluster is dissociated by the vibrational predissociation. Therefore, the IR transition can be measured by the decrease of the parent cluster. The same spectrum can be obtained by monitoring the enhancement of fragments (mass-selected multiphoton dissociation spectroscopy). In addition to these "dip" spectroscopies, the nonresonant ionization detected IR spectroscopy[2)] and the PFI-ZEKE photoelectron spectroscopy[3)] are also important tool to obtain the spectral information in the cation and the overtone states. Based on these spectroscopic techniques, we have measured the IR spectra of solvated clusters,[4)] such as phenol/ammonia,[5)] naphthol/alcohol,[6)] carbazole/water[7)] and 7-azaindole dimers,[8)] and have discussed the relation among geometrical structure, electronic state and intracluster reactions.

From 2001, we have been developing the new ultrafast time-resolved IR spectroscopy for the reactive clusters. The pico second time-resolved vibrational spectroscopy is one of the ideal way to reveal the reaction mechanism directly. Here, we will demonstrate its usefulness by applying the hydrogen transfer reaction in photoexcited PhOH-

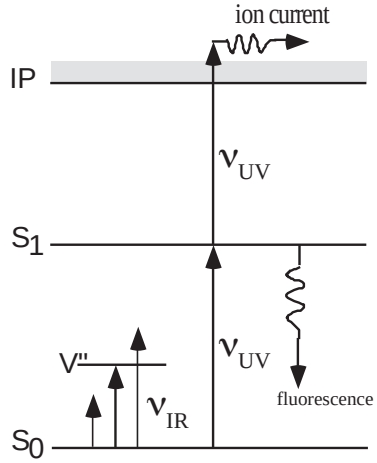

Figure 1. Principle of the IR Dip Spectroscopy. The IR transition in the ground state cluster can be measured.

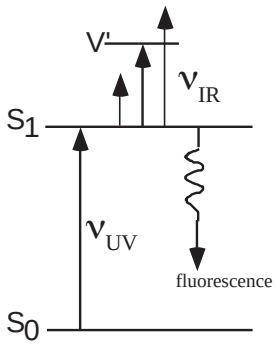

Figure 2. Principle of the UV-IR Fluorescence Dip Spectroscopy. The IR transition of the cluster in the S_1 state can be obtained.

$(NH_3)_n$ cluster.[9] Figure 4 shows the principle of the picosecond time-resolved UV-IR-UV ion dip spectroscopy. The reactive cluster (PhOH-$(NH_3)_n$ in present case) is excited to S_1 by a picosecond UV laser ν_{UV} and the photochemical reaction (hydrogen transfer) is triggered. The final reaction product, *i. e.* $(NH_3)_{n-1}NH_4$, is ionized by a nanosecond UV laser ν_{ION} which is irradiated after 100 ns from ν_{UV} and the population of the reaction product is monitored as a mass peak of $(NH_3)_{n-1}NH_4^+$. A picosecond tunable IR laser ν_{IR} is irradiated after *t* ps from ν_{UV} and is scanned over vibrational region. If ν_{IR} is resonant to vibrational levels of the transient species, the population of the final reaction product decreases due to the vibrational predissociation of the transient species. Therefore, the vibrational transitions of the transient species at t ps can be observed as decrease of ion current of the final reaction product.

Time resolved UV-IR-UV ion dip spectra of phenol-$(NH_3)_3$ are shown in Figure 5. The numbers in the left hand sides of each spectrum indicate the delay time from ν_{UV} to ν_{IR}. Here the spectrum at –20 ns corresponds to the IR spectrum of PhOH-$(NH_3)_3$ in S_0, in which the sharp bands around 3400 cm^{-1}, the broad bands at ~ 3200 cm^{-1} and the very broad background are assigned to the degenerated antisymmetric stretch vibration ν_3 in NH_3, the totally symmetric stretch vibration ν_1 in NH_3 and the OH stretch vibration ν_{OH} in phenol, respectively. The spectrum at + 180 ns shows the vibrational transitions of the final reaction product *via* S_1, *i.e.* $(NH_3)_2NH_4$, and 1) two intense bands at 3180 cm^{-1} and 3250 cm^{-1} and 2) a broad band at 2700 ~ 3100 cm^{-1} which have been assigned to

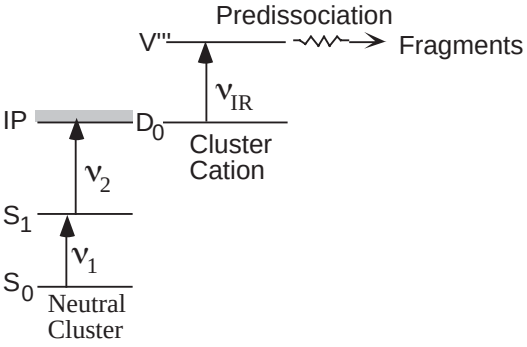

Figure 3. Principle of the mass-selected IR Ion Dip Spectroscopy. The IR transition of the cluster cation can be measured by the depletion of the parent cluster cation. The same spectrum can be measure by monitoring the enhancement of the fragments produced by the IR predissociation.

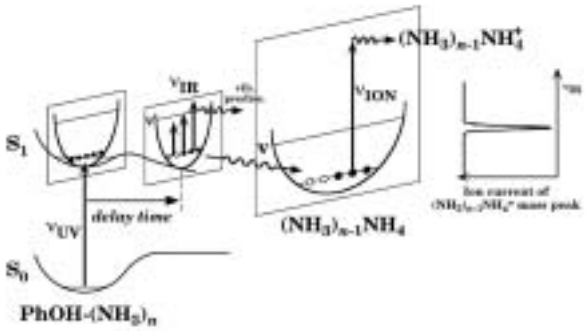

Figure 4. Principle of picosecond time-roselved UV-IR-UV ion dip spectroscopy. Potential curves of S_0 and S_1 are schematically drawn along O–H stretch coordinate. Potential curves in different sections on the S_1 O–H stretch coordinate are drawn along arbitrary N–H stretch coordinates.

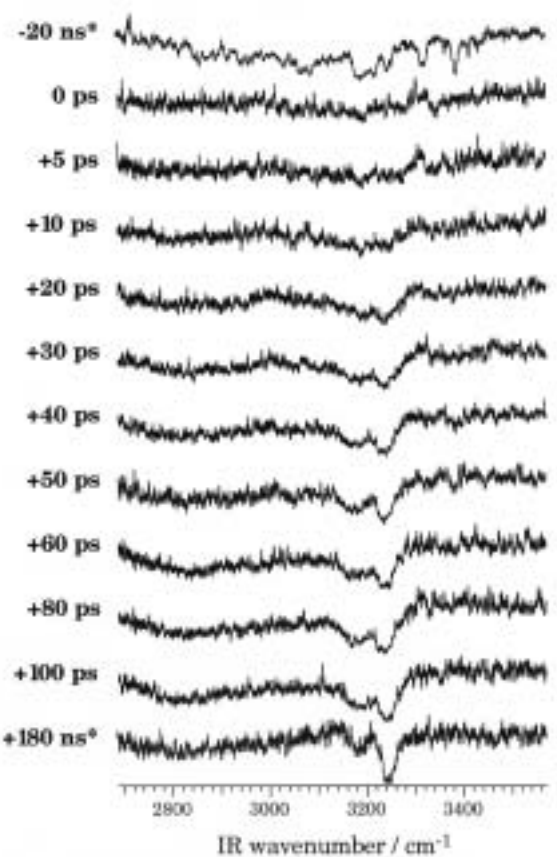

Figure 5. Picosecond time-resolved UV-IR-UV ion dip spectra of the transient species from the electronically excited PhOH-$(NH_3)_3$ which was observed by fixing ν_{UV} to the low vibronic band in the S_1 state of PhOH-$(NH_3)_3$ (281.49 nm) and monitoring $(NH_3)_2NH_4^+$ due to ν_{ION}(355 nm). Times indicated at the left side of each spectrum mean the delay times between ν_{UV} and ν_{IR}. The spectra whose delay times are –20 ns and +180 ns (indicated by *) are obtained by nanosecond laser system, which have been reported in the previous paper.[5]

vibrational transitions concerned with NH_4.

One can see that the vibrational bands rise with increasing delay time. The spectral feature at +100 ps is already similar to that of the final reaction product (+180 ns). Here, the intense band at 3250 cm^{-1} rises slower than the band at 3180 cm^{-1}. The relative intensities of the two bands become comparable at 40 ps, thereafter, the higher band at 3250 cm^{-1} clearly grows further. Thus, the rising time constant of the band at 3250 cm^{-1} is apparently different from that of the 3180 cm^{-1}-band. This remarkable difference between the two intense bands suggests that each vibrational transition is derived from different species. The existence of two transient species are naturally interpreted by considering the isomers of $(NH_3)_2NH_4$; the most stable NH_3–NH_4–NH_3 and the meta-stable NH_4–NH_3–NH_3. The co-existence of isomers is strongly supported by *ab initio* calculations.

As described above, we have successfully measured the picosecond time resolved IR spectra of the transient species for the ESHT of PhOH-$(NH_3)_3$ for the first time. It proves that the picosecond UV-IR-UV ion dip spectroscopy is a powerful tool to explore the dynamics of the intracluster reaction.

References

1) R. Yoshino *et al.*, *J. Phys. Chem. A* **102**, 6227 (1998).
2) T. Omi *et al.*, *Chem. Phys. Lett.* **252**, 287 (1996); S. Ishiuchi *et al.*, *Chem. Phys. Lett.* **283**, 243 (1998).
3) K. Takazawa *et al.*, *Chem. Phys. Lett.* **189**, 592 (1992); K. Müller-Dethlefs *et al.*, *Z. Naturforsch. Teil A* **39**, 1089 (1984); K. Müller-Dethlefs and M. C. R. Cockett, "*Zero Kinetic Energy (ZEKE) Photoelectron Spectroscopy*," Chapter 7, "Nonlinear Spectroscopy for Molecular Structure Determination," R. W. Field *et al.*, Eds., (Blackwell Science, Oxford, 1998), and references therein.; E. W. Schlag, "*ZEKE Spectroscopy*" (Cambridge University Press, Cambridge, 1998) , and references therein.
4) K. Suzuki, Y. Emura, S. Ishiuchi and M. Fujii, *J. Electron Spectrosc.* **108**, 13 (2000), K. Suzuki, S. Ishiuchi and M. Fujii, *Faraday Discuss.* **115**, 229 (2000), K. Sakota, N. Yamamoto, K. Ohashi, H. Sekiya, M. Saeki, S. Ishiuchi, M. Sakai and M. Fujii, *Chem. Phys. Lett.* **341**, 70 (2001).
5) S. Ishiuchi, M. Saeki, M. Sakai and M. Fujii, *Chem. Phys. Lett.* **322**, 27 (2000).
6) M. Saeki, S. Ishiuchi, M. Sakai and M. Fujii, *J. Phys. Chem. A* **105**, 10045 (2001).
7) M. Sakai, K. Daigoku, S. Ishiuchi, M. Saeki, K. Hashimoto and M. Fujii, *J. Phys. Chem. A* **105**, 8651 (2001).
8) H. Yokoyama, H. Watanabe, T. Omi, S. Ishiuchi and M. Fujii, *J. Phys. Chem. A* **105**, 9366 (2001).
9) S. Ishiuchi, M. Sakai, K. Daigoku, T. Ueda, T. Yamanaka, K. Hashimoto and M. Fujii, *Chem. Phys. Lett.* **347**, 87 (2001).

III-E-1 Hydrogen Transfer in Photo-Excited Phenol/Ammonia Clusters by UV-IR-UV Ion Dip Spectroscopy and Ab Initio MO Calculations I: Electronic Transitions

ISHIUCHI, Shun-ichi[1]; DAIGOKU, Kota[2]; SAEKI, Morihisa[3]; SAKAI, Makoto[4]; HASHIMOTO, Kenro[1]; FUJII, Masaaki[4]

([1]Tokyo Inst. Tech./JST-PRESTO; [2]Tokyo Metropolitan Univ./ACT-JST; [3]JAERI; [4]IMS and Tokyo Inst. Tech.)

[*J. Chem. Phys.* **117**, 7077–7082 (2002)]

The electronic spectra of reaction products *via* photo-excited phenol/ammonia clusters (1:2~5) have been measured by UV-near-IR-UV ion dip spectroscopy. Compared with the electronic spectra of hydrogenated ammonia cluster radicals the reaction products have been proven to be $(NH_3)_{n-1}NH_4$ (n = 2 ~ 5), which are generated by excited-state hydrogen transfer in PhOH-$(NH_3)_n$. By comparing the experimental results with *ab initio* molecular orbital calculations at multi-reference single and double excitation CI level, it has been found that the reaction products, $(NH_3)_{n-1}NH_4$ (for n = 3 and 4), contain some isomers.

III-E-2 Hydrogen Transfer in Photo-Excited Phenol/Ammonia Clusters by UV-IR-UV Ion Dip Spectroscopy and Ab Initio MO Calculations II: Vibrational Transitions

ISHIUCHI, Shun-ichi[1]; DAIGOKU, Kota[2]; SAEKI, Morihisa[3]; SAKAI, Makoto[4]; HASHIMOTO, Kenro[1]; FUJII, Masaaki[4]

([1]Tokyo Inst. Tech./JST-PRESTO; [2]Tokyo Metropolitan Univ./ACT-JST; [3]JAERI; [4]IMS and Tokyo Inst. Tech.)

[*J. Chem. Phys.* **117**, 7083–7093 (2002)]

The vibrational spectra of phenol/ammonia clusters (1:2~5) in S_0 and those of their photo chemical reaction products, $(NH_3)_{n-1}NH_4$ (n = 2 ~ 5), which are generated by excited-state hydrogen transfer, have been measured by UV-IR-UV ion dip spectroscopy. The geometries, IR spectra and normal modes of phenol-$(NH_3)_n$ (n = 1 ~ 5) have been examined by *ab initio* molecular orbital calculations, at the second-order Møller-Plesset perturbation theory level with large basis sets. For the n = 2 and 3 reaction products, similar vibrational analyses have been carried out. From the geometrical information of reactants and products, it has been suggested that the reaction products have memories of the reactant's structure, which we call "*memory effect*."

III-E-3 Picosecond Time-Resolved Nonresonant Ionization Detected IR Spectroscopy on 7-Azaindole Dimer

SAKAI, Makoto[1]; ISHIUCHI, Shun-ichi[2]; FUJII, Masaaki[1]

([1]IMS and Tokyo Inst. Tech.; [2]Tokyo Inst. Tech./JST-PRESTO)

[*Eur. J. Phys. D.* **20**, 399–402 (2002)]

The picosecond time-resolved IR spectrum of the 7-

azaindole dimer has been measured by picosecond time-resolved nonresonant ionization detected IR spectroscopy. This new time-resolved technique was developed by combining nonresonant ionization detected IR (NID-IR) spectroscopy with tunable picosecond IR and UV lasers. The time-resolved NID-IR spectrum from 2600 cm^{-1} to 3800 cm^{-1} shows a drastic change from 1.5 ps to 11 ps time evolution. A mode-specific vibrational redistribution has been suggested.

III-E-4 Construction of a Picosecond Time-Resolved IR Dip Spectrometer for Studying Structures and Dynamics of Solvated Clusters

SAKAI, Makoto[1]; UEDA, Tadashi; YAMANAKA, Takaya; FUJII, Masaaki[1]
([1]IMS and Tokyo Inst. Tech.)

[*Bull. Chem. Soc. Jpn.* **76**, 509–514 (2003)]

We have constructed a picosecond time-resolved IR dip spectrometer having a frequency resolution of < 20 cm^{-1} and an instrument response time of 25 ps, respectively. In this system, the second harmonic of the idler wave from the OPA pumped at 800 nm and the remaining light from a regenerative amplifier (< 2.5 mJ/pulse) were differentially mixed in a KTA crystal to generate tunable high-power IR light (2750–4000 cm^{-1}; > 60 μJ). The picosecond time-resolved IR dip spectra of phenol–$(H_2O)_1$ and carbazole–$(H_2O)_1$ are presented to demonstrate the capability of the constructed system. The spectral changes show clear vibrational structures of not only S_0, but also S_1 in the 2800–3800 cm^{-1} energy region. The system performance is also discussed.

III-E-5 Two-Color Far-Field Super-Resolution Microscope Using a Doughnut Beam

WATANABE, Takeshi[1]; IKETAKI, Yoshinori[2]; OMATSU, Takashige[3]; YAMAMOTO, Kimihisa[4]; ISHIUCHI, Shun-ichi[5]; SAKAI, Makoto[1]; FUJII, Masaaki[1]
([1]IMS and Tokyo Inst. Tech.; [2]Olympus Optical Co. Ltd.; [3]Chiba Univ.; [4]Keio Univ./JST-PRESTO)

[*Chem. Phys. Lett.* **371**, 634–639 (2003)]

We have demonstrated a realistic super-resolution scanning fluorescence microscope using conventional nanosecond lasers. This super-resolution microscope is based on the combination of two-color fluorescence dip spectroscopy and shape modulation to a doughnut beam. Only by introducing a doughnut erase beam, the resolution of the laser fluorescence microscope breaks the diffraction limit by two times without using any mechanical probe.

III-E-6 Investigation of the Fluorescence Depletion Process in Condensed Phase

IKETAKI, Yoshinori[1]; WATANABE, Takeshi[2]; ISHIUCHI, Shun-ichi[3]; SAKAI, Makoto[2]; OMATSU, Takashige[4]; YAMAMOTO, Kimihisa[5]; FUJII, Masaaki[2]; WATANABE, Tsutomu[6]
([1]Olympus Optical Co. Ltd.; [2]IMS and Tokyo Inst. Tech.; [3]Tokyo Inst. Tech./JST-PRESTO; [4]Chiba Univ.; [5]Keio Univ.; [6]Univ. Electro-Communications)

[*Chem. Phys. Lett.* **372**, 773–778 (2003)]

By using a two-color dip spectroscopy, we measured the fluorescence intensity from tryptophan in a water solution. The fluorescence intensity exponentially decreased as the laser intensity for the $S_n \leftarrow S_1$ excitation increased. The phenomenon was analyzed by a rate-equation for a three-state model. The analysis shows that tryptophan with the S_n state has a radiationless relaxation process without any process through the S_1 state, and that the $S_n \rightarrow S_1$ internal conversion does not have a 100% yield. The branching ratio of the process is estimated to be 20%. The presented result clarifies in detail the real meaning of Kasha's rule.

III-F Chemical Reaction Dynamics

The research group of Dr. Toshinori Suzuki has moved from IMS to RIKEN (Institute of physical and chemical research) in March 2003.

III-F-1 One- and Two-Color Photoelectron Imaging of the CO Molecule *via* the $B^1\Sigma^+$ State

KATAYANAGI, Hideki; MATSUMOTO, Yoshiteru; DE LANGE, Cornelis A.; TSUBOUCHI, Masaaki; SUZUKI, Toshinori

[*J. Chem. Phys.* **119**, 3737 (2003)]

This paper is concerned with photoelectron imaging following one-color (2+1) and two-color (2+1') resonance enhanced multiphoton ionization (REMPI) in the CO molecule. After the two-photon absorption step $B^1\Sigma^+$ (v' = 0) ←← $X^1\Sigma^+$ (v" = 0) or $B^1\Sigma^+$ (v' = 1) ←← $X^1\Sigma^+$ (v" = 0), the subsequent one-photon ionization $X^2\Sigma^+(v^+)$ ← $B^1\Sigma^+$ (v' = 0,1) shows deviations from the expected Δv = 0 Franck-Condon propensity rule. The results are in good agreement with a previous study using time-of-flight photoelectron spectroscopy (Sha *et al.*, *J. Chem. Phys.* **99**, 4334 (1993)). The experimental photoelectron kinetic energy spectra and their angular distributions are analyzed, and the essential role played by 'superexcited' Rydberg states with an $A^2\Pi$ ion core in this process is examined. Moreover, photoelectron imaging methods appear to be useful in extracting information about superexcited states.

III-G Structure and Properties of Carbon Nanotubes and Nanohorns

We studied growth of single-wall carbon nanotubes (SWNTs) and single-wall carbon nanhorns (SWNHs), and enabled their high-yield and structure-controlled growth. It is shown that the nanometer-scale tubule structures caused the unique behaviors such as one-dimensional fullurene-crystal growth inside SWNTs, size-selective adsorption of gas molecules inside SWNHs, and selective adsoprtion of polypeptides by the oxidized SWNHs. In some application of SWNTs and SWNHs, their immobilization on Si wafers was necessary, which was made possible by using bi-functional molecules with amine at one end and silane at the other end of the linear hydrocarbon molecules. We developed structure analyses methods of carbon nanotubes with electron diffraction analyses with transmission electron microscopy and Raman spectroscopy, and found there is no correlation between the symmetries of inner and outer tubes of double-wall carbon nanotubes.

III-G-1 Causes of Different Catalytic Activities of Metals in Formation of Single-Wall Carbon Nanotubes

YUDASAKA, Masako[1]; KASUYA, Yohko[1]; KOKAI, Fumio[2]; TAKAHASHI, Kunimitsu[3]; TAKIZAWA, Morio[4]; BANDOW, Shunji[5]; IIJIMA, Sumio[1,4,5]
([1]JST; [2]Mie Univ.; [3]IRI; [4]IMS; [5]Meijo Univ.)

[*Appl. Phys. A* **74**, 377–385 (2002)]

When single-wall carbon nanotubes (SWNTs) were formed by pulsed Nd:YAG laser ablation or arc discharge, the yield depended on the metal catalyst: NiCo > Ni ~ NiFe » Co ~ Fe > Pd ~ Pt. It appears that an effective catalyst for SWNT growth must satisfy three conditions: it must be a good graphitization catalyst, have low solubility in carbon, and have a stable crystallographic orientation on graphite. NiCo, Ni, and NiFe satisfy these three conditions. The poor catalytic activities of Co, Fe, Pd, and Pt for SWNT formation would be explained by the ineffectiveness of Pt and Pd as graphitization catalysts, crystallographic orientation instability of Co crystals on graphite, and high solubility of Fe in graphite.

III-G-2 Selective Production of Single-Wall Carbon Nanohorn Aggregates and Their Formation Mechanism

KASUYA, Daisuke[1]; YUDASAKA, Masako[1]; TAKAHASHI, Kunimitsu[2]; KOKAI, Fumio[3]; IIJIMA, Sumio[1,4,5]
([1]JST; [2]IRI; [3]Mie Univ.; [4]IMS; [5]Meijo Univ.)

[*J. Phys. Chem. B* **106**, 4947–4951 (2002)]

Single-wall carbon nanohorn (SWNH) aggregates can be produced by CO_2 laser vaporization of carbon, and a single aggregate can take either a “dahlia-like” or “bud-like” form. We found that “dahlia-like” SWNH aggregates were produced with a yield of 95% when Ar at 760 Torr was used as the buffer gas, while “bud-like” SWNH aggregates were formed with a yield of 70 or 80% when either He or N_2 at 760 Torr was used. The internal structures of both aggregates were studied by partially burning them in an O_2 atmosphere. We were then able to examine the mechanism for the formation of SWNH aggregates.

III-G-3 Fullerene Formation *via* Pyrolysis of Ragged Single-Wall Carbon Nanotubes

KOSHIO, Akira[1]; YUDASAKA, Masako[1]; OZAWA, Masaki[2]; IIJIMA, Sumio[1,3,4]
([1]JST; [2]Univ. Tokyo; [3]IMS; [4]Meijo Univ.)

[*Nano Lett.* **2**, 995–997 (2002)]

A new path of fullerene formation via pyrolysis of ragged single-wall carbon nanotubes (r-SWNTs) which were treated by ultrasonication with an organic solvent followed by heating in oxygen gas is reported. Mass spectrum and high-performance liquid chromatography results indicated that C_{60}, C_{70}, and higher fullerenes existed in products obtained through the pyrolysis of the r-SWNTs at above 800 °C in vacuum. We suggest that the pyrolysis of r-SWNTs originates from holes and defects in the r-SWNTs.

III-G-4 Diameter-Selective Resonant Raman Scattering in Double-Wall Carbon Nanotubes

BANDOW, Shunji[1]; CHEN, Gugang[2]; SUMANASEKERA, Gamini, Udaya[2]; GUPTA, Rajeev[2]; YUDASAKA, Masako[3]; IIJIMA, Sumio[1,3,4]; EKLUND, Peter Clay[2]
([1]Meijo Univ.; [2]Penn. State. Univ.; [3]JST; [4]IMS)

[*Phys. Rev. B* **66**, 075416 (8 pages) (2002)]

Double-wall carbon nanotubes (DWNT’s) have been studied by Raman scattering using different excitation wavelengths and their spectra compared to those of single wall nanotubes (SWNT’s) and C_{60}-SWNT peapods. Raman scattering from the radial and tangential vibrational modes of very small diameter d ~ 0.6–0.9 nm secondary (interior) semiconducting tubes within the DWNT can be unambiguously identified with 647.1 and 1064 nm excitations. The frequency of the tangential displacement vibrational modes identified with these secondary (interior) tubes is found to be downshifted by ~ 7 cm^{-1} relative to that of the larger primary (exterior) tubes that exhibit a diameter d ~ 1.3–1.6 nm. This downshift strongly suggests that at

small tube diameters (*i.e.*, $d \sim 0.7$ nm), the associated wall curvature of the nanotube may require an admixture of sp^3 character in the C–C interaction. Our results also show that the value $\gamma_0 = 2.90$ eV for the nearest C–C tight binding integral is consistent with the resonant enhanced Raman scattering from DWNT's.

III-G-5 Linking Chiral Indices and Transport Properties of Double-Walled Carbon Nanotubes

KOCIAK, Mathieu[1]; SUENAGA, Kazutomo[2]; HIRAHARA, Kaori[1]; SAITO, Yahachi[3]; NAKAHIRA, Takanori[3]; IIJIMA, Sumio[1,4,5]
([1]JST; [2]AIST; [3]Mie Univ.; [4]IMS; [5]Meijo Univ.)

[*Phys. Rev. Lett.* **89**, 155501 (4 pages) (2002)]

We performed *in situ* transport measurement in a transmission-electron microscope (TEM) on individual double-walled carbon nanotubes (DWNT). Using selected-area electron diffraction, the chiral indices of the two tubes constituting the DWNTs were determined through careful comparison with theory. We discuss the case of a DWNT whose two tubes have a gap at half filling and show a finite density of delocalized state at the Fermi level. The exact determination of chiral indices should be reachable in any transport-measurement experiment with samples that allow TEM characterization.

III-G-6 Diameter-Selective Removal of Single-Wall Carbon Nanotubes through Light-Assisted Oxidation

YUDASAKA, Masako[1]; ZHANG, Minfang[1]; IIJIMA, Sumio[1,2,3]
([1]JST; [2]IMS; [3]Meijo Univ.)

[*Chem. Phys. Lett.* **374**, 132–136 (2003)]

When single-wall carbon nanotubes (SWNTs) were treated with H_2O_2, rates of SWNT oxidative-degradation were found to be enhanced with irradiation of light. Raman spectroscopic study indicated that, when the irradiation periods were 2 and 5 min, the radial breathing modes of SWNTs having gap energies corresponding to the wavelength of the irradiated light selectively disappeared. This result suggests that SWNTs having a gap energy corresponding to the wavelength of the irradiated light were preferentially removed.

III-G-7 Single-Wall Nanostructured Carbon for Methane Storage

BEKYAROVA, Elena[1]; MURATA, Katsuyuki[1]; YUDASAKA, Masako[1]; KASUYA, Daisuke[1]; IIJIMA, Sumio[1,2,3]; TANAKA, Hideki[4]; KANOH, Hirofumi[4]; KANEKO, Katsumi[4]
([1]JST; [2]IMS; [3]Meijo Univ.; [4]Chiba Univ.)

[*J. Phys. Chem. B* **107**, 4681–4684 (2003)]

Open single-wall carbon nanohorns (SWNHs) were compressed repeatedly at 50 MPa to generate a nanocarbon material of high bulk density. TEM observations and Raman spectroscopy revealed a significant distortion in the structure of the compressed SWNHs. The obtained nanostructured disordered carbon exhibits a high methane storage capacity, reaching 160 cm^3/cm^3 of nanocarbon at 3.5 MPa and 303 K. Comparison of the experimental results with grand canonical Monte Carlo simulations indicates the importance of the adsorption in the interstitial channels for the high total adsorption capacity of the generated nanostructured carbon.

III-G-8 Nanowindow-Induced Molecular Sieving Effect in a Single-Wall Carbon Nanohorn

MURATA, Katsuyuki[1]; HIRAHARA, Kaori[1]; YUDASAKA, Masako[1]; IIJIMA, Sumio[1,2,3]; KASUYA, Daisuke[1]; KANEKO, Katsumi[4]
([1]JST; [2]IMS; [3]Meijo Univ.; [4]Chiba Univ.)

[*J. Phys. Chem. B* **106**, 12668–12669 (2002)]

Subnanoscale windows (nanowindows) were donated to the walls of single-wall carbon nanohorns (SWNHs) by oxidation in oxygen at different temperatures of 573–693 K. We determined the accessibility of internal nanospaces of the SWNHs through nanowindows to He, Ar, N_2, CH_4, SF_6, and C_{60}. An explicit molecular sieving effect of SWNHs due to the nanowindow was shown.

III-G-9 Binary Nano-Materials Based on Nano-Carbons: A Case for Probing Carbon Nanohorns' Biorecognition Properties

ZHU, Jin[1]; KASE, Daisuke[2]; SHIBA, Kiyotaka[2]; KASUYA, Daisuke[3]; YUDASAKA, Masako[1,3]; IIJIMA, Sumio[1,3,4,5]
([1]JST; [2]Cancer Inst.; [3]NEC; [4]IMS; [5]Meijo Univ.)

[*Nano Lett.* **3**, 1033–1036 (2003)]

A critical step toward the construction of complex architectures based on nanoscale carbonaceous materials is to interface these structures with other useful nanoscale building blocks. Herein we report the synthesis of a new class of binary nanomaterials from single-walled carbon nanohorns and nanoparticles by utilizing a bifunctional molecule as the bridging interconnect. Characterization of the materials by transmission electron microscopy, energy-dispersive X-ray spectroscopy, Raman spectroscopy, and thermogravimetric analysis unambiguously proves the formation of binary nanostructures. The strategy reported here is expected to be generic and readily applicable to carbon nanohorns' interfacing with other nanoscale materials, such as Pt, in the construction of fuel cells. Significantly, with these binary nanomaterials, distinct differences in peptide recognition properties have been identified for carbon nanohorns treated under different conditions through a phage-display enzyme-linked immunosorbent assay. Those peptide recognition motifs are important for exploiting this class of materials in

bioassembly, bioseparation, and biosensing applications.

III-G-10 A Surface Modification Approach to the Patterned Assembly of Single-Walled Carbon Nanomaterials

ZHU, Jin[1]; YUDASAKA, Masako[1,2]; ZHANG, Minfang[1]; KASUYA, Daisuke[2]; IIJIMA, Sumio[1,2,3,4]
([1]JST; [2]NEC; [3]IMS; [4]Meijo Univ.)

A surface modification strategy has been employed for the patterned assembly of single-walled carbon nano-materials onto oxide surfaces. The method relies on distinct molecular recognition properties of different functional groups toward the carbon graphitic structure. The surface modification starts with reactions between bifunctional molecules **1** (with amino and silane groups) and hydroxyl groups on an oxide substrate, generating an amine-covered surface. This is followed by a coupling step where bifunctional molecules **2** (with succinimidyl ester and pyrene groups) react with amines. With one area covered with pyrenyl groups and the other one with hydroxyl groups, patterned assembly of a single layer of single-walled carbon nanohorns (SWNHs) has been demonstrated. The strategy employed, herein, is quite generic and applicable to a variety of oxide substrates, including quartz, SiO_2 layer on Si, and Indium Tin oxide (ITO). Since silane chemistry is compatible with soft or lift-off lithography, an extension of this methodology to micrometer scale patterning has been achieved and a further reduction of the size feature should be possible. In addition, patterned assembly of single-walled carbon nanotubes (SWNTs) has also been realized. These surface immobilized structures should open up new possibilities in such areas as nano-electronics, chemical sensing, field emission displays, nano-tribology, and cell adhesion/bio-recognition investigations.

III-H Wave Packet Engineering Using a Phase-Programmable Femtosecond Optical Source

We proposed "wave packet engineering" which realizes mutual conversion between phase information of photonic and quantum wave packets by means of light-matter interaction. A phase-programmable femtosecond optical source is indispensable for such interactive control of photonic and quantum wave packets. We demonstrate control of quantum wave packets in organic molecules and semiconductors using phase-programmed pulses.

III-H-1 Three-Level Picture for Chirp-Dependent Fluorescence Yields under Femtosecond Optical Pulse Irradiation

HASHIMOTO, Naoyuki T.[1]; MISAWA, Kazuhiko; LANG, Roy[1,2]
([1]CREST(JST); [2]Tokyo Univ. Agric. Tech.)

[*Appl. Phys. Lett.* **82**, 2749–2751 (2003)]

We propose a simple model to account for chirp-dependent fluorescence yields from a substance under femtosecond optical pulse irradiation. The model is simple, consisting of a three-level system, and yet it explains the essential feature of the chirp-dependent fluorescence yields experimentally observed, for example, with cyanine dye molecules. Based on the model, the dependence of the fluorescence on the excitation pulse properties such as the chirp rate and pulse intensity has been examined in detail. The results indicate that chirp-dependent fluorescence can be utilized as a convenient means for characterizing phase distortions in optical pulses such as those in optical fiber communication systems.

III-H-2 Femtosecond Wave Packet Engineering in a Cyanine Dye Molecule

MISAWA, Kazuhiko; MATSUDA, Isao[1]; LANG, Roy[1]
([1]Tokyo Univ. Agric. Tech., CREST(JST))

[*Proc. SPIE–Int. Soc. Opt. Eng.* **4798**, 11–20 (2002)]

Quantum wave packet engineering is demonstrated using a phase-programmable femtosecond optical source. This paper describes development of a programmable phase modulator and coherent control of quantum wave packets. Wave packet motion in a cyanine dye molecule is observed to be dependent on the chirp direction and rate of excitation pulses. Strong reduction in excited state population is efficient for negatively chirped pulses in the cyanine dye molecule, which is explained in terms of a pump-dump process. We discuss a possibility of mutual conversion between the optical and electronic phase information by means of nonlinear light-matter interaction.

III-H-3 Femtosecond Chirp Variable Device Using a Chirped Mirror Pair for Quantum Coherent Control

MATSUDA, Isao[1]; MISAWA, Kazuhiko; LANG, Roy[1]
([1]Tokyo Univ. Agric. Tech., CREST(JST))

[*Appl. Phys. Lett.* submitted]

We demonstrate a femtosecond chirp variable device with a chirped mirror pair to manipulate the chirp rate of pulses precisely. The device is simple, easy-to-use, and compact with high energy durability and low insertion loss. Negative chirp can be added to the pulse digitally without a deviation of the output optical axis, which gives the group velocity dispersion of –42 fs^2 at each reflection on the chirped mirror. The whole device dimension is 180 mm × 76 mm. The reflectively and damage threshold of the chirped mirror are 99.5% and 0.6 J/cm^2, respectively. Using this chirp variable device, a chirp-dependent fluorescence in cyanine dye molecules (IR140) is observed. The device opens a new possibility to manipulate optical phase information.

RESEARCH ACTIVITIES IV
Department of Molecular Assemblies

IV-A Spectroscopic Study of Charge Carriers in Organic Conductors

The low-frequency reflectivity of an organic conductor provides us with a wealth of information on the nature of charge carriers. For instance, the anisotropy of a band structure, bandwidth, effect of electron-electron correlation, and electron-molecular vibration (*e-mv*) coupling parameters can be extracted from the analysis of the reflectivity or optical conductivity curve. We are investigating the polarized reflection spectra of various organic conductors in the spectral region of 50–33000 cm^{-1} and in the temperature range of 6–300 K. Usually the molecular vibrations (local phonons) are screened by strong electronic transition by charge carriers. Therefore, few local phonon bands are detected in the reflection spectrum. In this sense, the Raman spectroscopy is a complementary method to reflection spectroscopy for understanding molecular vibrations in a metallic state. Since some molecules have charge-sensitive vibrational modes, the Raman spectroscopic method is a powerful tool to detect the site-charge distribution (oxidation state of molecule). We are investigating the charge ordering (CO) phenomena in organic conductors using the technique of infrared and Raman spectroscopy. In the organic charge-transfer salts, CO is originated from the localization of the charge carriers. Since the charge carriers in organic crystal is located at the boundary between localized and extended (delocalized) states, CO will be widely found through the phase transition. The charge ordering was first found in inorganic narrow-band systems such as copper, manganese, and vanadium oxides. Recently, CO has been found in several organic conductors, and the electronic phase diagrams of typical organic conductors are re-examined taking CO into account. The CO state is drawing attention, since CO is theoretically considered as being related to the pairing mechanism in superconductivity. The Raman and infrared spectra change dramatically at the CO phase-transition temperature, since CO is accompanied by an inhomogeneous charge distribution. Our goal is the complete understanding of the CO phase transition through the interpretation of the vibrational spectra, and the drawing of a *P-T* phase diagram.

IV-A-1 Charge-Ordering Transition in Two Crystal Modifications of θ-(BEDT-TTF)$_2$TlZn(SCN)$_4$ Studied by Vibrational Spectroscopy

SUZUKI, Kenji[1]; YAMAMOTO, Kaoru; YAKUSHI, Kyuya
([1]GUAS)

[*Phys. Rev. B* submitted]

We are systematically investigating the phase diagram of θ-(BEDT-TTF)$_2$MM'(SCN)$_4$ (M = Tl, Rb, Cs; M' = Zn, Co). Subsequently to the thorough study of θ-(BEDT-TTF)$_2$RbZn(SCN)$_4$, we investigated the phase transitions of the orthorhombic and monoclinic modifications of θ-(BEDT-TTF)$_2$TlZn(SCN)$_4$ by the method of infrared and Raman spectroscopy with aid of electrical resistivity and x-diffraction experiments. Both modifications showed the phase transitions, which were accompanied by resistivity jumps, structural changes, and charge separation. The temperature dependence of vibrational spectra of orthorhombic salt showed abrupt peak splitting at around 240 K. Below this temperature, the polarization dependence of the infrared and Raman bands of the orthorhombic modification agreed with that of the low-temperature phase of θ-(BEDT-TTF)$_2$RbZn(SCN)$_4$, which had been elucidated to have a horizontal-type charge-ordering pattern (Figure 1a). The monoclinic salt also showed a resistivity jump at around 165 K. Below this temperature, the polarization dependence of infrared and Raman spectra and the pattern of the satellite peaks in x-ray diffraction were very different from those of orthorhombic modification. Analyzing these results, we concluded that the pattern of the charge order was a diagonal stripe (Figure 1b). The spectral change at the phase transition was rather gradual compared with that of orthorhombic modification. The precursory change was observed in the Raman spectrum above 165 K. This precursor was interpreted as the fluctuation of the site-charge density, namely, the charge carriers move incoherently.

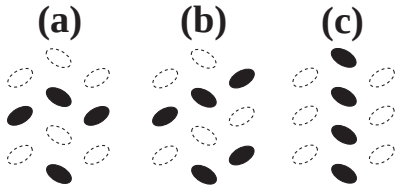

Figure 1. Schematic view of charge-ordered state in θ-type BEDT-TTF sals: (a) horizontal stripe, (b) diagonal stripe, and (c) vertical stripe. The ovals represent the arrangement of the BEDT-TTF molecules in a conducting layer. Above the phase transition temperature, the average charge (+0.5*e*/molecule) is homogeneously distributed at each site, whereas the charges are localized at the sites drawn by solid oval below the phase transition temperature.

IV-A-2 Dynamical Charge Localization in θ-(BEDT-TTF)$_2$MM'(SCN)$_4$ [M = Cs, Rb, Tl, M' = Zn,Co]

SUZUKI, Kenji[1]; YAMAMOTO, Kaoru;

YAKUSHI, Kyuya
([1]GUAS)

The high-temperature phase of θ-(BEDT-TTF)$_2$-MM'(SCN)$_4$ [M = Cs, Rb, Tl, M'=Zn, Co] (hereafter abbreviated as MM') exhibits an unusually broad Raman band. Although this phase is regarded as a metallic state, the temperature derivative of resistivity has a small negative value. The low-temperature phase has been characterized as a charge-ordered state, namely, the localized charge is ordered with a structural distortion. However, the nature of the high-temperature phase is not well understood. We found that the line shape of the Raman band of the charge-sensitive mode at room temperature changed systematically against the bandwidth. Figure 1a shows the line shapes of the Raman band of the charge-sensitive mode of CsZn, RbZn, and TlZn. As the high-pressure narrows the bandwidth in the θ-type BEDT-TTF salts, the various spectra are arranged in the descending sequence of bandwidth from the top to the bottom. In this spectral region, there are two charge-sensitive modes ν_2 and ν_3. We have experimentally and theoretically elucidated that ν_2 splits into two and the highest-frequency ν_3 among the split modes keeps the position, when the charge localization occurs. As shown in Figure 1a, the ν_2 band is broadened and split into two (shown by arrows), when the bandwidth is narrowed. We speculated that the systematic change of the line shape of the Raman band was ascribed to the hopping rate of the localized charge between the adjacent BEDT-TTF molecules. Figure 1b is the simulation of the linewidth based on the two-site motional-narrowing model. The agreement with the experimental results strongly suggests that the charge carrier in the high-temperature phase is not in a coherent state but is incoherently hopping between the adjacent sites in the time scale of a few ps. This state is regarded as a dynamically localized state of charge carrier. This interpretation is consistent with the non-metallic nature of the electrical resistivity.

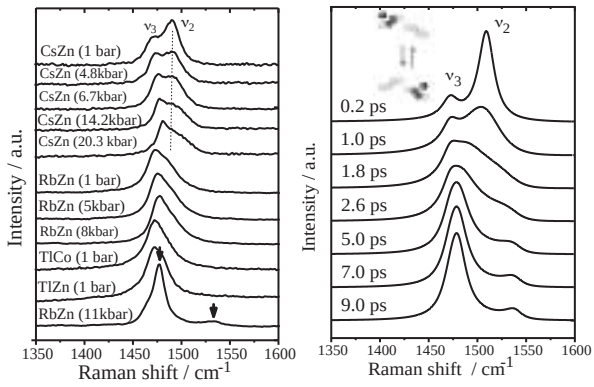

Figure 1. (a) Systematic change of the lineshape of the Raman band (λ_{ex} = 515 nm) of the title compounds at room temperature. The spectra are arranged in a descending order of bandwidth. (b) Raman spectra simulated by using a two-site motional-narrowing model. The time on each spectrum shows the hopping rate between the adjacent sites.

IV-A-3 Activation of Strong Overtone in the IR Spectrum of a Charge-Ordered Organic Conductor

YAMAMOTO, Kaoru; YAKUSHI, Kyuya

The infrared spectrum of charge ordered θ-(BEDT-TTF)$_2$RbZn(SCN)$_4$ exhibits a number of additional signals that are not present above the phase-transition temperature. The example of the additional signals is displayed by solid triangles of Figure 1a. Although the bandwidths of the activated signals seem to be of vibrational transitions, their frequencies are out of the characteristic range of ordinary vibrations. To understand the origin of these bands, we calculated the vibrational transition moment using a molecular dimer containing a single radical electron that is distributed asymmetrically as $M^{\rho+}$–$M^{(1-\rho)+}$. The vibrational transition moment is expressed by the series of the vibronic correction terms. Because the strongest newly activated signal (*ca.* 2750 cm^{-1}) is positioned around the twofold frequency of C=C stretching signal, we performed the numerical calculation including up to the second-order correction. We calculated the ratios of the oscillator strength of two overtones and one combination-tone to the vibronic fundamental. Figure 1b plots the ratios against the ionicity (ρ) at one site. This plot qualitatively explains that the overtones and combination tone are noticeable only when large charge disproportionation (ρ > 0.8) takes place.

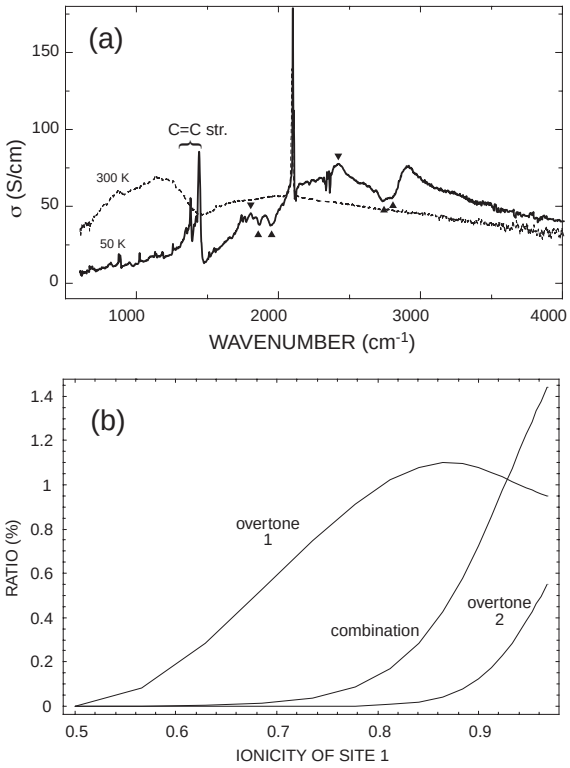

Figure 1. (a) Optical conductivity spectrum of θ-(BEDT-TTF)$_2$RbZn(SCN)$_4$ above (300 K) and below (50 K) the phase transition temperature. The solid triangles show the vibronic overtones and combination tones. (b) Intensity ratios of overtones and combination tones to the fundamentals are plotted against the site charge (ρ).

IV-A-4 Charge Ordered State in θ-(BEDT-TTF)$_2$Cu$_2$(CN)[N(CN)$_2$]$_2$

YAMAMOTO, Takashi; YAKUSHI, Kyuya; SHIMIZU, Hiroyasu[1]; SAITO, Gunzi[1]
([1]Kyoto Univ.)

θ-type BEDT-TTF salts are systematically studied according to the dihedral angle (φ_d) defined from BEDT-TTF molecules in adjacent BEDT-TTF stacks. In the temperature dependence of electrical resistivity, a metal-insulator transition is observed for the most of θ-salts. With increasing φ_d, the transition temperature increases. This phenomenon can be interpreted from the narrow bandwidth due to the small transfer integral. Theoretical studies predict that these compounds fall down to the charge ordered state since Coulomb repulsions play an important role for such a narrow band system. Among numerous θ-salts, which has been synthesized so far, θ-(BEDT-TTF)$_2$Cu$_2$(CN)[N(CN)$_2$]$_2$ has the largest φ_d (~ 132˚). We measured the temperature dependence of Raman spectra below 300 K, and analysed two kinds of C=C stretching modes abbreviated as ν_2 and ν_3. The ν_3 mode exhibited a factor group splitting with decreasing temperature. We were able to apply the factor group analysis exactly the same as those for θ-(BEDT-TTF)$_2$RbZn(SCN)$_4$. This result implied that the system fell down to the horizontally charge-ordered state. Interestingly, the ν_2 mode showed a peak splitting even at 300 K, which is higher than the transition temperature in the resistivity measurement (~ 220 K). This result suggests that the charges are already dynamically localized and the localized charges are incoherently hopping between the adjacent sites at room temperature. We estimated the site charge (ρ) from the peak positions of ν_2. The estimated values were ~ $+0.8_5$ and ~ $+0.1_5$, which were found to be independent of φ_d. Among the four ν_3 modes, the ν_{3D} mode was observed in the lowest energy through an *e-mv* interaction. The peak position of this mode showed a blue shift with the increase of φ_d. This result was explained by the decrease of the transfer integrals along the *a* direction.

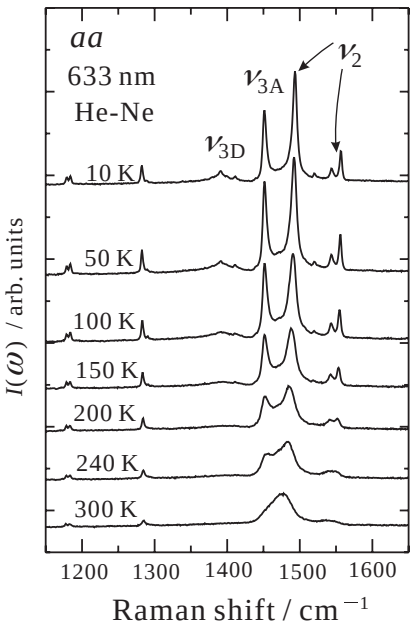

Figure 1. Temperature dependence of the Raman spectrum of θ-(BEDT-TTF)$_2$Cu$_2$(CN)[N(CN)$_2$]$_2$.

IV-A-5 Direct Evidence for the Inhomogeneous Charge Distributions and Charge Re-Distribution in β"-(ET)$_3$(ReO$_4$)$_2$

YAMAMOTO, Takashi; URUICHI, Mikio; YAKUSHI, Kyuya; YAMAURA, Jun-ichi[1]; TAJIMA, Hiroyuki[1]
([1]Univ. Tokyo)

The charge disproportionation in organic CT salt is drawing an attention since theoretical studies suggest the relation between charge fluctuation and pairing mechanism in superconductivity. An insulator-superconductor transition is observed for the several β"-type BEDT-TTF salts under the hydrostatic pressure or the ambient pressure. However, a few experimental studies were presented for the charge disproportionation in the insulating phase of BEDT-TTF salts. We measured the infrared and Raman spectra of β"-(BEDT-TTF)$_3$(ReO$_4$)$_2$ below 300 K. We analysed three kinds of C=C stretching modes abbreviated as ν_2, ν_{27} and ν_3. The ν_{27} mode shows triple peaks below 80 K, while ν_{27} exhibits a doublet above 81 K. The phase-transition temperature detected from the vibrational spectra agreed with those determined from the reflectivity and EPR experiments. In the low-temperature phase, the ν_2 mode was also observed as triple peaks. The site charges (ρ) estimated from the frequencies of ν_2 for non-equivalent BEDT-TTF were $+0.2$, $+0.8_5$ and $+0.9_5$. A mutual exclusion rule between the infrared and Raman spectra was broken for the three ν_3 modes. These results lead to the conclusion that an inversion center is lost below 80 K. This is in agreement with the result of the X-ray structural analysis solved at 22 K. The observed pattern of site charges in the unit cell was reproduced from the mean-field approximation of a Hubbard model. In the high temperature phase, the ν_2 mode was observed as doublets. The estimated ρ are $+0.7_3$ and $+0.5_3$. A mutual exclusion rule was found in the three ν_3 modes. These results imply that an inversion centre is kept above 81 K. This is also in agreement with the result from the X-ray structural analysis solved at 100 K. This inhomogeneous charge distribution above 81 K was reproduced from the mean-field calculation of the Hubbard model with a weak on-site Coulomb energy, where electron and hole pockets still exist in the semi-metallic band. The molecular arrangement slightly changed in this charge-ordering phase transition. This structural change brought about a re-distribution of the localized charge. It is interesting to note that the re-distribution of the charge accompanies the re-distribution of the transfer integrals.

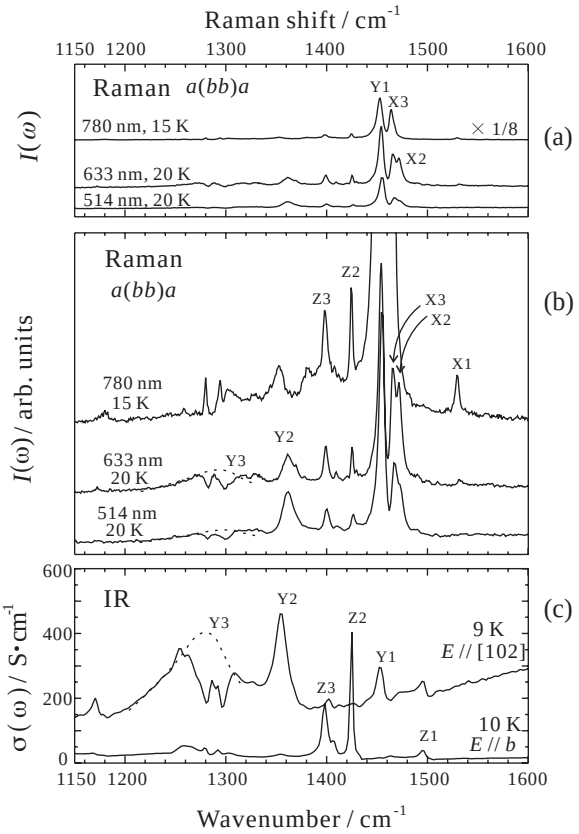

Figure 1. (a) and (b) Raman spectra at the lowest temperature we measured. X, Y and W correspond to the ν_2, ν_3 and ν_{27} modes. (c) Optical conductivity (IR) spectra. Z denotes the ν_{27} mode.

IV-A-6 Inhomogeneous Charge Distributions and Isotope Effect in β”-(BEDT-TTF)$_4$M(CN)$_4$H$_2$O (M = Ni, Pd, Pt) Group

YAMAMOTO, Takashi; URUICHI, Mikio; YAKUSHI, Kyuya; KAWAMOTO, Atushi[1]
([1]Hokkaido Univ.)

The charge disproportionation in organic CT salt is drawing attention since theoretical studies suggest the relation between charge fluctuation and pairing mechanism in superconductivity. Various studies have been concentrated on the θ-type BEDT-TTF salts. However, few studies have been presented for β”-type BEDT-TTF salts, although this family has a rich variety of electrical properties including superconductivity. The title compounds are 3/4-filled β”-salts. For M = Pd and Pt, superconductivities are observed under the hydrostatic pressures. No superconductivity is observed for M = Ni salt. However, resistivity curves for three compounds exhibit insulating behaviours under the ambient pressure below ~ 100 K. We studied temperature dependence of vibrational spectra under the ambient pressure. We analysed three C=C stretching modes abbreviated as ν_2, ν_{27} and ν_3. For M = Ni and Pd, ν_2 and ν_{27} have broad linewidth around 300 K. With decreasing temperature down to 10 K, both modes show peak splitting. This observation leads to an separation of charges. The separated site charges (ρ) are ~ +0.3 and ~ +0.7. Since more than two ν_3 modes are observed in the Raman spectra, the space group is changed from $P\bar{1}$ to $P1$ at low temperature. For M = Pt, ν_2 keeps a broad linewidth down to 10 K, but ν_{27} exhibits a peak splitting at 10 K. We also observed Raman spectra for the deuterium substituted M = Pt salt, where all the hydrogen atoms in BEDT-TTF were substituted by deuterium. Interestingly, the spectral shape becomes similar to that of M = Ni salt rather than that of M = Pt salt. Such a drastic isotope effect is firstly observed in β”-salts. Our results demonstrated that M = Pt salt was located at the region close to the phase boundary that separates the insulator, metal, and superconductor phases.

IV-A-7 Dynamical Fluctuation of Site-Charge Density in Metallic β”-(BEDT-TTF)(TCNQ)

URUICHI, Mikio; YAKUSHI, Kyuya; YAMAMOTO, Hiroshi[1]; KATO, Reizo[1]
([1]RIKEN)

Charge disproportionation (CD) and charge ordering (CO) in organic conductors originate from the localization of charge carriers. CO has been investigated in the insulating states of several charge-transfer salts. We present dynamically fluctuating CD in the metal-like state of the title compound, which are investigated by means of infrared and Raman spectroscopy. β”-(BEDT-TTF)(TCNQ) newly synthesized by Yamamoto *et al.* consists of a segregated stack structure, where TCNQ and BEDT-TTF separately form uniform chains.[1),2)] This compound is metallic with three resistance anomalies at 175 K, 80 K, and 20 K. We measured the polarized Raman and infrared spectra. First we estimated the charge-transfer degree as 0.5 using the C=C stretching mode (ν_4) of TCNQ. All of the Raman bands of TCNQ are independent of temperature. However, the C=C stretching modes (ν_2 and ν_3) of BEDT-TTF show clear splitting, and the low-frequency component of ν_3 exhibits a broad vibronic feature. This finding indicates that the holes of BEDT-TTF are nearly localized, and thus CD arises near the room temperature. We theoretically investigated the frequency shift and Raman intensity of ν_2 and ν_3 using an asymmetric dimer model, and verified that this observation is consistent with the generation of CD. Very interestingly, the split bands of ν_2 merge into a single broad band, and the broad band is sharpened on lowering temperature. The same phenomenon is found in the infrared-active C=C stretching mode ν_{27} as shown in Figure 1. This temperature dependence is well reproduced by motional narrowing model. This finding implies that the holes in BEDT-TTF chain change the nature at low temperature.

References

1) H. M. Yamamoto, M. Hagiwara and R. Kato, *Synth. Met.* **133-134**, 449 (2003).
2) H. M. Yamamoto, N. Tajima, M. Hagiwara, R. Kato and J.-I. Yamaura, *Synth. Met.* **135-136**, 623–624 (2003).

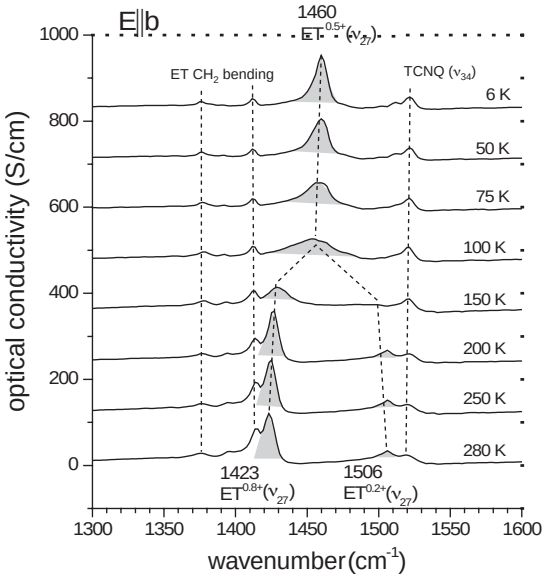

Figure 1. Temperature dependence of the infrared-active C=C stretching mode ν_{27}. The split bands merged at 100 K. This behavior was interpreted based on the motional narrowing model.

IV-A-8 Novel Type of $2k_F$ Bond-Charge-Density Wave in Quasi-One Dimensional 3/4 Filled (EDO-TTF)$_2$X (X = PF$_6$ and AsF$_6$)

DROZDOVA, Olga; YAKUSHI, Kyuya; YAMAMOTO, Kaoru; OTA, Akira[1]; YAMOCHI, Hideki[1]; SAITO, Gunzi[1]
([1]Kyoto Univ.)

[*Phys. Rev. B* submitted]

Recently, charge ordering (CO) in organic charge transfer solids (CTS) has received considerable interest. In quasi-1D 1/4-filled organic CTS, a large on-site (U) and inter-site (V) Coulomb repulsion would cause, intuitively, the alternating (Wigner type) pattern of charge distribution '1010' corresponding to a $4k_F$ CDW. For V smaller than some critical $V_c \sim 2t$ (t being the intra-stack transfer integral) the '0110' ground state ($2k_F$ BCDW-I, Chart 1) can be found, while further small V would lead to $2k_F$ BCDW-II. Whereas $2k_F$ BCDW-I was found experimentally in some 1:2 TCNQ salts, $2k_F$ BCDW-II was characterized for the first time in (EDO-TTF)$_2$X (X = PF$_6$ and AsF$_6$) below T_{MI} (268 K in PF$_6$ and 280 K in AsF$_6$). The stacking-axis optical conductivity spectrum at 300 K is consistent with the weak $4k_F$ BOW accompanied by *e-mv* coupling (Figure 1a). Below T_{MI} the spectrum is dominated by two charge transfer bands CT$_1$ and CT$_2$ corresponding to the electronic transition from the ground state (mainly, |0110>) to the first (|1100> (55%) and |1010> (41%)) and third (mainly, |0200>) excited states, respectively. The fact that CT$_2$ holds a large fraction of the total spectral weight in the nominally 1/4 filled (EDO-TTF)$_2$X (X = PF$_6$ and AsF$_6$) is unique to $2k_F$ BCDW-II state and can be explained by a cooperation of large site charge difference and the type of BOW where the largest transfer integral connects two charge-rich sites. From the vibrational analysis of three charge-sensitive C=C stretching modes of EDO-TTF, the site charges below T_{MI} were estimated as +0.04 and +0.96. Besides, there is evidence for strong *e-mv* coupling of the out-of-phase mode of vibration of the central pair of molecules to CT$_2$, in both infrared and Raman spectra. A kind of relationship between the molecular charge, molecular deformation, and intermolecular π-π overlap is thought to play a role in stabilizing the $2k_F$ BCDW-II state.

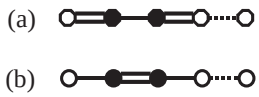

Figure 1. $2k_F$ BCDW-I (a) and $2k_F$ BCDW-II (b). Black and white circles represent charge-rich and charge-poor sites, respectively. The double, single and dotted lines denote the bond strength in descending order.

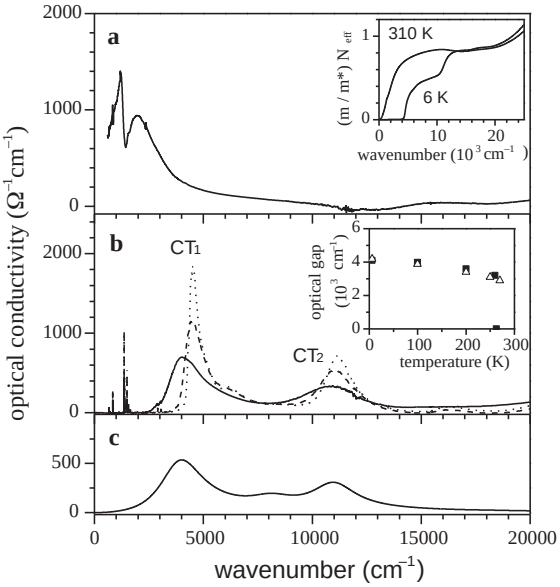

Figure 2. Stacking-axis optical conductivity spectra of (EDO-TTF)$_2$PF$_6$: (a) at 310 K; (b) at 270 K (solid line), 100 K (dashed line), and 6 K (dotted line); (c) spectrum calculated for a symmetric tetramer. Inset in (a) illustrates the sum rule calculation; inset in (b) the temperature dependence of the optical gap.

IV-A-9 Raman Spectra of (Me$_2$-DCNQI)$_2$Cu$_x$Li$_{1-x}$ ($0 \le x \le 1$)—Evidence for Charge Separation at Room Temperature in a One-Dimensional Conductor Having a Quarter-Filled Band

YAMAMOTO, Takashi[1]; TAJIMA, Hiroyuki[1]; KATO, Reizo[2]; URUICHI, Mikio; YAKUSHI, Kyuya
([1]Univ. Tokyo; [2]RIKEN)

[*J. Phys. Soc. Jpn.* **71**, 1956–1964 (2002)]

In the title alloys, the charge density on Me$_2$-DCNQI is expected to be varied as a function of x. These alloys are classified into three groups within $0 \le x \le 1$. For $x >$ 0.29, the alloy is classified into three-dimensional metal down to the liquid helium temperature. For $x \le 0.14$, a (metal-)insulator-insulator transition is observed in the resistivity measurement, and the system falls down to a

non-magnetic insulator below 60 K. For $0.14 < x \leq 0.29$, the system keeps a paramagnetic behaviour down to the liquid helium temperature, although a metal-insulator transition is observed in the resistivity measurement. Both groups ($x \leq 0.29$) are one-dimensional conductors. Observed physical properties for $x \leq 0.29$ around room temperature are interpreted in two different ways. One is a lattice dimerization through electron-phonon interaction, and another is the charge separation through Coulomb repulsion(s). Although the optical conductivity spectrum supports the latter, no direct evidence has been obtained. Raman spectroscopy is a powerful tool to evaluate the charge density on organic molecules. We have measured the Raman spectra of $(Me_2\text{-}DCNQI)_2\text{-}Cu_xLi_{1-x}$ ($0 \leq x \leq 1$) at room temperature, 200 K, 100 K and 5 K. The Raman band assigned to the a_g ν_{R8} fundamental mode (outer-ring C=N stretching) downshifts with an increase of x and exhibits a remarkable split for $0 \leq x \leq 0.29$. This frequency shift is attributable to the change of a charge density on a Me_2-DCNQI molecule. From the split of the ν_{R8} Raman band, it is concluded that charge disproportion occurs in $(Me_2\text{-}DCNQI)_2Cu_xLi_{1-x}$ ($x \leq 0.29$) even at room temperature, where the system exhibits a metallic behaviour.

IV-A-10 Vanadyl Phthalocyanine as a High-Pressure Sensor

SUZUKI, Kenji[1]; YAMAMOTO, Kaoru; YAKUSHI, Kyuya
([1]GUAS)

The ruby fluorescence is a useful pressure sensor, which is commonly used in transparent high-pressure cell, such as diamond and sapphire anvil cells. Since this fluorescence is located at around 694 nm, it appears at around 1400 cm^{-1} in a Raman spectrum when HeNe laser (632.8 nm) is used as an exciting light. Since the strong fluorescence is close to the frequency of the C=C stretching mode, it disturbs the measurement of the Raman bands, even if the focused HeNe laser is not directly irradiated to the ruby. In order to avoid this problem, we looked for some vibrational modes of vanadyl phthalocyanine as a pressure sensor, and examined the pressure dependence of these Raman bands. Among the strong Raman bands of vanadyl phthalocyanine, the breathing mode of macrocycle at around 835 cm^{-1} showed a large blue shift upon applying high pressure. On the other hand, the C–H bending mode at around 1002 cm^{-1} showed no shift at all. Therefore, the frequency difference $\Delta\omega$ between the CH stretching and breathing modes was used as a scale to measure the pressure. Since both modes showed similar temperature dependence, the frequency difference was independent of temperature as shown in Figure 1. We proposed the equation to relate $\Delta\omega$ to P, which was shown in the inset of Figure 1.

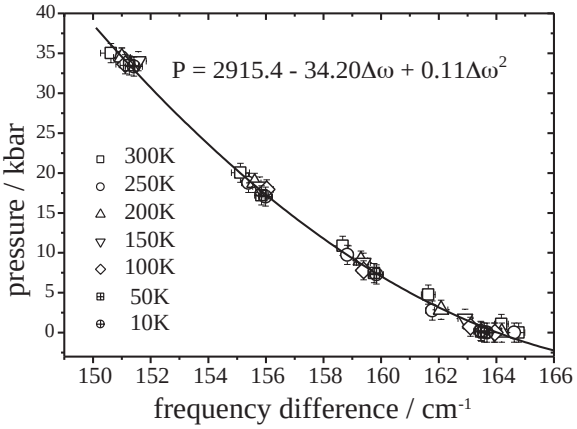

Figure 1. Pressure dependence of the frequency difference $\Delta\omega$ between the C–H bending mode (~ 1002 cm^{-1}) and the breathing mode of macrocycle (~ 835 cm^{-1}) in the Raman spectrum at various temperatures.

IV-A-11 Charge Ordering in the κ-Phase BEDT-TTF Salts with $Co(CN)_6$ and $Fe(CN)_6$ Anions Studied by Infrared and Raman Spectroscopy

SWIETLIK, Roman[1]; LAPINSKI, Andrzej[2]; OUAHAB, Lahcene[3]; YAKUSHI, Kyuya
([1]IMS and IMP, Poland; [2]IMP, Poland; [3]LCSIM-CNRS, France)

[*C. R. Acad. Sci. (Paris) Chimie* **3/6**, 395–403 (2003)]

We studied the temperature dependence of the Raman scattering spectra of two semiconducting isostructural charge-transfer salts κ-$[Et_4N](BEDT\text{-}TTF)_4M(CN)_6\cdot 3H_2O$ ($M = Co^{III}, Fe^{III}$) within the region of C=C stretching vibrations (1200–1700 cm^{-1}). Moreover, polarized reflectance spectra (600 to 10000 cm^{-1}) of the Co^{III} salt were recorded as a function of temperature and compared with previous infrared studies of the Fe^{III} salt. Both salts undergo a phase transition at T = 150 K related to a charge ordering inside the conducting BEDT-TTF layers. Due to the charge ordering new vibrational bands corresponding to $BEDT\text{-}TTF^{+1}$ cations are recorded both in Raman and infrared spectra. Infrared electronic bands also experience strong modifications at 150 K: a new energy gap is formed and a new charge-transfer band in the near-infrared region is observed. The most important difference is that the charge redistribution in Fe^{III} salt is developed gradually below about 240 K, whereas in Co^{III} salt this is an abrupt process related to the phase transition at 150 K.

IV-B Magnetic Resonance Studies for Molecular-Based Conductors

Molecular based conductors are one of the extensively studied materials. The development of the understanding of the electronic phases of these materials enables us systematic investigations of low-dimensional highly correlated electrons systems.

Magnetic resonance investigations are powerful microscopic investigations; they are advantageous for studying the fundamental electronic properties and for understanding the detailed electronic structures of molecular based compounds. Competition of the electronic phases in molecular based conductors has attracted much attention. Investigation of such electronic phases in molecular based conductors is important to understand the unsolved fundamental problems in the field of solid state physics.

In this project, we performed the ESR, and NMR measurements for molecular based conductors to clarify the low temperature electronic states.

IV-B-1 Low-Temperature Electronic Phases of EDT-TTF Based Molecular Conductors

NAKAMURA, Toshikazu

[*Mol. Cryst. Liq. Cryst.* **380**, 233–237 (2002)]

Magnetic investigation was carried out for low temperatures electronic phases in $(EDT\text{-}TTF)_2AuBr_2$, which undergoes an SDW transition at 16 K. In the SDW phase, we observed an abrupt change of ^{1}H-NMR absorption line around 6 K where the ^{1}H-NMR spin-lattice relaxation rate shows an anomalous second-peak. The electronic phase is discussed by microscopic point of view.

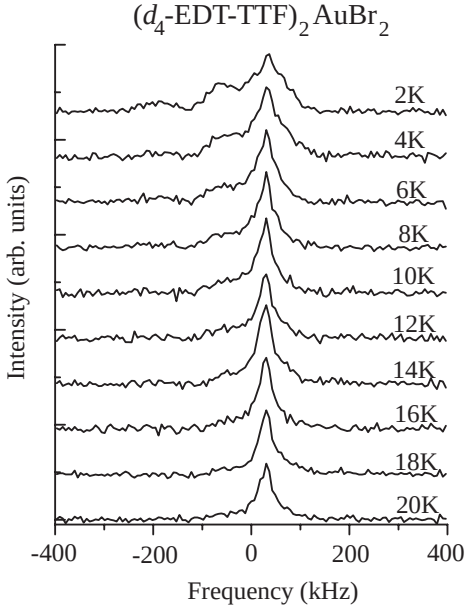

Figure 1. Temperature dependence of the ^{1}H-NMR absorption lines of the $(d_4\text{-}EDT\text{-}TTF)_2AuBr_2$ single crystal.

IV-B-2 Microscopic Investigation of a New Two-Component Organic Conductor with Itinerant and Localized Spins: $(CHTM\text{-}TTP)_2TCNQ$

NAKAMURA, Toshikazu; TANIGUCHI, Masateru[1]; MISAKI, Yohji[1]; TANAKA, Kazuyoshi[1]; NOGAMI, Yoshio[2]
([1]Kyoto Univ.; [2]Okayama Univ.)

[*J. Phys. Soc. Jpn.* **71**, 2208–2215 (2002)]

Low-temperature electronic phases in a new two-component organic conductor, a segregated-stack charge-transfer salt called $(CHTM\text{-}TTP)_2TCNQ$, are investigated. The ESR g tensor analyses indicate that there exist itinerant CHTM-TTP spins and localized TCNQ spins at R.T. The temperature dependence of the physical parameters reveals that this salt undergoes two drastic, successive phase transitions at low temperatures. The effective moment of the localized TCNQ spins decreases at the 245 K transition and completely disappears at the transition around 195 K. These curious physical properties are explained by the drastic changes in the electronic states of the two different types of spins. The spin susceptibility was decomposed into the contribution of each of the two spin species by using ESR, ^{1}H-NMR, and static susceptibility analyses. We present a microscopic investigation of the two-spin system with itinerant and localized moments.

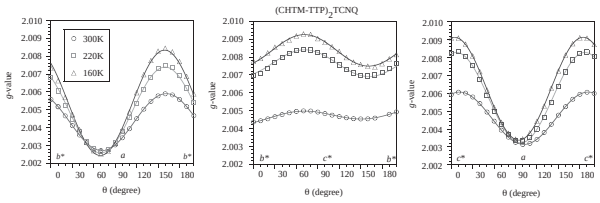

Figure 1. Angular dependence of the g values of $(CHTM\text{-}TTP)_2TCNQ$ at 300 K (circle), 220 K (square) and 150 K (triangle), applying the static field static field within the ab^*, b^*c^*, and c^*a planes, respectively. The solid curves are the least square fits to the measured data using the standard anisotropic g tensor equation.

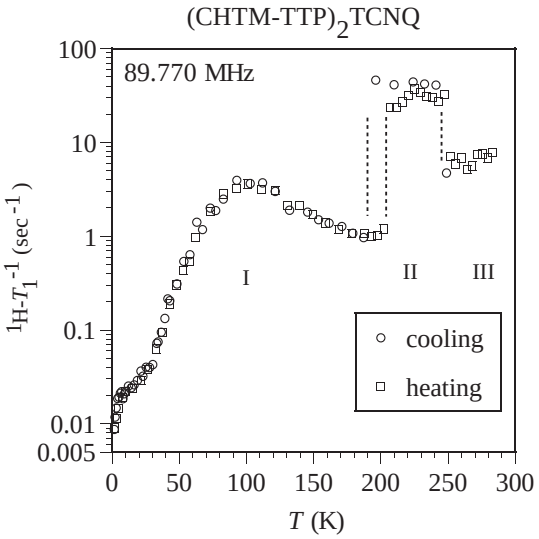

Figure 2. Temperature dependence of the ^{1}H-NMR spin-lattice relaxation rate, T_1^{-1}, of (CHTM-TTP)$_2$TCNQ, operated at 89.770 MHz, using a polycrystalline sample.

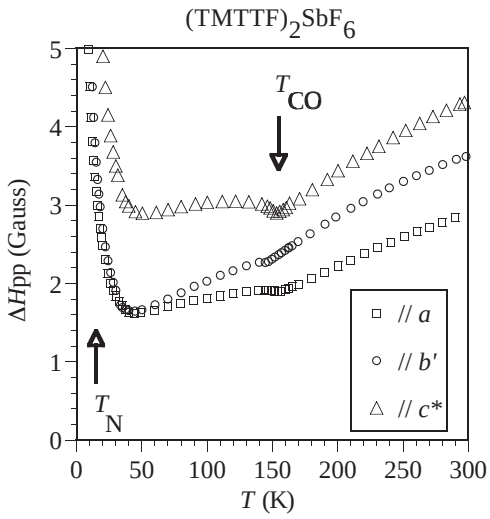

Figure 1. Temperature dependence of the peak-to-peak ESR linewidth, ΔHpp of (TMTTF)$_2$SbF$_6$ for a single crystal. The arrows indicate the charge-ordering and antiferromagnetic transitions.

IV-B-3 *g*-Tensor Analyses of β'-Type Pd(dmit)$_2$ Metal Complexes

NAKAMURA, Toshikazu; TAKAHASHI, Toshihiro[1]; AONUMA, Shuji[2]; KATO, Reizo[2,3]
([1]Gakushuin Univ.; [2]Univ. Tokyo; [3]IMS and Inst. Phys. Chem. Res.)

[*Mol. Cryst. Liq. Cryst.* **379**, 53–58 (2002)]

ESR measurements and *g*-tensor analyses were performed for metal complexes, β'-type Pd(dmit)$_2$. The ESR *g*-values of β'-type Pd(dmit)$_2$ are found to be beyond one radical description which is a good approximation for conventional molecular based conductors. In this paper we focus on the anomalous behavior of the ESR *g*-values in β'-type Pd(dmit)$_2$. We discuss the possible explanation of the electronic structure of β'-type Pd(dmit)$_2$ metal complexes from microscopic points of view.

IV-B-4 Possible Charge Ordering Patterns of the Paramagnetic Insulating States in (TMTTF)$_2$*X*

NAKAMURA, Toshikazu

[*J. Phys. Soc. Jpn.* **72**, 213–216 (2003)]

ESR investigations were performed for a series of quasi-one-dimensional organic conductors, (TMTTF)$_2$*X*. The ESR linewidth shows abrupt jumps or humps in the paramagnetic insulating region. The (TMTTF)$_2$*X* salts are roughly divided into three groups according to the anisotropy of the ESR linewidth at low temperatures. In this paper, we discuss the possible charge-ordered patterns of three typical salts (*X* = ReO_4, SbF_6 and Br) from the microscopic point of view.

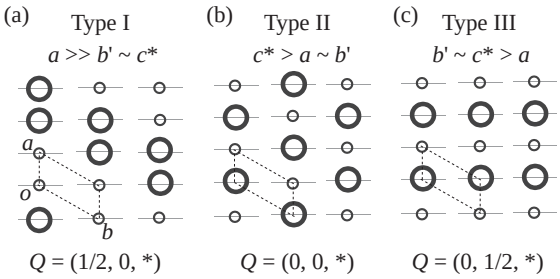

Figure 2. Schematic of possible charge-ordering patterns in the conducting *ab*' planes of TMTTF compounds: (a) Type I (ReO_4, ClO_4), (b) Type II (SbF_6, AsF_6) and (c) Type III (Br).

IV-B-5 NMR Investigation of (TMTTF)$_2$*X*: Charge Configurations and Spin Dynamics

FUJIYAMA, Shigeki; NAKAMURA, Toshikazu

[*Synth. Met.* **133-134**, 67–68 (2003)]

We performed ^{13}C NMR study for a quasi-one-dimensional organic conductor (TMTTF)$_2$Br. Although the resistivity has its minimum value around 100 K, the NMR spectra showed no significant change down to 30 K. Instead, we found slight broadening of the spectra above the magnetic phase transition temperature (T_N ~ 15 K). Similar anomaly is also observed for the uniform susceptibility (χ_s).

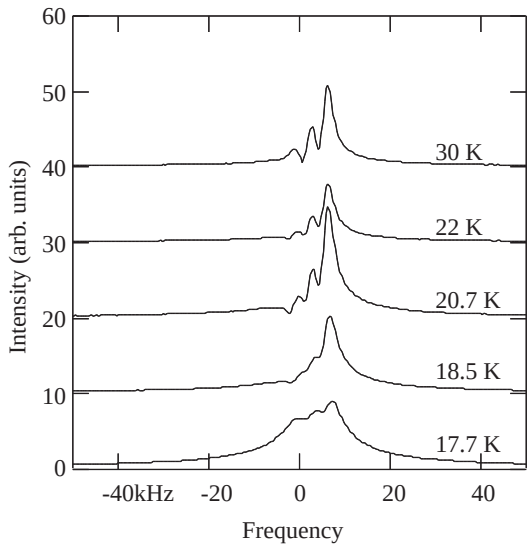

Figure 1. Temperature dependence of the ^{13}C NMR absorption line below 30 K.

IV-C Development of Multi-Functional Molecular Conductors

The molecules are usually assembled by weak intermolecular interactions and tend to retain their isolated electronic states even in the crystalline state. Consequently, the multi-functional systems may be constructed by assembling various molecules with different characters. Thus, the molecules are considered to be suitable building blocks for the bottom-up construction of the systems where various functions coexist and interplay with each other.

Recently, "dual-action system" such as magnetic molecular conductors has attracted a considerable interest. Though there exist well-known systems such as the paramagnetic organic superconductor and the ferromagnetic organic metals, there seems almost no significant interactions between conduction parts and magnetic parts. In contrast, we have discovered several novel organic superconductors exhibiting remarkable electro-magnetic properties originating from π-*d* coupling. κ-$(BETS)_2FeBr_4$ and κ-$(BETS)_2FeCl_4$ are the first and the second antiferromagnetic organic superconductors, respectively. Furthermore, κ-$(BETS)_2FeBr_4$ exhibits a metamagnetic (antiferromagnetic → ferromagnetic) transition around 1.6 T to give rise to a sharp switching behavior between superconducting and metallic states by tuning the external field around 1.6 T. In addition, due to the π-*d* interaction, a field-induced superconducting transition was observed around 12.5 T. But this is not the first observation of field-induced superconductivity in the organic conductors. We have previously reported the field-induced superconductivity in λ-$(BETS)_2FeCl_4$. Owing to the relatively large π-*d* interaction, λ-$(BETS)_2FeCl_4$ shows the field-induced superconductivity around 33 T, though the ground state is a π-*d* coupled antiferromagnetic insulating state. Moreover, the analogous system with diluted magnetic moments, λ-$(BETS)_2Fe_xGa_{1-x}Cl_4$ ($0.35 < x < 0.5$) undergoes the successive metal → superconductor → insulator transitions with decreasing temperature. The electromagnetic properties of these BETS conductors gave clear examples of organic conductors showing the π-*d* coupling. Besides these conductors, we have recently tried to develop another type of magnetic molecular conductors by using the π donor molecules incorporating stable organic radicals. When the magnetic anions such as $FeCl_4^-$ are adopted as counter anions, the magnetic organic conductors with two kinds of spin systems will be prepared where a variety of novel electromagnetic properties will be expected.

Until quite recently, it has been long believed that all the molecular metals are constructed of more than two chemical species because the intermolecular charge transfer phenomena have been used to generate charge carriers. The best example may be the first organic superconductor, $(TMTSF)_2PF_6$ where the hole carriers are generated in TMTSF columns by the charge transfer from TMTSF to PF_6^- (TMTSF → $TMTSF^{+0.5}$). Due to the charge transfer, the molecular metals have the character of ionic crystals. But we have recently developed molecular metals consisting of neutral single-component molecules where intermolecular charge transfer cannot be considered. More recently, the experimental evidence for the existence of Fermi surfaces in this single-component molecular crystal was obtained. The discovery of the single-component molecular metal disclosed the amphibious molecular crystal consisting of neutral single-component molecules and possessing 3D Fermi surfaces.

IV-C-1 Highly Conducting Crystals Based on Single-Component Gold Complexes with Extended-TTF Dithiolate Ligands

SUZUKI, Wakako[1]; FUJIWARA, Emiko[1]; KOBAYASHI, Akiko[1]; FUJISHIRO, Yuichi[2]; NISHIBORI, Eiji[2]; TAKATA, Masaki[2]; SAKATA, Makoto[2]; FUJIWARA, Hideki; KOBAYASHI, Hayao

([1]Univ. Tokyo; [2]Nagoya Univ.)

[*J. Am. Chem. Soc.* **125**, 1486 (2003)]

We have recently found the first metallic crystal consisting of neutral transition metal complex molecules with extended-TTF (tetrathiafulvalene) ligands, $[Ni(tmdt)_2]^{0+}$ (tmdt = trimethylenetetrathiafulvalene-dithiolate) with metallic behavior down to very low temperature. In terms of valence electrons, the neutral bis(dithiolato)gold complex is isoelectronic to the planar bis(dithiolato)nickel monoanion complex with one unpaired electron per molecule, which makes the electromagnetic properties of the neutral gold complex very attractive. It has been thought that these unpaired electrons or holes in the bis(dithiolato)gold complexes have a possibility to form a metallic band. We have prepared the crystals composed of single-component gold complexes with extended-TTF ligands, $[Au(dmdt)_2]^{0+}$ (dmdt = dimethyltetrathiafulvalene-dithiolate) and $[Au(tmdt)_2]^{0+}$ and examined their structural, electrical and magnetic properties. Since the crystals were very small, the synchrotron radiation X-ray powder experiments were performed by using the imaging plate detectors and the Large Debye-Scherrer camera at the facility SPring-8 BL02B2. Although the sufficient diffraction patterns could not be obtained on $[Au(dmdt)_2]$, an ideal X-ray powder pattern was obtained on $[Au(tmdt)_2]$, which revealed $[Au(tmdt)_2]$ to be isostructural to $[Ni(tmdt)_2]$. The crystal structure was successfully analysed by a self-consistent iterative analysis of a combination of the maximum entropy method (MEM) and Rietveld analysis. The lattice constants of $[Au(tmdt)_2]$ are: a = 6.4129(1) Å, b = 7.5514(2), c = 12.1543(3), α = 90.473(3)°, β = 96.698(2), γ = 103.008(3), V = 569.21(2) Å^3. The high conductivity of compacted crystalline powder sample (≈ 15 S cm^{-1} at room temperature) and the XPS and NEXAFS measurements suggested $[Au(tmdt)_2]$ to be essentially a metal. The temperature dependence of ESR intensity showed that $[Au(tmdt)_2]$ undergoes a magnetic transition around 100 K with keeping the highly conducting states. To our knowledge, there has been no molecular conductor exhibiting magnetic transition at the temperature as high as 100 K. The SQUID measure-

ments suggested the magnetic transition to be antiferromagnetic one.

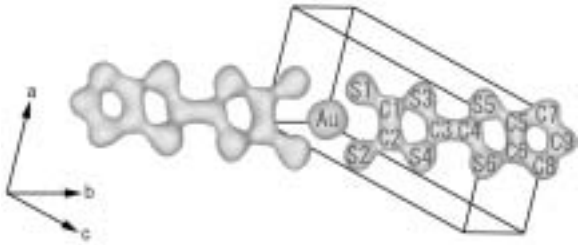

Figure 1. Structure of [Au(tmdt)$_2$] determined by MEM/Rietveld analysis of X-ray powder patterns.

IV-C-2 Structure and Physical Properties of Palladium Complexes with Extended-TTF Dithiolate Ligands

SUZUKI, Wakako[1]; FUJIWARA, Emiko[1]; KOBAYASHI, Akiko[1]; HASEGAWA, Ami[2]; MIYAMOTO, Takeshi[2]; KOBAYASHI, Hayao
([1]Univ. Tokyo; [2]Kitasato Univ.)

In the course of the studies on the development of single-component molecular metals, new dithiolato palladium complexes with an extended-TTF (tetrathiafulvalene) ligand (^{n}Bu$_4$N)[Pd(C3-tdt)$_2$](**1**) and [Pd(C3-tdt)$_2$] ((C3-tdt)$^{2-}$ = dipropylthiotetrathiafulvalenedithiolate)(**2**) were prepared and their crystal structures were determined. The electrochemical properties of **1** were investigated by cyclic voltammetry technique at 20 °C and scan rate of 200 mVs^{-1}. The cyclic voltammogram measured in dimethylformamide showed three pairs of reversible redox waves. The first, second and third potentials are –0.92, –0.30 and +0.47 V *vs.* Ag/AgCl, respectively. The first, second and third waves correspond to three electrons, two electrons and one electron oxidation, respectively, leading [Pd(C3-tdt)$_2$]$^{2-}$ to [Pd(C3-tdt)$_2$]$^{4+}$. The crystal structures of **1** and **2** were examined. **2** has three-dimensional S···S short contacts even though **2** has large steric hinderence through large propylthio groups. The molecular structure is almost planar except for four propylthio groups and more planar than that in **1**. The magnetic susceptibility of (^{n}Bu$_4$N)[Pd(C3-tdt)$_2$] gave good agreement with Bonner-Fisher model (J = –16 K), which suggests [Pd(C3-tdt)$_2$] anions form approximately a one-dimensional antiferromagnetic chain. On the other hand neutral [Pd(C3-tdt)$_2$] was found to be a semiconductor with a room temperature conductivity of 10^{-2} S·cm^{-1}.

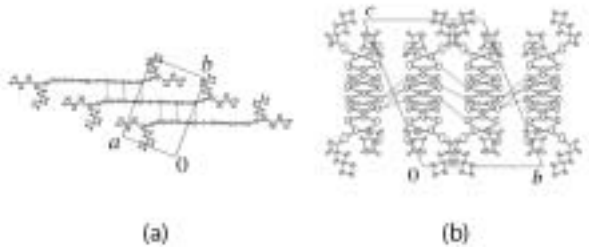

Figure 1. Crystal structure of [Pd(C3-tdt)$_2$] (**2**) projected onto (a) the *ac*-plane and (b) the *bc*-plane.

IV-C-3 Single-Component Molecular Crystal with Three-Dimensional Fermi Surfaces

TANAKA, Hisashi[1]; TOKUMOTO, Madoka[1]; ISHIBASHI, Shouji[1]; GRAF, David[2]; CHOI, Eun S.[2]; BROOKS, James S.[2]; YASUZUKA, Shyuma[3]; OKANO, Yoshinori; KOBAYASHI, Hayao; KOBAYASHI, Akiko[4]
([1]AIST; [2]Florida State Univ.; [3]Natl. Inst.Mater. Sci.; [4]Univ. Tokyo)

Recently a considerable attention has been attracted to the unconventional conducting molecular systems such as single component molecular conductors, nanowires , molecular wire junctions and even DNA. Though the intriguing reports on new types of molecular systems are rapidly increasing in number, there seem to be many systems whose origins of the charge carriers and/or transport mechanisms still remain unclear. The single-component molecular crystal, we reported recently, consisting of neutral metal complex molecules [Ni(tmdt)$_2$] (tmdt = trimethylenetetrathia-fulvalene-dithiolate) exhibits metallic behavior down to 0.6 K, but without Fermiological evidence of metallic nature. In order to prove definitely the existence of an amphibious molecular crystal consisting of single-component neutral molecules and possessing metal electrons, the torque magnetometry measurements of de Haas van Alphen oscillatory signals in a single crystal of [Ni(tmdt)$_2$] were performed by using a sensitive microcantilever at low temperatures in high magnetic fields to 45 T. Because of very small size of the crystals (of order 130 × 100 × 20 μm^3, and 0.5 μg in mass), we employed a commercial microcantilever for atomic force microscope (AFM). A simple resistance bridge circuit was used to cancel the background resistance of the two piezoresistive sensing cantilevers on the AFM assembly. The observed signals for all directions of magnetic field revealed unambiguously the presence of three-dimensional Fermi surfaces for both electrons and holes, which correspond well to the band structure calculated by local density approximation (LDA) and *ab initio* plane-wave norm-conserved pseudopotential method.

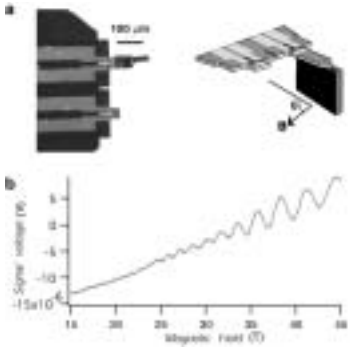

Figure 1. (a) AFM cantilever for torque magnetometry, (b) The raw torque magnetometer signal *versus* the applied magnetic field showing de Haas van Alphen oscillation of the single-component molecular metal, Ni(tmdt)$_2$.

IV-C-4 Infrared Electronic Absorption in Single-Component Molecular Metal

KOBAYASHI, Akiko[1]; SASA, Masaaki[1]; SUZUKI, Wakako[1]; FUJIWARA, Emiko[1]; TANAKA, Hisashi[2]; TOKUMOTO, Madoka[2]; OKANO, Yoshinori; FUJIWARA, Hideki; KOBAYASHI, Hayao
([1]Univ. Tokyo; [2]AIST)

[*J. Am. Chem. Soc.* in press]

It is commonly accepted that the electronic energy of a molecule is much higher than the vibrational energy of a molecule. If a molecule with electronic excitation in the *infrared* (*ir*) region can be designed, then the molecular system is expected to have unprecedented electronic properties. In order to develop a metallic crystal consisting of single-component molecules, we have tried to synthesize molecules with unprecedentedly low electronic excitations (or unprecedentedly small HOMO-LUMO gaps). In fact, as reported before, we could find the first single-component molecular crystal with stable metallic state down to 0.5 K. If our molecular design is correct, the transition metal complex molecules with extended TTF ligands (L) will have very small HOMO-LUMO gap. We have synthesized and examined the electronic absorption spectra of the crystals of $M(L)_2$[M = Ni, Pd; L = tmdt (trimethylenetetrathiafulvalenedithiolate), dmdt (dimethyl-tetrathiafulvalenedithiolate), ptdt (propylene-dithiotetrathia-fulvalenedithiolate) and dt (tetrathia-fulvalenedithiolate)]. Since a suitable solvent was not found, the *visible* (*vis*) and *ir* spectra were measured on crystalline powder samples. $Ni(tmdt)_2$ and $Ni(dmdt)_2$ exhibited the broadest absorption maxima around 2200 cm^{-1}. To our knowledge, this is the smallest electronic absorption energy ever reported for single-component closed-shell molecular systems. Although the electronic absorptions around 2200 cm^{-1} of $Ni(tmdt)_2$ and $Ni(dmdt)_2$ seem to suggest an extremely small HOMO-LUMO gap, the $M(L)_2$ peaks blue shifted as the semi-conducting properties of the crystal increased, which indicates that the band structure plays a crucial role. Based on the extended-Hückel tight-binding band parameters, the electronic spectra were calculated. The good agreement between observed and calculated spectra shows that the single-component molecular conductors are composed of molecules with unprec-edentedly small HOMO-LUMO gaps.

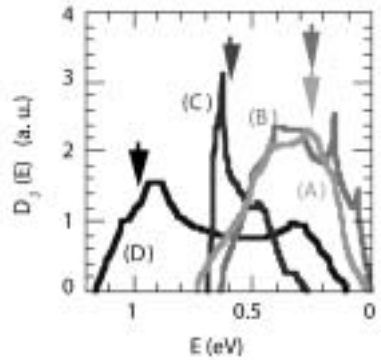

Figure 1. The calculated joint density of states $D_J(E)$: (A) $Ni(tmdt)_2$, (B) $Ni(dmdt)_2$, (C) $Ni(ptdt)_2$, and (D) $Pd(dt)_2$. The E-dependence of $D_J(E)$ is consistent with the observed electronic absorption spectra for each system. The arrows indicate the energy of observed absorption maxima.

IV-C-5 A Novel TTP Donor Containing a PROXYL Radical for Magnetic Molecular Conductors

FUJIWARA, Hideki; LEE, Ha-Jin; KOBAYASHI, Hayao; FUJIWARA, Emiko[1]; KOBAYASHI, Akiko[1]
([1]Univ. Tokyo)

[*Chem. Lett.* 482 (2003)]

The development of new electron donors for molecule-based conductors involving a magnetic centre are of quite interest to investigate the interplay between the π conducting electrons generated by an oxidation and the localized radical spins, and several donors containing a stable radical have been synthesized to try for novel conducting-magnetic bifunctional materials. Among them, to realize the metallic conductivity, we focused on the molecules with TTP skeleton [TTP = 2,5-bis(1,3-dithiol-2-ylidene)-1,3,4,6-tetrathiapenta-lene], which was regarded as a series of promising donors for the realization of stable metallic states. We synthesized a novel electron donor consisting of the TTP framework and a stable PROXYL radical part **1** and cleared its structure and physical properties. Furthermore, we reported the physical properties of its ClO_4^- and $FeCl_4^-$ salts. Among them, the $FeCl_4^-$ salts of **1** (D:A ratio ≈ 1:0.46) showed the highest conductivity record (1.1 S cm^{-1}) in the cation radical salts based on the donors containing stable organic radicals reported so far, even though it was measured on compressed pellets. This salt showed semiconducting behavior, however, the activation energy is quite small value of 0.02 eV. Therefore, the electrical conductivity of this salt can be considered to be essentially metallic if we could measure the conductivity using its single crystals. The χT values of this salt around room temperature correspond to the sum of the contributions from one PROXYL radical, high spin Fe^{3+} and conduction electrons, suggesting the coexistence of these three different magnetic moments. These results indicate that this salt is possibly the first example of paramagnetic organic metal with the coexistence of the conduction electrons and two kinds of the localized spins.

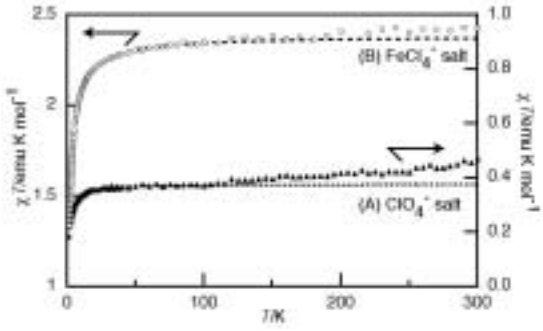

Figure 1. Magnetic properties of the cation radical salts of **1**.

IV-C-6 Synthesis, Structures and Physical Properties of a New Organic Conductor Containing a Stable PROXYL Radical

FUJIWARA, Hideki; LEE, Ha-Jin; CUI, Heng-Bo; KOBAYASHI, Hayao; FUJIWARA, Emiko[1]; KOBAYASHI, Akiko[1]
([1]Univ. Tokyo)

We have reported several π-extended donor molecules containing a stable organic radical part, and recently, we have discovered highly conducting cation radical salts by use of the bis-fused TTF skeleton called as TTP containing a PROXYL radical substituent. However we could not clear the crystal structures of the cation radical salts based on such TTP-based donor molecules because it was difficult to obtain suitably large crystals for crystallographic analysis so far. Very recently, we succeeded in the structure analysis of a quite small crystal of the AsF_6^- salt of a newly synthesized cyclopenteno-fused TTP derivative **1** carrying a stable PROXYL radical part by using a new X-ray diffractometer equipped with the confocal X-ray mirror system and the CCD detector. The AsF_6^- salt has a 4:1 stoichiometry of D:A. As shown in Figure 1, the TTP skeleton of the donor molecules formed the π-conduction layer along the *ab*-plane and the PROXYL radical parts of both the donors and the AsF_6^- anions formed the insulating layers sandwiched by the donor layers. The donor layer has a quite unique structure and each the donor molecules (A and B) constructed independent one-dimensional stackings I and II in the donor layer. Reflecting strong one-dimensionality of the intermolecular interactions along the *b*-axis, the calculated Fermi surface also indicates the one-dimensional electronic structure of this salt. Above 100 K, the χT values are larger than the value for one S = 1/2 spin per one donor molecule (0.375 emu K mol^{-1}), suggesting a small contribution from conduction electrons. That is, the localized spin of the PROXYL radical part and π conduction electrons seem to coexist at higher temperature. This salt showed relatively high room temperature conductivity of 1 S cm^{-1} and semiconducting temperature dependence of resistivities with a very small activation energy of 0.046 eV.

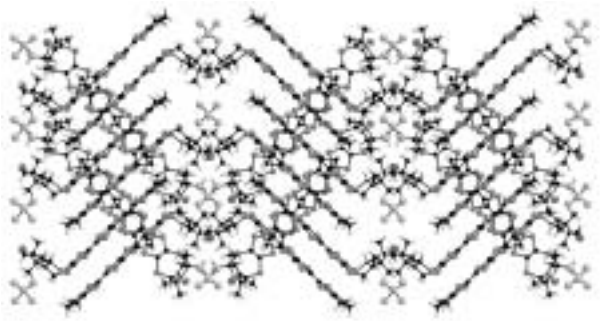

Figure 1. (a) Crystal structure of the AsF_6^- salt of **1** projected on to the *bc*-plane.

IV-C-7 Crystal Structures and Physical Properties of New Magnetic Conductors Based on π-Donor Molecule Containing a Stable Organic Radical

LEE, Ha-Jin; CUI, Heng-Bo; FUJIWARA, Hideki; KOBAYASHI, Hayao; FUJIWARA, Emiko[1]; KOBAYASHI, Akiko[1]
([1]Univ. Tokyo)

In the research for new molecular-based organic conductors, a considerable interest has been focused on the development of molecular conductors and superconductors containing magnetic transition metal anions to investigate the intrerplay between conduction electrons and localized magnetic moments in organic conductors. From this point of view, several donors containing a stable organic radical part such as TEMPO and NN, have been prepared with the aim of developing novel organic conducting-magnetic multifunctional materials and organic ferromagnetic metals. We have recently reported highly conducting radical salts, for example, the $FeCl_4^-$ (1:0.46) salt (σ_{RT} = 1 Scm^{-1}) of the donor (TTP-proxyl (**1**)) based on the bi-fused TTF skeleton named as TTP containing a PROXYL radical. However we could not solve the crystal structure of these cation radical salts because it was impossible to obtain single crystals suitable for crystallographic analysis. In this paper, we reported the preparation of the $FeCl_4^-$ and $GaCl_4^-$ salts of the donor **1**, which have a 1:1 stoichimoetry, and examined their structure, and magnetic and conductivity properties. Overall temperature dependence of the **1**·$FeCl_4$ indicates typical semiconducting behavior with an activation energy of *ca*. 0.13 eV. The room temperature electrical conductivity of this salt is low, with a value of about 10^{-3} Scm^{-1}, due to the 1:1 stoichiometry and strongly dimerized structure. The χT value of **1**·$FeCl_4$ at room temperature is 4.65 K·emu·mol^{-1} and slightly lower than 4.75 K·emu·mol^{-1} expecting from the sum of the contribution form one PROXYL radical (S = 1/2; 0.375 K·emu·mol^{-1}) and high spin Fe^{3+} (S = 5/2; 4.375 K·emu·mol^{-1}), and the value slightly increases as temperature decreases to 50 K.

Figure 1. Crystal structure of the $FeCl_4^-$ salt of **1** projected onto the *ac*-plane.

IV-C-8 An Unsymmetrical Donor Fused with Pyridazine Ring

OTSUBO, Saika; TAKAHASHI, Kazuyuki; CUI,

Heng-Bo; FUJIWARA, Hideki; KOBAYASHI, Hayao; FUJIWARA, Emiko[1]; KOBAYASHI, Akiko[1]
([1]Univ. Tokyo)

We have reported that the interaction between π conduction electrons and *d* magnetic anions plays an important role to realize novel electro-magnetic properties such as unprecedented superconductor-to-insulator transition and magnetic field-induced superconductivities of λ- and κ-type BETS salts containing high-spin Fe^{3+} ions. In order to enhance the interaction between donor and anion layers, we have prepared an EDST analogue fused with a pyridazine ring. The new thione unit, pyridazino-1,3-dithiole-2-thione was synthesized in 57% yield (3 steps). The new donor (**1**) was prepared by a phosphite-mediated cross-coupling reaction of the thione unit with 4,5-ethylenedithio-1,3-diselenol-2-one in 16% yield (Scheme 1). The cyclic voltammogram shows one reversible and one irreversible waves. The first and the second oxidation potentials were +0.86 and +1.21 V *vs*. Ag/AgCl, respectively. The crystal structure of the ReO_4^- salt showed that the D:A ratio was 1:1 and the donor molecules formed dimer with a head-to-tail overlap mode. There were anions between the donor dimers and no columnar structure was observed.

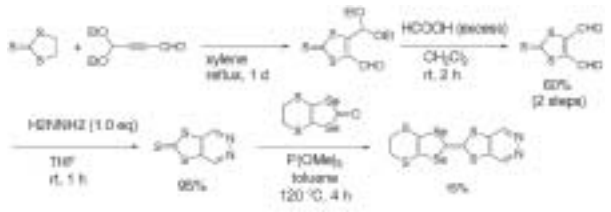

Scheme 1. Synthetic route of **1**.

IV-C-9 Structural, Electrical and Magnetic Properties of a Series of Molecular Conductors Based on BDT-TTP and Lanthanoid Nitrate Complex Anions [BDT-TTP = 2,5-bis(1,3-dithiol-2-ylidene)-1,3,4,6- tetrathiapentalene]

CUI, Heng-Bo; OTSUKA, Takeo; KOBAYASHI, Akiko[1]; TAKEDA, Naoya[1]: ISHIKAWA, Masayasu[1]; MISAKI, Yohji[2]; KOBAYASHI, Hayao
([1]Univ. Tokyo; [2]Kyoto Univ.)

[*Inorg. Chem.* **42**, 6114 (2003)]

The crystals of a series of novel molecular conductors, which are based on π donor molecules BDT-TTP [2,5-bis(1,3-dithiol-2-ylidene)-1,3,4,6-tetrathiapentalene] with a tetrathiapentalene skeleton and lanthanide nitrate complex anions $[Ln(NO_3)_x]^{3-x}$ (Ln = La, Ce, (Pr), Tb, Dy, Ho, Er, Tm, Yb, and Lu) with localized 4*f* magnetic moments, were synthesized. Except for the Ce complex, the salts were composed of $(BDT\text{-}TTP)_5[Ln(NO_3)_5]$ and were isostructural. Even though the Ce crystal had a different composition, $(BDT\text{-}TTP)_6[Ce(NO_3)_6](C_2H_5OH)_x$ ($x \approx 3$), the crystals all had the space group, $P\bar{1}$. Previously, we reported the crystal structures and unique magnetic properties of $(BDT\text{-}TTP)_5[Ln(NO_3)_5]$(Ln = Sm, Eu, Nd, Gd). Thus by combining the results of this work with previous one, we for the first time succeeded to obtain a complete set of organic conductors composed of the identical π-donors (BDT-TTP in this case) and all the lanthanide nitrate complex anions (except the complex with Pm^{3+}). The crystals were all metallic down to 2 K. Electronic band structure calculations resulted in two-dimensional Fermi surfaces, which was consistent with their stable metallic states. Except the Lu complex, which lacked paramagnetic moments, the magnetic susceptibilities were measured on the six heavy lanthanide ion complex salts by a SQUID magnetometer (Ln = Tb, Dy, Ho, Er, Tm, and Yb). The large paramagnetic susceptibilities, which were caused by the paramagnetic moments of the rare-earth ions, were obtained. The Curie-Weiss law fairly accurately reproduced the temperature dependence of the magnetic susceptibilities of $(BDT\text{-}TTP)_5[Ho(NO_3)_5]$ in the experimental temperature range (2–300 K) and a comparatively large Weiss temperature ($|\theta|$) was obtained [θ(Ho) = –15 K]. The fairly strong intermolecular magnetic interaction between Ho^{3+} ions, which was suggested by the $|\theta|$-value, is inconsistent with the traditional image of strongly localized 4*f* orbitals shielded by the electrons in the outer 5*s* and 5*p* orbitals.

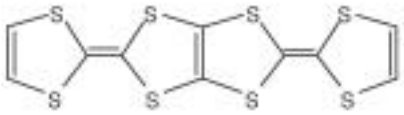

Figure 1. BDT-TTP [2,5-bis(1,3-dithiol-2-ylidene)-1,3,4,6-tetrathiapentalene].

IV-C-10 Anomalous 1:1 Salt with Metallic State down to 15 K, (BETS)$GaBr_4$

CUI, Heng-Bo; OKANO, Yoshinori; FUJIWARA, Hideki; KOBAYASHI, Hayao; KOBAYASHI, Akiko[1]
([1]Univ. Tokyo)

Except for a few conductors such as $(TTM\text{-}TTP)I_3$ with metallic state down to 160 K, almost all the 1:1 salt of π donors (D) and inorganic anions (A) have been considered to become insulators due to the large on-site Coulomb interactions. However, we have recently found a 1:1 salt of BETS (= bis(ethylenedithio)tetraselenafulvalene) and $GaBr_4^-$ with high room-temperature conductivity of about 20 S cm^{-1}. The resistivity decreased slowly but almost linearly with lowering temperature and increased rapidly below *ca.*15 K (T_{MI}). That is, (BETS)$GaBr_4$ is the anomalous 1:1 salt with stable metallic state down to about 15 K. The crystal has a very simple and unique structure. The lattice constants are: a = 7.050 Å, b = 8.489, c = 24.142, α = 85.63°, β = 83.79, γ = 68.85, V = 1338.5 $Å^3$, Z = 1. Similar to usual organic metals with the composition of D_2A, the crystal contains donor and anion layers. But due to 1:1 stoichiometry, the donor and anion layers are arranged as, DAADAA⋯ along the *a* direction. Considering the Coulomb repulsion between anions, this arrangement seems to be very unusual. In fact, (BETS)$FeBr_4$ has a completely different molecular arrangement, despite

that the 2:1 salts of $(BETS)_2FeBr_4$ and $(BETS)_2GaBr_4$ take the isomorphous structures to each other. Band structure calculation gave 2D electron and hole Fermi surfaces. ESR measurements suggested that the spin susceptibility, line width and *g*-value change their temperature dependencies around T_{MI}. The susceptibility increased below T_{MI} shows the low-temperature insulating state to be paramagnetic.

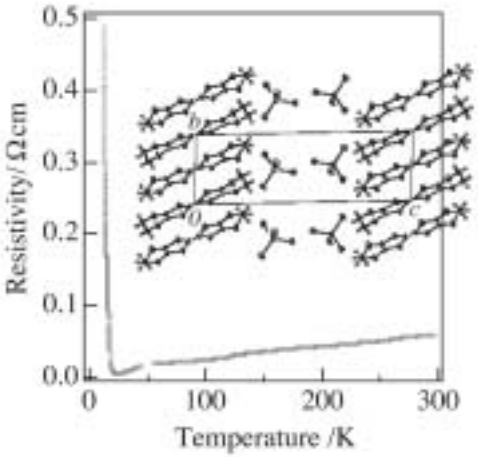

Figure 1. Crystal structure and temperature dependence of resistivity of $(BETS)GaBr_4$.

IV-C-11 High Pressure Effect on Conducting Behavior of an Antiferromagnetic Superconductor κ-$(BETS)_2FeBr_4$

OTSUKA, Takeo; FUJIWARA, Hideki; KOBAYASHI, Hayao; FUJIWARA, Emiko[1]; KOBAYASHI, Akiko[1]
([1]Univ. Tokyo)

κ-$(BETS)_2FeBr_4$, were found to show a unique successive phase transition from paramagnetic metal to antiferromagnetic metal to antiferromagnetic superconductor with lowering temperature. Recently, even the magnetic field induced superconductivity was discovered around 12.5 T. In order to acquire the key to solve the mechanism of these unique electro-magnetic properties, we measured the conduction behavior of this complex under high pressure.

At ambient pressure, a kink anomaly of the resistivity was observed at 2.4 K which is related with the Néel order of Fe^{3+} moments. Resistivity decrease at 1.4 K corresponds to the onset of superconducting phase transition. The pressure dependencies of T_N and T_C (onset) are summarized in Figure 1. The gradual increase of T_N could be attributed to the contraction of the lattice, which will be consequent on the increase of the magnetic interactions. On the other hand, the T_C decreases with increasing pressure, and around 3.5 kbar sharply shifted off lower than 0.6 K, which is the lowest measurement temperature. It is normal that the superconducting phase is suppressed by pressure, because of the stabilization of metallic state at high pressure. Although our preliminary experiments up to 15 T could not find the onset of reentrant field-induced superconducting state, the high-pressure resistivity behaviors under magnetic field will be informative for the understanding of the superconductivity of this unique *d*-π system.

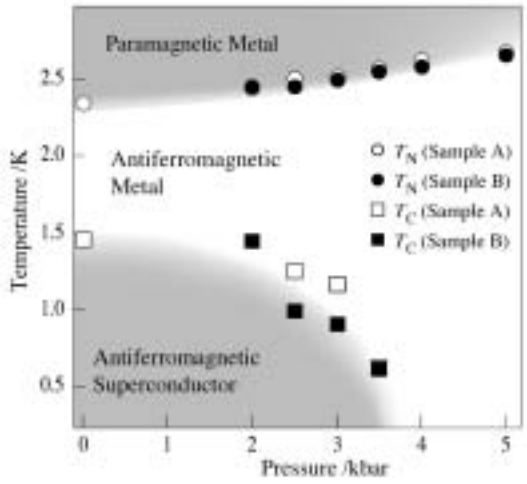

Figure 1. Pressure-temperature phase diagram of κ-$(BETS)_2FeBr_4$.

IV-D Development of Multi-Functional Porous Molecular Materials

The synthesis of new materials with new functions is the most important driving force for advancing molecular material sciences. The molecules are the smallest functional units of the materials and have been regarded as suitable building brocks for the bottom-up construction of multifunctional nano-systems. Recently, a large interest seems to be concentrated to the development of new functional molecular systems. Though increasing numbers of various intriguing molecular conducting systems such as molecular wires, atomic wires embedded in nano-porous molecular materials, molecular wire junctions and even DNA have been reported recently, there seems to be many systems whose underlying sciences seem to be very ambiguous. On the other hand, physics and chemistry of the bulk systems with typical electronic functions such as molecular superconductors and molecule-based magnets have been intensively studied in the last two decades. The *bi*functional molecular systems such as magnetic organic conductors have been developed by combining π donor molecules responsible for the electron conduction and magnetic anions, from which novel molecular systems exhibiting remarkable electro-magnetic properties such as

field-induced superconductivity and switchable superconductivity coupled with metamagnetism of the anion part, have been discovered recently. However, an innovative progress seems to be needed for further studies on the traditional molecular conducting systems. The recent progress in the development of the supramolecular systems seems to suggest a way to develop completely new types of multi-functional molecular systems. Nanoporous supramolecular systems have aroused rapidly growing interest because of their abilities on the constructions of potential hydrogen storage materials, gas sensors, molecular nano-devices, *etc*. We have recently launched to try to develop new molecular systems with multi-functionality by combining nano-porous frameworks and suitable guest molecules.

IV-D-1 Manganese(II)-Formate–a 3D Porous Homometallic Ferrimagnetic Diamond Network with Nodes of Mn-Centered $MnMn_4$ Tetrahedron

WANG, ZheMing; ZHANG, Bin; FUJIWARA, Hideki; KOBAYASHI, Hayao; KURMOO, Mohamedally[1]
([1]Inst. Physique Chimie Matériaux Strasbourg)

[*Chem. Commun.* in press]

Microporous coordination framework solids with high stability have been the focus of intense research activity because of their potential applications, associated with the porosity, in many fields. Chemists have been trying to add functionalities in addition to the porosity, such as magnetism, to these materials; thus new multifunctional materials are expected. We have examined a new form of metal(II)-formate. The novel 3D porous homometallic ferrimagnets based on manganese(II) with formate as the connector, $[Mn_3(HCOO)_6](CH_3OH)(H_2O)$ **1**, its desolvated form $[Mn_3(HCOO)_6]$ **2**, and the dioxane-inclusion compound **3**. Formic acid is the smallest and simplest carboxylic acid. It can form either a one-atom or a three-atom connector. The materials show a highly stable, unprecedented diamondoid framework based on octahedrally coordinated Mn-centered $MnMn_4$ tetrahedral nodes, and display porosity for guest exchange and 3D long-range magnetic ordering. At room temperature, **1** has a χT value of 12.41 cm^3Kmol^{-1}. The behavior is that of a ferrimagnet, with a minimum in χT at 21 K. The minimum χT reaches 6.53 cm^3Kmol^{-1} at 21 K then gradually rises to 12.24 cm^3Kmol^{-1} at 11.5 K. After that it rises sharply to the maximum of 374.4 cm^3Kmol^{-1} at 7.0 K. This work demonstrates a new, simple and easy approach to obtain magnetically porous materials.

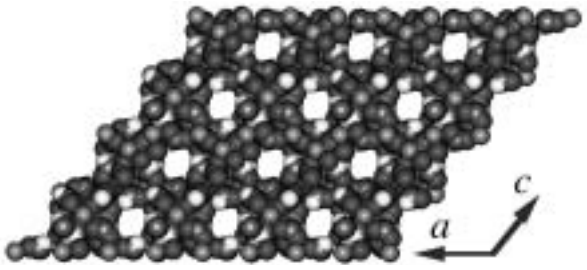

Figure 1. The space filling view of the framework with empty channels. The channels are occupied by methanol and water in **1** or dioxane in **3**.

IV-D-2 Magnetic Coordination Network Embedded in Polyiodide Matrix

WANG, ZheMing; ZHANG, Bin; OTSUKA, Takeo; FUJIWARA, Hideki; KOBAYASHI, Hayao; FUJIWARA, Emiko[1]; YAN, Chunhua[2]
([1]Univ. Tokyo; [2]Peking Univ.)

Crystal engineering of coordination networks has become a rapidly developing research area because of its importance in fundamental research and producing novel smart materials. Various bridging ligands have been employed to construct coordination networks. When they are neutral, the resultant networks are positive. Thus counter charged parts, *i.e.*, anions, coordinating directly to metal ions or acting as guest, are necessary to keep the whole system neutral, which have a strong influence on determining the structures of the produced network. Sometimes, the positive coordination networks can provide temprates for the formation of anion frameworks to produce, for example, novel organic-inorganic hybrid materials). However, to the best of our knowledge, polyiodides, a class of interesting and unique anionic species, have never been introduced in the crystal engineering of coordination networks.

In this work, we employ 4,4'-bipyridine-N,N'-dioxide (dpdo) to build the first series of architectures with positive coordination network and polyiodide, $[M(dpdo)_3](I_7)_2$, **1**, **2**, **3**, and **4** for M = Mn, Co, Ni, and Zn respectively, and examined their unusual structural and magnetic properties. All the compounds are isomorphic. As expected, the structure is composed of positive three-dimensional coordination network $[M(dpdo)_3{}^{2+}]_\infty$ of six-connected M nodes and the heptaiodide I_7^- anions. The Mn, Co, and Ni compounds show weak ferromagnetism due to anti-symmetric exchange interaction between magnetic metal ions. The critical temperatures, T_c's, are 5.7, 4.8 and 8.2 K for **1**, **2** and **3**, respectively. Thus, we have successfully developed a series of new magnetic and non-magnetic compounds by the assembly of positive coordination network with polyiodide through the concept of crystal engineering. The compounds with M^{2+} ions (M = Mn, Co, Ni) exhibit not only unusual structural characteristics, *i.e.*, the interwoven of 3D coordination network with polyiodide matrix, but also weak ferromagnetism.

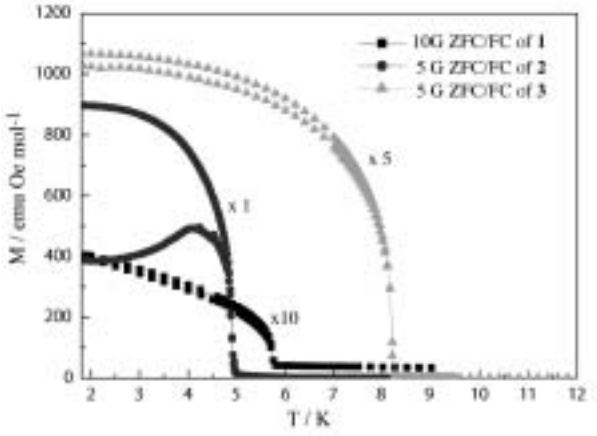

Figure 1. Zero-field (ZFC) and field-cooled (FC) *M-T* under low-field for **1**, **2** and **3**.

IV-E Control of Electronic States in Molecular Conductors with Chemical and Physical Methods

The electronic state of the molecular conductor is quite sensitive to molecular arrangement and orientation that are governed by the inter-molecular interaction. Design of the inter-molecular interaction is indispensable in the rational development of molecular conductors to still higher forms. An introduction of supramolecular chemistry is a possible solution to this problem. We have developed various molecular conductors containing supramolecular assemblies based on two types of supramolecular interactions, the iodine-based halogen bond and the tellurium-based secondary bond. It has been demonstrated that the supramolecular interaction has the ability to tune the molecular arrangement and orientation and thus provides a route for the formation of novel molecular materials.

On the other hand, the electronic state of molecular conductors can be quite sensitive to the pressure (including chemical pressure) application. Recent development of the uniaxial stress and strain methods has enabled selective or anisotropic regulation of the inter-molecular interaction and has provided a powerful means to search for novel electronic states. We have examined the uniaxial strain effect and have found unusual electronic states in the organic narrow-gap semiconductor, the supramolecular conductor, and the two-dimensional strongly correlated system based on the metal dithiolene complex.

IV-E-1 Structural and Physical Properties of New Conducting Cation Radical Salts with Te-Based Counter Anions, Tetraiodotellurate(II) and Hexaiododitellurate(II)

FUJIWARA, Masahiro[1]; TAJIMA, Naoya[2]; IMAKUBO, Tatsuro[2]; TAMURA, Masafumi[2]; KATO, Reizo
([1]Univ. Tokyo; [2]RIKEN)

[*J. Solid State Chem.* **168**, 396–407 (2002)]

We have prepared and characterized several cation radical salts of organic donors (TMTTF, EDT-TTF, ET, BETS and HMTSF; scheme) with two novel planar Te-based dianions, TeI_4^{2-} and $Te_2I_6^{2-}$. $(ET)_5Te_2I_6$ **1** and $(BETS)_5Te_2I_6$ **2** are isostructural. In these $Te_2I_6^{2-}$ salts, intermolecular short I···I contacts form a supramolecular corrugated anion sheet (Figure 1a). Donor arrangement is similar to the α-type (Figure 1b). With lowering temperature, the resistivity of **1** shows a gradual increase followed by a sharp upturn at 110 K. **2** is metallic down to 120 K and shows a gradual increase of the resistivity followed by a clear transition to an insulating state around 60 K. Crystal structure of $(ET)_4TeI_4$ **3** is based on the "herring bone" arrangement of ET molecules similar to the α-type. **3** shows a semiconductive behavior around room temperature followed by a transition to an insulating state at 210 K. $(EDT\text{-}TTF)_4TeI_4$ **4**, a semiconductor, exhibits a unique two-dimensional arrangement of dimerized EDT-TTF molecules.

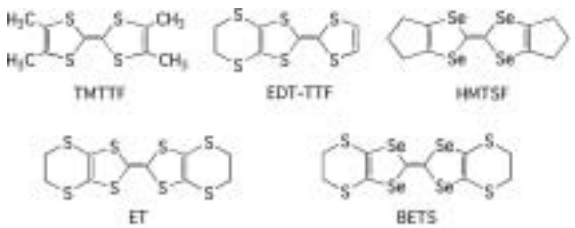

Scheme 1. Molecular structures of organic donors used in this work.

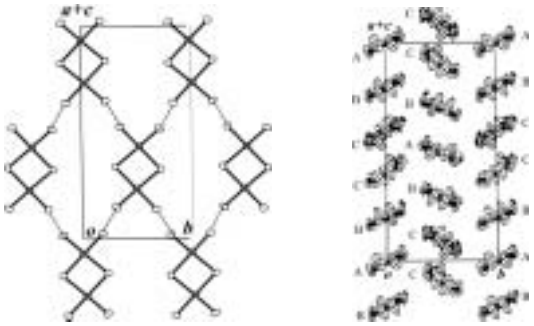

(a) (b)

Figure 1. Crystal structure of **1**: a) $Te_2I_6^{2-}$ anion network. b) end-on projection of ET molecules.

IV-F Electronic and Magnetic Properties of π-Electron-Based Molecular Systems

π-electrons are an interesting building block in architecting functionalized electronic and magnetic molecular systems. We have focused on nano-sized graphite and TTF-based organic charge transfer complexes, in which π-electrons play an important role, in developing new types of molecular electronic systems. In nanographene, single layer nanographite, which is defined as flat open π-electron system having edges and contrasted to closed π-electron systems of fullerenes and carbon nanotubes, non-bonding π-electronic state appearing around the Fermi level generates unconventional nanomagnetism. We have found an interesting magnetic switching effect in a nanographite network operated by water-adsorption/desorption processes. A combination of TTF-based π-electron donor and counteranion having localized spins is a useful way in producing molecular magnetic conductors, which are expected to have properties different from traditional metal magnets featured with *s-d* interaction. Under this scheme, we have developed a new class of TTF-based organic magnetic conductors. The interaction between the conducting π-electrons of donors and the localized *d*-electrons of magnetic anions are found to show interesting interplay between magnetism and electron transport.

IV-F-1 Drastic Effect of Water-Adsorption on the Magnetism of Carbon Nanomagnets

SATO, Hirohiko[1]; KAWATSU, Naoki[1]; ENOKI, Toshiaki; ENDO, Morinobu[2]; KOBORI, Ryoji[3]; MARUYAMA, Satoshi[3]; KANEKO, Katsumi[3]
([1]Tokyo Inst. Tech.; [2]Shinshu Univ.; [3]Chiba Univ.)

[*Solid State Commun.* **125**, 641–645 (2003)]

Activated carbon fibers (ACFs), composed of nanometer-size fragments of graphite (nanographites), show π-electron-based paramagnetism. Measurements of ESR and magnetic susceptibility revealed that adsorption of water molecules drastically suppresses the paramagnetism of ACFs. Considering also the structural change, this is interpreted in terms of a crossover from a paramagnetic state to a low-spin state of each nanographite due to a structural change of nanographite-network caused by internal pressure of adsorbed water molecules. This phenomenon serves us as a new method for in situ controlling of the condensed state of electrons in soft materials.

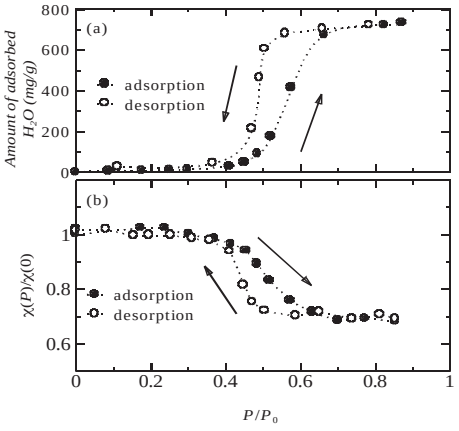

Figure 1. (a) Water adsorption isotherm of ACFs at room temperature, (b) adsorption dependence of the spin susceptivility obtained by ESR measurements. $P_0 \approx 20$ Torr is the saturation pressure of water at room temperature. The spin susceptibilities, $\chi_{spin}(P)$, were calculated from the peak heights and the line widths.

IV-F-2 Ferromagnetic Interaction and Metallic Conductivity of Radical Ion Salts (DIEDO)$_2$M(mnt)$_2$ (M = Ni, Pt)

NISHIJO, Junichi[1]; OGURA, Eiji[2]; YAMAURA, Jun-ichi[3]; MIYAZAKI, Akira[1]; ENOKI, Toshiaki; TAKANO, Takahiko[2]; KUWATANI, Yoshiyuki[2]; IYODA, Masahiko[2]
([1]Tokyo Inst.Tech.; [2]Tokyo Metropolitan Univ.; [3]Univ. Tokyo)

[*Synth. Met.* **133-134**, 539–541 (2003)]

(DIEDO)$_2$M(mnt)$_2$ (M = Ni, Pt; DIEDO = 4,5-diiodo-4',5'-ethylenedioxytetrathiafulvalene; mnt: maleonitriledithiolate) composed of transition metal complexes and iodine-bonded donor have a unique structure featured with strong coordination-bond-like interaction between iodo group of donor and cyano group of anion. It consists of two donor chains sandwiched between anion chains. The salts are metallic down to 100 K, followed by an onset of a metal-insulator (M-I) transition. T_{MI} becomes lowered at high pressures (21 K at P > 11 kbar). The magnetic susceptibility suggests the presence of ferromagnetic interactions ($J \sim 20$ K) between localized magnetic moments of M(mnt)$_2^-$, which interact with conduction electrons. The origin of ferromagnetic interactions is explained by McConnell's first model and small overlaps between SOMOs of M(mnt)$_2^-$.

IV-F-3 Crystal Structure and Physical Properties of (EDS-TTF)$_2$FeBr$_4$

MIYAZAKI, Akira[1]; ENOKI, Toshiaki[2]
([1]Tokyo Inst. Tech.; [2]IMS and Tokyo Inst. Tech.)

[*Synth. Met.* **133-134**, 543–545 (2003)]

Crystal structure, transport and magnetic properties of (EDS-TTF)$_2$FeBr$_4$ (EDS-TTF: ethylenediselenotetrathiafulvalene) are reported. Between one-dimensional columns of donors and quasi square-lattices of FeBr$_4$ anions, close Br···Se van der Waals contacts and CH···Br type hydrogen bonds are observed. This salt

shows high room-temperature conductivity and metal-insulator transition at *ca.* 250 K (σ_{RT} = 400 S cm^{-1}, E_A = 380 K). The magnetic susceptibility obeys the Curie-Weiss law (C = 4.58 emu K mol^{-1}, Θ = –0.9 K) without showing any magnetic transition down to 1.8 K. The weak π-*d* interaction can be due to the small contribution of Se 4*p* orbitals to the HOMO of EDS-TTF.

IV-F-4 Unconventional TTF-Based Molecular Magnets

ENOKI, Toshiaki; YAMAZAKI, Hisashi[1]; OKABE, Kazuki[1]; ENOMOTO, Kengo[1]; KATO, Takehiko[1]; MIYAZAKI, Akira[1]; OGURA, Eiji[2]; KUWATANI, Yoshiyuki[2]; IYODA, Masahiko[2]
([1]Tokyo Inst.Tech.; [2]Tokyo Metropolitan Univ.)

[*Synth. Met.* **133-134**, 296–272 (2003)]

Unconventional magnetic features are reported in charge-transfer complex-based molecular magnets. Quasi-1D metals $(DMET)_2FeBr_4$, $(EDTDM)_2FeBr_4$ and semiconductor $(EDS\text{-}TTF)_2FeBr_4$ are isostructural with alternating stacking of donor π-electron conducting sheets and square lattice *d*-spins of $FeBr_4^-$ anion sheets. The former two undergo an SDW transition at 15–40 K. For $(DMET)_2FeBr_4$, the magnetoresistance is strongly affected by Fe^{3+} spin arrangement, suggesting strong π–*d* interaction. Quasi-1D metal $(EDO\text{-}TTFBr_2)_3I_3$ undergoes an MI transition around T_{MI} ~ 150 K. The susceptibility is featured with 1D antiferromagnetic (AF) system with fractional magnetic moments. It takes a 3D AF ordered state below T_N = 15 K. The co-existence of metallic conduction and localised moments evidences features of strongly correlated electron system in the MI boundary.

IV-F-5 Novel π-*d* Interaction System $(DMET)_2FeCl_4$

ENOMOTO, Kengo[1]; MIYAZAKI, Akira[1]; ENOKI, Toshiaki[2]
([1]Tokyo Inst. Tech.; [2]IMS and Tokyo Inst. Tech.))

[*Synth. Met.* **135-136**, 561–562 (2003)]

The structure of $(DMET)_2FeCl_4$ is featured with an alternate stacking of quiasi-1D chain-based donor sheets and magnetic Fe^{3+} (S = 5/2) sheets. At ambient pressure, the salt shows metallic behavior down to ~ 100 K with the pressure of a resistivity anomaly around 7 K, at which the susceptibility has a broad maximum of magnetic short-renge ordering in the Fe^{3+} magnetic sheet of *d*-electrons. An antiferromagnetic transition takes place at T_N = 2.8 K. The large Weiss temperature Θ = –11 K and the field dependant anomalies in the magnetoresistance, which indicate the presence of a strong antiferromagnetic interation, suggest that the donor π-electrons mediate the interlayer interaction between the Fe^{3+} magnetic layers.

IV-F-6 Novel Magnetism of EDO-$TTFX_2$ Salts (X = Br, I),

ENOKI, Toshiaki; YAMAZAKI, Hisashi[1]; NISHIJO, Junichi[1]; UGAWA, Kouhei[2]; OGURA, Eiji[2]; KUWATANI, Yoshiyuki[2]; IYODA, Masahiko[2]; SUSHKO, Yuri V.[3]
([1]Tokyo Inst. Tech.; [2]Tokyo Metropolitan Univ; [3]Univ. Kentucky)

[*Synth. Met.* **137**, 1173–1174 (2003)]

Charge transfer complexes of EDO-$TTFX_2$(X = Br, I) form low-D structures featured with coordination-like bond formation of *X* with counter anions, giving unconventional magnetic conductive systems with magnetic anions. $(EDO\text{-}TTFI_2)_2M(mnt)_2$(M = Pt, Ni) are 1D conductors interacting with ferromagnetic 1D $M(mnt)_2$ chains. Applying pressure gives a unique ferromagnetic domain formation, 2D $(EDO\text{-}TTFBr_2)_2\text{-}FeBr_4$ is metallic, where 1D $FeBr_4$ chains taken an antiferromagnetic transition at a very high T_N(= 13.5 K) with a short-range-order effect around the resistivity minimum (30 K), suggesting the pressure of strong π-*d* interaction.

IV-F-7 Electronic and Magnetic Properties of Organic Conductors $(DMET)_2MBr_4$ (M = Fe, Ga)

ENOMOTO, Kengo[1]; YAMANAKA, Jun-Ichi[2]; MIYAZAKI, Akira[1]; ENOKI, Toshiaki
([1]Tokyo Inst. Tech.; [2]Univ. Tokyo)

[*Bull. Chem. Soc. Jpn.* **76**, 945–959 (2003)]

$(DMET)_2MBr_4$ (M = Fe, Ga) are isostructural organic conductors whose crystal structure consists of an alternate stacking of quasi one-dimensional chain-based donor layers and anion square lattices. The resistivity, ESR, magnetic susceptibility, magnetization, and magnetoresistance of these salts were investigated in order to clarify the correlation between the electronic structure and the magnetism. The electronic structures of both salts are metallic down to T_{MI} ~ 40 K, below which a Mott insulating state is stabilized, accompanied by an SDW transition at T_{SDW} ~ 25 K. The $FeBr_4$ salt with Fe^{3+} (S = 5/2) localized spins undergoes an antiferromagnetic transition at T_N = 3.7 K. In the $FeBr_4$ salt, the magnetization curves, which show field-direction-dependent anomalies in addition to a spin-flop transition, are demonstrated to have a participation of donor π-electron spins in the magnetization processes. The field dependence of the magnetoresistances below T_N tracks faithfully that of the magnetization, where the donor π-electrons and Fe^{3+} *d*-electrons are responsible for the former and the latter, respectively. This clearly demonstrates the presence of the π-*d* interaction that plays an important role in the interplay between electron transport and magnetism.

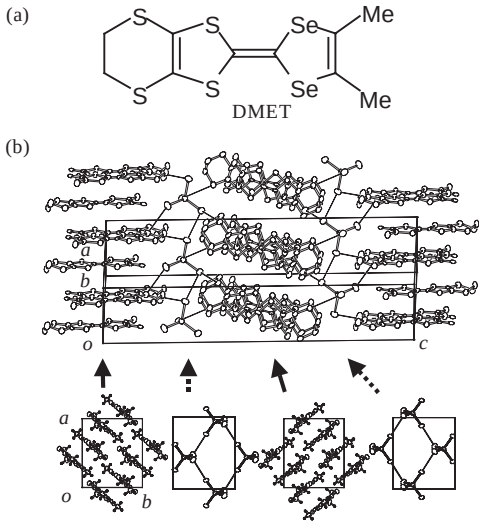

Figure 1. (a) Molecular structure of DMET donor. (b) The crystal structure of $(DMET)_2FeBr_4$. Cross sectional views of donor and anion layers are drawn. Solid lines in the both figures denote close intermolecular B···S and Br···Br contacts.

IV-F-8 Structure and Electronic Properties of a Nongraphitic Disordered Carbon System and Its Heat-Treatment Effects

TAKAI, Kazuyuki[1]; OGA, Meigo[1]; SATO, Hirohiko[1]; ENOKI, Toshiaki; OHKI, Yoshimasa[2]; TAOMOTO, Akira[2]; SUENAGA, Kazutomo[3]; IIJIMA, Sumio[3]
([1]Tokyo Inst. Tech.; [2]Matsushita Electric Industrial Co., Ltd.; [3]Meijo Univ.)

[*Phys. Rev. B* **67**, 214202 (11 pages) (2003)]

The heat-treatment effect on electronic properties is investigated in relation to structural change for pulsed-laser-deposited amorphous carbon thin films having sp^2/sp^3 ratio ≈ 9. The heat treatment at temperatures 200–400 °C increases conductivity and modifies the hopping conduction mechanism at low temperatures, resulting in the generation of a Coulomb gap at E_F. This is attributed to the heat-treatment-induced modification of the disorder nature of the structure from atomic-scale sp^2/sp^3 disorder to a disordered graphitic sp^2-domain network by the migration of sp^3 defects. In the heat-treatment temperature region above 600 °C, where the structure is featured with graphitic sp^2 domains, considerably small positive thermoelectric power is suggestive of carrier compensation by the competition of hole and electron carriers that originate from the inhomogeneous charge distribution caused by the difference of Fermi levels among graphitic sp^2 domains. In the high-heat-treatment-temperature region 800–1100 °C, the formation of an infinite percolation path network of the graphitic sp^2 domains induces an insulator-to-metal transition, where the electron transport in the sp^2-rich metallic state is featured by weakly temperature-dependent conductivity with majority hole and minority electron carriers.

IV-G Development of Molecular Materials Containing Photo-Reactive Species

The molecular materials are considered to be good candidates for advanced functional materials such as (nano-)devices. Their outstanding advantages include the wide variety of substances, possibility of molecular-level fine design, softness of lattices and unique and varied crystal structures. On the other hand, the physical properties of the molecular materials significantly depend on their crystal structures. The crystal structures are, however, not predictable or controllable thus far. Sometimes a pair of molecular materials with very similar crystal structures to each other exhibit qualitatively different physical properties for various or unknown reasons. Additionally many of the molecular charge-transfer salts are very difficult to change their Fermi level by standard methods of doping. Consequently one can hardly choose an appropriate molecular crystal which has favorable physical properties (band-filling) and a crystal structure with an enough good quality and sufficient size for study or other practical purposes. If one can obtain molecular radical salts with a photo-redox-reactive species, one could dope it by irradiation of light (permanent photo carrier injection) without unexpected structural change using solid state in situ reaction. In order to pursue a new possibility of molecular materials, we have started to develop molecular radical salts with photo-reactive species.

IV-G-1 Metastable State of MV[Ni(dmit)$_2$]$_2$ (MV = Methyl Viologene, dmit = 1,3-dithiol-2-thione-4,5-dithiolate)

NAITO, Toshio; INABE, Tamotsu[1]
([1]Hokkaido Univ.)

[to be published]

MV[Ni(dmit)$_2$]$_2$ has long attracted a special attention of several different research groups in terms of the strong photo-induced redox ability peculiar to MV. Yet most of the electrical, structural or optical data are based on the powder sample, and few details are known on its physical properties. We have recently obtained the single crystals of this material, and found that there exists a new phase as a metastable state. The fresh single crystals of the title compound exhibited clear metallic conductivity down to 1 K with anomaly below 100 K. The magnetic susceptibility was well described by Pauli paramagnetism with a small anomaly below 100 K corresponding to the electrical behavior. The thermoelectric power was constantly ~ 0 μVK^{-1} from RT–4 K, which is consistent with the fact that this material has a half-filled ("compensated") electronic band strucuture. The crystal consists of mixed stacking of [Ni(dmit)$_2$]$^-$ (A) and MV^{2+} (D) by repeating unit of D–A–A. The intermolecular interactions between A's are very weak but isotropic. This phase could be one of the rare examples of molecular version of naturally occurring (main group) metallic elements in that weak and isotropic inter-site interactions favor the metallic nature against correlation effect. The light irradiation effects on its electrical and magnetic properties are under study.

IV-G-2 Electrical Behavior of UV-VIS Irradiated Ag(DMe-DCNQI)$_2$

NAITO, Toshio; INABE, Tamotsu[1]
([1]Hokkaido Univ.)

[to be published]

The UV-VIS (200–1100 nm) irradiation effect on the electrical behavior of the title compound was examined with its single crystals and clear difference has been found depending on the duration of irradiation. The longer the irradiation time was, the higher RT resistivity it exhibited. The whole temperature-dependence also changed. With irradiation a sudden but small resistivity increase appeared well higher temperature than its original metal-insulator transition (100 K), and this temperature rapidly moved toward room temperature. These irradiation effects has been confirmed to be intrinsic by comparing the results of parallel measurements of non-irradiated samples. The overall behavior can be featured by sum of original bulk behavior (major part) and new metallic behavior with a possible transition at higher temperature (minor part). Further details are now under study.

RESEARCH ACTIVITIES V
Department of Applied Molecular Science

V-A Synthesis of Chiral Molecule-Based Magnets

Construction of molecule-based magnetic materials, which have additional properties such as conductivity or photo reactivity, is now becoming a challenging target. Specific goals aimed for these molecule-based magnets include: i) the ability to design the molecular building blocks and to organize them in the solid for desired dimensionality, ii) the optical transparency. The physical characteristic of current interest involves optical properties, particularly with respect to natural optical activity. When a magnet has optical transparency and chiral structure, the magnetic structure of crystal expects to be a chiral spin structure. These magnets will show an asymmetric magnetic anisotropy and magneto-chiral dichroism. This category of materials don't only have scientific interest but also have the possibility for use in new devices. When we construct chiral molecule-based magnets, chirality must be controlled not only in the molecular structure, but in the entire crystal structure. As a consequence of this difficulty, only few examples of this type of magnet exist. Up to the present reported chiral magnets have low dimensional magnetic structures, the magnetic ordering temperatures are below 10 K. To afford a high-T_C magnet, dimensionality of magnetic structure must be extended in two or three dimension. When we introduce magnetic bricks, which have more than three connections for the construction of magnets, we can expect to make two or three-dimensional magnets. To make high dimensionality molecule-based magnets, we recently discovered using cyano bridged complex with chiral organic ligands.

V-A-1 A Novel Two-Dimensional Chiral Complex; [Cu-II(*R*)-pn]$_2$[Ni-II(CN)$_4$]$_2$·H$_2$O ((*R*)-pn = (*R*)-1,2-Diaminopropane)

IMAI, Hiroyuki; INOUE, Katsuya; OHBA, Masaaki[1]; OKAWA, Hisashi[1]; KIKUCHI, Koichi[2]
([1]Kyushu Univ.; [2]IMS and Tokyo Metropolitan Univ.)

[*Synth. Met.* **137**, 919–920 (2003)]

The synthesis, single crystal X-ray structures and magnetic properties of a new two-dimensional chiral complex; [Cu-II(*R*)-pn]$_2$[Ni-II(CN)$_4$]$_2$·H$_2$O ((*R*)-pn = (*R*)-1,2-diaminopropane), are described. Blue plate crystals of [Cu-II(*R*)-pn]$_2$[Ni-II(CN)$_4$]$_2$·H$_2$O were obtained by the reaction between [Cu(*R*)-pn](SO$_4$) and K$_2$[Ni(CN)$_4$] in H$_2$O-EtOH(1:1). The structures consist of a two-dimensional cyano-metal network as shown in Figure 1 and 2. The temperature dependence of χT is shown in Figure 3. At low temperature χT decreases with lowering temperature. This tendency indicates a weak antiferromagnetic interaction dominates between copper ions. The magnetic susceptibility of this crystals can be reproduced by Curie-Weiss law with the parameters of C = 0.849 emu K mol^{-1} (g = 2.2) and θ = –1.27 K.

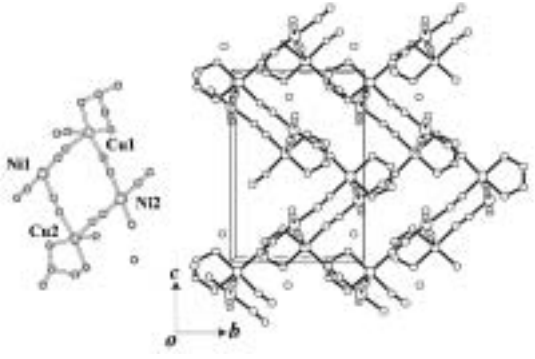

Figure 1. The asymmetric unit of [Cu^{II}(*R*)-pn]$_2$[Ni^{II}(CN)$_4$]$_2$ H$_2$O and the two-dimensional chiral network in the *bc*-plane.

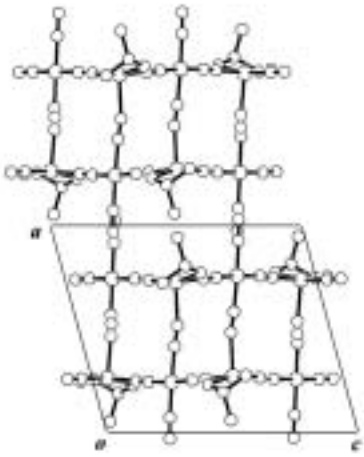

Figure 2. The side view of the two-dimensional sheet along *b*-axis.

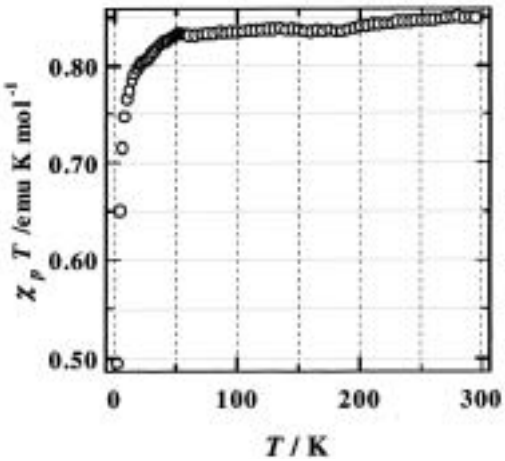

Figure 3. The temperature dependence of the χT.

V-B Hydrothermal Synthesis of Molecule-Based Magnets

Coordination polymers are attracting much interest due to the strength and rigidity of the extended lattices for gas absorption and intercalation and for the connectivity between magnetic ions in designing molecule-based magnets. They belong to a subset of organic-inorganic hybrid materials, and usually employ a central metal ion and a multitopic organic ligands or a coordination complex having ambidentate ligands, such as cyanide and oxalate. In some cases, other organic ligands are used to control the dimensionality or structure. The choice of the metals and of the ligands depends on the desired properties. On the one hand, there is strong interest by scientists studying catalysis and the absorption of gases originating from the possibility of creating structures with cavities, channels or pores and, consequently, large surface areas. On the other hand, there is increasing interest from magneto-chemists due principally to the realization of organizing the magnetic orbitals of the moment carriers to favor a particular magnetic ground state. The field of coordination polymers based on organic radicals is a very active area, indeed. Several ground states have been established and a clear molecular-orbital picture to explain the observations is emerging. For the realizing strong magnetic interaction, it is better to use simple and small organic ligands, such as cyanide or carboxylate ions. The metal complexes with such ligands are usually less solvability. The thermal synthesis is powerful method to make large single crystals for such complexes.

V-B-1 Synthesis and Characterization of One-Dimensional Mixed-Spin Cobalt(II) Metamagnet

OKA, Yoshimi; KUMAGAI, Hitoshi; INOUE, Katsuya

The hydrothermal synthesis, single crystal X-ray analysis and magnetic properties of a one-dimensional mixed-spin Co^{II} Metamagnet, $[Co_4(phcina)_6(OH)_2(H_2O)_4]\cdot 2H_2O$ (phcina = alpha-phenylcinnamate), is described. Pink needle crystals of $[Co_4(phcina)_6(OH)_2(H_2O)_4]\cdot 2H_2O$ was obtained at 120 °C. The x-ray structure analysis of **1** revealed the formation of 1-D chain along the *c*-crystal axis. (Figure 1 and 2). The asymmetric unit consists of two distorted octahedral Co^{II} ions (Co(1), Co(3)) and two octahedral Co^{II} ions (Co(2), Co(4)). Co(2) and Co(4) exhibit octahedral geometry comprising of three oxygen atoms of phcina ligands, one hydroxide and two waters. The O–Co–O bond angles in the $\{CoO_6\}$ octahedral site range from 81.37(8) ° to 98.18(10) ° and bond distances range from 2.029(2) to 2.163(3) Å (*av*. 2.10 Å). These values are similar to that found in octahedral Co^{II}(HS) complexes. In contrast, Co(1) and Co(3) exhibit distorted octahedral geometry, pseudo C_{4v} symmetry comprising of three oxygen atoms of phcina ligands, two hydroxides and one water. Co(1) has O(2), O(7), O(9) and O(15) in the basal plane and these O–Co(1)–O angles range from 82.16(10) ° to 94.37(10) °. These configurations are similar that found in Co^{II}(LS) complexes. The nearest intermetallic separation between Co···Co along*b*-axis is 3.095(2) Å and that along *a*-or *c*-axis is more than 14.406(4) Å. Figure 3 shows the temperature dependence of the magnetic susceptibility, the product of susceptibility and temperature and inverse susceptibility. The χT value is 9.87 emu K mol^{-1} at 300 K and reaches a local minimum at 35 K (7.18 emu K mol^{-1}) and then rapidly increases. The effective magnetic moment (μ_{eff}) per four cobalt ions is 9.87 μ_B at room temperature which is consistent with that expected for four Co^{II}(HS) ions. It is indicative that the value 7.58 μ_B of μ_{eff} at 35 K is assigned to two distorted octahedral Co^{II}(LS) and two octahedral Co^{II}(HS) ions, this complex shows gradual spin-crossover behavior of Co^{II} with C_{4v} symmetry and orbital contribution through spin-orbit coupling of octahedral Co^{II} ions as temperature increases. High-spin Co^{II} ions and low-spin Co^{II} ions interact ferrimagnetically and ferrimagnetic chains interact antiferromagnetically below T_N = 5.5 K. (Figure 4)

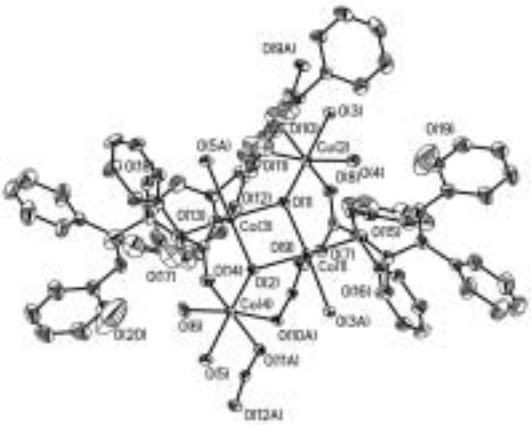

Figure 1. X-ray crystal structure of **1**.

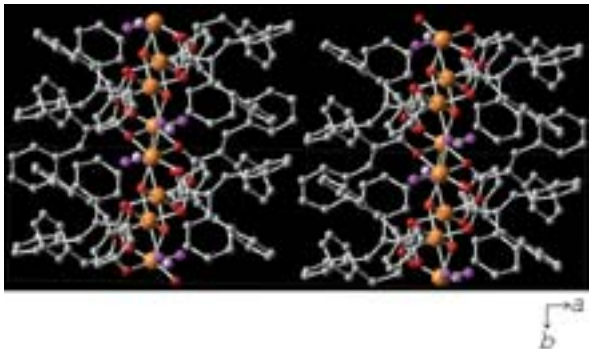

Figure 2. Packing diagram of the 1-D chain compound **1** along *c*-axis. Orange, red, dark red, purple, pink and gray represented Co, O(hydroxo), O(carboxylate), O(coordinated water), O(crystal water) and C, respectively.

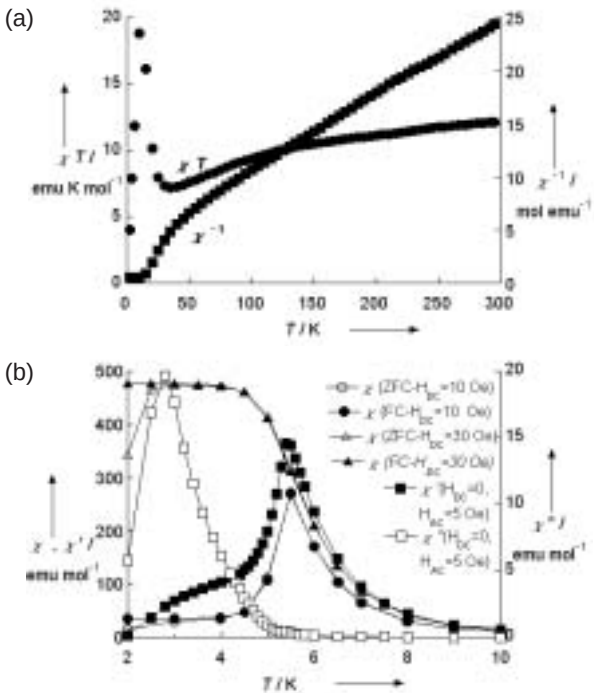

Figure 3. (a) Magnetic susceptibility of randomly oriented polycrystalline sample represented as χT and χ^{-1} per 4 Co ions. The applied field was 5 kOe. (b) Temperature dependence of the magnetic susceptibilities per 4 Co ions for oriented polycrystalline sample along *b*-axis. The applied DC field was 10 Oe and 30 Oe, and ZFC and FC refer to zero-field cooled and field-cooled, respectively. AC magnetic susceptibilities are also shown when applied DC field is 0 with AC field of 5 Oe and AC frequency of 1 Hz.

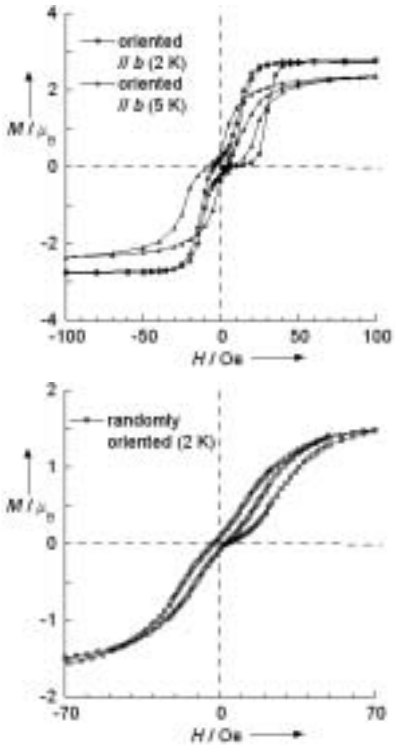

Figure 4. (a) Hysteresis loops for oriented polycrystalline sample along *b*-axis at 2 K and 5 K. (b) Hysteresis loop for randomly oriented sample at 2 K. Magnetic field was up to 70 kOe and magnetization values per 4 Co ions are shown.

V-B-2 Hydrothermal Synthesis, Structure and Magnetism of Square-Grid Cobalt(II)-Carboxylate Layered Compounds with and without Pillars

KUMAGAI, Hitoshi[1]; OKA, Yoshimi; INOUE, Katsuya; KURMOO, Mohamedally[2]
([1]IMS and Inst. Phys. Chem. Materials Strasbourg, France; [2]Inst. Phys. Chem. Materials Strasbourg, France)

[*J. Chem. Soc., Dalton Trans.* 3442–3446 (2002)]

The hydrothermal synthesis, single crystal X-ray structures and magnetic properties of two layered cobalt(II)-carboxylate complexes, $[Co^{II}(H_2O)_2(O_2C\text{-}CHCHC_6H_5)_2]$ (**1**) and $[Co^{II}(H_2O)_2(O_2CCHCHC_6H_4CO_2)_{2/2}]$ (**2**), are described. Pale red crystals of $Co(H_2O)_2L_2$, L = trans-cinnamate ($C_9H_7O_2^-$) (1) or L_2 = 4-carboxycinnamate($C_{10}H_6O_4^{2-}$) (**2**), were obtained at 120 °C. The structures consist of square-grid 2D-coordination polymeric sheets, ⋯–OCO–$Co(H_2O)_2$–OCO–$Co(H_2O)_2$–⋯, separated by C_6H_5–CH=CH– for (**1**) or pillared by –C_6H_4–CH=CH– for (**2**). (Figure 1, 2 and 3) The magnetism was studied as a function of temperature and magnetic field. In both cases the magnetic moment decreases on lowering the temperature due to spin-orbit coupling and no interaction between cobalt ions. The data can alternatively be fitted to an unrealistic quadratic layer model for S = 3/2 without taking into account the effect of spin-orbit.

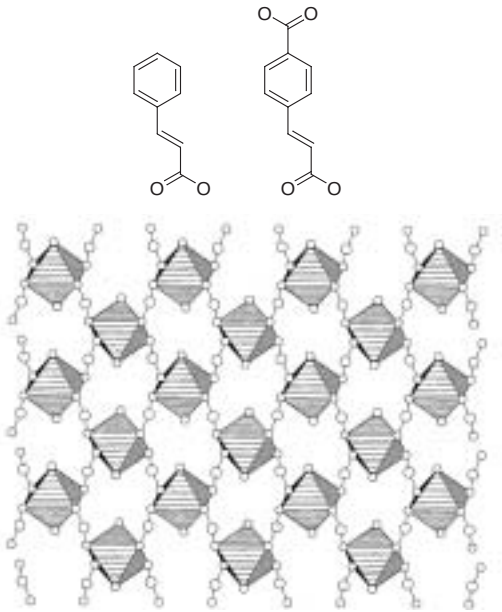

Figure 1. Crystal structure of **1** and **2** along *a* axis.

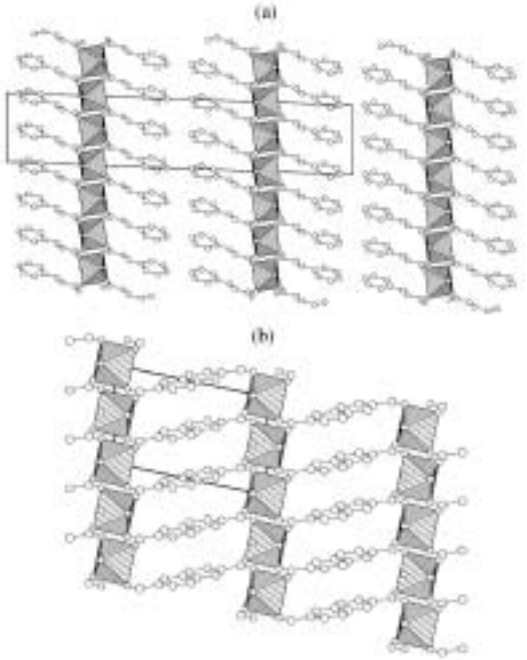

Figure 2. View of the *ab* plane arrangement of the organic backbone in the galleries in **1** (a) and **2** (b).

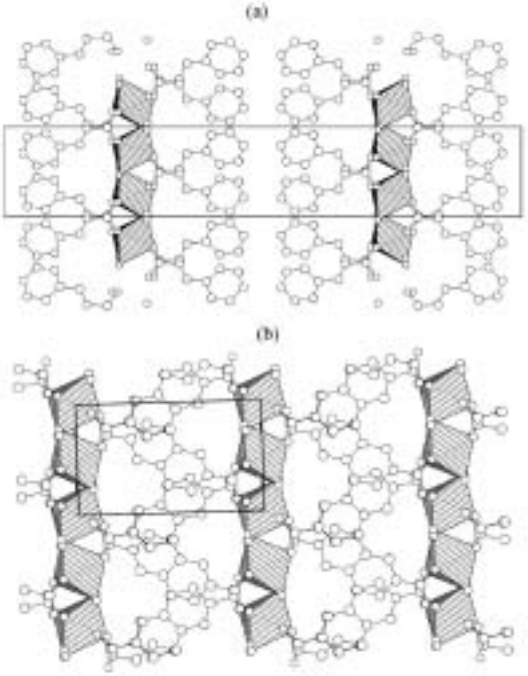

Figure 3. View of the *ac* plane arrangement of the organic backbone in the galleries in **1** (a) and **2** (b).

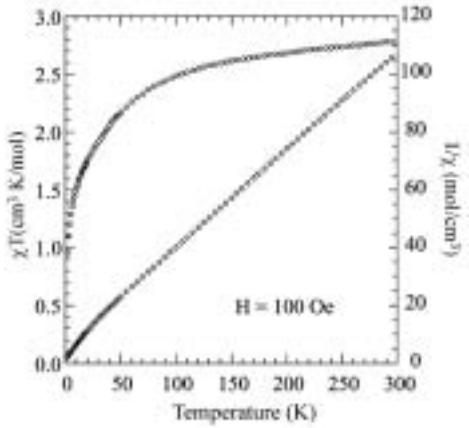

Figure 4. Temperature dependence of the product of susceptibility and temperature (circles) and the inverse susceptibility for **2** (diamonds).

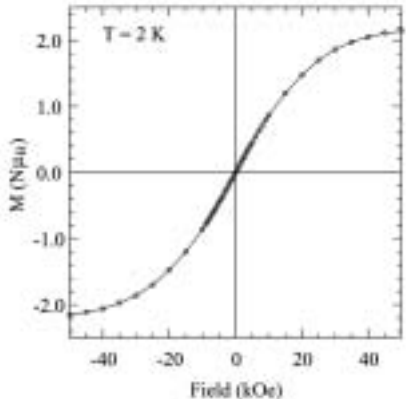

Figure 5. Isothermal magnetization of **2** at 2 K; line is a guide to the eye.

V-C Nano-Structure in Metal Oxides Prepared by Synchrotron Radiation and Swift Heavy Ions

In the project, micro-nano fabrication technique for metal oxide has been examined. The first one is the deep x-ray lithography and the liquid phase deposition method. Periodic arrangements of titanium dioxide (TiO_2) micro structure projections were fabricated in a supersaturated aqueous solution using ordered microcavities of poly(methylmethacrylate) as a template. The shape and periodicity of the TiO_2 projections were strictly controlled with the depth and arrangement of the cavities because crystalline TiO_2 was uniformly grown on the organic surface through heterogeneous nucleation. This biomimetic route is applicable to designed synthesis of three-dimensional architectures for photonic structures of various metal oxides. The other method is by using of the latent tracks introduced by the swift heavy ion. Micro structure having nano-order flatness was achieved after chemical etching. This method can be applied to create photonic crystal structure of titanium dioxide.

V-C-1 Nano/Micro-Structure in Metal Oxides Prepared by MeV Ions, Laser and Synchrotron Radiation

AWAZU, Koichi[1]; FUJIMAKI, Makoto[2]
([1]IMS and AIST; [2]AIST)

[*Handbook of Organic-Inorganic hybrid materials and Nanocomposites*, American Scientific Publishers, Chapter K, pp.1–29 (2002)]

As semiconductor device dimensions are scale down, there is also a parallel trend to minimized mechanical components and integrate these micro-mechanical components. Microelectronic devices to form micro-electro-mechanical systems (MEMS) and photonic crystals are typical examples. Especially, there has been increasing interest in photonic crystals in which the refractive index changes periodically. Various important scientific and engineering applications, such as control of spontaneous emission, sharp bending of light, trapping of photons, *etc*., may be realized by creating photonic band-gap. Recently, a few semiconductors like Si, InP, GaAs, and GaP have been shown to exhibit micrometer-size pores. However, it might be too difficult to use photonic crystals of semiconductors in the photonic network. Firstly, it is impossible to connect regular optical waveguide to semiconductor with low optical transmission loss because of the difference of refractive index. Reflection between photonic crystal of semiconductor and regular optical waveguide will cause the loss of light power. One of the most attractive application for photonic crystal is the super-prism effect. This is the reason why photonic crystal draws our attention as the substitute of arrayed wavelength grating (AWG). However, thermal expansion coefficient of semiconductor is too large to use in a conventional atmosphere. In contrast, thermal expansion coefficient in some ceramics is known as almost zero. For example, thermal expansion coefficient values of silicon, TiO_2 and $94SiO_2$:$6TiO_2$ are 7×10^{-6} /K, 7×10^{-7} /K, $\sim 0 \times 10^{-7}$ /K, respectively. In other words, photonic crystals of semiconductor must be used under constant temperature precisely controlled. Photonic crystal as well as AWG would lose the reliability when they must be used at a constant temperature. This is the second reason for why photonic crystals of semiconductor are hard to use as a photonic network device. A material having very low thermal expansion coefficient as well as a refractive index in the vicinity of 1.45 must be the best material for photonic crystal. We know that photonic crystal made of SiO_2:GeO_2 or SiO_2:TiO_2 materials would be satisfied such aspects, yet we do know little about micro (nano) fabrication technique for ceramics.

In the present review, periodic arrangements of titanium dioxide (TiO_2) micro projections were fabricated in a supersaturated aqueous solution using ordered microcavities of poly(methylmethacrylate) as a template. The shape and periodicity of the TiO_2 projections were strictly controlled with the depth and arrangement of the cavities because crystalline TiO_2 was uniformly grown on the organic surface through heterogeneous nucleation. This biomimetic route is applicable to designed synthesis of three-dimensional architectures for photonic structures of various metal oxides.

V-C-2 Structure of Latent Tracks Created by Swift Heavy Ions in Amorphous SiO_2 and Zinc Phosphate Glass

AWAZU, Koichi[1]; ROORDA, Sjoerd[2]; BREBNER, John L.[2]; ISHII, Satoshi[3]; SHIMA, Kunihiro[3]
([1]IMS and AIST; [2]Univ. Montréal; [3]Univ. Tsukuba)

[*Jpn. J. Appl. Phys.* **42**, 3950–3962 (2002)]

The structure of latent tracks introduced by swift-heavy-ion irradiation was examined on both amorphous SiO_2 and zinc phosphate glass ($68P_2O_5$:$25ZnO$:$4.5Al_2O_3$:$2.5Na_2O$). In amorphous SiO_2, the frequency of the infrared absorption assigned to the asymmetric stretching vibration of Si–O decreased with irradiation. This IR peak shift has been found to be related to the transition of normal six-membered rings of SiO_4 tetrahedra to planar three-membered rings. The high etching rate of the latent tracks is strongly related to planar three-membered rings. In the ion-irradiated zinc phosphate glass, two bridging oxygen atoms bound to a phosphorus atom turned into one bridging oxygen atom. Scission of the Zn–O bond was not observed. It was concluded that the high etching rate of the latent tracks in zinc-phosphate glass is related to P–O bond scission.

V-C-3 Structural Change Induced in TiO_2 by Swift Heavy Ions and Its Application to Three Dimensional Lithography

NOMURA, Ken-ichi[1]; NAKANISHI, Tetsuya[1]; OHKI, Yoshimichi[1]; AWAZU, Koichi[2]; FUJIMAKI, Makoto[1]; ISHII, Satoshi[3]; SHIMA, Kunihiro[3]
([1]Waseda Univ.; [2]IMS and AIST; [3]Univ. Tsukuba)

[*Phys. Rev. B* **68**, 64106 (2003)]

Rutile TiO_2 single crystal was irradiated by heavy ions with a high energy of the order of several tens of MeV. A good etching selectivity that only the irradiated surface is well etched by hydrofluoric acid is induced by the irradiation. Through X-ray diffraction and high-resolution electron microscopy, it became clear that the irradiated region lost crystallization. It is considered that this amorphous region and the surrounding region are dissolved in hydrofluoric acid. Through calculation of ion energy, it was found that the etching always stopped at the depth where the electronic stopping power of the ion decayed to a critical value of 6.2 keV/nm, regardless of the ion species in the case of I, Br, Cu, and Ti ions. However, in the case of Ca ions with energies higher than about 72 MeV or Cl ions with energies higher than about 77 MeV, the irradiated top surface was not etched with the hydrofluoric acid, but the inside several μm deep from the irradiated surface was etched. A calculation shows that the critical factor which determines whether the irradiated surface can be etched or not is the lateral energy density on the surface deposited by ions. The etched surface observed by atomic force microscopy is very smooth with a roughness of the order of nm. Therefore, combination of ion irradiation and etching can be used as a novel fabrication method of nanostructures in rutile.

V-C-4 Strained Si–O–Si Bonds in Amorphous SiO_2 Materials

AWAZU, Koichi[1]; KAWAZOE, Hiroshi[2]
([1]IMS and AIST; [2]Hoya Corp.)

[*J. Appl. Phys.* **94**, 6243 (2003)]

Amorphous SiO_2 (*a*-SiO_2), such as bulk silica glasses and thin films has been one of the key materials in modern opto-electronic industries. These materials are currently used in communication technologies as optical fibers, thin films for electrical insulation in dynamic random access memories (DRAM), and optical lenses for excimer laser lithography, for example. The property essential for these applications is the wide band gap amounting to ~ 9 eV. However, bulk silica glasses commercially available and silica thin films show photo-responses to sub-band gap lights in the vicinity of 5 eV and unexpected trapping of charges, and the behavior has a strong dependency on the preparation history.

A number of studies were carried out to clarify the relationship between the properties and structural imperfections in the materials and the formation mechanisms of the defects. There are two categories of the imperfections: one is dopant- or impurity-related imperfections and the other is non-stoichiometry related defects. These defects constitute gap states in *a*-SiO_2. The structural identification was usually performed by absorption- and emission spectroscopy in the visible-ultraviolet region and electron spin resonance (ESR). The experimentally proposed models were compared with the predictions by theoretical calculations of energy levels.

Recent development of the excimer laser lithography technique led us to recognize that a latent member, which has been unnoticed because of no response to the optical absorption or emission in the visible-uv range and ESR absorption, exists in the family of active centers in *a*-SiO_2, that is a strained Si–O–Si bond originating from the planar three membered ring. In contrast, the puckered four membered ring is unstrained. Although it has been pointed out that there was a wide distribution in Si–O–Si bond angle from 90° to 180° by X-ray analysis or ^{29}Si solid state NMR, the physical and chemical responses of the Si–O–Si bonds with a particular bond angle could not be differentiated.

Very recently it was clarified that a strained Si–O–Si bond, in other words chemically excited bonds, has an optical absorption locating on the band edge. The chemically excited bond can be scavenged by fluorine doping, because it is chemically reactive. In the present review we show that the unresolved optical and electric responses of silica glasses can be comprehensively understood by taking the presence of the strained bonds into consideration.

V-D Structures and Properties of Lanthanoid-Metallofullerenes

Lanthanoid-containing metallofullerenes with C_{82} cages, M@C_{82} (M is a lanthanoid metal atom), are the most widely investigated metallofullerenes. Accordingly to the oxidation state of the metal atom inside, they are classified into two groups; in one the metal atom takes the divalent state, and in the other it takes the trivalent state. Recently we investigated the cage structures and the motions of endohedral metal in metallofullerenes of the former group by ^{13}C NMR spectroscopy.

V-D-1 Structural Study of Four Ca@C_{82} Isomers by ^{13}C NMR Spectroscopy

KODAMA, Takeshi[1]; FUJII, Ryosuke[1]; MIYAKE, Yoko[1]; SAKAGUCHI, Koichi[1]; NISHIKAWA, Hiroyuki[1]; IKEMOTO, Isao[1]; KIKUCHI, Koichi[2]; ACHIBA, Yohji[1]
([1]Tokyo Metropolitan Univ.; [2]IMS and Tokyo Metropolitan Univ.)

[*Chem. Phys. Lett.* **377**, 197 (2003)]

The ^{13}C NMR spectra of four Ca@C_{82} isomers have been measured. The symmetry of isomers I, II, III and IV are assigned to be C_s, C_{3v}, C_2 and C_{2v}, respectively. For isomer IV, the cage is specified to be $C_{2v}(9)$. Our experimental results regarding the symmetry of cage structure coincide with the theoretical predictions.

V-E Development of Organic Superconductors

Since the discovery of superconductivity in a series of salts of TMTSF, TCF (tetrachalcogenafulvalene) derivatives have served as π-electron donors for the development of new organic superconductors. Although considerable research effort in this field has focused on the construction of TCF-type donors with extended π-conjugation, these donors, except for the DTEDT donor, failed to yield any organic superconductors. Besides TCF derivatives, our reported BDA-TTP donor gives three superconducting salts. And we succeeded in developing two superconductors from DODHT, with a less extended π-system that that of TCF derivatives. Recently other superconductors have been produced from these donors.

V-E-1 A New Organic Superconductor, $(DODHT)_2BF_4H_2O$

NISHIKAWA, Hiroyuki[1]; MACHIDA, Asami[1]; MORIMOTO, Takanobu[1]; KIKUCHI, Koichi[2]; KODAMA, Takeshi[1]; IKEMOTO, Isao[1]; YAMADA, Jun-ichi[3]; YOSHINO, Harukazu[4]; MURATA, Keizo[4]
([1]Tokyo Metropolitan Univ.; [2]IMS and Tokyo Metropolitan Univ.; [3]Himeji Inst. Tech.; [4]Osaka City Univ.)

[*Chem. Commun.* 494 (2003)]

In addition to two organic superconductors $(DODHT)_2X$ [DODHT = (1,4-dioxane-2,3-diyldithio)-dihydro-tetrathiafulvalene; X = PF_6 and AsF_6] previously reported by us, the BF_4 salt of DODHT containing one water molecule [$(DODHT)_2BF_4H_2O$] has been found to undergo a superconducting transition at 3.2 K under a hydrostatic pressure of 15.5 kbar.

V-E-2 A New Organic Superconductor, β-$(BDA\text{-}TTP)_2GaCl_4$ [BDA-TTP = 2,5-(1,3-Dithian-2-Ylidene)-1,3,4,6-Tetrathiapentalene]

YAMADA, Jun-ichi[1]; TOITA, Takashi[1]; AKUTSU, Hiroki[1]; NAKATSUJI, Shin'ichi[1]; NISHIKAWA, Hiroyuki[2]; IKEMOTO, Isao[2]; KIKUCHI, Koichi[3]; CHOI, Eun S.[4]; GRAF, David[4]; BROOKS, James S.[4]
([1]Himeji Inst. Tech.; [2]Tokyo Metropolitan Univ.; [3]IMS and Tokyo Metropolitan Univ.; [4]Florida State Univ.)

[*Chem. Commun.* 2230 (2003)]

The preparation, crystal structure and physical properties of β-$(BDA\text{-}TTP)_2GaCl_4$ has been investigated; the salt exhibits superconductivity at 3.1 K (onset) under a hydrostatic pressure of 7.6 kbar.

RESEARCH ACTIVITIES VI
Department of Vacuum UV Photoscience

VI-A Electronic Structure and Decay Mechanism of Inner-Shell Excited Molecules

In this project, we have two major subjects: (a) resonant photoelectron spectroscopy and (b) resonant inelastic soft X-ray emission spectroscopy following inner-shell excitations of simple molecules. We have already found some spin-forbidden ionized and excited states in (a) and (b) in collaboration with Uppsala University and Advanced Light Source. In the spectral assignments, angle(symmetry)-resolved photoion yield techniques and theoretical calculations are essential. We are now developing an original soft X-ray emission spectrometer for the recently upgraded UVSOR facility.

VI-A-1 Design and Development of a Novel Transmission Grating Spectrometer for Soft X-Ray Emission Studies

HATSUI, Takaki; SETOYAMA, Hiroyuki; SHIGEMASA, Eiji; KOSUGI, Nobuhiro

[*AIP Conference Proceedings* in press]

High resolution soft x-ray emission spectroscopy (XES) in combination with synchrotron radiation as an exciting source has been extensively studied. We propose a novel spectrometer design for high resolution soft-x-ray emission studies. Figure 1 shows the schematic layout of a transmission-grating spectrometer (TGS). In order to focus the emitted x-ray both horizontally and vertically, a Wolter type I mirror is introduced as the prefocussing mirror with a magnification of 10. The grazing-incidence angle of 1 degree gives a collection angle of 1.5×10^{-3} sr. A free-standing transmission plane grating with its groove density of 10000 lines/mm is placed at 67 mm downstream of the edge of the Wolter mirror, in the normal incidence geometry. A back-illuminated CCD, whose position is changed along the Rowland torus with scanning the photon energy, is located at 1400 mm downstream from the grating. In order to evaluate the aberrations of TGS, a ray-tracing code TGSGUI is developed by one of the authors (T.H.). Figure 2 shows a spot diagram of the 1st order diffracted rays of 320 eV at the detector with a rectangular source of 1(v.) × 200(h.) μm^2. The plane figure of the grating causes aberrations.[1)] The diagram however indicates that the resolving power better than 5000 is possible. The spatial resolution of the detector however should be very high, which is estimated to be about 1 μm, in order to achieve such a high resolution. The novel TGS is very promising because of its large collection angle and high energy resolution. Technical difficulties in realization of transmission gratings and high spatial resolution CCD still remain to be solved. The optical elements are now under development.

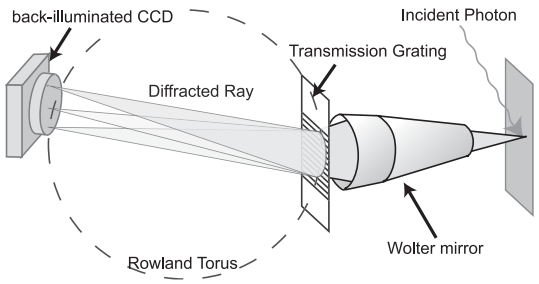

Figure 1. Schematic layout of the transmission-grating spectrometer (TGS).

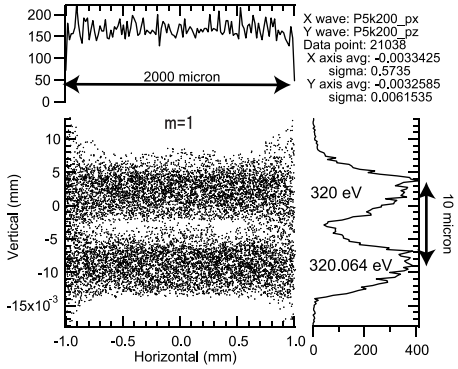

Figure 2. Spot diagram of the 1st order diffracted rays of 320 eV at the detector with a rectangular source of 1(v.) × 200(h.) μm^2.

VI-A-2 Symmetry-Resolved Photoion Yield Spectra of N_2 and C_2H_2

MASUDA, Suomi[1]; GEJO, Tatsuo[2]; KOSUGI, Nobuhiro
([1]GUAS; [2]Himeji Inst. Tech.)

In homonuclear systems, core excited states have a gerade-ungerade splitting. It has been discussed in term of delocalization of the core hole through the core-valence interaction between adjacent atoms.[1)] Relatively large g-u splitting is reported for N_2 and C_2H_2.[2)] In this work, we applied angle-resolved photoion yield spectroscopy (ARPIS) to core to Rydberg excitation of N_2 and C_2H_2 to study core excitation below the ionization thresholds. Because photo-excitation has the

References

1) K.P. Beuermann, *et al.*, *Appl. Opt.* **17**, 2304 (1978).

g-u selectivity, ARPIS can provide information on the symmetry of the excited states. ARPIS of N_2 and C_2H_2 near the N and C *K*-edge region are shown in Figure 1 and 2, respectively. In both the spectra, the parallel and perpendicular transitions are clearly resolved. Two ionization thresholds $^2\Sigma_g^+$ and $^2\Sigma_u^+$ are determined to have Δ_{gu} = 109 ± 8 meV and Δ_{gu} = 119 ± 15 meV for N_2 and C_2H_2 by extrapolating each Rydberg series by using Rydberg formula for a hydrogen-like system combined with constant quantum defects. In Figure 2, distinct difference is observed between vibrational progressions of $3p\sigma_u$ and those of $3p\pi_u$. In the $3p\sigma_u$ Rydberg excited state, the C–H symmetric stretching mode ν_1 is excited in addition to the C–C symmetric stretching mode ν_2. It can be attributed to perturbation in the $3p\sigma_u$ Rydberg excited state from the $3\sigma^*_u$ valence excited state, which has the C–H antibonding character.

References

1) N. Kosugi, *Chem. Phys.* **289**, 117 (2003).
2) B. Kempgens, *et al.*, *Phys. Rev. Lett.* **79**, 19 (1997).

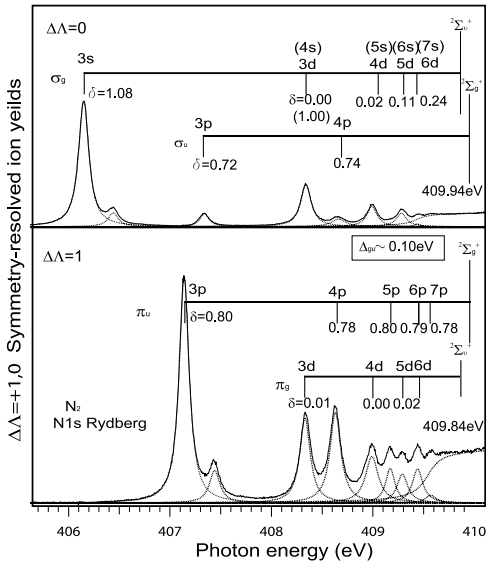

Figure 1. ARPIS of N_2 measured at near N *K*-edge region.

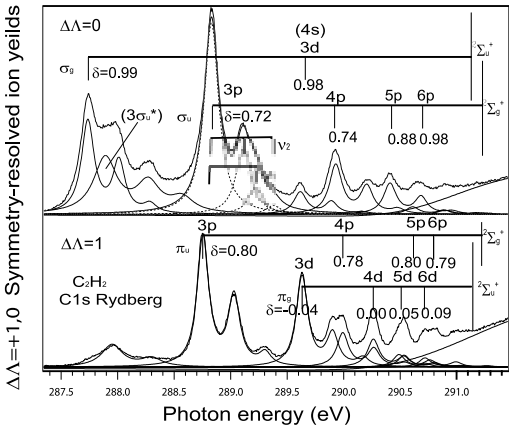

Figure 2. ARPIS of C_2H_2 measured at near C *K*-edge region.

VI-A-3 Ab Initio R-Matrix/MQDT Method for Near-Edge X-Ray Absorption Fine Structure

HIYAMA, Miyabi[1]; KOSUGI, Nobuhiro
([1]Univ. Tokyo)

[*Phys. Scr.* in press]

We have investigated feasibility of an ab initio polyatomic R-matrix/MQDT (multichannel quantum defect theory) method[1] using Gaussian type basis functions for the bound and continuum states to analyze the near edge feature of molecules. Test molecules here are N_2, C_2H_2, and NO. The R-matrix/MQDT method is revealed to be indispensable for the Rydberg states with the higher quantum number and the continuum states, both of which cannot be described by using Gaussian type functions in the outer region from an appropriate boundary. The close-coupling calculation augmented with the correlation term, which is carried out for the inner region, is powerful to describe the valence states and the interchannel coupling in several core-ionized states.

Reference

1) M. Hiyama and M. S. Child, *J. Phys. B* **35**, 1337 (2002).

VI-B Soft X-Ray Photoelectron-Photoabsorption Spectroscopy and Electronic Structure of Molecular Solids and Clusters

This project has been carried out in collaboration with Wuerzburg University. We have two subprojects: (a) molecules and radicals in condensed phase and in rare gas matrix, and (b) ionic fragmentations of molecular clusters following the inner-shell resonance excitation. In (a), we have measured Ar 2*p* excitation spectra in some matrix phases at the bending-magnet beamline BL4B of the UVSOR facility. In (b), we are developing a new cluster source for photoelectron measurements on a newly constructed undulator beamline BL3U.

VI-B-1 Ar 2*p* Excited States of Argon in Non-Polar Media

HATSUI, Takaki; NAGASONO, Mitsuru[1]; KOSUGI, Nobuhiro
([1]Kyoto Univ.)

[*J. Electron Spectrosc. Relat. Phenom.* in press]

Rydberg states in condensed phase are sensitive to external perturbation due to their large orbital radii. In the present study, Ar 2*p* excitations of solid Ar, and Ar:Kr, Ar:Xe and Ar:N_2 mixtures are investigated with high energy resolution in order to clarify the nature of Rydberg excited states in non-polar media. Figure 1 shows Ar 2*p* photoabsorption spectra of Ar gas, solid Ar, and Ar:Kr(1:4) and Ar:Xe(1:4) mixtures. The solid Ar spectrum shows Rydberg excitations blue-shifted compared with the Ar gas, as reported in the earlier work.[1)] The lowest Ar $2p_{3/2}$-4*s* band has a shoulder structure on the lower energy side. In order to discriminate surface contribution from bulk, fluorescence yield was measured for solid Ar (dotted line). The spectral features are very similar except for the shoulder and a weak band observed around 246.14 eV, which are clearly suppressed in the fluorescence yield spectra. They are hence assigned to the excitations arising from surface Ar atoms. The shoulder at ~ 244.6 eV can be assigned to the surface Ar $2p_{3/2}$-4*s* excitation. On the other hand, the weak band at ~ 246.14 eV can be assigned to the surface Ar $2p_{3/2}$-4*p* excitation, which becomes dipole allowed because of the lower local symmetry of surface Ar atoms. The bulk Ar $2p_{3/2}$-4*p* is not observable. The feature at 247–248.5 eV is broadened mainly because of the overlap of *nd* excitations. The bulk Ar $2p_{3/2}$-4*s* band in the Ar:Kr (1:9) spectrum locates at 244.82 eV with a red shift of 0.24 eV in comparison with the bulk Ar $2p_{3/2}$-4*s* band in the Ar solid. The red shift in the Ar:Kr mixture compared to the Ar solid can be explained as a combination of two effects, namely, decrease of ionization threshold and increase of term value. The ionization threshold is lowered in condensed phase by polarization stabilization. Based on a continuum model that treats all surrounding atoms as dielectric continuum, the ionization threshold for Ar:Kr mixture is predicted to be lower than that for Ar solid. On the other hand, the exchange repulsion of the excited Rydberg electron by the valence electrons of the neighboring atoms is predominantly determined by the distance between the core-excited atom and the neighboring atoms. Longer interatomic distance of Ar–Kr than Ar–Ar, results in smaller exchange repulsion. The excited states in Ar:Kr mixture hence have larger term values (lower excitation energies) than the Ar solid. Both the larger polarization stabilization and the smaller exchange repulsion make the excitation energies for Ar:Kr mixtures lower than those for Ar solid. Similar arguments are possible for Ar:Xe mixtures. Both the larger polarization stabilization and the smaller exchange repulsion contribute to larger red shift in Ar:Xe than in Ar:Kr. In the case of Ar:N_2 mixtures, Ar $2p_{3/2}$-4*s* band shows small red shift to the Ar solid, which is explained as a balance between the red shift by the polarization stabilization and the blue shift arising from the exchange repulsion. On the contrary, the Ar $2p_{3/2}$-*nd* band in Ar:N_2 mixtures shows a large blue shift to the Ar solid, which is explained by the strong exchange repulsion of spatially extended *nd* electrons by N_2 with short Ar–N distances.

Reference

1) R. Haensel, *et al.*, *Phys. Rev. B* **7**, 1577 (1973).

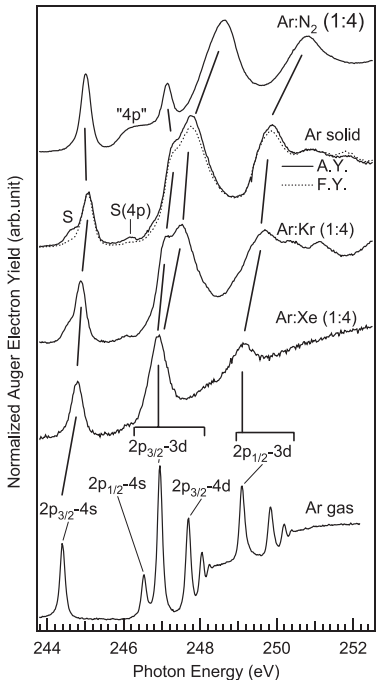

Figure 1. Ar 2*p* excitation spectra measured by using Auger electron yield method for Ar gas, Ar solid, and Ar:Kr(1:4), Ar:Xe(1:4) and Ar:N_2(1:4) mixtures. Fluorescence yield spectrum for Ar solid is shown as dotted line.

VI-B-2 Development and Construction of a Novel Undulator Beamline BL3U for Soft X-Ray Emission Studies

HATSUI, Takaki; SETOYAMA, Hiroyuki; MASUDA, Suomi; SHIGEMASA, Eiji; KOSUGI, Nobuhiro

[*AIP Conference Proceedings* in press]

A soft x-ray emission spectrometer (XES) generally requires small beam size at the sample position, because a smaller opening of the spectrometer entrance slit is needed to achieve higher energy resolution. Such a beam is usually produced by refocusing optics downstream of the exit slit. In our case, the adoption of such refocusing optics is impossible, due to a very limited space. On the other hand, a monochromator with short arm lengths is utilized with a small exit-slit opening for obtaining practical resolution. It is feasible to carry out XES studies at the exit slit position, if the monochromator has a constant exit-arm length. We have designed a varied-line-spacing plane (VLSP) grating monochromator in order to satisfy high energy resolution of $\lambda/\Delta\lambda = 10^4$ and small width of the exit slit opening. Figure 1 represents the layout of the beamline BL3U at the UVSOR facility. The cylindrical mirror M0 vertically focuses the beam on the entrance slit S0 with the demagnification of 1/7.57. Because of the short arm length, the entrance-slit opening corresponding to the resolving power of $\lambda/\Delta\lambda = 10^4$ becomes smaller than the beam size. This mismatch causes the beam loss of

12–63%. Varied-line-spacing parameters are calculated by minimizing the aberrations in the energy range of interest. The analytical solution of the aberrations for an S0-M1-VLSP-S1 optical system derived by Amemiya *et al.*[1] is used. The obtained parameters give resolving power higher than $\lambda/\Delta\lambda = 10^4$ in the photon energy range of 50–800 eV by using three interchangeable gratings with the center groove densities of 1200, 600, and 240 l/mm. In XES setup, the beam is horizontally focused on the exit slit by a plane-elliptical mirror M3, which is located downstream of the VLSP gratings. A sample is placed at 5–10 mm downstream of the exit slit S2. In the case of the multi-purpose setup, the beam is focused on the exit slit S1 only vertically and then refocused in the both directions on the sample by a toroidal mirror M2. The M3 mirror and the exit slit S2 are designed to be interchangeable with the exit slit S1. The calculated photon flux at the sample position in the multi-purpose setup is shown in Figure 2. The XES setup is also calculated to have very similar flux. The beam on the sample in the XES setup has a gaussian distribution with FWHM of 60 μm horizontally. The vertical beam size is close to the opening of the exit slit S2. Due to the diffraction by the exit slit S2, the vertical size of the beam cannot become smaller than ~ 10 μm. The beamline is now under commissioning and will be operated from March 2004.

Reference

1) K. Amemiya, *et al.*, *J. Synchrotron Radiat.* **3**, 282 (1996).

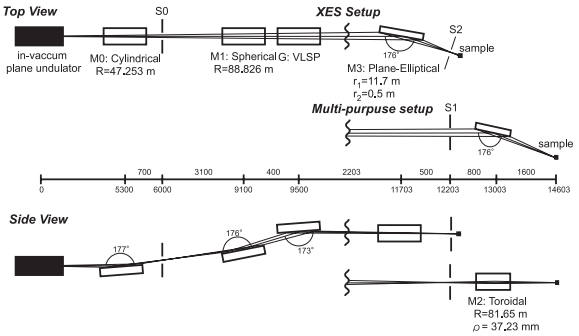

Figure 1. Schematic layout of the BL3U at UVSOR-II. The distances along the beam from the center of the in-vacuum plane undulator are shown in mm. S1X and M2X can be replaced with the other exit slit S1 so that experiments can be carried out at either the XES or multi-purpose endstation. In XES setup, the sample is placed at 5–10 mm downstream of S1X.

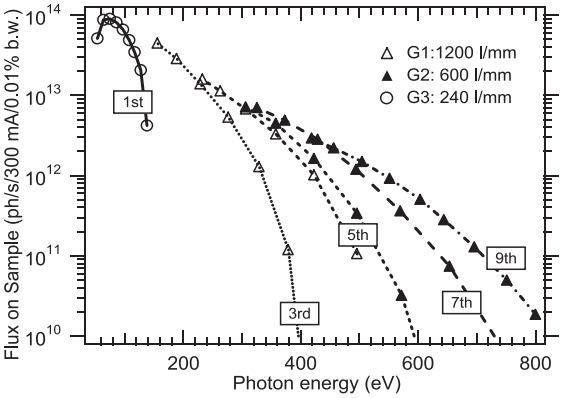

Figure 2. Calculated photon flux at the sample position in multi-purpose setup with the resolving power of $\lambda/\Delta\lambda = 10^4$.

VI-C Synchrotron Radiation Stimulated Surface Reaction and Nanoscience

Synchrotron radiation (SR) stimulated process (etching, CVD) has excellent characteristics of unique material selectivity, low damage, low contamination, high spatial resolution, and high precision *etc*. In this project, nano-level controlled structures are created by using synchrotron radiation stimulated process, and the reaction mechanisms are investigated by using STM and AFM. Concerning the SR etching, we are considering to apply this technique to the microfabrication of integrated protein transistor circuits.

VI-C-1 Design and Performance of Undulator Beamline (BL7U) for In-Situ Observation of Synchrotron Radiation Stimulated Etching by STM

NONOGAKI, Youichi; KATOH, Masahiro; SHIGEMASA, Eiji; MATSUSHITA, Kouji; SUZUI, Mitsukazu; URISU, Tsuneo

[*AIP Conference Proceedings* in press]

An undulator beamline of BL7U equipped with an ultra-high vacuum STM system is constructed at the UVSOR facility to investigate excitation energy dependence in synchrotron radiation stimulated etching. A schematic drawing of BL7U is shown in Figure 1. The SR beam is focused using two cylindrical mirrors on a sample surface just under the STM tip. The photon flux density is calculated to be 10^{19} photons (cm^2 sec 100mA)$^{-1}$ within the spot of 0.67 mm (H) × 0.17 mm (V) on the sample surface at the first harmonic tuned to 100 eV. The hydrogen adsorbed Si(111) surfaces were investigated using the STM apparatus before the undulator irradiation experiments were performed. We successfully observed the etching reaction from rest-atom monohydride surface by hydrogen exposure at room temperature.

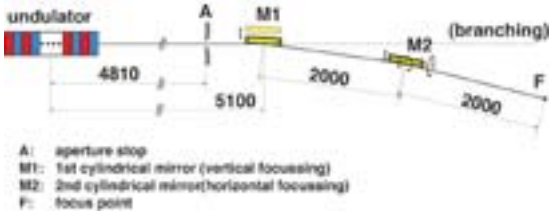

Figure 1. Schematic drawing of BL7U.

VI-C-2 Three-Dimensional Fine Structure on SOG/Si Surface Fabricated by Focused Ion Beam Mask Patterning and Synchrotron Radiation Etching

TERO, Ryugo; RAHMAN, Md. Mashiur; OKAWARA, Hiroshi[1]; NAGAYAMA, Kuniaki[1]; URISU, Tsuneo
([1]CIBS)

Synchrotron radiation (SR) etching of SiO_2 is a unique device process technique.[1)] The advantages of SR etching are unique material-selectivity, anisotropicity (vertical side wall) and low contaminations.[1),2)] When SiO_2 surfaces are patterned by SR etching using a contact mask,[2)] spatial resolution is limited by the available size of the photomask. Focused ion beam (FIB) is one of promising techniques which can make nano-scale patterning on metal, insulator and semiconductor materials.[3)] Therefore, nano-processing utilizing the advantages of SR etching will become practicable by applying FIB technique to patterning of etching mask. We have tried for the first time a new three dimensional fine process applying FIB and SR etching methods on spin-on glass (SOG), which is a widely used material in semiconductor processes because planar film with low dielectric constant is easily obtained.

SOG films with thickness of 450–500 nm were obtained after spin-coating on 14 mm square Si wafers followed by curing under flowing N_2 at 698 K for 30 min. SR etching was performed in UHV chamber in BL4A2, under mixture of 2.66×10^{-3} Pa of O_2 and 6.65×10^{-2} Pa of SF_6. Ion beam milling was carried out using 31 keV Ga FIB with a beam spot size of ~ 0.1 μm.

Experiments were performed as followed. First, the SOG film was covered by a Co layer with thickness of ~ 200 nm. Then, the Co photomask was patterned with FIB and the sample was exposed to SR. At last, the Co layer was removed by 0.01 M HNO_3 *aq*. Figure 1 shows an AFM image of the SOG surface after SR etching (2.0×10^4 mA min) followed by removal of the Co layer. Three-dimensional double-step well was successfully obtained in single irradiation process. The Co mask (~ 200 nm thick) was excavated by FIB before irradiation process in the region A and B; Co mask was penetrated to SOG therefore SOG was directly exposed to SR in A; Co mask in B was dug by only 95 nm, which meant FIB milling was stopped in the middle of the Co layer. The AFM profile in Figure 1 clearly shows that the SOG film has been removed and the Si substrate has appeared in the region A. In the region B, the SOG shrank maybe due to a curing effect by penetrating light through the thin Co layer.

Nanometer scale patterning by this combination method is aimed in the future. Effect of diffusion rate of etching gas and interference of light would also be investigated because these factors possibly become important in nano-scale processing.

References

1) T. Urisu and H. Kyuragi, *J. Vac. Sci. Technol., B* **5**, 1436–1440 (1987).
2) H. Akazawa, J. Takahashi, Y. Utsumi, I. Kawashima and T. Urisu, *J. Vac. Sci. Technol., A* **9**, 2653–2661 (1991).
3) S. Reyntjens and R. Puers, *J. Micromech. Microeng.* **11**,

287–300 (2001).

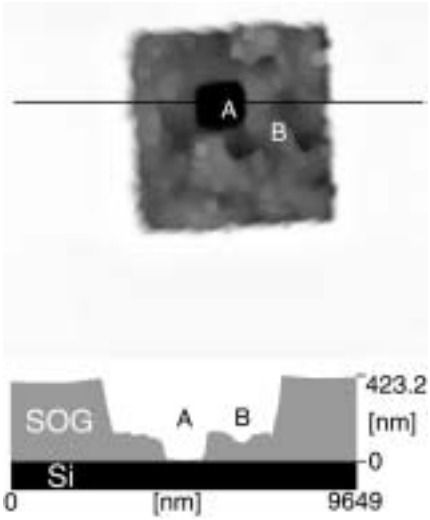

Figure 1. AFM image (10 × 10 μm^2) and a line profile of the SOG/Si surface after SR etching.

VI-C-3 Shrinking of Spin-on-Glass Films Induced by Synchrotron Radiation and Its Application to the 3-D Microfabrications

RAHMAN, Md. Mashiur; TERO, Ryugo; URISU, Tsuneo

[*Jpn. J. Appl. Phys.* to be submitted]

Spin-on-glass (SOG) is an important material in the semiconductor integrated circuit fabrication and widely used for flattening of the inter level dielectrics. Typical thicknesses of SOG films are hundreds of nanometers. It is usually cured with reducing the thickness by heating to high temperatures (for examples at 400 °C–500 °C) in the last stage of the processes. In the present work, we have found that the thickness is also reduced by the irradiation of the synchrotron radiation (SR) beam with covering the surface by Co mask. We are considering that this phenomenon is applied to three-dimensional microfabrications, since the degree of the shrinking depends on the thickness of the mask.

A commercial siloxane type SOG (Honeywell, Accuglass 312B) was used in this study. SOG was spun on 14 mm^2 silicon wafer at a spin speed of 3000 rpm for 10 sec. Immediately after spin coating, the film were subjected to three stages of soft baking on hot plates at 80 °C, 150 °C and 250 °C for 1 min at each temperature. The final curing was performed at 425 °C with a nitrogen gas flow of approximately 1.0 liters/min. After these curing process, thickness of SOG film was approximately 550 nm on Si wafer.

The SR etching of SOG was performed under mixture gas of SF_6 (0.05 Torr) and O_2 (0.002 Torr) at room temperature using a Co mask. The Co contact mask on SOG surface was fabricated by deposition of Co thin film (230 nm) on a resist pattern which was made by the photolithography and lift off technique. The thicker Co mask pattern area was formed by additional deposition of 330 nm Co film. After 20000 mA min dose of SR etching the Co mask was removed by 0.1 N HNO_3 for 3 min. The surface structure was measured by step profilometer (Dektak).

The open region of SOG film was completely etched and the etching was neatly stopped on the Si surface as reported by Urisu and Kyuragi. At the region covered by the thinner Co mask (230 nm), the thickness of SOG film reduced by 152 nm. At the region covered by thicker Co mask, no shrinkage was observed.

The SR etching rate of SOG was investigated. Etched depth of SOG gradually increased with the SR dose. In the present experiment we found that SOG thickness was reduced by the SR etching with thin Co mask and the SR shrinkage of SOG can be controlled with the Co mask thickness. Using this phenomenon we can make three-dimensional structures by one time of SR exposure.

VI-D Noble Semiconductor Surface Vibration Spectroscopy

As a new high sensitive and high resolution surface vibration spectroscopy technique, we are developing an infrared reflection absorption spectroscopy using buried metal layer substrate (BML-IRRAS), which have unique characteristics of high resolution and high sensitivity at finger print regions. Several Si surface chemical reactions are investigated using this BML-IRRAS. As a new fabrication technique of BML substrate, we have almost succeeded in developing the wafer bonding technique. It is considered that BML-IRRAS is also extremely useful in the research of bio-material integration on Si substrates.

VI-D-1 Three Pairs of Doublet Bands Assigned to SiH_2 Scissoring Modes Observed in H_2O-Induced Oxidation of Si(100) Surfaces

WANG, Zhi-Hong; URISU, Tsuneo; NANBU, Shinkoh; MAKI, Jun; GANGAVARAPU, Ranga Rao[1]; AOYAGI, Mutsumi[2]; WATANABE, Hidekazu[3]; OOI, Kenta[3]
([1]IMS and Indian Inst. Tech.; [2]Kyushu Univ.; [3]Natl. Inst. Adv. Ind. Sci. Tech.)

[*Phys. Rev. B* accepted]

Oxidation of Si(100) surfaces by H_2O has been investigated on 2H + H_2O/Si(100)-(2×1), H_2O + Si(100)-(2×1) as well as H_2O + H/Si(100)-(2×1) systems by infrared reflection absorption spectroscopy using $CoSi_2$ buried metal layer substrates (BML-

IRRAS). Three pairs of new doublet bands assigned to the scissoring modes of adjacent and isolated SiH_2 with zero, one and two inserted back bond oxygen atoms, respectively, have been reported for the first time. This is also the first report that has clearly shown the unique high sensitivity of BML-IRRAS for the perpendicular components in the finger print region compared to the multiple internal reflection and the external transmission arrangements. New oxidation mechanisms have been proposed. In the 2H + H_2O/Si(100)-(2×1) system, oxygen insertion into the back bond occurs easily. In the H_2O + H/Si(100) system, however, the tunneling effect is important to reach the oxygen inserted state.

VI-D-2 Assignment of Surface IR Absorption Spectra Measured in the Oxidation Reactions: 2H + H_2O/Si(100) and H_2O + H/Si(100)

WANG, Zhi-Hong; URISU, Tsuneo; GANGAVARAPU, Ranga Rao[1]; NANBU, Shinkoh; MAKI, Jun; AOYAGI, Mutsumi[2]; WATANABE, Hidekazu[3]; OOI, Kenta[3]
([1]IMS and Indian Inst. Tech.; [2]Kyushu Univ.; [3]Natl. Inst. Adv. Ind. Sci. Tech.)

[*Phys. Rev. B* to be submitted]

Infrared reflection absorption spectroscopy using buried metal layer substrates (BML-IRRAS) and density functional cluster calculations have been employed to study the water related oxidation reactions of 2H + H_2O/Si(100)-(2×1), 2D + H_2O/Si(100)-(2×1) and H_2O + H/Si(100)-(2×1). In addition to the oxygen inserted coupled monohydrides reported earlier in the former reaction system, we report several other oxidized Si hydride species in our BML-IRRAS experiments. Three pairs of new vibrational bands are identified between 900 and 1000 cm^{-1} region. These vibrational frequencies have been calculated using Si9 and Si10 cluster models which include all possible structures from zero to five oxygen insertions into the top layer silicon atoms using B3LYP gradient corrected density functional method with polarized 6-31G** basic set to all atoms. The three pairs of vibrational modes are assigned to the scissoring modes of adjacent and isolated SiH_2 with zero, one and two oxygen atoms inserted into the Si back bonds. All the other observed vibrational peaks related to Si oxidation have also been assigned in this study.

VI-D-3 A Comparative Infrared Study of H_2O Reactivity on Si(100)-(2x1), (2x1)-H, (1x1)-H and (3x1)-H Surfaces

GANGAVARAPU, Ranga Rao[1]; WANG, Zhi-Hong; URISU, Tsuneo
([1]IMS and Indian Inst. Tech.)

[*Surf. Sci.* submitted]

Water adsorption on bare and H-terminated Si(100) surfaces has been studied by BML-IRRAS technique. It is found that H-terminated surfaces are much less reactive compared to bare silicon surfaces. The (1×1)-H and (3×1)-H surfaces show similar and less reactivity pattern compared to the (2×1)-H surface. At higher exposures, water reaction with coupled monohydride species provides an effective channel for oxygen insertion into the back bonds of dihydride species.

VI-D-4 Theoretical Analysis of the Oxygen Insertion Process in the Oxidation Reactions of H_2O + H/Si(100) and 2H + H_2O/Si(100); Calculation of an Ab Initio Molecular Orbital Method and an Analysis of the Tunneling Reaction

WATANABE, Hidekazu[1]; NANBU, Shinkoh; WANG, Zhi-Hong; MAKI, Jun; URISU, Tsuneo; AOYAGI, Mutsumi[2]; OOI, Kenta
([1]Natl. Inst. Adv. Ind. Sci. Tech.; [2]Kyushu Univ.)

[*Chem. Phys. Lett.* submitted]

The reaction paths were analyzed, by an ab initio molecular orbital method, for the surface reaction systems, 2H + H_2O/Si(100)-(2×1) and H_2O + H/Si-(100)-(2×1), in which SiH_2 species with one or two oxygen atom-inserted back bonds have been observed as new stable reaction products. It was found that common metastable states exist in both systems, and the initial energy is sufficiently higher than all transition state energies in the former system, while in the latter system, the energy of the highest transition state is much higher than the initial energy, and thus a tunneling effect plays an important role.

VI-D-5 Structure-Optimized $CoSi_2$-Buried-Metal-Layer Substrates for IRRAS Fabricated by Wafer-Bonding

YAMAMURA, Shusaku; YAMAUCHI, Shouichi[1]; WATANABE, Satoru[2]; URISU, Tsuneo
([1]DENSO Res. Lab.; [2]Fujitsu Lab.)

The conventional infrared reflection absorption spectroscopy (IRRAS) is applicable only on the metal substrates. We are developing the IRRAS of semiconductor surfaces using buried metal layer (BML) substrates fabricated by wafer-bonding technique. To obtain high sensitivity in BML-IRRAS, it is essentially important to control the top Si layer thickness less than 200 nm. In this work, we have successfully fabricated BML substrates with 200 nm top Si layer by wafer-bonding technique for the first time using SOI wafers of which Si layer thickness is controlled definitely. Comparing with the ion implantation method, the wafer-bonding method has advantages of (1) atomically flat and (2) low-damaged top Si surfaces without epitaxial growth, which is essentially required in the ion implantation method to remove the ion implantation damage. The preliminary formation of thin (100 nm) SiO_2 layer on the SOI surface was effective to reduce the interface roughness between the top Si and the $CoSi_2$ layers. The self-assembled alkyl monolayer was deposited on the BML substrate, and its IRRAS was measured in the wide frequency range from stretching to bending regions.

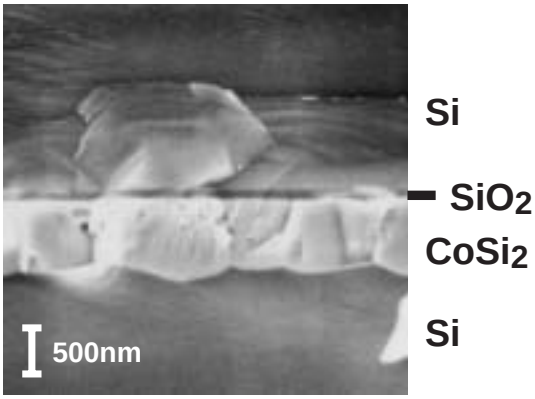

Figure 1. Cross-sectional SEM image of fabricated BML substrate by using preliminary formation of thin SiO_2 layer on the SOI surface.

VI-E Integration of Bio-Functional Materials on Silicon

Integration of bio-functional materials such as lipids and proteins are expected to find important applications in biosensors, development of new medicines, and diagnosis of intractable diseases *etc*. In this project, we are investigating the area selective modification of Si surfaces by depositing the self-assembled alkyl monolayers, and the integration of lipid bilayers supporting channel proteins keeping their bio-activities. Our special interests are developing "protein transistors" and co-integrating them together with the Si MOS FETs on the same Si chip.

VI-E-1 Deposition of Lipid DPPC Monolayer on SiO_2 Surface Using OTS Self-Assembled Monolayer Islands as Anchor Molecules

TAKIZAWA, Morio; KIM, Yong Hoon; TERO, Ryugo; URISU, Tsuneo

Bilayer lipid membranes (BLMs) supported on the solid surface are attractive research target from the viewpoint of application to the biosensors. The stability of the membrane can be increased significantly by using the *anchor molecules*. We have investigated the deposition of dipalmitoylphoshatidylcholine (DPPC) monolayer on SiO_2 surface using *n*-octadecyltrichlorosilane (OTS) self-assembled monolayer (SAM) islands as anchor molecules. After deposition of OTS SAM islands on SiO_2 surface, the DPPC monolayer was transferred to the surfaces by Langmuir-Blodgett method. The surface morphology observed by AFM shows that the flat DPPC monolayer is area-selectively deposited almost completely on the hydrophilic SiO_2 surface. On the hydrophobic OTS SAM surface, DPPC molecules were not observed as a form of monolayer. Bright protrusions were observed on and at the edges of the OTS islands, suggesting excess DPPC molecules accumulate and form three-dimensional islands. These results indicate that the OTS SAM islands have a potential of effective anchor molecules in DPPC BLM depositions on SiO_2 surfaces.

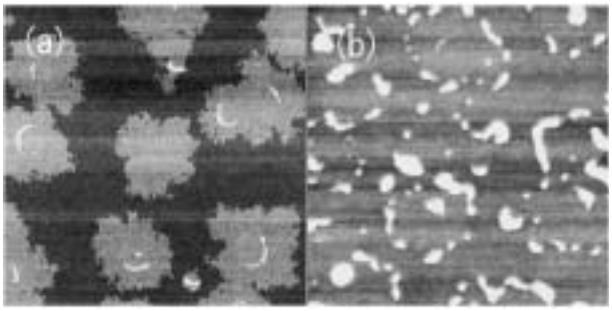

Figure 1. 5 μm × 5 μm AFM images of (a) OTS SAM islands and (b) DPPC monolayer deposition on OTS SAM/SiO_2 surface.

VI-E-2 Self-Assembled Monolayers on H-Si (111) Surfaces Studied by AFM Deposition of Undecenoic Acid

LI, Yanjun; TERO, Ryugo; NAGASAWA, Takayuki; NAGATA, Toshi; URISU, Tsuneo

A large number of studies have been conducted on the self-assembled monolayers (SAMs) from the view points of structure, formation process, and physical properties, for it is one of the promising candidates in applications such as adhesion promotion, surface modifications, surface protective films and the fabrication of devices such as field effect transistors.[1)–3)] The alkyl SAMs on Si substrates are relatively new topis and, among them, deposition of SAMs with a reactive group such as –COOH is especially interesting,[3)] since easiness of successive chemical treatments has potential applications to area selective immobilization of many kinds of bio-functional materials which is a key technology in the bioelectronics device fabrications. In

the present work, the undecenoic acid (CH_2=CH-C_8H_{16}-COOH) SAMs were deposited on the hydrogen-terminated Si (111) surface, and the surface morphology was successfully observed for the first time by AFM.

The B-doped *p*-type Si(111) wafers with a resistivity in the rang of 8.4–8.9 Ω cm were cleaned, thermally oxidized and after removal of the oxide layer, the undecenoic acid SAM layer was deposited and AFM observation was performed. The wafer cleaning process was wet method as follows; (1) H_2O_2:H_2SO_4 = 1:4 → NH_4OH:H_2O_2:H_2O = 1:4:20 → diluted HF treatments, (2) HCl:H_2O_2:H_2O = 1:1:6 → diluted HF treatments. In each step, copious rinsing with ultrapure water, (3) oxidation of the Si sample at 1000 °C for one hour, (4) removal of the thermal oxide layer by HF (2%) solution, and (5) the etching of the Si sample by the solution of NH_4F:NH_4OH (pH = 8) for 5 min. Then the H-terminated Si sample was immediately placed in the distilled the undecenoic acid solution. The deposition process was as follows: (1) bubbling of the undecenoic acid solution by N_2 gas for 30 min at RT. (2) dipping of the Si sample into the solution with continuous N_2 bubbling for 30 min at RT. (3) heating of the solution at 200 °C for requesting time with continuous N_2 bubbling, (4) cooling down to RT, and (5) rinsing of the sample by methanol and propanol. After these processes, the sample surface morphology was investigated by AFM in the tapping mode.

Figure 1(a) shows the AFM image of the Si sample surface just after the cleaning process. The step edges are clearly observed. Figures 1(b) and (c) show the AFM images after the undecenoic acid deposition for 20 min. The island growth was confirmed on the Si(111) terraces, and the islands show unique hexagonal shapes, which is considered to be the reflection of the deposition mechanisms. We will make a detailed analysis about the AFM data in the succeeding research.

References

1) J. B. Brzoska, N. Shadhidzadch and F. Rondclcz, *Nature* **360**, 719–721 (1992).
2) A. B. Sieval, A. L. Demirel, J. W. M. Nissink, M. R. Linford, J. H. ven der Maas, W. H. de Jeu, H. Zuilhof and E. J. R. Sudholter, *Langmuir* **14**, 1759–1768 (1998).
3) S. D. More, H. Graaf, M. Baune, C. Wang and T. Urisu, *Jpn. J. Appl. Phys.* **41**, 4390–4394 (2002).

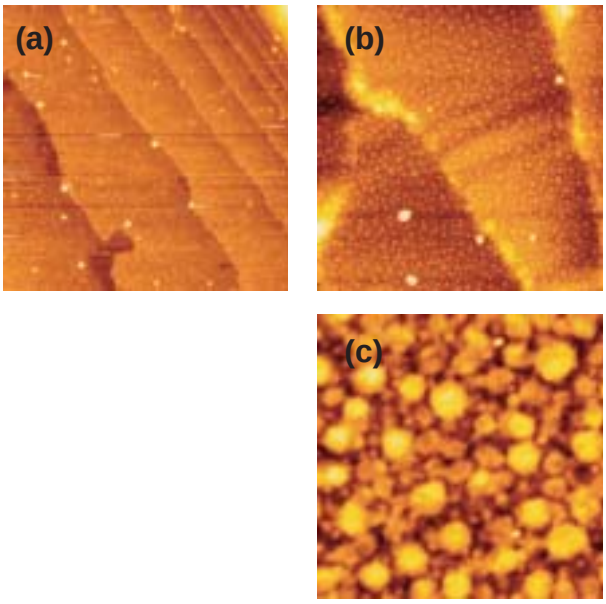

Figure 1. AFM images of the Si(111) sample surface, (a) just after the cleaning (800 μm × 800 μm) (b) after the undecenoic acid deposition (4 μm × 4 μm) and (c) in high magnification of (b) (800 nm × 800 nm).

VI-E-3 Characterization of Dipalmitoylphosphatidylcholine (DPPC)/Cholesterol Langmuir-Blodgett Monolayers by AFM and FT-IR

KIM, Yong Hoon; TAKIZAWA, Morio; URISU, Tsuneo

In advent of bio-nano technology, many experimental approaches have been performed to fabricate biosensors mimicking the ion channel system of cell membranes. In such system, intensity and lifetime of the ion channel current largely depend on membrane properties. Cholesterol is one of the major constituents in membranes and diminishes the gel to liquid crystalline phase transition. the chemical and physical properties and formation of the liquid-ordered phase (L_O), occurring at a certain cholesterol concentration, have been of considerable interest because the studies of this phase can provide important information related to the numerous biological functions in cell membranes, including signal transductions to immune systems and the activity of membrane proteins

It is the aim of this study to examine interactions of cholesterols with L_α phase of DPPC monolayer prepared by the Langmuir-Blodgett method. We have focused on effects of cholesterols, causing the formation of L_O phase, in relation to the conformational order of acyl chains of mixed (DPPC/cholesterol) monlayers and the behavior of phase separations in combination with FT-IR and AFM, respectively.

VI-F Photoionization and Photodissociation Dynamics Studied by Electron and Fluorescence Spectroscopy

Molecular photoionization is a major phenomenon in vacuum UV excitation and provides a large amount of information on fundamental electron-core interactions in molecules. Especially, neutral resonance states become of main interest, since they often dominate photoabsorption cross sections and lead to various vibronic states which are inaccessible in direct ionization. We have developed a versatile machine for photoelectron spectroscopy in order to elucidate dynamical aspects of superexcited states such as autoionization, resonance Auger decay, predissociation, vibronic couplings, and internal conversion. Two-dimensional photoelectron spectroscopy, allows us to investigate superexcited states in the valence excitation region of acetylene, nitric oxide, carbonyl sulfide, sulfur dioxide and so on. In a two-dimensional photoelectron spectrum (2D-PES), the photoelectron yield is measured as a function of both photon energy $E_{h\nu}$ and electron kinetic energy E_k (binding energy). The spectrum, usually represented as a contour plot, contains rich information on photoionization dynamics.

Photofragmentation into ionic and/or neutral species is also one of the most important phenomena in the vacuum UV excitation. In some cases, the fragments possess sufficient internal energy to de-excite radiatively by emitting UV or visible fluorescence. It is widely accepted that fluorescence spectroscopy is an important tool to determine the fragments and to clarify the mechanisms governing the dissociation processes of diatomic and polyatomic molecules. For several years we have concentrated upon fluorescence spectroscopy of H_2O in the photon energy region of 15–55 eV.

VI-F-1 Dissociation Mechanism of H_2O into $OH^+(\tilde{A}^3\Pi_\Omega)$ + H(n = 1) Manifested by Ultraviolet Dispersed Spectroscopy

MITSUKE, Koichiro

The photofragmentation of H_2O has been studied by fluorescence spectroscopy at photon energies between $h\nu$ = 16.9–54.5 eV. The primary photon beam was monochromatized undulator radiation supplied from BL3A2 of the UVSOR facility. The fluorescence in the wavelength range of 280–720 nm was dispersed with an imaging spectrograph.[1] Figure 1 shows the fluorescence excitation spectrum for the (0,0) vibrational band of the $OH^+(\tilde{A}^3\Pi_\Omega \rightarrow \tilde{X}_3\Sigma^-)$ transition. The intensity shows a slow onset at 25.5 ± 0.3 eV. This value is much higher than the dissociation limit of 21.5 eV and can be interpreted in terms of a highly repulsive potential energy surface of the excited H_2O^+ state along the dissociation coordinate. The correlation diagram of H_2O^+ proposed by Appell and Durup[2] predicts that the $OH^+(\tilde{A}^3\Pi_\Omega)$ + H(n = 1) limit correlates with a 2-hole 1-particle $^2A_1$ state of H_2O^+ with the electronic configuration of $[(1b_1)^{-2}(4a_1)^1]$. This doubly excited $H_2O^+(^2A_1)$ state was reported to be located at 27.6 ± 1 eV with respect to $H_2O(\tilde{X}^1A_1)$ in the Franck-Condon region. This vertical ionization energy rationalizes the present observation that the $OH^+(\tilde{A}^3\Pi_\Omega \rightarrow \tilde{X}^3\Sigma^-)$ band system begins to appear at $h\nu$ = 25.5 eV.

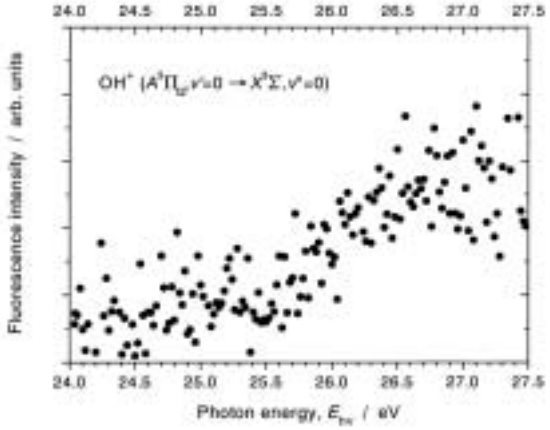

Figure 1. Fluorescence excitation spectrum for the (0,0) vibrational band of the $OH^+(\tilde{A}^3\Pi_\Omega \rightarrow \tilde{X}^3\Sigma^-)$ transition. The resolution of the synchrotron radiation was 2.4 Å.

References

1) K. Mitsuke, *J. Chem. Phys.* **117**, 8334–8340 (2002).
2) J. Appell and J. Durup, *Int. J. Mass Spectrom. Ion Phys.* **10**, 247–265 (1972/73).

VI-F-2 Autoionization of the Rydberg States Converging to $HI^+(A\,^2\Sigma^+_{1/2})$ below $h\nu$ = 12.7 eV

HIKOSAKA, Yasumasa[1]; MITSUKE, Koichiro
([1]Inst. Mater. Struct. Sci.)

[*J. Chem. Phys.* submitted]

Two-dimensional photoelectron spectroscopy of hydrogen iodide has been performed in the $E_{h\nu}$ range of 11.10–14.85 eV, in order to clarify autoionization mechanisms of the Rydberg states $HI^*(R_A)$ converging to $HI^+(\tilde{A}^2\Sigma^+_{1/2})$. The 2D-PES exhibits extensive vibrational excitation of $HI^+(\tilde{X}^2\Pi_{3/2}, v^+)$ over a $E_{h\nu}$ region from ~ 12 to 13.6 eV. The v^+ excitation below 12.7 eV is attributable to autoionizing features of the $5d\pi$ $HI^*(R_A)$ state. The potential energy curves of HI* and HI^+ are illustrated in Figure 1, where the curves of HI^+ are adopted from the literature.[1] Superexcitation and subsequent autoionization is usually governed by the Franck-Condon principle. Since the wave functions for excited vibrational levels have large amplitudes near

the potential wall, superexcitation into $5d\pi$ HI*(R_A) affords population to a few vibrational levels whose classical turning points at the repulsive branch of $5d\pi$ HI*(R_A) are included within the Franck-Condon region for transitions from HI($\tilde{X}^1\Sigma^+$). Then autoionization of these levels occurs either at near the repulsive branch or at the attractive branch, unless the lifetime with respect to autoionization is much shorter than the vibrational period of the $5d\pi$ state. The extensive vibrational excitation at $E_{h\nu}$ < 12.7 eV can be accounted for by autoionization at the attractive branch.

Reference

1) A. J. Cormack, *et al.*, *Chem. Phys.* **221**, 175–188 (1997).

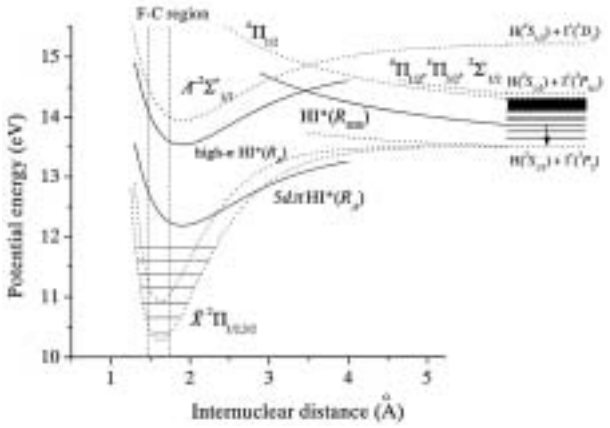

Figure 1. Schematic diagram for the potential energy curves of HI and HI^+. The solid and dashed lines designate the Rydberg and ionic states, respectively. The potential energy curves of HI*(R_A) states are assumed to have the same shape as those of $HI^+(\tilde{A}^2\Sigma^+_{1/2})$. The term values used for the $5d\pi$ and high-n Rydberg states are 1.76 and 0.44 eV, respectively. The Franck-Condon region is located between the two dashed vertical lines.

VI-F-3 Autoionization and Predissociation of the Rydberg States Converging to $HI^+(\tilde{A}^2\Sigma^+_{1/2})$ at $h\nu$ = 13.2–13.6 eV

HIKOSAKA, Yasumasa[1]; MITSUKE, Koichiro
([1]Inst. Mater. Struct. Sci.)

The 2D-PES of HI at $E_{h\nu}$ = 13.2–13.6 eV has been closely studied to understand dynamical properties on autoionization and predissociation of HI*(R_A) (see also Theme VI-F-2). The v^+ distribution of $HI^+(\tilde{X}^2\Pi_{3/2})$ shows an interesting left-side up pattern up to $v^+ \sim 12$. Namely, the relative population for a given v^+ reaches a maximum at $E_{h\nu} = E_{h\nu}^{max}$ whose value increases with increasing v^+. At first sight one would presume that this vibrational pattern results from autoionization of high-n HI*(R_A) Rydberg states with n » 5.

Figure 1 shows the constant-ionic-state (CIS) spectra for v^+ = 0–3 of $HI^+(\tilde{X}^2\Pi_{3/2})$ extracted from the 2D-PES. Panel (a) shows a broad resonance peak due to autoionization of $5d\pi$ HI*(R_A). With increasing v^+ the spectral features spread from ~ 12.0 to ~ 13.3 eV and become complicated as seen from the other three Panels. At $v^+ \geq 3$ the whole resonance splits into two broad peaks. The peak lying at higher energy shifts its maximum position from ~ 13.1 eV at v^+ = 3 to ~ 13.5 eV at v^+ = 12, being consistent with the left-side up pattern. At $E_{h\nu}$ = 13.2–13.6 eV, the integrated intensity for v^+ = 1 calculated from Figure 1(a) is no more than 4% of that for v^+ = 0. This ratio is much smaller than that at $E_{h\nu}$ = 12.2–12.7 eV, which implies that simple autoionization of the high-n HI*(R_A) states occur less efficiently than their conversion into predissociating repulsive states HI*(R_{Dis}). Then there is a probability that the system is converted from HI*(R_{Dis}) to low-n HI*(R_A) through avoided curve crossings. Autoionization of low-n HI*(R_A) states, such as the $5d\pi$ state; produced by double conversion can provide populations of HI^+ ($\tilde{X}^2\Pi_{3/2,1/2}$) at higher v^+ than expected from the Franck-Condon factors between HI($\tilde{X}^1\Sigma^+$) and HI*(R_A). From the relation between the potential energy curves of low-n HI*(R_A) and $HI^+(\tilde{X}^2\Pi_{3/2})$, autoionization can proceed mostly from the repulsive branch (see Figure 1 in Theme VI-F-2). The higher the n value of the primary high-n HI*(R_A) state becomes, the more the low-n HI*(R_A) state resulting from double conversion is vibrationally excited. Consequently, autoionizing transition occurs at a shorter nuclear distance and the final vibrational distribution of $HI^+(\tilde{X}^2\Pi_{3/2,1/2})$ shifts to higher v^+. The left-side up pattern at $E_{h\nu}$ = 13–13.7 eV in the 2D-PES obviously supports this expectation.

Reference

1) Y. Hikosaka and K. Mitsuke, *J. Chem. Phys.* submitted.

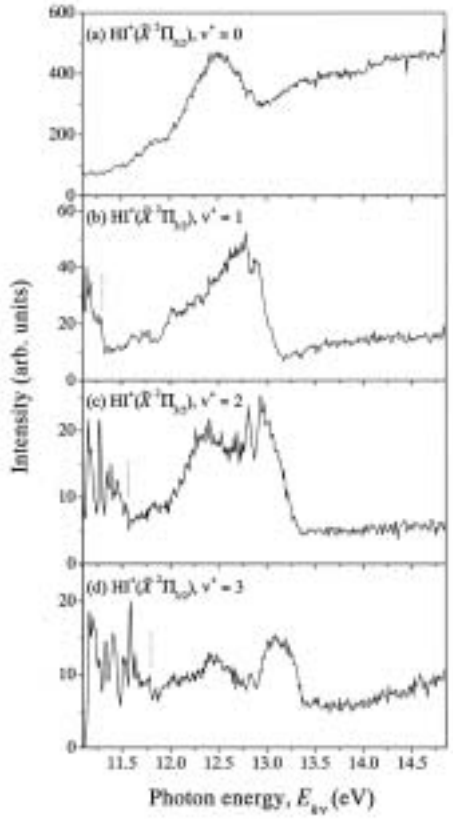

Figure 1. CIS spectra for the formation of v^+ = 0–3 vibrational levels of $HI^+(\tilde{X}^2\Pi_{3/2})$, which are extracted from the 2D-PES. The ionization energies for the v^+ = 1, 2 and 3 levels of $HI^+(\tilde{X}^2\Pi_{1/2})$ are indicated by the dotted lines in the spectra for v^+ = 1, 2 and 3, respectively.

VI-G Vacuum UV Spectroscopy Making Use of a Combination of Synchrotron Radiation and Laser

There is a growing interest in combining synchrotron radiation (SR) with the laser, since high resolution or ultrafast lasers are expected to open a new field for studies on dynamical behaviors of excited molecules in the VUV or soft X-ray region. Nevertheless, only a few attempts have been made on pump-probe experiments of gas-phase molecules using SR and a laser: photoelectron spectroscopy of atomic iodine produced from I_2 (Nahon *et al.*, 1990, 1991), photoelectron spectroscopy of N_2 and HCN produced from *s*-tetrazine (Nahon *et al.*, 1992), and photoionization of atomic iodine produced from CH_3I (Mizutani *et al.*, 1997). In UVSOR we have developed ultraviolet laser system which synchronizes precisely with the SR pulses from the storage ring to take maximum advantage of the features of the laser, *i.e.* its excellent spectral and temporal resolution, we employed the laser in detecting and analyzing products resulting from VUV or soft X-ray photoexcitation. The following combination studies have been performed: (1) two-photon ionization of helium atoms studied as the prototype of the time-resolved experiment (Mizutani *et al.*, 1997), (2) laser induced fluorescence (LIF) excitation spectroscopy of $N_2^+(X\ ^2\Sigma_g^+)$ ions or $CN(X\ ^2\Sigma^+)$ radicals produced by SR photoionization of N_2, N_2O, or CH_3CN (Mizutani *et al.*, 1998; Mitsuke *et al.*, 1998, 2001). This year another combination work commences as a new project, that is, SR photodissociation of vibrationally excited molecules prepared with irradiation of visible or infrared single frequency laser.

VI-G-1 Development of the Laser–SR Combination System for Photodissociation Studies of Highly Vibrationally Excited Molecules

MITSUKE, Koichiro

It is possible that the initial vibrational excitation in a molecule influences the chemical branching, if two different photodissociation channels are accessible. Much attention has been focused on the pioneering work of Crim and his collaborators,[1] who could accomplish the selective bond-breaking of heavy water, HOD. Very recently, Akagi and coworkers[2] reported that deuterized ammonia NHD_2 in the fourth N–H stretching overtone preferentially photodissociates into the ND_2 + H channel. In these two studies UV lasers were employed for vibrationally mediated photodissociation.

Instead, we are planning to use synchrotron radiation (SR) to promote vibrationally excited molecules to electronically excited states in the vacuum UV region. The main objectives are as follows: (1) Elucidating the properties of dissociative states by sampling a wide range of their potential energy surfaces, such as dynamics determining the final-state distributions of the products, nonadiabatic transitions on dissociation, and assignments and characterization of unknown multiply-excited states produced by Auger decay from core-excited states. (2) Aiming at more universal "vibrational state-specific" rupture of chemical bonds, which could be realized by changing the overlap between the wave-fucntions of the upper-state continuum and that of the ground state.

References

1) R. L. Vander Wal, J. L. Scott and F. F. Crim, *J. Chem. Phys.* **92**, 803–805 (1990).
2) H. Akagi, K. Yokoyama and A. Yokoyama, *J. Chem. Phys.* **118**, 3600–3611 (2003).

VI-G-2 Photodissociation of Vibrationally Excited H_2O in the $4\nu_{O-H}$ Region into $OH^+(X^3\Sigma^-)$ + H(n = 1)

MITSUKE, Koichiro; KOU, Junkei; MORI, Takanori

We have searched appropriate excited states through which photodissociation of vibrationally excited molecules can be investigated, on the basis of the correlation diagram in Figure 1 that we proposed in the dispersed fluorescence study for the extreme UV photoionization of H_2O.[1] First, we tackled the two $^2A_1$ states which correlate with the $OH^+(A^3\Pi_\Omega)$ + H(n = 1) and OH $(A^2\Sigma^+)$ + H^+ limits. Since the two states are highly repulsive, it is possible that significant decrease in the appearance energy is observed for the formation of $OH^+(A^3\Pi_\Omega)$ or $OH(A^2\Sigma^+)$ from vibrationally excited molecules. Here, spontaneous emission from these photofragments are detected.

A continuous titanium-sapphire laser was used in the wavenumber range between 13814–13819 cm^{-1}, with its bandwidth of 4×10^{-4} cm^{-1}. This energy range corresponds to excitation of the third O–H stretching overtone of water. However, when the visible laser was introduced together with SR, no additional peak feature of emission bands was detected in the dispersed spectra. Then we shifted the target to the dissociation channel of $OH^+(X^3\Sigma^-)$ + H(n = 1). The OH^+ ion was detected using mass spectrometry at SR photon energies near the dissociation threshold of 18.05 eV with respect to the neutral ground state. The difference between the normalized signal ion counts with and without the visible laser appears to exhibit multi-modal reflection structures due to the nodes of the vibrational wave function of the $4\nu_{O-H}$ stretch overtone of H_2O.

Reference

1) K. Mitsuke, *J. Chem. Phys.* **117**, 8334–8340 (2002).

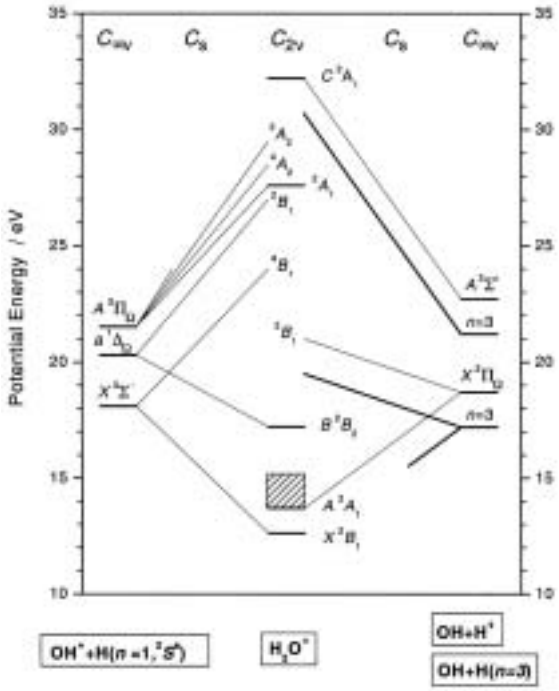

Figure 1. Correlation diagram between H_2O^+ and $OH^+ + H$ and between H_2O^+ and $OH + H^+$.

VI-H Extreme UV Photoionization Studies of Polyatomic Molecules and Fullerenes by Employing a Grazing-Incidence Monochromator

On the beam line BL2B2 in UVSOR a grazing incidence monochromator has been constructed which supplies photons in the energy region from 20 to 200 eV [M. Ono, H. Yoshida, H. Hattori and K. Mitsuke, *Nucl. Instrum. Methods Phys. Res., Sect. A* **467-468**, 577–580 (2001)]. This monochromator has bridged the energy gap between the beam lines BL3B and BL4B, thus providing for an accelerating demand for the high-resolution and high-flux photon beam from the research fields of photoexcitation of inner-valence electrons, *L*-shell electrons in the third-row atom, and 4*d* electrons of the lanthanides.

Since 2001 we have tried taking photoion yield curves of fullerenes. Geometrical structures and electronic properties of fullerenes have attracted widespread attention because of their novel structures, novel reactivity, and novel catalytic behaviors as typical nanometer-size materials. Moreover, it has been emphasized that the potential for the development of fullerenes to superconductors ($T_c \sim 50$ K) and strong ferromagnetic substances is extremely high. In spite of such important species spectroscopic information is very limited in the extreme UV region, which has been probably due to difficulties in obtaining enough amount of sample. The situation has been rapidly changed in these few years, since the techniques of syntheses, isolation, and purification have been advanced so rapidly that appreciable amount of fullerenes is obtainable from several distributors in Japan.

VI-H-1 Anisotropy of Fragment Ions from SF_6 by Photoexcitation between 23 and 210 eV

ONO, Masaki[1]; MITSUKE, Koichiro
([1]Louisiana State Univ.)

[*Chem. Phys. Lett.* **366**, 595–600 (2002)]

The anisotropy of the ionic photofragments produced from SF_6 has been measured using synchrotron radiation in the range of 23–210 eV. Despite the highly symmetrical molecule a strong anisotropy is observed below ~ 35 eV. The behavior of the asymmetry parameter involving all the fragment ions has been interpreted by simulation using partial oscillator strengths for the formation of individual species. Only SF_5^+ ions produced via superexcited states of valence type are assumed to have an anisotropic angular distribution. The observed decrease in the asymmetry parameter with increasing photon energy can be ascribed to the dominance of direct photoionization and the decrease in the branching ratio for SF_5^+ formation.

VI-H-2 Kinetic Energy Distribution and Anisotropy of Fragment Ions from SF_6 by Photoexcitation of a Sulfur 2*p*-Electron

ONO, Masaki[1]; MITSUKE, Koichiro
([1]Louisiana State Univ.)

[*Chem. Phys. Lett.* in press]

The kinetic energy (KE) distribution and asymmetry parameter β have been studied for photofragmentation of SF_6 near the sulfur 2*p* ionization edges at 170–208 eV by using synchrotron radiation. The relative yield of fast ions with KE > 5 eV is larger in the post-edge than in the pre-edge region (see Figure 1), whereas β of such ions is lower in the post-edge region. The β curve shows a sudden drop from 0.06–0.07 to zero near the edges and remains constant thereafter. These results are ascribed to *LVV* Auger decay occurring above the edges leading to SF_6^{2+} and SF_6^{3+} transiently. At KE > 2 eV the distribution curve for the S $2p \rightarrow 6a_{1g}$ resonance transition behaves in the same manner as that for the valence-electron ionization at 170 eV. This agreement, together with a similarity in β, suggests that the S $2p \rightarrow 6a_{1g}$ resonance and valence-electron ionization suffer similar formation pathways leading to ions with high KE.

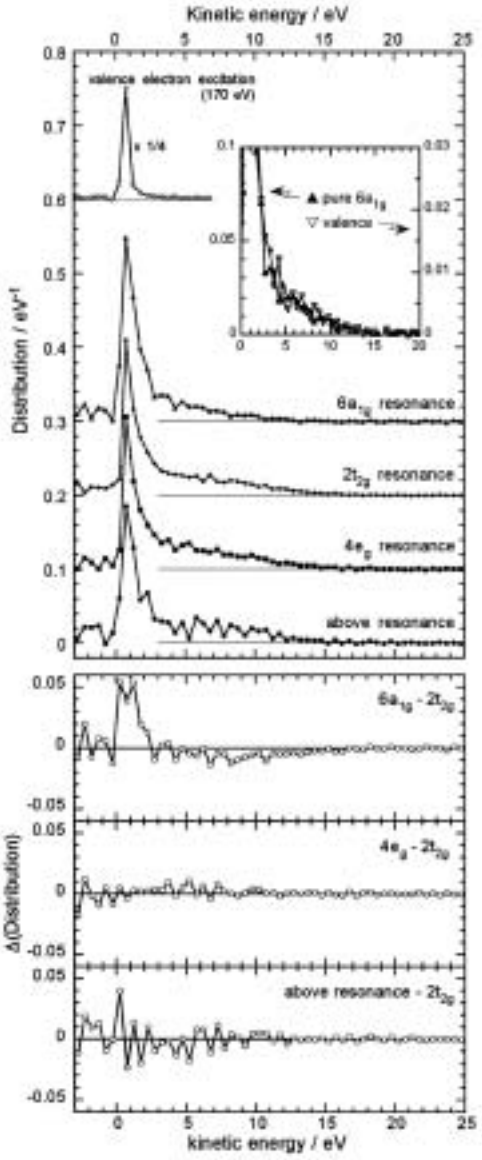

Figure 1. Upper panel: Kinetic energy distributions for sheer S 2*p*-electron excitation after subtracting the contributions of valence-electron photoionization. Inset shows expansion of the two distributions for the $6a_{1g}$ resonance at $h\nu$ = 173.5 eV and valence-electron ionization at 170 eV. Lower panel: Differences in distribution between the $2t_{2g}$ resonance and one of the three excitation energies (the $6a_{1g}$, $4e_g$ resonance and above the resonance).

VI-H-3 Molecular- and Atomic-Like Photoionization of C_{60} in the Extreme Ultraviolet

KOU, Junkei; MORI, Takanori; ONO, Masaki[1]; HARUYAMA, Yusuke[2]; KUBOZONO, Yoshihiro[3]; MITSUKE, Koichiro
([1]Louisiana State Univ.; [2]Okayama Univ.; [3]IMS and Okayama Univ.)

[*Chem. Phys. Lett.* **374**, 1–6 (2003)]

Photoion yield spectra of C_{60} in the gas phase have been measured from 23 to 180 eV by using synchrotron radiation. Two peaks at 26 and 34 eV and a flat area ranging from 40 to 50 eV are newly observed in the higher energy side of the giant resonance at ~ 20 eV, as shown in Figure 1. These features are assigned as resulting from the shape resonance on photoionization of valence electrons of C_{60} with large orbital angular momenta: the ionized electron is temporarily trapped inside a centrifugal barrier. Above ~ 50 eV the yield curve shows a steady decrease with increasing photon energy like the photoabsorption cross section of atomic carbon. Thus, the spectrum is considered to be determined by photoionization of the 2*s* orbitals of the carbon atoms.

Reference

1) P. Colavita, *et al.*, *Phys. Chem. Chem. Phys.* **3**, 4481–4487 (2001).

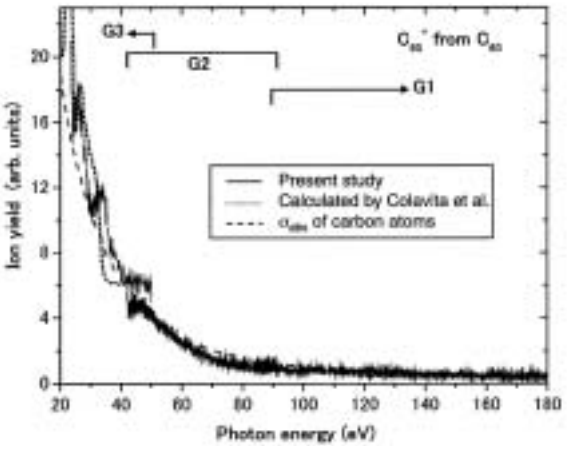

Figure 1. Solid curves: photoion yield of C_{60}^+ from C_{60} (present study). The dotted and dashed curves indicate the calculated photoabsorption cross sections of C_{60} and sixty carbon atoms, respectively, taken from Reference 1).

VI-H-4 Development of a Photoionization Spectrometer for Accurate Ion Yield Measurements from Gaseous Fullerenes

MORI, Takanori; KOU, Junkei; ONO, Masaki[1]; HARUYAMA, Yusuke[2]; KUBOZONO, Yoshihiro[3]; MITSUKE, Koichiro
([1]Louisiana State Univ.; [2]Okayama Univ.; [3]IMS and Okayama Univ.)

[*Rev. Sci. Instrum.* **74**, 3769–3773 (2003)]

A photoionization spectrometer has been developed for measuring the ion yields for fullerenes in the photon energy range of 23–200 eV (see Figure 1). Gaseous fullerenes were supplied from a high-temperature oven, ionized by irradiation of monochromatized synchrotron radiation and detected after analysis with a time-of-flight mass spectrometer. The fluxes of the synchrotron radiation and fullerene beams were monitored concurrently with the acquisition of the ion signal counts in order to obtain reliable photoionization efficiency curves. The performance of the apparatus was examined by measuring the efficiency curve of C_{60}^+ produced from C_{60}. The spectrum demonstrated better statistics than the previous results in the same photon energy region. Three distinct features were newly observed in the higher energy side of the prominent resonance at ~ 20 eV.

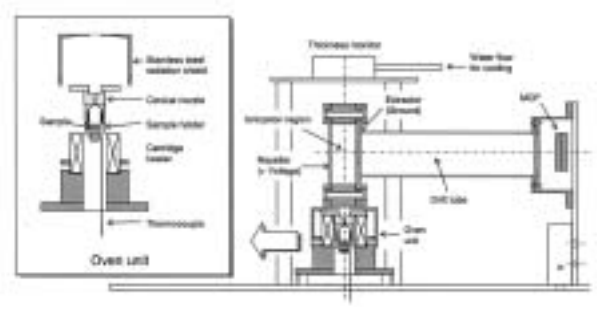

Figure 1. Apparatus of the photoionization spectrometer and an expansion of the oven unit.

VI-H-5 Production of Doubly Charged Ions in Valence Photoionization of C_{60} and C_{70} at $h\nu$ = 25–150 eV

KOU, Junkei; MORI, Takanori; S. V. K. Kumar[1]; HARUYAMA, Yusuke[2]; KUBOZONO, Yoshihiro[3]; MITSUKE, Koichiro
([1]IMS and Tata Inst. Fund. Res.; [2]Okayama Univ.; [3]IMS and Okayama Univ.)

[*J. Chem. Phys.* submitted]

Relative partial photoionization cross sections for production of singly and doubly charged ions of C_{60} and C_{70} have been measured at $h\nu$ = 25–150 eV. Figure 1 shows the photoionization yield curves of C_{60} for the formation of C_{60}^{n+} (n = 1 and 2). Since the yields for multiply charged ions with $n \geq 3$ are not significant in this energy region, one can regard the composite spectrum obtained by summing up the yields for C_{60}^+ and C_{60}^{2+} as the total photoionization yield of C_{60} or, to a good approximation, the total photoabsorption cross section of C_{60}. There are three peaks at $h\nu$ = 26, 34, and 49 eV in the composite spectrum. The total photoabsorption spectrum theoretically determined by Colavita and cowokers[1)] is depicted by the dotted curve in Figure 1. A comparison of the present total photoionization yield with the reported photoabsorption spectrum shows a large disagreement, probably because of the contribution of C_{60}^{2+} produced through the mechanism that has not been taken into account[1)] in the *ab initio* calculations. The most probable pathway to produce C_{60}^{2+} is considered to be spectator Auger decay of shape resonance states followed by cascade or electron tunneling, because there are many shape resonance states at various photon energies. In contrast, resonace Auger processes have been disregarded in the calculations.[1)] The partial and total photoionzation yield curves of C_{70} are similar to those of C_{60}. Ratio of the yields of C_{60}^{2+}/C_{60}^+ and C_{70}^{2+}/C_{70}^+ are found to be larger than unity at $h\nu$ > 50 eV. The observed yield curves and ratios quite differ from those reported in the electron impact ionization of C_{60} and C_{70}.

Reference

1) P. Colavita, *et al*., *Phys. Chem. Chem. Phys.* **3**, 4481–4487 (2001).

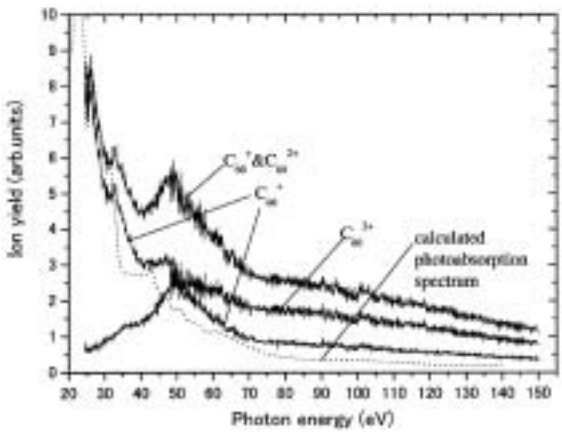

Figure 1. Partial and total photoionization yield curves of C_{60}.

RESEARCH ACTIVITIES VII
Coordination Chemistry Laboratories

Prof. Hiroyuki Matsusaka (Osaka Prefecture Univ.), Assoc. Prof. Keiji Ueno (Gunma Univ.) took the position of Laboratory of Coordination Bond from April 2003. Prof. Nobuhiro Tokito (Kyoto University) and Assoc. Prof. Kiyotaka Onizuka (Osaka University) finished their term as Adjunct Prof. of the Coordination Bond in March 2003. Their effort during their term is gratefully appreciated. Prof. Masahito Yamashita (Tokyo Metropolitan Univ.) and Prof. Naoto Chatani (Osaka Univ.) continue the position of the Laboratory of Synthetic Coordination Chemistry.

VII-A Nano-Sciences of Advanced Metal Complexes

Recently, nano-sciences or nano-technologies have been attracting much attention because they show very interesting physical properties based on the non-linearity and quantum effect. There are two methods to obtain the nano-size materials, that is, "top-down" and "bottom-up." The top-down method such as laser abrasion has a limitation to make particles with the size less than 100 nm. On the other hand, the bottom-up method is promising to control the nano-size since the chemical reactions are available. However, the researches based on the bottom-up methods are rare and such methods have not been accomplished so far. There are three types of the target materials such as inorganic compounds, organic compounds, and metal complexes. The inorganic compounds easily take three-dimensional bulk structures. The organic compounds easily take 0- and 1-dimesional bulk materials. Therefore, neither inorganic nor organic compounds are suitable for the nano-sciences. On the other hand, the metal complexes easily take nano-size clusters where they are surrounded with the organic ligands. Therefore, the nano-sciences of the advanced metal complexes are most promising. As for the non-linearity, we focus on the gigantic third-order optical non-linearity. As for the quantum effect, we focus on the single-molecule magnets, nano-wire molecule-magnets, and nano-network molecule-magnets.

VII-A-1 Out-of-Plane Dimers of Mn(III) Quadridentate Schiff-Base Complexes with Saltmen^{2-} and Naphtmen^{2-} Ligands: Structure Analysis and Ferromagnetic Exchange

MIYASAKA, Hitoshi[1]; CLERAC, Rodolphe[2]; ISHII, Tomohiko[1]; CHANG, Ho-Chol[3]; KITAGAWA, Susumu[3]; YAMASHITA, Masahiro[4]
([1]Tokyo Metropolitan Univ.; [2]Cent. Recherche Paul Pascal; [3]Kyoto Univ.; [4]IMS and Tokyo Metropolitan Univ.)

[*J. Chem. Soc., Dalton Trans.* **7**, 1528–1534 (2002)]

Six Mn(III) quadridentate Schiff base compounds with N,N'-(1,1,2,2-tetramethylethylene)bis(salicylideneiminato) dianion (saltmen^{2-}) and N,N'-(1,1,2,2-tetramethylethylene)bis(naphthylideneiminato) dianion (naphtmen^{2-}) were prepared and structurally characterized: [Mn(saltmen)(H_2O)]ClO_4 (1), [Mn(naphtmen)(H_2O)]ClO_4 (2), [Mn(saltmen)(NCS)] (3), [Mn(naphtmen)(NCS)] (4), [Mn(saltmen)(Cl)] (5) and [Mn(naphtmen)(Cl)] (6). Among them, 1 and 2 form phenolate-bridged out-of-plane dimers with Mn-Ophenolate bond distances of 2.434(2) and 2.662(3) Å, respectively. X-ray diffraction analyses show that compounds 3, 4 and 6 can also be considered as out-of-plane dimers in spite of long Mn-Ophenolate interacting distances (3.441(2) Å for 3, 3.758(3) Å for 4 and 3.505(5) Å for 6). In contrast with the above compounds, 5 is a discrete Mn(III) mononuclear complex with a square-pyramidal geometry. In the dimer series (compounds 1–4 and 6), the out-of-plane intermolecular distance varies dramatically according to equatorial ligands, saltmen^{2-} or naphtmen^{2-}, and axial ligands, H_2O, NCS^- and Cl^-. The relation between substitution of the ligands and structural parameters of the dimeric molecules are discussed. Magnetic susceptibility studies reveal interesting intra-dimer ferromagnetic interactions between Mn(III) ions. These new $S = 4$ building blocks open new possibilities in the design of magnetic molecule-based materials.

VII-A-2 Electron Spin Resonance Studies of Co(tbp)·C_{60} Single Crystal

TANAKA, Hisaaki[1]; MARUMOTO, Kazuhiro[1]; KURODA, Shin-ichi[1]; ISHII, Tomohiko[2]; KANEHAMA, Ryo[2]; AIZAWA, Naoko[2]; MATSUZAKA, Hiroyuki[2]; SUGIURA, Ken-ichi[2]; MIYASAKA, Hitoshi[2]; KODAMA, Takeshi[2]; KIKUCHI, Koichi[2]; IKEMOTO, Isao[2]; YAMASHITA, Masahiro[3]
([1]Nagoya Univ.; [2]Tokyo Metropolitan Univ.; [3]IMS and Tokyo Metropolitan Univ.)

[*J. Phys.: Condens. Matter* **14**, 3993–4000 (2002)]

ESR measurements were made on a newly synthesized cocrystallite of C_{60} with the Co^{II} complex of 5, 10, 15, 20-tetrakis[3, 5-(di-tert-butyl)-phenyl]porphyrin (tbp) single crystal to study the strong intermolecular interactions which are suggested by x-ray structural analyses. A single anisotropic ESR absorption line is observed. At room temperature with the principal g-values ($g_\perp$ = 2.423 and $g_\parallel$ = 2.005), which are typical values for the low-spin Co^{II} ions (S = 1/2). The antiferromagnetic superexchange interaction between Co^{II}

ions *via* C_{60} is confirmed from the observation of the finite Weiss temperature, which is further supported by the absence of the hyperfine splitting due to ^{59}Co (I = 7/2) nuclei. As the temperature is lowered, the $g_{\perp}$-value decreases monotonically suggesting an increase of the crystal-field splitting energy. This result is consistent with the fact that the intermolecular distance between Co^{II} and C_{60} becomes shorter as the temperature decreases. The peak-to-peak ESR linewidths ΔHpp along both principal axes increase with temperature due to the shorter spin-lattice relaxation time.

VII-A-3 Structure, Magnetic and Electronic Properties of Charge Transfer Complex Containing Hexacyanoferrate Chain and BEDT-TTF Column

NAKATA, Kazuya[1]; YOSHINO, Yuko[1]; HARA, Hatsune[1]; MANABE, Toshio[1]; ISHII, Tomohiko[1]; MIYASAKA, Hitoshi[1]; YAMASHITA, Masahiro[2]; MATSUZAKA, Hiroyuki[1]; KATADA, Motomi[1]
([1]Tokyo Metropolitan Univ.; [2]IMS and Tokyo Metropolitan Univ.)

[*Mol. Cryst. Liq. Cryst.* **380**, 117–122 (2002)]

A novel charge transfer complex containing of hexacyanoferrate ($Fe(CN)_6$) unit, which has been exhibited variety of magnetic topics in prussian blue systems, was synthesized. X-ray analysis of the single crystal obtained by electrolysis of BEDT-TTF (ET) and hexacyanoferrate suggests that this complex contains 1-dimensional magnetic hexacyanoferrate chain perpendicular to the conducting ET column. This significant structure implies that significant properties can be expected caused by the interaction between the spin momentum on *d*-electrons and a conducting π-electrons influenced vertically by the applied magnetic field. From the electronical conducting measurement, it is suggested that is a semiconductor, with the activation energy and the conductivity at room temperature to be 0.113 eV and 0.46 S/cm, respectively. Detailed x-ray analysis suggests that the occupancies of Fe and C elements in the 1-dimensional hexacyanoferrate chain are 0.5, that of N element is 1.0.

VII-A-4 Creations of Solitons and Polarons in MX-Chain Compounds, $\{[Pt(en)_2][PtX_2(en)_2]\}_3(CuX_4)_4$ (X = Cl and Br)

ASO, Hidemitsu[1]; MANABE, Toshio[1]; KAWASHIMA, Takuya[3]; ISHII, Tomohiko[1]; MIYASAKA, Hitoshi[1]; MATSUZAKA, Hiroyuki[1]; YAMASHITA, Masahiro[2]; KURODA, Noritaka[4]; SHIRO, Motoo[5]
([1]Tokyo Metropolitan Univ. and PRESTO(JST); [2]IMS and Tokyo Metropolitan Univ.; [3]Nagoya Univ.; [4]Kumamoto Univ.; [5]Rigaku Co.)

[*Mol. Cryst. Liq. Cryst.* **376**, 7–12 (2002)]

The creations of solitons and polarons in the $\{[Pt(en)_2][PtX_2(en)_2]\}_3(CuX_4)_4$ (X = Cl and Br) which consist of the double linear chain structures of the main one-dimensional halogen-bridged Pt(II)-Pt(IV) mixed-valence units and one-dimensional counteranions of trigonal bipyramidal Cu(I) ions, have been investigated by the absorption spectra, photoinduced absorption spectra, and ESR spectra. The ESR signals of the Pt(III) and Cu(II) species, which were introduced during the synthetic process, are observed in the compound. The relative intensities of *d-d* transitions and ESR spectra of Cu(II) species in counteranions are consistent with each other in the Cl-bridged compounds obtained by pH control. The photoinduced absorption of the Cl-bridged compound is observed in the mid-gap region, which is attributable to the soliton. The doping effect by Br_2 was investigated for the Br-bridged compound. The relative intensities of *d-d* transition and ESR spectra in Cu(II) increase with increasing exposure time. However, the electrical conductivities do not increase. Therefore, the induced Pt(III) species are attributable to neutral solitons.

VII-A-5 Syntheses and Physical Properties of Complexes of Fullerene with Magnetic Metal Porphyrins

AIZAWA, Naoko[1]; HARA, Hatsune[1]; ISHII, Tomohiko[1]; YAMASHITA, Masahiro[2]; MIYASAKA, Hitoshi[1]; MATSUZAKA, Hiroyuki[1]; KODAMA, Takeshi[1]; KIKUCHI, Koichi[1]; IKEMOTO, Isao[1]
([1]Tokyo Metropolitan Univ.; [2]IMS and Tokyo Metropolitan Univ.)

[*Mol. Cryst. Liq. Cryst.* **376**, 13–18 (2002)]

Crystals containing C_{60} and M(OEP) (M^{2+} = Pd, Cu, Ag; OEP^{2-} = octaethylporphinato) were synthesized. Crystal structures were determined for $Cu(OEP)\cdot C_{60}\cdot 2C_6H_6$, $Ag(OEP)\cdot C_{60}\cdot 2C_6H_6$ and $Pd(OEP)\cdot C_{60}\cdot 1.5C_6H_6$. From the x-ray analysis of the cocrystallites, the porphyrin molecules still retain their planar structures without deforming to the fit to the curved surface of the fullerene.

VII-A-6 Crystal and Electronic Structures of Quasi-One-Dimensional Halogen-Bridged Binuclear Platinum Complexes, $\{(C_nH_{2n+1})_2NH_2\}_4[Pt_2(pop)_4I]$ (n = 2–6)

TAKIZAWA, Kouichi[1]; ISHII, Tomohiko[1]; MIYASAKA, Hitoshi[1]; MATSUZAKA, Hiroyuki[1]; YAMASHITA, Masahiro[2]; KAWASHIMA, Takuya[3]; MATSUZAKI, Hiroyuki[4]; KISHIDA, Hideo[4]; OKAMOTO, Hiroshi[4]
([1]Tokyo Metropolitan Univ.; [2]IMS and Tokyo Metropolitan Univ.; [3]Nagoya Univ.; [4]Univ. Tokyo)

[*Mol. Cryst. Liq. Cryst.* **376**, 159–164 (2002)]

The crystal structures of $\{(C_nH_{2n+1})_2NH_2\}_4[Pt_2(pop)_4I]$ (pop = $O(PO_2H)_2^{2-}$, n = 2–6) were determined. Judging from the results of the x-ray structural analyses and Raman spectra, 1-dimensional electronic structures of these compounds are considered to be $\cdots Pt^{2+}–Pt^{3+}–X\cdots Pt^{2+}–Pt^{3+}–X\cdots$ charge-polarized states.

VII-A-7 Physical Properties of Quasi-One-Dimensional Mixed-Metal and Mixed-Halogen Complexes, $Ni_{1-x}Pd_x(chxn)_2Cl_yBr_{1-y}Y_2$

MANABE, Toshio[1]; YOKOYAMA, Kohei[1]; ISHII, Tomohiko[1]; MIYASAKA, Hitoshi[1]; MATSUZAKA, Hiroyuki[1]; YAMASHITA, Masahiro[2]; KAWASHIMA, Takuya[3]; MATSUZAKI, Hiroyuki[4]; KISHIDA, Hideo[4]; OKAMOTO, Hiroshi[4]; MARUMOTO, Kazuhiro[3]; TANAKA, Hisaaki[3]; ITOH, Hiroshi[3]; KURODA, Shin-ichi[3]
([1]Tokyo Metropolitan Univ.; [2]IMS and Tokyo Metropolitan Univ.; [3]Nagoya Univ.; [4]Univ. Tokyo)

[*Mol. Cryst. Liq. Cryst.* **376**, 165–170 (2002)]

Single crystals of quasi-one-dimensional Ni-Pd mixed-metal MX-chain compounds, $Ni_{1-x}Pd_x(chxn)_2Br_3$, and mixed-halogen MX-chain compounds, $Ni(chxn)_2Cl_yBr_{1-y}(NO_3)_2$ were obtained by electrochemical oxidation methods. To investigate the electronic states of these compounds, the optical conducting spectra were measured. The electronic states of the Ni compounds can be controlled by forming the mixed-metal or mixed-halogen systems.

VII-A-8 Magnetic/Conducting Hybrid Compound Composed of 1-D Chain $[Mn^{II}_2Cl_5(EtOH)]_\infty^-$ and BEDT-TTF Stacking Layer

MIYASAKA, Hitoshi[1]; YOSHINO, Yuko[1]; ISHII, Tomohiko[1]; KANEHAMA, Ryo[1]; MANABE, Toshio[1]; YAMASHITA, Masahiro[2]; NISHIKAWA, Hiroyuki[1]; IKEMOTO, Isao[1]; KISHIDA, Hideo[3]; MATSUZAKI, Hiroyuki[3]; OKAMOTO, Hiroshi[3]
([1]Tokyo Metropolitan Univ.; [2]IMS and Tokyo Metropolitan Univ.; [3]Univ. Tokyo)

[*J. Solid State Chem.* **168**, 418–426 (2002)]

An assembled compound $(BEDT\text{-}TTF)_2[Mn_2Cl_5(EtOH)]$ (1) consisting of two structural lattices of Mn(II)-Cl 1-dimensional (1-D) chains and bis(ethylenedithio)tetrathiafulvalene (BEDT-TTF) stacking layers was synthesized by electrochemical method. Compound 1 crystallized in triclinic space group with a = 13.1628(5), b = 20.3985(9), c = 7.4966(3) Å, α = 98.3498(8), β =104.980(1), γ = 74.602(2)°, and Z = 2. The 1-dimensional chains and the stacking layers are aligned along the c-axis of the unit cell. The 1-dimensional chain is described as $[Mn_2Cl_5(EtOH)]_\infty^-$ in which two Mn(II) ions and four Cl^- ions form a ladder-like chain with Kagome (cuboidal) sublattices, and the remaining Cl^- ion and an EtOH molecule cap the edge-positioned Mn(II) ions of the chains. The BEDT-TTF molecules are packed between the Mn-Cl chains (*ac*-plane), the intermolecules S···S contacts of which are approximately found in the range 3.440(2)–3.599(2) Å. The packing feature of BEDT-TTF molecule is very similar to that of $(BEDT\text{-}TTF)_2ClO_4(TCE)_{0.5}$ (TCE = 1,1,2-trichloroethane). Regarding the electronic state of each BEDT-TTF molecule, Raman spectroscopic analysis and ESR study revealed half-valence BEDT-TTF molecules (charge delocalization) in 1. Magnetic measurements clearly demonstrated that the paramagnetic spins on the 1-dimensional chain $[Mn_2Cl_5(EtOH)]_\infty^-$ arrange antiferromagnetically in the low-temperature region. Additionally, 1 exhibits metallic conduction in the temperature range 2.0–300 K (σ = 21 S cm^{-1} at 300 K and 1719 S cm^{-1} at 2.0 K), due to the contribution of the stacked BEDT-TTFs. Consequently, these peculiarities that correspond to antiferromagnetic/metallic conduction demonstrate the bifunctionality of 1.

VII-A-9 Structure and Electrochemistry of the Bridging-Ligand Mono-Substituted Diruthenium Compound, $[Ru_2(II,III)(O_2CCH_3)_3(admpym)(Cl)(MeOH)]$ (Hadmpym = 2-amino-4,6-dimethylpyrimidine)

KACHI-TERAJIMA, Chihiro[1]; MIYASAKA, Hitoshi[1]; ISHII, Tomohiko[1]; SUGIURA, Ken-ichi[1]; YAMASHITA, Masahiro[2]
([1]Tokyo Metropolitan Univ.; [2]IMS and Tokyo Metropolitan Univ.)

[*Inorg. Chim. Acta* **332**, 210–215 (2002)]

The ligand substitution reaction of $Ru_2(O_2CCH_3)_4Cl$ with 2-amino-4,6-dimethylpyrimidine (Hadmpym) under gentle refluxing conditions in MeOH gave a bridging-ligand mono-substituted compound, $[Ru_2(O_2CCH_3)_3(admpym)(Cl)(MeOH)]$ (**1**). **1** Crystallized in monoclinic space group $P2_1/n$ with a = 8.3074(8), b = 12.3722(8) Å, c = 18.913(1) Å, β =95.559(3)°, V = 1934.8(3) $Å^3$, and Z = 4. Temperature dependence of the magnetic susceptibility of 1 revealed it to be in a spin ground state S = 3/2 arising from the electronic configuration of $\sigma^2\pi^4\delta^2(\delta^*\pi^*)^3$. Compound 1 undergoes three metal-centered redox reactions in electrochem.: $E_{1/2}$ (ox) = +0.72 V (Ia/Ic < 1, ΔEp = 0.17 V); $E_{1/2}$ (1,red) = –0.65 V (Ia/Ic ≈ 1, ΔEp = 0.10 V); and $E_{1/2}$ (2,red) = –1.80 V (Ia/Ic.mchlt.1, ΔEp = 0.16 V). Then, the redox species produced by electrolysis were characterized by spectroscopic studies.

VII-A-10 Electrical Conduction of Halogen-Bridged Metal Complexes $Ni_{1-x}Pd_x(chxn)_2Br_3$

ITO, Hiroshi[1]; SUNATA, Makoto[1]; KURODA, Shin-ichi[1]; MANABE, Toshio[2]; YAMASHITA, Masahiro[3]
([1]Nagoya Univ.; [2]Tokyo Metropolitan Univ.; [3]IMS and Tokyo Metropolitan Univ.)

[*Mol. Cryst. Liq. Cryst.* **379**, 285–290 (2002)]

The resistance and thermopower of the quasi-one-dimensional halogen-bridged metal complexes $Ni_{1-x}Pd_x(chxn)_2Br_3$ were studied. Pressure dependence of the resistance indicates the crossover from SDW state to CDW state at x = 0.84–0.95. For almost all x region, thermopower is negative. For x < 0.5, thermopower is independent of temperature, while it is semiconducting for x > 0.6.

VII-A-11 Reactions of Mn(III) Quadridentate Schiff Base Compounds with TCNQ Anion to Form Unusual TCNQ Derivatives by Alcoholysis

MIYASAKA, Hitoshi[1]; SUGIMOTO, Kunihisa[2]; SUGIURA, Ken-ichi[1]; ISHII, Tomohiko[1]; YAMASHITA, Masahiro[3]
([1]Tokyo Metropolitan Univ.; [2]Rigaku Co. ; [3]IMS and Tokyo Metropolitan Univ.)

[*Mol. Cryst. Liq. Cryst.* **379**, 197–204 (2002)]

The reactions of Mn(III) quadridentate Schiff base compounds, $[Mn(saltmen)(H_2O)]ClO_4$ (1; saltmen^{2-} = N,N'-(1,1,2,2-tetramethylethylene)bis(salicylideneiminato)) and $[Mn(naphtmen)(H_2O)]ClO_4$ (2; naphtmen^{2-} = N,N'-(1,1,2,2-tetramethylethylene)bis(naphthylideneiminato)), with LiTCNQ gave three types of compounds depending on reaction conditions: $[Mn(saltmen)(H_2O)](TCNQ)$ (3), [Mn(saltmen)(MeOH)(TCNQ-OMe)] (4, TCNQ-OMe$^-$ = p-(α,α-dicyano-α-methoxytolyl)dicyanomethanide), and [Mn(naphtmen)(MeOH)(TCNQA-OMe)] (5, TCNQA-OMe$^-$ = p-(α-cyano-α-methoxy-a-methylamidotolyl)$^-$ dicyanomethanide). Compounds 3·MeOH and 5 were characterized by x-ray crystallography. Compounds 3 and 4 were prepared under anaerobic and aerobic conditions, respectively, in MeOH/H_2O. Compound 5 was synthesized under aerobic conditions analogous to 4. For 4 and 5, unusual additional reactions on the anionic TCNQ molecule occurred to form (TCNQ-OMe)$^-$ for 4 and (TCNQA-OMe)$^-$ for 5. Ferromagnetic and antiferromagnetic interactions in the prepared compounds were investigated.

VII-A-12 Out-of-Plane Dimer Structures and Magnetic Properties of Mn(III) Quadridentate Schiff Base Compounds with N,N'-(1,1,2,2-tetramethylethylene)bis(5-chlorosalicylideneiminato)

MIYASAKA, Hitoshi[1]; MIZUSHIMA, Kaori[1]; FURUKAWA, Sachie[1]; SUGIURA, Ken-ichi[1]; ISHII, Tomohiko[1]; YAMASHITA, Masahiro[2]
([1]Tokyo Metropolitan Univ.; [2]IMS and Tokyo Metropolitan Univ.)

[*Mol. Cryst. Liq. Cryst.* **379**, 171–178 (2002)]

Three Mn(III) quadridentate Schiff base compounds with N,N'-(1,1,2,2-tetramethylethylene)bis(5-chlorosalicylideneiminato) (5-Clsaltmen^{2-}) were prepared and characterized: $[Mn_2(5\text{-}Clsaltmen)_2(H_2O)_2](ClO_4)_2$ (1), $[Mn_2(5\text{-}Clsaltmen)_2(5\text{-}Clsal)_2]$ (2, 5-Clsal = phenol-bonded 5-chlorosalicylaldehyde), and $[NEt_4]_2[Mn_2(5\text{-}Clsaltmen)_2(MeOH)_2][Fe(CN)_6]ClO_4\cdot 2MeOH$ (3). All compounds contain Mn(III) out-of-plane dimer units. The magnetic measurements revealed intra-dimer ferromagnetic exchange interaction between Mn(III) ions via phenolate O, producing a $S = 4$ spin ground state. The structures of 2 and 3 were determined by x-ray crystallography.

VII-A-13 Synthesis, Structure and Magnetic Properties of the Antiferromagnetic Hexamanganese Cluster $[Mn_6(\mu_4\text{-}O)_2(O_2CC_6HF_4)_{10}(HO_2CCH_3)_4]\cdot(C_7H_8)$

NAKATA, Kazuya[1]; MIYASAKA, Hitoshi[1]; ISHII, Tomohiko[1]; YAMASHITA, Masahiro[2]; AWAGA, Kunio[3]
([1]Tokyo Metropolitan Univ.; [2]IMS and Tokyo Metropolitan Univ.; [3]Univ. Tokyo)

[*Mol. Cryst. Liq. Cryst.* **379**, 211–216 (2002)]

A hexanuclear Mn^{II}-Mn^{III}-cluster, $[Mn_6(O)_2(O_2CC_6HF_4)_{10}(HO_2CCH_3)_4]\cdot(C_7H_8)$ (1), was synthesized by a typical acetate-substitution reaction of the known Mn_{12}-cluster, $[Mn_{12}(O)_{12}(O_2CCH_3)_{16}(H_2O)_4]\cdot 2CH_3CO_2H\cdot 4H_2O$ in the presence of an excess of 2,3,5,6-tetrafluorobenzoic acid. Each unpaired spin on Mn(II) and Mn(III) ions is promoted as to be antiferromagnetically cancelled to produce an $S = 0$ ground state.

VII-A-14 Evidence for Single-Chain Magnet Behavior in a Mn^{III}-Ni^{II} Chain Designed with High Spin Magnetic Units: A Route to High Temperature Metastable Magnets

CLERAC, Rodolphe[1]; MIYASAKA, Hitoshi[2]; YAMASHITA, Masahiro[3]; COULON, Claude[1]
([1]Cent. Recherche Paul Pascal; [2]Tokyo Metropolitan Univ.; [3]IMS and Tokyo Metropolitan Univ.)

[*J. Am. Chem. Soc.* **124**, 12837–12844 (2002)]

The authors herein present the synthesis, crystal structure, and magnetic properties of a new heterometallic chain of Mn^{III} and Ni^{II} ions, $[Mn_2(saltmen)_2Ni(pao)_2(py)_2](ClO_4)_2$ (1) (saltmen^{2-} = N,N'-(1,1,2,2-tetramethylethylene)bis(salicylideneiminate) and pao$^-$ = pyridine-2-aldoximate). The crystal structure of 1 was studied by x-ray crystallography analysis: compound 1 crystallized in monoclinic, space group $C2/c$ with a = 21.140(3), b = 15.975(1), c = 18.6212(4) Å, β = 98.0586(4)°, and $Z = 4$. This compound consists of two fragments, the out-of-plane dimer $[Mn_2(saltmen)_2]^{2+}$ as a coordination acceptor building block and the neutral mononuclear unit $[Ni(pao)_2(py)_2]$ as a coordination donor building block, forming an alternating chain having the repeating unit $[–Mn–(O)_2–Mn–ON–Ni–NO–]_n$. In the crystal structure, each chain is well separated with a minimum intermetallic distance between Mn and Ni ions of 10.39 Å and with the absence of interchain π overlaps between organic ligands. These features ensure a good magnetic isolation of the chains. The *d.c.* and *a.c.* magnetic measurements were performed on both the polycrystalline sample and the aligned single crystals of 1. Above 30 K, the magnetic susceptibility of this 1-dimensional compound was successfully described in a mean field approximation as an assembly of trimers (Mn···Ni···Mn) with a $Ni^{II}\cdots Mn^{III}$ antiferromagnetic interaction (J = –21 K) connected through a ferromagnetic $Mn^{III}\cdots Mn^{III}$ interaction (J'). However, the mean field theory fails to describe the magnetic behavior < 30 K emphasizing the

1-dimensional magnetic character of the title compound. Between 5 and 15 K, the susceptibility in the chain direction was fitted to a 1-dimensional Ising model leading to the same value of *J'*. Hysteresis loops are observed < 3.5 K, indicating a magnet-type behavior. In the same range of temperature, combined *a.c.* and *d.c.* measurements show a slow relaxation of the magnetization. This result indicates a metastable state without magnetic long-range order. This material is the 1st experimental design of a heterometallic chain with S_T = 3 magnetic units showing a single-chain magnet behavior predicted in 1963 by R. J. Glauber for an Ising 1-dimensional system. This work opens new perspectives for 1-dimensional systems to obtain high temperature metastable magnets by combining high spin magnetic units, strong inter-unit interactions, and uniaxial anisotropy.

VII-A-15 Tuning of Spin Density Wave Strengths in Quasi-One-Dimensional Mixed-Halogen-Bridged Ni(III) Complexes with Strong-Electron Correlation, $[Ni^{III}(chxn)_2Cl_{1-x}Br_x](NO_3)_2$

MANABE, Toshio[1]; YOKOYAMA, Kohei[1]; FURUKAWA, Sachie[1]; KACHI-TERAJIMA, Chihiro[1]; NAKATA, Kazuya[1]; IWAHORI, Fumiyasu[1]; MIYASAKA, Hitoshi[1]; SUGIURA, Ken-ichi[1]; YAMASHITA, Masahiro[2]; KISHIDA, Hideo[3]; OKAMOTO, Hiroshi[3]
([1]Tokyo Metropolitan Univ.; [2]IMS and Tokyo Metropolitan Univ.; [3]Univ. Tokyo)

[*Inorg. Chem.* **41**, 4993–4995 (2002)]

This communication describes the syntheses of the quasi-one-dimensional mixed-halogen-bridged Ni^{III} complexes with strong electron correlation $[Ni(chxn)_2Cl_{1-x}Br_x](NO_3)_2$ and the tuning of the spin density wave strengths of these compounds. If the Cl 3*p* and Br 4*p* make one band in the compounds, we should observe a single peak in the electronic spectra. As a result, we should observe the single peak from 1.45 to 2.00 eV depending on the mixing ratios of Cl and Br ions. Therefore, the Cl 3*p* and Br 4*p* make one band. Then, we have succeeded in tuning the spin density wave strengths of the Ni^{III} complexes with the strong electron correlation by mixing the bridging halogen ions successively.

VII-A-16 Syntheses and Physical Properties of New Charge-Transfer Salts Consisting of a Conducting BEDT-TTF Column and Magnetic 1D or 2D Fe(III) Networks

KANEHAMA, Ryo[1]; YOSHINO, Yuko[1]; ISHII, Tomohiko[1]; MANABE, Toshio[1]; HARA, Hatsune[1]; MIYASAKA, Hitoshi[1]; MATSUZAKA, Hiroyuki[1]; YAMASHITA, Masahiro[2]; KATADA, Motomi[1]; NISHIKAWA, Hiroyuki[1]; IKEMOTO, Isao[1]
([1]Tokyo Metropolitan Univ.; [2]IMS and Tokyo Metropolitan Univ.)

[*Synth. Met.* **133-134**, 553–554 (2003)]

Two new molecular-based charge-transfer salts of bis(ethylenedithio)tetrathiafulvalene were prepared, that is $(BEDT\text{-}TTF)_3Fe(CN)_6\cdot 4H_2O$ and $(BEDT\text{-}TTF)_4Fe(C_2O_4)_3K\cdot PhCl$. Their crystal structures and physical properties were studied. Their structures consist of conducting columns of BEDT-TTF and magnetic 1-dimensional or 2-dimensional networks containing Fe(III) ions connected by cyano- or oxalate-bridges. The *d*-π interactions are discussed.

VII-A-17 Novel Optical and Magnetic Bistability and Photoinduced Transition in a One-Dimensional Halogen-Bridged Binuclear Pt Complex

MATSUZAKI, Hiroyuki[1]; MATSUOKA, Takashi[1]; KISHIDA, Hideo[1]; TAKIZAWA, Kouichi[2]; MIYASAKA, Hitoshi[2]; SUGIURA, Ken-ichi[2]; YAMASHITA, Masahiro[3]; OKAMOTO, Hiroshi[1]
([1]Univ. Tokyo; [2]Tokyo Metropolitan Univ.; [3]IMS and Tokyo Metropolitan Univ.)

[*Phys. Rev. Lett.* **90**, 046401 (4 pages) (2003)]

In I-bridged binuclear Pt compounds, $R_4[Pt_2(pop)_4I]nH_2O$ and $R'_2[Pt_2(pop)_4I]nH_2O$ (pop = $P_2O_5H_2^{2-}$), electronic structures on the PtPtI chains were controlled between a diamagnetic charge-density-wave (CDW) state and a paramagnetic charge-polarization (CP) state by modification of the counterions (R, R') located between chains. In the R = $Et_2NH_2^+$ compound, a pressure-induced CP to CDW transition with a drastic color change is identified. This transition is accompanied by a large hysteresis loop within which photo-induced transition between CDW and CP can be driven by selecting the excitation photon energy.

VII-A-18 Unprecedented Soliton Formation Mechanism in Quasi-One-Dimensional Chloro-Bridged Pt^{II}-Pt^{IV} Mixed-Valence Compound, $\{[Pt(en)_2][PtCl_2(en)_2]\}_3(CuCl_4)_4\cdot 12H_2O$

YAMASHITA, Masahiro[1]; ASO, Hidemitsu[2]; MATSUNAGA, Satoshi[2]; TAKIZAWA, Kouichi[2]; NAKATA, Kazuya[2]; KACHI-TERAJIMA, Chihiro[2]; IWAHORI, Fumiyasu[2]; ISHII, Tomohiko[2]; MIYASAKA, Hitoshi[2]; SUGIURA, Ken-ichi[2]; KAWASHIMA, Takuya[3]; TAKAI, Kenzi[3]; KURODA, Noritaka[4]; SHIRO, Motoo[5]; KISHIDA, Hideo[6]; OKAMOTO, Hiroshi[6]; TAKAHASHI, Hiroyuki[3]; TANAKA, Hisaaki[3]; MARUMOTO, Kazuhiro[3]; KURODA, Shin-ichi[3]
([1]IMS and Tokyo Metropolitan Univ.; [2]Tokyo Metropolitan Univ.; [3]Nagoya Univ.; [4]Kumamoto Univ.; [5]Rigaku Co.; [6]Univ. Tokyo)

[*Chem. Lett.* **32**, 278–279 (2003)]

A new type of complex consisting of double liner-chain structure $\{[Pt(en)_2][PtCl_2(en)_2]\}_3(CuCl_4)_4\cdot 12H_2O$ was synthesized. High concentration (*ca.* 200 times larger than the literature) of neutral soliton (Pt^{III} component) formation was found. This unprecedented soliton formation mechanism will be discussed.

VII-A-19 A Series of Ni(II) Pyridyloximato (pao^-) Compounds $[Ni(pao)_2(L)_2]$ (L = Unidentate Ligand): As a Coordination Donor Building Block in the Assembly with Mn(III) Salen Analogues

MIYASAKA, Hitoshi[1]; MIZUSHIMA, Kaori[1]; SUGIURA, Ken-ichi[1]; YAMASHITA, Masahiro[2]
([1]Tokyo Metropolitan Univ.; [2]IMS and Tokyo Metropolitan Univ.)

[*Synth. Met.* **137**, 1245–1246 (2003)]

A series of mononuclear Ni(II) compounds $[Ni(pao)_2(L)_2]$ (pao^- = 2-pyridyloximate, L = pyridine (1), 4-picoline (2), 4-ethylpyridine (3), 4-tert-butylpyridine (4), and N-methylimidazole (5)) were synthesized and characterized. The structures of 1–3 were determined by X-ray crystallography and revealed that all compounds have the same structural motif with trans coordination fashion for the identical ligands. For magnetic data, the best-fitting to an $S = 1$ ground state with the zero-field splitting effect found to have the zero-field splitting parameter $|D|$ of 3 as approximate 4 K in this series. These compounds are good coordination donor building blocks for assembly with Mn(III) salen analogs as coordination acceptor building blocks to form 1-D magnetic chains.

VII-A-20 Pressure Effects on an $S = 1$ Haldane Compound $Ni(C_5H_{14}N_2)_2N_3(PF_6)$

MITO, Masaki[1]; AKAMA, Hironori[2]; DEGUCHI, Hiroyuki[1]; TAKAGI, Seishi[1]; KAWAE, Tatsuya[2]; TAKEDA, Kazuyoshi[2]; ISHII, Tomohiko[3]; YAMASHITA, Masahiro[4]; NAKAO, Hironori[5]; MURAKAMI, Yoichi[5]; YAMAMOTO, Shoji[6]
([1]Kyushu Inst. Tech.; [2]Kyushu Univ.; [3]Tokyo Metropolitan Univ.; [4]IMS and Tokyo Metropolitan Univ.; [5]Tohoku Univ.; [6]Hokkaido Univ.)

[*J. Phys. Soc. Jpn.* **72**, 399–404 (2003)]

The pressure effects on an $S = 1$ Haldane compound $Ni(C_5H_{14}N_2)_2N_3(PF_6)$ (NDMAP) were studied through the magnetic susceptibility (χ) measurements using single crystal samples and the powder x-ray structural analysis experiment under pressure up to 11.5 kbar. The crystal-axis dependence of χ was analyzed with the results of quantum Monte Carlo simulation. Probably both the intrachain interaction (J) and single-ion anisotropy (D) are enhanced by pressure: $J = 31.5$ K ($P = 0$ kbar) $\rightarrow$ 90.0 K (10.0 kbar) and $D/J = 0.3$ ($P = 0$ kbar) $\rightarrow$ 0.4 (9.5 kbar). As for J, there is the linear increase against pressure as $dJ/dP = 2.0$ K/kbar in the pressure region below $P = 8.0$ kbar, at around which dJ/dP rapidly changes to $dJ/dP = 2.1 \times 101$ K/kbar. The ratio of D/J changes within 0.3–0.4, and probably D as well as J drastically change at around $P = 8.0$ kbar. Also, at $P = 9.5$ kbar, the development of paramagnetic moment on the easy plane is detected, and it is assumed that the interchain interaction may be also enhanced under pressure. The structural analysis shows that the interchain shrinkage is larger than the intrachain one. However, a result concerning the rapid changes of J and D at around $P = 8.0$ kbar was not observed, and the authors suppose that the changes of bond-angles such as –N–Ni–N– and –N–N–N– as well as interatomic shrinkage probably change under pressure. The authors assume that those bond-angles of NDMAP at around $P = 9.0$ kbar (J .simeq. 70 K) may become close to those of $Ni(C_5H_{14}N_2)_2N_3(ClO_4)$ (NDMAZ), where the value of J is 71.0 K.

VII-A-21 Platinum(II) Complex with $S = 1/2$ Organic Radical Ligand

IWAHORI, Fumiyasu[1]; MIYASAKA, Hitoshi[1]; ISHII, Tomohiko[1]; SUGIURA, Ken-ichi[1]; YAMASHITA, Masahiro[2]
([1]Tokyo Metropolitan Univ.; [2]IMS and Tokyo Metropolitan Univ.)

[*Synth. Met.* **135-136**, 355–356 (2003)]

A platinum(II) complex with organic radical ligand p-NNpy (= 2-(4'-pyridyl)-4,4,5,5-tetramethyl-imidazoline-1-oxyl-3-oxide) is synthesized. X-ray crystallographic analysis revealed that it has a square-planer four-coordinate anionic structure with formula of $[Pt(p\text{-}NNpy)Cl_3]^-$. Paramagnetic behavior which corresponds to $S = 1/2$ was observed with weak intermolecular antiferromagnetic interaction in the temperature range of 2–300 K. The structure, magnetic property and spectroscopic data will be reported.

VII-A-22 Tuning of Spin Density Wave Strength of Ni(III) Complexes with Strong Electron-Correlation

ONO, Takashi[1]; YAMASHITA, Masahiro[2]; YOKOYAMA, Kohei[1]; FURUKAWA, Sachie[1]; MANABE, Toshio[1]; SUGIURA, Ken-ichi[1]; ISHII, Tomohiko[1]; MIYASAKA, Hitoshi[1]; MATSUZAKA, Hiroyuki[3]; KISHIDA, Hideo[3]; OKAMOTO, Hiroshi[3]; MARUMOTO, Kazuhiro[4]; TANAKA, Hisaaki[4]; HASEGAWA, Yutaka[4]; KURODA, Shin-ichi[4]; ITOH, Hiroshi[4]
([1]Tokyo Metropolitan Univ.; [2]IMS and Tokyo Metropolitan Univ.; [3]Univ. Tokyo; [4]Nagoya Univ.)

[*Synth. Met.* **135-136**, 257–258 (2003)]

We have succeeded in synthesizing the Ni^{III} complexes doped by Co^{III} ions, $[Ni_{1-x}Co_x(chxn)_2Br]Br_2$ ($x = 0$, 0.044, 0.098, 0.118) by using an electrochemical oxidation method. The reflectance spectrum of $[Ni_{1-x}Co_x(chxn)_2Br]Br_2$ shows intense charge transfer bands about 0.5 eV, which are lower than that of $[Ni(chxn)_2Br]Br_2$. (1.3 eV).

VII-A-23 New Charge-Transfer Salts $(ET)_8(Mn^{II}Br_4)_2(DCE)_2$ and $(ET)_3Mn^{II}Br_4$: Preparations, Structures and Physical Properties (ET = BEDT-TTF, DCE = 1,2-Dichloroethane)

KANEHAMA, Ryo[1]; MIYASAKA, Hitoshi[1];

SUGIURA, Ken-ichi[1]; YAMASHITA, Masahiro[2]; ITOH, Hiroshi[3]; KURODA, Shin-ichi[3]; KISHIDA, Hideo[4]; OKAMOTO, Hiroshi[4]
([1]Tokyo Metropolitan Univ.; [2]IMS and Tokyo Metropolitan Univ.; [3]Nagoya Univ.; [4]Univ. Tokyo)

[*Synth. Met.* **135-136**, 633–634 (2003)]

New charge-transfer salts $(ET)_8(MnBr_4)_2(DCE)_2$ **1** and $(ET)_3MnBr_4$ **2** have been synthesized electrochemically and characterized. In both compounds, the magnetic $MnBr_4^{2-}$ anions exist between the conducting ET-layers. The shortest intermolecular Mn···Mn distances are 7.28 and 10.12 Å, respectively, which are too far to magnetically interact directly. But magnetic susceptibility measurements demonstrated that the antiferromagnetic interactions was observed at low temperature. This aniferromagnetic interactions between Mn ions may be operative *via* the π-electrons of conducting layers, that are so-called *d*-π interactions. The crystal structures and physical properties of these compounds are reported.

VII-A-24 Gigantic Third-Order Optical Nonlinearity in One-Dimensional Mott Insulators

KISHIDA, Hideo[1]; ONO, Masaki[1]; MATSUZAKI, Hiroyuki[1]; YAMASHITA, Masahiro[2]; TAGUCHI, Yutaka[3]; TOKURA, Yoshinori[1,4]; OKAMOTO, Hiroshi[1,4]
([1]Univ. Tokyo; [2]IMS and Tokyo Metropolitan Univ.; [3]Tohoku Univ.; [4]AIST)

[*Synth. Met*. **135-136**, 315–316 (2003)]

Third-order optical nonlinearity has been studied in one-dimensional Mott- insulators, Sr_2CuO_3, Ca_2CuO_3, and halogen-bridged Ni compounds $[Ni(chxn)_2X]Y_2$ (X = Br, Cl; Y = Br, Cl, NO_3), by electroreflectance (ER) spectroscopy. In $\chi(3)(-\omega;0,0,\omega)$ (ER) is evaluated to be $\chi(3) \approx 10^{-8}$ to 10^{-5} esu, which is significantly larger than those of conjugated polymers, $10^{-10} \approx 10^{-8}$ esu. An analysis of the ER spectral shape reveals that the strong enhancement of nonlinear optical response originates from the large transition dipole moments between nearly degenerate odd and even states.

VII-A-25 Structure and Magnetic Properties of the Two-Dimensional Ferrimagnet $(NEt_4)[\{Mn(salen)\}_2Fe(CN)_6]$: Investigation of Magnetic Anisotropy on a Single Crystal

MIYASAKA, Hitoshi[1]; IEDA, Hidenori[1]; MATSUMOTO, Naohide[2]; SUGIURA, Ken-ichi[1]; YAMASHITA, Masahiro[3]
([1]Tokyo Metropolitan Univ.; [2]Kumamoto Univ.; [3]IMS and Tokyo Metropolitan Univ.)

[*Inorg. Chem.* **42**, 3509–3515 (2003)]

The title compound, $(NEt_4)[\{Mn(salen)\}_2Fe(CN)_6]$ (1), was synthesized *via* a 1:1 reaction of $[Mn(salen)(H_2O)]ClO_4$ with $(NEt_4)_3[Fe(CN)_6]$ in a MeOH/EtOH medium ($NEt_4^+ = Et_4N^+$ cation, $salen^{2-}$ = N,N'-ethylenebis(salicylidene)iminate). The two-dimensional layered structure of 1 was revealed by x-ray crystallographic analysis: 1 crystallizes in monoclinic space group $P2_1/c$ with a = 12.3660(8), b = 15.311(1), c = 12.918(1) Å, β = 110.971(4)°, Z = 2 and is isostructural to the previously synthesized compound, $(NEt_4)[\{Mn(5\text{-}Clsalen)\}_2Fe(CN)_6]$ (5-$Clsalen^{2-}$ = N,N'-ethylenebis(5-chlorosalicylidene)iminate). The Mn ion is surrounded by an equatorial salen quadridentate ligand and two axial N atoms from the $[Fe(CN)_6]^{3-}$ unit, the four Fe-CN groups of which coordinate to the Mn ions of $[Mn(salen)]^+$ units, forming a two-dimensional network having $[-Mn-NC-Fe-CN-]_4$ cyclic repeating units. The network is spread over the *bc*-plane of the unit cell, and the layers are stacked along the *a*-axis. The counter-cation NEt_4^+ is located between the layers. Compound 1 is a ferrimagnet with T_c = 7.7 K and exhibits hysteresis with a remnant magnetization of 13.44 $cm^3\ mol^{-1}$ at zero field and a coercivity of 1000 Oe when the powder sample was measured at 1.9 K. Magnetic measurements of a direction-arranged single crystal were also carried out. The orientation of the crystallographic axes of a selected single crystal was determined by x-ray analysis, and magnetization was measured when an external field was applied in the *a**, *b*, and *c* directions. The magnetization in the *a** direction increased more easily than those in the *b* and *c* directions below the critical temperature. No hysteresis was observed only for the measurement in the *a** direction, indicating the presence of strong structural anisotropy with potential anisotropy on Mn(III) ions.

VII-A-26 LESR Studies of Long-Lived Photogenerated Spins in the MX-Chain Complex, $Pd(chxn)_2Br_3$

TANAKA, Hisaaki[1]; MARUMOTO, Kazuhiro[1]; KURODA, Shin-ichi[1]; YAMASHITA, Masahiro[2]
([1]Nagoya Univ.; [2]IMS and Tokyo Metropolitan Univ.)

[*Synth. Met.* **135-136**, 317–318 (2003)]

Light-induced ESR (LESR) measurements have been applied on the halogen-bridged metal complex (MX-chain), $Pd(chxn)_2Br_3$, to study the dynamics of the photogenerated spin such as neutral soliton and polaron. The time evolution of the LESR intensity is interpleted in terms of the pair-creation and recombination model of photo-generated spins which are separated by the finite potential barriers on the chain. The LESR intensity showed the same excitation power dependence with the one in the Pt-Cl compound.

VII-A-27 Heterometallic Hexanuclear Cluster with an S = 8 Spin Ground State: $Mn^{II}\{Mn^{II}(hfac)_2\}_3\{Ni^{II}(pao)_3\}_2$ ($hfac^-$ = Hexafluoroacetylacetonate, pao^- = Pyridine-2-aldoximate)

MIYASAKA, Hitoshi[1]; NEZU, Tomohiro[1]; IWAHORI, Fumiyasu[1]; FURUKAWA, Sachie[1]; SUGIMOTO, Kunihisa[2]; CLERAC, Rodolphe[3]; SUGIURA, Ken-ichi[1]; YAMASHITA, Masahiro[4]

([1]Tokyo Metropolitan Univ.; [2]Rigaku Co.; [3]Cent. Recherche Paul Pascal; [4]IMS and Tokyo Metropolitan Univ.)

[*Inorg. Chem.* **42**, 4501–4503 (2003)]

The heterometallic $Mn^{II}_4Ni^{II}_2$ title compound has been synthesized and characterized by X-ray crystallography. The compound consists of a Ni–Mn–Ni linear moiety, [{Ni-(μ-NO)$_3$}$_2$-Mn], linked by oximate bridges and three Mn(II) hfac terminal units attached by oximate oxygens in a di-μ-oxo fashion, forming a novel heterometallic cluster: Mn{Mn(hfac)$_2$}$_3$\{Ni(pao)$_3$\}$_2$ (1). Magnetic measurements reveal the antiferromagnetic nature of the oximate pathway between Mn(II) and Ni(II) metal ions, which imposes an unusual high-spin ground state (S = 8) for 1.

VII-B Development of New Carbonylation Reactions

Carbonylation reactions are recognized as useful and reliable transformations for the preparation of a variety of carbonyl compounds, such as aldehydes, ketones, esters, lactones, and lactams. Our research effort is directed towards the discovery of *novel* type of the catalytic carbonylation reactions; (i) direct carbonylation at C–H bonds and (ii) cycloaddition reaction using carbon monoxide as a one-atom assembling unit (carbonylative cycloaddition reaction).

VII-B-1 $Ru_3(CO)_{12}$-Catalyzed C–H/CO/Olefin Coupling of *N*-Pyridylindolines. Direct Carbonylation at a C–H Bond δ to the Pyridine Nitrogen

CHATANI, Naoto[1]; YORIMITSU, Shuhei[2]; ASAUMI, Taku[2]; KAKIUCHI, Fumitoshi[2]; MURAI, Shinji[2]
([1]IMS and Osaka Univ.; [2]Osaka Univ.)

[*J. Org. Chem.* **67**, 7557–7560 (2002)]

The reaction of *N*-pyridylindolines with CO and ethylene in the presence of $Ru_3(CO)_{12}$ results in direct carbonylation at a C–H bond δ to the pyridine sp^2 nitrogen, which represents a new type of C–H/CO/olefin coupling. The presence of a pyridine ring as a directing group on the substrates is essential for the reaction to proceed. The choice of *N*,*N*-dimethylacetamide (DMA) as the solvent is crucial for the reaction to proceed efficiently.

VII-B-2 Ruthenium-Catalyzed Reaction of α,β-Unsaturated Imines with Carbon Monoxide and Alkenes Leading to β,γ-Unsaturated γ-Butyrolactams: Involvement of Direct Carbonylation of Olefinic C–H Bonds as a Key Step

CHATANI, Naoto[1]; KAMITANI, Akihito[2]; MURAI, Shinji[2]
([1]IMS and Osaka Univ.; [2]Osaka Univ.)

[*J. Org. Chem.* **67**, 7014–7018 (2002)]

The reaction of α,β-unsaturated imines with CO and alkenes in the presence of $Ru_3(CO)_{12}$ as a catalyst results in a three-component coupling reaction that gives α,α-disubstituted β,γ-unsaturated γ-butyrolactams. The reaction proceeds *via* a two-step sequence involving the initial formation of ketone derivatives by catalytic carbonylation at the β-olefinic C–H bonds of α,β-unsaturated imines, followed by the (uncatalyzed) intramolecular nucleophilic attack of the imine nitrogen on the ketonic carbon to generate a tetrahedral intermediate, which then undergoes a 1,2-ethyl migration. The reaction of a cyclic unsaturated imine, derived from the reaction of (*1R*)-(–)-myrtenal with *tert*-butylamine, gives a β-aminocyclopentene derivative, which is formed by an aldol-type condensation of the initially formed ketone, indicating the initial formation of ethyl ketone.

VII-B-3 Ruthenium-Catalyzed Carbonylative Cycloaddition of α-Keto Lactones with Alkenes or Alkynes: The Participation of an Ester-Carbonyl group in Cycloaddition Reactions as the Two-Atom Assembling Unit

CHATANI, Naoto[1]; AMAKO, Katsuya[2]; TOBISU, Mamoru[2]; ASAUMI, Taku[2]; FUKUMOTO, Yoshiya[2]; MURAI, Shinji[2]
([1]IMS and Osaka Univ.; [2]Osaka Univ.)

[*J. Org. Chem.* **68**, 1591–1593 (2003)]

The reaction of benzofuran-2,3-dione derivatives with CO and alkenes (or alkynes) results in a carbonylative [2+2+1] cycloaddition in which the ester-carbonyl group is incorporated into a two-atom assembling unit to give spirolactone derivatives. This reaction provides the first example of an ester-carbonyl group participating in a carbonylative cycloaddition reaction.

VII-B-4 Palladium-Catalyzed Carbonylation of 2-(Propargyl)allyl Phosphates Leading to Highly Unsaturated γ-Lactones

KAMITANI, Akihito[2]; CHATANI, Naoto[1]; MURAI, Shinji[2]
([1]IMS and Osaka Univ.; [2]Osaka Univ.)

[*Angew. Chem. Int. Ed.* **42**, 1397–1399 (2003)]

The reaction of 2-(propargyl)allyl phosphates with CO in THF in the presence of $[(\eta^3\text{-allyl})PdCl]_2$ and dicyclohexylmethylamine results in the incorporation of two molecules of CO to give highly unsaturated bicyclic lactones in good to high yields. The reaction proceeds smoothly even under an ambient pressure of CO. The experimental data indicates the formation of π-allyl palladium complexes.

VII-C Development of $GaCl_3$-Catalyzed Reaction

We have interested in the development of new catalytic reactions based on a unique reactivity of $GaCl_3$. $GaCl_3$ is a Lewis acid, however it has higher affinity toward an alkyne than oxygen, unlike common Lewis acids, such as $AlCl_3$ and $TiCl_4$. We have already reported that the skeletal reorganization of enynes leading to 1-vinylcycloalkenes is achieved by the presence of a catalytic amount of $GaCl_3$ by taking advantage of a high affinity of $GaCl_3$ toward an alkyne (*J. Am. Chem. Soc.* **124**, 10294–10295 (2002)). Utilization of its lower oxophilicity would have a new possibility to explore new catalytic reactions.

VII-C-1 A $GaCl_3$-Catalyzed [4+1] Cycloaddition of α,β-Unsaturated Carbonyl Compounds and Isocyanides Leading to Unsaturated γ-Lactone Derivatives

CHATANI, Naoto[1]; OSHITA, Masayuki[2]; TOBISU, Mamoru[2]; ISHII, Yutaka[2]; MURAI, Shinji[2]
([1]IMS and Osaka Univ.; [2]Osaka Univ.)

[*J. Am. Chem. Soc.* **125**, 7812–7813 (2003)]

A $GaCl_3$-catalyzed reaction of α,β-unsaturated ketones with isocycanides leading to the formation of unsaturated lactone derivatives is described. This is the first example of the catalytic [4+1] cycloaddition of α,β-unsaturated ketones and isocycanides. $GaCl_3$ is an excellent catalyst due to its lower oxophilicity, which is desirable for all of the key steps, such as *E*/*Z* isomerization, cyclization, and deattachment from the products.

VII-D Reductive Activation of Carbon Dioxide and Oxidative Activation of Water Aiming at Reversible Conversion between CO_2 and Organic Molecules

Multi-electron reduction of CO_2 aiming at smooth conversion to organics is highly desired in the viewpoints of not only the utilization of C1 resources but also the decrease of the concentration in the air. Carbon dioxide easily reacts with coordinatively unsaturated low-valent metal complexes to form η^1- or η^2-CO_2 adducts, the former of which are easily converted to metal-CO complexes in protic media. Accumulation of much electrons on metal centers usually accelerates not only reduction of CO_2 but also metal-CO bond cleavages. As a result, CO is the main product in photo- and electro-chemical reduction of CO_2 catalyzed by metal complexes. It is, therefore, highly desired to develop new methodologies that can supply electrons to the carbonyl ligand of metal-CO complexes derived from CO_2 without accumulation of electrons at the central metals. Along the line, we are designing new types of metal complexes that have an ability to provide electrons to carbonyl carbon through metallacycle rings involving the CO groups aiming at catalytic generation higher organic molecules by the electro- and photochemical reduction of CO_2.

Oxygenations and oxidations of organic molecules by high valent metal-oxo complexes are of current interest from the viewpoints of the enzymatic activities of P-450. Mechanistic understandings of the reactivity of metal-oxo species derived from O_2, however, have been limited because of the difficulty of selective cleavage of the O–O bond of M–O_2 frameworks in artificial systems. Alternatively, high valent Ru=O complexes can be obtained by sequential electron and proton loss of the Ru–OH_2 frameworks, and some of Ru=O complexes have proven to work as oxidants of organic molecules. Introduction of quinone molecules, which are reduced to semiquinone and catecholate in a wide range of potentials, into M–OH_2 frameworks also induces sequential electron and proton loss of the Ru–OH_2 ones without addition of oxidizing agents. Such acid-base equilibria of the aqua ligands by taking advantages of smooth redox reactions of quinone ligands can be applied for energy conversion from pH gradients to electronic energy.

VII-D-1 Coordination Ability of 1,10-Phenanthroline-5,6-Dione: Syntheses and Redox Behavior of a Ru(II) Complex with an o-Quinoid Moiety and of Bridged Ru(II)-M(II) Complexes (M = Pd, Pt)

FUJIHARA, Tetsuaki[1]; OKAMURA, Rei[1]; WADA, Tohru; TANAKA, Koji
([1]IMS, CREST/JST)

[*Dalton Trans.* 3221–3226 (2003)]

The synthesis and electrochemical properties of Ru(II) complexes having 1,10-phenanthroline-5,6-dione (PD), [Ru(trpy)(PD-N,N')Cl](PF_6) ([**1**](PF_6)), mixed-metal complexes [$(PPh_3)_2$Pd(O,O'-PD-N,N')Ru(trpy)-Cl](PF_6) ([**2**](PF_6)), and [$(PPh_3)_2$Pt(O,O'-PD-N,N')Ru-(trpy)Cl](PF_6) ([**3**](PF_6)) (trpy = 2,2':6',2"-terpyridine) are presented. The PD ligand of $[\mathbf{1}]^+$, which was prepared by the reaction of Ru(trpy)(DMSO)Cl_2 with PD in hot ethanol, existed as the quinoid form and underwent two reversible ligand-based redox reactions. The quinoid group of $[\mathbf{1}]^+$ did not show any interactions with Pd(II) and Pt(II), whereas the ligand was endowed with coordination ability to metals by one- and two-electron reduction of the ligand-based redox reaction. Indeed, the mixed-metal complexes of $[\mathbf{2}]^+$ and $[\mathbf{3}]^+$ prepared by the reactions of $[\mathbf{1}]^+$ with M(PPh_3)$_4$ (M = Pd, Pt) have the $[\mathbf{1}]^-$ core bearing the two-electron reduced form of PD (catecolato form) and M(II) frameworks.

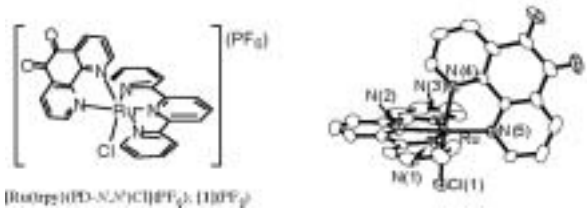

VII-D-2 Characterization of a Stable Ruthenium Complex with an Oxyl Radical

KOBAYASHI, Katsuaki[1]; OHTSU, Hideki[1]; WADA, Tohru; KATO, Tatsuhisa; TANAKA, Koji
([1]IMS, CREST/JST)

[*J. Am. Chem. Soc.* **125**, 6729–6739 (2003)]

The ruthenium oxyl radical complex, [Ru^{II}(trpy)-(Bu_2SQ)$O^{-\cdot}$] (trpy = 2,2':6',2"-terpyridine, Bu_2SQ = 3,5-di-tert-butyl-1,2-benzosemiquinone) was prepare for the first time by the double deprotonation of the aqua ligand of [Ru^{III}(trpy)(Bu_2SQ)(OH_2)](ClO_4)$_2$. [Ru^{III}-(trpy)(Bu_2SQ)(OH_2)](ClO_4)$_2$ is reversibly converted to [Ru^{III}(trpy)(Bu_2SQ)(OH^-)]$^+$ upon dissociation of the aqua proton (pKa 5.5). Deprotonation of the hydroxo proton gave rise to intramolecular electron transfer from the resultant O^{2-} to the Ru-dioxolene framework. The resultant [Ru^{II}(trpy)(Bu_2SQ)$O^{-\cdot}$] showed antiferro-magnetic behavior with a Ru^{II}-semiquinone moiety and oxyl radical, the latter of which was characterized by a spin trapping technique. The most characteristic structural feature of [Ru^{II}(trpy)(Bu_2SQ)$O^{-\cdot}$] is a long Ru–O bond length (2.042(6) Å) as the first terminal metal–O bond with a single bond length. To elucidate

the substituent effect of a quinone ligand, we prepared $[Ru^{III}(trpy)(4ClSQ)(OH_2)](ClO_4)_2$ (4ClSQ = 4-chloro-1,2-benzosemiquinone) and compared the deprotonation behavior of the aqua ligand with that of $[Ru^{III}(trpy)(Bu_2SQ)(OH_2)](ClO_4)_2$. Deprotonation of the aqua ligand of $[Ru^{III}(trpy)(4ClSQ)(OH_2)](ClO_4)_2$ induced intramolecular electron transfer from OH^- to the $[Ru^{III}(4ClSQ)]$ moiety affording $[Ru^{II}(trpy)(4ClSQ)(OH\cdot)]^+$, which then probably changed to $[Ru^{II}(trpy)(4ClSQ)O^{-}\cdot]$. The antiferromagnetic interactions (J values) between Ru^{II}-semiquinone and the oxyl radical for $[Ru^{II}(trpy)(Bu_2SQ)O^{-}\cdot]$ and for $[Ru^{II}(trpy)(4ClSQ)O\cdot]$ were $2J = -0.67$ cm^{-1} and -1.97 cm^{-1}, respectively.

VII-D-3 Terpyridine-Analogous (N,N,C)-Tridentate Ligands: Synthesis, Structures, and Electrochemical Properties of Ruthenium(II) Complexes Bearing Tridentate Pyridinium and Pyridinylidene Ligands

KOIZUMI, Take-aki[1]; TOMON, Takashi[1]; TANAKA, Koji
([1]IMS, CREST/JST)

[*Organometallics* **22**, 970–975 (2003)]

The cyclometalated complexes $[RuL(terpy)][PF_6]_2$ (**3**, L = N"-methyl-4'-methylthio-2,2':6',4"-terpyridinium; **4**, L = N"-methyl-4'-methylthio-2,2':6',3"-terpyridinium) with a (N,N,N)(N,N,C)-coordination mode were synthesized in good yields and fully characterized by x-ray crystallographic, spectroscopic, and electrochemical measurements. $^{13}C\{^1H\}$ NMR and electronic spectra revealed that the Ru–C bond of complex **4**, which has a quaternized N–Me unit at the para-position of the carbon atom bonding to the metal center in the terminal ring of the tridentate ligand, involves carbenic (Ru=C) character in solutions.

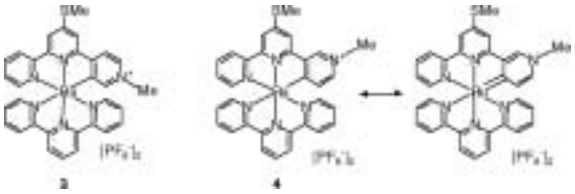

VII-D-4 Syntheses of a 6-(2-pyrrolyl)-2,2'-Bipyridine Derivative and its Ruthenium Complex

NAGATA, Toshi; TANAKA, Koji

[*Bull. Chem. Soc. Jpn.* **75**, 2469–2470 (2002)]

Syntheses of a new planar terdentate ligand, 6-(3,5-diphenyl-2-pyrrolyl)-2,2'-bipyridine (L^1H) and its Ru(II) complex ($[Ru(L^1)_2]$) are reported. The x-ray structure of $[Ru(L^1)_2]$ showed the distorted octahedral Ru(II) center similar to the structures of terpyridine complexes. The cyclic voltammograms revealed that $[Ru(L^1)_2]$ was more easily oxidized than $[Ru(terpy)_2]^{2+}$ by 1.10 V.

VII-D-5 Acid-Base Equilibrium of Aqua-Chromium-Dioxolene Complexes Aimed at Formation of Oxo-Chromium Complexes

SHIREN, Kazushi[1]; TANAKA, Koji
([1]IMS, CREST/JST)

[*Inorg. Chem.* **41**, 5912–5919 (2002)]

A series of aqua-Cr(III)-dioxolene complexes, $[Cr(OH_2)(3,5\text{-}Bu_2SQ)(trpy)](ClO_4)_2$ (**1s**), $[Cr(OH_2)(3,5\text{-}Bu_2Cat)(trpy)]ClO_4$ (**1c**), $[Cr(OH_2)(3,6\text{-}Bu_2SQ)(trpy)](ClO_4)_2$ (**2**), $[Cr(OH_2)(Cat)(trpy)]ClO_4$ (**3**), $[Cr(OH_2)(Cl_4Cat)(trpy)]ClO_4$ (**4**), $[Cr(OH_2)(3,5\text{-}Bu_2SQ)(Me_3\text{-}tacn)](ClO_4)_2$ (**5**), $[Cr(OH_2)(Cat)(Me_3\text{-}tacn)]ClO_4$ (**6**), and $[Cr(OH_2)(Cl_4Cat)(Me_3\text{-}tacn)]ClO_4$ (**7**) (Bu_2SQ = di-*tert*-butyl-*o*-benzosemiquinonate anion, Bu_2Cat = di-*tert*-butylcatecholate dianion, Cat = catecholate dianion, Cl_4Cat = tetrachlorocatecholate dianion, trpy = 2,2':6',2"-terpyridine, and Me_3-tacn = 1,4,7-trimethyl-1,4,7-triazacyclononane), were prepared. On the basis of the crystal structures, redox behavior, and elemental analyses of these complexes, dioxolene in **1c**, **3**, **4**, **6**, and **7** coordinated to Cr(III) as the catechol form, and the ligand in **1s**, **2**, and **5** was linked to Cr(III) with the semiquinone form. All the aqua-Cr(III) complexes reversibly changed to the hydroxo-Cr(III) ones upon dissociation of the aqua proton, and the *pKa* value of the aqua-Cr(III) complexes increased in the order **6** > **3** ≈ **1c** > **7** > **5** ≈ **4** > **1s**. Hydroxo-Cr(III)-catechol complexes derived from **1c**, **3**, **4**, **6**, and **7** did not show any signs of dissociation of their hydroxy proton. On the other hand, hydroxo-Cr(III)-semiquinone complexes were reduced to hydroxo-Cr(III)-catechol in H_2O/THF at pH 11 under illumination of visible light.

VII-D-6 Ruthenium Oxyl Radical Complex Containing *o*-Quinone Ligand Detected by ESR Measurements of Spin Trapping Technique

KOBAYASHI, Katsuaki[1]; OHTSU, Hideki[1]; WADA, Tohru; TANAKA, Koji
([1]IMS, CREST/JST)

[*Chem. Lett.* 868–869 (2002)]

Ru-quinone complex containing an aqua ligand, $[Ru(II)(trpy)(35tBu_2Q)(OH_2)](ClO_4)_2$ (trpy = 2,2':6',2"-terpyridine, $35tBu_2Q$ = 3,5-di-tert-butyl-1,2-benzoquinone) underwent deprotonation of an aqua ligand accompanied with intramolecular electron transfer from O^{2-} ligand to quinone ligand generating O^{-} ligand.

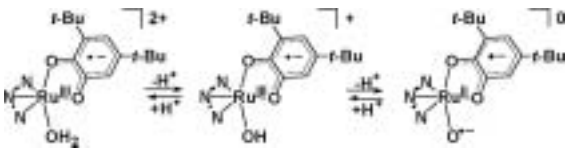

VII-D-7 Multi-Electron Reduction of CO_2 *via* Ru-CO_2, -C(O)OH, -CO, -CHO, and -CH_2OH Species

TANAKA, Koji; OOYAMA, Dai[1]
([1]Fukusima Univ., CREST/JST)

[*Coord. Chem. Rev.* **226**, 211–218 (2002)]

A review about preparations and the molecular structures determined by x-ray analyses of $[Ru(bpy)_2(CO)L]^{n+}$ (L = CO_2, C(O)OH, CO, CHO, CH_2OH, CH_3, and $C(O)CH_3$; n = 0, 1, 2) were presented. These complexes are reasonable models of reaction intermediates in the multi-electron reduction of CO_2 catalyzed by metal complexes, since reductive cleavage of the Ru–L bonds of the complexes in protic media affords HCOOH, CO, HCHO, CH_3OH, and CH_4 as two-, four-, six- and eight-electron reduction products of CO_2. Thermodynamically, the free energy required in the reduction of CO_2 progressively decreases with an increase of the number of electrons participating in the reduction of CO_2. The Ru–L bond character of $[Ru(bpy)_2(CO)L]^{n+}$ were assessed by the ν(Ru–L) bands and the Ru–L bond distances from the viewpoint of elucidation of a correlation between free energy changes in the multi-electron reduction of CO_2 catalyzed by metal complexes and the metal–C bond strength of each intermediate. The Ru–C bond distance of $[Ru(bpy)_2(CO)L]^{n+}$ largely depends on the hybrid orbital of the C atom bonded to Ru and lengthens in the order Ru–Csp < Ru–Csp_2 < Ru–Csp_3. An unusual shift of the ν(Ru–L) bands to higher wavenumber with decrease of the Ru–L bond distances is discussed in terms of σ- and π-character of the Ru–C bonds.

VII-D-8 Acid-Base Equilibria of Various Oxidation States of Aqua-Ruthenium Complexes with 1,10-Phenanthroline-5,6-Dione in Aqueous Media

FUJIHARA, Tetsuaki[1]; WADA, Tohru; TANAKA, Koji
([1]IMS, CREST/JST)

Synthesis and electrochemical behavior of aqua-ruthenium(II) complexes, $[Ru(trpy)(PDA\text{-}N,N')(OH_2)](ClO_4)_2$ ([**1**](ClO$_4$)$_2$) and $[Ru(trpy)(PD\text{-}N,N')(OH_2)](ClO_4)_2$ ([**2**](ClO$_4$)$_2$) (trpy = 2,2':6',2"-terpyridine, PDA = 6-acetonyl-6-hydroxy-5-oxo-1,10-phenanthroline, PD = 1,10-phenanthroline-5,6-dione) are presented. Treatment of $[Ru(trpy)(PD\text{-}N,N')Cl](PF_6)$ with $AgClO_4$ in a mixed solvent of acetone and H_2O selectively produced the acetonyl-PD complex [**1**](ClO$_4$)$_2$, and the similar treatment in a mixed solvent of 2-methoxyethanol and H_2O gave the PD complex [**2**](ClO$_4$)$_2$. The molecular structures of both complexes were determined by X-ray structural analysis. Simulation of pH dependent redox potentials ($E_{1/2}$) of $[\mathbf{1}]^{2+}$ and $[\mathbf{2}]^{2+}$ in H_2O revealed that the acetonyl-PD complex $[\mathbf{1}]^{2+}$ underwent closely successive Ru(II)/Ru(III) and Ru(III)/Ru(IV) redox reactions. In addition to the similar successive Ru(II)/Ru(III) and Ru(III)/Ru(IV) redox reactions, the aqua complex $[\mathbf{2}]^{2+}$ showed simultaneous two-electron quinone/catechol redox couple of the PD ligand.

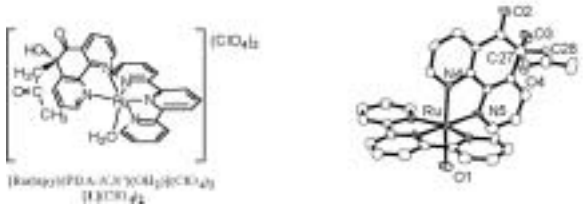

VII-D-9 Syntheses and Electrochemical Properties of Ruthenium(II) Polypyridyl Complexes with 4,4'-Bipyrimidine and Quaternized 4,4'-Bipyrimidinium Ligands

FUJIHARA, Tetsuaki[1]; WADA, Tohru; TANAKA, Koji
([1]IMS, CREST/JST)

The synthesis and electrochemical properties of novel ruthenium(II) polypyridyl complexes with 4,4'-bipyrimidine, [Ru(trpy)(bpm)Cl](X) ([**1**](X; X = PF_6^-, BF_4^-)), and with a quaternized bipyrimidinium ligand, $[Ru(trpy)(Me_2bpm)Cl](BF_4)_3$ ([**2**](BF$_4$)$_3$) (trpy = 2,2':6',2"-terpyridine, bpm = 4,4'-bipyrimidine, Me_2bpm = 1,1'-dimethyl-4,4'-byprimidinium) are presented. The bpm complex of $[\mathbf{1}]^+$ was prepared by the reaction of Ru(trpy)Cl_3 with 4,4'-bipyrimidine in $EtOH/H_2O$. The structural characterization of $[\mathbf{1}]^+$ revealed that the bpm ligand was coordinated to the ruthenium atom with the bidentate fashion. Diquaternization of the non-coordinating nitrogen atoms on bpm of $[\mathbf{1}]^+$ by $(CH_3)_3OBF_4$ in CH_3CN gave [**2**](BF$_4$)$_3$. The electrochemical and spectroelectrochemical properties of the complexes are described.

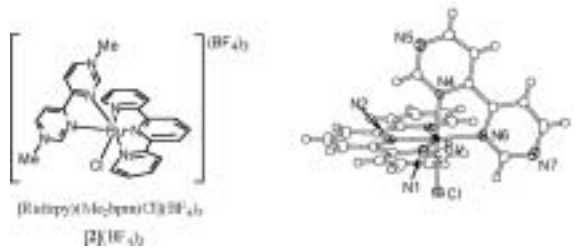

VII-D-10 Strong Interaction between Carbonyl and Dioxolene Ligands through Charge Distribution of Mono- and Dicarbonyl Ruthenium Complexes with Semiquinone

WADA, Tohru; FUJIHARA, Tetsuaki[1]; TOMORI, Mizuno[2] ; OOYAMA, Dai[2]; TANAKA, Koji
([1]IMS, CREST/JST; [2]Fukushima Univ., CREST/JST)

Monocarbonyl Ru(II) Complexes with semiquinone, $([Ru(CO)(sq)(L)])^n$ (sq = 3,5-di-*tert*-butyl-1,2-benzosemiquinone, L = terpyridine($[\mathbf{1}]^+$), 2,6-bis(*N*,*N*-dimethylaminomethyl)-pyridine($[\mathbf{2}]^+$), 2,6-dipyrid-2-ylphenyl($[\mathbf{3}]^0$), 2-(2,2'-bipyrid-6-yl)phenolato($[\mathbf{4}]^0$), n = 1+ or 0), and dicarbonyl Ru(II) complexes with two semiquinones, $[Ru(CO_2)_2(sq)_2]$ ($[\mathbf{5}]^0$) and $[Ru(CO)_2(phsq)_2]$ (phsq = 9,10-phenanthrasemiquinone, $[\mathbf{6}]^0$), were synthesized. Red shift of ν(CO) bands caused by one-electron reduction of semiquinone is in a range of –41 to –56 cm^{-1}. Unusual large red shift of ν(CO) bands

compared with analogous Ru(II)–polypyridyl results from the strong interaction between carbonyl and dioxolene across Ru(II).

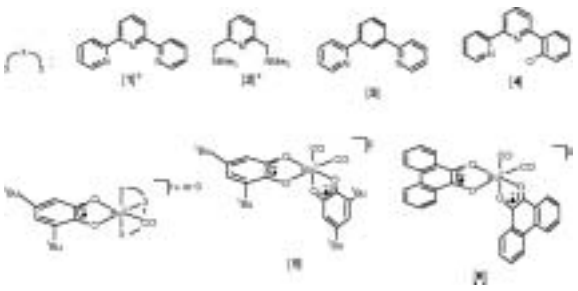

VII-D-11 Regulation of Inter- and Intra-Molecular A–D–A π-π Stacking. Solid State Structures of Bis(pyridinium) Compounds

KOIZUMI, Take-aki; TSUTSUI, Kanako; WADA, Tohru; TANAKA, Koji

The synthesis and molecular structures of bis(pyridinium) compounds, [1,4-(4-R-$C_5H_4N^+CH_2$-$CH_2CH_2)_2C_6H_4$][X^-]$_2$ (**1**, R = H, X = I; **2**, R = t-Bu, X = Br) are investigated. The compound **1** is a linear structure in the solid state and the crystal packing geometry of **1** is defined as isolated triplets formed by the phenylene ring of a molecule and two pyridinium rings of two neighboring molecules. On the other hand, compound **2** has an S-shaped arrangement, and an intra-molecular acceptor-donor-acceptor triplet is formed among the central phenylene ring and two terminal pyridinum rings in the same molecule. Such a distinct difference in the crystal structures of **1** and **2** is ascribed to the substituent in the pryridinium unit. The steric repulsion of the bulky tert-butyl group hinders intermolecular A–D–A π-π stacking.

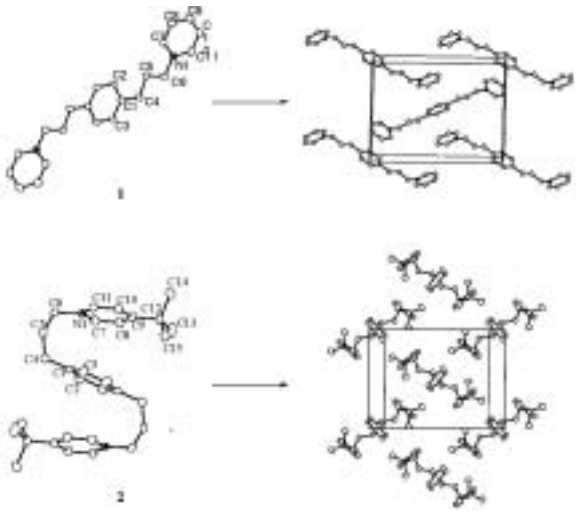

VII-D-12 Synthesis, Structures and Fluxional Behavior of Ruthenium(II) Complexes Bearing a Bidentate 1,8-Naphthyridine Ligand

KOIZUMI, Take-aki[1]; TOMON, Takashi[1]; TANAKA, Koji

([1]IMS, CREST/JST)

The ruthenium complexes bearing 1,8- naphthyridine (napy) and terpyridine analogous (N,C,N)-tridentate ligands were synthesized and characterized. Reaction of $RuCl_2(\eta^2$-napy$)(DMSO)_2$ with 2 equiv of $AgPF_6$ and subsequent addition of LH and CO gave [RuL(η^2-napy)(CO)][PF_6]$_n$ (**6a**: L = N-methyl-3,5-di(2-pyridyl)-4-pyridyl, n = 2; **6b**: L = 2,6-di(2-pyridyl)-phenyl, n = 1) *via* the formation of [RuL(η^2-napy)-(DMSO)][PF_6]$_n$ (**5a**: L = N-methyl-3,5-di(2-pyridyl)-4-pyridyl, n = 2; **5b**: L = 2,6-di(2-pyridyl)phenyl, n = 1). The crystal structures of **5a** and **6a** show that these complexes have distorted octahedral coordination with the tridentate (N,C,N)-ligand as mer-fashion, two nitrogen of bidentate napy and sulfur of DMSO (**5a**) or carbon of the CO (**6a**) ligand. Detailed irradiation and variable-temperature ^{1}H-NMR studies reveal fluxional process of the chelated napy ligand in solution.

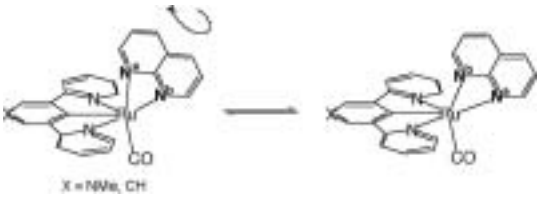

VII-D-13 Acid-Base Equilibrium of 6-Hydroxy-2,2'-Bipyridine Ligated on Ruthenium-Carbonyl Complexes and Cyclometalation Driven by Ligand Based Redox Reaction

TOMON, Takashi[1]; KOIZUMI, Take-aki[1]; TANAKA, Koji

([1]IMS, CREST/JST)

Two isomers of [Ru(trpy)(bpy-O)(CO)](PF_6) ([**1**]$^+$ and [**2**]$^+$) (trpy = terpyridine, bpy-O = 2-(2'-pyridyl)-6-pyridonato) were prepared; pyridonato in bpy-O of [**1**]$^+$ and [**2**]$^+$ is located in a position *trans* and *cis* to CO. Treatments of [**1**]$^+$ and [**2**]$^+$ with HPF_6 produced [**1**H]$^{2+}$ and [**2**H]$^{2+}$ with bpy-OH (bpy-OH = 6-hydroxy-2, 2'-bipyridine), and the reactions of [**1**H]$^{2+}$ and [**2**H]$^{2+}$ with Et_3N regenerated [**1**]$^+$ and [**2**]$^+$. The molecular structures of [**1**](PF_6), [**2**](PF_6)·H_2O and [**2**H](PF_6)$_2$·$2H_2O$ were determined by X-ray analysis. The cyclic voltammograms of [**1**]$^+$ and [**2**]$^+$ displayed one nearly reversible redox couple at $E_{1/2}$ = –1.65 V and –1.51 V, and one irreversible cathodic wave at $E_{p,c}$ = –1.97 and $E_{p,c}$ = –2.15 V, respectively. The complex of [**1**]$^+$ showed the υ(C≡O) band at 1979 cm^{-1}, which shifted to 1932 and 1853 cm^{-1} upon one- and two-electron reduction of [**1**]$^+$, respectively, and the intensity of the 1853 cm^{-1} band became weak compared with those of the 1979 and 1932 cm^{-1} bands due to loss of CO from [**1**]$^-$. [**2**]$^+$ and [**2**]^0 also displayed the υ(C≡O) band at 1997 and 1953 cm^{-1}, the latter of which moved to 1587 cm^{-1} upon one electron reduction of [**2**]^0. Reoxidation of [**2**]$^-$ at 0 V almost fully regenerated the IR spectra of [**2**]$^+$. Unusual large red shift of the υ(C≡O) band between [**2**]^0 and [**2**]$^-$ (Δυ = 345 cm^{-1}) is ascribed to a cyclometalation resulting from an attack of pyridonato oxygen to carbonyl carbon of [**2**]$^-$.

VII-E Silanechalcogenolato Complexes

The development of synthetic routes to mixed-metal chalcogenido clusters is a critical prerequisite for study of these important materials. It is well known that $(Me_3Si)_2E$ (E = S, Se, Te) is a good chalcogen transfer reagent, which can replace a halide, alkoxide, acetate, and oxide with a chalcogen ligand by taking advantage of formation of Si–Cl and Si–O bonds. Therefore the corresponding M–$ESiMe_3$ species hold great promise for synthetic precursors of chalcogenido clusters. However, because of the high lability of Si–E bond, there is a strong tendency to restrict the use of these complexes. Thus, their stabilization is required to develop cluster synthesis based on silanechalcogenolato complexes.

In this work, we have chosen to stabilize silanethiolato complexes by the chelating effect of the ligands. The chelating effect in coordination chemistry has most pronounced kinetic and thermodynamic consequences. This strategy could suppress the undesired degradation process of silanethiolato complexes *via* aggregation and/or ligand redistribution.

VII-E-1 Coordination Chemistry of Silanedithiolato Ligands Derived from Cyclotrisilathiane: Synthesis and Structures of Complexes of Iron(II), Cobalt(II), Palladium(II), Copper(I), and Silver(I)

KOMURO, Takashi[1]; MATSUO, Tsukasa; KAWAGUCHI, Hiroyuki; TATSUMI, Kazuyuki[1]
([1]Nagoya Univ.)

[*Inrog. Chem.* **42**, 5340 (2003)]

The coordination chemistry of chelating silanedithiolato ligands has been investigated on Fe(II), Co(II), Pd(II), Cu(I), and Ag(I). Treatment of $M(OAc)_2$ (M = Fe, Co, Pd) with cyclotrisilathiane $(SSiMe_2)_3$ in the presence of Lewis bases resulted in formation of $Fe(S_2SiMe_2)$(pmdeta) (**1**), $Fe(S_2SiMe_2)(Me_3tacn)$ (**2**), $Co(S_2SiMe_2)$(pmdeta) (**3**), and $Pd(S_2SiMe_2)(PEt_3)_2$ (**4**). The analogous reactions of M(OAc) (M = Cu, Ag) in the presence of PEt_3 gave rise to the dinuclear complexes $M\{(SSiMe_2)_2S\}(PEt_3)_3$ [M = Cu (**5**), Ag (**6**)]. Complexes were characterized in solution by ^1H, $^{31}P\{^1H\}$, and $^{29}Si\{^1H\}$ NMR and in the solid state by single-crystal X-ray diffraction. Mononuclear complexes **1**, **2**, and **3** have a four-membered MS_2SiMe_2 ring, and these five-coordinate complexes adopt trigonal-bipyramidal (for the pmdeta adducts) or square-pyramidal (for the Me_3tacn adduct) geometries. In dimer **6**, the $(SSiMe_2)_2S^{2-}$ silanedithiolato ligand bridges two metal centers, one of which is three-coordinate and the other four-coordinate. The chelating effect of silanedithiolato ligands leads to an increase in the stability of silylated thiolato complexes.

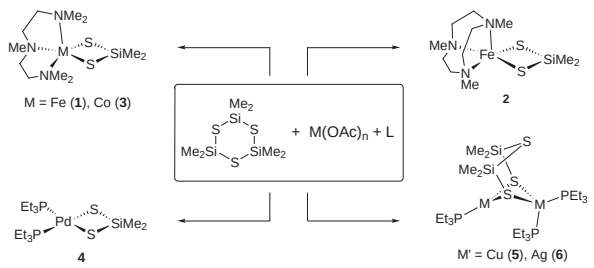

Figure 1.

VII-E-2 Copper and Silver Complexes Containing the $S(SiMe_2S)_2^{2-}$ Ligand: Efficient Entries into Heterometallic Sulfido Clusters

KOMURO, Takashi[1]; MATSUO, Tsukasa; KAWAGUCHI, Hiroyuki; TATSUMI, Kazuyuki[1]
([1]Nagoya Univ.)

[*Angew. Chem., Int. Ed.* **42**, 465 (2003)]

Reactions of copper and silver acetates with cyclotrisilathane in the presence of PEt_3 afforded the silanedithiolate-bridged dinuclear complexes $[M_2\{(SSiMe_2)_2S\}(PEt_3)_3]$ (M = Cu (**1a**), Ag (**1b**)) in high yields. Although these complexes are thermally stable in solution, they are found to react smoothly under mild conditions with metal halides, giving mixed-sulfido clusters. Treatment of **1a** with $[CpTiCl_3]$ and $[TiCl_4(thf)_2]$ produced copper-titanium sulfido clusters $[Cp_2Ti_2Cu_6S_6(PEt_3)_6]$ (**2**) and $[ClTiCu_3S_3(PEt_3)_4]$ (**3**), respectively. Addition of [CpLi] to **3** resulted in the formation of **2**. Structures of **1a**, **2**, and **3** have been determined by X-ray analysis.

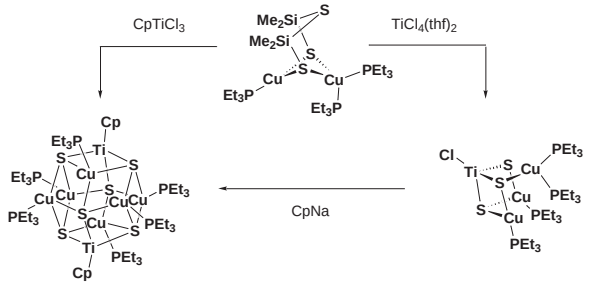

Figure 1.

VII-F Coordination Chemistry of Sterically Hindered Ligands and Multidentate Ligands and Activation of Small Molecules

This project is focused on the design and synthesis of new ligands that are capable of supporting novel structural features and reactivity. Currently, we are investigating multidentate ligands based on aryloxide, thiolate, and amidinate. In addition, we set out to study metal complexes with sterically hindered arylthiolate ligands. Our recent efforts have been directed toward activation of small molecules.

VII-F-1 Titanium N-Hetrocyclic Carbene Complexes Incorporating an Imidazolium-Linked Bis(phenol)

AIHARA, Hidenori; MATSUO, Tsukasa; KAWAGUCHI, Hiroyuki

[*Chem. Commun.* 2204 (2003)]

We synthesized and fully characterized titanium(II) complexes supported by a bis(aryloxido) ligand with an N-heterocyclic carbene (NHC) function. The use of NHC as ligands has attracted considerable attention, because their complexes are highly active and very stable catalysts for various organic reactions. However, the vast majority of NHC systems contain late transition metals. This is due to the lack of NHC derivatives suitable for studies of early transition metal chemistry. Thus we designed the aryloxido-functionalized NHC hybrid ligand, in which the carbene unit is flanked by two aryloxide groups. The aryloxido group acts as an anchor and reduces the tendency for NHC dissociation. This enables us to explore the effect of NHC on the properties of early transition metal complexes. In this context, we use this ligand (**L**) to prepare titanium complexes, which were fully characterized. Furthermore, another interesting aspect of this system is that these aryloxido-carbene complexes of titanium showed a high activity for ethylene polymerization. This is a first example of ethylene polymerization promoted by NHC complexes.

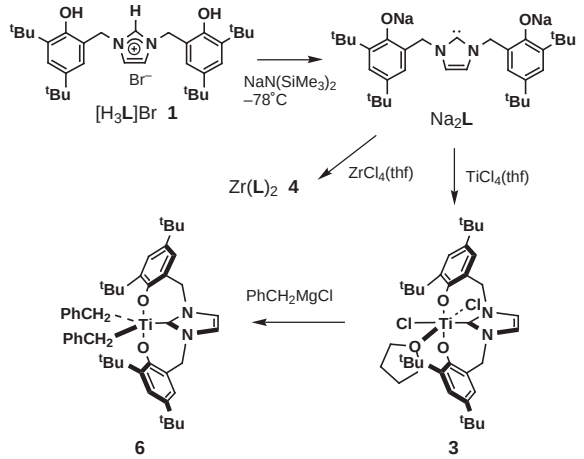

Figure 1.

VII-F-2 Unusual Coordination Modes of Arylthiolates in Mo{η^5-SC_6H_3-2,6-$(SiMe_3)_2$}{η^7-SC_6H_3-2,6-$(SiMe_3)_2$}

KOMURO, Takashi[1]; MATSUO, Tsukasa; KAWAGUCHI, Hiroyuki; TATSUMI, Kazuyuki[1]
([1]Nagoya Univ.)

[*J. Am. Chem. Soc.* **125**, 2070 (2003)]

Although arylthiolate ligands are ubiquitous in transition metal coordination chemistry, they are invariably S-bonded for either terminal or bridging coordination. This is probably because the affinity of transition metal elements to thiolate sulfurs is strong relative to the metal-aryl π interactions. In contrast, analogous aryloxide complexes have occasionally been found to assume π coordination geometries at the aryl substituents, in an η^5-pentadienyl or an η^3-allyl bonding manner, leaving the C=O portion intact. As a part of our ongoing study on activation of small molecules by means of coordinatively unsaturated transition metal complexes, we were interested in preparation of molybdenum complexes of the 2,6-disubstituted arylthiolates, SC_6H_3-2-Ph-6-$SiMe_3$ and SC_6H_3-2,6-$(SiMe_3)_2$. This work describes the reactions of $MoCl_3(thf)_3$ with the lithium salts of these arylthiolates, which resulted in isolation of the unexpected π-sandwiched bis-arylthiolato complex, Mo{η^5-SC_6H_3-2,6-$(SiMe_3)_2$}{η^7-SC_6H_3-2,6-$(SiMe_3)_2$} (**1**). We also report here that the π-bonding in **1** is labile and the treatment with acetonitrile gave rise to the S-bonded bis-arylthiolato complex carrying three acetonitrile molecules, one of which is coordinated in an η^2-mode, Mo{SC_6H_3-2,6-$(SiMe_3)_2$}$_2$(η^1-CH_3CN)$_2$(η^2-CH_3CN) (**2**).

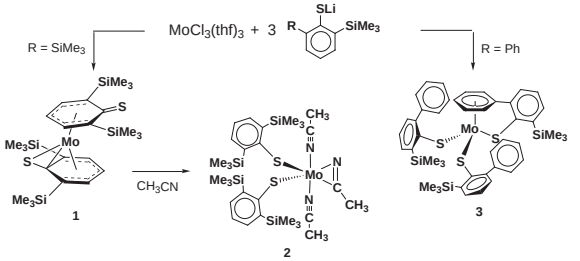

Figure 1.

VII-G Synthesis of Compounds Having a Novel Bonding Containing Heavier Main Group Elements

Double-bond compounds of main group elements of the second row such as olefins, carbonyl compounds, aromatic compounds, and azo compounds play very important roles in organic chemistry. However, the chemistry of their heavier element homologues has been undeveloped most probably due to their high reactivity and instability under ambient conditions. Since the first isolation of stable diphosphene (P=P), silene (Si=C), and disilene (Si=Si) in 1981 by taking advantage of steric protection, various double-bond compounds containing heavier main group elements have been synthesized and characterized.

On the other hand, we have developed an extremely bulky aromatic substituent, 2,4,6-tris[bis(trimethylsilyl)-methyl]phenyl (denoted as Tbt hereafter) and 2,6-bis[bis(trimethylsilyl)methyl]-4-[tris(trimethylsilyl)methyl]phenyl (denoted as Bbt hereafter). These substituents were found to be very effective steric protection groups for a variety of reactive species containing a heavier main group element. We have synthesized a variety of unprecedented low-coordinate compounds of heavier main group elements as stable compounds by taking advantage of kinetic stabilization using a new type of steric protection groups, Tbt and Bbt, and elucidated their properties.

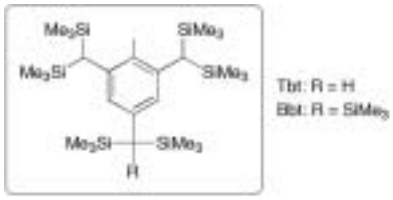

VII-G-1 Synthesis and Properties of the First Stable 1-Silanaphthalene

TAKEDA, Nobuhiro[1]; SHINOHARA, Akihiro[1]; TOKITOH, Norihiro[2]
([1]Kyoto Univ.; [2]IMS and Kyoto Univ.)

[*Organometallics* **21**, 4024–4026 (2002)]

Since aromatic compounds play very important roles in organic chemistry, much attention has been also paid to the chemistry of silaaromatic compounds. However, there are few reports on the synthesis and isolation of silaaromatic compounds stable at room temperature because of their high reactivity. Very recently, we have successfully synthesized the first stable silabenzene, 2-silanaphthalene, and 9-silaanthracene by taking advantage of an extremely bulky substituent, 2,4,6-tris[bis-(trimethylsilyl)methyl]phenyl (Tbt). On the other hand, there is no report for the synthesis of 1-silanaphthalene, which is a structural isomer of 2-silanaphthalene, although much attention has been focused on the similarities and differences between 1- and 2-silanaphthalenes.

The first 1-silanaphthalene **1** was successfully synthesized as moisture-sensitive, pale yellow crystals by taking advantage of Tbt group. The structure of **1** was determined based on its ^{1}H, ^{13}C, and ^{29}Si NMR, Raman, and UV/vis spectra together with theoretical calculations. These data clearly indicated that **1** has aromaticity comparable with naphthalene as well as Tbt-substituted 2-silanaphthalene. In contrast to the thermal stability of 2-Tbt-2-silanaphthalene, 1-Tbt-1-silanaphthalene (**1**) readily dimerizes in solution even at room temperature to give the corresponding [2+4] dimmer **2**.

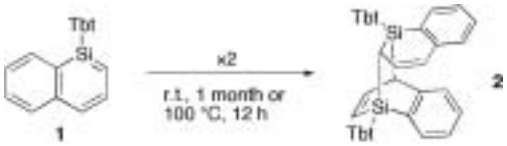

VII-G-2 Photochemical and Thermal Reactions of a Kinetically Stabilized 9-Silaanthracene: The First Spectroscopic Observation of a 9,10-Dewar-9-Silaanthracene Isomer

SHINOHARA, Akihiro[1]; TAKEDA, Nobuhiro[1]; TOKITOH, Norihiro[2]
([1]Kyoto Univ.; [2]IMS and Kyoto Univ.)

[*J. Am. Chem. Soc.* **125**, 10804–10805 (2003)]

In recent decades, much attention has been paid to the chemistry of silaaromatic compounds. Recently we have succeeded in the synthesis of novel silaaromatic species such as silabenzene, 1-silanaphthalene, 2-silanaphthalene, and 9-silaanthracene by taking advantage of an efficient steric protection group, 2,4,6-tris[bis(trimethylsilyl)methyl]phenyl (Tbt) group. In this paper we present the photochemical and thermal reaction of the stable 9-silaanthracene **1**.

Irradiation of **1** with the light of λ = 300–500 nm afforded the corresponding 9,10-Dewar-9-silaanthracene **2**, the formation of which was experimentally demonstrated by the ^{1}H, ^{13}C, and ^{29}Si NMR spectra. It should be noted that **2** is the first example of spectroscopically identified 9,10-Dewar-9-silaanthracene. Dewar isomer **2** was found to be a marginally stable species in solution and to undergo gradual thermal tautomerization into **1** even at –80 °C in hexane. On the other hand, thermal reactions of 9-silaanthracene **1** afforded the head-to-tail [4+4] dimer **3** either in solution or in the solid state. The dimer **3** was thermally very stable and its molecular structure was definitively determined by X-ray crystallographic analysis. The isolation and characterization of **3** are of particular note as the first unambiguous experimental evidence for the [4+4] dimer of 9-silaanthracene derivatives.

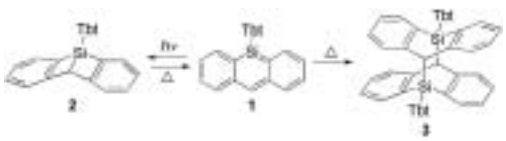

VII-G-3 Synthesis and Properties of the First Stable Neutral Germaaromatic Compound, 2-{2,4,6-Tris[bis(trimethylsilyl)methyl]phenyl}-2-Germanaphthalene

NAKATA, Norio[1]; TAKEDA, Nobuhiro[1]; TOKITOH, Norihiro[2]
([1]Kyoto Univ.; [2]IMS and Kyoto Univ.)

[*Organometallics* **22**, 481–489 (2003)]

While there have been relatively many informations on silaaromatic compounds, the studies on germaaromatic compounds are very few. In this paper, we present the synthesis and properties of the first stable 2-germanaphthalene.

The first stable neutral germaaromatic compound, 2-germanaphthalene **1** was synthesized by taking advantage of an extremely bulky and efficient steric protection group, 2,4,6-tris[bis(trimethylsilyl)methyl]phenyl (Tbt). The molecular structure and aromaticity of **1** were discussed on the basis of its NMR, UV-vis and Raman spectra, X-ray crystallographic analysis, and theoretical calculations, which indicate the delocalization of π-electrons in the 2-germanaphthalene ring of **1**. 2-Germanaphthalene **1** reacted with water, *t*-BuLi, mesitonitrile oxide, 2,3-dimethyl-1,3-butadiene, elemental sulfur, and elemental selenium to give the corresponding adducts **2**–**7** across the Ge–C double bond.

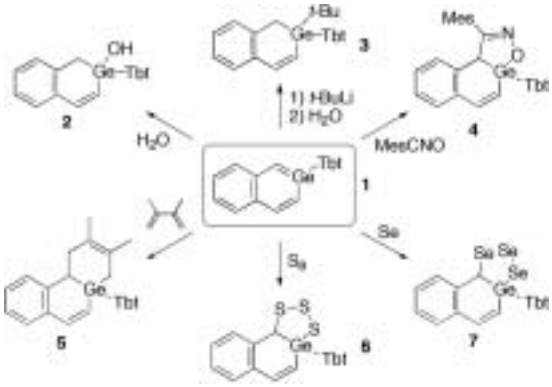

VII-G-4 η⁶-Germabenzene Complexes of Chromium and Molybdenum

NAKATA, Norio[1]; TAKEDA, Nobuhiro[1]; TOKITOH, Norihiro[2]
([1]Kyoto Univ.; [2]IMS and Kyoto Univ.)

[*Angew. Chem., Int. Ed.* **42**, 115–117 (2003)]

Germabenzenes are the most fundamental germaaromatic compounds having a simple 6π-electron ring system. However, very little has been known about the synthesis and characterization of germaaromatic compounds due to their extremely high reactivity. Very recently, we have succeeded in the synthesis and properties of the first stable germabenzene **1** bearing an efficient steric protection group, 2,4,6-tris[bis(trimethylsilyl)methyl]phenyl (Tbt). Meanwhile, in recent decades there has been considerable interest in the transition metal complexes containing sila- and germaaromatic compounds as ligands from the viewpoints of their coordination fashion and unique structure. However, the molecular structure and reactivity of η^6-sila- and germabenzene complexes have never been known.

The first η^6-germabenzene complexes, [M(η^6-C_5H_5GeTbt)$(CO)_3$] [M = Cr (**2**), Mo (**3**)], were synthesized by the ligand exchange reaction of the corresponding acetonitrile complexes, [M$(CH_3CN)_3(CO)_3$] (M = Cr, Mo) with **1**. These reactions are interesting also as the first examples showing the aromatic character of the germabenzene **1** from the standpoint of its reactivity. The low-temperature X-ray crystallographic analysis of Cr complex **2** revealed that the germabenzene ring was almost planar and η^6-coordinated to the $Cr(CO)_3$ group.

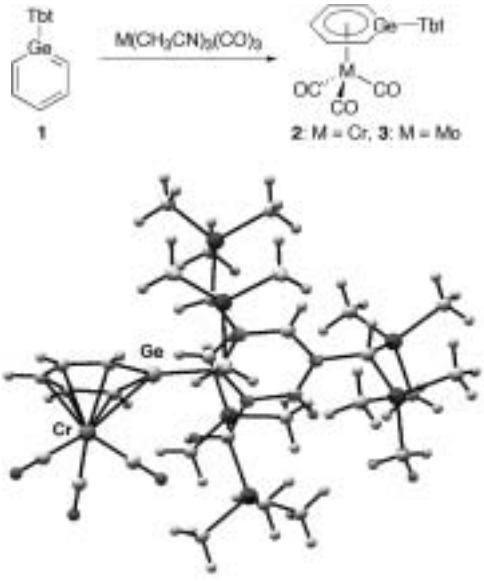

Figure 1. Molecular Structure of Germabenzene Complex of Chromium **1**.

VII-G-5 Reaction of Stable Germabenzene with Chalcogens: Synthesis and Structure of a Novel Germanium Analog of Pentathiepane, 1,2,3,4,5,6-Pentathiagermepane

NAKATA, Norio[1]; TAKEDA, Nobuhiro[1]; TOKITOH, Norihiro[2]
([1]Kyoto Univ.; [2]IMS and Kyoto Univ.)

[*J. Organomet. Chem.* **672**, 66–71 (2003)]

Much attention has been paid to the chemistry of cyclic polychalcogenides from the standpoints of chemical and physical properties as well as from that of biological activities. In contrast to the widely explored chemistry of transition metal polychalcogenido complexes, very little has been known for cyclic polychalcogenides containing a heavier group 14 element. We examined the synthesis of cyclic polychalcogenides containing germanium by the reactions of a stable germabenzene **1** bearing a 2,4,6-tris[bis(trimethylsilyl)methyl]phenyl (Tbt) group with elemental sulfur and selenium.

Treatment of a germabenzene **1** with elemental

sulfur gave a 1,2,3,4-trithiagermolane **2** together with a novel 1,2,3,4,5,6-pentathiagermepane **3**, which is the germanium analog of pentathiepane. On the other hand, the reaction of **1** with elemental selenium gave only 1,2,3,4-triselenagermolane **4**. All the newly obtained polychalcogenides containing a germanium atom were characterized by NMR spectroscopy and elemental analysis. The molecular structures of **2** and **3** were determined by X-ray crystallographic analysis. In addition, the thermal interconversion between pentasulfide **3** and trisulfide **2** plus 1/4 S_8 was confirmed.

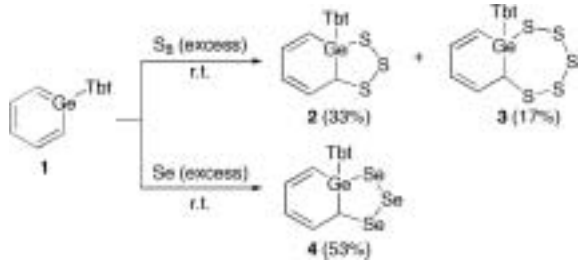

VII-G-6 Syntheses and Structures of Silicon Analogues of Cyclopropabenzenes

TAJIMA, Tomoyuki[1]; HATANO, Ken[2]; SASAKI, Takayo[1]; SASAMORI, Takahiro[1]; TAKEDA, Nobuhiro[1]; TOKITOH, Norihiro[3]; TAKAGI, Nozomi; NAGASE, Shigeru
([1]Kyoto Univ.; [2]Kyushu Univ.; [3]IMS and Kyoto Univ.)

[*Chem. Lett.* **32**, 220–221 (2003); *J. Organomet. Chem.* **686**, 118–126 (2003)]

Since the finding of significant deformation for the fused aromatic rings in the series of benzocycloalkanes, it has been one of the important subjects assigned to organic chemists to solve a riddle for such deformation. Cyclopropabenzene has attracted special attention because of the most severely enforced deformation in this series. However, there is no example for the synthesis of its heteroatom analogs, heteracyclopropabenzenes, as stable compounds until our project started. In this paper, we present the synthesis of the first stable silacyclopropazenzene and bis(silacyclopropa)benzenes, which are the first stable heteracyclopropabenzenes, by taking advantage of 2,4,6-tris[bis(trimethylsilyl)-methyl]phenyl (Tbt) group.

The reactions of an very crowded diaryldilithiosilane **1** with *o*-dibromobenzene and 1,2,4,5-tetrabromobenzene resulted in the formation of the first stable silacyclopropabenzene **2** and bis(silacyclopropa)-benzenes **3**, respectively. The crystallographic analyses and theoretical calculations revealed that the deformation in benzene rings of **2** ans **3** is less than that of cyclopropabenzenes, which show severe deformation of the benzene rings caused by the fused cyclopropane rings. The successful isolation of **2** is noteworthy because no carbon analogues, bis(cyclopropa)benzenes, have been synthesized yet.

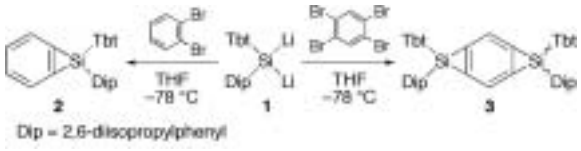

VII-G-7 Synthesis and Isolation of the First Germacyclopropabenzene: A Study to Elucidate the Intrinsic Factor for the Ring Deformation of Cyclopropabenzene Skeletons

TOKITOH, Norihiro[1]; HATANO, Ken[2]; SASAKI, Takayo[3]; SASAMORI, Takahiro[3]; TAKEDA, Nobuhiro[3]; TAKAGI, Nozomi; NAGASE, Shigeru
([1]IMS and Kyoto Uniiv.; [2]Kyushu Univ.; [3]Kyoto Univ.)

[*Organometallics* **21**, 4309–4311 (2002)]

Cyclopropabenzenes have attracted much attention because it is expected that the fused cyclopropane rings result in the severe deformation of the benzene rings. Recently, we have synthesized silacyclopropabenzene **1** as the first example of a stable heteracyclopropabenzene by the reaction of a sterically hindered dilithiosilane, Tbt(Dip)$SiLi_2$ (Tbt = 2,4,6-tris[bis(trimethylsilyl)-methyl]phenyl, Dip = 2,6-diisopropylphenyl), with 1,2-dibromobenzene. This successful synthesis of **1** naturally prompted us to examine the synthesis of germacyclopropabenzenes.

The treatment of an overcrowded diaryldilithiogermane, Tbt(Dip)$GeLi_2$, generated by exhaustive reduction of Tbt(Dip)$GeBr_2$, with 1,2-dibromobenzene resulted in the formation of the first stable germacyclopropabenzene **2**, which was fully characterized by ^1H and ^{13}C NMR spectra, FAB-MS, and X-ray structural analysis. As well as the case of silacyclopropabenzene **1**, the structural parameters of **2** indicated that the germacyclopropane ring can enjoy annelation with much less perturbation, in contrast to the severe distortion in cyclopropabenzene rings.

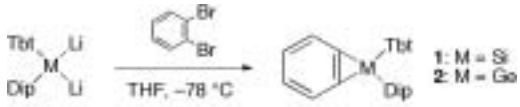

VII-G-8 Synthesis and Properties of the First Stable Silylene-Isocyanide Complexes

TAKEDA, Nobuhiro[1]; KAJIWARA, Takashi[1]; SUZUKI, Hiroyuki[2]; OKAZAKI, Renji[2]; TOKITOH, Norihiro[3]
([1]Kyoto Univ.; [2]Univ. Tokyo; [3]IMS and Kyoto Univ.)

[*Chem. Eur. J.* **9**, 3530–3543 (2003)]

Recently, various types of compounds containing a stable double bond to silicon have been synthesized by taking advantage of steric protection due to bulky substituents. On the other hand, the chemistry of compounds containing silicon as part of a cumulated double-bond system has been less explored. As for heavier analogues of ketenimines (>C=C=N–), it has

been reported that a stannaketenimine (>SnCN–) is rather stannylene-isocyanide complex (>Sn←CN–) than cumulative compound (>Sn=C=N–), while 1-phospha-3-silaallene (>SiCP–) and 1-phospha-3-germaallene (>GeCP–) represent allenic character (>M=C=P–). However, there is no report for stable silicon analogues (>SiCN–) and their properties have not been revealed, although their properties have attracted much interest.

We successfully synthesized Tbt(Mes)SiCNAr (Tbt = 2,4,6-tris[bis(trimethylsilyl)methyl]phenyl, Mes = mesityl) (**3a-c**), by the reactions of a kinetically stabilized disilene **1**, with bulky isocyanides **2a-c**. The spectroscopic data of **3a-c** and theoretical calculations indicated that the **3a-c** are not classical cumulative compounds but the first stable silylene-Lewis base complexes. The reaction with triethylsilane giving silylene adduct **4** indicated the dissociation of the complexes **3a-c** to the corresponding silylene [Tbt(Mes)Si:] and isocyanides **2a-c** at room temperature. In additrion, **3a** reacted with methanol to give methanol adduct **5** *via* electrophilic attack on the silicon atom, which is most likely resulted from the contribution of the zwitterionic resonance structures [Tbt(Mes)Si$^-$–C$^+$=N–Ar] and [Tbt(Mes)Si$^-$–C≡N$^+$–Ar].

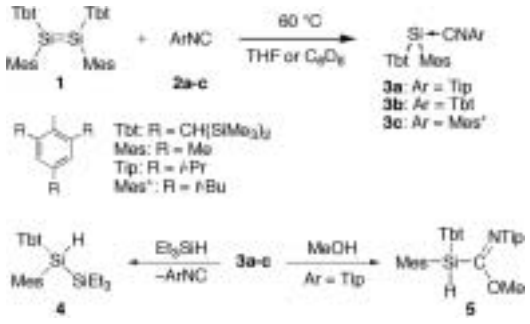

VII-G-9 Stable 2*H*-Azasilirene and 2*H*-Phosphasilirene: Addition Reaction of an Overcrowded Silylene to a Nitrile and a Phosphaalkyne

TOKITOH, Norihiro[1]; SUZUKI, Hiroyuki[2]; TAKEDA, Nobuhiro[3]; KAJIWARA, Takashi[3]; SASAMORI, Takahiro[3]; OKAZAKI, Renji[2];
([1]IMS and Kyoto Univ.; [2]Univ. Tokyo; [3]Kyoto Univ.)

[*Silicon Chem.* in press]

In recent decades, there has been much interest in the chemistry of divalent silicon species, silylenes, from the viewpoint of not only fundamental chemistry but also applied chemistry such as material science and organic syntheses. Much attention has been paid to their reactivities such as addition to olefins, alkynes, isocyanides, and so on in comparison with the reactivities of carbenes. On the other hand, we have succeeded in the formation of very crowded silylene **1** bearing a 2,4,6-tris[bis(trimethylsilyl)methyl]phenyl (Tbt) group by thermolysis of the corresponding disilene **2** at 60 °C or that of silylene–isocyanide complex **3** at room temperature.

In this paper, we present the reaction of an overcrowded silylene **1** with pivalonitrile and *t*-butylphosphaalkyne to give the corresponding [1+2]cycloadducts, 2*H*-azasilirene and 2*H*-phosphasilirene derivatives, **4** and **5**, respectively. This is the first example of the isolation of a stable 2*H*-azasilirene derivative, and the X-ray crystallographic analysis of **4** unambiguously revealed its three-membered ring structure in the solid state. In addition, DFT calculations supported three-membered ring character in the structures of the 2*H*-azasilirene **4** and 2*H*-phosphasilirene **5**.

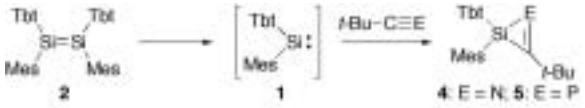

VII-G-10 Synthesis and Reactions of New Diphosphenes Bearing Extremely Bulky Substituents

SASAMORI, Takahiro[1]; TAKEDA, Nobuhiro[1]; TOKITOH, Norihiro[2]
([1]Kyoto Univ.; [2]IMS and Kyoto Univ.)

[*J. Phys. Org. Chem.* **16**, 450–462 (2003)]

Multiple-bond compounds between heavier group 15 elements have fascinated chemists for a long time. Since the first isolation of the diphosphene Mes*P=PMes* (Mes* = 2,4,6-tri-*t*-butylphenyl), intensive studies have been performed using several steric protection groups on the chemistry of a variety of diphosphenes.

In this paper, we present the synthesis of new diphosphenes, Tbt–P=P–Tbt (**1**) and Bbt–P=P–Bbt (**2**), having extremely bulky substituents, 2,4,6-tris[bis(trimethylsilyl)methyl]phenyl (Tbt) and 2,6-bis[bis(trimethylsilyl)methyl]-4-[tris(trimethylsilyl)methyl]phenyl groups (Bbt), which are effective to the stabilization of distibenes (Ar–Sb=Sb–Ar) and dibismuthenes (Ar–Bi=Bi–Ar). The X-ray crystallographic analysis revealed their unique structures in the solid state. Furthermore, the conformations of these extremely overcrowded diphosphenes, **1** and **2**, are twisted in different ways in spite of the close structural similarity between Tbt and Bbt groups. DFT calculations were performed to estimate the energy difference between the two conformations of diphosphenes. In addition, their structures and physical properties were compared with those of their heavier congeners, distibenes (Ar–Sb=Sb–Ar, Ar = Tbt and Bbt) and dibismuthenes (Ar–Bi=Bi–Ar, Ar = Tbt and Bbt) having the same substituents. Although the reactivities of the extremely hindered diphosphenes might be considerably suppressed owing to the severe steric congestion, it was found that they can react with elemental sulfur and selenium to give the corresponding thia- and selenadiphosphirane derivatives, respectively.

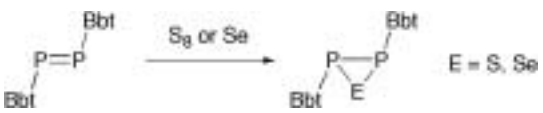

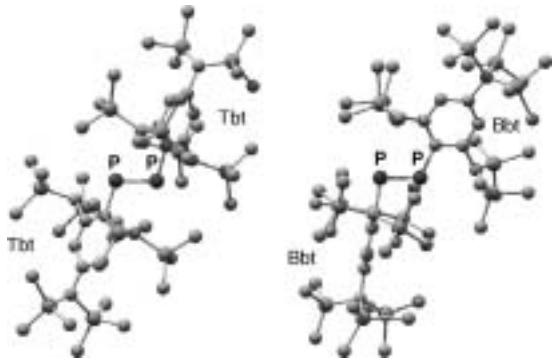

Figure 1. Molecular Structures of **1** (left) and **2** (right).

VII-G-11 Synthesis, Structure, and Properties of the First Disulfur and Diselenium Complexes of Platinum

NAGATA, Kazuto[1]; TAKEDA, Nobuhiro[1]; TOKITOH, Norihiro[2]
([1]Kyoto Univ.; [2]IMS and Kyoto Univ.)

[*Chem. Lett.* **32**, 170–171 (2003), *Bull. Chem. Soc. Jpn.* **76**, 1577–1587 (2003)]

Much attention has been focused on the chemistry of transition metal complexes having O_2, S_2, and Se_2 ligands from the viewpoints of not only fundamental chemistry but also catalysis and biochemistry. However, the disulfur and diselenium complexes of platinum remain unknown probably due to the strong propensity of sulfur and selenium ligands for bridging metal atoms.

We succeeded in the synthesis of the first disulfur and diselenium complexes of platinum, **1** and **2**, by taking advantage of bulky phosphine ligands bearing a 2,4,6-tris[bis(trimethylsilyl)methyl]phenyl (Tbt) or 2,6-bis[bis(trimethylsilyl)methyl]-4-[tris(trimethylsilyl)-methyl]phenyl (Bbt) group, which sterically protect the mononuclear complexes from the oligomerization. Complexes **1** and **2** were synthesized by the reaction of zerovalent platinum complexes **3** with elemental sulfur and selenium, respectively. Crystallographic analysis of **1b** and **2b** showed that their central Pt atoms have tetracoordinated, planar geometries, and their PtE_2 (E = S, Se) parts have three-membered-ring structures. The oxidation of **1b** and **2b** with an equimolar amount of *m*-chloroperbenzoic acid or *t*-butyl hydroperoxide in dichloromethane afforded the corresponding disulfur and diselenium monoxide complexes, **4** and **5**, respectively. An interesting difference in reactivity between **4** and **5** was shown in the further reactions with an excess of oxidants, which produced the corresponding *O*,*S*-coordinated thiosulfate complex **6** and the *O*,*O*-coordinated selenite complex **7**, respectively. The dynamic behavior in solution was revealed by the variable-temperature NMR spectroscopy for **1b**, **2b**, **6**, and **7**, which indicates the existence of the intramolecular CH···E (E = O, S, Se) interactions between the methine hydrogens of the *o*-bis(trimethylsilyl)-methyl groups and the Pt-bonded heteroatoms.

VII-H Preparation and Properties of the Homo- and Heterometallic Clusters

This project focuses on the development of a systematic synthetic route to a series of the homo- and heterometallic clusters as templates or catalysts for new types of activation and transformation of organic, inorganic, and organometallic molecules at the well-defined multimetallic reaction sites.

VII-H-1 Synthesis and Reactivities of Amido-Bridged Dinuclear Ruthenium Complexes

TAKEMOTO, Shin[1]; OSHIO, Shinya[1]; OGURA, Shin-ichiro[1]; MATSUZAKA, Hiroyuki[2]
([1]Osaka Prefecture Univ.; [2]IMS and Osaka Prefecture Univ.)

Novel dinuclear ruthenium 1,2-phenylenediamido complexes (**1a**) and (**1b**) were prepared and their reactivities have been examined in detail. Complex **1a** is cleanly converted to **1b** in refluxing acetonitrile. Treatment of 1b with 1 equiv of CO yields the carbonyl adduct (**2**), which further reacts with excess CO to form the amido/carbamoyl/carbonyl complex (**3**).

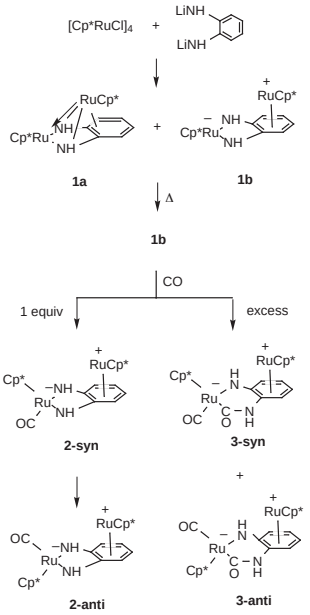

VII-H-2 Preparation, Structure, and Reactivity of the Benzenedithiolato-Bridged Ir/Ru Mixed-Metal Clusters

TAKEMOTO, Shin[1]; SHIMADZU, Daisuke[1]; OGURA, Shin-ichiro[1]; MATSUZAKA, Hiroyuki[2]
([1]Osaka Prefecture Univ.; [2]IMS and Osaka Prefecture Univ.)

A series of the iridium/ruthenium mixed-metal clusters containing a bridging benzenedithiolato ligand were selectively synthesized in good yields and their chemical reactivities have been examined in detail. Oxidation of the Ir(II) centers in the novel Ir_2R mixed-metal cluster **4** with I_2 readily proceeded to give the IrRu cluster **5** together with $[Cp^*IrI(\mu_2\text{-}I)]_2$. Direct treatment of $Cp^*Ir(\text{-}C_6H_4S_2\text{-}1,2)$ with $[Cp^*Ru(MeCN)_3]PF_6$ alternatively afforded **5**, whereas similar reaction in the presence of LiCl selectively produced **6**, the isomeric form of **5**, which was quantitatively converted to **5** in refluxing acetonitrile.

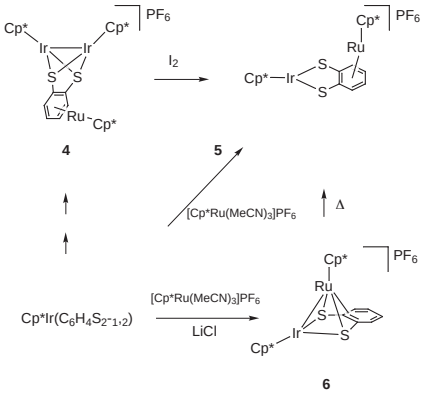

VII-H-3 Selective Transformation of the Oligomeric Ru_2Rh Cluster to the Ru_3Rh_2 and the Ru_4Rh_4 Framework

TAKEMOTO, Shin[1]; HAYASHI, Hirokazu[1]; KASHIWAKURA, Miki[1]; MATSUZAKA, Hiroyuki[2]
([1]Osaka Prefecture Univ.; [2]IMS and Osaka Prefecture Univ.)

Selective heteronuclear metal-metal bond formation reaction readily proceeded to give the Ru_3Rh and Ru_4Rh_4 mixed-metal clusters (**7** and **8**) from mononuclear precursors *via* oligomeric Ru_2Rh complex (**9**).

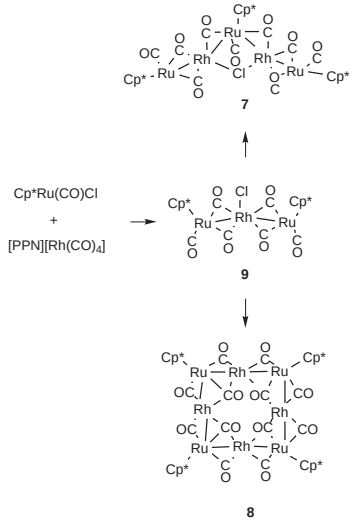

VII-I Precise Synthesis of Functional Macromolecules Using Organometallic Complexes

Macromolecules, in which not only molecular weight and chemical sequence but also secondary structures are well controlled, attract much attention due to their novel properties and functionalities. Precise synthesis of such macromolecules is one of the goals for the development of new functional materials. This project focuses on precise synthesis of helical or dendritic macromolecules using organometallic complexes, which act as living polymerization catalysts or building blocks. We also examined the physical and chemical properties of the resulting polymers.

VII-I-1 Platinum-Acetylide Dendrimers Possessing a Porphyrin Core

ONITSUKA, Kiyotaka[1]; KITAJIMA, Hotaka[2]; FUJIMOTO, Masanori[2]; IUCHI, Asako[2]; TAKEI, Fumie[2]; TAKAHASHI, Shigetoshi[2]
([1]IMS and Osaka Univ.; [2]Osaka Univ.)

[*Chem. Commun.* 2576 (2002)]

Intramolecular energy transfer from platinum-acetylide moieties to the porphyrin core was observed in novel organometallic dendrimers that were prepared from a tetra(4-ethynylphenyl)porphyrin-bridged tetranuclear platinum-acetylide core and platinum-acetylide dendrons by a convergent method.

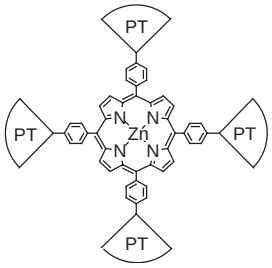

VII-I-2 A Divergent Approach to the Precise Synthesis of Giant Organometallic Dendrimers Using Platinum-Acetylides as Building Blocks

ONITSUKA, Kiyotaka[1]; SHIMIZU, Atsushi[2]; TAKAHASHI, Shigetoshi[2]
([1]IMS and Osaka Univ.; [2]Osaka Univ.)

[*Chem. Commun.* 280 (2003)]

Giant platinum-acetylides dendrimers were precisely synthesized by a divergent method; the sixth generation dendrimer, the diameter of which is larger than 10 nm, has 189 Pt atoms per molecule, and its molecular weight is as high as 139,750.

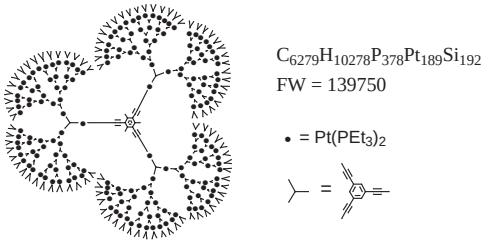

VII-I-3 Preparation and Photochemical Properties of Polyisocyanides with Regularly Arranged Porphyrin Pendants

TAKEI, Fumie[2]; NAKAMURA, Sugiko[2]; ONITSUKA, Kiyotaka[1]; ISHIDA, Akito[2]; TOJO, Sachiko[2]; MAJIMA, Tetsuro[2]; TAKAHASHI, Shigetoshi[2]
([1]IMS and Osaka Univ.; [2]Osaka Univ.)

[*Chem. Lett.* 506 (2003)]

A novel triblock polyisocyanide having free-base- and zincporphyrins as pendants was prepared by living polymerization with a Pt-Pd μ-ethynediyl complex as an initiator, and irradiated at 420 or 556 nm in a THF solution to cause intramolecular energy transfer from the zinc-porphyrin to the free-base-porphyrin.

VII-J Development of New Catalytic Reactions for Synthesis of N-Heterocyclic Compounds

Heterocyclic compounds are found in a wide variety of biologically active natural products, and considerable attention has been directed toward the development of new synthetic methods for useful heterocycles. Our research effort has been directed toward the discovery of new catalytic reactions for the synthesis of *N*-heterocyclic frameworks using *ortho*-functionalized aryl isocyanides.

VII-J-1 Structure and Reactivity of (η^3-Indolylmethyl)palladium Complexes Generated by the Reaction of Organopalladium Complexes with *o*-Alkenylphenyl Isocyanide

ONITSUKA, Kiyotaka[1]; YAMAMOTO, Mari[2]; SUZUKI, Shinobu[2]; TAKAHASHI, Shigetoshi[2]
([1]IMS and Osaka Univ.; [2]Osaka Univ.)

[*Organometallics* **21**, 581 (2002)]

The reaction of methylpalladium complexes with *o*-alkenylphenyl isocyanides results in the successive intramolecular insertion of the alkenyl and isocyano groups followed by the 1,3-migration of hydrogen to give (η^3-indolylmethyl)palladium complexes (**4**) in good yields. Treatment of **4** with diethylamine causes nucleophilic attack at the exo methylene carbon to give 2-methyl-3-aminomethylindole, whereas the reactions with HCl produce 2,3-dimethylindole derivatives.

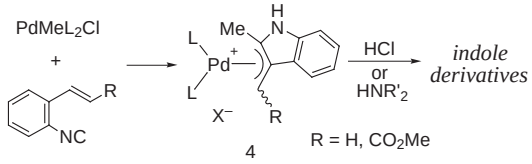

4

VII-J-2 A Novel Route to 2,3-Disubstituted Indoles *via* Palladium-Catalyzed Three-Component Coupling of Aryl Iodide, *o*-Alkenylphenyl Isocyanide and Amine

ONITSUKA, Kiyotaka[1]; SUZUKI, Shinobu[2]; TAKAHASHI, Shigetoshi[2]
([1]IMS and Osaka Univ.; [2]Osaka Univ.)

[*Tetrahedron Lett.* **43**, 6197 (2002)]

Three-component coupling reactions of aryl iodide, *o*-alkenylphenyl isocyanide and amine in the presence of palladium catalysts produced 2,3-substituted indoles in moderate yields.

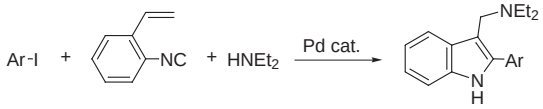

VII-K Synthesis of Transition Metal Complexes Containing a Novel Metal-Silicon and Metal-Gallium Bonding

Synthesis of transition metal complexes with unprecedented bonds between a metal and a heavy main group element is one of current topics on inorganic chemistry. In this project, we have investigated the synthesis, structure, and reactivities of metal complexes containing a metal-silicon unsaturated bonding and a metal-hydrogen-gallium 3c2e bonding. We also developed a versatile preparative method of anionic metal complexes $CpM(CO)_2^-$ (M = Fe, Ru).

VII-K-1 Synthesis of Self-Stabilized and Donor-Free Silyl(silylene)tungsten Complexes

UENO, Keiji[1]; WATANABE, Nobuhiko[2]; ASAMI, Satsuki[2]; SAKAI, Mihoko[2]; OGINO, Hiroshi[3]
([1]IMS and Gunma Univ.; [2]Tohoku Univ.; [3]Univ. Air)

[*Organometallics* **21**, 1326–1328 (2002)]

Photolysis of $Cp'W(CO)_3Me$ (**1a**: Cp' = η-C_5Me_5; **1b**: Cp' = η-C_5Me_4Et) in the presence of excess $HSiMe_2SiMe_3$ afforded a self-stabilized silyl(silylene)-tungsten complex with a dimeric structure, $[Cp'W(CO)_2(=SiMe_2)(SiMe_3)]_2$ (**2a**: Cp' = η-C_5Me_5; **2b**: Cp' = η-C_5Me_4Et), respectively. In contrast, photolysis of **1a** in the presence of $HSiMe_2SiMeMes_2$ (Mes = 2,4,6-$Me_3C_6H_2$) resulted in the formation of the first donor-free silyl(silylene) complex with only alkyl and aryl substituents on the silicon atoms $Cp'W(CO)_2(=SiMes_2)(SiMe_3)$ (**3**).

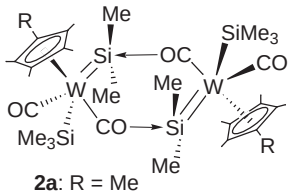

2a: R = Me
2b: R = Et

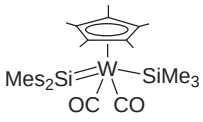

3

VII-K-2 Synthesis of the First Gallane-Coordinated Transition Metal Complex

UENO, Keiji[1]; YAMAGUCHI, Takeshi[2]; UCHIYAMA, Kei[2]; OGINO, Hiroshi[3]
([1]IMS and Gunma Univ.; [2]Tohoku Univ.; [3]Univ. Air)

[*Organometallics* **21**, 2347–2349 (2002)]

The first gallane-coordinated metal complex $(OC)_5W(\eta^1\text{-}GaH_3\cdot quinuclidine)$ (**2**) was synthesized by photolysis of a *ca.* 1:1 mixture of $W(CO)_6$ and quinuclidine-coordinated gallane $H_3Ga\cdot quinuclidine$ (**1**) in toluene and by the reaction of $(OC)_5W(THF)$ with 1 eq of gallane **1** in THF. X-ray crystal structure analysis of **2** revealed that gallane **1** is bound to the tungsten fragment *via* a W–H–Ga 3-center 2-electron bond.

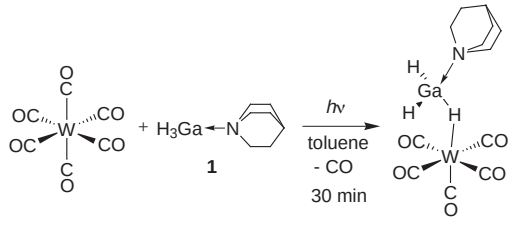

2

VII-K-3 Convenient Preparation of Li[(η^5-C_5Me_5)M(CO)$_2$] (M = Ru, Fe) by the Reaction of (η^5-C_5Me_5)M(CO)$_2$H with *n*-BuLi

OKAZAKI, Masaaki[1]; SATOH, Kazuyuki[1]; AKAGI, Tadahiro[1]; IWATA, Masatoshi[1]; JUNG, Kyeong A.[1]; SHIOZAWA, Rie[1]; UENO, Keiji[2]; TOBITA, Hiromi[1]; OGINO, Hiroshi[3]
([1]Tohoku Univ.; [2]IMS and Gunma Univ.; [3]Univ. Air)

[*J. Organomet. Chem.* **645**, 201–205 (2002)]

The anionic ruthenium and iron complexes Li[(η^5-C_5Me_5)M(CO)$_2$] (M = Ru (**1-Ru**), Fe (**1-Fe**)) were generated by deprotonation of the transition metal hydride (η^5-C_5Me_5)M(CO)$_2$H with *n*-BuLi in tetrahydrofuran (THF). The reaction proceeded at –45 °C immediately. Reactions of **1** with various electrophiles (Me_3SiCl, $pTol_2HSiCl$, Me_2SiCl_2, $MeSiCl_3$, $SiCl_4$, $Me_3SiSiMe_2Cl$, and Ph_2GeCl_2) afforded the corresponding nucleophilic substitution products (η^5-C_5Me_5)M(CO)$_2$$ER_3$ (E = Si, Ge) *via* salt-elimination.

RESEARCH ACTIVITIES VIII
Laser Research Center for Molecular Science

VIII-A Developments and Researches of New Laser Materials

Although development of lasers is remarkable, there are no lasers which lase in ultraviolet and far infrared regions. However, it is expected that these kinds of lasers break out a great revolution in not only the molecular science but also in the industrial world.

In this project we research characters of new materials for ultraviolet and far infrared lasers, and develop new lasers by using these laser materials.

VIII-A-1 High-Energy, All-Solid-State, Ultraviolet Laser Power-Amplifier Module Design and Its Output-Energy Scaling Principle

ONO, Shingo; SUZUKI, Yuji; KOZEKI, Toshimasa; MURAKAMI, Hidetoshi; OHTAKE, Hideyuki; SARUKURA, Nobuhiko; SATO, Hiroki[1]; MACHIDA, Susumu[1]; SHIMAMURA, Kiyoshi[1]; FUKUDA, Tsuguo[2]
([1]Tokin Corp.; [2]Tohoku Univ.)

[*Appl. Opt.* **41**, 7556 (2002)]

We demonstrated that a coaxially pumped, large-aperture ultraviolet power-amplifier module using solid-state tunable laser medium Ce^{3+}:$LiCaAlF_6$ has 98-mJ, 290-nm, and 3-ns output pulses with sufficient extraction efficiency of 25%. The detailed information of design parameters, including the gain-coefficient dependence on pump condition, is successfully accumulated for further energy scaling for a terawatt-class ultraviolet chirped pulse amplification laser system or a high-pulse-energy laser system.

VIII-A-2 Generation of Intense 25-fs Pulses at 290 nm by Use of a Hollow Fiber Filled with High-Pressure Argon Gas

LIU, Zhenlin[1]; ONO, Shingo; KOZEKI, Toshimasa[2]; SUZUKI, Yuji[2]; SARUKURA, Nobuhiko[2]; HOSONO, Hideo[1,3]
([1]ERATO; [2]IMS, ERATO; [3]Tokyo Inst. Tech.)

[*Jpn. J. Appl. Phys.* **41**, L986 (2002)]

Frequency-tripled pulses at 290 nm from a 100-fs, 1-kHz Ti:sapphire regenerative amplifier system are spectrally broadened in hollow fiber filled with high-pressure argon gas. The self-phase-modulated pulses are compressed to 25 fs through a prism pair. The compressed pulse has an energy of 15 μJ.

VIII-A-3 Anomalous Power and Spectrum Dependence of THz Radiation from Femtosecond-Laser-Irradiated InAs in a High Magnetic Field of 14 T

OHTAKE, Hideyuki; MURAKAMI, Hidetoshi; YANO, Takayuki; ONO, Shingo; SARUKURA, Nobuhiko; TAKAHASHI, Hiroshi[1]; SUZUKI, Yuji[1]; NISHIJIMA, Gen[2]; WATANABE, Kazuo[2]
([1]GUAS; [2]Tohoku Univ.)

[*Appl. Phys. Lett.* **82**, 1164 (2003)]

We report on the THz radiation from femtosecond-laser-irradiated InAs in a high magnetic field up to 14 T. It is found that the radiation power exhibits anomalous magnetic-field dependence, including saturation, decrease, and recovery up to 14 T. Moreover, the radiation spectrum possesses a clear periodic structure over 6 T, possibly due to differently phased radiation from holes with different masses.

VIII-A-4 Significant Enhancement of Terahertz Radiation from InSb by Use of a Compact Fiber Laser and an External Magnetic Field

TAKAHASHI, Hiroshi[1]; SUZUKI, Yuji[1]; SAKAI, Masahiro; ONO, Shingo; SARUKURA, Nobuhiko; SUGIURA, Toshiharu[2]; HIROSUMI, Tomoya[2]; YOSHIDA, Makoto[2]
([1]GUAS; [2]Aisin Seiki Co., Ltd.)

[*Appl. Phys. Lett.* **82**, 2005 (2003)]

We investigated the magnetic-field dependence of terahertz (THz) radiation power from InSb. Significant enhancement of THz-radiation power is observed by using a compact fiber laser that delivered 100 fs optical pulses at a center wavelength of 1560 nm. Additionally, applying external magnetic fields dramatically enhanced the THz-radiation power. THz-radiation power reaches a maximum value at around 1.2 T, and its enhancement factor exceeds 100. From an applications viewpoint, this is a significant finding for practical light source design, since it is easily achieved by using a compact fiber laser and a conventional magnet.

VIII-A-5 Micro-Character Printing on a Diamond Plate by Femtosecond Infrared Optical Pulses

TAKESADA, Masaki[1,2]; VANAGAS, Egidijus[3]; TUZHILIN, Dmitri[3]; KUDRYASHOV, Igor[3]; SURUGA, Shoji[3]; MURAKAMI, Hidetoshi; SARUKURA, Nobuhiko; MATSUDA, Kazunari[1]; MONONOBE, Shuji[1]; SAIKI, Toshiharu[1]; YOSHIMOTO, Mamoru[4]; KOSHIHARA, Shin-ya[1]

([1]KAST; [2]Hokkaido Univ.; [3]Tokyo Instrument Inc.; [4]Tokyo Inst. Tech.)

[*Jpn. J. Appl. Phys.* **42**, 4613 (2003)]

Processing of less than 400 nm has been performed on the surface of a diamond plate by means of a femtosecond infrared pulse laser. Various characters with a size of about 1 μm were drawn by the femtosecond pulse laser system in conjunction with a microscope equipped with a precisely controlled piezo-stage. The tightly focused laser light on the flat surface of the diamond made it possible to minimize the light-induced graphitization. The surface of the diamond plate after laser machining was analyzed by micro-Raman measurements to estimate the graphitization effect induced by laser irradiation. The obtained results indicate that graphitization increased with the number of irradiated laser pulses.

VIII-A-6 Mode-Locking Stability Adjustment of a Kerr-Lens Mode-Locked Ti:sapphire Laser, Analyzed by a Recently Developed Real-Time Spectrum Analyzer

TAKAHASHI, Hiroshi[1]; SUZUKI, Yuji[1]; MURAKAMI, Hidetoshi; ONO, Shingo; SARUKURA, Nobuhiko; NAKAMURA, Tadashi[2]
([1]GUAS; [2]Textronix Japan., Ltd.)

[*Jpn. J. Appl. Phys.* **42**, 4330 (2003)]

This is a report on the mode-locking stability of a Kerr-lens mode-locked Ti:sapphire, measured by a newly developed noise measurement method. Mode-locking stability is monitored *via* a power spectrum, which is obtained by irradiating optical pulses onto a fast photodiode, and by processing the detected signal using a recently developed real-time spectrum analyzer. The mode-locking stability of the Ti:sapphire laser strongly depends on pump power and becomes unstable as pump power decreases from an optimum power level. Amplitude fluctuation and Q-switched mode-locking are notably observed as the main causes for a break in a continuous-wave (CW) mode-locking operation. Moreover, chaotic frequency hopping is observed in a Q-switched mode-locking operation. A real-time spectrum analyzer provides a time-varying power spectrum, which enables easy adjustment for stable CW mode-locking operation of ultra-fast solid state lasers.

VIII-A-7 Magnetic-Field-Induced Enhancement of THz-Radiation Power from Femtosecond-Laser-Irradiated InAs up to 27 T

TAKAHASHI, Hiroshi[1]; SUZUKI, Yuji[1]; QUEMA, Alex; SAKAI, Masahiro; YANO, Takayuki; ONO, Shingo; SARUKURA, Nobuhiko; HOSOMIZU, Masato[2]; TSUKAMOTO, Takeyo[2]; NISHIJIMA, Gen[3]; WATANABE, Kazuo[3]
([1]GUAS; [2]SUT; [3]Tohoku Univ.)

[*Jpn. J. Appl. Phys.* **42**, L532 (2003)]

Magnetic-field dependence of THz-radiation power from InAs surface is investigated by using a hybrid magnet, which is capable of providing a magnetic field up to 28 T. It is found that THz-radiation power saturates at around 3 T and also at 13 T. Maximum THz-radiation power with high-frequency component spectrum is observed at 3-T. This result leads to the conclusion that a magnetic field of 3 T is optimum for the enhancement of THz-radiation power. Additionally, THz-radiation spectrum exhibits periodic structure at magnetic fields above 12 T. This can be attributed to the change of dielectric constant induced by the strong magnetic field resulting in the interference of THz-radiation pulses from the front and back surfaces of the InAs substrate.

VIII-A-8 Optical Properties of Ce^{3+} Ion Doped $LiCaAlF_6$ Crystal in Vacuum Ultraviolet Region

TAKAHASHI, Hiroshi[1]; SAKAI, Masahiro; ONO, Shingo[1]; SARUKURA, Nobuhiko; SATO, Hiroki[2]; YOSHIKAWA, Akira[2]; FUKUDA, Tsuguo[1]
([1]GUAS; [2]Tohoku Univ.)

[*Jpn. J. Appl. Phys.* **42**, L660 (2003)]

The optical properties of Ce^{3+} ion doped $LiCaAlF_6$ (Ce:LiCAF) crystal is investigated in vacuum ultraviolet (VUV) region. It is found that the optical excitation from the valence band of LiCAF crystal to the highest ^2D excited state of Ce^{3+} can be utilized as an efficient excitation channel to obtain the ultraviolet emission due to $4f$–$5d$ transition of Ce^{3+}. Furthermore, the energy level of ^2D state is found to be located near the conduction band of LiCAF crystal, which leads to the electron transfer from the LiCAF crystal to the active Ce^{3+} ion.

VIII-A-9 Identification of Potential Estrogenic Environmental Pollutants by Terahertz Transmission Spectroscopy

QUEMA, Alex; TAKAHASHI, Hiroshi[1]; SAKAI, Masahiro; GOTO, Masahiro; ONO, Shingo; SARUKURA, Nobuhiko; SHIODA, Ryu[2]; YAMADA, Norihide[2]
([1]GUAS; [2]Agilent Tech. Res. Cent.)

[*Jpn. J. Appl. Phys.* **42**, L932 (2003)]

Using magnetically enhanced terahertz radiation from InAs, various naphthols, which exhibits estrogenic like activity and are potentially mimic natural hormones, are studied. The experimental results show that the naphthols, depicted by the position of the hydroxyl (-OH) component at different carbon atom sites of the naphthalene compound, are distinguishable based on the absorption of THz radiation. It is found that the THz radiation absorption is strongly related to the crystal symmetry and dipole moment of these isomers.

VIII-A-10 Excitation Fluence Dependence of Terahertz Radiation Mechanism from Femtosecond-Laser-Irradiated InAs under Magnetic Field

TAKAHASHI, Hiroshi[1]; QUEMA, Alex; YOSHIOKA, Ryoichiro; ONO, Shingo; SARUKURA, Nobuhiko
([1]GUAS)

[*Appl. Phys. Lett.* **83**, 1068 (2003)]

The excitation fluence and magnetic field dependence of terahertz (THz) radiation power from InAs is investigated. At low excitation fluence, an enhancement of the THz-radiation power is observed independent of the magnetic-field direction. As the excitation fluence is increased, a crossover of terahertz radiation mechanism is observed. At excitation fluence above this crossover, the radiation power is either enhanced or reduced depending on the magnetic-field direction. These results are explained by considering the different THz-radiation mechanisms from the InAs surface with or without photoexcited carrier screening.

VIII-B Development and Research of Advanced Tunable Solid State Lasers

Diode-pumped solid-state lasers can provide excellent spatial mode quality and narrow linewidths. The high spectral power brightness of these lasers has allowed high efficiency frequency extension by nonlinear frequency conversion. Moreover, the availability of new and improved nonlinear optical crystals makes these techniques more practical. Additionally, quasi phase matching (QPM) is a new technique instead of conventional birefringent phase matching for compensating phase velocity dispersion in frequency conversion. These kinds of advanced tunable solid-state light sources, so to speak "Chroma Chip Lasers," will assist the research of molecular science.

In this projects we are developing Chroma Chip Lasers based on diode-pumped-microchip-solid-sate lasers and advanced nonlinear frequency conversion technique.

VIII-B-1 Highly Efficient Continuous-Wave 946-nm Nd:YAG Laser Emission under Direct 885-nm Pumping

LUPEI, Voicu[1]; PAVEL, Nicolaie[2]; TAIRA, Takunori

([1]IAP-NILPRP, Romania; [2]IMS and IAP-NILPRP, Romania)

[*Appl. Phys. Lett.* **81**, 2677 (2002)]

The quasi-three-level 946-nm emission of Nd^{3+} in YAG is important for construction of low-heat solid-state lasers at fundamental frequency or for doubling it by nonlinear processes to blue 473-nm radiation. Successful attempts to lase the Nd:YAG at 946 nm in continuous-wave (CW) or pulsed regimes have been reported;[1)–3)] however, the performances of these lasers are still limited and the full lasing potential is not yet exploited. This paper discusses some possibilities to improve the laser emission parameters and to reduce the generation of heat by pumping directly into the emitting level.

In a CW quasi-three-level laser the fractional thermal loading η_h (*i.e.* the fraction of absorbed power that is transformed into heat by non-radiative processes), contains specific contributions from the ions that participate in the lasing process as well as from those that do not lase. The quantum defect ratio for the 946-nm laser emission is much larger than that corresponding to the fluorescence emission, whose average wavelength $\bar{\lambda}$ is 1038 nm. The contribution to heating from each excited Nd^{3+} ion that does not lase would be then much larger than from each ion that participate to lasing; thus, a high laser extraction efficiency will contribute to the reduction of the heat generated in the pumped laser material. A complex interrelation exists between the laser emission parameters and the heat generation and an optimization of all these characteristics would be necessary in order to make a complete use of the quasi-three-level emission potential. Both the laser emission parameters and the generation of heat are influenced by the quantum defect ratio $\eta_{qd} = \lambda_p/\lambda_l$ between the pump and laser emission wavelengths. Traditionally the 946-nm Nd:YAG lasers are pumped at 808 nm into the level $^4F_{5/2}$: this induces a parasitic upper quantum defect of ~1000 cm^{-1} between the pump and the emitting laser levels that accounts for more than half of the total quantum defect. As evidenced by the spectroscopic investigations[4)–6)] very suitable for diode laser pumping the Nd:YAG is the double-peaked absorption band centred around 885 nm that collects the thermally activated transitions $Z_2 \rightarrow R_1$ and $Z_3 \rightarrow R_2$ of the absorption spectrum $^4I_{9/2} \rightarrow {}^4F_{3/2}$. This wavelength of pump determines an increase of the quantum defect ratio by ~ 9.5%, leading to a corresponding improvement of the laser emission parameters. Moreover, by restricting strongly the reabsorption losses η_h could be diminished by as much as 50 to 60% from the value corresponding to that of 808-nm pumping.

The 946-nm CW emission in a 1.0-at.% Nd:YAG crystal (3-mm thick) is investigated by using 885-nm Ti:sapphire longitudinal pumping. The crystal was AR coated for 808 and 885 nm (reflectivity, $R < 0.5\%$), and also 946 and 1064 nm ($R < 0.1\%$). A plane-concave resonator of 25-mm length and output mirror of 50-mm radius was employed. The Ti:sapphire laser is focused on the Nd:YAG in a 160-μm diameter spot. The 946-nm laser output power *vs.* the absorbed power at 885 nm is shown in Figure 1. This dependence reflects the increase of the slope efficiency $\eta_s^{(a)}$ with increasing absorbed power, owing to the saturation of the reabsorption. The output power depends on *R*: a high reflectivity leads to a lower threshold but also to lower slope efficiency. The best results are obtained with $R = 97\%$ output mirror: the absorbed power at threshold is ~ 120 mW and $\eta_s^{(a)}$ at absorbed power about 4 times larger than the threshold reaches as much as 68%. Output power of 180 mW resulted for ~ 500 mW absorbed power at 885-nm. In our knowledge this is the largest slope efficiency obtained for CW 946-nm Nd:YAG laser emission. At $R = 93\%$ the threshold increases to ~ 260 mW, but $\eta_s^{(a)}$ at pump ~ 2 times larger than the threshold is already 63%. For $R = 98.8\%$ $\eta_s^{(a)}$ was 47%, while the absorbed power at threshold was ~ 110 mW.

The 1064-nm emission at 885-nm pumping (Figure 2) gives $\eta_s^{(a)}$ of 72% and 30 mW absorbed power at threshold for a mirror with $R = 90\%$. Slope efficiencies of 64% and 31% were obtained for $R = 95$ and 99%, respectively, with absorbed pump power at threshold of ~ 13 and ~ 5 mW.

The laser emission at 946 nm and 1064 nm under 808-nm pumping shows similar trends. The highest $\eta_s^{(a)}$at absorbed power of ~ 4 times above the threshold, namely 48%, resulted for the $R = 93\%$ mirror; the threshold was ~ 300 mW and ~ 350 mW at 946 nm were obtained for an absorbed power of ~ 1.3 W. For *R*

= 97% $\eta_s^{(a)}$ = 45% and the threshold was ~ 200 mW, while for R = 98.8% these parameters were 24% and ~ 145 mW. The 1064-nm emission had slopes of 12%, 42%, 51% for the output mirror with R = 99, 95, and 90%, respectively, while the 808-nm power absorbed at threshold was 16, 26, and ~ 45 mW. It can be observed that under 808-nm pumping the emission threshold is larger and $\eta_s^{(a)}$ is smaller than for 885-nm pumping.

Pumping resonantly into the emitting level can sensibly enhance the laser emission parameters in absorbed power. However, the weaker absorption at 885 nm as compared to 808 nm for a component of given length could reverse the situation when the laser parameters are expressed in input power. Lengthening the active component in order to increase the pump absorption will increase the reabsorption losses. A suitable solution for increasing the absorption could be a decoupling of the lengths for pump absorption from that of reabsorption, which can be achieved in a laser configuration with multi-pass of the pumping radiation inside the laser component.[7] The use of more concentrated Nd:YAG components in such a multi-pass laser configuration could also improve the absorption. Once the reabsorption becomes very low, the effect of reduction of the emission quantum efficiency by concentration quenching on threshold in these materials could be completely compensated by the increased pump absorption efficiency, similar to the 1064-nm Nd:YAG lasers. Further calculation shows that in a multi-pass laser cavity the laser parameters in input power under 885 and 808-nm pumping are similar. Such multi-pass 885-nm pumped 946-nm Nd:YAG lasers would enable an optimum use of pump power, resulting in superior laser performances and low heat generation that could enable the scaling to higher powers.

References

1) T. Y. Fan and R. L. Byer, *J. Opt. Soc. Am. A* **3**, 109 (1986).
2) G. Holleman, E. Piek and H. Walther, *Opt. Lett.* **19**, 192 (1994).
3) P. Zeller and P. Peuser, *Opt. Lett.* **25**, 34 (2000).
4) R. Lavi and S. Jackel, *Appl. Opt.* **39**, 3093 (2000).
5) V. Lupei, A. Lupei, N. Pavel, T. Taira, I. Shoji and A. Ikesue, *Appl. Phys. Lett.* **79**, 590 (2001).
6) V. Lupei, A. Lupei, S. Georgescu, T. Taira, Y. Sato and A. Ikesue, *Phys. Rev. B* **64**, 092102 (2001).
7) A. Giesen, H. Hugel, A. Voss, K. Wittig, U. Braud and H. Opower, *Appl. Phys. B* **58**, 365 (1994).

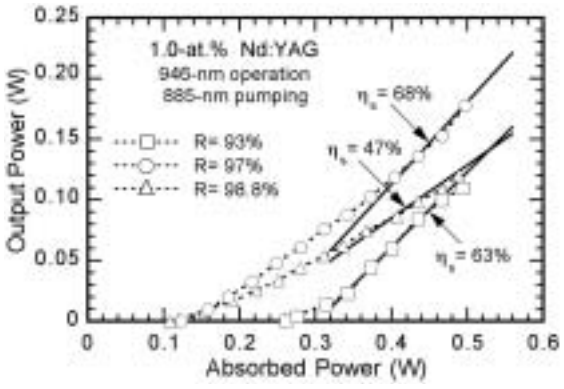

Figure 1. Output power at 946 nm function of the absorbed power under 885-nm Ti:Sapphire pumping.

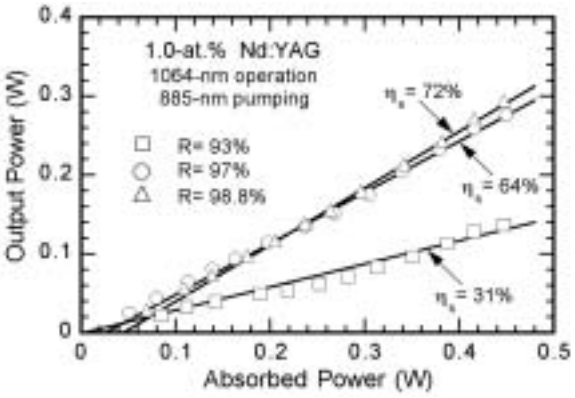

Figure 2. 1064-nm output power versus the absorbed power under 885-nm Ti:Sapphire pumping.

VIII-B-2 100-W Quasi-Continuous-Wave Diode Radially Pumped Microchip Composite Yb:YAG Laser

DASCALU, Traian[1,2,3]; TAIRA, Takunori; PAVEL, Nicolaie[2,3]

([1]CREATE-Fukui, Japan; [2]IAP-NILPRP, Romania; [3]IMS)

[*Opt. Lett.* **27**, 1791 (2002)]

The diode-pumped Yb:YAG medium has been demonstrated as a good candidate for high-power 1-μm laser systems as well as for tunable, single-axial-mode microchip configurations.[1)–3)] Besides of choice of gain medium, the configuration used for pumping, cooling and extraction plays a critical role in power scaling of a microchip laser. Recently, for scaling of a microchip Yb:YAG laser we proposed a new geometry that consists of a diode radial pumped composite Yb:YAG microchip.[4)] Theoretically was concluded that an output power of 100 W with overall optical-to-optical efficiency η_o of 39% could be obtained, employing an 13-at.% Yb-doped core of 2-mm diameter. Here we report first experimental results on this configuration: under quasi-continuous-wave (CW) pumping the best results of 112-W peak output power with η_o = 38% and slope efficiency in input power η_s of 63% were obtained.

The configuration of the diode radial pumped Yb:YAG microchip laser is shown in Figure 1. The composite crystal consists of a Yb:YAG doped core of square shape and that is diffusion bonded to an undoped YAG region. One side of the crystal was high reflectivity (HR) coated at the laser wavelength while the other surface was AR coated for this wavelength. The crystal is mounted with its HR coated side on a microchannel cooling system (water flow type, 20 °C temperature) and an indium based soldering technique was used to decrease the thermal impedance between them. The crystal was pumped by two JOLD-100-CAXF-15A diode fiber-coupled lasers (JenaOptik, Laserdiode GmbH, Germany) that delivers, each one, ~ 120 W maximum power at 940 nm ($\Delta\lambda$ ~ 4.0 nm FWHM) through a fiber of 0.6-mm core diameter and NA = 0.22. The pumping light was focused on the edge of the undoped YAG with a 1:1 achromatic optical system. Inside of the microchip it propagates by total

internal reflection through the Yb-doped core where is partially absorbed. The remained light propagates until it reaches the other edge of the undoped YAG slab: part of this light will be lost through the pumping window placed at that side, while the left light is scattered back into the microchip by a diffuse reflector.

Two crystals, one with core of 10-at.% Yb-doping level and 2 × 2-mm^2 square shape (sample #A) and the second of 1.2 × 1.2 mm^2 square 15-at.% Yb-doped core (sample #B) were used under a two diode lasers pumping, as in Figure 1. The slab shapes of 5-mm width and 0.8-mm thickness were obtained by cutting them from a 10-mm diameter rod.

The output *vs.* input power characteristics for these two crystals are presented in Figure 2, under quasi-CW pumping with rectangular pulses of 5 Hz repetition rate and 2.5% duty factor (pumping pulses of 5-ms duration). As output coupler a concave mirror of 0.1-m radius, placed 50-mm apart of the active medium, was employed. When the crystal #A is used with an output mirror of 97% reflectivity (R) a maximum output peak power of 66 W resulted at 220-W pumping power (Figure 2a); η_s was 49% (~ 58% in absorbed power). With an output mirror of R = 90% the threshold increases at ~ 33 W, however with an improved η_s of 54% (~ 64% in absorbed power). When crystal #B with R = 97% mirror was used we obtained maximum 63-W peak power with ~ 20-W absorbed at threshold and η_s far above threshold of 41% (~ 52% in absorbed power), as presented in Figure 2b. With the output mirror of R = 90% the threshold increased at ~ 33 W while η_s = 43% (~ 54% in absorbed power). The quasi-CW pumping with pulses of several milliseconds duration reduces the heat load of the crystals. The pulse duration is, however, long compared to the time necessary for the laser emission to reach the steady-state behavior. The obtained results suggest, therefore, the performances that could be obtained in CW operation if the heat is efficiently removed.

The power scalability of this microchip laser was investigated by using a third diode, placed perpendicular to the pumping directions of the first two (the inset of Figure 3). Figure 3 shows the input peak power *vs.* of pump peak power for the plane-concave resonator with R = 97% output mirror. A maximum of 112-W peak power for 298-W pump power, with η_s = 63%, was obtained for the crystal #B. For the crystal #A maximum peak power was 100 W and η_s was determined as 53%.

A future objective of this research is to demonstrate high-duty cycle or CW operation of Yb:YAG composite microchip by using this pumping scheme. As a first evaluation, the pumping repetition rate was increased, while the pumping pulse duration was kept at 5 ms. When the repetition rate increases from 10, to 30 and 60 Hz, the maximum peak output power for 298-W peak pump power decreases from 98, to 89 and 74 W, respectively, while η_s reduces from 52%, to 46% and 32% (output mirror with R = 90%). As much as 23-W average output power was obtained for 90-W average pump power (60 Hz repetition rate, 0.3 duty cycle). The temperature of the upper surface crystal was below 70 °C during all these experiments. An attempt of CW operation delivers 7.5 W for a pump power of 90 W; at this point an increase of the crystal temperature beyond 120 °C was however observed.

In conclusion a diode radial pumped composite Yb:YAG microchip laser is presented. Quasi-CW pumping of a 15-at.% Yb:YAG core (1.2 × 1.2 mm^2) with pulses of 5-Hz repetition rate and 2.5% duty cycle delivers 112-W peak power with 63% slope efficiency and 38% overall optical-to-optical efficiency. For further works, the temperature distribution into the Yb:YAG core was determined by a finite element method, while the output power was evaluated by taking into account the spatial variation of both the pump and the laser beams. The results show that efficient CW operation with 100-W power at room temperature could be obtained by using a 400-μm thick Yb:YAG chip and by improving the thermal impedance between the crystal and cooling head through an advanced soldering technique.

References

1) E. C. Honea, R. J. Beach, S. C. Mitchel, J. Skidmore, M. A. Emanuel, S. B. Sutton, S. A. Payne, P. V. Avizonis, R. S. Monroe and D. G. Harris, *Opt. Lett.* **25**, 805 (2000).
2) T. S. Rutherford, W. M. Tulloch, S. Sinha and R. L. Byer, *Opt. Lett.* **26**, 986 (2001).
3) T. Taira, J. Saikawa, T. Kobayashi and R. L. Byer, *IEEE J. Sel. Top. Quantum Electron.* **3**, 1000 (1997).
4) N. Pavel, J. Saikawa and T. Taira, *Jpn. J. Appl. Phys.* **40**, 146 (2001).

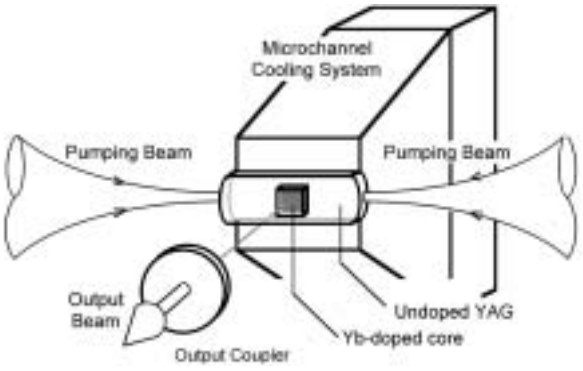

Figure 1. Schematic of the diode radial pumped composite Yb:YAG laser.

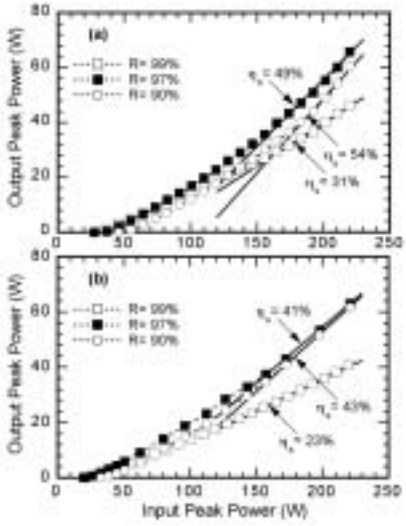

Figure 2. Output power *vs.* input power for composite Yb: YAG microchip laser with (a) crystal #A and (b) crystal #B.

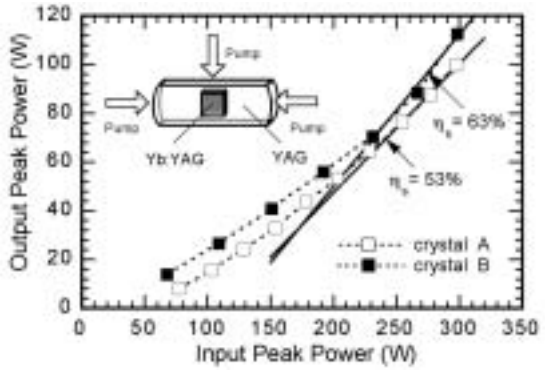

Figure 3. Performances of the microchip laser under pumping with three diodes, output coupler of 97% reflectivity.

VIII-B-3 Laser Operation with Near Quantum-Defect Slope Efficiency in Nd:YVO_4 under Direct Pumping into the Emitting Level

SATO, Yoichi; TAIRA, Takunori; PAVEL, Nicolaie[1]; LUPEI, Voicu[2]
([1]IMS and IAP-NILPRP, Romania; [2]IAP-NILPRP, Romania)

[*Appl. Phys. Lett.* **82**, 844 (2003)]

Construction of efficient solid-state lasers requires laser components able to absorb completely the pump radiation and to use it for high performance laser emission. These requirements are fulfilled by laser materials with broad and intense absorption bands that match the diode lasers emission spectrum, as well as with a high value for the product of the effective emission cross section σ_{eff} and the effective luminescence lifetime $\tau_f = \tau_{rad}\eta_{qe}$, where η_{qe} is the emission quantum efficiency. The Nd-doped crystals of the vanadate family, such as YVO_4 or $GdVO_4$, fulfill well these spectroscopic requirements.[1),2)] The Nd:YVO_4 lasers are traditionally pumped into the strongly absorbing $^4F_{5/2}$ level at 808.8 nm and this introduces a parasitic upper quantum defect (QD) between the pumping- and the emitting-laser level. The global QD in these lasers could be then reduced by elimination of this upper QD by pumping directly into the emitting level $^4F_{3/2}$. This modality of pumping was used in the first experiments to demonstrate the possibility of excitation of Nd^{3+} emission by resonant diode pumping.[3)] Recently, the pumping into the emitting level was reinvestigated for diluted Nd:YVO_4 crystals;[4)–6)] preliminary data on concentrated Nd:YVO_4 crystals were also reported.[5),6)] It was thus revealed that a suitable pump transition for Nd:YVO_4 is $^4I_{9/2}(Z_1) \rightarrow {}^4F_{3/2}(R_1)$, at 879.8 nm. The slope efficiency of the 1064-nm laser emission for both 809 and 880-nm pump was lower than the limit determined by η_{qd} for these wavelengths (0.760 and 0.827, respectively), even considering fairly large residual optical losses *L*. While for direct pumping this difference can be attributed[5),6)] to a less than unity efficiency of superposition between the pump and laser volumes η_m and to the use of uncoated crystals, in case of 809-nm pumping the possibility of a less than unity of η_p must be further checked. The aim of the present work is the improvement of laser parameters by using coated crystals and pump focusing conditions able to increase η_m. A method to determine the pump level efficiency η_p for 809-nm pumping based on pump saturation effects was developed.

The 1-μm CW laser emission of Nd:YVO_4 was investigated under end-pumping with 880-nm radiation of a Ti:Sapphire and of a diode laser. The laser crystal was a 1.0-mm thick *a*-cut plate with 1.0-at.% Nd, AR coated on both sides for 809, 880 and 1064-nm wavelengths. A plane-concave resonator of 45-mm length and 50-μm radius of the output mirror was used under Ti:Sapphire pumping. The Gaussian pump light was focused on crystal in a 50-mm diameter spot and the excitation was made with $E \| c$ crystal axis. Figure 1 shows the output power *vs.* Ti:Sapphire 880-nm input power. For a 10% transmission (T) output coupler the slope efficiency reached 80%, the threshold of emission was ~ 25-mW and for 1.0 W input power the laser emitted 0.79 W at 1064 nm. Slope efficiency of 74% and 67% resulted with T = 5 and 3%, respectively. These data give consistently round-trip residual losses L of ~ 0.9 % with η_m close of unity, and thus the difference between the obtained slope efficiency and that determined by the QD for this wavelength of pump can be fully accounted by the residual optical losses L. When the Ti:Sapphire laser wavelength was tuned to 809 nm the slope efficiency in the range of 70 to 650 mW input power was 70%, 63% and 57% for T = 10%, 5% and 3%, respectively.

Traditionally, for 809-nm pumping η_p has been considered as unity;[7)] however, other laser emission results[8)] indicate a lower value (~ 0.95) that could be, however, influenced by uncertainties in determining η_m. Here we show that η_p can be evaluated independently based on saturation effects in the pump transmission. Based on a rate equation modeling that accounts for this emission, a general equation for the dependence of the pump power on the distance *z* inside the active medium in absence of laser emission was obtained:

$$\frac{dP_{in}(z)}{dz} = -\alpha_a \frac{\pi w_p^2 \cdot I_p^{sat}}{2\beta} \times \ln\left[1 + \frac{2\beta}{\pi w_p^2 \cdot I_p^{sat}} P_{in}(z)\right] \qquad (1)$$

where $P_{in}(z)$ is the pump power, I_P^{sat} is the pump-saturation intensity, α_a is the absorption coefficient, and w_p the pump beam waist. The parameter β accounts for the mechanisms of excitation and de-excitation of the emitting level: for pumping above the emitting level (including 809-nm pumping), $\beta \equiv \eta_p$ while when pumping into the emitting level $\beta = 1 + f_2/f_0$, with f_2 and f_0 the fractional thermal population of the Stark sublevels $^4F_{3/2}(R_1)$ and $^4I_{9/2}(Z_1)$, respectively. Considering the energy level diagram of Nd:YVO_4 at the room temperature $f_0 = 0.4$, $f_2 = 0.52$ and $\beta = 2.3$.

Equation (1) integrated over the length of the crystal was used to estimate the parameter β from the fit of the measured transmission at various pump powers. In the experiments on saturation the Gaussian Ti:Sapphire radiation was focused on the 1-at.% Nd:YVO_4 crystal to a waist of 21-μm in case of 880 nm and 29-μm for 809-nm pumping. The absorption coefficients at 880 nm and

809 nm wavelengths, determined for low intensity of the Ti:Sapphire laser, were ~ 55 cm^{-1} and ~ 75 cm^{-1} respectively. In case of 809-nm pumping a good agreement was obtained for η_p = 1 (Figure 2); the inset of Figure 2 shows clearly the differences between the theoretical curves for η_p = 0.95 and 0.9 and the experimental data. At 880-nm pumping the effect of the induced emission on transmitted power at high pump intensity is evidenced by the good fit with β = 2.3.

A fiber array packed diode bars FAP-81-16C-800B laser (Coherent Co.) was next used to pump the Nd:YVO_4 crystal, in a 50-mm plane-plane resonator. A slope efficiency of 75% was obtained for T = 10% ($E||c$ pumping); the absorbed power at threshold was 0.55 W and 1.1-W output power resulted for 2.0-W absorbed power. The threshold absorbed power decreases to 0.33 and 0.16 W for T = 5 and 1%, respectively, however with a reduced slope efficiency of 69% and 28%.

In conclusion, one-micron highly efficient laser emission with 80% slope efficiency (~ 0.79 optical-to-optical efficiency) under Ti:sapphire and 75% slope efficiency relative to absorbed power under diode laser 880-nm pumping was obtained in a 1-mm thick, 1-at.% Nd:YVO_4 crystal; the first of these is close to the quantum defect limit. The pump-beam saturation effects on transmitted power under non-lasing condition indicate that η_p of the $^4F_{5/2}$ level is ~ 1.0. Directly-pumped highly Nd-doped vanadates have potential for construction of highly-efficient CW miniature lasers by using thinner active components with enhanced absorption and with extended capabilities to dissipate the heat or for scaling to higher powers; they could be also useful in the design of transversely-pumped Nd:YVO_4 lasers.

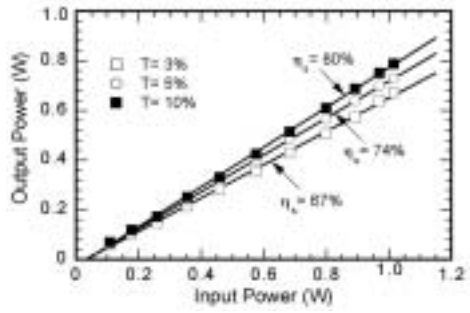

Figure 1. CW 1064-nm laser emission under 880-nm Ti:Sapphire pumping for 1-at.% Nd:YVO_4.

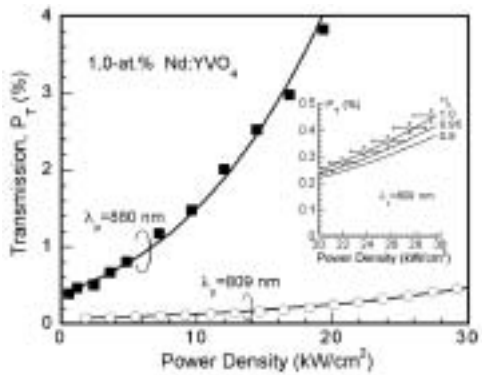

Figure 2. Transmitted power P_T *vs.* pump-beam intensity in absence of laser emission: symbols for experiments and curves from theory with β = 2.3 (880 nm) and η_p = 1 (809-nm pumping). The inset shows the fit of the 809-nm pump data with η_p = 1, 0.95, and 0.9.

References

1) R. A. Fields, M. Birnbaum and C. L. Fincher, *Appl. Phys. Lett.* **51**, 1885 (1987).
2) T. Jensen, V. G. Ostroumov, J. P. Meyn, G. Huber, A. I. Zagumennyi and I. A. Shcherbakov, *Appl. Phys. B* **58**, 373 (1994).
3) R. Newman, *J. Appl. Phys.* **34**, 437 (1963).
4) R. Lavi, S. Jackel, Y. Tzuk, M. Winik, E. Lebiush, M. Katz and I. Paiss, *Appl. Opt.* **38**, 7382 (1999).
5) V. Lupei, N. Pavel and T. Taira, *Opt. Commun.* **201**, 431 (2002).
6) V. Lupei, N. Pavel and T. Taira, *IEEE J. Quantum Electron.* **38**, 240 (2002).
7) A. W. Tucker, M. Birnbaum, C. L. Fincher and J. W. Erler, *J. Appl. Phys.* **48**, 4907 (1977).
8) R. A. Fields, T. S. Rose, M. E. Innochenzi, H. T. Yura and C. L. Fincher, *Proc. Advanced Solid State Lasers Conf.* (Optical Society of America, Washington, D.C.), 301 (1989).

VIII-B-4 High-Power Blue Generation in a Periodically Poled MgO:$LiNbO_3$ Ridge-Type Waveguide by Frequency Doubling of a Diode End-Pumped Nd:YAG Laser

PAVEL, Nicolaie[1]; SHOJI, Ichiro; TAIRA, Takunori; IWAI, Makato[2]; YOSHINO, Takeshi[2]; YAMAGUCHI, Shoichiro[2]; IMAEDA, Minoru[2]
([1]IMS and IAP-NILPRP, Romania; [2]NGK)

[*OSA, TOPS* **83**, 388 (2003)]

The $^4F_{3/2} \rightarrow {}^4I_{9/2}$ laser transition at 946 nm of Nd^{3+}:YAG opens the way for generation of continuous wave (CW) blue laser radiation that is of interest for various application, such us display technologies, obtaining of high-density optical disk systems, high-resolution printing, or biological applications. An attractive way to obtain a compact blue-light source is second-harmonic generation (SHG) by quasi-phase matching (QPM) interaction. Recently, MgO:$LiNbO_3$ (MgO:LN) was demonstrated to be a good nonlinear material for blue SHG: it presents higher resistance to photorefractive damage than LN, decreased coercive field compared with LN and a large nonlinear coefficient d_{33} ~ 25 (±2.5) pm/V.[1),2)] The key points for obtaining efficient and high-power SHG waveguide devices include strong confinement of the light wave into the waveguide, good overlap of fundamental and second-harmonic modes, prevention of nonlinear properties degradation, and maintaining of a high

optical-damage resistance, particularly in the shorter wavelength region. A CW blue power of 17.3 mW at 426 nm was demonstrated from a AlGaAs laser diode of 55-mW output power by using a MgO:LN proton-exchanged waveguide.[3] Proton-exchanged waveguides has, however some limitations, such as mode-field mismatching caused by dispersion and refractive index profiles, a trade-off between index change and non-linearity[4] and even degraded nonlinear properties.

A machining technique for processing three-dimensional waveguides[5] leads to a new waveguide technology: thus, a ridge-type waveguide QPM-SHG MgO:LN device that preserves the original performances of the nonlinear crystal was developed. CW SHG generation with 100 mW power at 412 nm using a Ti:Sapphire laser as a pumping source and with 14 mW output under diode laser pumping were demonstrated.[6] This work reports on our efforts toward scaling blue light obtained by frequency-doubling from a periodically polled MgO:LN ridge-type waveguide: using a diode end-pumped Nd:YAG laser operating at 946 nm as a fundamental source the maximum CW blue-light was 189 mW with a conversion efficiency of 49%.

A sketch of the experimental set-up is presented in Figure 1. A homemade diode-end pumped Nd:YAG laser was used in experiments. The 3-mm thick Nd:YAG crystal (1.0-at.% doping level) was AR coated for 809, 946 and 1064 nm. A 400-μm diameter, 0.22 NA fiber-coupled diode (HLU32F600, LIMO Co., Germany) was used for CW pumping. A plane-concave resonator of 30-mm length and output mirror of 100-mm radius was employed. With an output mirror of 97% reflectivity at 946 nm the laser delivered a random polarised beam of maximum 3.7 W for an absorbed power of 9.5 W in a beam characterised by a M^2 factor of 2.5. The slope efficiency was 44% with respect to the absorbed pump power. A glass plate positioned at the Brewster angle was used in order to achieve a polarised beam. For an absorbed power at 809 nm of 4.2 W the output was 1.1 W in a Gaussian beam (M^2 = 1.05). The laser spectrum, which was investigated with an Advantest Q8384 Spectrum Analyser (0.01-nm resolution), was centred at 946.2 nm and presented four longitudinal modes.

A periodically poled MgO:LN ridge-type waveguide of 8.5-mm length was used in experiments. Both the input and output surfaces were cut at 10° and AR coated at 946 nm by a SiO_2 monolayer; no coating was provided for the 473-nm wavelength. The MgO:LN ridge-type waveguide was placed on an aluminum plate whose temperature was controlled with 0.1 °C accuracy. The 946-nm radiation was varied by a rotating polarizer and focused into the waveguide with a lens of 8-mm focal length and NA = 0.55. For comparison, a Ti:Sapphire laser (Spectra Physics, Model 3900S) whose beam was characterized by M^2 ~ 1.03, was also used to pump the MgO:LN waveguide. Figure 2 presents the 473-nm blue light characteristics as a function of the 946-nm power coupled into the waveguide. The maximum blue power under Nd:YAG laser pumping was 189 mW with a conversion efficiency of 49%. If the Fresnel losses on the waveguide exit face are considered the maximum internal blue-light power is ~ 219 mW, corresponding to a conversion efficiency of ~ 57%. The measured temperature bandwidth was ΔT = 2.3 °C, in very good agreement with the predicted theoretical value of 2.35 °C. Under pumping by Ti:Sapphire laser the maximum blue power at 473-nm was 104 mW (conversion efficiency of 48%); the results were comparable with those obtained under pumping by Nd:YAG laser. The conversion efficiency saturation was attributed to the absorption of both the blue and fundamental radiations into the waveguide. Thus a slightly decrease of the phase-matching temperature with increasing of the blue output power was observed.

In conclusion, blue-light generation from a periodically polled $MgO:LiNbO_3$ ridge-type waveguide by frequency doubling of a diode end-pumped Nd:YAG laser is reported. To the authors best knowledge this is the first demonstration of such a system. The output power at 473 nm of 189 mW (internal power of 219 mW) was obtained, indicating the potential for high-power SHG of the ridge-type waveguide fabricated by ultra-precision machining.

References

1) I. Shoji, T. Kondo, A. Kitamoto, M. Shirane and R. Ito, *J. Opt. Soc. Am. B* **14**, 2268–2294 (1997).
2) A. Kuroda, S. Kurimura and Y. Uesu, *Appl. Phys. Lett.* **69**, 1565–1567 (1999).
3) T. Sugita, K. Mizuuchi, Y. Kitaoka and K. Yamamoto, *Opt. Lett.* **24**, 1590–1592 (1999).
4) K. Mizuuchi, H. Ohta, K. Yamamoto and M. Kato, *Opt. Lett.* **22**, 1217–1219 (1997).
5) T. Kawaguchi, K. Mizuuchi, T. Yoshino, J. Kondo, A. Kondo, M. Imaeda and K. Yamamoto, *Technical Digest of ISOM 2000* p. 66.
6) T. Kawaguchi, T. Yoshino, J. Kondo, A. Kondo, S. Yamaguchi, K. Noda, T. Nehagi, M. Imaeda, K. Mizuuchi, Y. Kitaoka, T. Sugita and K. Yamamoto, *Technical Digest of CLEO 2001 Conference*, 6–11 May 2001, Baltimore, USA, paper CTuI6, pp. 141–142.

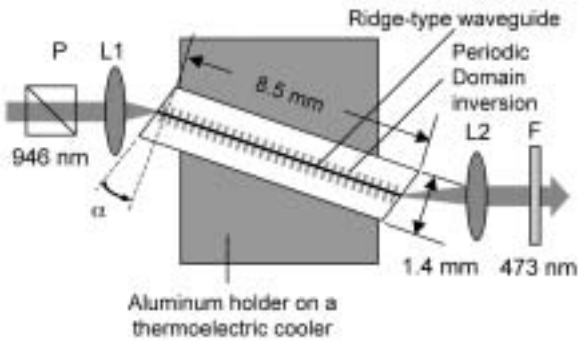

Figure 1. The experimental set-up for blue generation. P: polarizer; L1: focusing lens; L2: collimating lens; F: 946-nm cut filter.

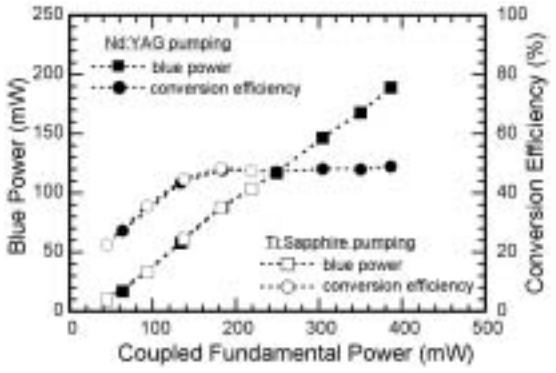

Figure 2. Blue laser characteristics vs. the 946-nm power coupled into the waveguide under pumping by Nd:YAG and Ti:Sapphire laser.

VIII-B-5 The Effect of Nd Concentration on Fundamental and Frequency-Doubled CW Laser Emission of Miniature Nd:YAG Lasers

LUPEI, Voicu[1]; PAVEL, Nicolaie[2]; TAIRA, Takunori
([1]IAP-NILPRP, Romania; [2]IMS and IAP-NILPRP, Romania)

[*CLEO/QELS 2003* paper CThM44]

This work discussed and demonstrated the benefit of using the direct pumping at 885 nm into the emitting level $^4F_{3/2}$ of concentrated Nd:YAG single crystals and ceramics for construction of efficient continuous-wave (CW) solid state lasers at the fundamental and frequency-doubled wavelength. Compared with the traditional 808-nm pumping into the strongly absorbing $^4F_{5/2}$ level, the direct pumping could improve the laser parameters (reduction of threshold and enhancement of slope efficiency) by ~ 10%, while the fraction of absorbed power transformed into heat for the 1064-nm laser emission can be diminished by ~ 30%. The reduced pump absorption of the emitting level can be compensated by using concentrated laser materials.[1)]

The laser components used in this investigation are 3-mm long Nd:YAG crystals with 1.0 or 2.4-at.% Nd and ceramics with 3.5-at.% Nd, coated as AR for 946 and 1064 nm and HT for the 808 and 885-nm wavelengths of pumping. The Gaussian radiation from a Ti:Sapphire laser was focused to a 50-μm diameter spot on the surface of the active media, for both pumping wavelengths. A plane-concave resonator of 35-mm length and output mirror of 50-mm radius was used for 1064-nm emission.

With an output mirror of 90% reflectivity the slope efficiency for the 1.0-at.% Nd sample under 885-nm pumping was 79%, close to the quantum defect limit of 83% (Figure 1). This is the largest slope efficiency reported so far for the CW Nd:YAG lasers. With increasing Nd concentration, C_{Nd} the slope efficiency diminishes slightly owing to increased residual losses: the value was 70% and 57% for the 2.4 and 3.5-at.% Nd:YAG, respectively. For the 808-nm pumping the slope efficiency for the 1.0, 2.4 and 3.5-at.% Nd:YAG components was 69%, 64%, and 52%, respectively. The best optical-to-optical efficiency in input power for 885-nm pumping is obtained with the 3.5-at.% Nd:YAG, which shows the largest absorption efficiency, while for 808-nm pumping the best results are obtained with the 2.4-at% Nd sample for which the absorption efficiency is already close to the unity. In case of 946-nm emission (output mirror of 97% reflectivity), the slope efficiency in absorbed power for the 1.0 and 2.4-at.% Nd under 885-nm pumping was 66% and 42%, respectively, while under 808-nm pumping the slope efficiency was 55% and 37%. For this wavelength of operation the increased reabsorption precludes the use of higher C_{Nd} for the single pump-pass lasers. However, as the theoretical modeling show, the direct pumping of the 946-nm emission of concentrated Nd:YAG can be much more efficient in case of multiple-pass-pumping.

The increased emission parameters at the fundamental frequency under direct pumping are expected to influence the performances of the intracavity frequency-doubling devices, such as a reduction of emission threshold and a more pronounced dependence on the absorbed pump power.[2)] This is evidenced with a end-pumped V-type frequency-doubling device for the Nd:YAG 1064-nm emission using a nonlinear LBO crystal (type I, critical phase matching, 25 °C temperature operation). A marked enhancement of the 532-nm emission in absorbed power was observed for the 1-at.% Nd:YAG crystal (Figure 2a). However, for a given input power the performances with 809-nm pumping are superior, although a strong limiting is observed for high pump powers. The green emission parameters in input power under 885-nm pumping are improved by using higher C_{Nd}, such as 2.4-at.% Nd, owing to the increased pump absorption efficiency (Figure 2b).

In conclusion, highly efficient fundamental (up to 79% slope efficiency) and frequency-doubled continuous-wave laser emission of Nd:YAG crystals and ceramics of various Nd concentration under 885-nm direct pumping with Ti:Sapphire laser is demonstrated. These results demonstrate the utility of direct pump of concentrated Nd laser materials for construction of efficient CW Nd lasers at the fundamental or doubled frequency.

References

1) V. Lupei, N. Pavel and T. Taira, *IEEE J. Quantum Electron.* **38**, 240 (2002).
2) V. Lupei, G. Aka and D. Vivien, *Appl. Phys. Lett.* **81**, 811 (2002).

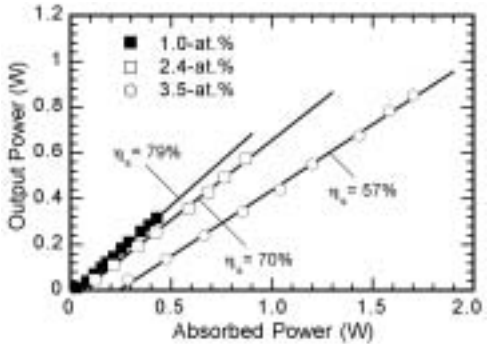

Figure 1. Output power at 1064 nm *vs.* absorbed power at 885-nm under Ti:Sapphire pumping.

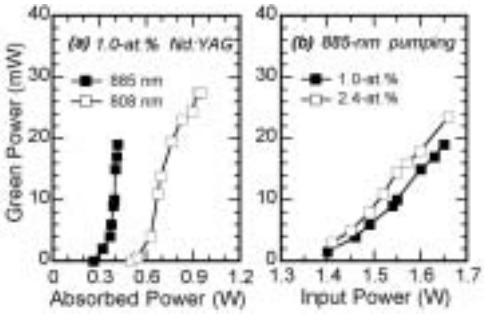

Figure 2. (a) Green power *vs.* absorbed power for the 1.0-at.% Nd:YAG crystal under 885 and 808-nm pumping, and (b) green power under 885-nm pumping for the 1.0 and 2.4-at.% Nd:YAG.

VIII-B-6 Great Reduction of Thermally-Induced-Birefringence Effect in Highly Nd^{3+}-Doped YAG Ceramics by Laser Oscillation

SHOJI, Ichiro; TAIRA, Takunori; IKESUE, Akio[1]; YOSHIDA, Kunio[2]
([1]JFCC; [2]Osaka Inst. Tech.)

[*CLEO/Europe* CA8-4-FRI (2003)]

Nd:YAG ceramics are promising materials for high-power and high-efficient microchip lasers because highly transparent and highly Nd^{3+}-doped ceramics are available with superior thermomechanical properties.[1)] We have investigated thermally-induced-birefringence effect in Nd:YAG ceramics and found that the depolarization loss of highly Nd^{3+}-doped ceramics is much larger than that of low-concentrated Nd:YAG single crystals even at the same absorbed pump power under non-lasing condition.[2)] This is mainly due to larger thermal loading, η_h, for higher Nd^{3+} concentration; η_h depends on the radiative quantum efficiency, η_r, which becomes smaller for higher Nd^{3+} concentration because of significant interaction between Nd^{3+} ions. Under lasing, however, η_h does not depend on η_r and then becomes a constant small value in an ideal case, reducing the depolarization to much smaller values than those under non-lasing. We experimentally investigated the reduction of depolarization under lasing condition.

The measurement was performed with the pump-probe measurement.[2)] A Ti:sapphire laser oscillating at 808nm was used as the pump source and a linearly polarized He-Ne laser was used as the probe. We used a 3.5at.% Nd:YAG ceramic, the thickness of which was 1.9mm, and also used a (111)-cut 3.0mm-thick 1.0at.% Nd:YAG single crystal as comparison. The laser output power as a function of the absorbed pump power for both the samples are shown in Figure 1. Lower output for the ceramic is supposed to be due to lower mode matching caused by more significant thermal-lens effect. Figure 2 shows the dependence of the depolarization on the absorbed pump power under non-lasing and lasing conditions. When lasing occurs, the depolarization of the 3.5at.% Nd:YAG ceramic reduced to 1/3 of that under non-lasing condition, which is nearly the same with that of the non-lasing single crystal. We also found that η_h is not constant even under lasing in a practical case, and the depolarization at each absorbed pump power can be estimated from the characteristics of the laser oscillation, as shown by the dotted curves in Figure 2.

In conclusion, we have experimentally verified that the depolarization of highly Nd^{3+}-doped YAG ceramics is greatly reduced by laser oscillation.

References

1) T. Taira, A. Ikesue and K. Yoshida, *OSA Trends in Optics and Photonics* **19**, 430 (1998).
2) I. Shoji, Y. Sato, S. Kurimura, V. Lupei, T. Taira, A. Ikesue and K. Yoshida, *Opt. Lett.* **27**, 234 (2002).

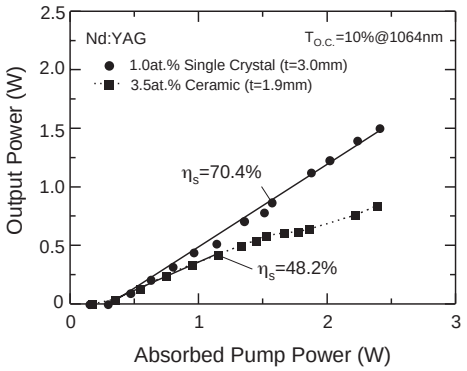

Figure 1. Laser output power as a function of the absorbed pump power for the ceramic and single-crystal.

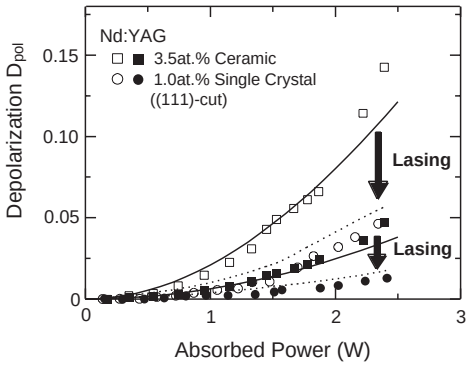

Figure 2. Dependence of the depolarization on the absorbed pump power under non-lasing and lasing conditions. The solid and dotted curves are the calculated depolarization under non-lasing and lasing conditions, respectively.

VIII-B-7 Periodical Poling Characteristics of Congruent MgO:$LiNbO_3$ Crystals at Elevated Temperature

ISHIZUKI, Hideki; SHOJI, Ichiro; TAIRA, Takunori

[*Appl. Phys. Lett.* **82**, 4062–4064 (2003)]

Quasi-phase matching (QPM) is an attractive technique for efficient nonlinear wavelength conversion, and various types of QPM devices have been demonstrated. A 5 mol% MgO-doped $LiNbO_3$ (MgO:LN) crystal has attracted much attention for the material of the QPM devices because of its higher resistance to photorefractive damage than that of non-doped LN. It has also a large nonlinear coefficient and a lower

coercive field to invert the sign of the nonlinear coefficient of the than that of non-doped LN. These features mean that MgO:LN is a suitable material for QPM devices with large cross-sections for high-power and/or short-pulse operation. However, few reports have been made on realizing bulk QPM devices by use of MgO:LN, and the maximum thickness was limited to 1mm. Here, we report the periodic poling characteristics of MgO:LN crystal at elevated temperature and demonstrate successful periodical poling of 3mm-thick MgO:LN crystals with 30 μm period.

The coercive field of MgO:LN was measured in an insulation-oil bath. An aluminum electrode of 0.2 μm thickness was prepared on the crystal surface by vacuum evaporation and photolithography. The measured coercive-field dependence on crystal temperature is shown in Figure 1. The open triangles are the estimated coercive field was measured by multipulse application totally longer than 100seconds, and the filled circles are the values obtained by applying only one high-field pulse of 1-second duration. The measured values by using 1-second pulse may have a little higher value than that by multipulse application because of the slow response time of the crystal. The coercive field decreased drastically with increasing temperature. The coercive fields at T = 250 °C were measured to be 1.2 kV/mm, which is about 1/4 compared with that for MgO:LN at room temperature(RT) and about 1/17 of that for non-doped LN at RT.

We tried to fabricate periodically poled structures of 30 μm grating period in 3-mm-thick MgO:LN at elevated temperature. At T = 170 °C, we achieved periodically poled structures with smooth surface by applying ~ 5 kV (~ 1.7 kV/mm) pulses as shown in Figure 2. Figure 2(a) shows the photograph of the *y*-face cross-section of obtained periodic structures after HF etching, and Fig. 2(b), 2(c) and 2(d) present the +*z* surface, *y*-face (expansion) and –*z* surface photographs, respectively. Periodic patterning with high aspect ratio (periodic-pattern width : crystal thickness) of 1:200 was realized.

In conclusion, we investigated the coercive field dependence on the crystal temperature for 5 mol% MgO:LN. The coercive field at 250 °C was found to reduce to about 1.2 kV/mm, which is about 1/4 of that at room temperature. We successfully fabricated periodic structures of 30 μm period with smooth surfaces in 3-mm-thick MgO:LN. The drastically reduced coercive field of MgO:LN crystals may enable us to realize much thicker QPM device than ever reported. This kind of thick QPM devices can be used as intracavity elements, and for high-power wavelength conversion, short-pulse amplification, and pulse compression.

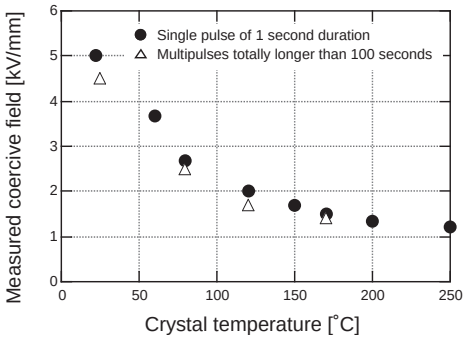

Figure 1.

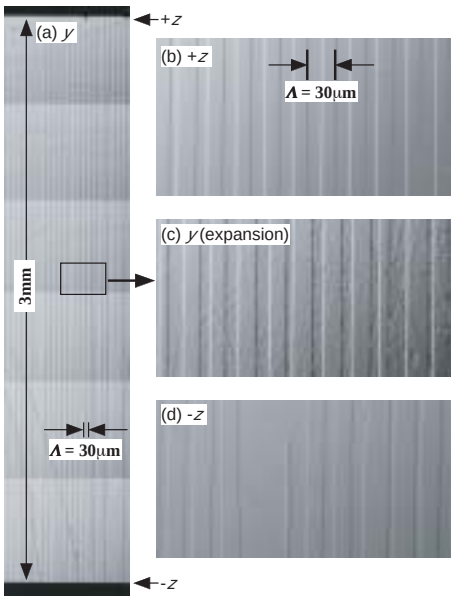

Figure 2.

VIII-B-8 Energy Transfer Processes of Nd^{3+} in Y_2O_3 Ceramic

LUPEI, Aurelia[1]; LUPEI, Voicu[1]; TAIRA, Takunori; SATO, Yoichi; IKESUE, Akio[2]; GHEORGHE, Cristian[1]
([1]Inst. Atomic Phys.; [2]JFCC)

[*J. Lumin.* **102-103**, 72–76 (2003)]

The paper presents spectroscopic and energy transfer results from the investigation of Nd^{3+}:Y_2O_3 transparent ceramics, as a new variant of a laser material. The positions of main Nd^{3+} lines (N) in ceramic Nd^{3+}:Y_2O_3, at low concentrations, are identical to those reported for single crystals. The absence of any other spectral satellites than those corresponding to Nd^{3+} pairs (M) as well as the relative intensity of M lines, show that no structural defects are present in the crystalline lattice of ceramic grains and that the distribution of Nd^{3+} ions at the available lattice sites is random. Thus, from spectroscopic and microstructural point of view, the ceramic Nd^{3+}:Y_2O_3 materials are similar to single crystals. At least two satellite lines were observed in high resolution absorption spectra and assigned to pairs of identical Nd^{3+} centers at nearest distances, C_2–C_2 pairs (8 sites at distances smaller than 4 Å) and dissimilar Nd^{3+} centers ,

C_2–C_{3i} pairs (4 sites at distances smaller than 4 Å).

The global emission decays of $^4F_{3/2}$ Nd^{3+} level at 300 K show strong concentration dependence. The decays for concentrations up to ~ 3 at% present a complex non-exponential behavior, that is interpreted in terms of a cross-relaxation process involving at least two types of interactions: a short range—probably superexchange—connected with interaction within near neighbor pairs and dipole–dipole and a migration term. Though the system contains two types of Nd^{3+} sites, no energy transfer or cross-relaxation to C_{3i} sites is considered for low concentrations since no magnetic dipole allowed transitions are involved in these processes. The efficient energy transfer for low concentrations (dipole-dipole microparameter $C_{DA} \sim 3.7 \times 10^{-39}$ cm^6 s^{-1} is ~ 20 times larger than that for Nd^{3+} in YAG[1]) and the additional transfer mechanisms at higher concentrations determines a strong drop of emission quantum efficiency with concentration and restricts the range of Nd^{3+} concentration in Y_2O_3 useful for laser emission to the range of ~ 1 at%.

Reference

1) V. Lupei, A. Lupei, S. Georgescu, T. Taira, Y. Sato and A. Ikesue, *Phys. Rev. B* **61**, 092102 (2001).

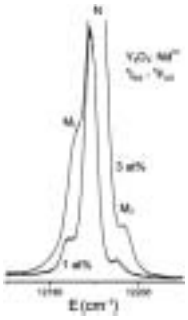

Figure 1. The absorption spectra corresponding to $^4I_{9/2} \rightarrow {}^4F_{5/2}$ (1) transition of Nd^{3+} in Y_2O_3 ceramic for 1 and 3 at%.

VIII-B-9 Second-Harmonic Nonlinear Mirror CW Mode Locking in Yb:YAG Microchip Lasers

SAIKAWA, Jiro; TAIRA, Takunori

[*Jpn. J. Appl. Phys.* **42**, L649 (2003)]

In recent years there has been great interest in sub-picosecond diode-pumped solid-state lasers with multi-watt average powers. Yb:YAG is the candidate for high power sub-picosecond lasers because it has wide emission bandwidth and large thermal conductivity. For high power sub-picosecond mode locked lasers, our approach is the second harmonic nonlinear mirror mode locking (NLM) technique. This technique is based on the second harmonic generation (SHG); thus it has no absorption losses and does not require interferometric cavity length control. In this paper we report the demonstration of a cw-pumped Yb:YAG laser that is passive mode-locked by the nonlinear mirror technique; the possibility to obtain high power sub-picosecond Yb:YAG lasers under diode laser pumping is discussed.

The experimental setup of NLM mode locked Yb:YAG laser is shown in Figure 1. A 15-at.% Yb:YAG chip (1 mm thickness) was used; the Yb:YAG crystal was sandwiched between two undoped YAG plates and is contact with a copper heatsink (~ 20 °C). The cavity length is ~ 2 m and excepting the output coupler M6, the other cavity mirrors were coated as high reflectivity around 1030 nm; moreover, the mirrors M5 and M6 were high reflectivity coated at the SH wavelength. Two LBO crystals (10 mm and 5-mm length) that were cut for type-I temperature tuned non-critical phase matching and antireflection coated for both the fundamental and SH wavelength were used. The LBO crystal was inserted into an oven whose temperature was controlled with 0.1 °C accuracy. The nonlinear mirror was composed of the LBO crystal and the output coupler M6.

In the mode locking operation (under phase-matching), the laser jumped from cw operation to self-start cw mode locking operation. The pulse duration was measured to 9 ps (5mm-LBO). This limitation of pulse width was due to bandwidth of nonlinear mirror. The pulse repetition rate was 82 MHz, and a maximum average power of 900 mW and an optical conversion efficiency of 54% were obtained.

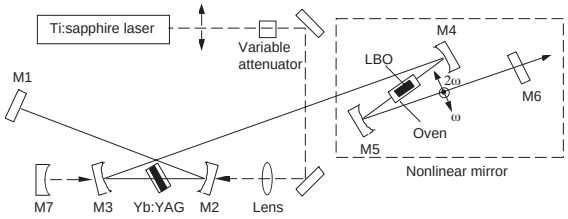

Figure 1. The cavity set up of NLM mode-locked Yb:YAG laser.

Research Center for Molecular-Scale Nanoscience

VIII-C Synthetic Approach Toward Molecular Scale Electronics

Electric properties of organic and in-organic nano structures are challenging field in material science. Those of aggregates, crystals, or polymers which are made from a large number of molecules or atoms have been well studied and established. In contrast, nano scale electronics is the forefront of science, and has been revealed gradually to have diverse phenomena such as quantum conductance, the Kondo effect, the Coulomb blockade, resonance tunneling and so on. In order to establish this field, we are synthesizing new organic and in-organic nano strucutures by using usual synthetic methods together with non-conventional lithographic technique, and measure their electric properties mainly.

VIII-C-1 Linear Functionalized Terthiophene Phenanthroline Polymer for Nanodevices

OGAWA, Takuji[1]; ENDO, Hiroaki[2]; ARAKI, Koiti[1]
([1]IMS, JST; [2]IMS and Ehime Univ.)

The development of molecular electronic devices requires the preparation of new funcional materials with suitable properties. Among them one have pursued the preparation of linear chain polymers constituted by porphyrins or ruthenium complexes that could be obtained in a controlled way. The redox and photophysical properties of those compounds are well known, such that one were atracted by the possibility of generating nanodevices by connecting a bunch or even a single strand of those polymers to a couple of nanogap electrodes. In this communication we report the synthesis and characterization of the monomer as well as the properties of the a new linear hexathiophene-phenanthroline based charge transfer polymer functionalized with $[Ru(bipy)_2(phen)]$ complexes, obtained by electropolymerization. The 1,10-phenanthroline with thiophene (tphen) and tertiophene (ttphen) radicals at the 3,8-positions were obtained by conventional Ni catalyzed coupling reactions and the complexes by reaction with $[Ru(bipy)_2(OH_2)]$ in DMF. Both complexes exhibited four reversible waves in the –1 to –2 V range assigned to the reduction of each of the bipy, phen and thiophene groups to the corresponding radical anion. In the anodic side a quite different behavior was observed. While the ttphen derivative exhibited a catalytic oxidation of ttphen ligand around 1.3 V responsible for the electropolymerization, a reversible Ru(III/II) wave was observed for the tphen derivative. One found out that the polymeric complex can be easily grown in between the nanogap electrodes. The conduction and photoconduction properties are being investigated.

VIII-C-2 Synthesis of Self-Standing Molecular Jacks Bearing Long Anchoring Arms

OGAWA, Takuji[1]; MIZUGUTI, Eisuke[2]
([1]IMS, JST; [2]IMS and Ehime Univ.)

A series of porphyrin derivatives bearing more than four lipoic acyl groups have been synthesized. The lipoic acyl group has disulfide moiety at the end of the acyl chain, and can be adsorbed to the gold surface. When rhodium metal is introduced in the center of the porphyrin, a variety of organic functional groups can be introduced as the axial group of the porphyrin plain. Thus, when the po rphyrin plain is anchored to the gold surface by the lipoic acyl groups, the axial organic functional groups will stand perpendicularly to the gold surface. We call the porphyirn part of the molecule as a "molecular jack," because a variety of molecular wires can be connected to the electrode metal surface through the molecule.

One merit of the molecular jack is that the occuping area of the molecule on the electrode surface can be controlled by changing the length of the alkyl group connecting to the lipoic acyl group. We have synthesized a tetraarylporphyrin derivative whose aryl groups are subsitituted with $(\text{-O-}(CH_2)_{11}\text{-OCO-}(CH_2)_4\text{-}C_3H_5(S\text{–}S))$ at their 3,5-positions. The distance between one S–S group to that of the oposite side is about 6 nm. Consequently the molecule will occupy circular area of about 6 nm diameter on the adsorbed metal surface. Thus when the molecules are adsorbed to the metal electrodes with the size of 60 nm × 60 nm, only 100 molecules will be present on it at the most. By reducing the number of molecules present on the electrodes, it will become much easier to discuss about the electronic properties of the individual molecules.

VIII-C-3 Synthesis and Self-Assembly of Novel Porphyrin Molecular Wires

OGAWA, Takuji[1]; KAWAO, Masahiro[2]
([1]IMS, JST; [2]IMS and Ehime Univ.)

Long π-conjugated molecular-wires have been focused much attentions because they can be used for organic conducting material, nonlinear optical material and molecular wire. The recently reported meso-meso-linked porphyrin wires were soluble in organic solvent in spite of their high molecular weight. The high solubility can be explained by the vertically crossed porphyrin π-plains to each other: because of the sterical requirement, intermolecular ππ-stacking was prevented. However at the same time because of the configuration, π-electronic conjugation was not effective, and the absorption band do not shift to the longer wavelength

even for the long oligomers. Because tunnel resistance is generally less when the molecule has lower HOMO-LUMO gap, we need molecules of lower HOMO-LUMO gap for good molecular conductor.

We prepared sub-micrometer long oligo-diethynylporphyrins by usual copper catalyzed oxidative coupling of diethynylporphyrins. The products were purified by repeating gel permeation chromatography (GPC) and analyzed by analytical GPC, absorption spectroscopy, matrix assisted laser dissorption time of flight mass spectroscopy (MALDI-TOFMS), and atomic force microscopy (AFM). Although with the MALDI-TOFMS no molecular peaks greater than ca. 100,000 could be detected, GPC and AFM data clearly indicated the presence of sub-micrometer long molecules.

These sub-micrometer π-conjugated molecules self-assembled on HOPG to make some kinds of ordered super structures as observed by AFM. When the length of the molecule is less than 100 nm and the concentration of the solution is relatively high, a regular network structure was formed in which the distance between each molecules is *ca.* 16 nm and the hight is *ca.* 0.9 nm in average. In longer molecules with less concentrated solution, a rectangular sheet structure was observed with the distance of 4 nm and the hight of 0.3 nm. Judging from the size, we postulate that in the regular network sturucture two or three molecular wires are stranded to make thicker molecular rope.

VIII-C-4 Synthesis and Characterization of Dendrimer Protected Sub-Micrometer Long Conjugated Porphyrin Wires

OGAWA, Takuji[1]; OZAWA, Hiroaki[2]
([1]IMS, JST; [2]IMS and Ehime Univ.)

Direct measurements of electronic properties of single molecule are still a challenging target of materials science, and have been reported in several papers by using scanning probe microscopic methods (SPM), or break junction methods. However, no one has ever succeeded in the electronic measurement with observing the molecules between the electrodes. One reason is that the roughness of electrodes surface, which was fabricated by usual electron beam lithographic methods, is larger than the diameter of the molecular wires, and it is difficult to observe the molecules clearly by SPM. In order to overcome the problem, we synthesized long (> 100 nm) and thick (3–5 nm) porphyrin wires surrounded by dendrimer moiety. Surrounding the wire with the dendrimer has several merits: (1) The diameter become enough large to observe them with AFM on the gapped electrodes, (2) solubility is increased, and (3) the wire may become rigid because of the steric hindrance between the adjacent moiety. Synthesized porphyrin wires were analyzed with gel permeation chromatography (GPC) and atomic force microscopy (AFM). The GPC analyses showed that the molecules have molecular weight greater than one million, which correspond to *ca.* 500 mer. The AFM images showed that the wires have the hight of *ca.* 5 nm, and in some molecules the lengths were nearly 1 μm.

VIII-D Development of Organic Semiconductors for Molecular Thin-Film Devices

Organic light-emitting diodes (OLEDs) and organic field-effect transistors (OFETs) based on π-conjugated oligomers have been extensively studied as molecular thin-film devices. Organic semiconductors with low injection barriers and high mobilities are required for highly efficient OLEDs and OFETs. Radical cations or anions of an organic semiconductor have to be generated easily at the interface with an electrode (or a dielectric), and holes or electrons must move fast in the semiconducting layer. Compared with organic *p*-type semiconductors, organic *n*-type semiconductors for practical use are few and rather difficult to develop. Recently, we found that perfluorinated oligomers are efficient electron-transport materials for OLEDs.

VIII-D-1 Oligo(2,6-Anthrylene)s: Acene-Oligomer Approach for Organic Field-Effect Transistors

ITO, Kaname; SUZUKI, Toshiyasu; SAKAMOTO, Youichi; KUBOTA, Daisuke[1]; INOUE, Youji[1]; SATO, Fumio[1]; TOKITO, Shizuo[1]
([1]NHK Sci. Technical Res. Labs.)

[*Angew. Chem., Int. Ed.* **42**, 1159–1162 (2003)]

Oligo(2,6-anthrylene)s (**2A** and **3A**) and their dihexyl derivatives (**DH-2A** and **DH-3A**) have been synthesized by the Suzuki coupling using palladium catalysts. Organic field-effect transistors (OFETs) of these anthracene oligomers were fabricated on SiO_2/Si substrates by high-vacuum evaporation. OFETs with **2A** exhibited FET activity, and the hole mobilities ranged from 0.0031 to 0.013 $cm^2V^{-1}s^{-1}$. The oligomer **3A** showed even higher mobilities (0.064–0.072 $cm^2V^{-1}s^{-1}$). Field-effect mobilities of **DH-2A** were greater than 0.1 $cm^2V^{-1}s^{-1}$. The highest mobilities (0.18 $cm^2V^{-1}s^{-1}$) were observed in **DH-3A** OFETs. X-ray diffraction studies on the films indicated a high degree of lamellar ordering and crystallinity.

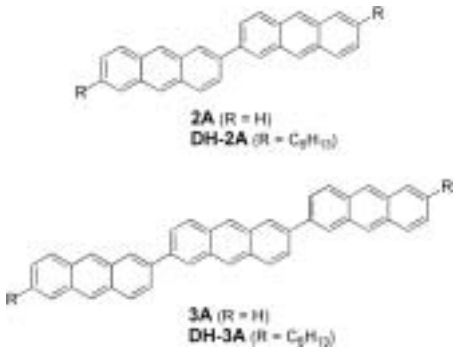

Figure 1. Structures of anthracene oligomers.

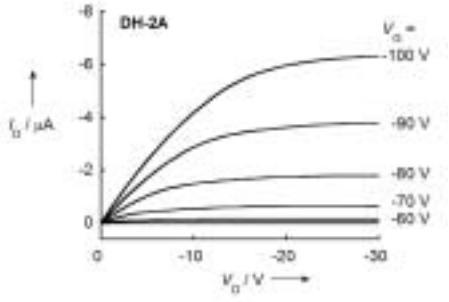

Figure 2. Drain current (I_D) *vs* drain voltage (V_D) as a function of gate voltage (V_G) for an OFET with **DH-2A** (T_{sub} = 70 °C). Channel length L = 100 μm and channel width W = 1 mm (W/L = 10).

VIII-D-2 Color Tunable Organic Light-Emitting Diodes Using Pentafluorophenyl-Substituted Iridium Complexes

TSUZUKI, Toshimitsu[1]; SHIRASAWA, Nobuhiko; SUZUKI, Toshiyasu; TOKITO, Shizuo[1]
([1]NHK Sci. Technical Res. Labs.)

[*Adv. Mater.* **15**, 1455–1458 (2003)]

Novel iridium complexes with perfluorophenyl-substituted phenylpyridine ligands have been developed. The figure shows the photoluminescence (PL) spectra of four complexes in the doped films. By changing the position of substitution, the peaks in the PL spectra are tuned in the wavelength region 513–578 nm. Light-emitting diodes using these complexes as the emitting material show an external quantum efficiency of 10–17%.

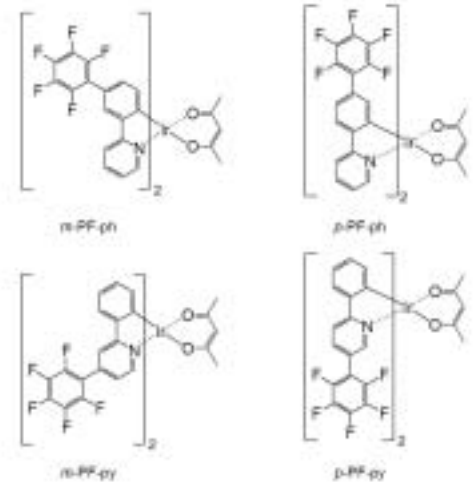

Figure 1. Structures of iridium complexes.

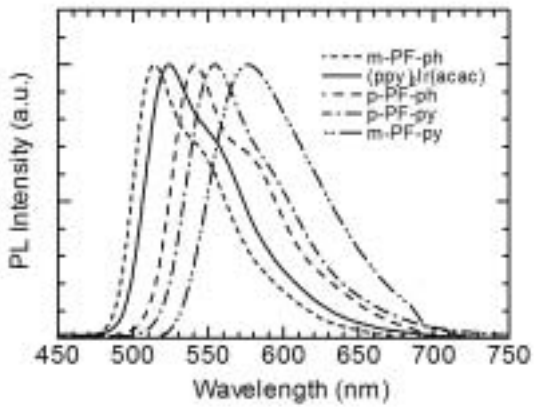

Figure 2. PL Spectra for films of the complexes (6%) doped in CPB.

VIII-E Field-Effect Transistors with Organic Semiconductors

Considerable attention has recently focused on organic field-effect transistors (OFET) because of their potential use in low-cost flexible electronic devices. In order to improve output characteristics, carrier transport in organic semiconductors is the most important subject to be elucidated.

VIII-E-1 Carrier Transport in Field-Effect Transistors Based on Single-Crystalline Wires of Bis-(1, 2, 5-thiadiazolo)-*p*-Quinobis(1, 3-dithiole) (BTQBT)

FUJIWARA, Eiichi; TAKADA, Masaki[1]; YAMASHITA, Yoshiro[2]; TADA, Hirokazu
([1]GUAS; [2]Tokyo Inst. Tech.)

We prepared single-crystalline wires of bis(1, 2, 5-thiadiazolo)-*p*-quinobis(1, 3-dithiole), whose ends were anchored to the drain and source electrodes of bottom-contact-type field-effect transistors. Figures 1 shows the SEM image of BTQBT wires grown on the substrates at 360 K. Molecular crystalline wires bridge the gaps between electrodes. It is noted that wires are anchored selectively to the electrodes and no aggregates exist on SiO_2 surface under appropriate growth conditions. Figure 2 shows the temperature dependence of the field-effect mobilities of the devices composed of nanowires and small grains in the temperature range from 5 K to 300 K. The tunnel transport and thermally activated hopping were found to be dominant at $T < 30$ K and 30 K $< T <$ 150 K, respectively, in both devices. While hopping behavior was still dominant in the device of small grains at $T >$ 150K, the mobility of wires varied as $T^{-1.3}$, indicating that phonon scattering governed carrier transport in single-crystalline wires.

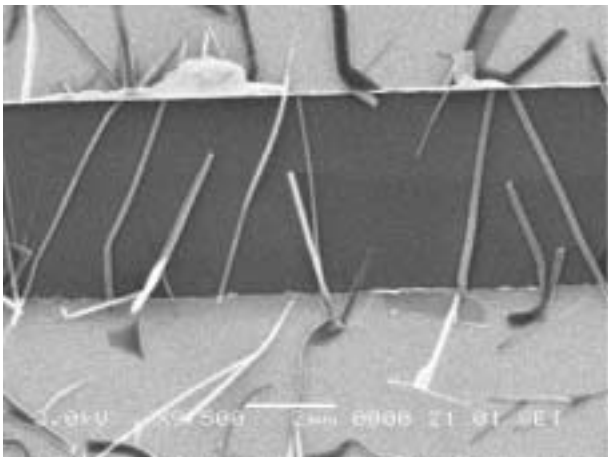

Figure 1. SEM image of BTQBT wires on FET electrodes with spacing of 5 μm.

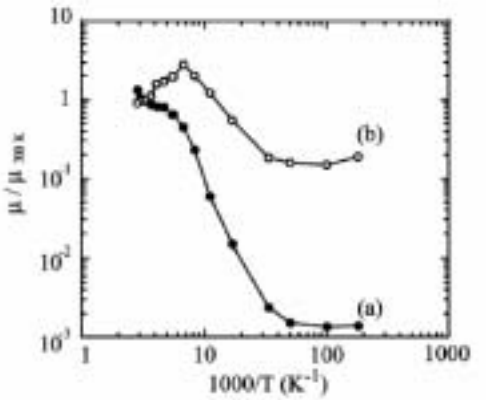

Figure 2. Temperature dependence of field-effect mobilities of small grains (a) and wires (b).

VIII-E-2 Field-Effect Transistors of $F_{16}CuPc$ with Bottom- and Top-Contact Electrodes

MINARI, Takeo[1]; FUJIWARA, Eiichi; TAKADA, Masaki[2]; TADA, Hirokazu; NEMOTO, Takeshi[1]; ISODA, Seiji[1]
([1]Kyoto Univ.; [2]GUAS)

Output characteristics of organic field-effect transistors depend strongly upon device structures. We have prepared bottom- and top-contact FET devices based on hexadecafluoro-copperphthalocyanine ($F_{16}CuPc$) films and studied electrical properties. It was found that electron mobilities of the top contact FETs were higher than those of the bottom contact FETs probably due to the difference in electric field distribution. Electron mobility of top contact FETs increased with increasing grain size of $CuPcF_{16}$ films, but large grains cause lower mobility owing to poor contact at the interface between the electrodes and the organic film in the bottom contact FETs. The FET with thick $CuPcF_{16}$ films resulted in the higher mobility in the bottom contact FETs because of less influence of air. In top contact FET, however, the thicker film gave rise to the less drain current because of the increase of resistance between source electrode and accumulation layer.

VIII-F Molecular Assemblies on Silicon Surfaces *via* Silicon-Carbon Covalent Bonds

Preparation of molecular assemblies on inorganic semiconductors such as silicon and germanium has received a growing interest because of their potential application to stable regist for nano-patterning. We have prepared organic monolayers on silicon by wet process and studied film structures with IR and AFM.

VIII-F-1 Molecular Conformation of *n*-Alkyl Monolayers Covalently Bonded to Si(111) Probed by Infrared-Visible Sum-Frequency Spectroscopy

ISHIBASHI, Taka-aki[1]; ARA, Masato[2]; TADA, Hirokazu; ONISHI, Hiroshi[1]
([1]KAST; [2]GUAS)

[*Chem. Phys. Lett.* **367**, 376–381 (2003)]

Infrared-visible sum-frequency spectra of *n*-alkyl (C_nH_{2n+1}; n = 10–13, 18) monolayers anchored on the Si(111) surface through a Si–C covalent bond were measured for the C–H stretch region. Spectral shapes exhibited azimuthorientation dependence compatible with the C_{3v} symmetry of the substrate as shown in Figure 1, indicating that the monolayers were epitaxially constructed on the substrate. Three methyl bands dominated each spectrum, and two-weak methylene bands were identified. Two distinct intensity patterns of the methyl bands were observed depending on n as shown in Figure 2. The observed spectra were interpreted with reference to reported molecular models of the monolayer that consist of alkyl chains with an all-trans head part and a twisted stem.

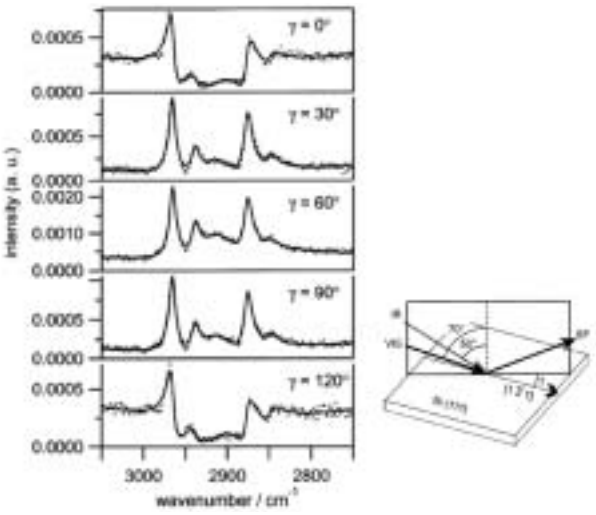

Figure 1. Azimuth dependence of SF spectra of tridecyl ($C_{13}H_{27}$) monolayer on Si(111). The spectra were measured at room temperature.

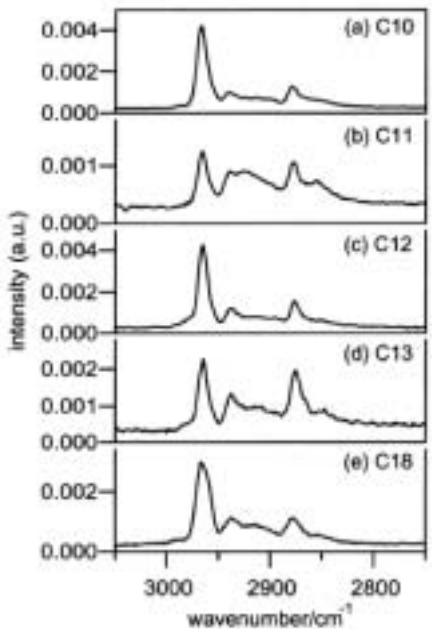

Figure 2. SF spectra of *n*-alkyl (C_nH_{2n+1}; n = 10–13, 18) monolayers on Si(111) measured at the azimuth $\gamma = 60°$.

VIII-F-2 Study on Phase Transition of Alkyl-Monolayers Anchored Covalently to Silicon by Temperature Dependent ATR-FT-IR

YAMADA, Ryo; ARA, Masato[1]; TADA, Hirokazu
([1]GUAS)

The phase behavior of alkyl-monolayers formed on Si(111) surface was investigated by an attenuated total reflection Fourier transform infra-red spectroscopy from room temperature to 590 K (Figure 1). A continuous disordering process of the monolayer was indicated from the gradual peak shifts toward higher frequency in C–H stretching modes with small decrease in the peak intensities as temperature was increased to 440 K. The rapid decrease in peak intensity was observed above 440 K. The observed changes in the spectrum were reversible by 440 K while the peak intensity was decreased and peak position became higher when the substrate was cooled to room temperature after heated above 440 K, indicating the destruction of the monolayer above 440 K. The temperature limit for the reversible phase transition was much higher than that for alkanethiol monolayer on Au(111) surface (*ca.* 350K), showing that the monolayer formed by Si–C covalent bond was more stable than that of alkanethiols on Au(111) surface due to the stronger anchoring of the molecules to the substrate.

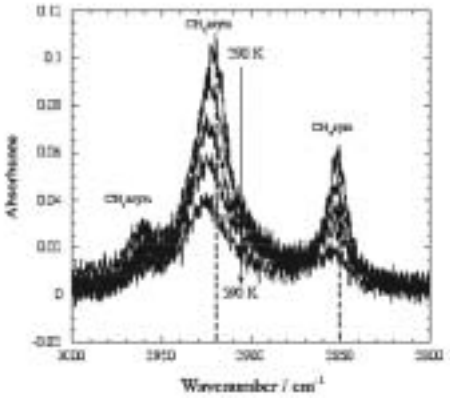

Figure 1. Temperature dependent ATR-FT-IR spectra in the C–H stretching region of octadecene-monolayer on Si(111) surface.

VIII-F-3 Friction Force Microscopy Using Silicon Cantilevers Covered with Organic Monolayers *via* Silicon-Carbon Covalent Bonds

ARA, Masato[1]; TADA, Hirokazu
([1]GUAS)

[*Appl. Phys. Lett*. **83**, 578–580 (2003)]

Cantilevers covered with hydrocarbon (CH) and fluorocarbon (CF) monolayers *via* Si–C covalent bonds were prepared and used for adhesion force measurements and friction force microscopy of the surface patterned also with CH and CF areas. The adhesion and friction forces on CF areas were larger than those on CH areas, especially using CF cantilevers as shown in Figure 1. Large polarizabilities of CF molecules compared to CH molecules are found to enhance the contrast in adhesion and friction images. The cantilevers covered with organic monolayers *via* covalent bonds are useful for chemical force microscopy with contact and noncontact mode atomic force microscopy in various atmospheres since the interface between molecules and cantilevers is thermally and chemically stable.

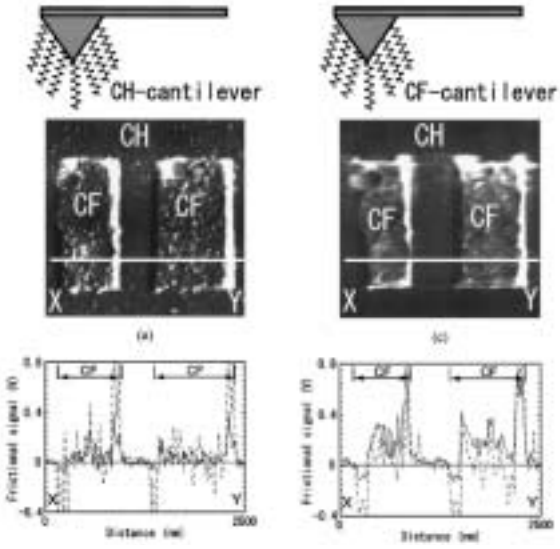

Figure 1. FFM images (a) and (c) (2.5 mm × 2.5 mm) and the friction profiles (b) and (d) of the patterned surface on Si(111) with a CH (a, b) and a CF cantilever (c, d). Spring constants of both cantilevers were 0.6 N/m. Typical loads applied were 30 nN. Solid curves and dashed curves were the profiles measured in air and *in vacuo*, respectively.

VIII-G Development of Precisely-Defined Macromolecules and Their Organization on Substrate Surfaces for Planar Molecular-Scale Electronics Circuits

The concept of molecular-scale electronics is now realized for individual components such as wire, diode, switch, and memory cell, but the fabrication of complete molecular-scale circuits remains challenging because of the difficulty of connecting molecular modules to one another. Molecular monolithic technology, which integrates the wiring, transistors and the required passive elements on a single macromolecule, has been proposed as a promising solution to this problem. In this project we have been trying to establish both the architecture of this novel class of macromolecules and the protocols for their purposive organization on metal/semiconductor substrate surfaces.

VIII-G-1 Characterization of Electronic Properties of Molecular Enamel Wires

TANAKA, Shoji

The precisely-defined "insulated molecular wire," in which rigid insulators are placed around a π-conjugated backbone except the "electrical connections," is one of the key modules for realizing ultra-dense molecular-scale electronic circuits. The well known approach to this special class of molecular wire is based on the supramolecular complex between π-conjugated oligomers and cyclodextrin molecules. As an alternative approach, we have proposed "molecular enamel wire" concept, in which the insulator mantle is covalently bonded to the backbone. The stability of insulator-attachment of molecular enamel wire will be superior to that of supramolecular wire due to the intrinsic toughness of a covalent bond. So far, we have established the synthetic approaches to molecular enamel wires based on building blocks **1** (Figure 1). Here we report the effects of the insulator mantles on electronic behaviors of these molecular enamel wires.

Figure 2 shows the absorption spectra of the vacuum-deposit thin films of oligomers **2**–**5** on quartz substrate as well as those in THF. Generally photopysical process of a π-conjugated molecule in solid state is complicated due to the intermolecular π-π interactions. The electronic spectra of the thin film of non-insulated oligothiophenes **2**–**3** are apparently dissimilar to those in the THF solution. In contrast, the thin film spectra of insulated oligothiophenes **4**–**5** are nearly identical to the THF solution spectra. These results indicate that the intermolecular π-π interactions are efficiently prevented by the insulator mantle of **4**–**5**. This conclusion is supported by the electrochemical data. Typical cyclic voltammograms of insulated and non-insulated α-12T derivatives **6**–**7** are shown in Figure 3. The voltammogram of non-insulated α-12T **6** is broad and ill-defined in contrast to that of insulated α-12T **7**, where three reversible waves are obtained. In general the ill-resolved cyclic voltammogram of long oligothiophenes has its origin in i) adsorption of charged species on the electrode surface and/or ii) π-complex formations such as "π dimer" and "dimer radical ion." Therefore the reversible electrochemical behavior of insulated α-12T **7** can be attributed to the steric inhibitions of adsorption and/or complex formation *via* π-system of the oligomers by the insulator mantle.

In conclusion these experimental data clearly demonstrate the availability of our "molecular enamel wire" concept in molecular-scale engineering.

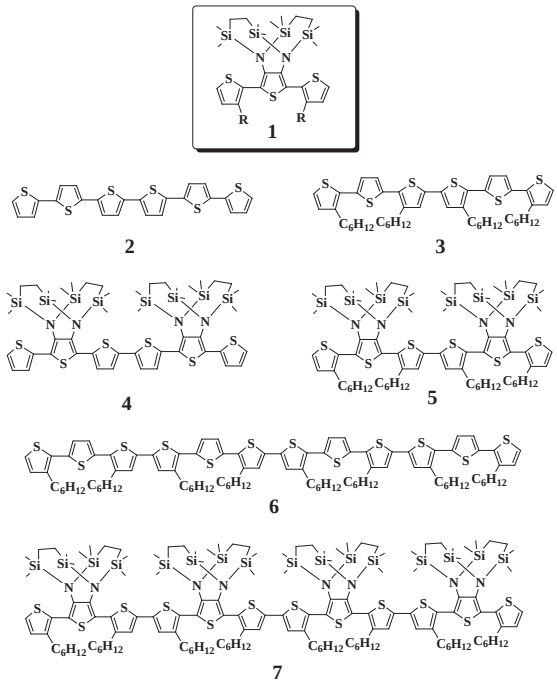

Figure 1. Molecular Structure of oligomers.

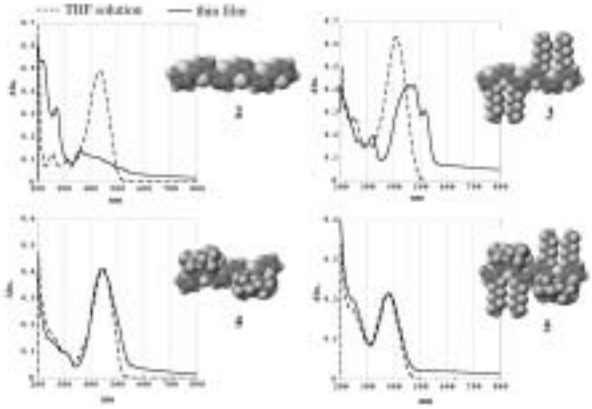

Figure 2. UV/Vis spectra of oligomers.

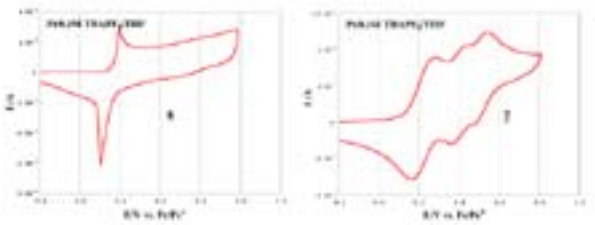

Figure 3. Cyclic voltammograms of oligomers.

VIII-G-2 Combined Spectroscopic and Theoretical Study of Narrow-Bandgap Heterocyclic Cooligomers Containing Alternating Aromatic-Donor and *o*-Quinoid-Acceptor Units

RUIZ DELGADO, Mari Carmen[1]; HERNÁNDEZ, Víctor[1]; LÓPEZ NAVARRETE, Juan T.[1]; TANAKA, Shoji; YAMASHITA, Yoshiro[2]
([1]Univ. Malágo.; [2]Tokyo. Inst. Tech.)

In this paper we analyze, with the help of Density Functional Theory calculations, the relationship between the molecular structure and the optical and vibrational properties of two narrow-bandgap π-conjugated cooligomers containing an alternating sequence of aromatic-donor and *o*-quinoid acceptor units. The optimized molecular geometries of these cooligomers reveal that short inter-ring S···N contacts occur in their minimum-energy structure between the two types of constituiting units, and that the resulting rigid coplanar arrangement of the rings enhances the degree of π-conjugation and lowers the bandgap.

VIII-G-3 Electrochemical Synthesis and Properties of Poly[1,4-bis(*N*-pyrrolylalkoxy)benzene]s with a Three-Dimentional Crosslinked Structure

ONO, Katsuhiko[1]; YAMADA, Satsuki[1]; OHKITA, Masakazu[1]; SAITO, Katsuhiro[1]; TANAKA, Shoji; HANAICHI, Takamasa[2]
([1]Nagoya Inst. Tech.; [2]Hanaichi UltraStruc. Res. Inst.)

[*Chem. Lett.* 516–517 (2003)]

The title polymers, which were composed of π-conjugated pyrroles and dialkoxybenzene crosslinkers, were prepared by electrochemical polymerization to afford amorphous thin films, which were characterized by cyclic voltammetry (CV), scanning electron microscope (SEM), and redox stability.

VIII-H Development of Novel Heterocyclic Compounds and Their Molecular Assemblies for Advanced Materials

Heterocycles containing sulfur and/or nitrogen atoms are useful as components of functional materials since heteroatoms in their rings are helpful to stabilize ions or ion-radical species, and extended π-conjugation decreases Coulombic repulsion. In addition intermolecular interactions caused by heteroatom contacts can be expected to form novel molecular assemblies. In this project new electron acceptors, donors, and donor-acceptor compounds based on heterocycles such as 1,2,5-thiadiazole and 1,3-dithiole were synthesized and their properties including those of the charge-transfer complexes or ion-radical salts were investigated. Unique crystal structures were constructed by using weak intermolecular interactions such as hydrogen bonding or heteroatom contacts.

VIII-H-1 Non-Planar BEDT-TTF Derivatives Fused with Tetrahydrofuran Rings Affording Cation Radical Salts with Unusual Crystal Structures

YAMASHITA, Yoshiro[1]; TOMURA, Masaaki; IMAEDA, Kenichi[2]
([1]IMS and Tokyo Inst. Tech.; [2]IMS and Chubu Univ.)

[*Mol. Cryst. Liq. Cryst.* **380**, 203–207 (2002)]

The title non-planar electron donors **1** and **2** were prepared by the several steps involving the addition reaction of oligo(1,3-dithiole-trithione) with 2,5-dihydrofuran. They afforded the cation radical salts as single crystals whose unusual crystal structures were revealed by X-ray analysis.

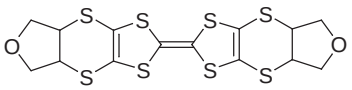

1

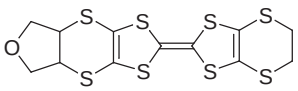

2

VIII-H-2 Synthesis and Characterization of New π-Conjugated Molecules Containing Bis(ethynylpyridine) Units with a Benzothiadiazole Spacer

AKHTARUZZAMAN, Md.[1]; TOMURA, Masaaki; ZAMAN, Md. Badruz[2]; NISHIDA, Jun-ichi[1]; YAMASHITA, Yoshiro[3]
([1]Tokyo Inst. Tech.; [2]IMS and Steacie Inst. Mol. Sci.;

[3]IMS and Tokyo Inst. Tech.)

[*J. Org. Chem.* **67**, 7813–7818 (2002)]

Three novel 4,7-bis(*n*-pyridylethynyl)-2,1,3-benzothiadiazoles (*n* = 2, 3 and 4) were synthesized by using the Sonogashira cross-coupling reaction of 4,7-dibromo-2,1,3-benzothiadiazole with the corresponding ethynylpyridines in the presence of a Pd(II) catalyst. The viologen analogues were also prepared by methylation of pyridyl nitrogen atoms. X-ray structure analysis of these compounds revealed the linear molecular structures with unusual columnar crystal structures. Insertion of a benzothiadiazole moiety into the acetylene-pyridine skeleton brings about a large increase in electron affinity and the bispyridyl compounds obtained here show high fluorescence quantum yields.

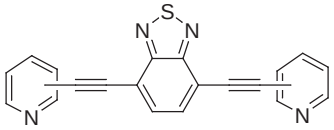

2,2'-dipyridyl, 3,3'-dipyridyl, 4,4'-dipyridyl

VIII-H-3 Preparation and Structures of Dication Salts of Phenyl Substituted TTF Vinylogues

YAMASHITA, Yoshiro[1]; TOMURA, Masaaki
([1]IMS and Tokyo Inst. Tech.)

[*J. Solid State Chem.* **168**, 427–432 (2002)]

Some TTF vinylogues **1a-l** containing phenyl groups at the vinyl positions were synthesized. The redox properties were investigated by cyclic voltammograms, showing that they are strong electron donors and the Coulomb repulsion is decreased in the dication states. Some of the donors afforded their dication salts as single crystals by electrochemical oxidation or the reaction with $CuCl_2$. X-ray structure analysis has revealed that the dication molecules have structures with planar TTF vinylogue units and twisted phenyl groups. The crystal structures are unusual to avoid the steric interactions of the phenyl groups.

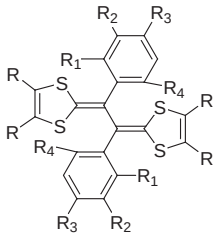

1

	R,R	R_1	R_2	R_3	R_4
1a	$(CH{=}CH)_2$	H	H	H	H
1b	$(CH{=}CH)_2$	F	H	H	F
1c	$(CH{=}CH)_2$	H	H	Cl	H
1d	$(CH{=}CH)_2$	CN	H	H	H
1e	$(CH{=}CH)_2$	H	H	CN	H
1f	$(CH{=}CH)_2$	OCH_2O		H	H
1g	SCH_2CH_2S	F	H	H	F
1h	SCH_2CH_2S	Cl	H	H	H
1i	SCH_2CH_2S	CN	H	H	H
1j	SCH_2CH_2S	H	H	CN	H
1k	SCH_2CH_2S	OCH_2O		H	H
1l	H, H	F	H	H	F

VIII-H-4 Unsymmetrical Tetrathiafulvalene with a Fused 1,2,5-Thiadiazole Ring and an Ethylenedioxy Group

TOMURA, Masaaki; YAMASHITA, Yoshiro[1]
([1]IMS and Tokyo Inst. Tech.)

[*Acta Crystallogr., Sect. E* **59**, o145–o147 (2003)]

In the crystal structure of the title compound, 4,5-ethylenedioxy[1,2,5]thiadiazolotetrathiafulvalene, $C_8H_4N_2O_2S_5$, a large number of short intermolecular S···S contacts are observed [3.519(5)–3.610(5) Å]. The molecules stack along the *c* axis in a face-to-face fashion.

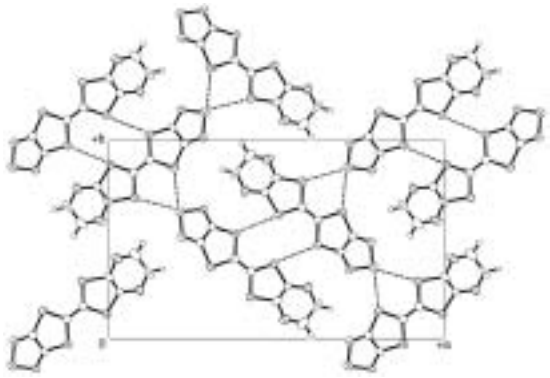

Figure 1. Packing diagram of the title compound viewed along the *c* axis. Dotted lines indicate the short intermolecular S···S contacts.

VIII-H-5 Novel Electron Acceptors Containing Nitrogen, Sulfur-Heterocyclic Units

YAMASHITA, Yoshiro[1]; SUZUKI, Kazuharu[2]; TOMURA, Masaaki
([1]IMS and Tokyo Inst. Tech.; [2]IMS and Inst. Res. Innov.)

[*Synth. Met.* **133-134**, 341–343 (2003)]

A tetracyanodiphenoquinodimethane (TCNDQ) analog **1** containing fused thiadiazole rings is a stronger electron acceptor than tetra-cyanoquinodimethane (TCNQ). The single crystals of this TCNDQ analog were found to exhibit semiconductive behaviors as a single component whose structures were revealed by X-ray structure analysis. The anion radical salts with Et_4N and Me_4P ions were obtained as single crystals by electrochemical reduction. They are 1:1 salts and showed semiconductive behaviors. The structures include tape-like networks formed by S···N contacts. Furthermore, one of the benzothiadiazole rings was replaced with a thiophene unit to give new π-extended quinonoid acceptors **2** which are highly polarized and exhibit their absorption maxima above 500 nm.

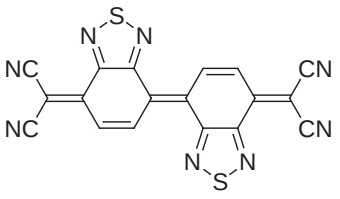

1

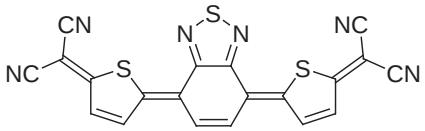

2

VIII-H-6 Linear Molecules with Ethynylpyridine and Bisbenzothiadiazole Units

AKHTARUZZAMAN, Md.[1]; TOMURA, Masaaki; NISHIDA, Jun-ichi[1]; YAMASHITA, Yoshiro[2]
([1]Tokyo Inst. Tech.; [2]IMS and Tokyo Inst. Tech.)

[*Synth. Met.* **137**, 873–874 (2003)]

7,7'-Bis(pyridylethynyl)-4,4'-bis(2,1,3-benzothiadiazole) derivatives were synthesized using the Sonogashira reaction. X-ray crystallographic analysis of the 4,4'-dipyridyl derivative revealed the linear molecular structure with an unusual tape-like crystal structure. They show high electron affinity and fluorescence with large Stokes shifts. The viologen analogues were also prepared by methylation of the pyridyl nitrogen atoms.

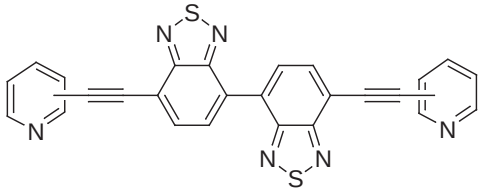

3,3'-dipyridyl, 4,4'-dipyridyl

VIII-H-7 Hydrogen Bonding Networks Consisted of Conjugation-Extended 4,4'-Bipyridines and Chloranilic Acid

AKHTARUZZAMAN, Md.[1]; TOMURA, Masaaki; TAKAHASHI, Kazuko[2]; NISHIDA, Jun-ichi[1]; YAMASHITA, Yoshiro[3]
([1]Tokyo Inst. Tech.; [2]Tohoku Univ.; [3]IMS and Tokyo Inst. Tech.)

[*Supramol. Chem.* **15**, 239–243 (2003)]

Hydrogen-bonding networks of π-extended 4,4'-bipyridines, 2,5-di(4-pyridyl)thiophene **1**, 2,5-di(4-pyridyl)furan **2** and 1,4-di(4-pyridyl)benzene **3** with 2,5-dichloro-3,6-dihydroxy-1,4-benzoquinone (chloranilic acid, **CA**) have been investigated. The dipyridyl compounds afforded three complexes, (dication of **1**)·(monoanion of **CA**)$_2$, (dication of **2**)·(dianion of **CA**)·(MeOH) and **3**·(dication of **3**)·(dianion of **CA**)·$(H_2O)_6$ with **CA**. X-ray structure analyses revealed the formation of unusual molecular tape and sheet structures involving N–H···O, O–H···O, C–H···O and N–H···N hydrogen bonds, where the aromatic spacer groups play an important role in constructing the unique crystal structures.

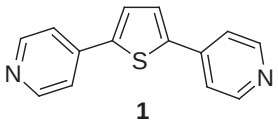

1

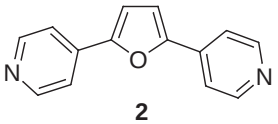

2

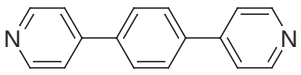

3

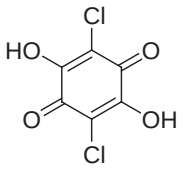

CA

VIII-I Green and Risk-Free Catalysis

Catalytic organic transformations under mild, safe, and green conditions is an important goal in synthetic organic chemistry. We recently reported that several palladium-catalyzed reactions, including π-allylic substitution, carbonylation, the Heck reaction, and Suzuki-Miyaura cross-coupling, took place in water by use of palladium-phosphine complexes bound to an amphiphilic polystyrene-poly(ethylene glycol) graft copolymer (PS-PEG) resin. Rhodium-catalyzed hydroformylation, cyclotrimerization of alkynes, and Michael-type addition of arylboronic acids were also found to proceed smoothly in water. Here we wish to report that Heck reaction, Sonogashira reaction, Wacker reaction were successfully examined in water by use of PS-PEG resin-supported transition metal complexes.

VIII-I-1 Heck Reaction in Water with Amphiphilic Resin-Supported Palladium-Phosphine Complexes

UOZUMI, Yasuhiro; KIMURA, Tsutomu

[*Synlett* 2045–2048 (2002)]

The Heck reaction of various aryl halides and alkenes took place in water in the presence of an amphiphilic polystyrene-poly(ethylene glycol) resin-supported palladium-phosphine complex to give the corresponding styrene derivatives in quantitative yields.

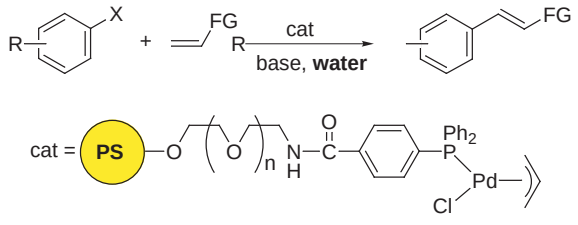

Scheme 1.

VIII-I-2 The Sonogashira Reaction in Water with an Amphiphilic Resin-Supported Palladium-Phosphine Complex under Copper-Free Conditions

UOZUMI, Yasuhiro; KOBAYASHI, Yukinari

[*Heterocycles* **59**, 71–74 (2003)]

The Sonogashira reaction of aryl halides with terminal alkynes was catalyzed by an amphiphilic polystyrene-poly(ethylene glycol) (PS-PEG) resin-supported palladium-phosphine complex in water to give the corresponding aryl-substituted alkynes in high yields under copper-free conditions. Reaction of *o*-iodophenol with terminal alkynes under Sonogashira conditions gave benzofuran derivatives in one step.

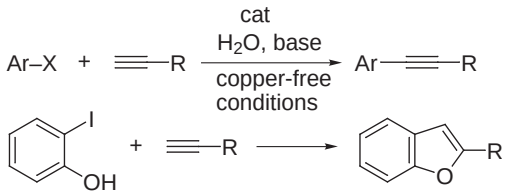

Scheme 1.

VIII-I-3 Polymer-Supported 2,2'-Bis(oxazolin-2-yl)-1,1'-Binaphthyls (boxax): Immobilized Chiral Ligands for Asymmetric Wacker-Type Cyclizations

HOCHE, Heiko; UOZUMI, Yasuhiro

[*Synlett* 2049–2053 (2003)]

Homochiral 2,2'-bis(oxazolin-2-yl)-1,1'-binaphthyl (boxax) ligands were anchored on various polymer supports including PS-PEG, PS, PEGA, and MeO-PEG *via* selective monofunctionalization at the 6-position of the binaphthyl backbone. Palladium(II) complexes of the supported boxax ligands catalyzed Wacker-type cyclization of 2-(2,3-dimethyl-2-butenyl)phenol to give 2-methyl-2-isopropenyl-2,3-dihydrobenzofuran with up to 96% ee.

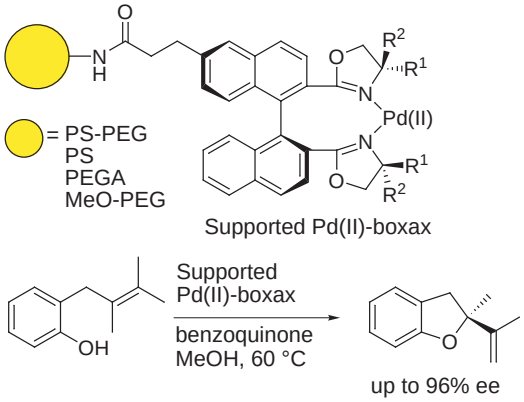

Scheme 1.

VIII-J Designing Artificial Photosynthesis at Molecular Dimensions

Photosynthesis is one of the finest piece of molecular machinery that Nature has ever created. Its ultrafast electron transfer and following well-organized sequence of chemical transformation have been, and will continue to be, challenging goals for molecular scientists. We are trying to mimic the function of photosynthesis by assembling molecular units that perform individual physical/chemical action. The molecular units include porphyrins, redox active organic molecules, and transition metal complexes. Our ultimate goal is to design artificial molecular systems that effect multiple chemical reactions triggered by light on the basis of molecular rationale.

VIII-J-1 Photooxidation of Alcohols by a Porphyrin/quinone/TEMPO System

NAGATA, Toshi; ITO, Hajime; NAGASAWA, Takayuki

Photoinduced electron transfers involving porphyrins are widely studied, but utilizing the high-energy radical ion pairs for driving chemical reactions remains to be a great challenge. We reported preliminary results on photooxidation of alcohols by a porphyrin/quinone/TEMPO system in AR2002. This year we report the mechanistic detail of this reaction system.

When a solution of porphyrin **1** (1 μmol), TEMPO (25 μmol), 2,5-di-*tert*-butyl-1,4-benzoquinone (100 μmol), benzyl alcohol (300 μmol) and *n*-dodecane (50 μmol; an internal standard for the gas chromatography) in 0.5 ml of dry pyridine was irradiated with visible light (λ > 500 nm), benzaldehyde was formed with concurrent formation of 2,5-di-*tert*-butyl-1,4-hydroquinone. The substrate dependence experiments revealed following order of reactivity: benzylic ≈ allylic > primary >> secondary (no reaction). This is in accordance with other reported TEMPO-mediated oxidation.

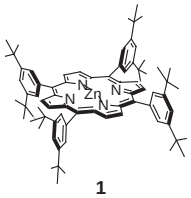

1

With benzyl alcohol as a substrate, the initial rates of product formation were examined under various conditions (Figure 1). As shown in parts (a) and (b), the rate increases with increasing concentrations of $PhCH_2OH$ and TEMPO. Particularly interesting is the dependence on the quinone concentration, shown in part (c). Here the initial rates decrease with increasing quinone concentration. The dependence on the porphyrin concentration (part (d)) also shows a similar trend.

The negative dependence on quinone concentration can be explained by considering the quantum yields of the triplet radical pairs. When the concentration of quinone becomes higher, the quantum yield of the triplet radical pair is lowered because the singlet state is more likely to be quenched prior to intersystem crossing. On the other hand, the negative dependence on porphyrin concentration is ascribed to the electron-transfer equilibrium between the porphyrin cation radical and TEMPO (Equation 1). As the concentration of porphyrin becomes higher, the equilibrium is pushed to the left and the steady-state concentration of the oxoammonium cation $TEMPO^+$ becomes lower. The proposed reaction mechanism is shown in Scheme 1.

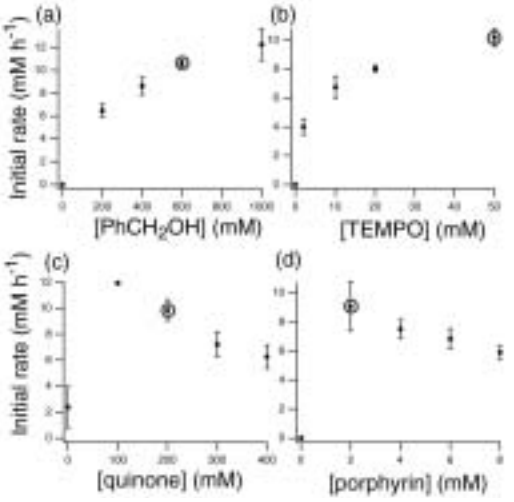

Figure 1. The initial rates of formation of PhCHO under various conditions.

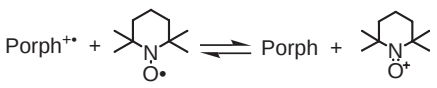

Equation 1.

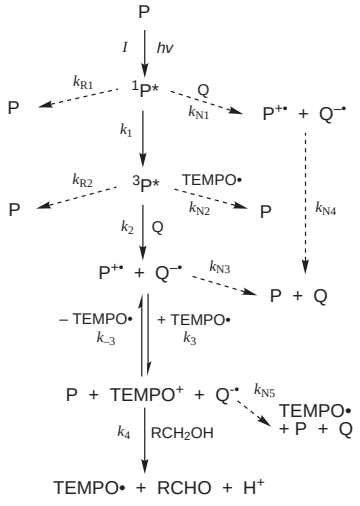

Scheme 1. Proposed reaction mechanism.

VIII-K Development of New Nanomaterials as Components in Advanced Molecular Systems

Nanometer-sized materials exhibit unique electronic behavior. In the quest of advanced redox catalysis, we are currently interested in combining nanometer-sized materials into molecular redox systems. Herein we report two attempts to develop new nanomaterials that potentially suit for combination with advanced molecular system.

VIII-K-1 Development of New Spatially-Relaxed Dendrimers and Their Application as Precursor to Redox Pool Molecules

KIKUZAWA, Yoshihiro; NAGATA, Toshi

We synthesized a series of new dendrimers with up to fourteen "internal" carboxyl groups. These dendrimers (**G$^{1–3}$**) are made from a branching unit and a spacer unit with a carboxyl group. Introduction of the spacer groups makes the internal carboxyl groups more spatially relaxed than previously reported dendrimers.

This type of dendrimer was used as a building framework of new redox pool molecules. The dendrimer **G^3** was connected to a porphyrin, the internal carboxyl groups were converted to alcohols, and ferrocene-carbonyl groups were introduced via ester linkages to give **P-G^3(Fc)$_{14}$**. This molecule will be useful for examination of photoinduced electron transfer between a porphyrin and multiple electron donor molecules.

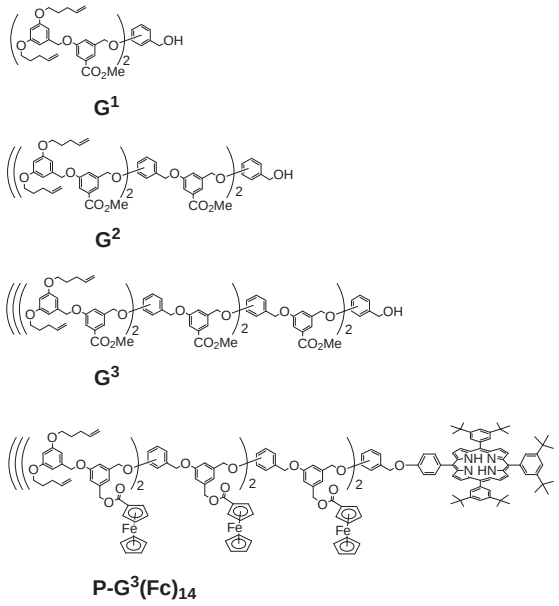

VIII-K-2 Synthesis and Size Control of Gold Sub-Nanoparticles Stabilized by Tripod Organic Molecules

HOSOKAWA, Youichi; NAGATA, Toshi

Recently, gold nanoparticles have received much attention as potentially useful materials showing novel electronic, optical, optoelectronic, and magnetic properties derived from the quantum size effect. One promising application of these materials is utilization as one of the functional "components" in molecular systems. To realize this idea we are developing techniques to treat metal nanoparticles as if they were "molecules."

We synthesized new tripod molecule **1**–**3** (Figure 1) and examined stabilization of of gold sub-nanoparticles stabilized by them. These molecules are designed so that a single molecule can enclose a single metal nanoparticle to give a "molecular" nanoparticle complex (Figure 2). The multi-point interaction by arylthioether units will produce the stabilization, and the different "leg" length will also result in size-selection of metal nanoparticles. Figure 3 shows the TEM pictures and the observed diameter distribution of gold nanoparticles derived from **1**–**3**. The most frequent values of the diameter distribution became larger with increasing numbers of the benzyl thioether units.

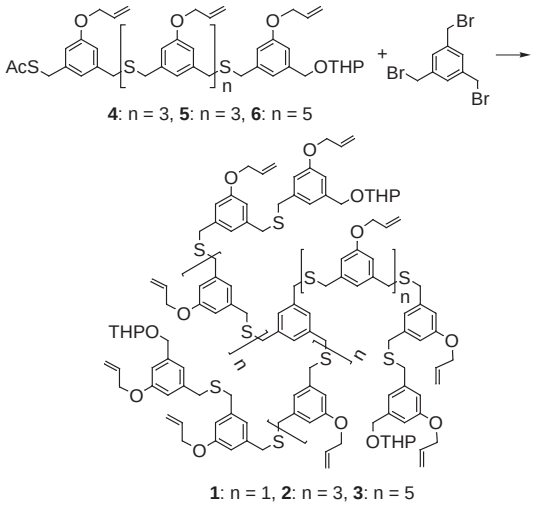

Figure 1. Preparation of the tripod molecules **1**–**3**.

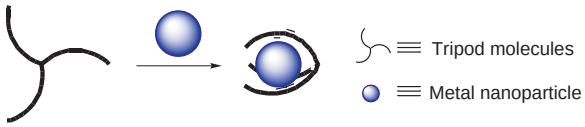

Figure 2. A schematic representation of the complex between the tripod molecule and the metal nanoparticle.

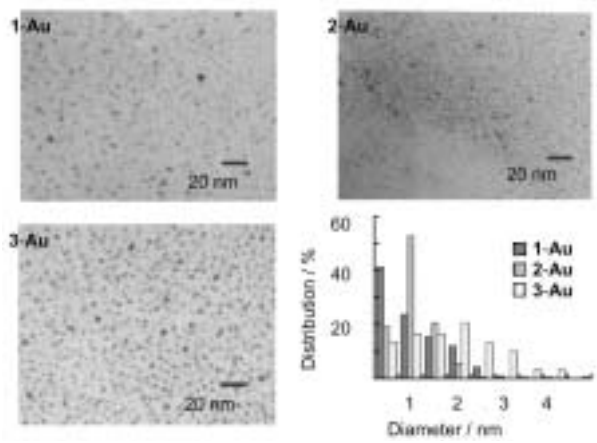

Figure 3. TEM images and the diameter distribution of **1-**, **2-**, and **3-Au**.

VIII-L Photochemistry on Well-Defined Surfaces

Upon the irradiation of light in the wavelength range from visible to ultraviolet, a number of adsorbed molecules on metal surfaces reveal variety of photochemical processes, including photo-stimulated desorption, rearrangement of adsorbed states, photodissociation, and photo-initiated reactions with coadsorbates. A central and fundamental question in the surface photochemistry is to clarify how adsorbate-substrate systems are excited by photon irradiation. In addition, since photo-initiated reactions can be induced without any thermal activation of reactants, they may provide good opportunities for studying a new class of surface reactions that may not be induced thermally. We have studied photochemistry of various adsorption systems on well-defined metal and semiconductor surfaces mainly by temperature-programmed desorption (TPD), x-ray photoelectron spectroscopy (XPS), work function measurements, near edge x-ray absorption fine structure (NEXAFS) and angular-resolved time-of-flight (TOF) mass spectrometry of photodesorbed species associated with pulsed laser irradiation.

VIII-L-1 Photo-Induced Oxygen Elimination on Silver Surfaces

NAKAGOE, Osamu[1]; OHTA, Michiharu[1]; WATANABE, Kazuya[1]; TAKAGI, Noriaki[1]; MATSUMOTO, Yoshiyasu
([1]GUAS)

[*Surf. Sci.* **528**, 144–150 (2003)]

We have investigated the structural changes in the added-rows of Ag–O chains at a Ag(110)(2×1)-O surface due to photo- and CO-induced elimination of O by using scanning tunneling microscopy. The photo-induced elimination occurs only on the surface containing carbidic carbon, resulting in the structural change of the added-rows from (2×1) to (4×1) according to the reduction of O coverage (θ_O). The structural change due to the CO-induced elimination depends on the carbon coverage: the (2×1) structure is retained in spite of the decrease of θ_O for the C-contained surface, while the structure changes sequentially from (2×1) to (4×1) and (6×1) for the carbon-free surface. Furthermore, the CO-induced elimination rate in the low θ_O on the carbon-free surface is much faster than that on the C-contained surface. These results indicate that the small amount of C atoms play an important role not only in the structural changes associated with the oxygen elimination reactions but also in the kinetics of the oxidation reaction of CO.

VIII-M Ultrafast Dynamics at Well-Defined Surfaces

To understand the mechanism of surface photochemistry, it is vital to know how photoinduced electronic excitation induces adsorbate nuclear motions that ultimately lead to chemical reactions. We demonstrate the real-time observations of substrate surface phonons and adsorbate-substrate vibrational modes by fs time-resolved second harmonics generation (TRSHG). If an excitation light pulse has a duration sufficiently shorter than a period of a vibrational mode or a phonon mode, it can excite the mode with a high degree of temporal and spatial coherence. This coherent nuclear motion modulates the second-order susceptibility $\chi^{(2)}$. Thus, by monitoring the intensity modulation of the second harmonics (SH) generation of a probe pulse, we can observe the evolution of the coherent nuclear motion subsequent to the electronic excitation at the surfaces.

VIII-M-1 Coherent Surface Phonon at a GaAs(100)-c(8x2) Surface

WATANABE, Kazuya[1]; DIMITROV, Dimitre T.[1]; TAKAGI, Noriaki[1]; MATSUMOTO, Yoshiyasu
([1]GUAS)

[*Phys. Rev. B* **65**, 235328 (7 pages) (2002)]

Coherent surface phonon at a GaAs(100)-c(8×2)-Ga reconstructed surface has been investigated by time resolved TRSHG. The phonon mode is impulsively excited by an ultrashort laser pulse and subsequent coherent nuclear motion is monitored through the intensity modulation of the second harmonics of a probe pulse. Oscillatory traces are clearly observed in TRSHG signals and their Fourier transformation show two peaks at 8.2–8.6 THz and 8.9 THz. Fitting these traces with two oscillatory components shows that the oscillatory signals are contributed by the bulk LO-phonon at 8.8 THz and the surface phonon at 6.0–8.6 THz. The relative amplitude of the surface phonon modes is sensitive to sputtering and annealing of the surface. Clear dips appear at 8.7 THz in the Fourier spectra, which is caused by the initial phase difference between the surface phonon and the bulk phonon modes. The frequency of the surface component shows red shifts as the pumping power increases. The shifts are indicative of a marked electron phonon interaction or anharmonicity of the surface phonon modes.

VIII-M-2 Impulsive Excitation of a Vibrational Mode of Cs on Pt(111)

WATANABE, Kazuya[1]; TAKAGI, Noriaki[1]; MATSUMOTO, Yoshiyasu
([1]GUAS)

[*Chem. Phys. Lett.* **366**, 606–610 (2002)]

We have performed TRSHG measurements regarding a Cs–Pt stretching mode on a Cs-covered Pt(111) surface under an ultrahigh vacuum condition. The TRSHG trace obtained from the clean surface shows an instantaneous sharp rise right after the excitation. This is followed by a fast decaying component (t < 1 ps) and a slowly decaying one persistent to the longest delay (t = 6 ps) of the measurements. When the surface is covered with Cs, SH signals are enhanced by about 70 times and strongly modulated waveforms are superimposed on the TRSHG traces. The power spectrum obtained from the Cs-covered Pt(111) surface shows a strong peak at 2.3 THz; this is assigned to the Cs–Pt stretching mode. The dephasing time of the coherent vibration was estimated to be 1.4 ps. The strong modulation is observed only the Cs-coverages larger than 0.24 ML. At these coverages alkali metal adsorbates are known to make metallic quantum wells. Thus, the resonant impulsive Raman process between quantum well states is responsible for the creation of the vibrating nuclear wavepacket motion in phase along the Cs–Pt stretching coordinate.

VIII-N Multiphoton Photoelectron Spectroscopy of Electronic States of Nano-Structured Materials on Surfaces

Electronic structure and excited state dynamics of nano-structured materials on surfaces are very important for exploring their properties, thermal reactivity and nonthermal processes including photochemistry and photo-induced charge transfer. For this purpose, we performed multiphoton photoelectron spectroscopy with fs lasers. This year we applied this method to a single-layered nano-graphite crystalline grown on a metal surface.

VIII-N-1 Anomalous Quenching of Electronic States of Nanographene on Pt(111) by Deuterium Edge Termination

KINOSHITA, Ikuo[1]; INO, Daisuke[2]; NAGATA, Kaoru[1]; WATANABE, Kazuya[2]; TAKAGI, Noriaki[2]; MATSUMOTO, Yoshiyasu
([1]Yokohama City Univ.; [2]GUAS)

[*Phys, Rev. B* **65**, 241402R (4 pages) (2002)]

The electronically excited state and its decay dynamics of graphite nano-crystals on metal surfaces have been investigated by fs time-resolved multi-photon photoelectron spectroscopy. Single-layer graphite nano-crystals are formed on a Pt(111) surface. The 3-photon photoelectron spectra taken from this surface reveal two peaks whose intensities are strongly correlated with the graphite coverage. By combining with the measurements of photoemission of adsorbed xenon used as another probe for local work functions, we can clearly identify for the first time that one of the peak is due to the electronically excited σ^* state of the graphite nano-crystal. Moreover, this state is extremely sensitive to hydrogen termination of the edge of the nano-crystal in contrast to the occupied π state. These findings clarify the properties of the electronic states of graphene and finally settle the controversy on the location of the interlayer band and its split-off state of bulk graphite.

VIII-O Chemistry of One-Dimensional Nano-Surface Compounds Studied by Scanning Tunneling Microscopy

The fluctuating configurations of low-dimensional structures can be thermodynamically favorable at finite temperatures, because the energy gain overcomes the energy cost that accompanies local structural fluctuation. In particular, one-dimensional (1D) systems have a propensity to be sensitive to these fluctuations as described by one of the maxims of condensed matter physics, *i.e.*, one chain does not make a crystal. Thus, the dynamical formation of active species and sites by these fluctuations is a key factor in establishing a microscopic model for chemical reactions at surfaces and nano-structured compounds.

VIII-O-1 Role of Structural Fluctuation in a Surface Reaction Studied by Scanning Tunneling Microscopy: The CO + O → CO_2 Clean-Off Reaction on Ag(110)(2x1)-O

NAKAGOE, Osamu[1]; WATANABE, Kazuya[1]; TAKAGI, Noriaki[1]; MATSUMOTO, Yoshiyasu
([1]GUAS)

[*Phys. Rev. Lett.* **90**, 226105 (4 pages) (2003)]

It is well known that the adsorption of O on Ag(110) results in the formation of quasi-1D structures, AgO chains, accompanied by the mass transfer of substrate atoms.

AgO chains arrange periodically to form (n×1) (n = 2 ~ 7) depending on the fractional O coverage due to repulsive inter-chain interactions. While the chains appear as rigid straight lines in the (2×1) structure at room temperature, the structures fluctuate to appear as segmented and sometimes "frizzy" chains in the (n×1) ($n \geq 4$) structures. Energetically-equivalent structures of different configurations of segments exist, reflecting the 1D nature of the chains. Thus, chains fluctuate between configurations rather than freezing into a single configuration, and consequently segmented or frizzy chains are observed. Therefore, AgO chains on Ag(110) is a good system for investigating the effects of structural fluctuation on reactivity.

The kinetics of the clean-off reaction of O adatoms by CO on Ag(110)(2×1)-O is investigated by scanning tunneling microscopy. The reaction is accelerated in the lower O coverage range where AgO chains with (n×1) ($n \geq 4$) configurations show significant structural fluctuation. Simulations based on the Ising model are used to provide a quantitative understanding of the acceleration, which originates from the dynamical formation of active O adatoms by fluctuation of AgO chains.

VIII-P Adsorbate Structure and Surface Chemistry on Well-Defined Surfaces

Surface reactions have been playing an important role in production of many useful compounds and also fabrication of electronic devices. In particular, investigations on the structures of adsorbates and their reactivity are the first step for understanding more complicated catalytic reactions. We investigate surface reactions and kinetics by means of various techniques including temperature-programmed desorption (TPD), x-ray photoelectron spectroscopy (XPS), ultraviolet photoelectron spectroscopy (UPS), work function measurements, Auger electron spectroscopy (AES), infrared reflection absorption spectroscopy (IRAS) and scanning tunneling microscopy (STM).

VIII-P-1 Thermal Decomposition of Acetylene on Pt(111) Studied by Scanning Tunneling Microscopy

NAKAGOE, Osamu[1]; TAKAGI, Noriaki[1]; MATSUMOTO, Yoshiyasu
([1]GUAS)

[*Surf. Sci.* **514**, 414–419 (2002)]

The adsorption and the thermal decomposition processes of C_2H_2 on Pt(111) have been investigated by the use of STM. For a high C_2H_2 coverage, a (2×2) structure is observed locally after the C_2H_2-covered Pt(111) surface is heated to 120 K. By heating to 220 K, the sample surface is covered with the (2×2) structure separated with brighter lines. After heating up to 370 K, (2×2) domains related to ethylidyne species appear with larger and brighter protrusions. For a low C_2H_2 coverage, adsorbates are located randomly and no ordered islands are observed after heating to 120 K. In contrast, heating to 220 K leads to the formation of (2×2) islands. This indicates that the adsorbate-adsorbate interaction in the (2×2) structure observed by 120 K heating is different from that in the (2×2) structure observed by 220 K heating; the former is repulsive, but the latter attractive. Therefore, it is suggested that different surface species are formed by the decomposition of C_2H_2 at 220 K. The detail of the decomposition processes of C_2H_2 and the relation between the adsorbate-adsorbate interaction and the surface species are discussed. The results are also reported measured by heating up to higher temperatures above 400 K.

VIII-P-2 Reaction Intermediates in the Oxidation of Methanol on a Pt(111)-(2x2)O Surface

LIU, Zhengxin[1]; SAWADA, Takeshi[1]; TAKAGI, Noriaki[1]; WATANABE, Kazuya[1]; MATSUMOTO, Yoshiyasu
([1]GUAS)

[*J. Chem. Phys.* **119**, 4879–4886 (2003)]

The oxidation of methanol on a Pt(111)-(2×2)O surface has been investigated by infrared reflection absorption spectroscopy and temperature-programmed desorption. Methanol is dehydrogenated to produce methoxy species in the annealing temperature range from 130 to 170 K. At above 170 K, the reaction proceeds differently, depending on methanol coverage. At the saturation coverage, methanol adsorbates partly desorb molecularly and partly react with precovered

oxygen atoms to produce CO, H_2 and H_2O. No detectable formaldehyde or formate is formed. In contrast, at submonolayer coverages, methoxy species is dehydrogenated to yield formaldehyde at ~ 180 K and further oxidized to formate at ~ 200 K. Formate is decomposed by 300 K. Defect sites such as steps are not relevant to the formation of the intermediates. When CO is coadsorbed on the surface, it destabilizes the reaction intermediates. The destabilization by coadsorbed CO makes the reaction intermediates short lived as not to be detectable at high initial coverages of methanol.

VIII-Q Structures and Photophysical Properties of Monolayer–Protected Metal Clusters

For the last decade, the monolayer-protected metal clusters (MPCs) have gained much attention both as prototype systems to study the size dependent evolution of the electronic properties of the metal clusters and as promising candidates for elementary units of nano-scale devices. The emergence of novel optical and electronic properties is expected for small-sized MPCs because their electronic energy levels become quantized due to the electron confinement into the small dimensions. For example, it is anticipated that the small MPCs exhibit photoluminescence since the radiative process of the photoexcited state can compete with the phonon-mediated nonradiative relaxation processes. Our interests are focused on the following issues on the MPCs: (1) preparation and characterization of the small MPCs with core diameters of ~ 1 nm range (~ 40 atoms/cluster) which may exhibit molecular–like electronic and charging properties, (2) determination of structural dimensions (core diameters and monolayer thickness), (3) development of size–selection method, and (4) clarification of the effects of the core size, core shape, and thiolate ligation on the optical and electronic properties.

VIII-Q-1 One-Pot Preparation of Subnanomerter-Sized Gold Clusters *via* Reduction and Stabilization by *meso*-2,3-Dimercaptosuccinic Acid

NEGISHI, Yuichi; TSUKUDA, Tatsuya

[*J. Am. Chem. Soc.* **125**, 4046–4067 (2003)]

We report herein a simple method to prepare subnanometer-sized gold clusters by the reactions between hydrogen tetrachloroaurate ($HAuCl_4$) and *meso*-2,3-dimercaptosuccinic acid (DMSA; $HO_2CCH(SH)CH(SH)CO_2H$) in water. It is demonstrated that DMSA molecules efficiently reduce the Au(III) species and stabilize the resultant gold clusters. The Au:DMSA clusters, which tend to aggregate into assemblages in water, can be well-isolated each other by ion-pair formation between the carboxyl groups of DMSA and tetraoctylammonium (TOA) cations. This surface modification enables us to examine the core size distributions of the individual clusters by mass spectrometry and TEM. It is revealed that the gold clusters comprised of 10–13 atoms (*ca.* 0.8 nm) are the main products of the reactions.

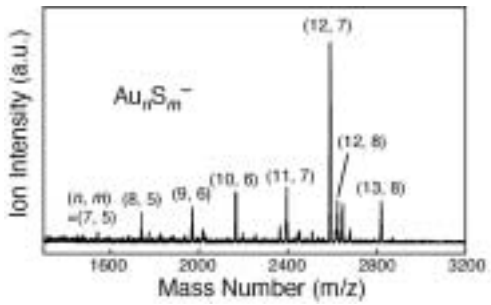

Figure 1. Laser desorption ionization mass spectrum of Au:DMSA-TOA clusters.

VIII-Q-2 Photoluminescence from Nearly Monodispersed Au_{12} Clusters Protected by *meso*-2,3-Dimercaptosuccinic Acid

NEGISHI, Yuichi; TSUKUDA, Tatsuya

[*Chem. Phys. Lett.* **383**, 161–165 (2004)]

Nearly monodispersed gold clusters ($Au_{\sim 12}$) protected by *meso*-2,3-dimercaptosuccinic acid (DMSA) exhibit luminescence at 630 nm with a quantum yield of 1×10^{-6} upon the photoexcitation at 390 nm into the lowest electronic excited state. The large Stokes shift (1.2 eV) suggests that the visible PL is assigned to phosphorescence originating from a triplet-like excited state. The PL quantum yield was enhanced up to 0.9%, greater by 8 orders of magnitude than that of bulk gold, by thickening the protecting layer and freezing of the solvent at 77 K. The emission peak energy is discussed within the context of core-size dependent electronic structures by comparing with those of other gold MPCs reported in literatures.

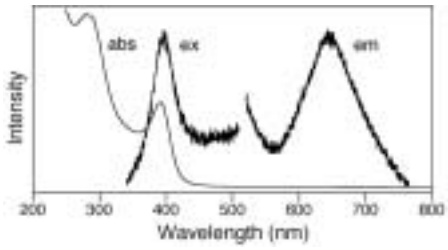

Figure 1. Optical absorption, emission and excitation spectra of Au:DMSA clusters at 298 K; λ_{ex} = 400 nm, λ_{em} = 630 nm.

VIII-Q-3 Isolation and Characterization of Subnanometer-Sized Gold Clusters

NEGISHI, Yuichi; SATO, Seiichi[1]; TAKASUGI, Yoshimitsu[1]; YAO, Hiroshi[1]; KIMURA, Keisaku[1]; SCHAAFF, T. Gregory[2]; WHETTEN, Robert L.[3]; TSUKUDA, Tatsuya

([1]Himeji Inst. Tech.; [2]Oak Ridge Natl. Lab.; [3]Georgia Inst. Tech.)

The Au:SG clusters with the core diameters of 0.8–1.0 nm were synthesized in Kimura group by reducing $AuCl_4^-$ with $NaBH_4$ in the presence of glutathione GSH molecules ($AuCl_4^-$:GSH = 1:2).[1)] The Au:SG clusters thus prepared were further fractionated into five distinct components by using polyacrylamide gel electrophoresis (PAGE).[2),3)] In order to characterize the chemi-

cal composition of these components, the electrospray ionization (ESI) mass spectra were recorded by using an apparatus constructed at IMS. The negative-ion mode ESI mass spectra of these fractions are comprised of series of multiply charged ions of $Au_{21}(SG)_{12}$, $Au_{25}(SG)_{14}$, $Au_{28}(SG)_{16}$, $Au_{32}(SG)_{20}$, $Au_{38}(SG)_{23}$, respectively, demonstrating the isolation of nearly singly-sized clusters. It is found that these isolated clusters exhibit visible photoluminescence with quantum yields in the order of 10^{-3}.

References

1) S. H. Chen and K. Kimura, *Langmuir* **15**, 1075–1082 (1999).
2) T. G. Schaaff, G. Knight, M. N. Shafigullin, R. F. Borkman and R. L. Whetten, *J. Phys. Chem. B* **102**, 10643–10646 (1998).
3) T. G. Schaaff and R. L. Whetten, *J. Phys. Chem. B* **104**, 2630–2641 (2000).

VIII-Q-4 Construction of Apparatus for Photoelectron and Photodissociation Studies of Mass-selected Organometallic Clusters

NEGISHI, Yuichi; NARUSHIMA, Takashi[1]; TSUKUDA, Tatsuya
([1]GUAS)

The electronic structures of the MPCs, especially in the subnanometer-sized regime, are significantly influenced by the thiolate (RS) coordination against the metallic cores as well as their core sizes. In order to study such effects, it is necessary to prepare and isolate the mass selected $M_n(SR)_m$ clusters ($m \geq 0$) in the gas phase, since the clusters with small m are unstable against the aggregation in liquid dispersion. To this end, we have developed a new apparatus, which consists of a cluster ion source, a tandem time-of-flight mass spectrometer, and a photoelectron spectrometer. In the cluster source, the bare metal clusters produced by laser vaporization of the metal target are allowed to react with the thiol molecules, RSH, to form organometallic clusters. The anionic clusters, $M_n(SR)_m^-$, are mass-selected by the first TOF mass spectrometer and then irradiated by pulsed laser light. The photoelectrons and photofragments are detected by the magnetic-bottle type photoelectron spectrometer and the secondary TOF mass spectrometer, respectively.

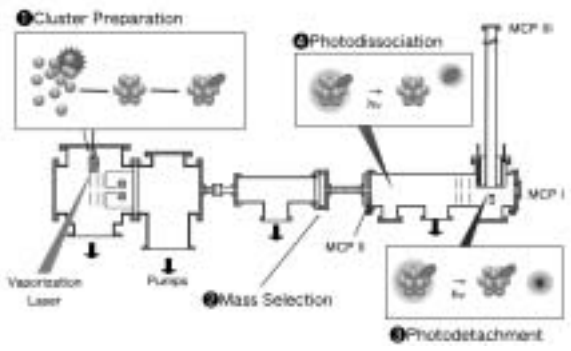

Figure 1. Schematic diagram of the experimental setup.

VIII-Q-5 EXAFS Study on Interfacial Structure between Pd Cluster and *n*-Octadecanethiolate Monolayer: Formation of Mixed Pd–S Interlayer

MURAYAMA, Haruno; ICHIKUNI, Nobuyuki[1]; NEGISHI, Yuichi; NAGATA, Takashi[2]; TSUKUDA, Tatsuya
([1]Chiba Univ.; [2]Univ. Tokyo)

[*Chem. Phys. Lett.* **376**, 26–32 (2003)]

The geometrical structure of a Pd cluster (diameter of ≈ 3.1 nm) protected by *n*-octadecanethiolate monolayer has been investigated by high-resolution TEM (HRTEM), XRD, and EXAFS spectroscopy. The HRTEM and XRD measurements have revealed that the cluster core is comprised of an *fcc* single crystal of Pd. The mean coordination numbers of the Pd–Pd and Pd–S shells determined by the Pd *K*-edge EXAFS analysis suggest that the surface of the Pd core is sulfurized to form a mixed Pd–S layer underneath the thiolate monolayer.

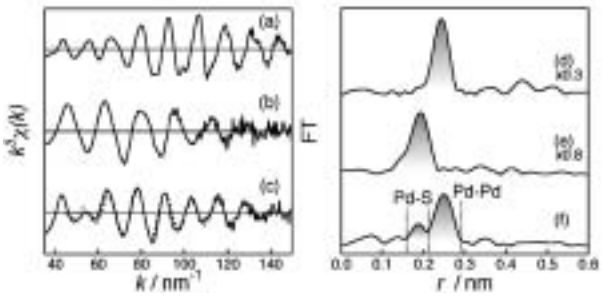

Figure 1. k^3-weighted Pd *K*-edge EXAFS spectra after background subtraction; (a) Pd foil, (b) PdS pellet, (c) Pd:SC_{18} clusters. The broken line in panel (c) represents the best-fit result. Fourier-transforms of the EXAFS spectra; (d) Pd foil, (e) PdS pellet, (f) Pd:SC_{18} clusters.

VIII-Q-6 Structures and Stabilities of Alkanethiolate Monolayers on Palladium Clusters as Studied by Gel Permeation Chromatography

MURAYAMA, Haruno; NARUSHIMA, Takashi[1]; NEGISHI, Yuichi; TSUKUDA, Tatsuya
([1]GUAS)

[*J. Phys. Chem. B* submitted]

Palladium clusters protected by a series of *n*-alkanethiolates, Pd:SC_n (SC_n = *n*-$C_nH_{2n+1}S$, n = 10, 12, 14, 16, and 18), were prepared by a ligand exchange approach: Pd clusters protected by poly (*N*-vinyl-2-pyrrolidone) (PVP) were transferred from aqueous phase to the toluene phase containing the thiols. The structures and stabilities of the thiolate monolayers of the Pd:SC_n clusters were investigated by gel permeation chromatography (GPC) together with TEM, XPS, and FT-IR. The thicknesses of the thiolate layers formed on the Pd clusters were evaluated from the differences between the hydrodynamic diameters and core diameters of the Pd:SC_n clusters, determined by GPC and TEM, respec-

tively. The thicknesses thus obtained are in good agreement with the lengths of the corresponding thiolates in the all-*trans* conformations, illustrating that the alkanethiolates in nearly straight configurations are aligned almost perpendicularly to the core surfaces. Fractionation of the Pd:SC_{18} clusters by GPC yielded a series of the purified samples: the clusters in each fraction are different in their core sizes. The GPC measurements on the Pd:SC_n clusters with small n revealed the decomposition of the monolayers through spontaneous etching and their reconstruction by heat treatment in the presence of the free thiols. The mechanism of these processes is discussed. The present study demonstrates that the GPC provides an elemental and versatile means to characterize and purify the monolayer-protected clusters.

VIII-R Mass Spectroscopic Studies on Nanoscale Materials

Information on the size, shape, and dispersity is of fundamental importance in understanding natures and functions of nanoscale materials. Traditionally, transmission electron microscope (TEM) and powder X-ray diffraction have been employed to measure size, shape and size distributions of the nanoscale materials. We have applied an alternative technique, mass spectrometry, to provide more detailed insight into the structures of these fascinating materials.

VIII-R-1 Self-Assembly of Si Clusters into Single Crystal Arrangements: Formation of Si_{10} Cluster Crystals

SATO, Seiichi[1]; YAMAMOTO, Naoaki[1]; NAKANISHI, Kentaro[1]; YAO, Hiroshi[1]; KIMURA, Keisaku[1]; NARUSHIMA, Takashi[2]; NEGISHI, Yuichi; TSUKUDA, Tatsuya
([1]Himeji Inst. Tech.; [2]GUAS)

[*Jpn. J. Appl. Phys.* **42**, L616–L618 (2003)]

Single crystals at an air/solution interface or a solution/hydrogen-terminated Si substrate interface were created using a self-assembly process, which originated from the hydrophobic nature of Si clusters. Mass analysis indicated that the components of the cluster crystals were partially oxidized hydrogenated Si_{10} clusters. At either interface the nearest-neighbor distances between lattice points in the Si cluster crystals were 0.53 nm or 0.60 nm, which is consistent with the diameters of the Si_{10} clusters. The slight difference in these values seems to be due to variations in the surface passivation of the component Si_{10} clusters.

VIII-R-2 Highly Oxygenated Fullerene $C_{60}O_n$ formed by Corona Discharge Ionization in the Gas Phase

TANAKA, Hideki[1]; TAKEUCHI, Kazuo[1]; NEGISHI, Yuichi; TSUKUDA, Tatsuya
([1]RIKEN)

[*Chem. Phys. Lett.* in press]

Oxygenated fullerenes were produced by a vaporization source equipped with a corona discharge ionizer in the presence of a trace amount of oxygen. *In situ* mass analysis revealed that the species formulated as $C_{60}O_n$ ($n \leq 30$) are formed in the source and that the degree of oxygenation can be altered through the discharge current. Formation of the epoxidized structure in the $C_{60}O_n$ was confirmed by XPS measurements of the thin films of $C_{60}O_n$ and semi-empirical PM3 calculations for $C_{60}O_{30}$. The structures and formation processes for higher analogues $(C_{60})_mO_n$ (m = 2, 3) are briefly discussed.

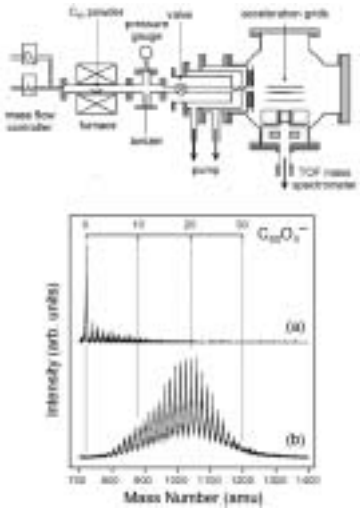

Figure 1. Schematic diagram of experimental setup (top) and typical mass spectra of the negative ions produced by the corona discharge ionizer (bottom) operated at 100 mA under Ar gas flow (a) without oxygen and (b) with 1% oxygen.

VIII-S Structures and Reactions of Molecular Cluster Ions

Molecular clusters, intermediate states of matter between the bulk and the molecule, provide us unique opportunities to study how the chemical and physical properties evolve with a degree of aggregation. We have studied reactions of hydrated anions with a simple molecule by using mass spectrometry, photoelectron and photodissociation spectroscopies and *ab initio* calculations.

VIII-S-1 Gas-Phase Reaction of Hydrated $CO_2^{\cdot-}$ Anion Radicals with CH_3I

TSUKUDA, Tatsuya; NAGATA, Takashi[1]
([1]Univ. Tokyo)

[*J. Phys. Chem. A* **107**, 8476–8483 (2003)]

Hydrated $CO_2^{\cdot-}$ anion radicals, $CO_2^{\cdot-}(H_2O)_n$, are selectively prepared in an electron-impact free jet of $CO_2^{\cdot-}$ containing H_2O. Mass spectrometric measurement reveals that $CO_2^{\cdot-}(H_2O)_n$ reacts with CH_3I to form an anion with $[(CO_2)(H_2O)]^-$ stoichiometry. The product $[(CO_2)(H_2O)]^-$ is further identified as the anion of acetyloxy iodide, $CH_3CO_2I^-$, based on the observation that $[(CO_2)(H_2O)]^-$ photodissociates at 532 nm into $CH_3CO_2^-$ + I or CH_3CO_2 + I^- channels. The $CO_2^{\cdot-}(H_2O)_n$ + CH_3I reaction thus presents a sharp contrast to the corresponding reaction in solution: the gas-phase $CO_2^{\cdot-}(H_2O)_n$ behaves as a carboxylation reagent for alkyl halide (RX), whereas in aqueous solutions the reaction proceeds as $CO_2^{\cdot-}$ + RX → CO_2 + R + X^-. *Ab initio* calculations suggest that $CO_2^{\cdot-}(H_2O)_n$ can take on structures preferable for radical reactions: the hydraion occurs on the O atoms of $CO_2^{\cdot-}$ and the unpaired electron on the C atom remains uncovered with H_2O solvents. The reaction mechanism of the $CO_2^{\cdot-}(H_2O)_n$ + CH_3I process is discussed in conjunction with previous results of $(CO_2)_n^{\cdot-}$ + CH_3I.[1)]

Reference

1) T. Tsukuda, M. Saeki, S. Iwata and T. Nagata, *J. Phys. Chem. A* **101**, 5103–5110 (1997).

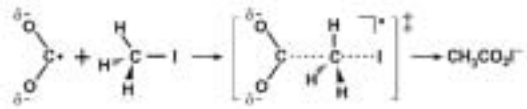

Scheme 1.

VIII-T Nanoscale Characterization of Heterogeneous Catalyst Surfaces

Heterogeneous catalysis occurs on a surface of a solid catalyst. Active centers for heterogeneous catalysis commonly consist of clusters of several surface atoms, and thus a long-range order of surface atoms is not normally required. Therefore, when using precious metals as catalysts, nanometer-scale superfine particles are commonly employed in order to increase its surface area and to decrease the amount of catalysts. This introduces difficulties in characterizing the catalyst surfaces and their active centers, because characterization techniques of solid surfaces at nanometer-scale are not well established. Here we mainly used scanning probe microscopes, in conjunction with other surface characterization techniques, to characterize catalytically active centers as well as the nature of catalyst-support interactions.

VIII-T-1 Monte Carlo Simulation of Pyridine Base Adsorption on Heulandite (010)

YOKOI, Yasuto[1]; YELKEN, Gulnihal[2]; OUMI, Yasunori[3]; KOBAYASHI, Yasunori[1]; KUBO, Momoji[1]; MIYAMOTO, Akira[1]; KOMIYAMA, Masaharu[4]
([1]Tohoku Univ.; [2]Izmir Inst. Tech.; [3]Japan Inst. Sci. Tech.; [4]IMS and Yamanashi Univ.)

[*Appl. Surf. Sci.* **188**, 377–380 (2002)]

Adsorption of pyridine base molecules (pyridine and α-, β- and γ-picolines) on a surface of a natural zeolite, heulandite (010), was examined by Monte Carlo simulations. Two types of adsorption areas were identified on heulandite (010) bound by surface OH arrays, and each area showed different influence on the adsorption and orientation for pyridine base molecules. The presence of methyl group and its position within the adsorbed molecule also influenced its adsorption characteristics. For pyridine adsorption, molecular dynamics simulation was also performed. The results were compared with existing experimental data obtained through atomic force microscopy.

VIII-T-2 Apparent Local Structural Change Caused by Ultraviolet Light on a TiO_2 Surface Observed by Scanning Tunneling Microscopy

KOMIYAMA, Masaharu[1]; LI, Yanjun; YIN, Donghong[2]
([1]IMS and Yamanashi Univ.; [2]Funan Normal Univ.)

[*Jpn. J. Appl. Phys.* **41**, 4936–4938 (2002)]

An apparent local surface structural change at nano-scale was observed by scanning tunneling microscopy on a TiO_2 surface upon irradiation with ultraviolet (UV) light. This phenomenon was reversible with UV light irradiation, and was interpreted to be due to the local accumulation of photoexcited states. This is the first real-space observation of inhomogeneous local charge distribution under UV light irradiation at nanoscale on a semiconductive photocatalyst surface, which may help identify the photocatalytic active sites and elucidate their reaction mechanisms.

VIII-T-3 Electronic Structure Change on TiO_2 Surface due to UV Light Irradiation

KOMIYAMA, Masaharu[1]; YIN, Donghong[2]; LI, Yanjun
([1]IMS and Yamanashi Univ.; [2]Funan Normal Univ.)

[*Stud. Surf. Sci. Catal.* **145**, 153–156 (2003)]

Photocatalysts have been paid extensive attentions for their environmental as well as energy applications. Although each photocatalytic processes may be different in terms of their kinetics and surface reactions involved, they are all initiated with the photoexcitation of TiO_2 electrons, the process commonly understood and explained by the so-called band model which assumes an infinite array of crystallographic lattice points. In contrast, catalytic reactions involved in photocatalysis are highly local in nature: some reactant may need particular local arrangements of atoms that are present on the catalyst surface, and others may need particular local electronic states of the surface atoms to provide unique adsorption or reaction sites. Despite this gap that exist in between the two descriptions involved in heterogeneous photocatalysis (band model and local catalysis), no efforts to address and bridge this gap are known to the authors. The present report is the first of such attempts, and examines the local electronic characters of TiO_2 surface upon UV-light illumination by means of scanning tunneling microscopy (STM).

VIII-T-4 In Situ Observations of Tetraamineplatinum (II) Hydroxide Adsorption from Its Aqueous Solution on Heulandite (010) Surface by Atomic Force Microscopy

KOMIYAMA, Masaharu[1]; LI, Yanjun; GU, Ning[2]
([1]IMS and Yamanashi Univ.; [2]Southeast Univ.)

Adsorption of tetraamineplatinum (II) hydroxide, a Pt catalyst precursor, from its aqueous solution on a (010) surface of a natural zeolite heulandite was observed, in situ, by atomic force microscopy (AFM). The Pt complex exhibited certain adsorption habits on the surface, frequently forming a short chain along the zeolite *a* axis, separated by three times the *c* unit cell length in the *c* direction. Possible adsorption sites on the surface were identified and discussed. The present work constitutes the first in situ atomic-level observation of a

liquid-phase preparation process of supported metal catalysts.

VIII-T-5 Defect Creation on Rutile TiO_2 (110)-(1x1) Surface due to Light Irradiation Observed by Scanning Tunneling Microscopy

LI, Yanjun; MATSUMOTO, Taki; GU, Ning[1]; KOMIYAMA, Masaharu[2]
([1]Southeast Univ.; [2]IMS and Yamanashi Univ.)

Laser light irradiation created atomic-scale structures on rutile TiO_2 (110)-(1×1) surface, the number of which increased with irradiation time. The created bright structures appear to be cross-shaped, each bridging two titanium [001] rows, and having dark areas in the front and in the back. The structure is interpreted as an oxygen deficiency on the (1×1) surface, and the one of the dark spots around the structure as the oxygen atom displaced from its original position. The structure often appears as a pair aligned along [1-10] direction, which could be viewed as a local (2×3) structure.

VIII-T-6 Crater Structures on a Molybdenite Basal Plane Observed by Ultra-High Vacuum Scanning Tunneling Microscopy

KOMIYAMA, Masaharu[1]; KIYOHARA, Kohei[2]; LI, Yanjun; KUBOTA, Takeshi[2]; OKAMOTO, Yasuaki[2]
([1]IMS and Yamanashi Univ.; [2]Shimane Univ.)

Atomic structure of a natural molybdenite (MoS_2) single crystal basal plane was examined by ultra-high vacuum scanning tunneling microscopy (UHV-STM). After high-temperature (473 K) resulfidation, numbers of crater structures with diameters ranging from 6 to 8 nm were observed. Atomic structures within these craters were continuous from the surrounding terrace, with no step structures at the rims of the craters. Atoms in the bottom of the craters showed higher corrugations compared to the terrace atoms, indicating perturbed electronic states in the craters. Its implication in hydrodesulfurization activity over MoS_2 basal plane is discussed.

VIII-U Fundamental Study on Electrostatic Manipulation of Biomolecules and its Application to Gene Analysis

Since conventional DNA sequencing method can determine up to 1000 base pairs at one time, longer DNA must be cut into small fragments. However, order information among these fragments is inevitably lost resulting in tremendous post sequencing process to do a puzzle. To cope with the problem, we have studied DNA sequencing method based on one-by-one DNA handling. The method includes (1) electrostatic manipulation of genomic DNA, (2) fixation in a stretched from, (3) cut from the terminus, (4) recovery and amplification of the fragments.

VIII-U-1 Manipulation of Single Coiled DNA Molecules by Laser Clustering of Microparticles

HIRANO, Ken[1]; BABA, Yoshinobu[1]; MATSUZAWA, Yukiko[2]; KATSURA, Shinji[2]; MIZUNO, Akira
([1]Tokushima Univ.; [2]Toyohashi Univ. Tech.)

A method of manipulating single DNA molecules for application in single-molecule analysis was developed. Manipulation of laser clustered beads allowed manipulation of a single DNA molecule without modification. Figure 1 shows sequential photographs of a DNA molecule anchored at both end to a glass surface. The DNA molecule was tweezed at one point and successfully stretched (figure1(b)–(d)). The stretched DNA molecule returned to its original form after releasing by turning off the laser beam (figure1(e)).

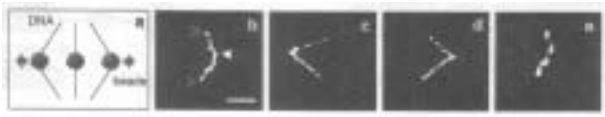

Figure 1. Sequential images of the manipulation of a single DNA molecule using laser clustering of 0.2 μm latex beads.

VIII-U-2 One-End Immobilization of Individual DNA Molecules on a Functional Hydrophobic Glass Surface

MATSUURA, Shun-ichi[1]; KURITA, Hirofumi[1]; NAKANO, Michihiko[1]; KOMATSU, Jun[1]; TAKASHIMA, Kazunori[1]; KATSURA, Shinji[1]; MIZUNO, Akira
([1]Toyohashi Univ. Tech.)

An extremely simple technique of DNA immobilization on a hydrophobic glass surface was developed. The technique includes hydrophobic processing of a cover slip with dichlorodimethylsilane and modification of the terminus of DNA with sulfhydryl group. Dichlorodimethylsilane reacts with silanol groups on a cover slip surface (figure1(a)) and forms hydrophobic monolayer of dichlorodimethylsilane (figure1(b)). Sulfhydryl group of DNA molecule modified at one terminus reacts on the dichlorodimethylsilane layer resulting in anchoring of a single DNA molecule to the cover slip (figure1(c))

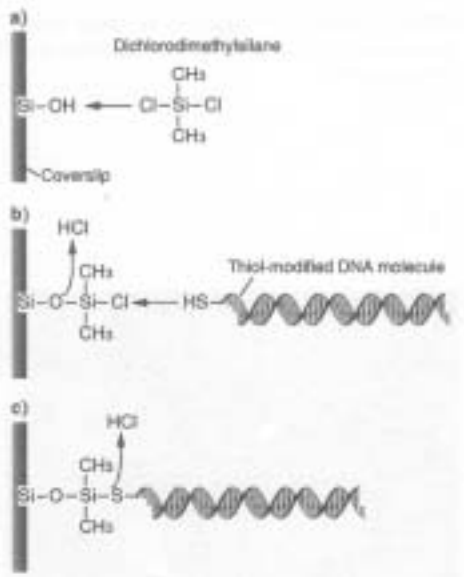

Figure 1. Schematic diagram of reaction mechanism of DNA immobilization on a dichlorodimethylsilane-coated surface.

VIII-U-3 Single-Molecule PCR using Water-in-Oil Emulsion

NAKANO, Michihiko[1]; KOMATSU, Jun[1]; MATSUURA, Shun-ichi[1]; TAKASHIMA, Kazunori[1]; KATSURA, Shinji[1]; MIZUNO, Akira
([1]Toyohashi Univ. Tech.)

[*J. Biotechnology* **102**, 117–124 (2003)]

A simple PCR method utilizing a water-in-oil (W/O) emulsion was developed. Numerous numbers of droplets serving as reaction mixture are included in bulk oil phase in this system. The method allows amplification of very low concentration DNA samples because such droplets increase effective concentration of template DNA. In this method, PCR was started with emulsified samples, in which template DNA was amplified to sufficient amount applicable to conventional PCR next step. After the first PCR in emulsified state was completed, W/O emulsion was broken by centrifuging to start the conventional PCR. By using this method consisting of 13 and 25 cycles in the first and the second step, target DNA of which concentration is 1molecule/tube was successfully amplified.

VIII-U-4 FIM Observation of DNA Molecules

FURUMAKI, Takuya[1]; TSUJI, Yuuta[1]; NAKANO,

Michihiko[1]; TAKASHIMA, Kazunori[1]; UCHIDA, Hironaga[1]; KATSURA, Shinji[1]; MIZUNO, Akira
([1]Toyohashi Univ. Tech.)

An application of field ion microscope (FIM) to DNA sequencing has been experimentally studied. By applying a DC voltage to a FIM tip on which a DNA molecule is attached, the bases may be released and carried along the electric field. Ultra high-speed genome analysis will be feasible by detecting the digested bases. We constructed a DNA sequencing system based on a field ion microscope. An electro-polished gold was used as a substrate. DNA molecules modified with sulfhydryl (-SH) group prepared by PCR (polymerase chain reaction) were attached on the needle tip. High voltage up to 7 kV was applied to DNA-bound tip to observe the FIM images. It was found that binding of DNA on samples decreased on-set voltage of FIM images suggesting the existence of an atomically rough surface.

VIII-U-5 Micro Reactor System Based on Water-in-Oil Emulsion

NAKANO, Michihiko[1]; NAKAI, Naohito[1]; TAKASHIMA, Kazunori[1]; KATSURA, Shinji[1]; MIZUNO, Akira
([1]Toyohashi Univ. Tech.)

A method called as “combinatory chemistry” has been proposed to create useful enzymes higher active and stable. Since the combinatory chemistry is based on multiple mutations of enzymes and evaluation of those mutants, high through-put production and analysis of enzymes is required to promote this method. For this purpose, miniaturization of reactors has been developed by using micro fabrication techniques. However, the miniaturization accompanies with difficulty of liquid handling, therefore size of reactors was limited by liquid handling technique.

To overcome this problem, we have been engaged in development of reaction system based on water-in-oil emulsion. W/O emulsion contains large amount of water droplets in continuous oil phase. Because many biological molecules are hydrophilic, those can be enclosed in the droplets. This indicates that the droplets play a role of small reactors, however reaction control of the droplets has not been established. We are developing unit operations such as transport, fusion to achieve reaction control of the droplets. In this term, we have developed transport methods based on electro-osmosis and charge injection. We have succeeded to drive the droplets by both methods. Now, we are engaged in improving controllability of droplet transport.

VIII-V Studies of Electronic Structure of Organic Thin Films

Electronic structures of organic film surface and organic/inorganic interface are expected to play an important role in organic-device properties. It is important to clarify the characteristics of not only occupied states but also unoccupied states for organic thin films, since the device properties such as the efficiency of the electron and/or the hole injection depend on the position and/or the distribution of these electronic states. We have investigated the electronic structure of organic film surface and organic/inorganic interface using surface sensitive spectroscopies such as photoelectron spectroscopy and near-edge x-ray absorption fine structure (NEXAFS). To help the assignment of NEXAFS spectra, we use the photon energy dependence of photon-stimulated ion desorption, since the chemical bond scission by inner-shell excitation depends on the electronic configuration of the excited state.

VIII-V-1 Photodegradation of Poly(Tetrafluoroethylene) and Poly(Vinylidene Fluoride) Thin Films by Inner Shell Excitation

OKUDAIRA, K. Koji; YAMANE, Hiroyuki[1]; ITO, Kazuyuki[1]; IMAMURA, Motoyasu[2]; HASEGAWA, Shinji; UENO, Nobuo[1]
([1]Chiba Univ.; [2]AIST)

[*Surf. Rev. Lett.* **9**, 335–340 (2002)]

Ion time-of-flight (TOF) mass spectra of poly(tetrafluoroethylene) (PTFE) and poly(vinylidene fluoride) (PVDF) thin films near fluorine and carbon *K*-edges were observed. For PTFE thin films peaks corresponding to F^+, CF^+, and CF_3^+ appeared, while for PVDF F^+ and H^+ were mainly observed. They indicate that for PTFE the polymer chain (C–C bonds) as well as C–F bonds are broken by irradiation of photons near fluorine and carbon *K*-edges, while for PVDF the bond scission occurs mainly at the C–F and C–H bond. In Figures 1 (a), (b), and (c) partial ion yield (PIY) spectra of F^+, CF^+ and CF_3^+ for PTFE thin films are compared with total electron yield (TEY) near the fluorine *K* absorption edge. PIY spectra of F^+, CF^+ and CF_3^+ are different from the TEY spectrum. The intense PIY feature of F^+ appears at $h\nu$ = 689 eV corresponding to the transition from F1*s* to σ(C–F)*. The PIY intensity of F^+ at $h\nu$ = 689 eV is much stronger than at $h\nu$ = 693 eV corresponding to the transition from F1*s* to σ(C–C)*, while the TEY intensity at $h\nu$ = 689 eV is slightly stronger than that at $h\nu$ = 693 eV. That is, the C–F bond scission by irradiation of photons at $h\nu$ = 689 eV (F1*s* → σ(C–F)*) is expected to occur more effectively than at $h\nu$ = 693 eV(F1*s* → σ(C–C)*). For the case of PVDF, the intense PIY feature of F^+ appears at the transition from F1*s* to σ(C–F)*. The excitation from fluorine 1*s* to σ(C–F)* is specially efficient for F^+ ion production for both PTFE and PVDF.

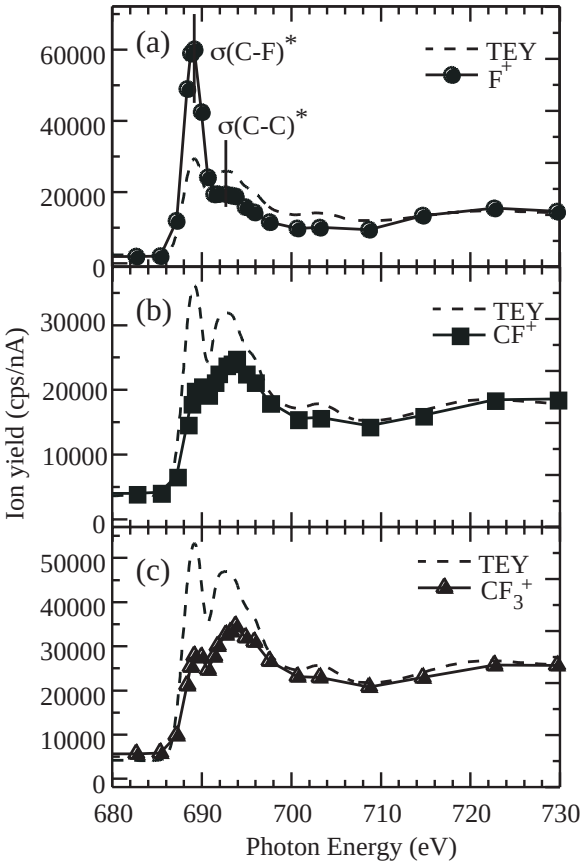

Figure 1. PIY spectra of (a) F^+, (b) CF^+ and (c) CF_3^+ for PTFE thin film near the fluorine *K* absorption edge. TEY spectra (broken curve) are also shown for comparison. TEY spectra are renormalized at $h\nu$ = 682.5 eV and at $h\nu$ = 730 eV to fit PIY intensities.

VIII-V-2 Excited States of Perfluorinated Oligo(p-phenylene) by Inner-Shell Excitation

OKUDAIRA, K. Koji; OHARA, Kosuke[1]; SETOYAMA, Hiroyuki[1]; SUZUKI, Toshiyasu; SAKAMOTO, Youichi[1]; IMAMURA, Motoyasu[2]; HASEGAWA, Shinji; MASE, Kazuhiko[3]; UENO, Nobuo[1]
([1]Chiba Univ.; [2]AIST; [3]IMSS)

[*Nucl. Instrum. Methods Phys. Res., Sect. B* **199**, 265–269 (2003)]

Ion time-of-flight (TOF) mass spectra and near edge x-ray absorption fine structure (NEXAFS) spectra of

perfluorinated oligo(*p*-phenylene) (PF-8P) films near fluorine (F) and carbon (C) *K*-edges were observed. In ion TOF mass spectra near F and C *K*-edges, F^+, CF^+, and CF_3^+ were intensely observed. It indicates that C–C bonds of phenyl ring as well as C–F bonds are broken by irradiation of photons near F and C *K*-edges. Partial ion yield (PIY) spectra of PF-8P show clear $h\nu$ dependence near F and C *K*-edges. Especially, near F *K*-edge, the PIY spectra of F^+ increases remarkably at $h\nu$ = 689.2 eV, which corresponds to the lowest peak in NEXAFS. The lowest peak in the NEXAFS near fluorine *K*-edge is assigned to the transition from F1*s* to σ(C–F)*. Furthermore, from the analysis of PIY spectra of PF-8P near carbon K-edge, the peak at $h\nu$ = 289.5 eV is ascribed to the transition from C1*s* to σ(C–F)*.

VIII-W Electronic Structure and Collision Dynamics of Atoms and Molecules Studied by Electron Impact near the Bethe Ridge

Binary (*e*,2*e*) or electron momentum spectroscopy (EMS), based on the so-called electron Compton scattering, is a high-energy electron-impact ionization experiment in which kinematics of all the electrons are fully determined by coincident detection of the two outgoing electrons. The ability to measure electron momentum distribution for each molecular orbital, square modulus of the momentum-space wavefunction, is a remarkable feature of this technique. Since momentum-space and position-space are uniquely related to each other by Fourier transformation, electron momentum distribution is highly sensitive to diffuse parts of the position-space wavefunction that are important in chemical reaction and molecular recognition. However, the potential of EMS has not been fully achieved as yet, due mainly to the extremely small cross sections involved. For these reasons, together with various improvements to spectrometers we are aiming at developing next-generation EMS for chemistry, which would give quite unique and versatile information on electronic structure of molecules.

VIII-W-1 A High Sensitivity Electron Momentum Spectrometer with Simultaneous Detection in Energy and Momentum

TAKAHASHI, Masahiko; SAITO, Taku[1]; MATSUO, Motoaki[1]; UDAGAWA, Yasuo[1]
([1]Tohoku Univ.)

[*Rev. Sci. Instrum.* **73**, 2242 (2002)]

A new apparatus for electron-electron coincidence experiments has been developed to examine molecular orbital patterns quantitatively by electron momentum spectroscopy. Using a spherical analyzer and position-sensitive detectors, it enables one to measure energy and angular correlations between the two outgoing electrons simultaneously. The design and performance of the apparatus is reported together with results on Ar to show extensive improvements in coincidence count rates and statistical precision, covering a wide range of binding energies and momenta.

VIII-W-2 The Impact Energy Dependence of Momentum Profiles of Glyoxal and Biacetyl and Comparison with Theory at Their High-Energy Limits

TAKAHASHI, Masahiko; SAITO, Taku[1]; HIRAKA, Jyunya[1]; UDAGAWA, Yasuo[1]
([1]Tohoku Univ.)

[*J. Phys. B: At., Mol. Opt. Phys.* **36**, 2539 (2003)]

We report an electron momentum spectroscopy study of the two outermost orbitals of dicarbonyls, glyoxal and biacetyl. The experiments were performed at impact energies of 800, 1200 and 1600 eV by using a recently developed multichannel (*e*,2*e*) spectrometer. The experimental momentum profiles clearly show remarkable variations in the low momentum region with increase in impact energy. Furthermore, it has been found that the two molecules reach their high-energy limits at different impact energies, indicating that the range of the validity of the plane-wave impulse approximation (PWIA) largely depends on the target in question. The results at 1600 eV are employed for comparisons with PWIA calculations using Hartree-Fock and density functional theory (DFT). While the DFT calculations reproduce well the observations for glyoxal, considerable discrepancies between experiment and theory exist in biacetyl.

VIII-W-3 (*e*,2*e*) Ionization-Excitation of H_2

TAKAHASHI, Masahiko; KHAJURIA, Yugal; UDAGAWA, Yasuo[1]
([1]Tohoku Univ.)

[*Phys. Rev. A* in press]

Binary (*e*,2*e*) measurements are reported for simultaneous ionization-excitation processes of H_2. The experiments were performed at impact energies of 1200, 1600 and 2000 eV using an energy- and momentum-dispersive spectrometer. Momentum profiles for transitions to the $2s\sigma_g$ and $2p\sigma_u$ excited final ion states are presented as normalized intensities relative to the cross section of the primary ionization to the $1s\sigma_g$ ground ion state. The results are compared with theoretical calculations of Lermer *et al.* [*Phys. Rev. A* **56**, 1393 (1997)] using the first-order plane-wave impulse approximation. Certain features of the discrepancies between experiment and theory can be explained by incorporating contributions from the second-order two-step mechanisms into the (*e*,2*e*) cross sections. Furthermore, the present results suggest that $2s\sigma_g$ and $2p\sigma_u$ cross sections approach their high-energy limits in different ways.

VIII-W-4 Electron Momentum Spectroscopy of N_2O

KHAJURIA, Yugal; TAKAHASHI, Masahiko; UDAGAWA, Yasuo[1]
([1]Tohoku Univ.)

[*J. Electron Spectrosc.* in press]

An electron momentum spectroscopy study of the outer valence orbitals of N_2O is reported. The experi-

ments were performed at impact energies of 1000, 1200, 1600 and 1800 eV by using a recently developed multichannel (*e*,2*e*) spectrometer. The experimental momentum profiles are compared with each other to examine their impact energy dependence. The results are used for comparisons with Hartree-Fock (HF) and density functional theory (DFT) calculations using various basis sets. The DFT and HF calculations with large basis sets are in good agreement with the measured electron momentum profiles, with the exception of that of the 6σ orbital for which the HF method underestimates the cross sections in the low momentum region.

VIII-W-5 A High Sensitivity Electron Momentum Spectrometer with Two-Dimensional Detectors and Electron Momentum Distributions of Several Simple Molecules

TAKAHASHI, Masahiko; UDAGAWA, Yasuo[1]
([1]Tohoku Univ.)

[*J. Electron Spectrosc.* submitted]

Electron momentum spectroscopy (EMS) makes it possible to examine orbital patterns of individual molecular orbitals in momentum space. A new spectrometer for electron-electron coincidence experiments for EMS has been developed to obtain orbital patterns quantitatively. Using a spherical analyzer and position-sensitive two-dimensional detectors combined with fast electronics, simultaneous measurements of energy and angular correlations between the two outgoing electrons can be made. This spectrometer features high sensitivity and an ease of changing impact energies. Details of the apparatus are described and impact energy dependence of electron momentum distributions of the HOMO of H_2 and biacetyl are compared.

VIII-W-6 Electron-Impact Double Ionization Mechanisms in the Impulsive Regime

VAN BOEYEN, Roger W.[1]; WATANABE, Noboru; DOERING, John P.[1]; MOORE, John H.[2]; COPLAN, Michael A.[2]; COOPER, John W.[2]
([1]Johns Hopkins Univ., USA; [2]Univ. Maryland, USA)

[*Phys. Rev. Lett.* submitted]

Five-fold differential cross sections (5DCS) for the electron-impact double ionization of the 3*s* electrons of magnesium have been measured in a high-impact-energy, high-momentum-transfer regime within the ionization mechanisms can be accurately described by simple models in which the ionization processes and the initial-state atomic properties can be separated. In the unique experimental geometry, the form of the measured cross sections provides strong evidence for impulsive two-collision ionization mechanisms. Second Born calculations are in agreement with the experimental data providing further evidence for the mechanisms. The implications for the measurement of two-electron densities are discussed.

VIII-W-7 Second Born Approximation Calculations of Double Ionization of Mg

WATANABE, Noboru; COOPER, John W.[1]; VAN BOEYEN, Roger W.[2]; MOORE, John H.[1]
([1]Univ. Maryland, USA; [2]Johns Hopkins Univ., USA)

Electron impact double ionization, also called the (*e*,3*e*) reaction, can provide direct information on correlated motion of atomic electrons, provided that the collision mechanism is known. Possible mechanisms for the (*e*,3*e*) reaction include shake-off (SO), two-step 1 (TS1), and two-step 2 (TS2). The SO and TS1 are of the first order in the projectile-target interaction, while the TS2 is a second-order process. In this study we theoretically examine contributions from TS2 in the scattering geometry chosen for the (*e*,3*e*) experiments of the Maryland group, which investigate correlated motion of the 3*s* electrons in the magnesium atom. It has been found that dominant contribution from the Second Born term is involved in the observed (*e*,3*e*) cross sections of Mg. Electron correlation effects in the initial target state are also studied using a configuration interaction wave function.

VIII-W-8 Orbital Momentum Profiles and Binding Energy Spectra for the Complete Valence Shell of CO

SAITO, Taku[1]; TAKAHASHI, Masahiko; UDAGAWA, Yasuo[1]
([1]Tohoku Univ.)

Electron momentum profiles and binding energy spectra for the complete valence shell of CO have been measured using an energy- and momentum-dispersive (*e*,2*e*) spectrometer at an impact energy of 1600 eV. It has been found that shapes of the orbital momentum profiles are well reproduced by Hartree-Fock calculations. Binding energy spectra and momentum profiles in the satellite region beyond 22 eV binding energy of CO are studied in detail, determining pole sterngth distributions of the molecule. Comparisions are made for the pole strength distributions with theoretical predictions of Ehara and Nakatsuji using the SAC-CI general-R method. The agreement between experiment and theory is generally good, but some discrepancies remain for ionization transitions with small pole strength lower than about 0.1.

VIII-W-9 (*e*,2*e*) Study on Ionization-Excitation and Double Ionization of He

TAKAHASHI, Masahiko; UDAGAWA, Yasuo[1]
([1]Tohoku Univ.)

A binary (*e*,2*e*) study has been carried out for He at an impact energy of 2000 eV using a recently developed energy- and momentum-dispersive spectrometer. Binding energy and momentum ranges up to about 100 eV and 4 au were then covered. Momentum distributions of the individual ionization-excitation transitions, converging to the double ionization threshold, have been compared with first-order plane-wave impulse

calculations of Mitroy *et al.* [*J. Phys. B* **18**, 4149 (1985)]. For the primary ionization that leaves the residual He^+ ion in the $n = 1$ ground state, agreement between experiment and theory is satisfactory. On the other hand, for ionization-excitation that leads to change of state of both the two target electrons the experiments always exhibit larger intensity than theory, suggesting noticeable contributions from the second-order two step mechanisms.

VIII-W-10 Development of a Triple Coincidence Spectrometer for a Complete Three-Dimensional Mapping of Electron Momentum Densities in Gaseous Molecules

TAKAHASHI, Masahiko; WATANABE, Noboru; UDAGAWA, Yasuo[1]; ELAND, John H. D.[2]
([1]Tohoku Univ.; [2]Oxford Univ., England)

Electron momentum spectroscopy has been developed as a powerful means for the investigation of electronic structure and electron correlation. In particular, the ability to measure electron momentum distribution for each molecular orbital, square modulus of the momentum-space wavefunction, is a remarkable feature of this technique. It is unfortunate, however, that experimentally observable electron momentum distribution is spherically averaged due to random orientation of gaseous targets, smearing out details of electronic structure inherently involved in the experiments.

To overcome the experimental difficulty a new apparatus has been developed for a complete three-dimensional mapping of electron momentum densities in gaseous molecules. Based on the axial recoil, measurements of vector correlations among the two outgoing electrons and fragment ion correspond to (*e*,2*e*) experiments with oriented molecules. Dissociation of molecular ions perpendicular to the incident electron momentum vector are detected with seven independent channeltrons, while the two outgoing electrons are detected with a pair of position-sensitive detectors. A schematic diagram of the kinematics of our experiments is shown in Figure 1.

Although there are substantial backgrounds due to a huge number of fragment ions produced by forward scattering of electron projectile, we have successfully measured genuine triple coincidence signals for the first time. Figure 2 shows an example of the results, which plots directional electron momentum densities obtained for the $2\sigma_g$ ionization of O_2. While the statistics of the data is not satisfactory, we can clearly see anisotropy of electron momentum densities. For establishing this method developments in detection of the outgoing electrons in the momentum dispersive plane around full 2π azimuth are now in progress to increase sensitivity of two additional orders of magnitude.

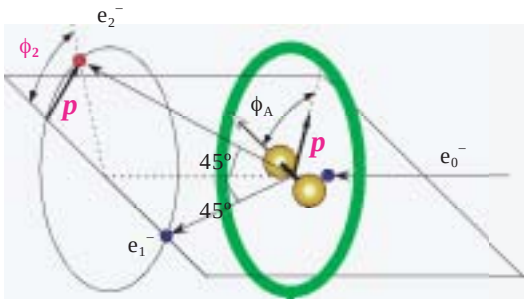

Figure 1. Schematic diagram of the kinematics of the (*e*,2*e*) directional momentum density experiment. The spectrometer records only the component of momentum perpendicular to the scattering plane. When dissociation takes place in the perpendicular plane, the channeltron detectors will record the arrival of the dissociation products.

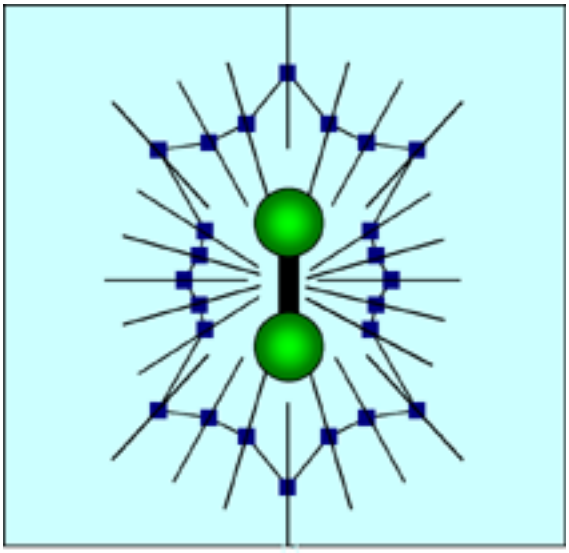

Figure 2. Directional electron momentum densities for the $2\sigma_g$ orbital ionization of O_2.

VIII-X Electronic Structure and Collision Dynamics of Atoms and Molecules Studied by Photon Impact

The group takes another, photon-impact, approach to issues of electronic structure and collision dynamics, since photon-impact and electron-impact or photoelectric effects and Compton scattering are complementary to each other.

VIII-X-1 Multilayer Polarizers for the Use of He-I and He-II Resonance Lines

HATANO, Tadashi[1]; KONDO, Yuzi[1]; SAITO, Katsuhiko[1]; EJIMA, Takeo[1]; WATANABE, Makoto[1]; TAKAHASHI, Masahiko
([1]Tohoku Univ.)

[*Surf. Rev. Lett.* **9**, 587 (2002)]

Multilayer polarizers for the use of He resonance lines have been developed. Si/Mg and SiC/Mg multilayers were designed and fabricated for the He-I and He-II resonance lines, respectievely. The performance was checked by the use of synchrotron radiation. The polarizance and *s*-reflectance of the He-II polarizer measured at an angle of incidence of 40° were 0.98 and 41%, respectievely. The polarizance of the He-I polarizer measured at an angle of incidence of 31.5° was 0.96.

VIII-X-2 Polarization Measurements of Laboratory VUV Light: A First Comparison between Multilayer Polarizers and Photoelectron Angular Distributions

TAKAHASHI, Masahiko; HATANO, Tadashi[1]; EJIMA, Takeo[1]; KONDO, Yuzi[1]; SAITO, Katsuhiko[1]; WATANABE, Makoto[1]; KINUGAWA, Tohru[2]; ELAND, John H. D.[2]
([1]Tohoku Univ.; [2]Oxford Univ., England)

[*J. Electron Spectrosc.* **130**, 79 (2003)]

The use of photoelectron angular distributions to determine the linear polarization of VUV light over a wide range of photon energies is demonstrated. Light at wavelengths from 25.6 to 73.6 nm, partially polarized by large angle reflections in a toroidal grating monochromator and at a refocus mirror, has been analyzed. The results are validated by comparison measurements at spot wavelengths using multilayer polarizers.

VIII-X-3 Carbon *K*-Shell Photoelectron Angular Distribution from Fixed-in-Space CO_2 Molecules

SAITO, Norio[1]; FANIS, Albert De[2]; KUBOZUKA, Kenichiro[3]; MACHIDA, Masatake[3]; TAKAHASHI, Masahiko; YOSHIDA, Hiroaki[4]; SUZUKI, Isao H.[1]; CASSIMI, Amine[5]; CZASCH, Achim[6]; DÖRNER, Reinhard[6]; WANG, Kwanghsi[7]; ZIMMERMANN, Björn[7]; MCKOY, Vincent[7]; KOYANO, Inosuke[3]; UEDA, Kiyoshi[2]
([1]Natl. Metrology Inst.; [2]Tohoku Univ.; [3]Himeji Inst. Tech.; [4]Hiroshima Univ.; [5]Univ. Caen, France; [6]Univ. Frankfurt, Germany; [7]California Inst. Tech., USA)

[*J. Phys. B: At., Mol. Opt. Phys.* **36**, L25 (2003)]

Measurements of photoelectron angular distributions for carbon *K*-shell ionization of fixed-in-space CO_2 molecules with the molecular axis oriented along, perpendicular and at 45° to the electric vector of the light are reported. The major features of these measured spectra are fairly well reproduced by calculations employing a relaxed-core Hartree-Fock approach. In contrast to the angular distribution for *K*-shell ionization of N_2, which exhibits a rich structure dominated by the f-wave (l = 3) at the shape resonance, the angular distribution for carbon *K*-shell photoionization of CO_2 is quite unstructured over the entire observed range across the shape resonance.

VIII-X-4 N 1*s* Photoionization Cross Sections of the NO Molecules in the Shape Resonance Region

HOSAKA, Kouichi[1]; ADACHI, Junichi[1,2]; TAKAHASHI, Masahiko; YAGISHITA, Akira[1,2]
([1]Tokyo Univ.; [2]KEK-PF)

[*J. Phys. B: At., Mol. Opt. Phys.* in press]

The N 1*s* partial photoionization cross sections of NO leading for the $^3\Pi$ and $^1\Pi$ ionic states have been measured in the shape resonance region for the first time. The twin local maxima in the cross sections have been tentatively assigned, based on the simple models for the photoabsorption intensities and for the branching ratio of the $^3\Pi$ and $^1\Pi$ ionic states from the σ^* shape resonance state.

VIII-X-5 Multiplet-Specific N 1*s* Photoelectron Angular Distributions from the Fixed-in-Space NO Molecules

HOSAKA, Kouichi[1]; ADACHI, Junichi[1,2]; TAKAHASHI, Masahiko; YAGISHITA, Akira[1,2]; LIN, Ping[3]; LUCCHESE, Robert R.[3]
([1]Tokyo Univ.; [2]KEK-PF; [3]Texas A&M Univ., USA)

[*Phys. Rev. Lett.* submitted]

Angular distributions of multiplet-specific N 1*s* photoelectrons from the fixed-in-space NO molecules have been measured for the first time. The dynamics of the σ^* shape resonance appeared in the channel leading to the $^3\Pi$ and $^1\Pi$ ionic states has been made clear from the analyses of the angular distributions. Multiplet-specific multichannel calculations have reproduced the observed angular distributions fairy well.

VIII-X-6 Shape-Resonance-Enhanced Vibrational Effects in the Angular Distributions of C 1*s* Photoelectrons from Fixed-in-Space CO Molecules

ADACHI, Junichi[1,2]; HOSAKA, Kouichi[1]; FURUYA, Shuusaku[3]; SOEJIMA, Kouich[3]; TAKAHASHI, Masahiko; YAGISHITA, Akira[1,2]; SEMENOV, Sergei K.[4]; CHEREPKOV, Nikolai A.[4]
([1]Tokyo Univ.; [2]KEK-PF; [3]Niigata Univ.; [4]State Univ. Aerospace Instrum., Russia)

[*Phys. Rev. Lett.* in press]

Angular distributions of C1*s* photoelectrons from fixed-in-space CO molecules have been measured with

vibrational resolution. A strong dependence of the angular distributions on the vibrational states of the residual molecular ion has been found for the first time in the region of the shape resonance. Calculations in the relaxed core Hartree-Fock approximation have reproduced the angular distributions fairly well in the general shapes of the angular distributions due to the correct description of nuclear motion as an average of the internuclear-distance-dependent dipole amplitudes.

VIII-X-7 Angular Distributions of Vibrationally Resolved C 1*s* Photoelectrons from Fixed-in-Space CO Molecules: Vibrational Effect in the Shape-Resonant C 1*s* Photoionization of CO

ADACHI, Junichi[1,2]; HOSAKA, Kouichi[1]; FURUYA, Shuusaku[3]; SOEJIMA, Kouich[3]; TAKAHASHI, Masahiko; YAGISHITA, Akira[1,2]; SEMENOV, Sergei K.[4]; CHEREPKOV, Nikolai A.[4]
([1]Tokyo Univ.; [2]KEK-PF; [3]Niigata Univ.; [4]State Univ. Aerospace Instrum., Russia)

[*J. Electron Spectrosc.* submitted]

We have measured molecular-frame photoelectron angular distributions (MF-PAD) for the vibrationally resolved C1*s* photoelectron from CO molecule in the s shape resonance region. The MF-PAD's for the v_f = 0,1, and 2 levels in the C1*s* → ε*l*σ channel are apparently different each other at each incident photon energy. These MF-PAD's agree woth the present theoretical results from the averaging the nuclear distance dependent dipole matrix elements with the relaxed core Hartree-Fock calculations. The present results show that the internuclear distance dependences of the phase and of the magnitude of the dipole matrix element play a crucial role in the C1*s* photoionization of CO.

VIII-X-8 Coulomb Hole in N_2, CO and O_2 Deduced from X-Ray Scattering Cross Sections

WATANABE, Noboru; KAMATA, Yohei[1]; YAMAUCHI, Kota[1]; UDAGAWA, Yasuo[1]; MÜLLER, Thomas[2]
([1]Tohoku Univ.; [2]Res. Cent. Jülich, Germany)

Total (elastic + inelastic) x-ray scattering cross sections $\sigma_{ee}(q)$ are very sensitive to electron correlation effects, since they are related to the Fourier transform of the radial electron-electron pair distribution function $P(r_{12})$.[1)] X-ray scattering experiments can hence provide a crucial check of whether or not a theoretical wave function takes electron correlation properly into consideration.

In this study, accurate $\sigma_{ee}(q)$ of N_2, CO and O_2 were measured by the use of the energy dispersive method up to a momentum transfer of q =12 *a.u.* $P(r_{12})$ was extracted from the cross sections. The Coulomb hole, defined as the difference between the exact $P(r_{12})$ and the corresponding function evaluated at Hartree-Fock limit, has been derived from experimental data. Comparison with configuration interaction calculations shows small but systematic differences between the theoretical and experimental results.

Reference

1) N. Watanabe *et al.*, *Review of Modern Quantum Chemistry*, K. D. Sen, Ed., World Scientific; Singapore, 553 (2002).

VIII-X-9 Absolute Surface Coverage Measurement Using a Vibrational Overtone

PIPINO, Andrew C. W.[1]; HOEFNAGELS, Johan P. M.[2]; WATANABE, Noboru
([1]Natl. Inst. Standards Tech., USA; [2]Eindhoven Univ. Tech., Netherland)

Sub-monolayer absolute surface number densities are obtained by cavity ring-down spectroscopy (CRDS) for trichloroethylene, cis-dichloroethylene, and trans-dichloroethylene adsorbed on silica using the first C–H stretching overtones, which are probed with the idler of a seeded optical parametric amplifier having a 0.075 cm^{-1} line width. The absolute surface number densities are found by invoking conservation of the integrated band intensity with adsorption together with knowledge of the transition moment orientation as derived from the adsorbate polarization anisotropy. The evanescent wave CRDS (EW-CRDS) measurements employ a fused-silica monolithic folded resonator with a peak finesse of ≈ 28,500 at 1650 nm. The absolute coverage of trichloroethylene on SiO_2 is also obtained by a mass-spectrometer-based surface-uptake technique, which is briefly contrasted with the EW-CRDS method. The sensitivity of EW-CRDS for trichloroethylene detection with an unclad resonator is found to be comparable to that obtained with a long-effective-path-length waveguide having a trichloroethylene-enriching polysiloxane coating.

VIII-Y Study on Compact X-Ray Sources

Electron storage rings are useful devices as x-ray sources. However, these synchrotron radiation facilities usually occupy large area and cost much. So that there have been many works to investigate compact x-ray sources using small electron accelerators. It is also useful to use laser undulator radiation or backward Compton scattering caused by the interactions of electron beams with laser photons, if we provide enough electrons to produce practical intensity of x-rays. RF-photocathode would produce high peak intensity electron beam so that it is a useful candidate of a electron source. It is necessary to search good materials as the photocathode for construction of a practical compact x-ray source. Cesium telluride has reported to have a good quantum efficiency, so that we have studied about it.

In order to generate high brilliant x-rays using small electron accelerators, we propose metal multi-foils as the target irradiated by the electron beam. We have studied x-ray intensity generated from the multi-foil target using Monte Carlo simulation code.

VIII-Y-1 Feasibility Study of X-Ray Generation by Using Metal Multi-Foil Target Irradiated by High Energy Electron Beam

TAKASHIMA, Yoshifumi; KOBAYAKAWA, Hisashi[1]; MATSUBARA, Masahide[1]
([1]Nagoya Univ.)

We performed feasibility study of x-ray source using metal multi-foil target irradiated by high energy electrons. Figure1 shows the sketch of the setup. High energy electron beams extracted from small accelerators are incident on metal multi-foil targets with small angles. X-rays generated in the foils by bremsstrahlung are reflected on the surface of the next foils if the incident angle is small enough to satisfy the total reflection condition.

We calculate the spectrum and angular spread of the x-rays radiated from the multi-foil targets by using EGS4[1)] simulation code. Figure 2 shows the geometry used in the EGS4 calculation. We use stacks of copper foils as the target. The thickness, width and length of a foil are 0.1 μm, 100 mm and 500 mm, respectively. We stack 100 foils as the target for EGS4 calculation. Incident electron energy was 150 MeV and the incident angle of the electron on the surface of the target was 1 mrad.

Figure 3 shows the angular spread of 5keV x-rays using multi-foil and bulk targets. The total thickness of the multi-foil is 10 μm which is the same thickness of the bulk target. The yield of the x-rays from multi-foil target is larger than that from the bulk target because of the reflection of x-rays between the foils.

The energy spectra of x-rays from the multi-foil and bulk targets are shown in Figure 4. X-ray intensity radiated from multi-foil is larger than bulk target in the low energy region, because low energy x-rays have large total reflection angles so that it is not absorbed in the target material but extracted by reflection between foils.

We calculated the spectrum and angular distribution of x-rays generated from metal multi-foils irradiated by high energy electrons using EGS4 simulation code. For further study, we should include the effect of transition radiation in the calculation in order to estimate x-ray intensity more precisely.

Reference

1) W. R. Nelson, H. Hirayama and D. W. O. Rogers, SLAC-Report-256, (1985).

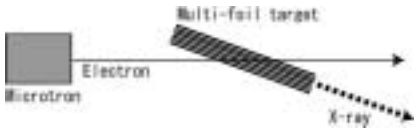

Figure 1. Sketch of experimental setup using multi-foil target.

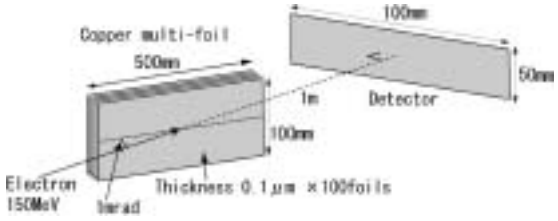

Figure 2. Geometry used in EGS4 simulation.

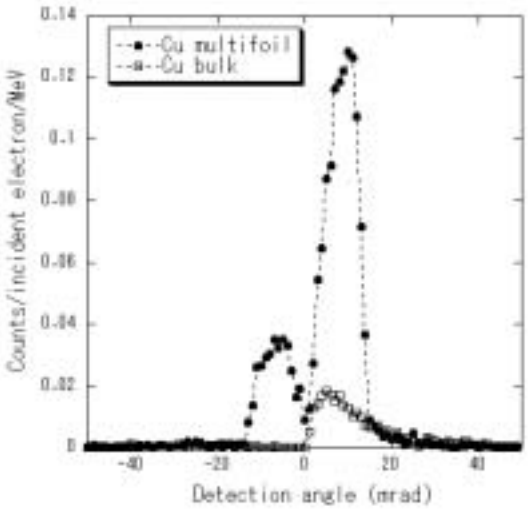

Figure 3. Angular distribution of x-rays generated from multi-foil and bulk targets.

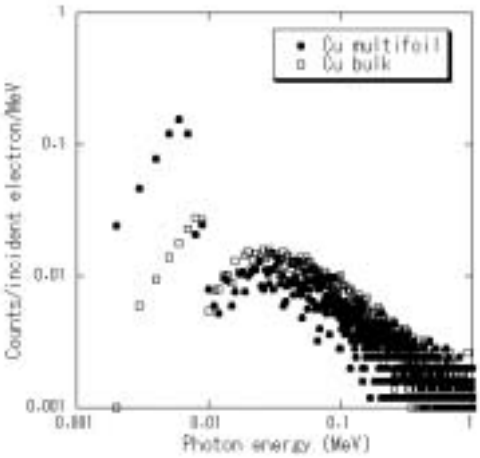

Figure 4. Energy spectrum of x-rays generated from multi-foil and bulk targets.

VIII-Z Syntheses of Fullerene-Based New Materials with Novel Physical Properties and Their Application toward New-Generation Electronic Devices

Fullerene-based new materials are synthesized and their structures and electronic properties are studied in solid, thin film and nanometer scale. The crystal structures of metallofullerene solids are determined by Rietveld refinements for X-ray diffraction patterns with synchrotron radiation. The resistivity and field effect transistor (FET) characteristics are studied with thin films of metallofullerens and higher-fullerenes. Furthermore, the scanning tunneling microscopy (STM) and scanning tunneling spectroscopy (STS) of metallofullerenes deposited onto the well-defined semiconducting surfaces are studied under ultrahigh vacuum.

VIII-Z-1 Crystal Structure and Electronic Transport of Dy@C_{82}

KUBOZONO, Yoshihiro; TAKABAYASHI, Yasuhiro[1]; SHIBATA, Kana[2]; KANBARA, Takayoshi[2]; FUJIKI, Satoshi; KASHINO, Setsuo[2]; FUJIWARA, Akihiko[3]; EMURA, Shuichi[4]
([1]IMS and Okayama Univ.; [2]Okayama Univ.; [3]JAIST; [4]Osaka Univ.)

[*Phys. Rev. B* **67**, 115410 (2003)]

The crystal structure of Dy@C_{82} isomer I at 298 K has been determined by Rietveld refinement for x-ray powder diffraction with synchrotron radiation. Isomer I shows a simple cubic structure (sc: $Pa\bar{3}$) with a lattice constant a of 15.78(1) Å. The C_2 axis of a C_{2v}-C_{82} cage aligns along the [111] direction of this crystal lattice. The C_{82} cage is orientationally disordered to satisfy a $\bar{3}$ symmetry along [111], which is requested in this space group. The large thermal parameter for the Dy atom estimated from the x-ray diffraction probably reflects a large disorder caused by a floating motion of the Dy atom inside the C_{82} cage as well as a ratchet-type motion of the Dy@C_{82} molecule. The electronic transport of thin film of Dy@C_{82} shows a semiconducting behavior. The energy gap E_g is estimated to be 0.2 eV. Further, the variation of valence from Dy^{3+} to Dy^{2+} is found by metal doping into the Dy@C_{82} crystals.

VIII-Z-2 Synthesis, Structure, and Magnetic Properties of the Fullerene-Based Ferromagnets, Eu_3C_{70} and Eu_9C_{70}

TAKENOBU, Taishi[1]; CHI, Dam Hieu[2]; MARGADONNA, Serena[3]; PRASSIDES, Kosmas[4]; KUBOZONO, Yoshihiro; FITCH, Andrew N.[5]; KATO, Ken-ichi[6]; IWASA, Yoshihiro[1]
([1]Tohoku Univ.; [2]JAIST; [3]Univ. Cambridge; [4]Univ. Sussex; [5]European Synchrotron Radiation Facility; [6]JASRI)

[*J. Am. Chem. Soc.* **125**, 1897 (2003)]

Intercalation of C_{70} with europium affords two kinds of magnetic compounds, a canted antiferromagnet Eu_xC_{70}($x \approx 3$) and a ferromagnet Eu_xC_{70}($x \approx 9$) with transition temperatures (T_c) of 5 and 38 K, respectively. The Curie constants in the paramagnetic phase and the saturation moment in the ferromagnetic phase are both understood by the full moment of Eu^{2+} for both systems. The structure of $Eu_{3-\delta}C_{70}$ ($\delta \approx 0.27$) is pseudo-monoclinic, derived by a simple deformation of the parent face-centered cubic (*fcc*) structure. $Eu_{9-\delta}C_{70}$ ($\delta \approx 0.2$) forms an *fcc* structure, in which cuboctahedral clustering of Eu^{2+} ions is observed in the enhanced size octahedral holes. The observed T_c of the $Eu_{9-\delta}C_{70}$ ferromagnet is comparable to or larger than those of simple binary Eu-based ferromagnets, such as Eu chalcogenides or carbides, despite the low atomic ratio of Eu in the chemical formulas. This can be understood by the short Eu^{2+}–Eu^{2+} distances and high coordination numbers permitted by the multiple occupation by Eu^{2+} ions of the expanded octahedral interstitial sites in higher fullerene-based solids.

VIII-Z-3 Pressure-Induced Structural Phase Transition in Fullerides Doped with Rare Earth Metals

CHI, Dam Hieu[1]; IWASA, Yoshihiro[1,2]; UEHARA, Katsuyuki[1]; TAKENOBU, Taishi[2]; ITO, Takayoshi[1]; MITANI, Tadaoki[1]; NISHIBORI, Eiji[3]; TAKATA, Masaki[3,4]; SAKATA, Makoto[3]; OHISHI, Y.[4]; KATO, Ken-ichi[4]; KUBOZONO, Yoshihiro
([1]JAIST; [2]Tohoku Univ.; [3]Nagoya Univ.; [4]JASRI)

[*Phys. Rev. B* **67**, 94101 (2003)]

Rare-earth-metal-doped fullerides with nominal composition of R_3C_{70} (R = Sm, Eu) adopt a pseudo-monoclinic structure in which C_{70} dimers glued with rare-earth ions are involved. High-pressure powder x-ray diffraction experiments revealed that these compounds undergo a reversible first-order structural phase transition at 1.5 GPa, associated with 2.7%–2.9% reduction of the unit cell volume. Structural analyses showed that the rare-earth ions, which are located close to the edge of tetrahedral sites at ambient pressure, move back to the center of the tetrahedral sites. Simultaneously, C_{70} molecules are realigned so that the fivefold (long) axes are perpendicular to the $(10\bar{1})$ or $(11\bar{1})_{fcc}$ plane at high pressure. The derived charge density map indicates that the transition is regarded as a structural change from dimers to three-dimensional polymers of fullerenes. These features are ascribed to the unique bonding nature in rare-earth C_{70} compounds.

VIII-Z-4 Molecular- and Atomic-Like Photoionization of C_{60} in the Extreme Ultaviolet

KOU, Junkei; MORI, Takanori; ONO, Masaki; HARUYAMA, Yusuke[1]; KUBOZONO, Yoshihiro[2]; MITSUKE, Koichiro
([1]Okayama Univ.; [2]IMS and Okayama Univ.)

[*Chem. Phys. Lett.* **374**, 1 (2003)]

Photoion yield spectra of C_{60} in the gas phase were measured from 23 to 180 eV by synchrotron radiation. Two peaks at 26 and 34 eV and a flat area ranging 40–50 eV are newly observed in the high-energy side of the giant resonance at ~ 20 eV. These features are assigned to the shape resonance on photoionization of the valence electrons of C_{60}; the ionized electron is temporarily trapped inside a centrifugal barrier. Above ~ 50 eV the yield curve shows a steady decrease with increasing photon energy like the photoabsorption cross section of atomic carbon. Thus, the spectrum is interpreted as essentially determined by photoionization of the 2*s* orbitals of carbon atoms.

VIII-Z-5 A Complex Fulleride Superstructure-Decoupling Cation Vacancy and Anion Orientational Ordering in $Ca_{3+x}C_{60}$ with Maximum Entropy Methods

CLARIDGE, J. B.[1]; KUBOZONO, Yoshihiro; ROSSEINSKY, M. J.[1]
([1]Univ. Liverpool)

[*Chem. Mater.* **15**, 1830 (2003)]

The structure of the alkaline-earth fulleride $Ca_{3.01}C_{60}$ is refined using maximum entropy data analysis of synchrotron powder diffraction data. Despite the size and complexity of the structural problem, the fulleride anion orientations and the details of multiple occupancy of the octahedral interstitial sites in the fcc anion array are determined. The power of the maximum entropy technique in solving underdetermined problems in powder crystallography is thus demonstrated.

VIII-Z-6 Development of a Photoionizaion Spectrometer for Gaseous Fullerenes in the Extreme Ultraviolet

MORI, Takanori; ONO, Masaki; KOU, Junkei; HARUYAMA, Yusuke[1]; KUBOZONO, Yoshihiro; MITSUKE, Koichiro
([1]Okayama Univ.)

[*Rev. Sci. Instrum.* **74**, 3769 (2003)]

A photoionization spectrometer has been developed for measuring the ion yields for fullerenes in the photon energy range of 23–200 eV. Gaseous fullerenes were supplied from a high-temperature oven, ionized by irradiation of monochromatized synchrotron radiation, and detected after analysis with a time-of-flight mass spectrometer. The fluxes of the synchrotron radiation and fullerene beams were monitored concurrently with the acquisition of the ion signal counts in order to obtain reliable photoionization efficiency curves. The performance of the apparatus was examined by measuring the efficiency curve of C_{60}^+ produced from C_{60}. The spectrum demonstrated better statistics than the previous results in the same photon energy region. Three distinct features were newly observed in the higher-energy side of the prominent resonance at ~ 20 eV.

VIII-Z-7 Structural and Electronic Properties of $Ce@C_{82}$

SHIBATA, Kana[1]; RIKIISHI, Yoshie[1]; HOSOKAWA, Tomoko[1]; HARUYAMA, Yusuke[1]; KUBOZONO, Yoshihiro[2]; KASHINO, Setsuo[1]; URUGA, Tomoya[3]; FUJIWARA, Akihiko[4]; KITAGAWA, Hiroshi[5,6]; TAKANO, Takumi[7]; IWASA, Yoshihiro[7]
([1]Okayama Univ.; [2]IMS, JST and Okayama Univ.; [3]JASRI; [4]JAIST; [5]Univ. Tsukuba; [6]PRESTO/JST; [7]Tohoku Univ.)

[*Phys. Rev. B* **68**, 94104 (2003)]

X-ray diffraction patterns for a solid sample of $Ce@C_{82}$ that contains a mixture of two isomers, I and II, can be indexed in a face-centered cubic lattice with a lattice constant of 15.88(5) Å, while x-ray diffraction patterns for $Ce@C_{82}$ isomer I alone indicate a simple cubic lattice with a lattice constant of 15.78(1) Å. Rietveld refinement for the x-ray diffraction pattern of the latter, $Ce@C_{82}$ isomer I, has been carried out with a space group of $Pa\bar{3}$. Thin films of $Ce@C_{82}$ were first prepared by thermal deposition under ~ 10^{-7} Torr. The Raman spectra for these thin films show a peak ascribable to a Ce-C_{82} cage-stretching mode at ~ 160 cm^{-1}, implying that the valence of Ce in this structure is +3. This valence of +3 is supported by Ce L_{III}-edge XANES for a thin film of $Ce@C_{82}$. Furthermore, the local structure around the Ce ion could be determined by Ce L_{III}-edge EXAFS for a thin-film. Transport properties of a thin film of $Ce@C_{82}$ have been studied by a four-probe method, and these demonstrate a semiconducting behavior with a small gap of 0.4 eV.

VIII-Z-8 N-Channel Field Effect Transistors with Fullerene Thin Films and Their Application to a Logic Gate Circuit

KANBARA, Takayoshi[1]; SHIBATA, Kana[1]; FUJIKI, Satoshi; KUBOZONO, Yoshihiro[2]; KASHINO, Setsuo[1]; URISU, Tsuneo; SAKAI, Masahiro; FUJIWARA, Akihiko[3]; KUMASHIRO, Ryotaro[4]; TANIGAKI, Katsumi[4]
([1]Okayama Univ.; [2]IMS and Okayama Univ.; [3]JAIST; [4]Osaka Univ.)

[*Chem. Phys. Lett.* **379**, 223 (2003)]

N-channel field effect transistors (FETs) were fabricated with thin films of C_{60} and $Dy@C_{82}$. A typical enhancement-type FET property was observed in C_{60} FET above 220 K. The mobility of C_{60} FET increased with increasing temperature. This fact suggests hopping

transport as the conduction mechanism, with the activation energy of 0.29 eV. The Dy@C_{82} FET was found to be a normally-on type FET, which has a property different from that for C_{60} and C_{70} FETs. A complementary metal oxide semiconductor (CMOS) logic gate circuit was first fabricated with C_{60} and pentacene thin-film FETs.

VIII-Z-9 Scanning Tunneling Microscopy of Dy@C_{82} and Dy@C_{60} Adsorbed on Si(111)-(7x7) Surfaces

FUJIKI, Satoshi[1]; KUBOZONO, Yoshihiro[1]; HOSOKAWA, Tomoko[2]; KANBARA, Takayoshi[3]; FUJIWARA, Akihiko[4]; NONOGAKI, Youichi; URISU, Tsuneo
([1]IMS and Okayama Univ.; [2]Okayama Univ.; [3]Tohoku Univ.; [4]JAIST)

[*Phys. Rev. B* in press]

Dy@C_{82} and Dy@C_{60} adsorbed on Si(111)-(7×7) surface are investigated by scanning tunneling microscopy (STM) at 295 K. The Dy@C_{82} molecules in the first layer are adsorbed on Si(111)-(7×7) surface without formation of islands and nucleation, and the internal structure of the Dy@C_{82} molecule is first observed on the surface at 295 K. The average heights of the Dy@C_{82} molecule in the first and second layers are estimated to be 7.2 and 10.8 Å, respectively, by STM. These results suggest strong interactions between the Si atoms and the Dy@C_{82} molecules in the first layer. The STM image reveals that Dy@C_{60} molecule is nearly spherical, showing that the metal endohedral C_{60} possesses a cage-form structure.

VIII-Z-10 Preferred Locations of Metal Ions in Two M@C_{82} Isomers

TAKABAYASHI, Yasuhiro[1]; HARUYAMA, Yusuke[1]; RIKIISHI, Yoshie[1]; HOSOKAWA, Tomoko[1]; SHIBATA, Kana[1]; KUBOZONO, Yoshihiro[2]
([1]Okayama Univ.; [2]IMS and Okayama Univ.)

[submitted]

Location of metal ion in the minor isomer of M@C_{82} (M: metal ion with valence of +3) was determined for the first time by Dy L_{III}-edge EXAFS of Dy@C_{82}. The Dy ion lied near the fused bond between two hexagon rings. On the other hand, the EXAFS showed that the Dy ion in the major isomer of Dy@C_{82} lied near the center of a hexagon ring. The locations found in the minor and major isomers were consistent with those predicted theoretically for the respective isomers.

VIII-Z-11 Fabrication and Characterization of a New Type of Carbon Cluster Field Effect Transistor

SHIBATA, Kana[1]; KUBOZONO, Yoshihiro[2]; KANBARA, Takayoshi[1]; HOSOKAWA, Tomoko[1]; FUJIWARA, Akihiko[3]; SHINOHARA, Hisanori[4]; ITO, Yasuhiro[4]
([1]Okayama Univ.; [2]IMS and Okayama Univ.; [3]JAIST; [4]Nagoya Univ.)

[submitted]

A new type of carbon cluster field effect transistor (FET) was fabricated with thin film of C_{84}, and *n*-channel normally-on depletion-type FET characteristics were found in this FET device. The C_{84} FET device exhibited the highest mobility, μ, of 1.3×10^{-3} $cm^2V^{-1}s^{-1}$ among normally-on carbon cluster FETs. The carrier transport of this FET device suggested a thermally-activated hopping transport. Carrier type (*n*-channel) and transport mechanism (hopping) reflect the electronic properties of the C_{84} molecule. This is the first report of the FET with higher-fullerene thin-film.

VIII-Z-12 Structural and Electronic Characterizations of Two Ce@C_{82} Isomers

RIKIISHI, Yoshie[1]; HOSOKAWA, Tomoko[1]; SHIBATA, Kana[1]; HARUYAMA, Yusuke[1]; TAKABAYASHI, Yasuhiro[1]; KUBOZONO, Yoshihiro[2]
([1]Okayama Univ.; [2]IMS and Okayama Univ.)

[submitted]

X-ray diffraction patterns for the Ce@C_{82} isomers I and II, which refer to major and minor isomers, respectively, are studied in a wide temperature region. The diffraction patterns observed at 295 K can be indexed based on a simple cubic (sc) structures with the lattice constants, *a*'s of 15.78(1) Å for the isomer I and 15.74(4) Å for the isomer II. Rietveld analyses are achieved for these X-ray diffraction patterns with a space group of $Pa\bar{3}$. Temperature dependence of *a* for the isomer I shows a drastic change around 150 K which implies an existence of structural phase transition. The structural phase transition above 300 K cannot be detected for the Ce@C_{82} isomer I in contrast with the fact that the phase transition at 400 K was previously reported for La@C_{82} isomer I by a differential scanning calorimetry and dielectric constant measurements. Temperature dependence of *a* for the isomer II indicates no structural phase transition from 100 to 300 K. Pressure dependence of *a* for the isomer I exhibits a monotonous decrease with an increase in pressure. This result implies no pressure-induced structural phase transition for the isomer I.

VIII-AA Study of Electronic Structure of Organic Thin film and Organic/Inorganic Interface

Organic semiconductors have gained increasing interest because of their potential use in various optoelectronic devices In order to understand electronic processes at interface in the organic devices, many surface sensitive techniques such as high-resolution ultraviolet photoemission spectroscopy (UPS) have been performed for organic thin films, because origins of the energy position and the bandwidth of ultraviolet photoelectron spectra are keys to understand interface properties, such as the energy level alignment at the interface and molecule-molecule and/or molecule-substrate interaction. The energy-band structure is a fundamental basis for the understanding of electronic and optical properties of solids. The intermolecule band dispersion for the organic thin film is observed using angle-resolved UPS using synchrotron radiation, since the width of band dispersion depends the intermolecular interaction.

VIII-AA-1 Intermolecular Energy-Band Dispersion in PTCDA Multilayers

YAMANE, Hiroyuki[1]: KERA, Satoshi; YOSHIMURA, Daisuke; OKUDAIRA, K. Koji; SEKI, Kazuhiko[2]; UENO, Nobuo[1]
([1]Chiba Univ.; [2]Nagoya Univ.)

[*Phys. Rev. B* **68**, 033102 (4 pages) 2003]

The electronic structure of a well-oriented perylene-3,4,9,10-tetracarboxylic acid-dianhydride multilayer prepared on MoS_2 single crystal surface were studied by angle-resolved ultraviolet photoemission spectroscopy using synchrotron radiation. From the photon energy dependence of normal emission spectra, we observed an intermolecular energy-band dispersion of about 0.2 eV for the highest occupied molecular orbital (HOMO) band of single π character. The observed energy-band dispersion showed a cosine curve, which originates from the intermolecular π-π interaction. Analyses using the tight-binding model gave that the transfer integral of about 0.05 eV for the π-π interaction, the effective mass of HOMO hole $m_h^* = 5.28m_0$, and the hole mobility $\mu_h > 3.8$ cm^2/V s. This is the first observation of the intermolecular energy-band dispersion of a conventional single-component organic semiconductor only with the weak intermolecular van der Waals interaction.

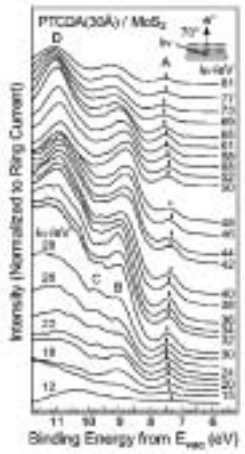

Figure 1. Photon energy ($h\nu$) dependence of SR-ARUPS spectra along the surface normal for the 30-Å-thick PTCDA multilayer (~ 8 ML) prepared on the MoS_2 surface. The binding energy (E_B)scale refers to the vacuum level (E_{vac}).

VIII-AA-2 Very Narrow Photoemission Bandwidth of the Highest Occupied State in a Copper-Phthalocyanine Monolayer

KERA, Satoshi; YAMANE, Hiroyuki[1]; SAKURAGI, Isamu[1]; OKUDAIRA, K. Koji; UENO, Nobuo[1]
([1]Chiba Univ.)

[*Chem. Phys. Lett.* **364**, 93–98 (2002)]

We observed a very narrow bandwidth of the highest occupied molecular orbital (HOMO) state in ultraviolet photoemission spectra (UPS) of copper-phthalocyanine monolayer deposited on graphite. The HOMO band in UPS consists of three components which may originate from the vibrational coupling. The full width at half maximum of each component was found to be ~ 150 meV at 295 K. This HOMO-bandwidth leads to an estimation that the lifetime of the HOMO hole should be at least longer than 2.2 fs, which may be dominated by the electron transfer rate from the substrate to the molecule.

VIII-BB Effects of High Magnetic Field on Chemical and Physical Processes

We have studied the effects of high magnetic field on chemical reaction and physical processes of diamagnetic and paramagnetic materials to unravel the mechanisms of the interaction of matter and magnetic field and to develop unique methods controlling chemical and physical processes and improving chemical and physical properties of functional materials. Currently we are using a vertical superconducting magnet which can generate high magnetic fields (15 T, 1500 T^2/m) in a 40 ϕ bore tube. Magnetic levitation of a water droplet and others is capable using the magnet. It is shown that many chemical reactions and physical processes are significantly affected by the magnetic field. For example, we have succeeded, for the first time, to induce 3D-morphological chirality in zinc silicate membrane tube using a high magnetic field. The results are interpreted in terms of the Lorentz force on ions thermally moving in an aqueous solution. In NaCl:Eu crystals, dislocation mobility is affected by a magnetic field.

VIII-BB-1 3D-Morphological Chirality Induction in Zinc Silicate Membrane Tube Using a Magnetic Field

UECHI, Ichiro[1]; KATSUKI, Akio[2], DUNIN-BARKOVSKIY, Lev R.; TANIMOTO, Yoshifumi
([1]IMS and Hiroshima Univ.; [2]Shinshu Univ.)

[*J. Phys. Chem.* in press]

We report *three-dimensional morphological* chirality induction using a vertical magnetic field. Right-handed *circular* helix of zinc silicate membrane tube was *selectively* induced by application of a magnetic field (5–15 T), whereas the tube grew straightly upward at zero field as shown in Figure 1. Left-handed circular helix was also selectively obtained by changing experimental condition. *Square* and *triangular* helixes were also prepared. The results are interpreted in terms of the boundary-assisted magnetohydrodynamics mechanism in which cyclotron motion of ions in solution results in one-way convection of the solution near the boundary.

Figure 1. Magnetic field effects on the growth of zinc silicate membrane. (a) 0 T, (b) 6 T, (c) 13.5 T.

VIII-BB-2 Effects of a High Magnetic Field on the Growth of 3-Dimensional Silver Dendrites

KATSUKI, Akio[1]; UECHI, Ichiro[2]; TANIMOTO, Yoshifumi
([1]Shinshu Univ.; [2]IMS and Hiroshima Univ.)

[*Bull. Chem. Soc. Jpn.* in press]

A liquid/solid redox reaction between silver ion and copper metal was investigated under a *vertical* and *inhomogeneous* high magnetic field (maximum field strength: 15 T). 3-Dimensional silver dendrites produced *via* the reaction were affected drastically by the magnetic field. Black and round dendrites were obtained in the magnetic field, whereas metallic silver crystals were grown under the gray dendrites at zero field. The yields of silver dendrite and copper ion increased significantly in the magnetic fields. The results are interpreted in terms of magnetic convection of the solution which is induced by the magnetic force on paramagnetic copper ions generated in the reaction as well as the Lorentz force on ions.

VIII-BB-3 Magnetic Field Effects on TiO_2 Photocatalytic Reaction

KAMOCHI, Masataka[1]; FUJIWARA, Yoshihisa[1]; TANIMOTO, Yoshifumi
([1]Hiroshima Univ.)

We attempted to examine whether a magnetic field could affect photo-catalytic reaction of titanium oxide, as little was known about the magnetic field effect (MFE) on catalytic reaction. The reaction studied here is as follows,

$$CH_3OH + H_2O + h\nu + TiO_2/Pt \rightarrow 3H_2\uparrow + CO_2\uparrow$$

A methanol-water (1:1) solution containing titanium oxide powder and chloroplatinic (IV) acid hexahydrate was irradiated with light from a xenon lamp in the absence and presence of a magnetic field and the volume of the photo-generated gas was determined. The yield of the gas decreased gradually with increasing a magnetic field from zero to 4 T (*ca.* –10% at 4 T). Similar MFE was observed on the photocurrent of the photo-galvanic cell, $TiO_2(s)|NaOH(aq)||H_2SO_4(aq)|Pt(s)$.

The present MFE is tentatively explained in terms of

a radical pair model (Δg mechanism). Upon photo-excitation of TiO_2, excited singlet TiO_2, $^1TiO_2$*, is generated. While $^1TiO_2$* undergoes intersystem crossing (ISC) to $^3TiO_2$*, singlet electron-hole pair is generated from $^1TiO_2$*. The free electron and hole will be formed by the dissociation of the singlet pair. In a magnetic field, the singlet-to-triplet ISC in the pair is accelerated due to the difference in *g*-values of electron and hole, leading the depression in the yield of free electron and hole by which the succeeding redox reaction is initiated.

VIII-BB-4 On the Movement of Paramagnetic Ions in an Inhomogeneous Magnetic Field

FUJIWARA, Masao; CHIE, Kenjiro[1]; SAWAI, Jun[1]; SHIMIZU, Daisuke[1] ; TANIMOTO, Yoshifumi
([1]Hiroshima Uinv.)

[*J. Phys. Chem.* submitted]

The movement of transition metal ions was observed in an inhomogeneous magnetic field. The solution containing Cr^{3+}, Mn^{2+}, Co^{2+}, Ni^{2+}, and Cu^{2+} ions was spotted on a silica gel support, and exposed to magnetic fields up to 410 kOe^2cm^{-1}. The distribution of the metal ions was measured, and the frictional coefficient of the movement was analyzed in relation to the susceptibility and concentration of the metal ions as well as to the size of the silica gel particles. When the concentration is higher, the metal ions move to a larger the distance. It is shown that a large group composed of the metal ions and water molecules moves in a magnetic field.

VIII-BB-5 Magnetic Separation of Metal Ions

CHIE, Kenjiro[1]; FUJIWARA, Masao; FUJIWARA, Yoshihisa[1]; TANIMOTO, Yoshifumi
([1]Hiroshima Univ.)

[*J. Phys. Chem.* in press]

The magnetic separation was investigated for Co^{2+}(9500 × 10^{-6} cm^3mol^{-1}) and Fe^{3+} (14600 × 10^{-6} cm^3mol^{-1}) ions and for Cr^{3+} (6200 × 10^{-6} cm^3mol^{-1}) and Al^{3+} (–2 × 10^{-6} cm^3mol^{-1}) ions. The metal ion solutions were spotted on a silica gel support and exposed to a magnetic field of 410 kOe^2cm^{-1} intensity × gradient. The Co^{2+} ions move to a larger distance toward the maximum field than the Fe^{3+} ions. The result is explained by the fact that the Fe^{2+} ions are adsorbed more strongly on the silica gel support than the Co^{2+} ions. The Cr^{3+} ions move farther toward the field center than the Al^{3+} ions. This occurs because the Cr^{3+} ions are attracted more strongly by the magnetic force than the Al^{3+} ions. It is demonstrated that the separation makes effective use of the adsorption activities as well as the magnetic susceptibilities.

VIII-BB-6 Influence of Magnetic Field up to 15 T on Luminescence of NaCl:Eu Crystals

BASKAKOV, A. A.[1]; DUNIN-BARKOVSKIY, Lev R.[2]; MORGUNOV, Roman B.[2]; TANIMOTO, Yoshifumi
([1]ISSP, Chernogolovka; [2]IMS and ISSP, Chernogolovka)

Variations of Eu^{2+} luminescent spectra during Eu aggregation in NaCl crystal lattice has been found. These variations caused by extremely high sensitivity of electronic levels splitting to intracrystalline electrical field and Eu^{2+} environment continuously changing during aggregation process. Influence of magnetic field on luminescent excitation spectra in nonequilibrium quenched crystals during the aggregation acted was found (Figure 1). Redistribution of luminescent bands intensity in the excitation spectra gradually increases with the sample exposure in magnetic field (Figure 1). It is unreasonable to suppose that Eu^{2+} ions being paramagnetic can take part in a spin-dependent solid state reaction controlled by magnetic field.

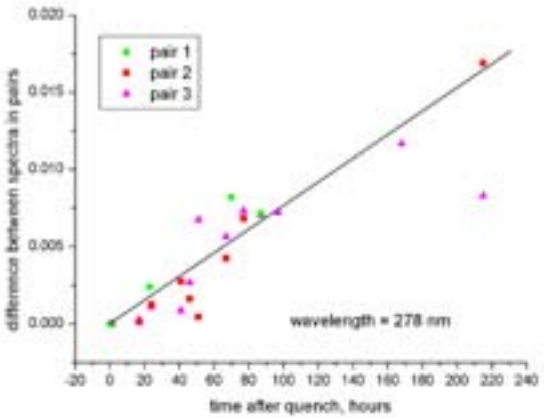

Figure 1. Dependencies of difference between luminescence intensity in reference sample and identical crystal stored in magnetic field after quenching on storage duration for 3 pairs of the identical NaCl:Eu crystals.

VIII-BB-7 Magnetic Field Effect on Dislocation Mobility in NaCl:Eu Crystals

BASKAKOV, A. A.[1]; DUNIN-BARKOVSKIY, Lev R.[2]; MORGUNOV, Roman B.[2]; TANIMOTO, Yoshifumi
([1]ISSP, Chernogolovka; [2]IMS and ISSIP, Chernogolovka)

Recent investigation shown that mobility of dislocations (elementary carriers of plastic deformation) could be considered as an electron spin-dependent process. Magnetic field and its influence on dislocation displacements can serve as a facilities to distinguish spin-dependent part of dislocation interaction with the obstacles. All experiments in this area were carried out early in magnetic fields up to 2 T or in pulsed fields. In this work comparatively strong static magnetic field 15 T was used. It is important because identification of concrete mechanism of spin state mixing in magnetic field as a rule based on correct field dependencies of the magnetic effects.

Displacements of individual dislocation and movement of dislocation in slip bands after exposure of

diamagnetic NaCl:Eu crystals in magnetic field with an induction 15 T were found (Figure 1). Since there was no an external loading of crystals during experiments, the internal stress were the main reason of dislocation displacements. Magnetic field initiates unpinning of dislocations from local obstacles that are Eu aggregates. After magnetic field was switched off increased mobility of the dislocations takes place during 1–2 days. Obtained results open a new possibilities to reliable comparison of theory predictions with the experimental data.

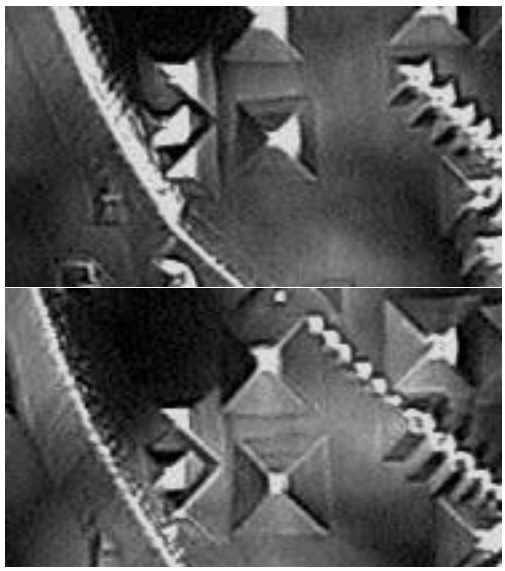

Figure 1. Surface of NaCl crystal a) before, b) after exposure in MF. Big pyramidal pits are initial position of dislocation lines entering on the surface. Small pits are new dislocation line positions after displacement.

VIII-BB-8 Imprinting Magnetic Memory Cells in Molecular Based $NiL_2(C_2H_5OH)_2$ Heterospin Crystals

BASKAKOV, A. A.[1]; FOKIN, S. V.[2]; GUDOSHNIKOV, S. A.[3]; MORGUNOV, Roman B.[4]; OSSIPYAN, YU. A.[1]; OVCHARENKO, V. I.[2]; SAGDEEV, R. Z.[2]; SKOMARVSKII, V. S.[3]; TANIMOTO, Yoshifumi
([1]ISSP, Chernogolovka; [2]Intl. Tomography Cent., Novosibirsk; [3]Inst. Terrestrial Magnetism, Troitsk; [4]IMS and ISSP, Chernogolovka)

Magnetic studies of molecular based crystals have stirred great interest in the magnetic properties of structural defects induced by plastic deformation. In our experiments local deformation of molecular based magnet was carried out by diamond indentor. Local magnetic field around indentation pit was measured by scanning SQUID magnetometer. It has been found that local deformation causes ferromagnetic exchange interaction in $NiL_2(C_2H_5OH)_2$ heterospin single crystals at unusually high temperatures (≥ 77 K). These magnetization temperatures are much higher than the temperature observed for the same, but undeformed crystals (~ 5 K). Ferro- and antiferromagnetic ordering around dislocation cores arise from lattice distortions and changes in distances between the magnetic atoms. Near structural defects high pressure will strongly affect exchange interactions in many spin paramagnetic crystals. Thus, in spite of usual aspiration for perfect crystals grows our experiment shown that disordering can give fruitful results. Local plastic deformation should be considered as a method of control over the magnetic properties of molecular based crystals and as a technique for improving their magnetic characteristics. It offers a nice possibility to imprint the magnetic structure and to distribute magnetic memory cells on the surface premeditatedly. Nanoindentation technologies will probably allow the imprinting of separate magnetic cells ~ 1–10 nm in size.

VIII-BB-9 Localization of Conduction-Band Electrons in β”-(BEDT-TTF)$_4NH_4[Cr(C_2O_4)_3]$·DMF Single Crystals

MORGUNOV, Roman B.[1]; BASKAKOV, A. A.[2]; DUNIN-BARKOVSKIY, Lev R.[1]; KHASANOV, S. S.[1]; SHIBAEVA, R. P.[2]; PROKHOROVA, T. G.[3]; YAGUBSKIY, E. B.[3]; KATO, Tatsuhisa; TANIMOTO, Yoshifumi
([1]IMS and ISSP, Chernogolovka; [2]ISSP, Chernogolovka; [3]Inst. Problems Chem. Phys., Chernogolovka)

Temperature dependence of EPR spectrum of β”-(BEDT-TTF)$_4NH_4[Cr(C_2O_4)_3]$·DMF single crystals, which consists of two separate lines characterizing magnetic features of BEDT-TTF and Cr^{3+} ions, was studied within the range 1.5–300 K. It was found that reconstruction of the EPR spectrum occurs under decrease of the temperature down to $T \approx 20$ K. The reconstruction consists in change of Lorentzian shape of the BEDT-TTF line to Gaussian one and in decrease of the effective magnetic moment of Cr^{3+} ions. Analysis of temperature and orientation dependencies of parameters of the EPR spectra allows one to suppose that localization of conduction electrons within regions with dimensions close to the size of individual BEDT-TTF molecules occurs at $T \approx 20$ K. Exchange interactions between Cr^{3+} ions change towards antiferromagnetic spin correlations as well.

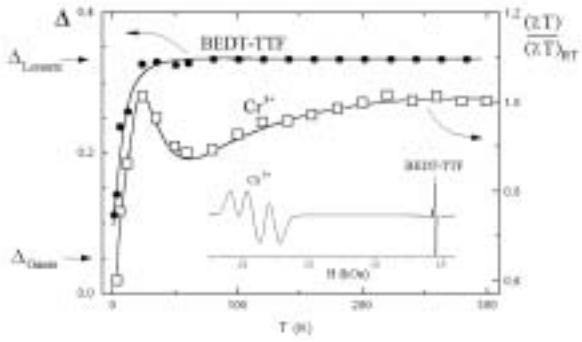

Figure 1. Dependencies of χT and line-shape parameter Δ (Δ = 0.05 for pure Lorenz line and Δ = 0.33 for pure Gauss one) on temperature *T*. ESR spectrum of the salt at room temperature is shown on the insert.

VIII-CC Theoretical and Computational Study on Gas Phase Reactions and Chromic Molecules

1. Quantum chemical calculations are used to produce potential energy surface (PES) to do reaction dynamics simulations. We develop the methodology to generate PES efficiently and automatically using quantum chemical calculation results. The method does not need any derivative information in quantum chemical calculations.
2. Another interest of our group is theoretical explanation and prediction of structural and spectral changes of photochromic and electrochromic substances.
3. We also search a reasonable pathway to form H_2 from H atoms *via* PAH related catalysts to solve why H_2 is abundant in interstellar space.

VIII-CC-1 Theoretical Study on Photoinduced Color Change and Charge Transfer of Methylviologen

ISHIDA, Toshimasa; MURAKAMI, Makoto[1]; WATANABE, Go[1]; YOSHIKAWA, Hirofumi[2]; NISHIKIORI, Shin-ichi[2]
([1]Shizuoka Univ.; [2]Univ. Tokyo)

[*Internet Electronic J. Mol. Design* **2**, 14–23 (2003)]

Methylviologen dication is easily reduced to a monocation radical, and turned to be blue, forming a charge-transfer complex with a donor molecule. Yoshikawa *et al*. recently reported photo-induced reduction and charge transfer complexes in poly-cyano–polycadmate host clathrates. We study this reduction using quantum chemical calculations. The energy changes with the torsion angle of the two cations and the spectral change, solvent effect and the charge transfer between the dication and other guest molecules in the clathrates are investigated. The Hartree-Fock, DFT, CI singles, time dependent DFT calculations are carried out for the ground state and excited states of the two cations. Solvation effect is treated with the polarizable continuum model, and the charge transfer in the clathrates is modeled based on crystal structures determined experimentally. The optimized geometry of the monocation radical was found to be planar while that of the dication is twisted. These results are consistent with recent calculations for related compounds. The color change upon the photoreduction was reproduced by the calculation. The solvent effect of acetonitrile was found to be small. Charge transfer absorption was reproduced for the mesitylene–methylviologen dication complex in the clathrate host using a small model. The geometry modification and the color change were reproduced satisfactorily. The TDDFTscheme reproduces the observed spectra better than the CIS scheme, but the latter scheme is still valuable to evaluate qualitative feature of spectra.

VIII-CC-2 Crystal Structure and Spectroscopic Properties of the CT Complex of Methyl Viologen Dication and *o*-Dimethoxybenzene Included in a Polycyano-Polycadmate Host, and Theoretical Study on Its Red Shifted CT Absorption

YOSHIKAWA, Hirofumi[1]; NISHIKIORI, Shin-ichi[1]; ISHIDA, Toshimasa
([1]Univ. Tokyo)

[*J. Phys. Chem. B* **107**, 9261–9267 (2003)]

Using the polycyano-polycadmate host that is a negative charged Cd cyanide complex with a framework structure built with Cd^{2+} ions and bridging cyanide ligands, we synthesized a clathrate including methyl viologen dication (MV^{2+}) and *o*-dimethoxybenzene (ODMB) as guests. The color of the clathrate was red and its origin was considered to be charge transfer (CT) interaction of a CT complex formed with MV^{2+} as an acceptor and ODMB as a donor in the host. The wavelength at the CT absorption maximum was largely red shifted compared with that of the CT complex in an acetonitrile solution. The single crystal X-ray diffraction analysis revealed a π-π stacking structure of the CT complex and a 1D arrangement of the CT complexes in a channel-like cavity of the framework host. In the array of the CT complexes, MV^{2+} ions are adjacent to each other and their separation is short. The direction of the transition moment of the CT absorption determined from the structural information and the spectrum measured on a crystalline sample agreed with that derived from *ab initio* calculations at the CIS/6-31+G* level. Our calculations also showed that the red shift of the CT absorption is mainly due to electrostatic effects between the CT complexes, not due to the shortening of the distance between MV^{2+} and ODMB, which is generally believed to be the reason. The negative charged host stabilizes the ground state of the CT complex, but the electrostatic interaction between the CT complexes heightens the ground state and lowers the excited state. In this clathrate, due to the CT complex array with the short separation the effect from the guests overcomes that from the host and the red shift appears.

VIII-CC-3 A Local Interpolation Scheme Using No Derivatives in Potential Sampling: Application to $O(^1D) + H_2$ System

ISHIDA, Toshimasa; SCHATZ, George C.[1]
([1]Northwestern Univ.)

[*J. Comput. Chem.* **24**, 1077–1086 (2003)]

We recently proposed a local interpolation scheme, in which interpolant moving least squares (IMLS) and Shepard interpolation are employed to describe potential

energy surfaces. This IMLS/Shepard scheme is applicable to do potential interpolation with quantum chemical results for which analytical derivatives are not available. In this study, we apply the scheme to the highly exothermic $O(^1D) + H_2 \rightarrow H + OH$ reaction and compare it with results based on Shepard interpolation using second order Taylor expansions. An analytical surface is used to define the potential function so that errors in the interpolation function may accurately be determined. We found that the present scheme reproduces the correct reactive cross sections more accurately than the Shepard scheme, and with rms errors for energy and gradients that are significantly smaller than those from Shepard interpolation. This occurs even though the present scheme does not utilize derivative and hessian information whereas the Shepard interpolation does. The Bayesian approach proposed by Bettens and Collins does not improve the IMLS/Shepard results significantly although it does the Shepard-only approach. The accuracy in the IMLS/Shepard scheme is surprising, but can be explained by the more global nature of the interpolation.

VIII-CC-4 Possible Molecular Hydrogen Formation Mediated by the Radical Cations of Anthracene and Pyrene

HIRAMA, Mutsumi[1]; ISHIDA, Toshimasa; AIHARA, Jun-ichi[1]
([1]Shizuoka Univ.)

[*J. Comput. Chem.* **24**, 1378–1382 (2003)]

Hydrogen molecules cannot be formed readily by the association of gaseous hydrogen atoms. Possible H_2 formation mediated by the radical cations of typical polycyclic aromatic hydrocarbons (PAHs), anthracene and pyrene, was studied at the B3LYP/6-31G** level of theory. We presumed that H_2 is formed by way of two elementary reactions, the addition of an H atom to a PAH molecular cation and the H abstraction from the resulting monohydro-PAH cation (*i.e.*, arenium ion) by a second H atom to yield H_2. The first reaction takes place without any activation energy. The second reaction is also predicted to proceed along almost barrierless pathways although it is far from being a typical ion-molecule reaction. There is a possibility that these reactions might constitute one of the mechanisms for H_2 formation in extremely cold interstellar space. Deuterium enrichment in PAH cations is possibly accompanied by such H_2 formation since deuteration lowers the energies of polyatomic PAH cations appreciably.

VIII-CC-5 Molecular Hydrogen Formation Mediated by a Naphthalene Radical Cation

TOKOSUMI, Takaaki[1]; HIRAMA, Mutsumi[1]; TERADA, Yoshihiro[1]; HAGIWARA, Noriko[1]; ISHIDA, Toshimasa; AIHARA, Jun-ichi[1]
([1]Shizuoka Univ.)

[*Phys. Chem. Chem. Phys.* submitted]

Hydrogen molecules cannot be formed readily by the association of gaseous hydrogen atoms. Bauschlicher and we independently proposed a possible molecular hydrogen formation mediated by polycyclic aromatic hydrocarbon (PAH) radical cations in space. We studied such a reaction process at the B3LYP/6-31G** level of theory and for the first time succeeded in determining the entire reaction pathway for the H_2 formation mediated by the naphthalene radical cation. We presumed that H_2 is formed by way of two elementary reactions, the addition of an H atom to a naphthalene cation and the H abstraction from the resulting naphthalenium ion by a second H atom to yield H_2. The first reaction takes place without any activation energy. The second reaction is predicted to proceed *via* a van der Waals complex but with little activation energy. These reactions are supposed to enhance the deuteration of the naphthalene cation. Neutral naphthalene also mediates the H_2 formation but needs some activation energy.

VIII-CC-6 Possible Molecular Hydrogen Formation Mediated by the Inner Carbon Atoms of PAH Radical Cations

HIRAMA, Mutsumi[1]; ISHIDA, Toshimasa; AIHARA, Jun-ichi[1]
([1]Shizuoka Univ.)

[in preparation]

Molecular hydrogen in space is believed to form from atomic hydrogen. During the past few years, we have been performing density functional theory (DFT) calculations to explore the possibility of H_2 formation mediated by the radical cations of gaseous polycyclic aromatic hydrocarbons (PAHs). As a continuation of this study, we explored the catalytic ability of inner carbon atoms of some typical PAH cations at the B3LYP/6-31G** level of theory. We presumed as before that H_2 is formed by way of two elementary reactions, the addition of an H atom to a PAH cation and the H abstraction from the resulting arenium ion by another H atom to yield H_2. We found that both reactions proceed without any activation energy. It follows that almost all carbon atoms of a PAH cation give sites for moelcular hydrogen formation. Since there are large compact PAHs abundantly in space, the H_2 formation at the inner carbon atoms of such PAH cations can never be overlooked. Even if inner carbon atoms might be less reactive than peripheral ones, there are many inner carbon atoms in large compact PAH cations.

VIII-DD Macromolecular Self-Assembly Opens the Way for Development of Novel Materials that Have Characteristics of Cellular Systems

Self-assembly is a principle to integrate molecular devices into a cellular supramolecular system. Exchangeability of the components, characteristic of assembled structures, allows the system to be repairable, reusable and modifiable on demand, and enables metabolism, adaptation, and evolution of the system. This insight may open new perspective for artificial photoelectronic apparatuses at the nano scale. Development and integration of molecular devices have been focuses for downsizing and energy-saving in the field of photoelectronics. For global, sustainable development, in our opinion, the future materials should also be "entropy-saving" (reusable, repairable, and bio-degradable) that has not been considered to date. We thus aimed at development of an artificial photosynthetic system that allows on-demand reuse (Figure 1); for their basis, we also study on molecular mechanisms of photosynthesis. Our study should serve a new design concept for nano- and molecular-scale intelligent materials (see also Special Research Project (c)).

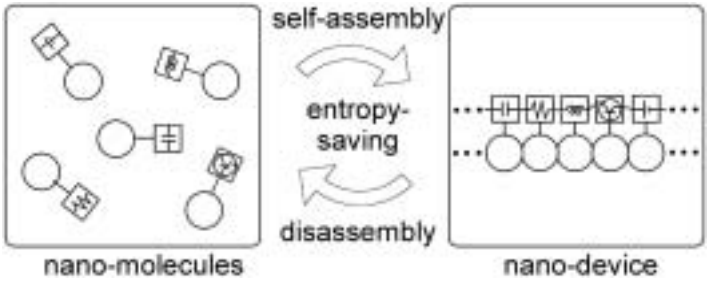

Figure 1. A concept of the "entropy-saving" nano-devices. The device does not function until on-demand self-assembly of nano functional blocks, and the device can easily be decomposed into the reusable components on demand.

VIII-DD-1 Engineering of Tobacco Mosaic Virus

OBA, Toru; TAKATOYA, Haruki[1]; MINABE, Masahiro[1]
([1]Utsunomiya Univ.)

Green photosynthetic bacteria possess rod-shaped nano-elements (4 ~ 5 nmϕ × 200 ~ 300 nm) as cores of light-harvesting antenna function. The rod-element is thought to be a self-assembled chlorophylls whose details remain yet unclear. Such a supramolecule may be useful as unique devices for future photoelectronics and biotechnology, but (1) it is impossible to obtain intact rod-elements from the cell and (2) it is quite difficult to build artificial tubule supramolecules by self-assembly of chlorophylls. We aimed at construction of nano-tubule of self-assembled chlorophylls by using tobacco mosaic virus (TMV) as a template. TMV possesses a tubule structure with an outer diameter of 15 nm, inner diameter of 4 nm, and length of 300 nm: the size of the channel matches that of the chlorosomal rod-element. We synthesized novel hydrophilic chlorophyll derivatives, and examined their affinities for the inner surface of TMV and their self-assemblies in the channel.

VIII-DD-2 Synthesis and Properties of Novel Biotin Derivatives

OBA, Toru; TOBITA, Hiromi[1]; MINABE, Masahiro[1]
([1]Utsunomiya Univ.)

Arrangement and connection of functional molecules in desired sequences and shapes are basic techniques for future fabrication of elaborate molecular systems including nano-devices and nano-computers. We aimed at development of a new method to arrange functional molecules sequentially in a desired order by utilizing specific interaction between avidin and biotin. Avidin is a 6.8 kDa protein (*ca.* 5 × 5 × 6 nm in size) that can bind four biotin molecules. The topology of the biotin binding sites is appropriate to link avidin molecules linearly when using a linear molecule that possesses two biotin moieties at both ends. Syntheses of novel bitoin derivatives and examination of their abilities to control the assembly of avidin molecules are now under way.

VIII-DD-3 Physicochemical Studies on the Molecular Mechanism of Photosynthesis

OBA, Toru; TAMIAKI, Hitoshi[1]
([1]Ritsumeikan Univ.)

[*Photosynth. Res.* **74**, 1–10 (2002)]

Since chlorophylls (Chls) and bacteriochlorophylls (BChls) are highly asymmetric molecules, an external ligand can coordinate to the central Mg atom of (B)Chls either from the chlorin macrocycle side where the C13^2-methoxycarbonyl moiety protrudes (denoting as the "back" side) or from the other side (the "face" side, Figure 2). We found that the "back" side is favored for the ligand coordination, by survey of the highly resolved crystal structures of photosynthetic proteins and by theoretical calculations of model molecules. The calculations reveal that stability of the (B)Chl-ligand

complex is sensitive to distortion of the macrocycle, and the distortion is affected by steric repulsion between particular peripheral substituents as well as flexibility of the macrocycle. We note that not only the static pigment-protein (pigment-pigment) interactions but also dynamics of the pigment-protein (pigment-pigment) assembly should be clarified for better understanding of the role of the planar chirality of (B)Chls *in vivo*.

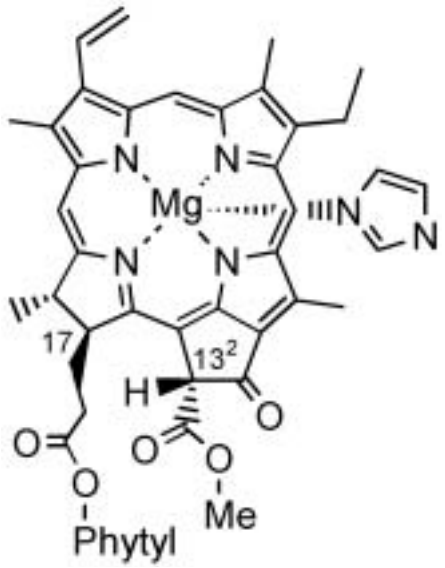

Figure 1. Molecular structure of the "back" type chlorophyll *a*-imidazole complex.

Equipment Development Center

VIII-EE Development of "Special Machine"

The technical staff of the Equipment Development Center is partly engaged in planning, researching, designing and constructing "Special machine." This machine, is a high-tech experimental instrument, with emphasis on newtechnical idea and co-operative work with members inside and outside the Institute including those in industries.

VIII-EE-1 Construction of the Evaluation Endstation Dedicated for Transmission Gratings

HATSUI, Takaki; KOSUGI, Nobuhiro; KONDOH, Takuhiko[1]; MATSUSHITA, Kouji; YANO, Takayuki; UTCHIYAMA, Kouichi; SUZUI, Mitsukazu
([1]Nagoya Univ.)

A novel endstation dedicated for the evaluation of free-standing transmission grating have be en constructed at BL4B of the UVSOR facility in the course of the development project of soft x-ray emission spectrometer in collaboration with the department of vacuum UV photoscience. The transmission grating are planned to be used in a novel soft x-ray emission spectrometer, which covers 100–1000 eV region. The endstation is capable to measure the absolute diffraction efficiency as well as energy resolution limited by the imperfect grating structure. Figure 1 shows the schematic overview of the endstation, which consists of a chamber for target grating (a), a Si diode detector for the diffraction efficiency measurement (b), and a gas cell for the measurement of the energy resolution of the grating (c). The grating chamber is capable to move the grating along 5 axes by using a linear feedthrough and three micrometers. The position of the gas cell is controlled by a manupilator, and monitored by a laser interferrometer so that x-ray absorption spectra of gaseous sample can be measured by scanning the gas cell. The high precision slit located upper stream to the gas cell have two blades. The blades are manufactured by grinding using Electrolytic in-process dressing (ELID) method, which was introduced to the equipment development center through the collaboration with Nagoya university. First results have been obtained for a test grating chip in March 2003.

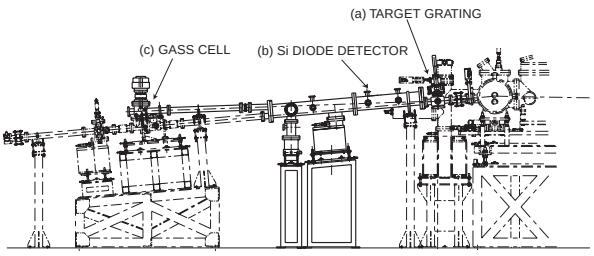

Figure 1. Schematic overview of the endstation at BL4B.

Ultraviolet Synchrotron Orbital Radiation Facility

VIII-FF Development of the UVSOR Light Source

VIII-FF-1 UVSOR Upgrade Project

KATOH, Masahiro; HOSAKA, Masahito; MOCHIHASHI, Akira; YAMAZAKI, Jun-ichiro; HAYASHI, Kenji; HORI, Yoichiro[1]; HONDA, Toru[1]; HAGA, Kaiichi[1]; TAKASHIMA, Yoshifumi[2]; KOSEKI, Tadashi[3]; KODA, Shigeru[4]; KITAMURA, Hideo[5]; HARA, Toru[5]; TANAKA, Takashi[5]
([1]KEK-PF; [2]Nagoya Univ.; [3]RIKEN; [4]Saga Sync. L. S.; [5]RIKEN/SPring-8)

UVSOR was successfully converted to UVSOR-II, which has eight straight sections and small emittance of 27 nm-rad. The magnetic lattice was modified without changing the circumference of 53.2 m. All the magnets and their beam ducts except for the bending magnets were replaced. An undulator and a super-conducting wiggler were replaced with two new in-vacuum undulators. Some parts of the injector were replaced and upgraded. Some beam-lines were reconstructed. All the reconstruction works were completed within three months, from April to June 2003. In July, UVSOR-II was successfully commissioned. Some preliminary measurements on the beam parameters suggested that the design goal of the emittance, 27 nm-rad, was likely achieved. Vacuum conditioning with beams are in progress. Users experiments will start in September.

VIII-FF-2 UVSOR Free Electron Laser

HOSAKA, Masahito; KATOH, Masahiro; MOCHIHASHI, Akira; YAMAZAKI, Jun-ichiro; HAYASHI, Kenji; TAKASHIMA, Yoshifumi[1]; HAMA, Hiroyuki[2]
([1]Nagoya Univ.; [2]Tohoku Univ.)

Q-switching operation of the storage ring FEL provides high peak power and is therefore very attractive to application experiments. On the UVSOR, the Q-switching is performed by modulation of RF frequency. In the operation, an excitation of a coherent synchrotron oscillation of electron beam is observed. However, observed damping of the oscillation is faster than one due to synchrotron radiation by factor 100 and, therefore the influence on the FEL lasing is very small. Detailed analysis reveals that the phenomenon is explained with the Robinson damping.

VIII-FF-3 Ion Trapping at UVSOR

MOCHIHASHI, Akira; KATOH, Masahiro; HAYASHI, Kenji; HOSAKA, Masahito; TAKASHIMA, Yoshifumi[1]; YAMAZAKI, Jun-ichiro
([1]Nagoya Univ.)

A vertical tune shift depending on a beam current in multi-bunch condition was observed in the UVSOR electron storage ring. The vertical tune increased as decrease in the beam current, and the slope of the tune shift depended on the condition of the vacuum in the ring. Such change in the vertical tune was explained by change in stability condition of trapped ions on the beam current. The experimental results were consistent with the results from analytic and tracking calculations.

VIII-FF-4 Improvements of the Vacuum System for the UVSOR II

HORI, Yoichiro; YAMAZAKI, Jun-ichiro; KATOH, Masahiro; HAYASHI, Kenji; HOSAKA, Masahito; MOCHIHASHI, Akira; HAGA, Kaiichi[1]
([1]KEK-PF)

In the upgrading to the UVSOR II, all straight chambers and three bend chambers except some elements such as RF cavities and insertion devices should be replaced to new ones. Those were designed and fabricated considering to increase the pumping speed as much as possible in the bend section and the just downstream. The reconstruction work of the ring was started in April 2003. New beam position monitors were additionally equipped for the reinforcement of the focusing magnets in the UVSOR II. After the installation of all chambers, the ring was re-evacuated and baked. Beam injection to the ring was started in the middle of July. The following vacuum conditioning so-called beam scrubbing has been satisfactorily advanced for the user run scheduled to resume in September.

VIII-FF-5 A New Auger Electron Spectroscopy in Coincidence with Photoelectrons

ITO, Kenji; SHIGEMASA, Eiji

Auger photoelectron coincidence spectroscopy, which involves measuring Auger lines in coincidence with the corresponding photoelectron line, reveals a new trend for doubly charged atomic and molecular ions. The experimental resolution in this spectroscopy can be made as good as the instrument resolution permits; the spectral resolution is limited by a lifetime of the inner-shell hole produced by the photoelectron emission. However, the simultaneous measurements of the two electrons can make the situation such that, due to the energy conservation of the whole process, the instrumental resolution instead of the core-hole lifetime governs the spectral resolution. We are preparing for the experimental investigation that will be carried out at a newly constructed undulator beamline BL3U; a high-resolution and high-efficiency analyzer for threshold photoelectrons with a penetration field, and a high-resolution hemi-spherical analyzer or high-resolution time-of-flight spectrometer for Auger electrons. We have already tested the threshold photoelectron analyzer at UVSOR, and found that the energy resolution of a

few meV can be attained easily.

VIII-GG Researches by the USE of UVSOR

VIII-GG-1 Angle-Resolved Photoion Spectroscopy of NO_2 and SO_2

GEJO, Tatsuo[1]; TAKATA, Yasutaka[2]; HATSUI, Takaki; NAGASONO, Mitsuru; OJI, Hiroshi; KOSUGI, Nobuhiro; SHIGEMASA, Eiji
([1]IMS and Himeji Inst. Tech.; [2]IMS and RIKEN)

[*Chem. Phys.* **289**, 15–29 (2003)]

Based on recent conceptual and technological improvements for soft x-ray monochromators, a varied-line-spacing plane grating monochromator of the Hetrrick type is installed on the bending-magnet beamline BL4B in the UVSOR facility with a second generation VUV ring of the beam energy of 0.75 GeV. The BL4B has enabled us to realize various spectroscopic investigations under high resolution in the energy range of 90 to 800 eV. High-resolution angle-resolved photoion-yield spectra (ARPIS) of NO_2 and SO_2 have been measured in the N and O *K*-shell excitation regions. The fragment-ion yield spectra measured at 0° and 90° relative to the electric vector of the light reveal excitation symmetries of complicated electronic states. The spectral features are interpreted in comparison with other transition systems and quantum chemical calculations show strong or weak Rydberg-valence mixing depending on the excitation site in the molecule.

VIII-GG-2 Atmospheric Lifetime of SF_5CF_3

TAKAHASHI, Kenshi[1]; NAKAYAMA, Tomoki; MATSUMI, Yutaka[1]; SOLOMON, Susan[2]; GEJO, Tatsuo; SHIGEMASA, Eiji; WALLINGTON, Tim J.[3]
([1]Nagoya Univ.; [2]Natl. Oceanic Atmospheric Admin.; [3]FORD Res. Lab.)

[*Geophys. Res. Lett.* **29**, 10.1029/2002GL015356, 7-1–4 (2002)]

The vacuum ultraviolet (VUV) absorption spectrum of SF_5CF_3 was measured over the range 106–200 nm. At 121.6 nm, $\sigma(\text{base } e) = (7.8 \pm 0.6) \times 10^{-18}$ cm^2 molecule^{-1}, in which quoted uncertainty includes two standard deviation from the least-square fit in the Beer-Lambert plot and our estimate of potential systematic errors associated with measurements of the reactant concentrations. The VUV spectrum and literature data for electron attachment and ion-molecule reactions were incorporated into a model of the stratosphere, mesosphere, and lower thermosphere. This information provides better constraints on the atmospheric lifetime and hence on the potential of this highly radiatively-active trace gas to influence the climate system. The atmospheric lifetime of SF_5CF_3 is dominated by dissociative electron attachment and is estimated to be approximately 950 years. Solar proton events could reduce this to a lower limit of 650 years.

VIII-GG-3 Pump /Probe Experiments with FEL and SR Pulses at UVSOR

GEJO, Tatsuo[1]; SHIGEMASA, Eiji; NAKAMURA, Eiken; HOSAKA, Masahito; MOCHIHASHI, Akira; KATOH, Masahiro; YAMAZAKI, Jun-ichiro; HAYASHI, Kenji; TAKASHIMA, Yoshifumi; HAMA, Hiroyuki[2]
([1]IMS and Himeji Inst. Tech.; [2]IMS and Tohoku Univ.)

Storage Ring Free Electron Laser (SRFEL or FEL) has been developed at many synchrotron radiation (SR) facilities all over the world as a powerful light source owing to its high power, high coherence and unique temporal feature. Pump and probe experiments using FEL and SR pulses have been tried to perform for the last decade, since the FEL pulse naturally synchronizes with the SR one. Recently, we have successfully carried out the two-photon double-resonant excitation on Xe atoms, utilizing an SR pulse as a pump and an FEL pulse as a probe light.

In the present work, separate experiments were implemented at two different beamlines of BL3A1 and BL7B at UVSOR. At BL3A1, no monochromator is installed. Therefore, an LiF filter was employed to suppress higher order harmonics of the undulator radiation. The FEL pulses were extracted through the backward mirror of the optical klystron at BL5 and transported to experimental stations through series of multi-layer mirrors. The flight path of FEL, which was adjusted to synchronize timing between the FEL and the SR pulses, was about 30 m. A focusing mirror (f = 10 m) was placed in the center of the flight path to keep the beam size of FEL small throughout the transport. About 69 % of the extracted power was transferred to the experimental station. Fine-tuning of the delay timing was made by using a movable optical delay system (50 cm) at the experimental station. The FEL and SR pulses introduced, coaxially crossed an effusive jet of Xe atoms from a gas nozzle. The singly charged Xe ions produced in the interaction region were detected by means of a conventional channeltron. During the experiment, there were serious background signals due to scattered stray light of SR pulses (typically about 10^5 counts/sec), which made it difficult to detect the real ion signals. In order to overcome such a difficulty, we temporarily employed the Q-switching technique. With use of this technique, much larger peak power of FEL than that in the normal operation is provided, although the duration of lasing becomes relatively short (~ 0.2 msec). However, if events are selected only during this duration, the improvement of signal to noise ratio (S/N)

by a factor of 100 can be achieved.

Figure 1 shows the excitation spectrum near the Xe* $5p^5 5d$ resonance region obtained by setting the FEL wavelength to the maximum of the $5d \rightarrow 4f'$ transition. The background pressure indicated in the figure was kept constant during the measurement. The clear enhancement just below the Xe* $5p^5 5d$ resonance around 117.5 nm is observed in Figure 1, which has not been detected in the previous measurements at a lower pressure. This result strongly suggests that the newly found structure indicated by the arrow is relevant to the formation of Xe clusters, mainly dimers. From the consideration of the excitation energy, it seems to be safe to say that an excited state of Xe_2 exists near the $5p \rightarrow 5d$ transition of the Xe atom, which act as intermediate states in the present experiments.

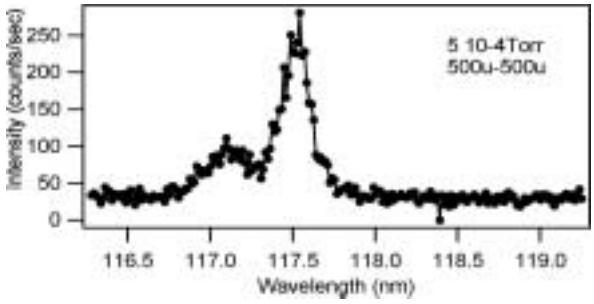

Figure 1. Two-photon ionization signal of Xe as a function of the wavelength of SR.

VIII-GG-4 Photoemission Study of Mixed-Valent Tm-Monochalcogenides: Evidence of Electron-Correlation Effect in Different Tm-Core Levels

NATH, Krishna G.[1]; UFUKTEPE, Yuksel[2]; KIMURA, Shin-ichi; HARUYAMA, Yuichi[3]; KINOSHITA, Toyohiko[4]; MATSUMURA, Takeshi[5]; SUZUKI, Takashi[5]; OGASAWARA, Haruhiko[4]; KOTANI, Akio[4]

([1]JAERI.; [2]Univ. Cukurova, Turkey; [3]Himeji Inst. Tech.; [4]Univ. Tokyo.; [5]Tohoku Univ.)

[*J. Phys. Soc. Jpn.* **72**, 1792–1799 (2003)]

Systematic results of the photoemission spectra for different core levels such as, Tm 4*p*, 5*p* and 3*d* in the mixed valent Tm-monochalcogenides (TmS, TmSe and TmTe) obtained by both experimentally and theoretically are reported. The effects of the electron–electron correlation due to the interaction between core-holes and 4*f*-electrons or the interaction between different configurations are considered to explain the spectral features, depending on the principal (n) and orbital quantum numbers of the core levels. Any sharp peak corresponding to a spin–orbital term is not observed especially from the $n = 4$ states. Instead, the multiplet structures are dominantly observed, and the physical identity of the spin–orbital peaks is totally or partially dissolved into the multiplets. Moreover, the electron-correlation effect is found to be dependent on the valence components (Tm^{2+} and Tm^{3+}). In the case of the Tm 4*p* core level, in which the principal quantum number is identical with the valence 4*f*, the correlation effect is stronger, and the configuration interaction is therefore considered to explain the spectral features. The photoemission spectra for the shallow core level Tm 5*p* also show the effect of electron correlation, but weaker than that for Tm 4*p*. This has been confirmed bythe resonant photoemission spectroscopy taken at Tm 4*d*–4*f* absorption edges. In addition, the feature of Tm 3*d* photoemission spectra is discussed. All the experimental spectra are compared with the calculated ones. It is therefore understood that the electron correlation effect plays an important role on determining the various features in Tm 4*p*, 5*p* and 3*d* photoemission spectra.

VIII-GG-5 Infrared Spectroscopy under Extreme Conditions

KIMURA, Shin-ichi; NISHI, Tatsuhiko[1]; TAKAHASHI, Toshiharu[2]; HIRONO, Toko[3]; IKEMOTO, Yuka[3]; MORIWAKI, Taro[3]; KIMURA, Hiroaki[3]

([1]GUAS; [2]Kyoto Univ.; [3]JASRI/SPring-8)

[*Physica B* **329-333**, 162–1626 (2003)]

We constructed a magneto-optical microspectroscopy apparatus in the infrared region using a synchrotron radiation, SPring-8. In the apparatus, an infrared microscope with the spatial resolution of 11 mm is combined with low temperatures of 3.5 K and high magnetic fields of 14 T. The purpose is to investigate the electronic structure under extreme conditions of tiny materials such as organic conductors and of small region and the spatial distribution of electronic structures. After the installation of high pressure cells, optical measurements under multiple-extreme conditions is available.

VIII-GG-6 Collapse of Kondo Lattice in $Ce_{1-x}La_xPd_3$ (x = 0, 0.03)

KIMURA, Shin-ichi; IWATA, Hideki[1]; KANAI, Kaname[2]; SHIN, Sik[2]; SCHMERBER, G.[3]; KAPPLER, J. P.[3]; PARLEBAS, J. C.[3]

([1]Kobe Univ.; [2]Univ. Tokyo; [3]Univ. Luis Pasteur, France)

[*Acta Physica Polonica B* **34**, 975–978 (2003)]

The change of the electronic structure as well as the hybridization between the localized 4*f* state and the conduction band (cf hybridization) of $Ce_{1-x}La_xPd_3$ (x = 0, 0.03) due to the La-substitution has been studied by the optical conductivity spectra in the infrared region. The width of the optical transition of Pd $4d \rightarrow$ Ce $4f$ states that was mainly observed in the energy region shrinks by the La-substitution. This means that the cf hybridization is strongly suppressed by the absence of the periodicity of the Ce-ion.

VIII-GG-7 Optical Reflectivity of the Clathrate Compound Ba_6Ge_{25}

SICHELSCHMIDT, Jourg[1]; VOEVODIN,

Vladimir[1]; PASCHEN, Silke[1]; CARRILLO-CABRERA, W.[1]; GRIN, Yu.[1]; STEGLICH, Franck[1]; KIMURA, Shin-ichi
([1]Max-Planck-Inst. Chem. Phys. Stoffe, Germany)

[*Acta Physica Polonica B* **34**, 613–616 (2003)]

We report optical investigations of the electronic properties of the clath-rate compound Ba_6Ge_{25} in which at room temperature Ba atoms "rattle" in Ge-network cavities. When lowering the temperature across T_S ~ 200 K a lock-in of the Ba-atoms to split-site positions in the cages is observed. The low energy Drude type of reflectivity is characterized by a low charge carrier density which smoothly varies with temperature. However, the Drude relaxation time of the charge carriers is found to be almost temperature independent, especially when cooling below T_S where, according to thermopower data, the effective mass is enhanced. This behavior could indicate a formation of polaronic quasi particles below T_S which is also supported by previous measurements of magnetic susceptibility of Ba_6Ge_{25}.

VIII-GG-8 Infrared Magneto-Optical Imaging of κ-(BEDT-TTF)$_2$Cu[N(CN)$_2$]Br

NISHI, Tatsuhiko[1]; KIMURA, Shin-ichi; ITO, Takahiro; TAKAHASHI, Toshiharu[2]; MIYAGAWA, Kazuya[3]; KANODA, Kazushi[3]
([1]GUAS; [2]Kyoto Univ.; [3]Univ. Tokyo)

Since the ground state of κ-(BEDT-TTF)$_2$Cu-[N(CN)$_2$]Br locates in the vicinity of the boundary of the Mott transition, the weak perturbations of the deuteration and the rapid cooling make the phase transition from the superconductor to the antiferro-magnetic insulator. The phase separation is expected to appear on the boundary by the magnetic susceptibility data. Then we observed the spatial distribution of the optical spectrum in the infrared region because the peak at around $h\nu$ = 0.3 eV reflects the physical properties. At the result, the spectral distribution on the sample surface at T = 4 K was observed in spite that no distribution appears at 50 K. The result indicates that the phase separation appears at 4 K.

VIII-GG-9 Construction of Angle-Resolved Photoemission Apparatus for Solids

ITO, Takahiro; KIMURA, Shin-ichi; SODA, Kazuo[1]; TAKEUCHI, Tsunehiro[1]; TAKAHASHI, Kazutoshi[2]
([1]Nagoya Univ.; [2]Saga Univ.)

We have constructed a new high-energy-resolution angle-resolved photoemission apparatus shown in Figure 1 for the helical undulator beam line, BL5U. The main purpose is the investigation of the electronic structure near the Fermi level as well as the topological shape of the Fermi surface, so-called "fermiology," of solids, thin films and surfaces. The apparatus consists of a photoelectron analyzer (MBS-Toyama A-1), a main chamber, a sample preparation chamber, a liquid-He flow-type cryostat (JANIS ST-400 UHV) with a manipulator, a He lamp with UV monochromator (GAMMADATA VUV5000 + VUV5040) and several vacuum pumps. Samples are transferred to the preparation chamber from a load-lock chamber, a molecular beam epitaxy system or other chambers that can be replaced by users.

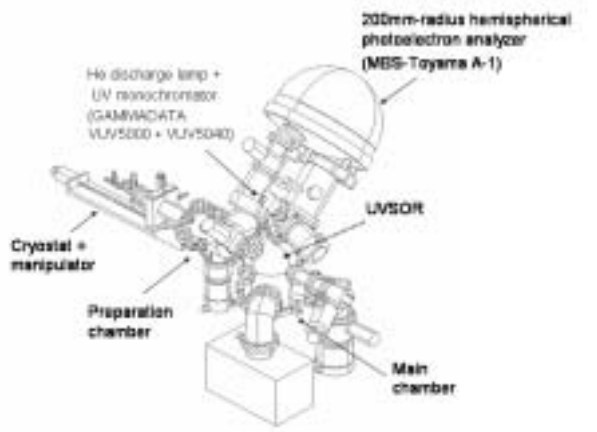

Figure 1. High-energy-resolution angle-resolved photo-emission apparatus for BL5U.

Computer Center

VIII-HH Computer Simulation of Quantum Systems in Condensed Phase

VIII-HH-1 An Analysis of Molecular Origin of Vibrational Energy Transfer from Solute to Solvent Based upon Path Integral Influence Functional Theory

MIKAMI, Taiji; OKAZAKI, Susumu

[*J. Chem. Phys.* **119**, 4790–4797(2003)]

Molecular process of vibrational energy relaxation of CN^- ion in the aqueous solution has been investigated based upon path integral influence functional theory. In order to obtain a molecular-based picture, bath normal coordinates were retransformed to Cartesian coordinate, Eulerian coordinate, and intramolecular vibrational coordinate of the solvent molecule. Then, based upon this retransformation matrix, coupling of the solute with the normal modes may be assigned to the couplings with the solvent molecules. Further, with respect to two-phonon process which is dominant in the relaxation of the present system, the relaxation may be divided into single- and dual-molecular processes. We show that the single-molecular relaxation is dominant in the relaxation. Further, water molecules in the first hydration shell play an essential role in the relaxation, whereas the solvent molecules outside the first hydration shell make little contribution. The solvent molecules located in the direction of CN^- bond axis were found to make great contribution to the relaxation.

VIII-HH-2 Mixed Quantum-Classical Molecular Dynamics Study of Vibrational Relaxation of CN^- Ion in Water: An Analysis of Coupling as a Function of Time

SATO, Masahiro; OKAZAKI, Susumu

[*J. Chem. Phys.* submitted]

Mixed quantum-classical molecular dynamics method has been applied to vibrational relaxation of CN^- in water. The calculated relaxation time was in good agreement with that based upon Fermi's golden rule with classical interaction. Flexible water model adopted here enhanced the relaxation rate by a factor of about 5 compared with the rigid rotor model. This supports our previous result of path integral influence functional theory that intramolecular bending of water plays an essential role in the relaxation. Time-dependent interaction between the solute vibrational degree of freedom and the solvent water shows random-noise-like behavior, no collisional or stationary coupling observed in gas or solid, respectively, being found in the liquid. The interaction has been analyzed in detail defining the effective coupling for the relaxation. The relaxation mechanism in the liquid may be described by a variety of effective couplings, *i.e.*, relaxing and exciting as well as strong and weak, which arise successively as a function of time.

VIII-II Molecular Dynamics Study of Classical Complex Systems

VIII-II-1 A Molecular Dynamics Study of Single Molecular Manipulation by AFM Cantilever—Mechanical Extension of Polyalanine—

IWAHASHI, Kensuke; MIKAMI, Taiji; IKAI, Atsushi[1]; OKAZAKI, Susumu
([1]Tokyo Inst. Tech.)

Potential of mean force of polyalanine in water has been calculated as a function of molecular length by molecular dynamics calculations simulating mechanical extension of the molecule by AFM cantilever. When the molecule keeps alpha helix structure, it behaves like a spring following Hooke's law. After the helix is broken, the force becomes large with increasing extension. Hydrophobic interaction and conformational entropy must play an important role for this force-extension curve. At the extension of about 100%, the force curve rises sharply, showing the increase of molecular bending energy of all trans conformation.

VIII-JJ Development of Simulation Algorithms for Quantum Many-Body Systems

VIII-JJ-1 Path Integral Hybrid Monte Carlo Algorithm for Correlated Bose Fluids

MIURA, Shinichi; TANAKA, Junji

[*J. Chem. Phys.* in press]

Path integral hybrid Monte Carlo (PIHMC) algorithm for strongly correlated Bose fluids has been developed. This is an extended version of our previous method applied to a model system consisting of non-interacting bosons. Our PIHMC method for the correlated Bose fluids is constituted of two trial moves to sample path-variables describing system coordinates along imaginary time and a permutation of particle labels giving a boundary condition with respect to imaginary time. The path-variables for a given permutation are generated by a hybrid Monte Carlo method based on path integral molecular dynamics techniques. Equations of motion for the path-variables are formulated on the basis of a collective coordinate representation of the path, staging variables, to enhance the sampling efficiency. The permutation sampling to satisfy Bose-Einstein statistics is performed using the multilevel Metropolis method developed by Ceperley and Pollock. Our PIHMC method has successfully been applied to liquid helium-4 at a state point where the system is in a superfluid phase. Parameters determining the sampling efficiency are optimized in such a way that correlation among successive PIHMC steps is minimized.

VIII-KK Theoretical Studies on Electronic Structure and Dynamics of Electronically Excited States

VIII-KK-1 Millimeter-Wave Spectroscopy of the Internal-Rotation Band of the X-HCN Complex (X = He, Ne, and Ar) and the Intermolecular Potential Energy Surface

HARADA, Kensuke[1]; TANAKA, Keiichi[1]; TANAKA, Takehiko[1]; NANBU, Shinkoh; AOYAGI, Mutsumi[1]
([1]Kyusyu Univ.)

Millimeter-wave absorption spectroscopy combined with a pulsed-jet expansion technique was applied to the measurement of the internal-rotation band of the X-HCN (X = He, Ne, and Ar) in the frequency region of 95–125 GHz. The observed transition frequencies were analyzed including their hyperfine splitting to yield an intermolecular potential energy surface, as improved from the one given by a coupled-cluster single double (triple) ab initio calculation. Regarding the He complex, the surface obtained has a global minimum in the linear configuration (He···H–C–N) with a well depth of 30.2 cm^{-1}, and the saddle point located in the anti-linear configuration (H–C–N···He) is higher by 8.174 cm^{-1} in energy than the global minimum. The distance R_m between the He atom and the center of mass of HCN along the minimum energy path shows a strong angular dependence; R_m = 4.169 Å and 4.040 Å in the linear and anti-linear forms, respectively, while it is 3.528 Å in a T-shaped configuration. The energy level diagram is consistent with the millimeter-wave observation. And now, we are trying to measure the stretching motion located just below the dissociation limits.

VIII-KK-2 Theoretical Study of Vibrational Spectra of *p*-Tert-Butylcalix[4]crown-6-Ether Complexed with Ethyl Ammonium Cations

MINAMINO, Satoshi; CHOE, Jong-In[1]; CHANG, Suk-Kyu[1]; MIZUTANI, Fumiyasu; NANBU, Shinkoh
([1]Chung-Ang Univ.)

[*Chem. Phys. Lett.* **374**, 572–576 (2003)]

Theoretical infrared (IR) absorption spectra were calculated for *p-tert*-butylcalix[4] crown-6-ether (1) in the cone conformer and its ethyl ammonium complex. The IR spectra were obtained by restricted Hartree-Fock (RHF) calculations with the 6–31 G basis set. For the purpose of an absorption band assignment on the host molecule, guest molecule, and complexes thereof, we discussed a way to distinguish a specific molecule by comparing the calculated vibrational spectra. The theoretical result for the host molecule and its ethyl ammonium complex were preliminarily compared with the experimental result, and found that the calculated result agrees well with the features of the experimental spectra.

VIII-KK-3 He*(2^3S) Penning Ionization of H_2S I. Theoretical Franck-Condon Factors for the $H_2S(X^1A_1, v' = 0) \rightarrow H_2S^+ (X^2B_1, A^2A_1)$ Ionization and the H_2S^+ (A-X) Transitions

TOKUE, Ikuo[1]; YAMASAKI, Katsuyoshi[1]; NANBU, Shinkoh
([1]Niigata Univ.)

[*J. Chem. Phys.* in press]

In order to elucidate the ionization dynamics, in particular the vibrational distribution, of $H_2S^+(\tilde{A})$ produced by the Penning ionization of H_2S with He*(2^3S) atoms, the Franck-Condon factors (FCFs) were presented for the $H_2S(\tilde{X}) \rightarrow H_2S^+(\tilde{X}, \tilde{A})$ ionization and the $H_2S^+(\tilde{A}–\tilde{X})$ transition, and Einstein's A coefficients were presented for the latter transition. The FCFs were obtained by quantum vibrational calculations using the global potential energy surfaces (PESs) of $H_2S(\tilde{X}\,^1A_1)$ and $H_2S^+(\tilde{X}\,^2B_1, \tilde{A}\,^2A_1, \tilde{B}\,^2B_2)$ electronic states. The global PESs were determined by the multi-reference configuration interaction calculations with the Davidson correction (MRCI+Q) and the interpolant moving least squares (IMLS) method combined with the Shepard interpolation. The obtained FCFs exhibit that the $H_2S^+(\tilde{X})$ state primarily populates the vibrational ground state since its equilibrium geometry is almost equal to that of $H_2S(\tilde{X})$, while the bending mode (ν_2) is strongly enhanced for the $H_2S^+(\tilde{A})$ state; the maximum in the population is around ν_2 = 6–7. In the same manner, the bending progressions are expected to consist of the great part of the $H_2S^+(\tilde{A}–\tilde{X})$ emission. A detailed comparison with the experimental study for this system is reported in the accompanying paper, Paper II.

VIII-KK-4 He*(2^3S) Penning Ionization of H_2S II. Formation of $SH^+(A^3\Pi)$ and H_2S^+ (A^2A_1) Ions

TOKUE, Ikuo[1]; YAMASAKI, Katsuyoshi[1]; NANBU, Shinkoh
([1]Niigata Univ.)

[*J. Chem. Phys.* in press]

Emissions in the 200–750 nm region produced by the collision of He(2^3S) with H_2S were studied under single-collision conditions. The hydrogen Balmer lines and the $SH^+(A^3\Pi–X^3\Sigma^-)$ and $H_2S^+(\tilde{A}\,^2A_1–\tilde{X}\,^2B_1)$ bands were assigned. The total emission cross section (σ_{em}) was evaluated to be $(1.7 \pm 0.3) \times 10^{-20}$ m^2 at a collision energy of 150 meV. The σ_{em}'s of the $SH^+(A–X)$ and $H_2S^+(\tilde{A}–\tilde{X})$ bands decreased with increase in the collision energy in the 115–200 meV range, indicating that attractive forces are effective for the incident channels with regard to the formation of these species. The rotational distribution of $SH^+(A^3\Pi, v' = 0)$ is represented by a Boltzmann temperature of 870 ± 80 K. The $H_2S^+(\tilde{A}\,^2A_1–\tilde{X}\,^2B_1)$ emission, which was assigned

for the first time in the Penning ionization of H_2S, primarily consists of the bending progressions. The internal populations of $H_2S^+(\tilde{A})$ were analyzed using the vibrational energies and Einstein's *A* coefficients calculated in this study. The details of the calculation and derived spectroscopic constants are reported in the accompanying paper, Paper I. The populations obtained for the bending vibration (ν_2') of $H_2S^+(\tilde{A})$ show an inverted distribution with a peak at v_2' = 3. This distribution is shifted lower compared that with a peak at v_2' = 4–5 observed by He(2^3S) Penning ionization electron spectroscopy and that with a peak at v_2' = 6–7 predicted by the theoretical Franck-Condon factors (FCFs) for the $H_2S(\tilde{X})$–$H_2S^+(\tilde{A})$ ionization. The origin of the difference is discussed concerning the formation mechanism of $H_2S^+(\tilde{A}^2A_1)$.

VIII-KK-5 Theoretical Analysis of the Oxygen Insertion Process in the Oxidation Reactions of H_2O + H/Si(100) and 2H + H_2O/Si(100); Calculation of an Ab Initio Molecular Orbital Method and an Analysis of the Tunneling Reaction

WATANABE, Hidekazu[1]; NANBU, Shinkoh; MAKI, Jun[2]; WANG, Zhi-Hong; URISU, Tsuneo; AOYAGI, Mutsumi[2]; OOI, Kenta[1]
([1]Niigata Univ.; [2]Kyusyu Univ.)

[*Chem. Phys. Lett.* submitted]

The reaction paths were analyzed, by an ab initio molecular orbital method, for the surface reaction systems, 2H + H_2O/Si(100)-(2×1) and H_2O + H/Si(100)-(2×1), in which SiH_2 species with one or two oxygen atom-inserted back bonds have been observed as new stable reaction products. It was found that common metastable states exist in both systems, and the initial energy is sufficiently higher than all transition state energies in the former system, while in the latter system, the energy of the highest transition state is much higher than the initial energy, and thus a tunneling effect plays an important role.

VIII-KK-6 Optimal Control of Quantum Chaotic Dynamics

TAKAMI, Toshiya; FUJISAKI, Hiroshi[1]; MIYADERA, Takayuki[2]
([1]Boston Univ.; [2]Tokyo Univ. Sci.)

We numerically investigate how chaos affects controllability of wavepacket dynamics using the monotonically convergent method of optimal control theory introduced by Zhu, Bonita, and Rabitz [*J. Chem. Phys*. **108**, 1953 (1998)]. We find that a quantized kicked rotor in a bounded phase space is successfully controlled with the method, *i.e.*, an initial Gaussian wavepacket can be steered to a target Gaussian wavepacket with a high probability, even in strongly chaotic regions when the target time T is larger than a minimal time $T_{\min}$. We also find that $T_{\min}$ saturates to a certain value as the system becomes a random matrix system.

RESEARCH ACTIVITIES IX
Center for Integrative Bioscience

IX-A Single-Molecule Physiology

A single molecule of protein (or RNA) enzyme acts as a machine which carries out a unique function in cellular activities. To elucidate the mechanisms of various molecular machines, we need to observe closely the behavior of individual molecules, because these machines, unlike man-made machines, operate stochastically and thus cannot be synchronized with each other. By attaching a tag that is huge compared to the size of a molecular machine, or a small tag such as a single fluorophore, we have been able to image the individual behaviors in real time under an optical microscope. Stepping rotation of the central subunit in a single molecule of F_1-ATPase has been videotaped, and now we can discuss its detailed mechanism. RNA polymerase has been shown to be a helical motor that rotates DNA during transcription. Myosin V is another helical motor that moves as a left-handed spiral on the right-handed actin helix. Single-molecule physiology is an emerging field of science in which one closely watches individual, "live" protein/RNA machines at work and examines their responses to external perturbations such as pulling and twisting. I personally believe that molecular machines operate by changing their conformations. Thus, detection of the conformational changes during function is our prime goal. Complementary use of huge and small tags is our major strategy towards this end.

http://www.k2.ims.ac.jp/

IX-A-1 The ATP-Waiting Conformation of Rotating F_1-ATPase Revealed by Single-Pair Fluorescence Resonance Energy Transfer

YASUDA, Ryohei[1]; MASAIKE, Tomoko[2,3]; ADACHI, Kengo; NOJI, Hiroyuki[4]; ITOH, Hiroyasu[5]; KINOSITA, Kazuhiko, Jr.
([1]Cold Spring Harbor Laboratory; [2]ERATO; [3]Tokyo Inst. Tech.; [4]Univ. Tokyo; [5]Hamamatsu Photonics)

[*Proc. Natl. Acad. Sci. U.S.A.* **100**, 9314–9318 (2003)]

F_1-ATPase is an ATP-driven rotary motor in which a rod-shaped γ subunit rotates inside a cylinder made of $\alpha_3\beta_3$ subunits. To elucidate the conformations of rotating F_1, we measured fluorescence resonance energy transfer (FRET) between a donor on one of the three βs and an acceptor on γ in single F_1 molecules. The yield of FRET changed stepwise at low ATP concentrations, reflecting the stepwise rotation of γ. In the ATP-waiting state, the FRET yields indicated a γ position ≈ 40° counterclockwise (= direction of rotation) from that in the crystal structures of mitochondrial F_1, suggesting that the crystal structures mimic a metastable state before product release.

IX-A-2 Single Molecule Imaging of the Rotation of F_1-ATPase

ADACHI, Kengo; NOJI, Hiroyuki[1]; KINOSITA, Kazuhiko, Jr.
([1]Univ. Tokyo)

[*Methods in ENZYMOLOGY* **361**, 211–227 (2003)]

A single molecule of F_1-ATPase has been shown to be a rotary motor, driven by adenosine triphosphate (ATP) hydrolysis, in which the central γ subunit rotates against a surrounding cylinder made of alternately arranged three α and three β subunits. Together with another (yet putative) proton-driven rotary motor F_o, it constitutes the F_oF_1-ATP synthase that synthesizes ATP from adenosine diphosphate (ADP) and inorganic phosphate using proton flow as the energy source. Isolated F_1 composed of $\alpha_3\beta_3\gamma_1\delta_1\varepsilon_1$ subunits only hydrolyzes ATP, and hence is called F_1-ATPase. Its subcomplex $\alpha_3\beta_3\gamma$ suffices for rotation driven by ATP hydrolysis. Single-molecule imaging of this subcomplex has revealed detailed mechanical and kinetic properties of the motor1 activity, and high-resolution atomic structures of F_1 are already available. At present, F_1-ATPase is one of the best characterized molecular motors, or nucleotide-driven molecular machines. It is possible to learn a lot from this rotary machine about the molecular mechanism of chemo-mechanical energy transduction.

Because all molecular machines work stochastically, their operations can never be synchronized with each other in a rigorous sense. Thus, it is necessary to watch the individual behaviors closely. With F_1-ATPase, for example, we have been able to show that it rotates in a unique direction, that it does so in discrete 120° steps, and that 120° steps are resolved into ~ 90° and ~ 30° substeps at low ATP concentrations. We have also been able to measure its rotary torque, and have shown that its energy conversion efficiency can reach ~ 100%. We believe that it would be very difficult, if not impossible, to obtain these results without dealing with individual molecules. Here we describe in detail the techniques involved, hoping that they may also be applicable to other molecular machines, in particular to the detection of conformational changes underlying their function (note that a conformational change accompanies reorientation, or partial rotation, of one part against the other).

For the detection of rotation (or conformational changes), we recommend the complementary use of large and small probes. Here we describe two examples, an actin filament as a probe that is large compared to the rotary motor, and a single fluorophore as a small and

less perturbing probe. We begin with the preparation of materials, and proceed to the setting of functional motor molecules on a glass surface and then to imaging and analysis.

IX-B Bioinorganic Chemistry of Heme-Based Sensor Proteins

Heme-based sensor proteins are a newly recognized class of heme proteins, in which the heme acts as a sensor of gaseous effector molecules such as O_2, NO, and CO. Our research interests focus on the CO-sensing transcriptional activator CooA and the O_2-sensing signal transducer HemAT. We have elucidated the structure and function relationships of CooA and HemAT by mutagenesis and some spectroscopic studies.

IX-B-1 Characterization of the Heme Environmental Structure of Cytoglobin, a Fourth Globin in Humans

SAWAI, Hitomi[1]; KAWADA, Norifumi[1]; YOSHIZATO, Katsutoshi[1]; NAKAJIMA, Hiroshi; AONO, Shigetoshi; SHIRO, Yoshitsugu[1]
([1]RIKEN HARIMA Inst./SPring 8)

[*Biochemistry* **42**, 5133–5142 (2003)]

Cytoglobin (Cgb) represents a fourth member of the globin superfamily in mammals, but its function is unknown. Site-directed mutagenesis, in which six histidine residues were replaced with alanine, was carried out, and the results indicate that the imidazoles of His81 (E7) and His113 (F8) bind to the heme iron as axial ligands in the hexacoordinate and the low-spin state. The optical absorption, resonance Raman, and IR spectral results are consistent with this conclusion. The redox potential measurements revealed an *E*' of 20 mV (*vs* NHE) in the ferric/ferrous couple, indicating that the imidazole ligands of His81 and His113 are electronically neutral. On the basis of the ν(Fe–CO) and ν(C–O) values in the resonance Raman and infrared spectra of the ferrous–CO complexes of Cgb and its mutants, it was found that CO binds to the ferrous iron after the His81 imidazole is dissociated, and three conformers are present in the resultant CO coordination structure. Two are in closed conformations of the heme pocket, in which the bound CO ligand interacts with the dissociated His81 imidazole, while the third is in an open conformation. The ν(Fe–O_2) in the resonance Raman spectra of oxy Cgb can be observed at 572 cm^{-1}, suggesting a polar heme environment. These structural properties of the heme pocket of Cgb are discussed with respect to its proposed *in vivo* oxygen storage function.

IX-B-2 Structure and Function of the CO-Sensor Protein CooA

AONO, Shigetoshi; KOBAYASHI, Katsuaki; INAGAKI, Sayaka

CooA from a photosynthetic bacterium, *R. rubrum*, is the only example of CO-sensor protein so far. We have found a CooA homologue in a thermophilic CO oxidizing bacterium, *Carboxydothermus hydrogenoformans*, and constructed an expression system of CooA from *C. hydrogenoformans* (Ch-CooA) as described below. The gene encoding Ch-CooA was prepared by PCR with a chromosomal DNA of *C. hydrogenoformans* as the template and the two primers (5'-AGG AGA GGA CTA TGG CCA CCC AAA TGA GAT TAA CCG AC-3' and 5'- TTA CTA AAC GCC TGA GGA AAA CTC-3'). The DNA fragment containing *Ch-cooA* was subcloned in pCR4-TOPO vector and then inserted at the EcoRI-site in pKK223-3 vector to construct an expression vector. Ch-CooA was expressed in the soluble fraction of *E. coli* and purified to a homogeneous state by using Q-Sepharose, Hitrap Heparin, and Sephacryl S-100 column chromatography. The purified Ch-CooA showed typical uv/vis spectra for 6-coordinate, low-spin heme proteins. Characterization of the biochemical and biophysical properties of Ch-CooA is now in progress.

IX-B-3 Structure and Function of the Oxygen Sensing Signal Transducer Protein HemAT from *Bacillus subtilis*

AONO, Shigetoshi; KOBAYASHI, Katsuaki; YOSHIMURA, Hideaki

HemAT-Bs is a heme-containing signal transducer protein responsible for aerotaxis of *Bacillus subtilis*. The recombinant HemAT-Bs expressed in *E. coli* is purified as the oxy form in which oxygen is bound to the ferrous heme. HemAT-Bs as isolated gives the Soret, α and β peaks at 414, 578, and 543 nm, respectively. This spectrum is typical of 6-coordinate, low-spin hemoproteins and resembles that of the oxy form of Mb. On deoxygenation with sodium dithionite, HemAT-Bs shows a spectrum with the Soret peak at 431 nm and a single peak at 563 nm in the Q-band region. This spectrum is typical of 5-coordinate, high-spin ferrous hemoproteins, which shows the formation of deoxy HemAT-Bs. CO-bound HemAT-Bs is formed upon the reaction of dithionite reduced HemAT-Bs with CO, which shows the Soret, α and β peaks at 422, 567, and 543 nm, respectively.

HemAT-Bs consists of two domains, *i.e.*, the N-terminal sensor domain that contains a heme and the C-terminal signaling domain. When the C-terminal signaling domain is truncated, the resulting mutants show a different oxygen affinity and a heme environmental structure from those of wild-type HemAT-Bs. These results suggest that a conformational change around the heme pocket is responsible for the intramolecular signal transduction from the sensor domain to the signaling domain.

IX-C Electronic Structure and Reactivity of Active Sites of Metalloproteins

Metalloproteins are a class of biologically important macromolecules that have various functions such as oxygen transport, electron transfer, oxidation, and oxygenation. These diverse functions of metalloproteins have been thought to depend on the ligands from amino acid, coordination structures, and protein structures in immediate vicinity of metal ions. In this project, we are studying the relationship between the structures of the metal active sites and functions of metalloproteins.

IX-C-1 Trigonal Bipyramidal Ferric Aqua Complex with Sterically Hindered Salen Ligand as a Model for Active Site of Protocatechuate 3,4-Dioxygenase

FUJII, Hiroshi; FUNAHASHI, Yasuhiro

[*Angew. Chem., Int. Ed.* **41**, 3638–3641 (2002)]

Protocatechurate 3,4-dioxygenase (3,4-PCD) has been found in soil bacteria and is known to play a role in degrading aromatic molecules in nature. The enzyme is classified as an intradiol dioxygenase and cleaves catechol analogues bound to the iron(III) site into aliphatic products with incorporation of both atoms of molecular oxygen. It has been proposed that the enzyme does not activate an iron-bound oxygen molecule, but rather induces an iron-bound catecholate to react with O_2. Therefore, knowledge of the structure and electronic state of the iron site is essential to understanding the unique reaction of 3,4-PCD. A previous crystalstructu re analysis of 3,4-PCD from Pseudomonas putida revealed a distorted trigonal-bipyramidal ferric iron center with four endogenous protein ligands (Tyr 408, Tyr 447, His 460, and His 462) and a solvent-derived water molecule (see Figure 1). To understand the structure±function relationship of 3,4-PCD, attempts have been made over several decades to prepare inorganic modelcompl exes of 3,4-PCD. However, no iron(III) complex that reproduces the active site of 3,4-PCD has been characterized. We report here the first example of a distorted trigonal-bipyramidal ferric aqua complex with a sterically hindered salen ligand that not only duplicates the active site but also mimics the spectral characteristics of 3,4-PCD.

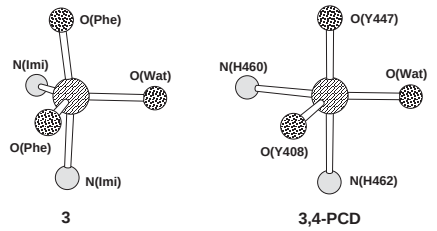

Figure 1. Comparison of Active Site Structures of Our Model Complex and 3,4-PCD.

IX-C-2 An Oxidizing Intermediate Generated from a Salen Iron Complex, Related to the Oxygen Activation by Mononuclear Nonheme Iron Enzymes

KURAHASHI, Takuya; KOBAYASHI, Yoshio[1]; NAGATOMO, Shigenori; KITAGAWA, Teizo; FUJII, Hiroshi
([1]RIKEN)

High-valent iron-oxo species are proposed to be the key reactive intermediate in oxidation reactions catalyzed by the oxygen-activating iron enzyme. In the case of heme enzymes, porphyrin model complexes have been extensively investigated. However, an insight into the nonheme oxidizing intermediate is still limited. Very recently, Wieghardt *et al.* reported the first example of the high-valent iron(IV) species from a nonheme model complex, utilizing the cyclam iron complex. In 2003, Que Jr. *et al.* succeeded in the X-ray crystallographic analysis of the iron(IV) μ-oxo species, using the similar nonheme iron complex. On the other hand, we have been attempting to prepare the nonheme Compound I analog from a salen iron complex. Herein we report the detailed electronic structure and the reactivity of the oxidizing intermediate generated from a salen iron complex and *m*CPBA. To model the monomeric iron center of enzymes, bulky mesityl substituents are introduced to the salen iron complex. Indeed, the aquo complex **1** is found in a monomeric form, due to the steric repulsion by the mesityl group, as already reported. Addition of *m*CPBA to the purple solution of the salen iron complex **1** in dichloromethane at –80 °C produced a blue-green solution (Figure 1). This solution gave a distinct UV-Vis spectrum (λ_{max} = 815 nm) from the starting solution. The intensity of the signal at 815 nm was totally attenuated at room temperature. These results suggest that oxidation of **1** with *m*CPBA generates a transient intermediate having a distinct electronic structure from **1**. The detailed structure of the blue-green intermediate is now being investigated by means of Mössbauer, EPR, NMR and resonance Raman spectroscopy.

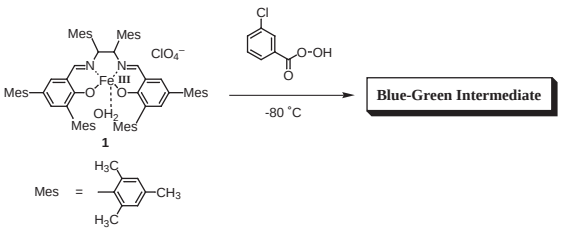

Figure 1. Formation of Blue-Green Intermediate from **1**.

IX-C-3 A Superoxo-Ferrous State in a Reduced Oxy-Ferrous Hemoprotein and Model Compounds

DAVYDOV, Roman[1]; SATTERLEE, James[2]; FUJII, Hiroshi; SAUER-MASARWA, Alexandra[3]; BUSCH, Daryle H.[3]; HOFFMAN, Brian M.[1]
([1]Northwestern Univ.; [2]Washington State Univ.; [3]Univ. Kansas)

[*J. Am. Chem. Soc.* in press]

Cryoreduction of the $[FeO_2]^6$ (n = 6 is the number of electrons in 3*d* orbitals on Fe and π* orbitals on O_2) dioxygen-bound ferroheme through (irradiation at 77 K generates an $[FeO_2]^7$ reduced oxy-heme. Numerous investigations have examined $[FeO_2]^7$ centers that have been characterized as peroxo-ferric centers, denoted $[FeO_2]^7_{per}$, in which a ferriheme binds a dianionic peroxo-ligand. The generation of such an intermediate can be understood heuristically if the $[FeO_2]^6$ parent is viewed as a superoxo-ferric center and the injected electron localizes on the O–O moiety. We here report EPR/ENDOR experiments which show quite different properties for the $[FeO_2]^7$ centers produced by cryoreduction of monomeric oxy-hemoglobin (oxy-GMH3) from *Glycera dibranchiata*, which is unlike mammalian globins in having a leucine in place of the distal histidine, and of frozen aprotic solutions of oxy-ferrous octaethyl porphyrin and of the oxy-ferrous complex of the heme model, cyclidene. These $[FeO_2]^7$ centers are characterized as superoxo-ferrous centers, ($[FeO_2]^7_{sup}$), with nearly unit spin density localized on a superoxo moiety which is end-on coordinated to a low-spin ferrous ion. This assignment is based on their *g* tensors and ^{17}O hyperfine couplings, which are characteristic of the superoxide ion coordinated to a diamagnetic metal ion, and on the absence of detectable endor signals either from the in-plane ^{14}N ligands or from an exchangeable H-bond proton. Such a center would arise if the electron that adds to the $[FeO_2]^6$ superoxo-ferric parent localizes on the Fe ion, to make a superoxo-ferrous moiety. Upon annealing to T > 150 K the $[FeO_2]^7_{sup}$ species recruit a proton and converts to peroxo/hydroperoxo-ferric ($[FeO_2H]^7$) intermediates. These experiments suggest that the primary reduction product is $[FeO_2]^7_{sup}$, and that the internal redox transition to $[FeO_2]^7_{per}/[FeO_2H]^7$ states is driven at least in part by Hbonding/ proton donation by the environment.

IX-C-4 Preparation of Artificial Metalloenzymes by Insertion of Chromium(III) Schiff Base Complexes into Apomyoglobin Mutants

OHASHI, Masataka[1]; KOSHIYAMA, Tomomi[1]; UENO, Takafumi[1]; YAMASE, Manabu[1]; FUJII, Hiroshi; WATANABE, Yoshihito[1]
([1]Nagoya Univ.)

[*Angew. Chem., Int. Ed.* **42**, 1005–1008 (2003)]

Construction of artificial metalloenzymes is one of the most important subjects in bioinorganic chemistry, because metalloenzymes catalyze chemical transformations with high selectivity and reactivity under mild conditions. There are several reports on protein design: introduction of metal binding sites, design of substrate binding cavities, chemical modification of prosthetic groups, and covalent attachment of metal cofactors. In particular, the covalent modification of proteins is a powerful tool for the generation of new metalloenzymes, while the efficiency of the modification is very much dependent on the position and reactivity of the cysteinyl thiol functional group. Herein, we describe a novel strategy for the preparation of artificial metalloenzymes by noncovalent insertion of metal-complex catalysts into protein cavities. The resulting semisynthetic metalloenzymes, apo-myoglobin (apo-Mb) reconstituted with Cr(III) Schiff base complexes, are able to catalyze enantioselective sulfoxidation.

IX-C-5 ^{63}Cu Study of Copper(I) Carbonyl Complexes with Various Tridentate Ligands

KUJIME, Masato; FUJII, Hiroshi

Copper is an essential trace element that plays an important role in a variety of biological functions. We have been studying coordination chemistry of copper complexes ligated by various tridentate ligands as synthetic models for the active site of copper protein which has three imidazolyl groups involved in the histidine residues. Previously we found that the copper(I) carbonyl complexes bearing hydrotris-(pyrazolyl)borates (TPB) exhibit the sharp ^{63}Cu NMR signal in contrast to the other CuL_3L' type complexes, and these chemical shifts were found to be related to the electron donating or withdrawing capabilities of TPB as supported by the dependence of the C≡O stretching vibration. The other copper(I) carbonyl complexes with a series of triazacyclononanes (TACN), tris(4-imidazolyl)carbinols (TIC), trispyrazolylmethanes (TPM), and tris(2-pyridyl)carbomethoxide (TPC) also have shown the good correlations between the δ(^{63}Cu) and C≡O stretching vibration as observed in the TPB system (Figure 1). On the other hand, no meaningful differences were observed for δ(^{13}C) of coordinating carbon monoxide for each complexes, which appears in narrow range around 175 ppm from TMS. These results shows that δ(^{63}Cu) is the sensitive sensor of the extent of back-donation of the Cu-*d* electrons to the antibonding C≡O orbitals, *i.e.*, electron density at the metal center affected by the tridentate ligands. This study also shows the possibility that ^{63}Cu NMR can be the useful tool for the investigation of copper proteins.

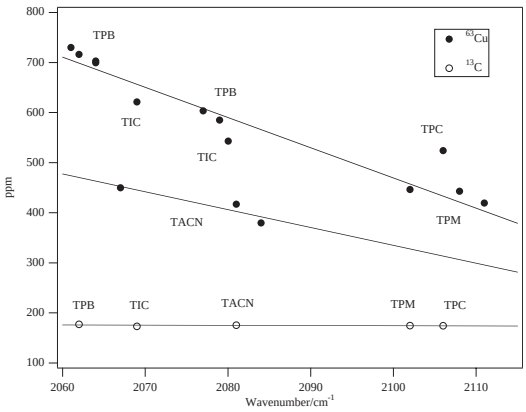

Figure 1. Electronic Effect of Tridentate Ligand on ^{63}Cu- and ^{13}C-NMR Signals of Copper(I) Carbonyl Complexes.

IX-D Molecular Mechanism of Heme Degradation and Oxygen Activation by Heme Oxygenase

Heme oxygenase (HO), an amphipathic microsomal proteins, catalyzes the regiospecific oxidative degradation of iron protoporphyrinIX (heme) to biliverdinIXa, carbon monoxide, and iron in the presence of NADPH-cytochrome P-450 reductase, which functions as an electron donor. Heme oxygenase reaction is the biosynthesis processes of bile pigments and CO, which is a possible physiological messenger. Recent development in the bacterial expression of a soluble form of heme oxygenase has made it possible to prepare in the large quantities for structural studies. In this project, we are studying the molecular mechanism of heme degradation and the oxygen activation by heme oxygenase using various spectroscopic methods.

IX-D-1 Regiospecificity of Each of the Three Steps of Heme Oxygenase Reaction from Hemin to *meso*-Hydroxyhemin, from *meso*-Hydroxyhemin to Verdoheme, and from Verdoheme to Biliverdin

ZHANG, Xuhong[1]; FUJII, Hiroshi; MANSFIELD-MATERA, Kathryn[2]; MIGITA, Catharina Taiko[2]; SUN, Danyu[1]; SATO, Michihiko[1]; IKEDA-SAITO, Masao[2]; YOSHIDA, Tadashi[1]
([1]Yamagata Univ.; [2]Tohoku Univ.)

[*Biochemistry* **42**, 7418–7426 (2003)]

Heme oxygenase catalyzes the regiospecific oxidation of hemin to biliverdin IXα with concomitant liberation of CO and iron by three sequential monooxygenase reactions. The α-regioselectivity of heme oxygenase has been thought to result from the regioselective oxygenation of the heme α-*meso* position at the first step, which leads to the reaction pathway *via meso*-hydroxyheme IXα and verdoheme IXα intermediates. However, recent reports concerning heme oxygenase forming biliverdin isomers other than biliverdin IXα raise a question whether heme oxygenase can degrade *meso*-hydroxyhemin and verdoheme isomers other than the α-isomers. In this paper, we investigated the stereoselectivity of each of the two reaction steps from *meso*-hydroxyhemin to verdoheme and verdoheme to biliverdin, by using a truncated form of rat heme oxygenase-1 and the chemically synthesized four isomers of *meso*-hydroxyhemin and verdoheme. Heme oxygenase-1 converted all four isomers of *meso*-hydroxyhemin to the corresponding isomers of verdoheme. In contrast, only verdoheme IXα was converted to the corresponding biliverdin IXα. We conclude that the third step, but not the second, is stereoselective for the α-isomer substrate. The present findings on regioselectivities of the second and the third steps have been discussed on the basis of the oxygen activation mechanisms of these steps.

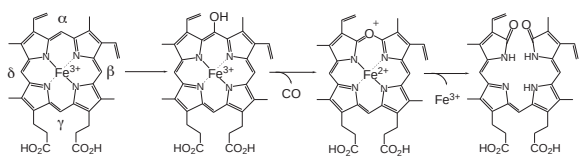

Figure 1. α-Regioselective Heme Catabolism by Heme oxygenase.

IX-E Biomolecular Science

Elucidation of a structure-function relationship of metalloproteins and structural chemistry of amyloid are current subjects of this group. The primary technique used for the first project is the stationary and time-resolved resonance Raman spectroscopy excited by visible and UV lasers. IR-microscope dichroism analysis and AFM are the main techniques for the second project. The practical themes that we want to explore for the first project are (1) mechanism of oxygen activation by enzymes, (2) mechanism of active proton translocation and its coupling with electron transfer, (3) structural mechanism of signal sensing and transduction by heme-based sensor proteins, (4) higher order protein structures and their dynamics, and (5) reactions of biological NO. In category (1), we have examined a variety of terminal oxidases, cytochrome P450s, and peroxidases, and also treated their enzymatic reaction intermediates by using the mixed flow transient Raman apparatus and the Raman/absorption simultaneous measurement device. For (2) the third-generation UV resonance Raman (UVRR) spectrometer was constructed and we are going to apply it to a giant protein like cytochrome *c* oxidase. Recently, we succeeded in pursuing protein folding of apomyoglobin by combining UV time-resolved Raman and rapid mixing device. We also determined the carboxylic side chains of bovine cytochrome oxidase which undergo protonation/deprotonation changes and hydrogen-bonding status changes in response with electron transfers between metal centers or ligand dissociation from heme a_3. Currently, we focus our attention on detecting tyrosine radical for the P intermediate of terminal oxidases. Some positive evidence was obtained for cytochrome *bo*. In (3) we are interested in a mechanism of ligand recognition specific to CO, NO or O_2 and communication pathway of the ligand binding information to the functional part of the protein. For (4) we developed a novel technique for UV resonance Raman measuremnts based on the combination of the first/second order dispersions of gratings and applied it successfully to 235-nm excited RR spectra of several proteins including mutant hemoglobins and myoglobins. Nowadays we can carry out time-resolved UVRR experiments with nanosecond resolution to discuss protein dynamics. With the newly developed third generation UV Raman spectrometer, we have succeeded in isolating the spectrum of tyrosinate in ferric Hb M Iwate, which was protonated in the ferrous state, and the deprotonated state of Tyr244 of bovine cytochrome *c* oxidase. As a model of Tyr244, an imidazole-bound *para*-cresol was synthesized and its UV resonance Raman was investigated. For (5) we purified soluble guanylate cyclase from bovine lung and observed its RR spectra. To further investigate it, we are developing an expression system of this protein. For the amyloid study, we examined FTIR spectra of β_2-microglobulin and its #11-21 peptides which form a core part of amyloid fibril.

IX-E-1 FTIR Detection of Protonation/Deprotonation of Key Carboxyl Side Chains Caused by Redox Change of the Cu_A-Heme *a* Moiety and Ligand Dissociation from the Heme a_3-Cu_B Center of Bovine Heart Cytochrome *c* Oxidase

OKUNO, Daichi[1]; IWASE, Tadashi; SHINZAWA-ITOH, Kyoko[2]; YOSHIKAWA, Shinya[2]; KITAGAWA, Teizo
([1]GUAS; [2]Himeji Inst. Tech.)

[*J. Am. Chem. Soc.* **125**, 7209–7218 (2003)]

FTIR spectral changes of bovine cytochrome *c* oxidase (CcO) upon ligand dissociation from heme a_3 and redox change of the Cu_A-heme *a* moiety (Cu_AFe_a) were investigated. In a photosteady state under CW laser illumination at 590 nm to carbonmonoxy CcO (CcO–CO), the C–O stretching bands due to $Fe_{a3}^{2+}CO$ and $Cu_B^{1+}CO$ were identified at 1963 and 2063 cm^{-1}, respectively, for the fully reduced (FR) state [$(Cu_AFe_a)^{3+}Fe_{a3}^{2+}Cu_B^{1+}$] and at 1965 and 2061 cm^{-1} for the mixed valence (MV) state [$(Cu_AFe_a)^{5+}Fe_{a3}^{2+}$-$Cu_B^{1+}$] in H_2O as well as in D_2O. For the MV state, however, another band due to $Cu_B^{1+}CO$ was found at 2040 cm^{-1}, which was distinct from the α/β conformers in the spectral behaviors, and therefore was assigned to the $(Cu_AFe_a)^{4+}Fe_{a3}^{3+}Cu_B^{1+}CO$ generated by back electron transfer. The FR-minus-oxidized difference spectrum in the carboxyl stretching region provided two negative bands at 1749 and 1737 cm^{-1} in H_2O, which were apparently merged into a single band with a band center at 1741 cm^{-1} in D_2O. Comparison of these spectra with those of bacterial enzymes suggests that the 1749 and 1737 cm^{-1} bands are due to COOH groups of Glu242 and Asp51, respectively. A similar difference spectrum of the carboxyl stretching region was also obtained between $(Cu_AFe_a)^{3+}Fe_{a3}^{2+}Cu_B^{1+}CO$ and $(Cu_AFe_a)^{5+}Fe_{a3}^{2+}Cu_B^{1+}CO$. The results indicate that an oxidation state of the (Cu_AFe_a) moiety determines the carboxyl stretching spectra. On the other hand, CO-dissociated minus CO-bound difference spectra in the FR state gave rise to a positive and a negative peaks at 1749 and 1741 cm^{-1}, respectively, in H_2O, but mainly a negative peak at 1735 cm^{-1} in D_2O. It was confirmed that the absence of a positive peak is not caused by slow deuteration of protein. The corresponding difference spectrum in the MV state showed a significantly weaker positive peak at 1749 cm^{-1} and an intense negative peak at 1741 cm^{-1} (1737 cm^{-1} in D_2O). The spectral difference between the FR and MV states is explained satisfactorily by the spectral change induced by the electron back flow upon CO dissociation as described above. Thus, the changes of carboxyl stretching bands induced both by oxidation of (Cu_AFe_a) and dissociation of CO appear at similar frequencies (~ 1749 cm^{-1}) but are ascribed to different carboxyl side chains.

IX-E-2 Core Structure of Amyloid Fibril Proposed from IR-Microscope Linear Dichroism

HIRAMATSU, Hirotsugu; GOTO, Yuji[1]; NAIKI,

Hironobu[2]; KITAGAWA, Teizo
([1]Osaka Univ.; [2]Fukui Medical Univ.)

[*J. Am. Chem. Soc.* submitted (2003)]

A new approach for studying a peptide conformation of amyloid fibril has been developed. It is based on infrared linear dichroism analysis using an IR-microscope for aligned amyloid fibril. The polarization directions of amide I and II bands were perpendicular similarly for β_2-microglobulin and its #21-31 peptide. Furthermore, this approach has shown that the #21-31 peptide consists of two C=O bonds in the β-sheet that makes 0° with the fibril axis, three C=O bonds in the β-sheet inclined by 27° with respect to the fibril axis, four residues in the random coil by 47°, and two residues in possible β-bulge structure by 32°. Plausible structures of the amyloid core in the fibril is proposed by taking account of these results.

IX-E-3 Resonance Raman Characterization of the P Intermediate in the Reaction of Bovine Cytochrome *c* Oxidase

OGURA, Takeshi[1]; KITAGAWA, Teizo
([1]Himeji Inst. Tech.)

[*Biochim. Biophys. Acta* in press (2003)]

Reduced cytochrome *c* oxidase binds molecular oxygen, yielding an oxygenated intermediate first (Oxy) and then converts it to water *via* the reaction intermediates of P, F, and O in the order of appearance. We have determined the iron-oxygen stretching frequencies for all the intermediates by using time-resolved resonance Raman spectroscopy. The bound dioxygen in Oxy does not form a bridged structure with Cu_B and the rate of the reaction from Oxy to P (P_R) is slower at higher pH in the pH range between 6.8 and 8.0. It was established that the P intermediate has an oxo-heme and definitely not the Fe_{a3}–O–O–Cu_B peroxy bridged structure. The Fe_{a3}=O stretching ($\nu_{Fe=O}$) frequency of the P_R intermediate, 804/764 cm^{-1} for $^{16}O/^{18}O$, is distinctly higher than that of F intermediate, 785/750 cm^{-1}. The rate of reaction from P to F in D_2O solution is evidently slower than that in H_2O solution, implicating the coupling of the electron transfer with vector proton transfer in this process. The P intermediate (607 nm form) generated in the reaction of oxidized enzyme with H_2O_2 gave the $\nu_{Fe=O}$ band at 803/769 cm^{-1} for $H_2{}^{16}O_2$/$H_2{}^{18}O_2$ and the simultaneously measured absorption spectrum exhibited the difference peak at 607 nm. Reaction of the mixed valence CO adduct with O_2 provided the P intermediate (P_M) giving rise to an absorption peak at 607 nm and the $\nu_{Fe=O}$ bands at 804/768 cm^{-1}. Thus, three kinds of P intermediates are considered to have the same oxo-heme a_3 structure. The ν_4 and ν_2 modes of heme a_3 of the P intermediate were identified at 1377 and 1591 cm^{-1}, respectively. The Raman excitation profiles of the $\nu_{Fe=O}$ bands were different between P and F. These observations may mean the formation of a π cation radical of porphyrin macrocycle in P.

IX-E-4 Heme Strctures of Five Hemoglobin Ms Probed by Resonance Raman Spectroscopy

JIN, Yayoi[1]; NAGAI, Masako[1]; NAGAI, Yukifumi[1]; NAGATOMO, Shigenori; KITAGAWA, Teizo
([1]Kanazawa Univ.)

[*Biochemmistry* submitted (2003)]

The α-abnormal Hb Ms show physiological properties different from the β-abnormal Hb Ms, that is, extremely low oxygen affinity of the normal subunit and extraordinary resistance to both enzymatic and chemical reduction of the abnormal met-subunit. In order to get insight into contribution of the heme structure to these differences among Hb Ms, we examined the 406.7-nm excited resonance Raman (RR) spectra of five Hb Ms in the frequency region from 1700 to 200 cm^{-1}, which afford some essential information on the heme structure. The spectra of the abnormal met-subunit in the high frequency region were extracted by the difference calculations between the spectra of the fully-met Hb Ms and of metHb A to eliminate overlaps of the RR bands of the fully-met Hb Ms with those of normal met-subunits. For the half-met Hb Ms (abnormal subunits in the met-form and normal subunits in the deoxy-form), RR bands due to abnormal met-subunits could be clearly distinguished from those of normal deoxy-subunits except for ν_7. In the high frequency region, profound differences between met-α abnormal subunits and met-β abnormal subunits were observed for the in-plane skeletal mode (the $\nu_{C=C}$, ν_{37}, ν_2, ν_{11} and ν_{38} bands), probably reflecting different distortion of the heme structure by the displacement of the heme iron due to tyrosine coordination. Below 900 cm^{-1}, Hb M Iwate (αF8-Tyr) exhibited a distinct spectral pattern for ν_{15}, γ_{11}, $\delta(C_bC_aC_b)_{2,4}$, and $\delta(C_bC_cC_d)_{6,7}$ compared to that of Hb M Boston (αE7-Tyr), although both heme irons are coordinated by Tyr. The β-abnormal Hb Ms, namely, Hb M Hyde Park (βF8-Tyr), Hb M Saskatoon (βE7-Tyr) and Hb M Milwaukee (βE11-Glu), displayed RR band patterns similar to that of metHb A, but with some minor individual differences. The RR bands characteristic of the met-subunits of Hb Ms totally disappeared by chemical reduction and the ferrous heme of abnormal subunits was no more bonded with Tyr or Glu. They were bound to the distal (E7) or proximal (F8) His, and this was confirmed by the presence of the $\nu_{Fe–His}$ mode at 215 cm^{-1} in the 441.6-nm excited RR spectra. A possible involvement of heme distortion in differences of reducibility of abnormal subunits and oxygen affinity of normal subunits is discussed.

IX-E-5 Heme-Regulated Eukaryotic Initiation Factor 2a Kinase (HRI) Activation by Nitric Oxide Is Induced by Formation of Five-Coordinated NO-Heme Complex: Optical Absorption, Electron Spin Resonance and Resonance Raman Spectral Studies

IGARASHI, Jotaro[1]; SATO, Akira; KITAGAWA, Teizo; YOSHIMURA, Tetsuhiko[2]; YAMAUCHI, Seigo[1]; SAGAMI, Ikuko[1]; SHIMIZU, Toru[1]
([1]Tohoku Univ.; [2]Yamagata Public Co. Develop. Ind.)

[*J. Biol. Chem.* submitted (2003)]

Heme-regulated eukaryotic initiation factor 2a (eIF2a) kinase (HRI) regulates the synthesis of hemoglobin in reticulocytes in response to heme availability. HRI has tightly bound heme at the N-terminal domain. Nitric oxide (NO) has been reported to regulate HRI catalysis, but its mechanism remains unclear. In the present study, we examined *in vitro* kinase assay, optical absorption, electron spin resonance (ESR) and resonance Raman spectra of full-length HRI to elucidate regulation mechanism by NO. HRI was activated *via* heme upon NO binding and the Fe(II)HRI(NO) complex had 5-fold eIF2a kinase activity compared to the Fe(III)HRI complex. The Fe(III)HRI complex had Soret peak at 415 nm and exhibited a rhombic ESR signal with *g* values of 2.49, 2.28 and 1.87, suggesting that the Fe(III)HRI complex would be coordinated with His and Cys as axial ligands. Upon addition of NO to the Fe(II)HRI complex, the Soret peak shifted from 423 nm to 398 nm, indicating formation of 5-coordinate NO-heme complex. ESR spectra of the Fe(II)HRI(NO) complex showed a hyperfine triplet, characteristic of 5-coordinate NO-heme complex. Resonance Raman studies showed that Fe–NO and N–O stretching frequencies were located at 527 and 1677 cm^{-1}, respectively in the Fe(II)HRI(NO) complex and that Fe–His stretching frequency was observed at 219 cm^{-1}, immediately after photolysis from the Fe(II)HRI(CO) complex. The spectral findings obtained with full-length HRI were totally different from those obtained with the isolated N-terminal heme-binding domain. We will discuss roles of NO and heme in catalysis with HRI, taking account of heme-based sensor proteins.

IX-E-6 Structural and Spectroscopic Features of a *cis* (Hydroxo)-Fe^{III}-(Carboxylato) Configuration as an Active Site Model for Lipoxygenases

OGO, Seiji[1]; YAMAHARA, Ryo[2]; ROACH, Mark; SUENOBU, Tomoyoshi[3]; AKI, Michihiko; OGURA, Takashi[4]; KITAGAWA, Teizo; MASUDA, Hideki[5]; FUKUZUMI, Shunichi[3]; WATANABE, Yoshihito[6]
([1]IMS and Osaka Univ.; [2]Osaka Univ. and Nagoya Inst. Tech.; [3]Osaka Univ.; [4]Univ. Tokyo; [5]Nagoya Inst. Tech.; [6]Nagoya Univ.)

[*Inorg. Chem.* **41**, 5513–5520 (2002)]

In our preliminary communication (Ogo, S.; Wada, S.; Watanabe, Y.; Iwase, M.; Wada, A.; Harata, M.; Jitsukawa, K.; Masuda, H.; Einaga, H. *Angew. Chem., Int. Ed.* **37**, 2102–2104 (1998)), we reported the first example of X-ray analysis of a mononuclear six-coordinate (hydroxo)iron(III) non-heme complex, $[Fe^{III}(tnpa)(OH)(RCO_2)]ClO_4$ [tnpa = tris(6-neopentylamino-2-pyridylmethyl)amine; for **1**, R = C_6H_5], which has a characteristic *cis* (hydroxo)-Fe^{III}-(carboxylato) configuration that models the *cis* (hydroxo)-Fe^{III}-(carboxylato) moiety of the proposed (hydroxo)iron(III) species of lipoxygenases. In this full account, we report structural and spectroscopic characterization of the *cis* (hydroxo)-Fe^{III}-(carboxylato) configuration by extending the model complexes from **1** to $[Fe^{III}(tnpa)(OH)(RCO_2)]ClO_4$ (**2**, R = CH_3; **3**, R = H) whose *cis* (hydroxo)-Fe^{III}-(carboxylato) moieties are isotopically labeled by $^{18}OH^-$, $^{16}OD^-$, $^{18}OD^-$, $^{12}CH_3{}^{12}C^{18}O_2^-$, $^{12}CH_3{}^{13}C^{16}O_2^-$, $^{13}CH_3{}^{12}C^{16}O_2^-$, $^{13}CH_3{}^{13}C^{16}O_2^-$, and $H^{13}C^{16}O_2^-$. Complexes **1**–**3** are characterized by X-ray analysis, IR, EPR, and UV-vis spectroscopy, and electrospray ionization mass spectrometry (ESI-MS).

IX-E-7 Low-Temperature Stopped-Flow Studies on the Reactions of Copper(II) Complexes and H_2O_2: The First Detection of a Mononuclear Copper(II)-Peroxo Intermediate

OSAKO, Takao[1]; NAGATOMO, Shigenori; TACHI, Yoshimitsu[1]; KITAGAWA, Teizo; ITOH, Shinobu[1]
([1]Osaka City Univ.)

[*Angew. Chem., Int. Ed.* **41**, 4325–4328 (2002)]

Mononuclear copper-active oxygen complexes are key reactive intermediates in many biological and catalytic oxidation processes, but no information is presently available from model systems about mononuclear Cu^{II}-peroxo species. Herein, low-temperature stopped-flow studies are described for the reactions of copper(II) complexes supported by tridentate ligands (L1 and L2) with H_2O_2 to demonstrate that a mononuclear Cu^{II}-peroxo complex is generated from an initially formed Cu^{II}-hydroperoxo intermediate [Equations. (2) and (3)]. The results represent the first example of the direct detection of a mononuclear Cu^{II}-peroxo complex, which provides important information about the reactive intermediates involved in biological and industrial oxidation processes.

$$H_2O_2 + Et_3N \underset{}{\overset{K_1}{\rightleftharpoons}} HO_2^- Et_3NH^+ \quad (1)$$

$$[LCu^{II}]^{2+} + HO_2^- Et_3NH^+ \xrightarrow{k_1} [LCu^{II}\text{-}OOH] + Et_3NH^+ \quad (2)$$
(A)

$$LCu^{II}\text{-}OOH \xrightarrow{k_2} LCu^{II}(O_2) \xrightarrow{k_3[Cu^{II}(L)]} LCu^{II}(O_2)Cu^{II}L \quad (3)$$
(A) (B) (C)

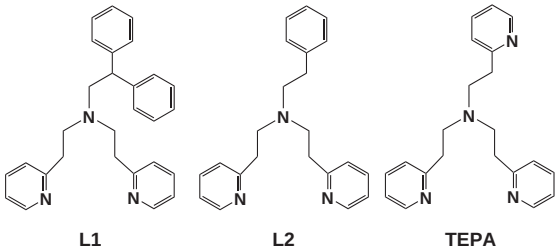

Figure 1.

IX-E-8 Ligand Effect on Reversible Conversion between Copper(I) and Bis(μ-oxo)Dicopper(III) Complex with a Sterically Hindered Tetradentate Tripodal Ligand and Monooxygenae Activity of Bis(μ-oxo)Dicopper(III) Complex

MIZUNO, Masayasu[1]; HAYASHI, Hideki[1];

FUJINAMI, Shuhei[1]; NAGATOMO, Shigenori; OTAKE, Shigenori[1]; UOZUMI, Kounosuke[1]; SUZUKI, Masatatsu[1]; KITAGAWA, Teizo
([1]Kanazawa Univ.)

[*Inorg. Chem.* submitted (2003)]

A new sterically hindered tetradentate tripodal ligand (Me_2-etpy) and its deuterated ligand of the methylene hydrogens (d_4-Me_2-etpy) were synthesized, where Me_2-etpy is bis(6-methyl-2-pyridylmethyl)(2-pyridylethyl)amine. Copper(I) complexes $[Cu(Me_2\text{-etpy}$ or $d_4\text{-}Me_2\text{-etpy})]^+$ (**1** and **1**-d_4, respectively) reacted with dioxygen at –80 °C in acetone to give bis(μ-oxo)dicopper(III) complexes $[Cu_2(O)_2(Me_2\text{-etpy}$ or $d_4\text{-}Me_2\text{-etpy})_2]^{2+}$ (**1**-oxo and **1**-d_4-oxo respectively), the latter of which was crystallographically characterized. Unlike a bis(μ-oxo)dicopper(III) complex with a closely related Me_2-tpa ligand having a 2-pyridylmethyl pendant, **1**-oxo possessing a 2-pyridylethyl pendant is not fully formed even under 1 atm of O_2 at –80 °C and is very reactive toward the oxidation of the supporting ligand. **1**-oxo has a regioselective monooxygenase activity toward the methylene group of the supporting ligand to give a *N*-dealkylated ligand in yield ~ 80% based on a dimer and a corresponding aldehyde. The deuterated ligand d_4-Me_2-etpy greatly stabilizes the bis(μ-oxo)dicopper(III) complex **1**-d_4-oxo, indicating that the rate determining step of the *N*-dealkylation is the hydrogen abstraction from the methylene group. The reversible conversion between **1**-d_4 and **1**-d_4-oxo in acetone was observed depending on the temperature and the thermodynamic parameters (ΔH and ΔS) of the equlibrium were determined to be -53 ± 2 kJ mol^{-1} and -187 ± 10 J mol^{-1}K^{-1}, respectively. The effect of the 2-pyridylethyl pendant in comparison with the 2-pyridylmethyl and 6-methyl-2-pyridylmethyl pendants on the physicochemical properties of the copper(I) and bis(μ-oxo)dicopper(III) species is discussed. (X-ray crystallography (Crystal data for **1**·ClO_4: monoclinic, *C2/c*, a = 20.305(4) Å, b = 12.705(2) Å, c = 16.867(3) Å, β = 100.123(4) Å, V = 4283(1) Å^3, Z = 8, R = 0.044 and R_W = 0.064 ($I \geq 0.0\sigma(\boldsymbol{I})$); for **1**-$d_4$-oxo·$ClO_4$: triclinic, *P*1, a = 10.910(4) Å, b = 11.259(4) Å, c = 14.986(5) Å, α = 82.38(2)°, β = 71.48(2)°, γ = 84.69(2)°, V = 1727(1) Å^3, Z = 1, R = 0.118 and R_W = 0.123($I \geq 0.0\sigma(\boldsymbol{I})$); for **1**-OMe·$ClO_4$: monoclinic, $P2_1/c$, a = 11.642(3) Å, b = 16.689(4) Å, c = 12.885(4) Å, β = 97.700(6)°, V = 2480(1) Å^3, Z = 2, R = 0.031 and R_W = 0.040($\boldsymbol{I} \geq 3\sigma(\boldsymbol{I})$)).

IX-E-9 Dinuclear Copper-Dioxygen Intermediates Supported by Polyamine Ligands

TERAMAE, Shinichi[1]; OSAKO, Takao[2]; NAGATOMO, Shigenori; KITAGAWA, Teizo; FUKUZUMI, Shunichi[1]; ITOH, Shinobu[2]
([1]Osaka Univ.; [2]Osaka City Univ.)

[*J. Inorg. Biochem.* submitted (2003)]

Reactivity of the dicopper(I) and dicopper(II) complexes supported by novel polyamine ligands L1 (*N*,*N*'-dibenzyl-*N*-{3-[benzyl-(6-methyl-pyridin-2-ylmethyl)-amino]-propyl}-*N*'-(6-methyl-pyridin-2-ylmethyl)-propane-1,3-diamine) and L2 (*N*-benzyl-*N*-{2-[bis-(6-methyl-pyridin-2-ylmethyl)-amino]-ethyl}-*N*',*N*'-bis-(6-methyl-pyridin-2-ylmethyl)-ethane-1,2-diamine) towards O_2 and H_2O_2, respectively, have been investigated in order to shed light on the ligand effects on Cu_2/O_2 chemistry. The dicopper(I) complex of L1 (**1a**) readily reacted with O_2 in a 2 : 1 ratio at a low temperature (~ –90 °C) in acetone to afford a mixture of (μ-η^2:η^2-peroxo)dicopper(II) and bis(μ-oxo)dicopper(III) complexes. The formation of these two species has been confirmed by the ESR-silence of the solution as well as their characteristic absorption bands in the UV-vis region [λ_{max} = 350 and 510 nm due to the peroxo complex and ~ 400 nm due to the bis(μ-oxo) complex] and the resonance Raman bands at 729 cm^{-1} [$\Delta\nu(^{16}O_2\text{–}^{18}O_2)$ = 38 cm^{-1} due to the peroxo complex] and at 611 and 571 cm^{-1} [$\Delta\nu(^{16}O_2\text{–}^{18}O_2)$ = 22 cm^{-1} and 7 cm^{-1}, respectively, due to the bis(μ-oxo) complex]. The peroxo and bis(μ-oxo) complexes were unstable even at the low temperature, leading to oxidative *N*-dealkylation at the ligand framework. The dicopper(I) complex of L2 (**2a**) also reacted with O_2 to give (μ-hydroxo)-dicopper(II) complex ($\mathbf{2b^{OH}}$) as the product. In this case, however, no active oxygen intermediate was detected even at the low temperature (–94 °C). With respect to the copper(II) complexes, treatment of the (μ-hydroxo)dicopper(II) complex of L1 ($\mathbf{1b^{OH}}$) with an equimolar amount of H_2O_2 in acetone at –80 °C efficiently gave a (μ-1,1-hydroperoxo)dicopper(II) complex, the formation of which has been supported by its ESR-silence, UV-vis (370 and 650 nm) and resonance Raman spectra [881 cm^{-1}; $\Delta\nu(^{16}O_2\text{–}^{18}O_2)$ = 49 cm^{-1}]. The (μ-1,1-hydroperoxo)dicopper(II) intermediate of L1 also decomposed slowly at the low temperature to give similar oxidative *N*-dealkylation products. Kinetic studies on the oxidative *N*-dealkylation reactions have been performed to get insight into the reactivity of the active oxygen intermediates.

IX-F Molecular Mechanism of Photosensory Protein Function, Excitation Energy Transfer and Electron Transfer in Biological Systems

We are interested in photochemistry, photophysics, photoenergy conversion and photosignal transduction in living orgamisms. Above all, the primary interest in our laboratory is the molecular mechanism of photosensory proteins including rhodopsin and photoactive yellow protein. Using theoretical/computational techniques, we study what happens in these photosensory proteins after light illumination and how these proteins convert light energy into conformational changes.

Excitation energy transfer is a significant process in biophysics. The light-harvesting antenna system in photosynthetic purple bacteria collects and transfers photoenergy efficiently by its unique mechanism. We study this mechanism theoretically.

The electron transfer in biological systems is mostly long-range electron transfer that occurs by the electron tunneling through the protein media. Using theoretical/computational methods, we calculate the electron tunneling current in the protein matrix and analyze how intraprotein electron transfer occurs.

IX-F-1 Role of Protein in the Primary Step of the Photoreaction of Yellow Protein

YAMADA, Atushi[1]; ISHIKURA, Takakazu[1]; YAMATO, Takahisa[2]
([1]Nagoya Univ.; [2]IMS and Nagoya Univ.)

[*Proteins: Struct., Funct., Genet.* in press]

We show the unexpectedly important role of the protein environment in the primary step of the photoreaction of the yellow protein after light illumination. The driving force of the *trans*-to-*cis* isomerization reaction was analyzed by a computational method. The force was separated into two different components: the term due to the protein-chromophore interaction and the intrinsic term of the chromophore itself. As a result, we found that the contribution from the interaction term was much greater than that coming from the intrinsic term. This accounts for the efficiency of the isomerization reaction in the protein environment in contrast to that in solution environments. We then analyzed the relaxation process of the chromophore on the excited-state energy surface and compared the process in the protein environment and that in a vacuum. Based on this analysis, we found that the bond-selectivity of the isomerization reaction also comes from the interaction between the chromophore and the protein environment.

IX-F-2 Direct Measure of Functional Importance Visualized Atom-by-Atom for Photoactive Yellow Protein

YAMADA, Atushi[1]; ISHIKURA, Takakazu[1]; YAMATO, Takahisa[2]
([1]Nagoya Univ.; [2]IMS and Nagoya Univ.)

[Proteins: Struct., Funct., Genet. submitted]

Photoreceptor proteins serve as efficient nanomachines for the photoenergy conversion and the photosignal transduction of living organisms. For instance, the photoactive yellow protein derived from a halophilic bacterium has the *p*-coumaric acid chromophore, which undergoes an ultrafast photoisomerization reaction after light illumination. To understand the structure-function relationship at the atomic level, we used a computational method to find *functionally important atoms* for the photoisomerization reaction of the photoactive yellow protein. In the present study, a "direct" measure of the functional significance was quantitatively evaluated for each atom by calculating the *partial atomic driving force* for the photoisomerization reaction. As a result, we revealed the reaction mechanism in which the specific role of each functionally important atom has been well characterized in a systematic manner. In addition, we observed that this mechanism is strongly conserved during the thermal fluctuation of the photoactive yellow protein.

IX-F-3 A Computational Study on the Stability of the Protonated Schiff Base of Retinal in Rhodopsin

YAMADA, Atushi[1]; KAKITANI, Toshiaki[1]; YAMAMOTO, Shigeyoshi[2]; YAMATO, Takahisa[3]
([1]Nagoya Univ.; [2]Chukyo Univ.; [3]IMS and Nagoya Univ.)

[*Chem. Phys. Lett.* **366**, 670–675 (2003)]

We investigated the effect of amino acids in rhodopsin on the protonation state of the Schiff base (SB) retinal. We constructed a model system consisting of SB retinal, Glu113(counterion), and eight residues. For this model, we considered two states of the SB retinal, namely, the protonated/deprotonated state. We then performed *ab initio* MO calculations at the RHF/6-31g* level. As a result, the protonated state was stabler than the deprotonated state. Interestingly, we observed an additive rule for the contribution to the stabilization energy due to each amino acid. Above all, it turned out that Ser186 and Cys187 play a significant role in the stability.

IX-F-4 Destructive Interference in the Electron Tunneling through Protein Media

KAWATSU, Tsutomu[1]; KAKITANI, Toshiaki[2]; YAMATO, Takahisa[3]
([1]Duke Univ.; [2]Nagoya Univ.; [3]IMS and Nagoya Univ.)

[*J. Phys. Chem. B* **106**, 11356–11366 (2002)]

We investigated the origin of the very rapid and large fluctuation of the electron tunneling matrix element T_{DA} due to the thermal fluctuation of protein conformation which was recently observed by the simulation study (Daizadeh, I.; Medvedev, E. S.; Stuchebrukhov, A. A. *Proc. Natl. Acad. Sci. U.S.A.* **94**, 3703 (1997)). We made analysis of this phenomena by using the interatomic tunneling current map of Ru-modified azurins. We defined a new index, degree of destructive interference Q, by making an average of the intermediate level for the interatomic tunneling currents. We found an empirical relation that $|T_{DA}|$ is proportional to Q^{-1} holds true in the course of thermal fluctuation of protein conformation. Comparing maps of the interatomic tunneling currents with different values of Q, we found that the very rapid (in much less than 1 ps) and large amount (maximally 2 orders of magnitude) of fluctuations in T_{DA} are caused by the reconnection and the change in the direction of interatomic tunneling currents with considerable amplitudes. By taking the statistical average for the dynamics effect of $\log|T_{DA}|$, we found that the range of the averaged dynamic modification of electron transfer rate amounts to more than 2 orders of magnitude in the Ru-modified azurins. In the systems with a large range of dynamic modification, this nuclear dynamics effect contributes to enhance the thermally averaged electron transfer rate considerably.

IX-F-5 Unique Mechanism of Excitation Energy Transfer, Electron Transfer and Photoisomerization in Biological Systems

KAKITANI, Toshiaki[1]; KAWATSU, Tsutomu[2]; KIMURA, Akihiro[1]; YAMADA, Atushi[1]; YAMATO, Takahisa[3]; YAMAMOTO, Shigeyoshi[4]
([1]Nagoya Univ.; [2]Duke Univ.; [3]IMS and Nagoya Univ.; [4]Chukyo Univ.)

[*J. Biol. Phys.* **28**, 367–381 (2002)]

We discuss unique mechanisms typical in the elementary processes of biological functions. We focus on three topics. Excitation energy transfer in the light-harvesting antenna systems of photosynthetic bacteria is unique in its structure and the energy transfer mechanism. In the case of LH2 of *Rhodopseudomonas acidophila*, the B850 intra-ring energy transfer and the inter-ring energy transfer between B800 and B850 take place by the intermediate coupling mechanism of energy transfer. The excitonic coherent domain shows a wave-like movement along the ring, and this property is expected to play a significant role in the inter-ring energy transfer between LH2's. The electron transfer in biological systems is mostly long-range electron transfer that occurs by the electron tunneling through the protein media. There is a long-standing problem that which part of protein media is used for the electron tunneling root. As a result of our detailed analysis, we found that the global electron tunneling root is a little winded with a width of a few angstrom, reflecting the property of tertiary and secondary structures of the protein and it is affected by the thermal fluctuation of protein structure. Photoisomerization of rhodopsin is very unique: The *cis-trans* photoisomerization of rhodopsin occurs only around the C11=C12 bond in the counterclockwise direction. Its molecular mechanism is resolved by our MD simulation study using the structure of rhodopsin which was recently obtained by the X-ray crystallographic analysis.

IX-F-6 Analysis of Cis-Trans Photoisomerization Mechanism of Rhodopsin Based on the Tertiary Structure of Rhodopsin

YAMADA, Atushi[1]; YAMATO, Takahisa[2]; KAKITANI, Toshiaki[1]; YAMAMOTO, Shigeyoshi
([1]Nagoya Univ.; [2]IMS and Nagoya Univ.; [3]Chukyo Univ.)

[*J. Photosci.* **9**, 51–54 (2002)]

We propose a novel mechanism (Twist Sharing Mechanism) for the *cis-trans* photoisomerization of rhodopsin, based on the molecular dynamics (MD) simulation study. New things devised in our simulations are (1) the adoption of Mt. Fuji potentials in the excited state for twisting of the three bonds C9=C10, C11=C12 and C13=C14 which are modeled using the detailed ab initio quantum chemical calculations and (2) to use the rhodopsin structure which was resolved recently by the X-ray crystallographic study. As a result, we found the followings: Due to the intramolecular steric hindrance between 20-methyl and 10-H in the retinal chromophore, the C12–C13 and C10–C11 bonds are considerably twisted counterclockwise in rhodopsin, allowing only counterclockwise rotation of the C11=C12 in the excited state. The movement of 19-methyl in rhodopsin is blocked by the surrounding three amino acids, Thr118, Met207 and Tyr268, prohibiting the rotation of C9=C10. As a result only all-*trans* form of the chromophore is obtainable as a photoproduct. At the 90 degrees twisting of C11=C12 in the course of photoisomerization, twisting energies of the other bonds amount to about 20 kcal/mol. If the transition state for the thermal isomerization is assumed to be similar to this structure, the activation energy for the thermal isomerization around C11=C12 in rhodopsin is elevated by about 20 kcal/mol and the thermal isomerization rate is decelerated by 10^{-14} times than that of the retinal chromophore in solution, protecting photosignal from the thermal noise.

RESEARCH FACILITIES

The Institute for Molecular Science includes five research facilities. This section describes their latest equipment and activities. For further information please refer to older IMS Annual Review issues (1978–2002).

Laser Research Center for Molecular Science

This center was established in 1997 by reorganization of a part of the Instrument Center. The new Center is composed of three research groups which are asked to develop new lasers suitable for pioneering researches in the new field of molecular science. The three groups are

1. Advanced Lasers for Chemical Reaction Studies,
2. Advanced Lasers for Synchrotron Radiation Applications, and
3. Advanced UV and IR Tunable Lasers.

The Laser Research Center is equipped with excimer lasers and solid-state light sources in various temporal and spectral regions, including femtosecond optical parametric oscillators (OPO). The synchronously pumped femtosecond (OPO) (OPAL; Spectra Physics) is tunable from 1.1 μm up to 1.6 μm.

The Laser Center also has general instruments and spectrophotometers. A fluorescence spectrophotometer (Fluorolog II; Spex) is composed of a xenon lamp house for excitation, double and single monochromators for spectroscopy, and changeable detectors (CCD and photomultiplier tube). Other instruments are UV-VIS and IR spectrophotometers, circular dichroism dispersion photometer, and general-purpose electronic instruments. Using these instruments, researchers can carry out various experiments not only in the ultrafast temporal region but also in the steady state regime.

Research Center for Molecular-scale Nanoscience

This Center was established in April 2002 after reorganization including the Research Center for Molecular Materials, the Department of Electronic Structure and the Department of Molecular Assemblies. The Center is supposed to play a principal role to integrate the innovative progress that IMS has achieved in the fields of molecular science and materials science. Its mission is to develop a new frontier of science that aims at constructing novel nanometer-scale materials, and elucidating the behavior thereof, on the basis of understanding the structure and dynamics of each molecular component.

The scientific research in this Center is carried out in the five laboratories: (A) Molecular-scale Electronics, (B) Nanocatalysis and Biomolecular Devices, (C) Nano-scale Photoscience, (D) Interface Molecular Science, and (E) Molecular Clusters, where the latter two laboratories consist of the faculty members transferred from other universities. The respective research activities of these laboratories are reported in the other sections in this Review. The Center also contains the supporting facilities, which manage the instruments (EPR, SQUID, NMR, *etc.*) for inter-university use, provide liquid N_2 and He for research and machine maintenance, and take care of the elemental analyses and the mass spectrometric measurements of chemical materials.

Equipment Development Center

A number of research instruments have been designed and constructed at the mechanical, electronic and glasswork sections in this Facility. Examples of our works in this fiscal year are listed below.

400MHz Gain-of-10 High-speed Signal Amplifier
Internet Compatible Remote Data Acquisition System
Multi-channel Micro-ampere Constant Current Source
Fast Rising High-voltage Pulse Generator
Interlock Circuit for Vacuum Chambers.
Thin-window X-ray cell
Quartz Cell
Microphone cell
Conections for crystals cooling system
Diodelaser focusing line
Two-stage vacuum chamber for precise alignment of the visible laser with extreme
UV light beam
Z axis stage used in scannig near-field optical microscope
Double stage acceleration time-of-flight mass spectrometer
A mount for corner-cube prism chain
A magnetic coil mount for trapping of He atoms
Insertion device for 28T Hybrid MagnetSample holder
Buffer chamber

Development of Special Machine

Equipment Development Center is also engaged in developing Special Machine. This activity is described in

detail in section “RESEARCH ACTIVITIES.”

Ultraviolet Synchrotron Orbital Radiation Facility

The UVSOR accelerator complex consists of a 15 MeV injector linac, a 600 MeV booster synchrotron, and a 750 MeV storage ring. The magnet lattice of the storage ring is the so-called double-bend achromat. The double RF system is routinely operated for the user beam time, and the lifetime of the electron beam has been improved to about 6 hours at 200 mA. The storage ring is normally operated under multi-bunch mode with partial filling. The single bunch operation is also conducted about two weeks per year, which provides pulsed synchrotron radiation (SR) for time-resolved experiments. Initial beam currents stored under multi-bunch and single-bunch modes are 350 mA and 70 mA, respectively.

The upgrade project, which is intended to realize much smaller emittance (27nm-rad) and create new straight sections, was funded in FY2002 and the construction of accelerator components has begun in 2002. All the quadrupole and sextupole magnets installed previously have been replaced with combined function magnets, which can generate both quadrupole and sextupole fields. Sixteen vertical steers that is almost twice as large in number than before, have been installed. All the power supplies for the storage ring magnets and their control system, all the beam ducts at the quadrupoles and sextupoles, three of the beam ducts at the bending magnets, the electron-gun for the injection linac and its power supplies, and the pulse modulator of the klystron have been replaced. By the end of March 2003, the fabrications of all these components were completed and their installation was initiated in April 2003, which was a month behind schedule due to the vacuum accident in November 2002 as described below.

Eight bending magnets and two insertion devices are available for utilizing SR. The bending magnet with its radius of 2.2 m provides SR, whose critical energy is 425 eV. After completing the upgrade project, there will be a total of 18 beamlines operational at UVSOR, which can be classified into two categories. 9 of them are so-called “Open beamlines,” that are open to scientists of universities and research institutes belonging to the government, public organizations, private enterprises and those of foreign countries. The rest of the 9 beamlines are so-called “In-house beamlines,” which are dedicated to the use of the research groups within IMS. We have 1 soft X-rays (SX) station equipped with a double-crystal monochromator, 8 EUV and SX stations with a grazing incidence monochromator, 4 VUV stations with a normal incidence monochromator, 1 (far) infrared station equipped with FT interferometers, 1 station with a multi-layer monochromator, and 3 non-monochromatized stations for irradiation of white-light.

The replacement of the old planar undulator into an in-vacuum type one with 2-m long has been successfully accomplished in Spring 2003. The length of the undulator period and the number of the periods are 38 mm and 50, respectively. This new undulator will cover the spectral region from 50 to 120 eV with its first harmonic radiation. The carbon, nitrogen, and oxygen *K*-edge regions, which are main targets on the novel in-house beamline BL3U, will be covered with the use of the third and fifth harmonics. The helical undulator was installed in 1996, which can also be used as the helical optical klystron for free electron laser (FEL) experiments. The undulator supplies the perfect circular polarization in the photon energy range of 2–45 eV, and the elliptic polarization up to 200 eV. In order to demonstrate the capability of FEL, the combination experiments of the non-monochromatized undulator radiation at BL3A1 with FEL have been continued last year. Further development related to the practical usability of FEL is in the planning stage.

Discussion with users, concerning the improvements and upgrades of the beamlines at UVSOR, has been continuously made as series of UVSOR workshops. Discussion for the rebuilt and rearrangement of several old beamlines has been initiated more recently, on the basis of the review and evaluation report on the present status of UVSOR in 2000. According to the decision through the discussion, the reconstruction of BL3U and BL6, and the introduction of high-resolution photoelectron spectrometer to BL5U have begun in 2002.

In 13th November 2002, a vacuum leakage happened. The origin of the leakage was a beam shutter at the front-end of BL1B, whose cooling water came into the ultra-high vacuum (UHV) system through a pinhole between the water channel and the surface of the shutter in UHV. The water vapor spread immediately inside the whole UHV ducts of the storage ring, and many components of the UHV system of the storage ring have been seriously damaged. As a result, the users’ beamtime for approximately a month has been canceled. The great effort by the UVSOR staff, especially the machine group, has led to quick recovery from such a serious accident, and enabled the operation of the ring to be restarted in the middle of December 2002. Finally, the user time was resumed on 24th December 2002 and was terminated by the end of March 2003. All the reconstruction work as mentioned above has been completed by the end of July, and the commissioning of the upgraded UVSOR, UVSOR-II, has begun in July 2003. The alignment of the optical elements at each beamline using visible light is under progress.

All users are required to refer to the beam-line manuals and the UVSOR guidebook (latest revision in 1999), on the occasion of conducting the actual experimental procedures. Those wishing to use the open and in-house beamlines are recommended to contact with the stationmaster/supervisor and the representative, respectively. For updated information of UVSOR, http://www.uvsor.ims.ac.jp/.

Computer Center

Since April, 2000, Computer Center of IMS has been reorganized as Research Center for Computational Science in Okazaki National Research Institute. The main super-computers at the Center consist of a vector parallel system

of Fujitsu VPP5000 and a scalar parallel system of SGI 2800. The VPP5000 system has 30 vector CPU-nodes and 256 GB of main memory. The SGI system has 320 CPUs and 320 GB of memory. NEC SX-7 and NEC TX-7 are also installed for general-purpose computations. These computers are linked to international networks through Science Information Network (SINET).

We have two types of application categories: (a) Use-of-Facility Program is open to all the domestic scientists in molecular science and related fields; (b) Advanced Research Project is for large-scale computational projects which require resources in excess of the limit for (a) Use-of-Facility Program. The projects applying for the category (b) must be expected scientifically significant achievements. About 20% of the CPU time is used by research staffs in the Institute, while the remaining 80% is given out as research grants described above to outside scientists. As of March 2003, the number of project groups was 191 with 587 users. Some of the famous package programs in Molecular Orbital Theory, *e.g.* Gaussian98, Molpro2000, Hondo, *etc.*, are kept updated as Library Programs for immediate use on the super-computers of the Center. The information for each program can be found on our Web page (http://ccinfo.ims.ac.jp/).

The Quantum Chemistry Literature Database (QCLDB) has been developed by the Quantum Chemistry Database Group in collaboration with staff members of the Center. The latest release, QCLDB Release 2002, contains 57,037 data. This database is accessible through the Web page (http://qcldb.ims.ac.jp/).

SPECIAL RESEARCH PROJECTS

IMS has special research projects supported by national funds. Three projects in progress are:
(a) Chemical Reaction Dynamics
(b) Molecular Photophysics and Science
(c) Novel Materials Science

These three projects are being carried out with close collaboration between research divisions and facilities. Collaborations from outside also make important contributions. Research fellows join these projects.

(a) Chemical Reaction Dynamics

Folding Mechanism of Protein Molecules Studied by Generalized-Ensemble Algorithms

OKAMOTO, Yuko; OKUMURA, Hisashi; YODA, Takao[1]; KAWASHIMA, Yukio; NISHINO, Masamichi; KOKUBO, Hironori[2]; MURATA, Katsumi[2]; SAKAE, Yoshitake[2]; ITO, Satoru[2]
([1]Nagahama Inst. Bio-Sci. Tech.; [2]GUAS)

Proteins are the most complicated molecules that exist in nature. Since protein structures are closely related to their biological functions, the understanding of their folding mechanism from the first principles is not only very challenging but also very important. To be more specific, it is widely believed that three-dimensional structures of proteins are determined by their amino-acid sequence information. However, nobody has completely succeeded in predicting it solely from the amino-acid-sequence information (prediction from the first principles).

There are two elements for the difficulty. One element is that the inclusion of accurate solvent effects is non-trivial because the number of solvent molecules that have to be taken into account is very large. The other element for the difficulty is that there exist a huge number of local minima in the energy function, and simulations by conventional techniques will necessarily get trapped in one of the local minima without ever finding the energy global minimum. Generalized-ensemble algorithms are new simulation algorithms that can alleviate this second difficulty (for reviews, see Refs.1-3). We have been developing new generalited-ensemble algorithms. We found that the combination of multicanonical algorithm and replica-exchange method is particularly promising.[2),3)]

The goal of the present project is to further develop and test the effectiveness of generalize-ensemble algorithms in the protein folding problem and to succeed eventually in the prediction of tertiary structures of proteins from the first principles.

References

1) U. H. E. Hansmann and Y. Okamoto, *Ann. Rev. Comput. Phys. VI*, D. Stauffer, Ed., World Scientific, pp. 129–157 (1999).
2) A. Mitsutake, Y. Sugita and Y. Okamoto, *Biopolymers (Pept. Sci.)* **60**, 96–123 (2001).
3) Y. Sugita and Y. Okamoto, *Lecture Notes in Computational Science and Engineering*, T. Schlick and H. H. Gan, Eds., Springer-Verlag, pp. 304–332 (2002).

Theoretical Studies of Chemical Dynamics

NAKAMURA, Hiroki; MIL'NIKOV, Gennady V.; KONDORSKIY, Alexey[1]; OLOYEDE, Ponmile[2]; KAMISAKA, Hideyuki[3]; FUJISAKI, Hiroshi[4]
([1]IMS and Lebedev Physical Inst.; [2]GUAS; [3]Univ. Tokyo; [4]Boston Univ.)

Various chemical quantum dynamics have been studied analytically as well as numerically. Quantum dynamics calculations have been carried out for the reactions in the O(^{1}D)HCl system which is a prototypical electronically nonadiabatic triatomic reaction system.[1)–3)] Three potential energy surfaces are involved and reaction mechanisms on each surface are clarified. Effects of nonadiabatic transitions are planned to be further analyzed. In order to attack large chemical and biological nonadiabatic systems two types of semiclassical methodologies are developed with the Zhu-Nakamura theory of nonadiabatic transition[4)] incorporated into the formalisms. These are the TSH (trajectory surface hopping) and the semiclassical Herman-Kluk type of frozen Gaussian propagation method.

New powerful theories have been developed for treating two kinds of multi-dimensional tunneling effects. One is the energy splitting in a symmetric double well potential[5),6)] and the other is the decay of metastable state through tunneling.[7)] The first one was applied to nine atomic malonaldehyde molecule with use of the high level of ab initio quantum chemical calculations and an excellent agreement with experiment was obtained.[8)] A novel method to defect caustics along classical trajectory has also been successfully formulated. These theories can be incorporated into the TSH and the semiclassical prepagation method to take into account the tunneling effects.

Finally, new ideas of laser control of molecular processes have been devised. It was demonstrated that the photodissociation branching ratio of HI molecule can be controlled with use of the complete reflection phenomenon.[9)] Another idea is to use a sequence of chirped pulses to control nonadiabatic transitions among dressed states. This can be used to achieve selective and complete excitation of a particular state.[10)]

References

1) S. Nanbu, M. Aoyagi, H. Nakamura, H. Kamisaka, W. Bian

and K. Tanaka, *J. Theor. Comput. Chem.* **1**, 263–273 (2002).
2) H. Kamisaka, H. Nakamura, S. Nanbu, M. Aoyagi, W. Bian and K. Tanaka, *J. Theor. Comput. Chem.* **1**, 275–284 (2002).
3) H. Kamisaka, H. Nakamura, S. Nanbu, M. Aoyagi, W. Bian and K. Tanaka, *J. Theor. Comput. Chem.* **1**, 285–293 (2002).
4) H. Nakamura, *Nonadiabatic Transition: Cencepts, Basic Theories, and Applications*, World Scientific; Singapore, (2002).
5) G. V. Mil'nikov and H. Nakamura, *J. Chem. Phys.* **115**, 6881–6897 (2001).
6) C. Zhu, G. V. Mil'nikov and H. Nakamura, X. Yang and K. Liu, Eds., World Scientific; Singapore, **Chap 10** (2003).
7) G. V. Mil'nikov and H. Nakamura, *J. Chem. Phys.* **117**, 10081–10087 (2002).
8) G. V. Mil'nikov, K. Yagi, T. Taketsugu, H. Nakamura and K. Hirao, *J. Chem. Phys.* **119**, 10 (2003).
9) H. Fujisaki, Y. Teranishi and H. Nakamura, *J. Theor. Comput. Chem.* **1**, 245–253 (2002).
10) K. Nagaya, Y. Teranishi and H. Nakamura, *J. Chem. Phys.* **117**, 9588–9604 (2002).

Two-Dimensional Raman and Infrared Vibrational Spectroscopy for a Harmonic Oscillator System Nonlinearly Coupled with a Colored Noise Bath

KATO, Tsuyoshi; TANIMURA, Yoshitaka

Multi-dimensional vibrational response functions of a harmonic oscillator are reconsidered by assuming nonlinear system-bath couplings. In addition to a standard linear-linear(LL) system-bath interaction, we consider a square-linear(SL) interaction. The LL interaction causes the vibrational energy relaxation, while the SL interaction mainly responsible for the vibrational phase relaxation. The dynamics of the relevant system are investigated by the numerical integration of the Gaussian-Markovian Fokker-Planck equation under the condition of strong couplings with a colored noise bath, where the conventional perturbative approach cannot be applied. The response functions for the fifth-order non-resonant Raman and the third-order infrared (or equivalently the second-order infrared and the seventh-order non-resonant Raman) spectra are calculated under the various combinations of the LL and the SL coupling strengths. Calculated two-dimensional response functions demonstrate that those spectroscopic technique are very sensitive to the mechanism of the system-bath couplings and the correlation time of the bath fluctuation. We discuss the primary optical transition pathways involved to elucidate the corresponding spectroscopic features and to relate them to the microscopic sources of the vibrational nonlinearity which is induced by the system-bath interactions. Optical pathways for the fifth-order Raman spectroscopies from an "anisotropic" medium were newly found in this study, which were not predicted by the weak system-bath coupling theory or the standard Brownian harmonic oscillator model.

Experimental Exploration of Chemical Change at the Most Detailed Level

SUZUKI, Toshinori; KOHGUCHI, Hiroshi; KATAYANAGI, Hideki

Molecular reaction dynamics was explored at the level of state-to-state differential cross sections for photoionization, photodissociation, and molecular collisions using electron and ion imaging techniques. We introduced photoion imaging polarization analysis into the study of photodissociation dynamics and established theoretical frame work to analyze electron orbital alignment. Molecular scattering was investigated by using crossed beam ion imaging that provided the most accurate and detailed experimental results on open-shell collision dynamics. Femtosecond time-resolved photoelectron imaging was developed as a novel experimental means to visualize time-evolving molecular electronic state and electron configuration.

Computational Study of Quantum Dynamics of a Solute in Solution

OKAZAKI, Susumu; MIURA, Shinichi; IWAHASHI, Kensuke; TANAKA, Junji; MIKAMI, Taiji; SATO, Masahiro

Molecular mechanism of vibrational energy relaxation of a solute molecule in solution has been analyzed based upon path integral influence functional theory. Then, solvent normal modes were transformed to each molecular motion in order to examine the couplings in terms of solvent molecules. Coupling which has large contribution to relaxation could be attributed to a particular water molecule. Mixed quantum-classical molecular dynamics method has also been applied to the analysis of dynamic aspects of the coupling Component which is resonant with the solute wave function was extracted from the solute-solvent interaction <0|V|1>. In a short time-scale, *i.e.* sub ps, it shows almost random behavior. However, in longer time-scale, ~ps, it clearly shows relaxation.

Simulation method for quantum liquids has been investigated, too. A new hybrid Monte Carlo method has been developed to simulate liquid helium in superfluid state.

Ultrafast Protein Dynamics Probed by Time-Resolved Resonance Raman Spectroscopy

KITAGAWA, Teizo

Ultrafast protein dynamics were examined with myoglobin (Mb) using picosecond time-resolved resonance Raman spectroscopy with a stress on structural changes and vibrational energy relaxation of heme. Studies on the structural relaxation of Mb following CO photolysis revealed that the structural change of heme itself (core expansion), caused by CO photodissociation, is completed within the instrumental response time of the time-resolved resonance Raman apparatus used (~ 2 ps). In contrast, changes in the intensity and frequency of the iron-histidine (Fe–His) stretching mode upon dissociation of the trans ligand were found to occur in the picosecond regime. The Fe–His stretching band is absent for the CO-bound form, and its appearance upon photodissociation was not instantaneous, in contrast with that observed in the vibrational modes of heme, suggesting appreciable time

evolution of the Fe displacement from the heme plane. The intensity reflected the out-of-plane displacement of iron, and 80% of the movement occurred in 2 ps but the remaining 20% occurred in 40 ps. The band position of the Fe–His stretching mode changed with a time constant of about 100 ps, indicating that tertiary structural changes of the protein occurred in a 100-ps range. This rate was dependent on viscosity of solvent ($k = \eta^{-0.3}$), indicating that the small change at the Fe–His bond is communicated to the protein surface through a conformation change, and conversely the change of Fe-His bond is controlled by the surface of the protein. Temporal changes of the aniti-Stokes Raman intensity of the ν_4 and ν_7 bands demonstrated immediate generation of vibrationally excited heme upon the photodissociation and successive decay of excited populations, whose time constants were 1.1 ± 0.6 and 1.9 ± 0.6 ps, respectively. This technique has been applied to identify an axial residue of a sensor protein, CooA, for which geminate recombination of photodissociated CO is very fast (τ = 70 ps) and therefore the Fe–His (His77) stretching Raman band could be detected only transiently with this technique.

(b) Molecular Photophysics and Science

Development of Dynamic Spectroscopy Apparatus Having Nanometer Spatial Resolution

IMURA, Kohei; NAGAHARA, Tetsuhiko; OKAMOTO, Hiromi

Recent technological progress in scanning near-field optical microscope (SNOM) has made it possible to perform optical measurements with very high spatial resolution beyond the diffraction limit. We have constructed apparatus for space- and time-resolved spectroscopic measurements, by combining SNOM and ultrafast time-resolved technique. With the apparatus, we have achieved ~ 100 nm spatial and ~ 100 fs temporal resolution at the same time. Various photophysical phenomena probed under such extremely high space and time resolution can be of considerable significance not only in physics and chemistry but also in biology, and thus will open a new research activity. We make use of this experimental methodology to investigate basic problems on chemical processes of mesoscopic systems. This technique also has a potential to shed a new light on nanoscale material science. Right now we have performed measurements to understand basic local optical properties of porphyrin aggregates and metal nanoparticles. The details of the apparatus and experimental results are reported in II-A.

Studies on Laser Cooling and Trapping of Metastable Helium Atoms and Laser Spectroscopic Studies of Atoms and Ions in Liquid Helium

MORITA, Norio; MORIWAKI, Yoshiki[1]
([1]Toyama Univ.)

In "studies on laser cooling and trapping of metastable helium atoms," we have been constructing a new laser trapping apparatus for realizing the Bose-Einstein condensation of metastable helium atoms. Especially, we have developed a new metastable atomic beam source cooled by liquid helium, which can provide a metastable helium beam with a very small initial velocity. With this metastable source, it is greatly expected that the number of trapped atoms will dramatically be increased, and that Bose-Einstein condensation will more easily be realized (see II-B-1). On the other hand, in "laser spectroscopic studies of atoms and ions in liquid helium," for both ^{4}He and ^{3}He we have extensively investigated the helium pressure dependence of inner shell transition spectra of Eu atoms over a very wide pressure range including the solidification region. We have found that some interesting differences in spectral behaviors between ^{4}He and ^{3}He in both liquid and solid states (see II-C-1). In addition, from the pressure dependence of the sideband profile of the spectra, we have found a proof for the inference that an unknown structure of the phonon sideband seen in our previous experiments for liquid ^{4}He is due to the roton spectrum (see II-C-2).

Structure, Relaxation and Control of Reactive Cluster Studied by Two-Color Laser Spectroscopy

FUJII, Masaaki

A molecular cluster is a microscopic system of solution and/or crystal, and is thought to provide detailed information on relaxation and reaction dynamics in condensed phase. However the molecular clusters which have been studied are mainly static system which has no reaction pathway after photoexcitation, and consequently spectroscopic information which concerns the reaction mechanism has not been obtained sufficiently. In this research project started from 2000, we will apply various laser spectroscopy to the reactive clusters to reveal detailed mechanism of intracluster reaction. The originally developed spectroscopies, such as nonresonant ionization detected IR spectroscopy, UV-IR-UV ion dip spectroscopy, and the picosecond time-resolved IR dip spectroscopy, are described in the Research Activities of this group. By using these method, we have measured the IR spectra of solvated clusters, such as phenol/ammonia, naphthol/water and alcohol, carbazole/water and 7-azaindole dimers, and have discussed the relation between the structure and intracluster reactions. We also investigated the vibrational dynamics of those clusters in S_0 by picosecond time-resolved nonresonant ionization detected IR (NID-IR) spectroscopy and picosecond time-resolved transient fluorescence detected IR (TFD-IR) spectroscopy.

Dynamics of Superexcited States of Molecules and Fullerenes Studied by Electron, Fluorescence, and Laser Spectroscopy

MITSUKE, Koichiro

One of our main interests is to elucidate the spectroscopy and dynamics of superexcited states of molecules and fullerenes. Though these states often play crucial role in photoexcitation and bimolecular reactions in the VUV and soft X-ray regions, the knowledge of their characteristics is very limited. Owing to autoionization in a very short period and strong perturbation from neighboring neutral states, superexcited states experience various decay pathways such as neutral dissociation, internal conversion, and intramolecular vibrational redistribution. We have employed three experimental methods which serve as a means of providing insights into such processes: Photoelectron spectroscopy, dispersed fluorescence spectroscopy, and SR-laser pump-probe spectroscopy. Taking maximum advantage of the tunability of synchrotron radiation, we have obtained hundreds of spectra at different primary photon energies. Assembling and comparing these one-dimensional spectra enable us to uncover novel decay pathways. For example, superexcited states are often subject to neutral dissociation into electronically excited fragments. These fragments release their internal energy

by emitting fluorescence. Dispersed fluorescence spectroscopy is helpful for us in assigning the dissociation products and determining their vibrational distribution. However, this is not sufficient. If we wish to decide on which precursor state gives rise to the fragments, we should carry on excitation spectroscopy for the particular emission band with changing the primary photon energy. Namely, the fluorescence intensity should be measured as a function of two variables, the initial synchrotron radiation photon energy and final fluorescence wavelength. Two-dimensional plots thus obtained allow us to investigate involved dissociation mechanism of a superexcited state, to evaluate the magnitudes of the electronic coupling with other neutral or ionic states, and to achieve description on the potential energy surface of the relevant dissociative state.

Theoretical Study on Photochromic Molecules and Electrochromic Amorphous

ISHIDA, Toshimasa; YOSHIKAWA, Hirofumi[1]; NISHIKIORI, Shin-ichi[1]; MURAKAMI, Makoto[2]; WATANABE, Go[2]; KIMURA, Kenji[2]; KITAO, Michihiko[2]
([1]Univ. Tokyo; [2]Shizuoka Univ.)

Methylviologen dication is easily reduced to a monocation radical, and turned to be blue, forming a charge-transfer (CT) complex with a donor molecule. It is reported that photo-induced reduction and charge transfer complexes of this molecule in clathrates. We study this reduction and CT using quantum chemical calculations. The energy changes with the torsion angle of the two cations and the spectral change, solvent effect and the charge transfer between the dication and other guest molecules in the clathrates are investigated. The optimized geometry of the monocation radical was found to be planar while that of the dication is twisted, which is consistent with recent calculations for related compounds. The color change upon the photoreduction and CT was reproduced by the calculation. The solvent effect of acetonitrile was small for photoreduction but significant for the CT complex.

It is known that WO_3 films show color change when the charge was injected and remarkable change of its IR spectrum. With increasing of injected protons, the intensity of peak of ν(W–OH) increased and its position shifted hugely from 3200 to 2400 cm^{-1}. We calculated various bond-patterns of OH vibrations. Then OH vibrations accompanied with hydrogen bonds are plausible for observed OH peaks. On the other hand, with increasing of injected protons the intensity of peak of ν(W=O) bond also increased, but its position shifted a little. It is considered that parts of W–O–W–O–W bonds were broken by injected protons and then W=O bonds were brought about. It is suggested that the color change is associated with radical formation.

Decay and Dissociation Dynamics of Core Excited Molecules

SHIGEMASA, Eiji; GEJO, Tatsuo[1]
([1]IMS and Himeji Inst. Tech.)

The dynamics of molecular inner-shell photoexcitation, photoionization, and subsequent decay processes is much more complex, in comparison to outer-shell photoionization which is still largely within the scope of the single electron picture. For instance, the excitation and ionization of valence electrons accompanies the inner-shell photoionization, which manifest themselves as shake-up and shake-off satellite structures in the corresponding photoelectron spectrum. The multi-electron processes due to the electron correlation are known to happen not only in the primary inner-shell hole creation processes, but also in their relaxation processes. It is advantageous to use various experimental techniques together with a high performance monochromator in the soft x-ray region, in order to investigate the related phenomena from different points of view. The high performance of the Varied-Line-Spacing Plane Grating Monochromator (VLS-PGM) at BL4B of the UVSOR facility provides us opportunities for performing various spectroscopic studies on molecular core-levels with high-resolution.

A high luminosity double toroidal analyzer (DTA) equipped with a two-dimensional detector enables the simultaneous measurement of the angular distribution and kinetic energy of electrons/ions. In the first performance test of DTA at BL4B, the LMM Auger spectra of Ar atoms have been observed at last. However, considerable a considerable amount of noise after the accidental discharge of the microchannel plates were experienced, which may lead to inhomogeneous and unexpected geometrical patterns on the images around the symmetry axis of DTA. In order to obtain threshold electron spectra including the symmetry information on the excited states, symmetry-resolved threshold electron spectra, which are based on the combination between a threshold electron spectroscopy and an angle-resolved photoion spectroscopy, have been measured on BL27SU at the SPring-8 after the careful tuning of the apparatus on BL4B and BL7B. The results obtained so far are not yet close to satisfaction, and further improvement of our experimental setup is obviously necessary for achieving a much higher counting rate for the coincidence signals.

A new project towards the practical usability of the free electron laser (FEL) developed at UVSOR has been continued since 2000. Two-photon double-resonant excitation spectrum of the autoionization Xe* $5p^5 4f$ resonance via the Xe* $5p^5 5d$ intermediate state has been successfully derived in 2001. Recently we have performed pressure-dependent measurements concerning the same system. The results gained, strongly suggest the formation of Xe dimmers in the intermediate states prepared by the initial pump processes.

(c) Novel Materials Science

Parallel Algorithm of Semi-In-Core Calculations of Large Molecular Systems

ISHIMURA, Kazuya; NAGASE, Shigeru

In material science, it is currently of great interest to perform reliable and high-speed calculations for large molecular systems using ab initio molecular orbital or density functional methods. An important bottleneck for high-speed calculations is time-consuming two-electron integrals. By using effectively many distributed memories available for large PC clusters and parallelization algorithm, we have developed a semi-in-core method to calculate two-electron integrals, which is essential for the high-speed ab intio and density functional calculations of large molecular systems. The method is implemented in the representative quantum chemistry program packages such as GAMESS.

Statistical Mechanics of Interfacial Fluids

HIRATA, Fumio; KOVALENKO, Andriy F.; YAMAZAKI, Takeshi; TANIMURA, Ayumi; OMELYAN, Ihor

Microscopic structure of fluid interfaces has been drawing a lot of attention due to recent development in the experimental techniques devised particularly to probe the interface. However, there are many open questions remained unanswered. For example, how wide is the interfacial region, how does it depend on the chemical species consisting the solution? Is the interface more or less homogeneous in terms of density or concentration of the two fluids, or is it spatially inhomogeneous? If it is inhomogeneous, what is the spatial extent of the inhomogeneity?

Answering those questions is the most difficult and challenging tasks for theoretical physics and chemistry, and not much progress has been made in the past, especially from a molecular view point. The difficulty arises from the fact that the interface makes the density of fluid non-uniform, which violates the standard requirement for the liquid state theory, or the uniformity of the system. The requirement can be removed by applying a density functional theory for a non-uniform fluids.

In the present project, we develop the theory of non-uniform fluids, which employs a density functional theory of fluids developed by Lovett, Mou, Buff, and Wertheim (LMBW). The basic idea of the theory is to solve the problem in two stages. The first stage is to obtain the one-particle density along the direction normal to the fluid interface, which is a functional of a pair correlation function of the fluids. The second stage is to obtain the pair correlation function in the fluid, which, in tern, is a functional of the one-particle density. Therefore, the two equations which relate the one-particle density and the pair correlation function should be solved iteratively.

We have applied the theory to two problems concerning interfacial fluids, which are essentially the same in terms of the theoretical view point: a Lennard-Jones fluid at vapor-liquid interface, and molecular fluids at liquid-liquid interface.

The density profile at the vapor-liquid interface is shown in Figure 1. The density profile indicates that the width of the interfacial region is about 1 nano-meter for the system in concern. The pair correlation functions (PCF) in planes parallel to the interface are shown in Figure 2. The thin solid line, thick solid line and dashed line depict, respectively, the PCF in the plane at $z = -10\sigma$(vapor), $z = +10\sigma$(liquid), and $z = 0$(interface), where z denotes the distance from the interface, and σ is the Lennard-Jone diameter of a molecule. The behavior of PCFs at $z = -10\sigma$ at $z = +10\sigma$ are typical to those in bulk gas and liquids, respectively, while the PCF at $z = 0$ has an unusually long lasting tail. The long range behavior in PCF is a characteristic of the "critical point" of fluids, which is a manifestation of the density fluctuation in pheno-menological scale.

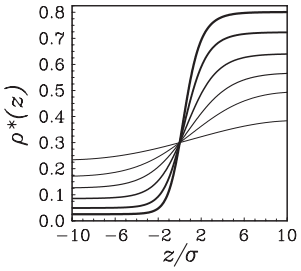

Figure 1.

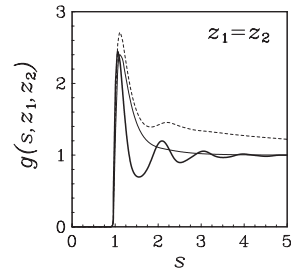

Figure 2.

Theory for Equilibrium and Non-Equilibrium Properties of Low-Dimensional Molecular Materials with Strong Correlation

YONEMITSU, Kenji; KISHINE, Jun-ichiro[1]; OTSUKA, Yuichi; INOUE, Hitoshi; MIYASHITA, Naoyuki[2]
([1]Kyushu Inst. Tech.; [2]Univ. Tokyo)

In low-dimensional molecular materials, the effects of different interactions appear not only in their ground states or in their equilibrium phases but also in the non-equilibrium time-evolution of their inhomogeneous domains. i) In the mixed-stack organic charge-transfer complex, TTF-CA, neutral-ionic and dimerization-induced ferroelectric phase transitions are observed. At ambient pressure, they occur simultaneously and

discontinuously. Under high pressure, these transitions take place at different temperatures, that is, its phase diagram contains a paraelectric ionic phase in addition to the ferroelectric ionic and neutral phases. To treat both the ionicity (*i.e.*, degree of charge transfer from the donor to acceptor molecules) and the dimerization, which causes a finite polarization, we employ a classical spin-1 model called Blume-Emery-Griffiths model. To reproduce the observed solid-liquid-gas phase diagram, we show the inter-stack electrostriction effect is necessary. This complex shows ionic-to-neutral and neutral-to-ionic transitions after sufficiently strong photoirradiation. We have solved the time-dependent Schrödinger equation for an extended Peierls-Hubbard model under an oscillating electric field during the photoirradiation. In the ionic-to-neutral transition, there is threshold photo-absorption intensity above which the ionicity globally changes. In the neutral-to-ionic transition, however, the degree of charge transfer is proportional to the number of absorbed photons, although it is still a highly nonlinear function of the amplitude and duration time of the oscillating electric field. ii) Among halogen-bridged binuclear metal complexes, the iodine-bridged binuclear platinum complexes with ligand pop show a discontinuous transition from the charge-polarization to charge-density-wave phases upon increasing pressure. A photo-induced transition is observed in the hysteresis loop, but only from the metastable charge-density-wave to stable charge-polarization phases. The threshold photo-absorption intensity is explained by drawing the diabatic potentials of the two phases in a Peierls-Hubbard model. The one-way transition is shown to be due to very different inter-unit charge-transfer processes for the two transitions. iii) Among organometal spin-crossover complexes, some show two-step transitions from a high-temperature high-spin phase to a mid-temperature mixed-spin phase to a low-temperature low-spin phase due to a short-range interaction favoring high-spin-low-spin neighbors. We study a two-sublattice Ising-like model accompanied with intra-dimer "antiferromagnetic" coupling and inter-dimer "ferromagnetic" coupling. Monte Carlo simulations show complex behavior under continuous photo-excitation, *i.e.*, threshold behavior, phase separation, and step-like evolution of the high-spin fraction.

UHV Systems for MOKE, MSHG, XMCD and XAFS Measurements

NAKAGAWA, Takeshi; YOKOYAMA, Toshihiko; MARUYAMA, Koichi; WATANABE, Hirokazu

The magneto-optical Kerr effect (MOKE) is usually the most suitable method to characterize magnetic properties of ultrathin films. In the case of in-plane magnetization, however, the rotation angle is sometimes too small to discuss detailed magnetic properties. The magnetic second-harmonic generation (MSHG) method is superior for such purposes. Since last year we have been constructing an ultrahigh vacuum (UHV) MOKE system containing an UHV electromagnet (max. 3000 G, static). The installation was completed and some experiments are being conducted. For MSHG, a Ti: sapphire laser (800 nm) and the detection system were installed in autumn 2003. Using the UHV MOKE-MSHG system, we will investigate magnetic properties of ultrathin metal films, nanowires and nanodots, especially control of magnetism using surface chemical techniques such as gas deposition.

The x-ray magnetic circular dichroism (XMCD) technique is also quite useful since it provides information on element-specific magnetization and on the orbital magnetic moment because of its importance for discussion on magnetic anisotropy. The up-grade project of UVSOR was almost completed and we have installed a new surface analysis chamber at Beamline 4B. In the UHV system, we can perform typical sample treatments for surface analysis (sputtering, annealing, cooling, evaporation of metals, gas adsorption, *etc.*) and verify the surface order and cleanliness of the single crystal substrate using LEED, RHEED (reflection high energy electron diffraction), and XAFS (x-ray absorption fine structure). In order to measure XMCD a similar UHV-compatible electromagnet is installed. The XMCD and XAFS spectra are recorded by the partial electron yield mode using a microchannel plate (for zero magnetic field) or by the total electron yield mode (drain current, for applied field). The installation was completed in autumn 2003.

Pulsed Methods of Electron Spin Resonance Spectroscopy

KATO, Tatsuhisa; FURUKAWA, Ko

Electron spin resonance (ESR) spectroscopy has been a powerful technique for the characterization of radical species. The modern development of ESR spectroscopy enables us to investigate the transient phenomena in detail. The pulsed ESR spectroscopy gives us the prototyped demonstration of the time-dependent spectroscopy. Some time-dependent measurements were experimentally performed and compared with the theoretical model calculation. The advanced ESR method was applied to the study on the high spin state of Eu@C_{82} and Eu@C_{74} described in section II-I-1, of water soluble C_{60} and metallofullerenes described in section II-I-3,of a discrete self-assembled metal array in artificial DNA described in section II-J-1, and of multi-cations of aromatic amines in section II-J-4. The spin state of anion species of La_2@C_{80} was characterized by X-band and W-band ESR observation combined with the detailed simulation analysis as described in section II-I-2. Hyperfine Interactions in La@C_{82} was studied by W-band ESR and ENDOR spectroscopy described in section II-I-5.

Charge Ordering in Organic Conductors

YAKUSHI, Kyuya; YAMAMOTO, Kaoru; URUICHI, Mikio; YAMAMOTO, Takashi; DROZDOVA, Olga; SUZUKI, Kenji

The charge ordering is originated from the localization of charges owing to the on-site and inter-site Coulomb interactions which are stronger than the energy gain by the delocalization charges. Since these competing energies are comparable with each other,

many organic conductors are situated in the boundary between delocalized and localized states. Organic conductors exhibits various electronic states such as charge-density wave (CDW), spin-density wave (SCD), antiferromagnetic state (AF), spin-Peierls state (SP), and superconducting state (SC) *etc*. through the electron-phonon, Coulomb, and exchange interactions. Recently, the charge-ordered state (CO) participates in the ground state. The boundary with a superconducting state has been drawing attention, since theoretical studies suggest a charge-fluctuation-mediated superconducting mechanism. We are investigating the charge ordering (CO) in organic conductors using the technique of infrared and Raman spectroscopy, and obtained the following achievements. (1) Subsequently to the thorough study of θ-(BEDT-TTF)$_2$RbZn(SCN)$_4$, we have investigated θ-type BEDT-TTF salts that has more narrow bandwidth than θ-(BEDT-TTF)$_2$RbZn(SCN)$_4$ such as orthorhombic and monoclinic θ-(BEDT-TTF)$_2$TlZn(SCN)$_4$ and θ-(BEDT-TTF)$_2$Cu$_2$(CN)-[N(CN)$_2$]$_2$. All of these compounds showed a metal-insulator phase transition accompanying charge order and structural change. We characterized the CO pattern of orthorhombic θ-(BEDT-TTF)$_2$TlZn(SCN)$_4$ and θ-(BEDT-TTF)$_2$Cu$_2$(CN)[N(CN)$_2$]$_2$ as a horizontal stripe and that of monoclinic θ-(BEDT-TTF)$_2$TlZn(SCN)$_4$ as a diagonal stripe. The latter compound is the first example for the diagonal stripe. (2) We found a precursory phenomenon of charge ordering above the CO transition temperature in the very narrow-bandwidth system, monoclinic θ-(BEDT-TTF)$_2$TlZn(SCN)$_4$ and θ-(BEDT-TTF)$_2$Cu$_2$(CN)[N(CN)$_2$]$_2$. (3) We found a similar precursory phenomenon at room temperature in the metallic phase of β”-(BEDT-TTF)(TCNQ). Very interestingly, this precursory phenomenon continuously disappeared at low temperature, where the resistivity continuously decreased from the room temperature. We consider that our spectroscopic experiment catches the dynamics of the charges in organic conductors. (4) We examined the β”-type BEDT-TTF salts such as β”-(BEDT-TTF)$_3$(ReO$_4$)$_2$ and β”-(BEDT-TTF)$_4$M(CN)$_4$-H$_2$O (M = Ni, Pd, Pt), and found that the metal-insulator phase transitions of all these compounds were accompanied by charge ordering. It is known that the latter compounds shows superconductivity under high pressure. Therefore, we confirmed that the latter compounds are the candidate for the materials at the boundary between CO and SC. (5) We elucidated that the charges in the insulating phase of (EDO-TTF)$_2$X (X = PF$_6$, AsF$_6$) were almost completely localized at the inner two molecules in a tetramer unit. This unique CO pattern with BOW (bond order wave) was verified in these compounds for the first time. (6) We have conducted a theoretical consideration of the frequency and intensity of the Raman-active and infrared-active vibronic band that are interacting with electronic excited state through the electron-molecular-vibration (*e-mv*) interaction. We provided a theoretical support that the charge disproportionation induces a strong Raman-active vibronic band and infrared-active overtone and combination tone, when the vibrational mode has a large *e-mv* coupling constant.

Broad-Line Solid State NMR Investigation of Molecular-Based Conductors

NAKAMURA, Toshikazu; FUJIYAMA, Shigeki

Magnetic resonance measurements may be mature techniques as devices of the so-called chemical analyses. However, from the viewpoint of the solid state material science, magnetic resonance measurement is challenging area still in under the special condition such cases as the extreme low temperature, strong magnetic field, high pressure, electric field ,optical response and so on. Moreover they are advantageous for studying the fundamental electronic properties and for understanding the detailed electronic structures of molecular based compounds. Soft materials such as molecule based conductors show huge response to environments from the outside. In fact, competition of the electronic phases in molecular based conductors has attracted much attention. Magnetic resonance measurements under the special condition are absolutely necessary to search of the materials with new functions.

The development of the understanding of the electronic phases of molecular based conductors enables us systematic investigations of low-dimensional highly correlated electrons systems. For example, (TMTTF)$_2$*X*, have been extensively studied so far because of their various ground states such as spin-Peierls, AF, IC-SDW and superconductivity. However the origin of the para-magnetic insulating states is an open question. Recent progress of the investigation shows possibility of charge ordering and/or charge disproportionation states also in this family. We performed ^{13}C NMR measurements to investigate the charge configurations and spin dynamics in the low temperature phases of (TMTTF)$_2$*X* in which the two central carbon sites were labeled with ^{13}C.

In this project, we are constructing our third NMR system. We also try to carry out experiments with new devices under unconventional circumstance.

The following projects are also now going on.

[1] Charge Configurations and Spin Dynamics of (TMTTF)$_2$*X*
[2] ^{13}C NMR study of two-component spins system, (BEDT-TTF)-TCNQ
[3] Charge and spin dynamics in organic conductors
[4] Low temperature electronic phases in (EDT-TTF)$_2$*X*

Development of New Molecular Conductors

KOBAYASHI, Hayao; FUJIWARA, Hideki; CUI, Heng-Bo; OKANO, Yoshinori; OTSUKA, Takeo; LEE, Ha-jin; WANG, ZheMing; ZHANG, Bin; FUJIWARA, Emiko[1]; KOBAYASHI, Akiko[1]
([1]Univ. Tokyo)

Since the discovery of the first organic superconductors more than two decades ago, extremely large number of the organic conductors including many superconductors have been developed based on the π donor molecules with TTF (tetrathiafulvalene) skeletons and inorganic anions. Though the development of new organic superconductors is still promoted very actively especially in Japan, traditional Bechgaard-type organic superconductors, D$_2$X (D = TTF-like π donor, X =

inorganic anion) seem to become rather trivial. The development of the completely new types of molecular systems with novel electronic functions will be highly desired for further progress. We have continued to try to develop new functional molecular systems. The main results are as follows. (1) Recently a considerable attention has been attracted to the unconventional conducting molecular systems such as single-component molecular conductor, nano-wires, molecular wire junctions and even DNA. Though the intriguing reports on these new types of molecular systems are rapidly increasing in number, there seem to be many systems where the origins of the charge carriers and/or transport mechanisms still remain unclear. We have observed the de Haas van Alphen oscillation in the recently discovered first single-component molecular metal, $Ni(tmdt)_2$ by using piezoresistive cantilever technique, which revealed unambiguously the presence of the single-component neutral molecular crystal with three-dimensional Fermi surfaces. The angle dependence of the oscillation frequencies agrees well to the band structure calculated by local density approximation (LDA) and *ab initio* plane-wave norm-conserved pseudo potential method. We have also observed the extremely low energy electronic excitations in the single-component molecular conductors. To our best knowledge, the absorption maxima observed around 2200 cm^{-1} in $Ni(tmdt)_2$ and $Ni(dmdt)_2$ are the smallest absorption energy ever reported for single-component molecular systems. The general feature of the *ir* electronic spectra of $Ni(tmdt)_2$ and analogous systems, especially the blue shift of the electronic absorption spectra in the semiconducting systems was well explained by the calculated joint density of states. (2) We have developed single-component molecular metal, $Au(tmdt)_2$ which has the crystal structure isostructural to $Ni(tmdt)_2$. The ESR and SQUID measurements revealed that $Au(tmdt)_2$ undergoes a magnetic transition around 100 K without loss of its high conductivity, indicating the possibility of the future development of molecular metals with magnetic order around room temperature. We have also prepared new types of magnetic organic conductors based on the p donor molecules with stable organic radical parts. In the system with magnetic anions such as $FeCl_4^-$, the first example of organic π conductors with two kinds of spin systems could be obtained. (3) We have tried to develop new *bi*-functional molecular systems by using the microporous frame works constructed of magnetic transition metal atoms and organic ligands and suitable guest molecules. Several ferrimagnetic porous molecular materials have been prepared.

Deposition of Phospholipid Layers on SiO_2 Surface Modified by Alkyl-SAM Islands

TERO, Ryugo; TAKIZAWA, Morio; LI, Yanjun; YAMAZAKI, Masakazu[1]; URISU, Tsuneo
([1]Shizuoka Univ.)

Nano-bioelectronics is one of the most attractive and desirable fields in these days. The surface modification with self-assembled monolayers (SAMs), on semiconductor or insulting materials such as Si and SiO_2 is one of the key-techniques. It plays an important role for anchoring and/or immobilization of supported membranes and many kinds of biofunctional materials. In this study, we will report about dipalmitoyl phosphatidylcholine (DPPC) monolayers and bilayers on the SiO_2 surface modified with SAM islands of octadecyltrichlorosilane (OTS) by means of atomic force microscopy (AFM).

The SiO_2 layers were formed by thermal oxidation of cleaned Si wafers at 1000 degree C, followed by immersion into the H_2O_2/H_2SO_4 solution. It resulted in the flat and hydrophilic SiO_2 layer. OTS was deposited in water-saturated toluene at 22 degree C for 3–5 sec. Unilamellar vesicles of DPPC were prepared by extruding the DPPC suspension in buffer solution (150 mM NaCl, 1.0 mM $CaCl_2$, 10 mM HEPES/NaOH (ph 7.0)) through a 100 nm polycarbonate filter. The suspension was kept above 41 degree C during vesicle preparation. After the sample wafer was incubated in the vesicle suspension at 45 degree C for 2 h, the DPPC layer was deposited on the surface. AFM observations were performed under the buffer solution using an SPI3800 scanning probe microscopy system (Seiko Instruments Inc.) in contact mode.

Figure 1 shows AFM images of OTS-modified SiO_2/Si surfaces before and after deposition of DPPC. OTS islands with typical shapes and heights[1)] were successfully prepared as shown in Figure 1a. After the DPPC deposition, the height of OTS islands regions increased from 2.9 nm to 4.1 nm as shown in Figure 1b. It indicates the deposition of the DPPC membrane on OTS islands. The height increment of 1.2 nm corresponds to the half value of DPPC monolayer, therefore DPPC would be sparsely deposited on OTS islands. Whether DPPC was deposited on SiO_2 region or not was confirmed by scratching the surface with the AFM tip applying a strong force.[2)] In the case of as filtered vesicles (Figure 1b), no scratch trace was observed, indicating that depositions did not occur on the SiO_2 region. In the case of vesicles with the smaller size, which were obtained by the sonication of 100 nm-filtered vesicles, DPPC layers were formed on the SiO_2 region as well as on OTS islands. It will be due to the difference in adhesion and fusion processes between on OTS islands and on SiO_2 regions.

References

1) T. Komeda, K. Namba and Y. Nishioka, *J. Vac. Sci. Technol., A* **16**, 1680–1685 (1998).
2) J. Mou, J. Yang, C. Huang and Z. Shao, *Biochemistry* **33**, 9981–9985 (1994).

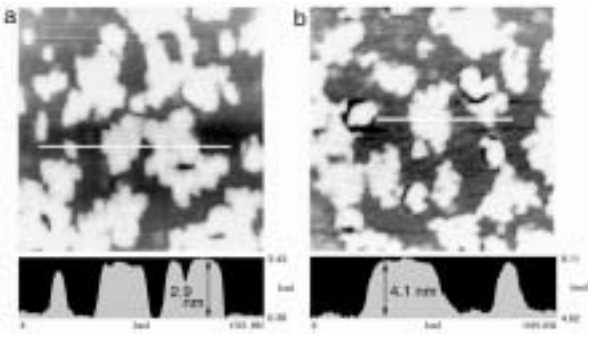

Figure 1. AFM images (2.0 × 2.0 nm^2) and line profiles of OTS/SiO_2 surfaces (a) before and (b) after deposition of DPPC vesicles. The images were successively obtained using the same tip.

Reductive Activation of Carbon Dioxide and Oxidative Activation of Water Aiming at Reversible Conversion between CO_2 and Organic Molecules

TANAKA, Koji

Multi-electron reduction of CO_2 aiming at smooth conversion to organics is highly desired in the viewpoints of not only the utilization of C1 resources but also the decrease of the concentration in the air. Carbon dioxide easily reacts with coordinatively unsaturated low-valent metal complexes to form η^1- or η^2-CO_2 adducts, the former of which are easily converted to metal-CO complexes in protic media. Accumulation of much electrons on metal centers usually accelerates not only reduction of CO_2 but also metal–CO bond cleavages. As a result, CO is the main product in photo- and electro-chemical reduction of CO_2 catalyzed by metal complexes. It is, therefore, highly desired to develop new methodologies that can supply electrons to the carbonyl ligand of metal-CO complexes derived from CO_2 without accumulation of electrons at the central metals. Along the line, we are designing new types of metal complexes that have an ability to provide electrons to carbonyl carbon through metallacycle rings involving the CO groups aiming at catalytic generation higher organic molecules by the electro- and photo-chemical reduction of CO_2.

Oxygenations and oxidations of organic molecules by high valent metal-oxo complexes are of current interest from the viewpoints of the enzymatic activities of P-450. Mechanistic understandings of the reactivity of metal-oxo species derived from O_2, however, have been limited because of the difficulty of selective cleavage of the O–O bond of $M–O_2$ frameworks in artificial systems. Alternatively, high valent Ru=O complexes can be obtained by sequential electron and proton loss of the $Ru–OH_2$ frameworks, and some of Ru=O complexes have proven to work as oxidants of organic molecules. Introduction of quinone molecules, which are reduced to semiquinone and catecholate in a wide range of potentials, into $M–OH_2$ frameworks also induces sequential electron and proton loss of the $Ru–OH_2$ ones without addition of oxidizing agents. Such acid-base equilibria of the aqua ligands by taking advantages of smooth redox reactions of quinone ligands can be applied for energy conversion from pH gradients to electronic energy.

Coordination Chemistry of New Multidentate Ligands and Activation of Small Molecules

KAWAGUCHI, Hiroyuki; MATSUO, Tsukasa

The ability of RE^- (E = O, S) ligands to support and promote various important organic/inorganic reactions at metal centers has been known for many years. In this context, they complement the well-studied cyclopentadienyl-based systems, with the major difference being the greater reactivity of the former complexes due to their relatively higher unsaturation and lower coordination numbers for a $(RE)_nM$ fragment. However, ligand redistribution reaction is a common reaction pathway through which coordinatively unsaturated metal complexes decompose. These undesired ligand redistribution reactions are occasionally a severe obstacle to synthetic efforts. One of strategies for overcoming this problem is to use covalently linked ancillary ligands, thereby limiting ligand mobility and leaving little possibility to reorganize the molecule. This strategy has been a very useful concept in coordination chemistry and has allowed the isolation of transition metal complexes in unstable oxidation states or in unusual coordination geometries, and many with diverse highly-reactive functionalities. In this scenario, we prepared complexes of group 4, 5, and 6 transition metal complexes incorporating linear linked aryloxide trimers. Additionally we have designed and synthesized arylthiolate multidentate ligands new ancillary ligands. Studies the coordination chemistry of these complexes and their derivatives are in progress.

Developments and Researches of New Laser Materials

SARUKURA, Nobuhiko; ONO, Shingo; GOTO, Masahiro; QUEMA, Alex; OUENZERFI, Riadh; TAKAHASHI, Hiroshi; HOSOMIZU, Masato[1]
([1]Tokyo Univ. Sci.)

Although development of lasers is remarkable, there are no lasers which lase in ultraviolet and far infrared regions. However, it is expected that these kinds of lasers break out a great revolution in not only the molecular science but also in the industrial world.

In this project we research characters of new materials for ultraviolet and far infrared lasers, and develop new lasers by using these laser materials.

Development and Research of Advanced Tunable Solid State Lasers

TAIRA, Takunori; SHOJI, Ichiro; PAVEL, Nicolaie; DASCALU, Traian; ISHIZUKI, Hideki; SATO, Yoichi; SAIKAWA, Jiro

The use of diode lasers to pump solid-state lasers opens new horizon in laser science. Diode-pumped solid-state lasers are compact, reliable, and efficient sources of coherent radiation. They can provide

excellent spatial mode quality and narrow linewidths. The high spectral power brightness of these lasers has allowed high efficiency frequency extension by nonlinear frequency conversion. Moreover, the availability of new and improved nonlinear optical crystals makes these techniques more practical. Recently attention has been directed to the trivalent ytterbium ion doped YAG. The advantages of Yb:YAG lasers for a high power, high stability and wide tunability laser operation are well recognized due to its small quantum defect, long upper-state life time and wide gain width.

On the other hand, quasi phase matching (QPM) is a new technique instead of conventional birefringent phase matching for compensating phase velocity dispersion in frequency conversion. Inasmuch as the pool of mature nonlinear optical materials is limited and development of new materials takes time and cost, QPM is a useful method for extending the range of available nonlinear optical materials. The ability to pattern a QPM structure allows the nonlinear materials to be engineered for desired interactions, meaning molecular-science-specified lasers are obtainable through these artificial materials.

In this projects we research and develop new diode-pumped-solid-sate lasers and new frequency conversion devices. Especially, we will focus on the combination of microchip lasers and QPM devices. These kinds of advanced tunable solid-state light, so to speak "Chroma-Chip Lasers," will assist the research of molecular science.

Synthesis of Perfluorinated Tetracene and Pentacene and Applications for Organic Field-Effect Transistors

SAKAMOTO, Youichi; SUZUKI, Toshiyasu

We have synthesized perfluorotetracene (**PF-TC**) and perfluoropentacene (**PF-PC**). These compounds are reddish orange and dark blue crystalline solids, respectively. **PF-TC** is slightly soluble in some organic solvents, but **PF-PC** is almost insoluble in common organic solvents. Their reduction potentials shifted positively by 500–600 mV relative to parent acenes, indicating that they should be good candidates for the *n*-type semiconductors of OFETs.

Friction Force Microscopy Using Silicon Cantilevers Covered with Organic Monolayers *via* Silicon-Carbon Covalent Bonds

ARA, Masato[1]; TADA, Hirokazu
([1]GUAS)

[*Appl. Phys. Lett.* **83**, 578–580 (2003)]

Cantilevers covered with hydrocarbon (CH) and fluorocarbon (CF) monolayers *via* Si–C covalent bonds were prepared and used for adhesion force measurements and friction force microscopy of the surface patterned also with CH and CF areas. The adhesion and friction forces on CF areas were larger than those on CH areas, especially using CF cantilevers. Large polarizabilities of CF molecules compared to CH molecules are found to enhance the contrast in adhesion and friction images. The cantilevers covered with organic monolayers via covalent bonds are useful for chemical force microscopy with contact and noncontact mode atomic force microscopy in various atmospheres since the interface between molecules and cantilevers is thermally and chemically stable.

Development of Multi-Function Integrated Macromolecules Directed toward Molecular Scale Electronics

TANAKA, Shoji

The emerging field of molecular-scale electronics is the new frontier of molecular science and technology. In recent years there have been demonstrations worldwide of molecular-scale diode, switches, transistors, logic circuits, and memory cells. However, the fabrication of ultra-dense molecular-scale circuits remains extremely challenging because of the difficulty in assembling a large number of molecular functional modules. As a promising solution to this problem, molecular monolithic technology based on "planar and multi-function integrated" π-conjugated macromolecules has become a subject of intensive research. In this project we have been trying to establish practical architecture for this novel class of tailor-made macromolecules. As the building blocks we have developed and characterized i) "insulated molecular modules," ii) "energy-gap tuning modules," iii) "molecule-anchor modules," and iv) "molecule-junction modules" for constructing planar grid-type molecular frameworks. Furthermore we have composed various type of "processible" and "multifunctional" oligoheterocyles based on these modules, and characterized them on substrate surfaces using the high-resolution STM/STS.

Asymmetric Transition Metal Catalysis

UOZUMI, Yasuhiro

Catalytic asymmetric reactions have attracted significant interest for their synthetic utility. One of the most exciting and challenging subjects in research on the catalytic asymmetric synthesis is development of the novel and basic chiral units. Homochiral organic molecules bearing hetero atoms (*e.g.* nitrogen, phosphorus, *etc*.) occupy a prominent position in organic chemistry as both useful synthetic reagents and molecules of biological interest. In this specail project, highly functionalized optically active pyrrolo[1,2-*c*] imidazolone framework was identified as a novel basic chiral unit through a diversity-based approach. Selective functionalization of unsymmetrical binaphthyl skeleton was also successfully achieved.

New chiral ligands having a pyrrolo[1,2-*c*] imidazolone backbone were prepared by condensation of anilides of homochiral cyclic amino acids with 2-(diphenylphosphino)benzaldehyde. Of these ligands, (3*R*,9a*S*)-(3-(2-diphenylphosphino)phenyl-2-phenyl)-tetrahydro-1*H*-imidazo[1,5-*a*]indole-1-one was found to be effective for palladium-catalyzed asymmetric allylic alkylation of cycloalkenyl carbonates with dimethyl

malonate to give the corresponding dimethyl cycloalkenylmalonates with up to 89% *ee*.

Various homochiral binaphthyl derivatives having functional groups at the 6-position are important key intermediates for the immobilization of binaphthyl compounds on various solid-supports and have been prepared from commercially available 1,1'-bi-2-naphthol *via* controlled monopivalation of the 2-hydroxyl group and electrophilic aromatic substitution at the 6-position. (*S*)-2,2'-Bis-((*S*)-4-alkyloxazol-2-yl)-6-(2-methoxycarbonyl)ethyl-1,1'-binaphthyls (6-functionalized (*S,S*)-boxax)) were prepared and immobilized on various polymer supports including PS-PEG, PS, PEGA and MeO-PEG resin.

Construction of Advanced Redox Materials Based on Organic Molecules and Metal Complexes, as Basis of Chemical Energy Conversion Systems

NAGATA, Toshi; KIKUZAWA, Yoshihiro; HOSOKAWA, Youichi; NAGASAWA, Takayuki

The goal of this project is to develop advanced redox catalysis reactions suitable for chemical energy conversion. Our current interest focuses on modeling photosynthesis, that is, driving endothermic chemical transformation by using light energy via photoinduced electron transfer. Progress has been made in the following topics during the last year:

A. Mechanistic details of light-driven oxidation of alcohols by a TEMPO/quinone/porphyrin system were investigated. The kinetic analyses were consistent with the intermediacy of the triplet radical pair of porphyrin and quinone, followed by one-electron oxidation of TEMPO by the porphyrin cation radical.

B. A new series of dendrimers were prepared. These dendrimers have "internal" carboxylate functionality that are readily accessible from exterior even after construction of the dendritic framework. We demonstrated introduction of up to fourteen ferrocenyl groups inside the dendrimer. These materials will serve as single-molecular models of biological redox pools.

C. New tripod molecules for stabilization of metal nanoparticles were developed. These molecules are designed so that a single molecule can enclose a single metal nanoparticle to give a "molecular" nanoparticle complex.

Fabrication of Model Catalytic Systems with the Use of Monolayer-Protected Metal Clusters as Starting Materials

NEGISHI, Yuichi; NARUSHIMA, Takashi[1]; TSUKUDA, Tatsuya
([1]GUAS)

The size-dependent catalytic properties of metal clusters have been one of the most important subjects in nanoscience. In order to study the catalytic properties, it is necessary to be able to prepare samples of monodispersed clusters supported on well-characterized substrates. The most elegant method for the preparation of such model catalytic systems is based on the soft landing of the size-selected metal clusters onto the clean surface placed in the UHV condition. In this project, we aim to develop an alternative approach to this subject by using the monodispersed metal clusters prepared by chemical methods. The monolayer-protected metal clusters (MPCs) are chosen as the starting materials because of the following reasons: (1) they can be prepared in a large quantity as stable entities; (2) the core size can tuned through the synthetic conditions and further selected by chromatographic method; (3) they are self assembled into two dimentional crystal on a flat surface. One obvious difficulty in the fabrication of the catalytic system lies in the removal of the thiolate ligands from the cluster surfaces. To this end, we have constructed an apparatus which accommodates a plasma source, where the MPCs on a surface are exposed to the oxygen and/or hydrogen plasma. The etching processes of the organic layers of the MPCs will be monitored by XPS and AFM.

Local Distribution of Photoexcited States on a Semiconductor Surface as Observed by Scanning Tunneling Spectroscopy

KOMIYAMA, Masaharu; GU, Ning[1]; LI, Yanjun; MATSUMOTO, Taki; KISHIRUSAGER, Rajendra
([1]IMS and Southeast Univ.)

The photocatalytic processes occurring on a semiconductor catalyst surface may be divided into two parts: physical processes that are initiated by photoexcitation of titania electrons, and following chemical processes which are the so-called heterogeneous catalysis. The former physical processes are commonly described within the framework of band model which assumes infinite array of three-dimensional (3-D) unit cells that give rise to a periodic potential, with which the electronic band structure is defined. Thus upon UV light illumination electrons in the valence band of titania are excited to its conduction band, leaving holes in the valence band, and they migrate within each band following the energy gradient until they annihilate each other, trapped in some (defect) sites, or consumed by subsequent chemical processes. However, at the solid surfaces and in superfine particles which are the common forms of practical photocatalysts, this infinite array of unit cells in three dimensions no longer exist, and their electronic band structure are known to be quite different from that of bulk.

This very surface is where the chemical part, namely heterogeneous catalysis, occurs. It is a highly local process: individual reactant molecules adsorb on a solid catalyst surface, react in one or more steps, and the product molecules leave the surface in the process called desorption. The adsorption and/or reaction sites in heterogeneous catalysis are often very specific, in terms of their atomic and/or electronic configuration: some reactant may need particular arrangements of atoms that is present on the catalyst surface, and others may need particular electronic states of the surface atoms to provide unique adsorption or reaction sites.

Despite these vastly different descriptions between the two processes occurring in heterogeneous photocatalysis, namely the physical process that is

described by infinite 3-D or 2-D array of unit cells, and the chemical process that necessitates very local description of catalyst surface, no efforts to bridge this gap are known to the authors. The present work is the first of such attempts, and examines the local electronic characters of titania surface upon UV-light illumination by means of scanning tunneling microscopy (STM).

Photoexcited states on rutile TiO_2(110) surface have been examined with ultrahigh vacuum scanning tunneling microscopy. Mesoscopic as well as atomic level excitation was observed. The observed excitation appeared to be associated with oxygen deficiency on the surface. The results were interpreted in terms of reported experimental as well as theoretical band structures.

Electronic Structures of Excited States for Organic Thin Films by Inner-Shell Excitation

OKUDAIRA, Koji K.

Organic devices such as organic light-emitting diodes (OLEDs) in general consist of *p*-type and *n*-type organic thin films. However, there are not so many *n*-type organic materials which are stable and show high electron mobilities. To develop highly efficient organic devices, it is important to clarify the characteristics of unoccupied states of electron-transport layer. As the inner shell electron is excited in the near-edge absorption fine structure (NEXAFS) spectroscopy, the character of unoccupied state can be easily studied. However, the assignment is not so easy due to the interaction between photogenerated holes and electrons. The analysis of photon energy ($h\nu$) dependence of photon-stimulated ion desorption (PSID) is expected to help the assignment of NEXAFS spectra, since the chemical bond scission by inner-shell excitation depends on the electronic configuration of the excited state.

We reported that partial ion yields (PIY) for poly(tetrafluoroethylene) (PTFE) and poly(vinylidene fluoride) (PVDF) thin films show strong photon energy dependencies near fluorine(F) and carbon(C) *K*-edges. The excitation from fluorine 1*s* to σ(C–F)* is specially efficient for F^+ ion production for both PTFE and PVDF.

The PIY of perfluorinated oligo(*p*-phenylene) (PF-8P) which is an efficient *n*-type semiconductor with high electron mobilities were observed near F and C *K*-edges PIY spectra of PF-8P show clear hn dependence near F and C *K*-edges. Especially, near F *K*-edge, the PIY spectra of F^+ increase remarkably at $h\nu$ = 689.2 eV, which corresponds to the lowest peak in NEXAFS. From the comparison with the results of PIY of PTFE and PVDF, the lowest peak in the NEXAFS near F *K*-edge is assigned to the transition from F1*s* to σ(C–F)* not to π*. Furthermore, from the analysis of PIY spectra of PF-8P near carbon *K*-edge, the peak at $h\nu$ = 289.5 eV is ascribed to the transition from C1*s* to σ(C–F)*.

Preliminary Study on Photoemission Thickness Dependence of Cesium Telluride Irradiated by Polarized Photon

TAKASHIMA, Yoshifumi; SUGIYAMA, Harue[1]; KOBAYAKAWA, Hisashi[1]; FURUTA, Fumio[1]; NAKANISHI, Tsutomu[1]
([1]Nagoya Univ.)

Cesium telluride is a good candidate for a material to be used as a photocathode for RF-gun because of its high quantum efficiency and long life. The quantum efficiency of the photocathode measured with changing the thickness of the cesium telluride gives us important information about the effective thickness of the photocathode.

We measured the quantum efficiency of cesium telluride by using linear polarized photon. Figure 1 shows a sketch of our experimental set up. A Xe lamp was used as a light source. The light from the Xe lamp passed through a monochrometer and polarized light enter a vacuum chamber in which cesium telluride was evaporated on molybdenum block as a photocathode.

Figure 2 shows the thickness dependence of the quantum efficiency of the cesium telluride irradiated by the light of 250nm wavelength. Closed circles show the experimental data and solid line shows a function proportional to (1-R), where R is reflectivity of the incident light from the photocathode surface.

We assume that the quantum efficiency is proportional to (1-R) in order to estimate the most effective thickness of the photocathode of cesium telluride. The maximum quantum efficiency is given at 10 nm for 250nm light.

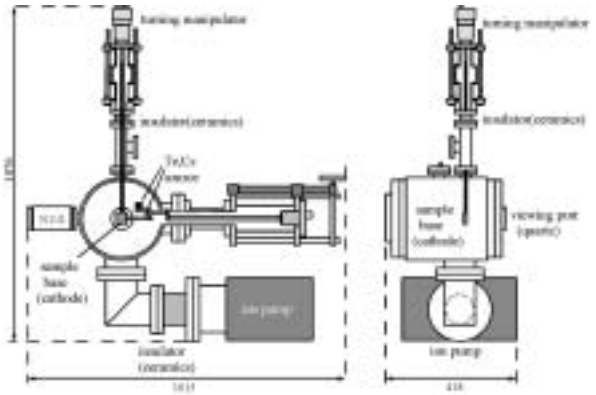

Figure 1. Sketch of experimental set up.

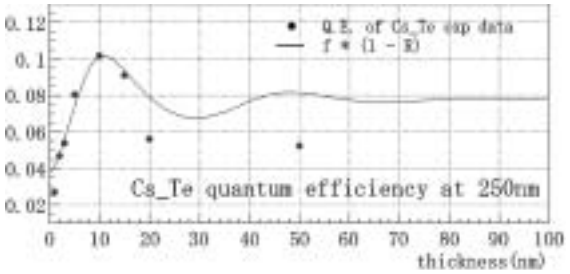

Figure 2. Quantum efficiency of cesium telluride with the thickness the cathode. The wavelength of the light is 250 nm. Closed circles show the quantum efficiency for the experimental data and solid line shows the calculation.

Development of New Materials Based on Fullerenes and Carbon Nanotubes in Nanometer Scale

KUBOZONO, Yoshihiro[1]; TAKABAYASHI, Yasuhiro[2]; FUJIKI, Satoshi[2]; KANBARA, Takayoshi[2]; RIKIISHI, Yoshie[2]; HOSOKAWA, Tomoko[2]; SHIBATA, Kana[2]; HARUYAMA, Yusuke[2]
([1]IMS and Okayama Univ.; [2]Okayama Univ.)

New materials based on fullerenes with novel physical properties were studied in various scales from bulk to nanometer size. The structures for the isomer-separated Dy@C_{82} and Ce@C_{82} crystals have been studied by powder X-ray diffraction with synchrotron radiation, and the electronic properties have also been clarified from the resistivity and Raman of their thin films. The crystals of these metallofullerenes exhibited simple cubic structures with space groups of $Pa\bar{3}$. The temperature dependence of resistivity showed a narrow-gap semiconducting behavior for these metallofulleres. The gap energies were 0.2–0.5 eV. These experimental studies led to new stage of solid state physics and chemistry of metallofullerenes.

The field effect transistors (FETs) have been fabricated with thin films of C_{60}, C_{70}, C_{84} and Dy@C_{82}. The C_{60} and C_{70} FETs showed normally-off enhancement-type properties, while the C_{84} and Dy@C_{82} FETs showed normally-on depletion-type properties. The C_{84} FET exhibited the highest mobility (~ 10^{-3} $cm^2V^{-1}s^{-1}$) among normally-on fullerene FETs. This will open a way to practical devices such as logic gate circuits for computing and memory.

The STM/STS has been studied for metallofullerenes deposited on Si(111)-7×7 surface, and the adsorption pattern of Dy@C_{82} has been clarified. The Dy@C_{82} molecule preferred an adsorption site surrounded by three Si adatoms. This origin is an ability to form strong Si–C interaction in this site. Further, the high-resolution STM image showed a charge distribution ascribable to the fullerene cage in Dy@C_{82}. These STM/STS studies opened the first step of nanoscale materials-science based on metallofullerene.

Effects of Vertical Magnetic Field in Material Science

TANIMOTO, Yoshifumi; UECHI, Ichiro; FUJIWARA, Masao; KATSUKI, Akio[1]
([1]Shinshu Univ.)

Magnetic control of chemical processes has been one of the most interesting and hot topics in material science. This is partly because a superconducting magnet, which generates a high magnetic field, is now commercially available and partly because new phenomena, which can not be observed in a low magnetic field, emerge in a high magnetic field. We have studied the effect of vertical magnetic field (up to 15 T and 1500 T^2/m) on various processes. It is shown that we can control natural convection of aqueous solution and levitate various materials using a vertical magnetic field. It is considered that vertical magnetic field can provide us a novel composite environment useful in material science where influence of gravity is negligibly small and various mechanisms of magnetic field effects are operative.

Many chemical reactions occur at the solid-liquid interface. In order to examine the influence of microgravity created by a strong magnetic field, the following chemical reactions are examined in a vertical magnetic field.

$$Cu + 2Ag^+ \rightarrow Cu^{2+} + 2Ag\downarrow \quad (1)$$

$$Zn + 2Ag^+ \rightarrow Zn^{2+} + 2Ag\downarrow \quad (2)$$

The reaction was carried out in a plastic plates (2 mm × 20 mm × 55 mm) between which a thin metal plate (0.1 mm × 20 mm × 5 mm) was placed and silver nitrate aqueous solution was charged in the space between them. The 2D-dendrite grows at the upper and lower sides of the plate. The plates are placed in a vertical magnetic field. At zero field, the dendrite grows at the upper side of the copper plate more efficiently than that at the lower one for both reactions. In the presence of a magnetic field, the yield at the lower side of the plate is larger than that at the upper one. The efficiency is reversed. At zero field natural convection of the solution due to gravity determines the efficiency of the dendrite yield, whereas in the presence of a magnetic field it is controlled by the magnetic field-induced convection. Furthermore, the dendrites grown by the reaction (2) are tilted by *ca*. 30° in a magnetic field. This could be ascribed to the magnetic anisotropy due to its shape.

It is capable to levitate diamagnetic materials by using an intense vertical magnetic field when the magnetic force (F_{mag}) is equal to gravity,

$$F_{mag} = mg \quad (3)$$

where m is the mass, and g is gravity. Furthermore, F_{mag} is given,

$$F_{mag} = (1/\mu_0)\chi BdB/dz \quad (4)$$

where μ_0 is the magnetic permeability of vacuum, χ is the magnetic susceptibility of a material, B is the magnetic intensity, and dB/dz is its gradient in the vertical direction.

In case of water, this condition will be satisfied when F_{mag} = 1360 T^2/m. Since our magnet can generate the intense magnetic force of 1500 T^2/m, magnetic levitation of several materials were attempted. As expected, we succeeded to levitate water droplet, cherry tomato, nylon ball, polyethylene chip, polystyrene chip, and frog. Furthermore it is succeeded to separate polyethylene chip and polystyrene chip simply by levitating them by the magnetic force. It is clearly shown that magnetic levitation is a useful technique for processing various materials without vessel.

Development of "Entropy-Saving" Nano-Materials

OBA, Toru; HANASAKI, Mitsuru[1]; FUJIWARA, Umihito[1]; MINABE, Masahiro[1]
([1]Utsunomiya Univ.)

Integration of molecular devices has been of much interest for miniaturization in the field of electronics and photonics. For global, sustainable development, in our opinion, such future materials should also be "entropy-saving": reusable, repairable, and bio-degradable. By

utilizing a cytoskeleton, "microtubule" (MT), we fabricated an artificial photosynthetic system as a prototype of such nano-devices. Because formation and maintenance of MT require hydrolysis of GTP, MT is not in an equilibrium but in a dissipative process called dynamic instability: our functionalized MT is the first artificial system that functions in a dissipative process. In view that self-fabrication, self-healing, adaptation and learning, that are characteristics of living organisms, may occur in dissipative processes, utilization or functionalization of the dynamic instability may afford, *e.g.*, self-healing artificial nano-device. We now examine this possibility in addition to further characterization of the functionalized MT and improvement of efficiencies of excitation energy transfer and charge separation (see VIII-DD).

Commissioning of In-Vacuum Undulators at UVSOR

KATOH, Masahiro; HAYASHI, Kenji; HORI, Yoichiro[1]; HOSAKA, Masahito; TAKASHIMA, Yoshifumi; YAMAZAKI, Jun-ichiro; KITAMURA, Hideo[2]; HARA, Toru[2]; TANAKA, Takashi[2]
([1]KEK-PF; [2]Nagoya Univ.; [3]RIKEN/SPring-8)

In-vacuum undulators have been installed in the UVSOR-BL3U and BL7U. Due to the improvement of the UVSOR, the insertion devices with narrow magnetic gaps such as the in-vacuum undulators have become available. The undulators have the period length of 36/38mm and the minimum gap of 15 mm, which results in wide tunability in VUV and soft X-ray region. Influence on the stored beam, especially for the resistive wall instability, has been estimated and it has found that the disturbance for the stored beam can be negligible even in the minimum gap height.

Optical and Photoelectrical Studies on Fermiology of Strongly Correlated Electron Systems

KIMURA, Shin-ichi; ITO, Takahiro; NISHI, Tatsuhiko

Strongly correlated electron systems attract much attention because of their various physical properties. Since the origin is the interaction between the carriers and the localized magnetic moments, we are investigating the electronic structure near the Fermi level (fermiology) by infrared and photoemission spectroscopies using synchrotron radiation. In this year, we measured optical reflectivity spectra of $Ce_{1-x}La_xPd_3$, $YbRh_2Si_2$ and Ba_6Ge_{25}, infrared magneto-optical spectra of κ-(BEDT-TTF)$_2$Cu[N(CN)$_2$]Br and angle-resolved photoemission spectrum of CeSb. A new high-energy-resolution angle-resolved photoemission instrument has been fixed and will be installed at BL5U of UVSOR in the autumn of 2003. The apparatus combined with UVSOR is useful for the three dimensional fermiology of strongly correlated electron systems including organic conductors.

Regulation of Biological Function by the Heme-Based Gas-Molecule Sensor Proteins

KOBAYASHI, Katsuaki; INAGAKI, Sayaka; YOSHIMURA, Hideaki; AONO, Shigetoshi

A variety of gas molecules serve as substrates and/or reaction products in many enzymatic reactions including oxygen respiration, denitrification, nitrogen fixation and methanogenesis. Recently, a novel physiological function of gas molecules, that act as a signaling molecules, has been elucidated and studied extensively. For example, ethylene, O_2, NO, and CO are known to act as physiological effectors in the control of various biological functions. The corresponding receptor (sensor) proteins are required for these gas molecules to act in this way. The external signal is sensed by a sensor domain and then an intramolecular signal transduction proceed to express a physiological function of the sensor protein. A gas molecule that plays the role of the input signal is sensed by an active site of a sensor domain. An intramolecular signal transduction is induced following the detection of the gas molecule, which controls the functional activity in response to the input signal. Generally, a conformational change in the sensor protein facilitates this intramolecular signal transduction.

All of the gas sensor proteins so far reported have a metal-containing prosthetic group at the sensor active site. Specific interactions between protein and gas, for which the metal-containing prosthetic group is used, are required for the gas sensor protein to detect its physiological effector gas. Heme groups have been widely found at the active sites of the O_2, NO, and CO gas sensor proteins. This is not surprising as heme can bind O_2, NO, and CO reversibly.

In this project, we elucidate the structure and function relationships of the heme-based CO and O_2 sensor proteins, CooA and HemAT-Bs, respectively.

Molecular Mechanism of Oxygen Activation by Metalloenzymes

FUJII, Hiroshi; KURAHASHI, Takuya; KUJIME, Masato

Metalloenzymes are a class of biologically important macromolecules that have various functions such as oxygen transport, electron transfer, oxidation, and oxygenation. These diverse functions of metalloenzymes have been thought to depend on the coordination structure of the active site in the protein matrices; the ligand donors, the geometry, and the coordination mode of reactant and substrate. Furthermore, it has been thought that protein structures in immediate vicinity of active metal ion are related to enzymatic function, regio-selectivity, and stereo-selectivity. In this project, we are studying the molecular mechanism of activation of molecular oxygen mediated by metalloenzymes.

(1) High-valent iron-oxo species are proposed to be the key reactive intermediate in oxidation reactions catalyzed by the oxygen-activating iron enzyme. In the case of heme enzymes, porphyrin model complexes have been extensively investigated. However, an insight

into the nonheme oxidizing intermediate is still limited. We have been attempting to prepare the nonheme Compound I analog from a salen iron complex. To model the monomeric iron center of enzymes, bulky mesityl substituents are introduced to the salen iron complex. We found that a blue-green intermediate is formed at –80 °C by the oxidation of the ferric aqua complex of the salen with mCPBA.

(2) Copper is an essential trace element that plays an important role in a variety of biological functions. We have been studying coordination chemistry of copper complexes ligated by various tridentate ligands as synthetic models for the active site of copper protein which has three imidazolyl groups involved in the histidine residues. The results in this study show that $\delta(^{63}Cu)$ is the sensitive sensor of the extent of back-donation of the Cu-*d* electrons to the antibonding C≡O orbitals, *i.e.*, electron density at the metal center affected by the tridentate ligands. This study also shows the possibility that ^{63}Cu NMR can be the useful tool for the investigation of copper proteins.

(3) Heme oxygenase catalyzes the regiospecific oxidation of hemin to biliverdin IXα with concomitant liberation of CO and iron by three sequential mono-oxygenase reactions. We investigated the stereo-selectivity of each of the two reaction steps from *meso*-hydroxyhemin to verdoheme and verdoheme to biliverdin, by using a truncated form of rat heme oxygenase-1 and the chemically synthesized four isomers of *meso*-hydroxyhemin and verdoheme. Heme oxygenase-1 converted all four isomers of *meso*-hydroxyhemin to the corresponding isomers of verdo-heme. In contrast, only verdoheme IXα was converted to the corresponding biliverdin IXα. We conclude that the third step, but not the second, is stereoselective for the α-isomer substrate. The present findings on regioselectivities of the second and the third steps have been discussed on the basis of the oxygen activation mechanisms of these steps.

OKAZAKI CONFERENCE

Okazaki COE Conference

Okazaki IMS Conference 2002 "Search for Frontier of Biomolecular Science"

The series of conferences which had been called "IMS COE Conference" until last year, is renamed henceforth to "Okazaki IMS Conference, (year)." The series of international conferences will be held once a year with a focus on some selected area of molecular science. This year the organization of the conference was left to Profs. Kazuhiko Kinosita, Yoshihito Watanabe (moved to Nagoya Univ. afterward), and Teizo Kitagawa of Center for Integrative Bioscience. Accordingly, they organized a symposium on "Dynamical Structures and Molecular Design of Metalloproteins," which was held on November 19 through 21, 2002 at Okazaki Conference Center. Twenty one invited talks including nine oversea lecturers, and thirty-five poster presentations were involved. The number of registered participants were 114 including 22 foreigners.

An amino acid sequence of a given protein is determined by gene and idividual proteins adopt a specific three dimensional structure to perform their physiological functions. The characteristics of proteins include that they are flexible macromolecules whose structures are dynamical and that the structure itself changes with a progress of reaction in the case of enzymes. It is the purpose of this conference to discuss the dynamical structures of proteins determined with time-resolved techniques in nano- or pico-second time regimes and their relations with physiological functions. The discussion is further extended to design an arrangement of amino acid residues so that nonactive protein could be converted to an active enzyme along a given reaction.

The symposium started from a sonorous lecture by Prof. S. G. Sligar, who covered comprehensively heme enzymes. Structure and reaction mechanism of cytochrome P450 attracted attention and it was demonstrated that myoglobin, an oxygen carrier protein, can be converted to cytochrome P450 with a specific enzymatic activity by using site-directed mutagenesis. Various enzymatic activities were generated by different site-directed mutations to a single protein and these facts led us to reconsider the idea that protein functions were developed with evolution of organisms. Bioenergetic sessions involved a coupling mechanism of electron/proton transfers in terminal oxidases and an active biomotor movement of ATPase. The latter was demonstrated as a movie of a single molecule. Thus, the cutting-edge results were introduced in this conference and young participants were stimulated greatly. The program was as follows;

PROGRAM

November 18 (Monday)
15:00–18:30 Registration
18:30–20:00 Get-Together Party

November 19 (Tuesday)
9:00– 9:10 Welcome Greeting
K. Kaya (Director, IMS)
Opening Remarks
T. Kitagawa (Center for Integrative Bioscience)

Chair: M. Ikeda-Saito (Tohoku University)
9:10– 9:50
S. G. Sligar (University of Illinois, Urbana):
The Cytochrome P450 Dynamic Landscape: A Case of Complex Adaptive Matter
9:50–10:30
Y. Watanabe (Nagoya University):
Introduction of P450, Peroxidase, and Catalase Activities into Myoglobin by Site-Directed Mutagenesis

10:30–10:50 Coffee Break

Chair: Y. Shiro (RIKEN)
10:50–11:30
V. Srajer (Argonne National Laboratory):
Nanosecond Time-Resolved X-Ray Diffraction Study of Protein Relaxation and Ligand Migration in Myoglobin and *Scapharca* Hemoglobin
11:30–12:10
M. Nakasako (Keio University):
Hydration Structure of Proteins

12:10–13:30 Lunch
13:30–15:00 Poster Discussion

Chair: K. Akasaka (Kinki University)
15:00–15:40
H. Kandori (Nagoya Institute of Technology):
Internal Water Molecules of Rhodopsins at Work
15:40–16:20
R. B. Dyer (Los Alamos National Laboratory):
The Role of Fast Protein Motions in Enzymatic Catalysis
16:20–16:40 Coffee Break

Chair: Y. Naruta (Kyushu University)
16:40–17:20
I. Hamachi (Kyushu University):
Bioorganic Engineering of Native Proteins
17:20–18:00
D. B. Goodin (Scripps Research Institute):
Engineering Heme Enzymes to Bind Novel Ligands, Substrates and Molecular Wires

November 20 (Wednesday)
Chair: T. Hase (Osaka University)
9:00– 9:40
S. Yoshikawa (Himeji Institute of Technology):
The Reaction Mechanism of Cytochrome *c* Oxidase
9:40–10:20
Y. Lu (University of Illinois, Urbana):
Designing a Cytochrome *c* Oxidase: Structural and Kinetic Study of Cu_A and Heme-Cu_B Model Proteins

10:20–10:40 Coffee Break

Chair: N. Go (Institute of Atomic Energy)
10:40–11:20
Y. Okamoto (IMS):
Molecular Simulations of Protein Folding.
11:20–12:00
S. Hayward (University of East Anglia):
A Database Approach to Understanding and Predicting Functional Domain Movements in Proteins

12:00–13:20 Lunch
13:20–14:50 Poster Discussion

Chair: K. Yoshihara (JAIST)
14:50–15:30
M. Terazima (Kyoto University):
New Time-resolved Detections on Energy and Protein Structures of Some Photoactive Proteins
15:30–16:10
R. J. D. Miller (University of Toronto):
Advent of Few Cycle Optical Pulses: Mapping the Transduction of Reaction Forces from the Quantum to Mesoscale Motions of Protein Functions

16:10–16:30 Coffee Break

Chair: K. Nagayama (Center for Integrative Bioscience)
16:30 – 17:10
A. Ikai, M. T. Alam, R. Afrin and H. Arakawa (Tokyo Institute of Technology):
Force Spectroscopy of Metallo-protein Dynamics
17:10–17:50
K. Kinosita Jr. (Center for Integrative Bioscience):
Single-Molecule Physiology under an Optical Microscope: How Molecular Machines May Work

18:30–20:30 Banquet: Okazaki New Grand Hotel

November 21 (Thursday)
Chair: M. Go (Nagoya University)
9:00– 9:40
I. Morishima (Kyoto University):
Module as the Structural and Functional Unit in Hemoproteins and Its Application to Design of Novel Hemoproteins
9:40– 10:20
T. Yomo (Osaka University):
Experimental Evolution of Function from Random Sequences

10:20–10:40 Coffee Break

Chair: T. Iizuka (Hosei University)
10:40–11:20
L. -L. Wong (Oxford University):
Molecular Recognition in Catalysis by Cytochrome P450cam
11:20–12:00
T. Kitagawa (Center for Integrative Bioscience):
Time-Resolved Resonance Raman Study on Vibrational and Structural Relaxations of Carbonmonoxy Myoglobin
12:00–12:40
P. Anfinrud (National Institutes of Health):
Watching a Protein as Its Functions with Picosecond Time-Resolved X-Ray Crystallography and Femtosecond Time-Resolved IR Spectroscopy

12:40–12:45 Concluding Remarks
K. Kinosita Jr. (Center for Integrative Bioscience)

JOINT STUDIES PROGRAMS

As one of the important functions of an inter-university research institute, IMS undertakes joint studies programs for which funds are available to cover research expenses as well as travel and living expenses of individuals. The proposals from domestic scientists are reviewed and controlled by an inter-university committee.

The programs are carried out under one of the following categories:

(1) Joint Studies on Special Projects (a special project of significant relevance to the advancement of molecular science can be carried out by a team of several groups of scientists).
(2) Research Symposia (a symposium on timely topics organized by collaboration between outside and IMS scientists).
(3) Cooperative Research (a research program carried out by outside scientists with collaboration from an IMS scientist).
(4) Use of Facility (a research program carried out by outside scientists at the research facilities of IMS except the UVSOR facility).
(5) Invited Research Project
(6) Joint Studies Programs using beam lines of UVSOR Facility.
(7) Use of Facility Program of the Computer Center (research programs carried out by outside scientists at research facilities in Computer Center).

In 2002 Oct.–2003 Sep., the numbers of joint studies programs accepted for the categories (1)–(7) were 5, 13, 119, 59, 0, 126, and 146, respectively.

(1) Special Projects

A. Ultrafast Time-Resolved Study on Photochromic Reactions in the Isolated State and Condensed Phase

SEKIYA, Hiroshi[1]; OKABE,Chie[1]; INOKUCHI, Yoshiya[1]; NAKABAYASHI, Takakazu[2]; IRIE, Masahiro[1]; NISHI, Nobuyuki
([1]Kyushu Univ.; [2]Hokkaido Univ.)

Recently, a lot of photochromic molecules have been synthesized to design functional materials such as molecular switching devices. However, the excited state dynamic of photochromic molecules has not been fully understood. The investigation of excited-state dynamics of typical photochromic molecules, diarylethene derivatives and *N*-salicylideneaniline (SA), is important to understand the mechanism of photochromic reactions. In this research project, we have investigated the excited-state potentials and the relaxation processes by applying picosecond time-resolved Raman spectroscopy[1)] as well as steady-state electronic and FT-Raman spectroscopy.[2),3)]

Spectroscopic studies of SA showed that the excited-state intramolecular proton transfer (ESIPT) plays a crucial role in the *cis*-*trans* isomerization process (Scheme 1). We have first to observe the electronic spectrum of jet-cooled SA.[3)] The fluorescence excitation spectrum of the enol form is very broad and shows no resolved vibronic structure. This result has been ascribed to the lifetime broadening due to an ultrafast process in addition to the ESIPT. Theoretical calculations predicted that a $^1(n\pi^*)$ state reaction is located very close to the lowest $^1(\pi\pi^*)$ state.[4)] However, no direct experimental result has been presented. In the present work, we have applied the time-resolved ionization detection spectroscopy to obtain quantitative information on the excited-sate dynamics.

A time-of-flight mass spectrometer combined with a supersonic molecular beam and a femtosecond laser system was used to monitor the ultrafast reaction dynamics of SA in the gas phase. Gas mixture of sample molecules and helium is expanded into the vacuum chamber through a continuous nozzle. The product ions are mass analyzed in the time-of-flight mass spectrometer and are detected using a multichannel plate detector. The instrumental response function is determined by the pump-probe ionization experiments on pyrazine and benzene, which are known to exhibit an instrument-limited rise. It is estimated to be a Gaussian function with a full width at half maximum of 230 fs. Time-resolved multiphoton ionization intensities of SA have been observed by using this spectrometer.

Figure 1 displays the intensities of the REMPI (Resonance-Enhanced Multi-Photon Ionization) signal of SA against the delay time measured with the probe wavelengths of 395 nm and 790 nm, respectively. The time profile significantly depends on the probe wavelength. The time profile in Figure 1a is reproduced with three decay components < 230 fs, 1.5 ps, and > 100 ps, while that in Figure 1b is fitted with two decay components < 230 fs and 3.5 ps. The ESIPT reaction proceeds 210 fs in cyclohexane solution.[5)] The fast component is due to the ion signal from the enol form of SA, and the < 230 fs component is assigned to the ESIPT reaction. The existence of the *cis*-keto and *trans*-keto forms has been suggested from experimental and theoretical studies.[3)] The transient absorption of the enol form of SA was observed at 400 nm,[6)] which corresponds to the transition from the lowest $^1(\pi\pi^*)$ state to a higher excited electronic state of the *cis*-keto form. Thus, the two components 1.5 ps and > 100 ps are ascribed to the decays of the excited electronic states of the *cis*-keto form produced *via* the ESIPT reaction. On the other hand no transient absorption has been detected from the $^1(\pi\pi^*)$ state of the *cis*-keto form with the probe wavelength of 790 nm. In this work, strong ion signal was observed with the probe wavelength at 790 nm.

Therefore, we have assigned the 3.5 ps decay component to the ion signals from the $^1(n\pi^*)$ state of the enol form. This is the first observation of the $^1(n\pi^*)$ state of the eno form of SA.

We have examined the decay profile by varying the probe wavelength in the range of 360–373 nm. Figure 2 shows the changes of the decay profile as a function of the probe wavelength. The four decay profiles are reproduced with a fast component (< 230 fs) and a slow component (1.5 ~ 8.5 ps). The decay constant of the slow component remarkably changes from 8.5 to 1.5 ps by decreasing the wavelength from 370 nm to 365 nm. This suggests that a decay channel exists in the range of 370–365 nm. The decay channel is predicted to be the internal conversion (IC) from the $^1(\pi\pi^*)$ state to the $^1(n\pi^*)$ state of the *cis*-keto form. The quantum yield of the *trans*-keto form remarkably depends on the excitation wavelength. The quantum yield is three times larger when the enol form is excited with 334 nm light than that with 365 nm light.[5)] Theoretical calculations by Zgierski *et al.* predicted that the $^1(n\pi^*)$ state is located above the $^1(\pi\pi^*)$ state of the *cis*-keto form, and the *trans*-keto form may be produced from the $^1(n\pi^*)$ state.[4)] When the enol form of SA is excited with the pump wavelength of 370 nm, the following processes may occur; (i) radiative process and internal conversion from the $^1(\pi\pi^*)$ state to the electronic ground state of the *cis*-keto form and (ii) IC to the ground state of the *trans*-keto form. The excitation of the enol form with the pump wavelength of 365 nm induces (iii) IC from the $^1(\pi\pi^*)$ state to the $^1(n\pi^*)$ state of the *cis*-keto form in addition to processes (i) and (ii), which enhances the quantum yield of the *trans*-keto form.

References

1) C. Okabe, T. Nakabayashi, N. Nishi, T. Fukaminato, T. Kawai, M. Irie and H. Sekiya, *J. Phys. Chem. A* **107**, 5384–5390 (2003).
2) N. Otsubo, C. Okabe, H. Mori, K. Sakota, K. Amimoto, T. Kawato and H. Sekiya, *J. Photochem. Photobiol., A* **154**, 33–39 (2002).
3) C. Okabe, N. Tanaka, T. Fukaminato, T. Kawai, M. Irie, Y. Nibu, H. Shimada, A. Goldberg, S. Nakamura and H. Sekiya, *Chem. Phys. Lett.* **357**, 113–118 (2002).
4) M. Z. Zgierski and A. Grabowska, *J. Chem. Phys.* **112**, 6329–6337 (2000).
5) S. Mitra and N. Tamai, *Chem. Phys. Lett.* **282**, 391–397 (1998) and references therein.

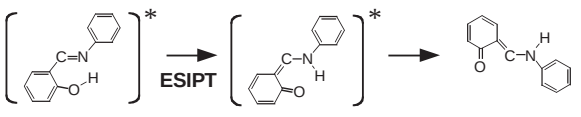

Scheme 1.

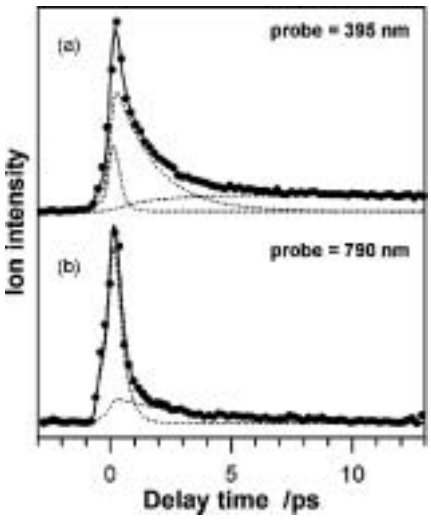

Figure 1. Decay profiles of ion signal of SA detected by femtosecond REMPI with the pump wavelength of 320 nm and two different probe wavelengths of 395 nm (a) and 790 nm (b). The decay profiles (a) and (b) drawn with solid lines are fitted with three and two decay components (dotted lines), respectively.

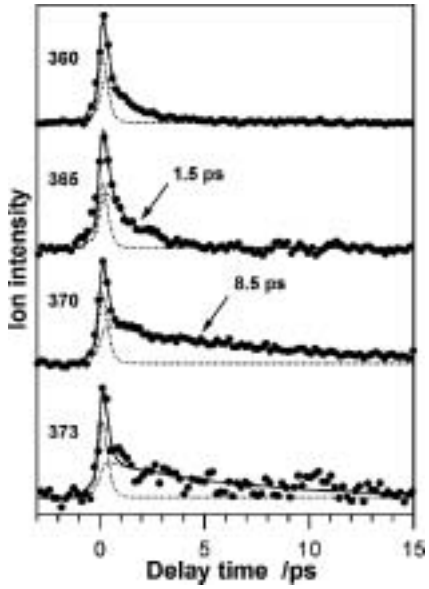

Figure 2. Decay profiles of ion signal of SA as a function of the probe wavelengths of 360 ~ 373 nm. Each decay profile shown by solid line is fitted with two decay components (dotted lines).

B. Development of Effective Generalized-Ensemble Algorithms for Complex Systems with Many Degrees of Freedom

OKAMOTO, Yuko; SUGITA, Yuji[1]; NAGASIMA, Takehiro[2]; MITSUTAKE, Ayori[3]; NAKAZAWA, Takashi[4]; YUMINAGA, Hiroko[4]; BERG, Bernd A.[5]
([1]Tokyo Univ.; [2]Natl. Inst. Genetics; [3]Keio Univ.; [4]Nara Women's Univ.; [5]Florida State Univ.)

Complex systems with many degrees of freedom such as spin glasses and biopolymers have a huge number of local minima in potential energy. Conven-

tional constant-temperature simulations based on canonical ensemble will thus tend to get trapped in states of energy local minima. Generalized-ensemble algorithms, which are based on artificial non-Boltzmann weight factors, alleviate this multiple-minima problem by performing random walks in potential energy space, allowing the simulation to explore a much wider range of the configurational space than by conventional methods. The advantage of generalized-ensemble algorithms lies in the fact that from only one simulation run, one can obtain not only the global-minimum state in potential energy but also various thermodynamic quantities as a function of temperature. Multicanonical algorithm, simulated tempering, and replica-exchange method are well-known examples of generalized-ensemble algorithms and have been widely used in simulations of spin systems and protein systems. However, as the system becomes complex, the application of these algorithms faces technical difficulties. In the first two methods, the determination of the non-Boltzmann weight factors becomes very time-consuming. In the third method, on the other hand, the weight factor determination is trivial, but much more simulation time is required for the production run than in the first two methods. Recently, we have developed new effective generalized-ensemble algorithms that combine the merits of these three generalized-ensemble algorithms (for a recent review, see A. Mitsutake, Y. Sugita, and Y. Okamoto, *Biopolymers (Peptide Science)* **60**, 96–123 (2001)). The purpose of the present project is to further test the effectiveness of these new methods by performing simulations of spin systems and protein systems and to develop even more powerful generalized-ensemble algorithms.

B-1 Replica-Exchange Multicanonical and Multicanonical Replica-Exchange Monte Carlo Simulations of Peptides. I. Formulation and Benchmark Test

[*J. Chem. Phys.* **118**, 6664–6675 (2003)]

The replica-exchange multicanonical algorithm and the multicanonical replica-exchange method for molecular dynamics simulations have recently been developed. In the former method the multicanonical weight factor is determined from a short replica-exchange simulation with the multiple-histogram reweighting techniques. A long multicanonical production run with high statistics is then performed with this weight factor. In this method, the process of determining the multicanonical weight factor is faster and simpler than that in the usual iterative determination. The multicanonical replica-exchange method is a further extension of the first in which a replica-exchange multicanonical simulation is performed with a small number of replicas. In this paper, we give the formulations of these two methods for Monte Carlo simulations and demonstrate the effectiveness of these algorithms for a penta peptide in gas phase.

B-2 Replica-Exchange Multicanonical and Multicanonical Replica-Exchange Monte Carlo Simulations of Peptides. II. Application to a More Complex System

[*J. Chem. Phys.* **118**, 6676–6688 (2003)]

In Paper I of this series the formulations of the replica-exchange multicanonical algorithm and the multicanonical replica-exchange method for Monte Carlo versions have been presented. The effectiveness of these algorithms were then tested with the system of a penta peptide, Met-enkephalin, in the gas phase. In this article the detailed comparisons of performances of these algorithms together with the regular replica-exchange method are made, taking a more complex system of a 17-residue helical peptide. It is shown that these two new algorithms are more efficient than the regular replica-exchange method.

B-3 Multioverlap Simulations for Transitions between Reference Configurations

[*Phys. Rev. E* **68**, 036126 (2003)]

We introduce a new procedure to construct weight factors, which flatten the probability density of the overlap with respect to some pre-defined reference configuration. This allows one to overcome free energy barriers in the overlap variable. Subsequently, we generalize the approach to deal with the overlaps with respect to two reference configurations so that transitions between them are induced. We illustrate our approach by simulations of the brain peptide Met-enkephalin with the ECEPP/2 energy function using the global-energy-minimum and the second lowest-energy states as reference configurations. The free energy is obtained as functions of the dihedral and the root-mean-square distances from these two configurations. The latter allows one to identify the transition state and to estimate its associated free energy barrier.

C. Development of the Advanced Materials with Photo-Switching Molecules

HAYAMI, Shinya[1]; INOUE, Katsuya
([1]Kyushu Univ.)

The design of molecules, which can be utilized for information processing and information storage, is one of the main challenges in molecular materials science. The molecules for such purpose must exhibit bistability, which may be defined as the property of a molecular system being able to exist in two different electronic states in a certain range of external perturbation. Typical example of molecular species exhibiting such molecular bistability is spin crossover complexes. Since the discovery of the first spin-crossover complex, a variety of d^n (n = 4–7) transition metal compounds exhibiting bistability between high-spin (HS) and low-spin (LS) states have been reported. Usually, the spin transition phenomena can be induced by a variation of temperature or of pressure. On the other hand, Decurtine *et al.* show that the spin transition can be induced by illumi-

nation in 1984. This finding shows that the spin-crossover compounds have potential applications for optical switches and data storage devices. Here we purpose to develop the optical switching molecular devices.

C-1 Photo-Induced Spin Transition for an Iron(III) Pyruvic Acid Thiosemicarbazone Compound

HAYAMI, Shinya[1]; INOUE, Katsuya
([1]Kyushu Univ.)

[submitted]

Recently, we have succeeded in observing the LIESST effect for an iron(III) complex $[Fe(pap)_2]ClO_4 \cdot H_2O$ (Hpap = 2-hydroxyphenyl-(2-pyridyl)-methaneimine) by using enhanced cooperative behavior and strong intermolecular interactions for the first time. The planar ligand, pap, with corresponding π electrons, has a potential ability to interact with neighboring ligands by π-π interactions. In this time, we have succeeded in observing the LIESST effect for an iron(III) compound [Fe(thpu)(Hthpu)] (**1**) with intermolecular hydrogen bonds. We believe that our approach, *i.e.*, the introduction of strong intermolecular interactions to trap the metastable HS state can be applied in the design of metal complexes with LIESST effects.

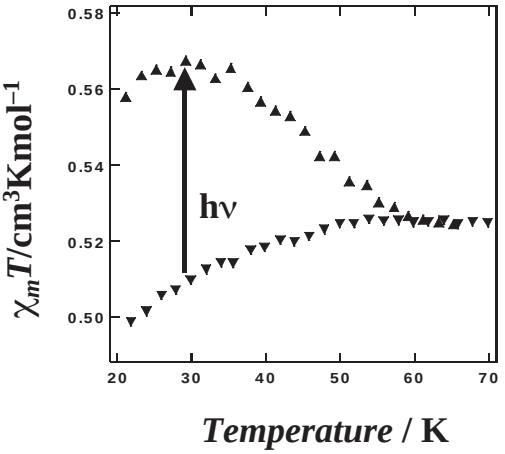

Figure 1. $\chi_m T$ *versus* T plots for the complex **1** was recorded in the warming or cooling mode after the sample was exposed to light illumination for 1 hour.

C-2 Thermal and Optical Switching of Iron(III) Complexes

HAYAMI, Shinya[1]; INOUE, Katsuya
([1]Kyushu Univ.)

[*J. Radio. Nucl. Chem.* **255**, 443–447 (2003)]

Binuclear iron(III) spin-crossover complexes, $[Fe_2(salten)_2(az)](BPh_4)_2$ (**1**) and $[Fe_2(salten)_2(cc)](BPh_4)_2$ (**2**) (H_2salten = 2,2'-[iminobis(3,1-propanediylnitrilomethylidyne)]bis-phenol, az = 4,4'-azobispyridine and cc = 4,4'-(1,2-ethenediyl)bis-pyridine), and mononuclear iron(III) spin-crossover complexes $[Fe(pap)_2]ClO_4 \cdot H_2O$ (**3**) (Hpap = 2-(2-Pyridylmethyleneamino)phenol) and $[Fe(qsal)_2]NCSe \cdot CH_2Cl_2$ (**4**) (Hqsal = 2-[(8-quinolinylimino)methyl]-Phenol) were synthesized and characterized by single-crystal X-ray diffraction, Mössbauer spectra, magnetic susceptibilities and electronic spectra. The structures of $[Fe_2(salten)_2(az)](BPh_4)_2$ (**1**) and $[Fe_2(salten)_2(cc)](BPh_4)_2$ (**2**) were determined in the low-spin state at 100 K and high-spin states at 298 K. The complexes **1** and **2** exhibited the spin-crossover behavior; gradual and rapid spin interconversion was observed by means of Mössbauer spectroscopy at 293 K. The structure of $[Fe(pap)_2]ClO_4 \cdot H_2O$ (**3**) in the high-spin state was determined at 293 K. The complex **3** exhibited the abrupt spin transition with thermal hysteresis ($T_{1/2}\uparrow$ = 180 K and $T_{1/2}\downarrow$ = 165 K). The time dependence of the magnetism and the frozen-in effect were observed for the complex **3**, furthermore, light-induced excited spin state trapping (LIESST) effect was observed for the first time for iron(III) complexes. The structure of $[Fe(qsal)_2]NCSe \cdot CH_2Cl_2$ (**4**) in the low-spin state was determined at 200 K. The complex **4** exhibited a wide thermal hysteresis loop of 180 K ($T_{1/2}\uparrow$ = 392 K and $T_{1/2}\downarrow$ = 212 K) in the first cycle, although the hysteresis loop observed for the first cycle is apparent ones. Following the first loop, it shows a two-step spin transition in warming mode ($T_{1/2(S1)}\uparrow$ = 215 K and $T_{1/2(S2)}\uparrow$ = 282 K) and a one-step spin transition in cooling mode ($T_{1/2}\downarrow$ = 212 K).

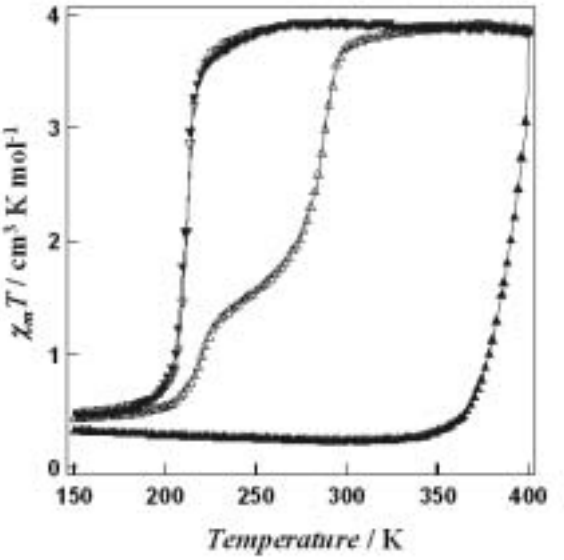

Figure 1. $\chi_m T$ *versus* T plots for 4. The sample was warmed from 5 K to 400 K (▲) and then cooled from 400 K to 5 K (▼) in the first cycle, and then the sample was warmed from 5 K to 400 K (△) and then cooled from 400 K to 5 K (▽) in the second cycle at a rate of 2 K min^{-1}.

C-3 New Cobal(II) Spin Crossover Compounds

HAYAMI, Shinya[1]; INOUE, Katsuya
([1]Kyushu Univ.)

[*Chem. Lett.* **32**, 882–883 (2003)]

The metal-ligand bond lengths changes for iron(II) compounds following the transition are significantly

larger than those of the cobalt(II) compounds. Since the structural changes as well as the volume changes are small, the abrupt spin-transition is rare for cobalt(II) compounds, and the issue of cooperative interaction in these materials have not been discussed extensively, yet. The reported compounds do not only represent novel cobalt(II) spin-crossover compounds, but they offer a good opportunity to investigate the role of intermolecular interactions in spin-transition. The two compounds have similar cores around the cobalt(II) ions, however there is a big difference in their ability to form intermolecular interactions. The compound $[Co^{II}(phimpy)_2](ClO_4)_2$ (**1**) has phenyl groups that can build intermolecular connections by π stacking to the nearest neighbors, as it was proved by the crystallographic measurement. Compound $[Co^{II}(ipimpy)_2](ClO_4)_2$ (**2**) has only bulky and apolar iso-propyl groups, for that reason only interactions based on "image pressure" and of steric origin can have take place. The investigations showed that in compound **1** the intermolecular π stacking result in a negative feedback between the molecules overcompensating any cooperative-type behavior, while in compound **2** the spin transition is only weakly influenced by cooperativity. The strong negative feedback is rare among the reported spin-crossover compounds, either iron(II) or cobalt(II) ones, that is why we believe that our study is to be of wide appeal.

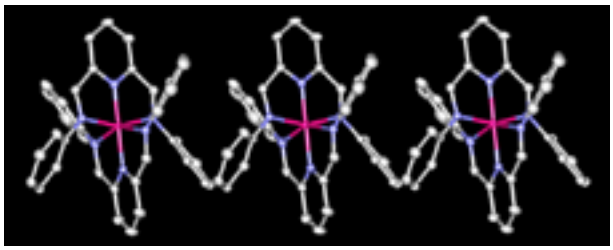

Figure 1. The structure of **1**: the position of two neighbor $[Co(phimpy)_2]^{2+}$ units. The hudrogen atoms are omitted.

C-4 Structure and Magnetic Property of a Mononuclear Helical Iron(II) Complex

HAYAMI, Shinya[1]; INOUE, Katsuya
([1]Kyushu Univ.)

[submitted]

The high-spin mononuclear helical iron(II) complex $[Fe(bis\text{-}dimphen)_2(NCS)_2]$ (**1**) has been prepared from the dimeric ethane-bridged ligand; bis-dimphen (bis-dimphen = 1,2-bis(9-methyl-1,10-phenanthorolin-2-yl)ethane). The complex **1** shows monohelical structure around an iron(II) center. The ferromagnetic interaction between the complexes through the π-π interaction and S···S contact has been observed in the magnetic measurement for **1**.

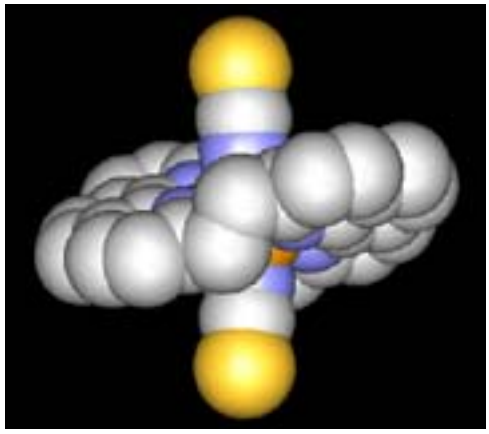

Figure 1. The structure of **1**. The comples **1** shows monohelical structure around an iron(II) center.

C-5 Liquid-Crystal Properties of a Photo-Induced Spin transition Metal Complex

HAYAMI, Shinya[1]; INOUE, Katsuya
([1]Kyushu Univ.)

[submitted]

The iron(II) complex $[Fe(3C16\text{-}L)_2(NCS)_2]$ has been synthesized and characterized by polarizing optical microscopy, differential scanning calorimetry, and X-ray scattering, where 3C16-L is 3,4,5-tris(hexadecyloxy)-N-(2-pyridinylmethylene)-benzenamine. The iron(II) complex exhibits liquid-crystal properties in the temperature range from 345 to 400 K. Variable-temperature magnetic susceptibility measurements and Mössbauer studies reveal that this compound exhibits spin-crossover behavior between high-spin and low-spin states, and photo-induced spin transition effect from a low-spin state to a metastable high-spin state. Therefore the iron(II) complex can undergo spin-crossover, photo-induced spin transition and liquid-crystal properties in a single compound. The compounds with multifunction, *i.e.* spin-crossover and photo-induced spin transition material with liquid-crystal properties, are important in the development of molecular switches and optical materials.

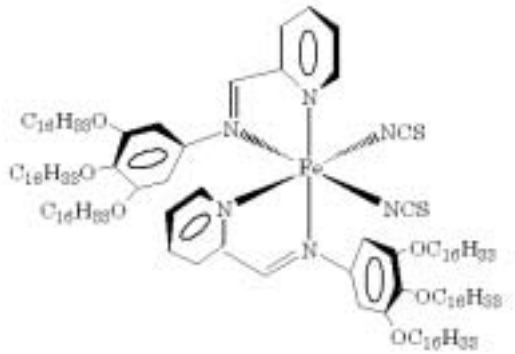

Figure 1. Chemical structure oh the comples **1**. An iron(II) ion is surrounded by six nitrogen atoms of tow 3C16-L ligands and two NCS^- groups in *cis* position.

D. Theoretical Study for Self-Organization of Nano-Assembly in Solution

HIRATA, Fumio; KOVALENKO, Andriy; KINOSHITA, Masahiro[1]; OKAMURA, Emiko[1]; IMAI, Takashi[2]; UEOKA, Ryuichi[3]; HOLOVKO, Myroslav[4]; OMELYAN, Ihor[4]
([1]Kyoto Univ.; [2]Ritsumeikan Univ.; [3]Sojo Univ.; [4]Inst. Cond. Matt. Phys.)

Outline of the project:

Formation of molecular assemblies taking place in solutions is a popular phenomenon in our daily life, *e.g.*, detergent. It is also quite important problem in biological applications, *e.g.*, membrane and blood cell. In spite of its importance, the status of theoretical study has been very poor, and it has stayed in the phenomenological level at its best.

The eventual goal of the project is to build up a molecular theory which enables us to explain the thermodynamic stability of molecular assemblies, *e.g.*, micelles and vesicles, especially to describe the size distribution of the assembly. The stability of the molecular assemblies is determined by many physicochemical parameters, *i.e.*, temperature, pressure, the chemical composition of the surfactant, solvent (water), electrolytes, and so on. We tackle the problem with the RISM-KH theory which we have been developing in the past few years.

As the initial step of the project, we have carried out the analysis of thermodybamic stability of the water-alcohol mixture by calculating the compressibility of the solution and its temperature dependence. The results have been published in *JTCC*, **vol. 2**, page 193 (2003). What follows is the summary of the results.

Summary of the results:

The isothermal compressibility χ_T of binary mixtures of water and *tert*-butyl alcohol (TBA) was calculated using the reference interaction site model (RISM) integral equation theory. The calculations were performed over the whole concentration from $x = 0$ to 1 and a wide temperature from $T = 283$ to 313 K ranges employing an extended point charge model for water and optimized site-site potentials for TBA molecules. The results obtained were compared *versus* available experimental data. It was demonstrated that, despite an approximate character of the model potentials and closure relation applied, the theory was able to reproduce qualitatively all main features of the *x*- and *T*-dependencies of χ_T inherent in real experiment. (Figure (a) (b)) Such features include the decrease of compressibility with increasing *T* in the low TBA concentration limit *x* to 0 (pure water), and the increase of χ_T with rising *T* in the opposite regime *x* to 1 (pure alcohol); the presence of a concentration region where the function $\chi_T(x,T)$ does not depend much on *T*; as well as the existence of a minimum in χ_T with respect to *x* at each given *T*. The question of how to achieve a quantitative agreement between the theoretical and experimental values by correcting the closure relation was also discussed.

Reference

1) I. Omelyan, A. Kovalenko and F. Hirata, *J. Theor. Comput. Chem.* **2**, 193 (2003).

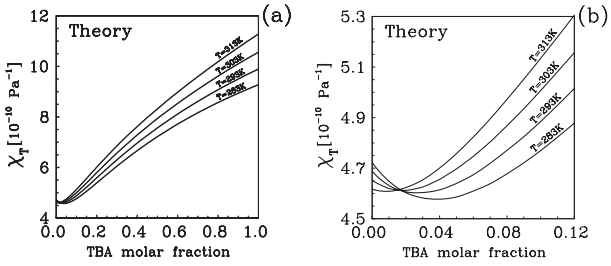

Figure 1.

E. Collaborative Project Research, "Structural Chemistry of High Oxidation State Intermediate of Terminal Oxidases"

KITAGAWA, Teizo

This project research is carried out by eight members including three from Tokyo University (Prof. Takashi Ogura, Ph.D. student Kenji Oda, and Ms. student Toshinari Takahashi), one from each of Himeji Institute of Technology (Prof. Shinya Yoshikawa), Kyoto Univ. (Dr. Satoshi Takahashi), Univ. of Crete (Prof. Constantinos Varotsis), Hankuk Univ. of Foreign Studies (Prof. Younkyoo Kim) and me. The purpose of this project is to characterize the P intermediate of cytochrome *c* oxidase. Ogura's group carried out time-resolved resonance Raman as well as time-resolved absorption spectroscopy. Yoshikawa analyzed x-ray crystallographic structure of this enzyme. Kitagawa examined IR spectra of the protein moiety of this enzyme to elucidate the proton pumping mechanism. Kim produced the P intermediate by incubation of oxidized enzyme with CO and investigated UV resonance Raman spectra. Varotsis brought bacterial terminal oxidase with him from Crete Univ. to Okazaki and measured its resonance Raman spectra. Prof. Peter Kozolowski of Lousville Univ. also joined this collaborative research to perform DFT calculations on the P intermediate. The all members got together on December 12, 2002 to discuss the structure of P intermediate.

It was pointed out that although the P intermediate generated by incubation of oxidized enzyme with CO exhibits the absorption and resonance Raman spectra quite similar to those of the P intermediate generated in reduction of O_2 by fully reduced enzyme, the two P intermediates are distinct from each other, because the former becomes ferric state without showing the F intermediate but the latter shows it. The presence of an extra oxidation equivalent of the P intermediate on a heme was suggested from the DFT calculations and its compatibility with resonance Raman spectra became a highlight of discussion.

(2) Research Symposia

(From 2002 Oct. to 2003 Sep.)

1. Molecular Science of Complex Condensed System
   (Nov. 8–10, 2002)
   Chair: **UDAGAWA, Yasuo**

2. Present Status and Future Plan of Infrared Synchrotron Radiation
   (Nov. 13–14, 2002)
   Chair: **NANBA, Takao**

3. New Frontier of Molecular Science by Highly Reliable and Large Scaled Computations
   (Nov. 29–Dec. 1, 2002)
   Chair: **SAKAKI, Shigeyoshi**

4. Recent Progress in Magneto-Science—Application of Magnetic Field Effects in Chemical Reaction and Material Processing
   (Dec. 13–14, 2002)
   Chair: **YAMAGUCHI, Masuhiro**

5. Molecular Science of Cluster, Giant-Cluster, and Nanoparticles: Studies on Structural, Electronic and Magnetic Properties for Designing Their Functionalities
   (Feb. 18–19, 2003)
   Chair: **NAKAJIMA, Atsushi**

6. Molecular Materials with Novel Electronic Functions
   (March 3–5, 2003)
   Chair: **KOBAYASHI, Hayao**

7. Molecular Science of Structures and Properties of Copper Proteins
   (March 5–6, 2003)
   Chair: **KOHZUMA, Takamitsu**

8. Symposium on Molecular Science
   (May 16–17, 2003)
   Chair: **TERAZIMA, Masahide**

9. Molecular Science of Rhodopsin
   (May 30–31, 2003)
   Chair: **KANDORI, Hideki**

10. Symposium on Physical Chemistry for Young Researchers of Molecular Science
    (June, 9, 2003)
    Chair: **OHNO, Koichi**

11. Vibrational Relaxation Dynamics in Condensed Phases, from Simple Molecules to Complex Systems
    (June 24–26, 2003)
    Chair: **EBATA, Takayuki**

12. New Development of Hydrogen Bonds and Dynamics of Biomolecules
    (July 11–12, 2003)
    Chair: **SEKIYA, Hiroshi**

13. Chemistry of Nonthermal Electronic Excitation on Solid Surfaces
    (Aug. 21–22, 2003)
    Chair: **YAMASHITA, Koichi**

(3) Cooperative Research

This is one of the most important categories that IMS undertakes for conducting its own research of the common interest to both outside and IMS scientists by using the facilities at IMS. In 2002 Oct.–2003 Mar., 131 outside scientists from 63 research groups joined the Cooperative Research programs, and 121 outside scientists from 56 research groups in 2003 Apr.–2003 Sep. The names and affiliations of those collaborations are found in the Research Activities sections in this Review.

(4) Use of Facility

The number of projects accepted for the Use of Facility in 2002 Oct.–2003 Mar. amounted 3, 28, and 0 for the Laser Research Center for Molecular Science (LRCMS), for the Research Center for Molecular-scale Nanoscience (RCMN) and for the Equipment Development Center (EDC), respectively. In 2003 Apr.–2003 Sep., the number of projects accepted amounted 3, 25, and 0 for LRCMS, for RCMN, and for EDC, respectively.

(5) Invited Research

Under this joint-study program, several scientists were invited from other institutions of help for construction and improvement of instruments in IMS. The total number of the projects in this category was 0.

(6) Use of UVSOR Projects

In the UVSOR Facility with the 750 MeV electron storage ring, there are twenty beam lines available for synchrotron radiation research (see UVSOR ACTIVITY REPORT 2001). Under the Use of UVSOR Projects, many synchrotron radiation experiments have been carried out by outside scientists on eleven beam lines in close cooperation with the UVSOR staff. The total number of the projects in this category was 126 (71 in 2002 Oct.–2003 Mar., and 55 in 2003 Apr.–2003 Sep.).

(7) Use of Facility Program of the Computer Center

Computer Center provides three types of research programs for outside scientists: (a) Use-of-Facility Program; (b) Cooperative Research Program; (c) Advanced Research Program. The numbers of projects accepted for each programs during the fiscal year of 2002 were (a) 146 with 461 users, (b) 10 with 18 users and (c) 3 with 4 users. Computer time distributed for these projects amounted to 80% of the total annual CPU time available.

FOREIGN SCHOLARS

Visitors from abroad are always welcome at IMS and they have always played an important role in the research activities of the Institute. The foreign scientists who visited IMS during the past year (September 2002–August 2003) are listed below.

The mark *1 indicates attendance at an Okazaki Conference; *2 a MONBUSHO (the Ministry of Education, Science, Sports and Culture, Japan) or JSPS (the Japan Society for the Promotion of Science) Invited Fellow; *3 an IMS councillor; *4 an IMS visiting professor or associate professor from abroad (period of stay from 6 to 12 months); *5 a JSPS Post-Doctoral or Ronpaku Fellow; *6 an IMS visiting scientist and *7 a visitor to IMS.

Scientists who would like to visit IMS under programs *2 and *4 are invited to make contact with IMS staff in their relevant field.

Prof. Evgeni Solovijev*2	Macedonian Acad. of Arts and Sci.	(Macedonian)	Sep. '02–Jun. '03
Prof. T. Reetz Manfred*1	Max-Plank-Inst.	(Germany)	Sep. '02
Prof. Rainer Weinkauf*1	Inst. fur Physikalische	(Germany)	Sep.–Oct. '02
Dr. Gennady V. Mil'nikov*6	Inst. of Structural Macrokinetics,	(Russia)	May–Oct. '02
Prof. Cornelis de Lange*2	Univ. of Amsterdam	(Holland)	Oct.–Nov. '02
Prof. Hong Maochun*2	Chinese Acad. of Sci.	(China)	Oct. '02
Prof. Serguei Brazovski*1	Paris South Univ.	(France)	Nov. '02
Dr. Oliver Kuhn*2	Free Univ. Berlin	(Germany)	Nov. '02–Mar. '03
Dr. Balwant K. Rajendra*6	Univ. of Pune Ph.D.	(India)	Nov. '02–Mar. '03
Prof. Luet-Loc Wong*1	Oxford Univ.	(England)	Nov. '02
Prof. R.J.Dwayne Miller*1	Univ. of Toronto	(Canada)	Nov. '02
Dr. Vukica Srajer*1	Argonne Natl. Laboratory	(U.S.A.)	Nov. '02
Prof. Stephan G. Sligar*1	Univ. of Illinois	(U.S.A.)	Nov. '02
Prof. Lu Yi*1	Univ. of Illinois	(U.S.A.)	Nov. '02
Prof. David B. Goodin*1	Scripps Res. Inst.	(U.S.A.)	Nov. '02
Dr. Philip Anfinrud*1	Natl. Inst. of Health	(U.S.A.)	Nov. '02
Prof. Richard B Dyer*1	Los Alamos Natl. Laboratory	(U.S.A.)	Nov. '02
Prof. Steven Hayward*1	Univ. of East Anglia	(England)	Nov. '02
Dr. Danilo Roccatano*1	Univ. of L'Auila	(Italy)	Nov. '02
Mr. Tom Makris *1	Univ. of Illinois	(U.S.A.)	Nov. '02
Mr. Thomas Pfister*1	Univ. of Illinois	(U.S.A.)	Nov. '02
Dr. Aaronn T. Setterdahl*1	Osaka Univ.	(Japan)	Nov. '02
Mr. Rukman Hertadai*1	Tokyo Inst. of Tech.	(Japan)	Nov. '02
Dr. Rehana Afrin*1	Tokyo Inst. of Tech.	(Japan)	Nov. '02
Dr. Mohammad T. Alam*1	Tokyo Inst. of Tech.	(Japan)	Nov. '02
Dr. Ihor P. Omelyan*6	Condensed Matter of Phsics	(Ukraine)	Nov. '02–Mar. '03
Prof. Zdenek Slanina*2	Inst.of Chemistry, Acad. Sinica	(Taiwan)	Dec. '02–Sep. '03
Dr. LEV Dunin-Barkovskiy*6	Moleculare Clusters	(Russia)	Dec. '02–Mar. '04
Prof. P.T. Manoharan*7	Indian Inst. of Tech.	(India)	Mar. '03
Dr. Hanpei Yang*6	Nanjing Univ. Ph.D.	(China)	Dec. '02–Mar. '03
Prof. Younkyoo Kim*6	Hankuk Univ. of Foreign Studies	(Korea)	Dec. '02–Feb. '03
Prof. SangKyu Kim*2	Inha Univ.	(Korea)	Jan.–Mar. '03
Prof. Subbarao V. K. Kumar*2	Tata Inst. of Fundamental Res.	(India)	Jan.–Jun. '03
Prof. Oro Luis*7	Univ. of Zaragoza	(Spain)	Feb. '03
Dr. Nicolaie Pavel*2	Inst. of Atomic Phisics	(Rumania)	May–Aug. '03
Prof. Chun-Woo Lee*6	Ajou Univ.	(Korea)	Feb. '03
Prof. Minggi Cui*7	BSRF Inst. of High Energy Physics	(China)	Feb. '03
Prof. Peiping Zhu*7	Beijing Synchrotron Radiation Facility Inst.	(China)	Feb. '03
Prof. Lammertsma Koop*2	Univ. of Amsterdam	(Holland)	Feb. '03
Prof. Kizhakeyil L Sebastian*7	AIST	(Japan)	Feb. '03
Dr. Petra V. Prokop*7	Tokyo Koka Univ.	(Germany)	Feb. '03
Dr. Seung H. Huh*7	Keiou Gijuku Univ.	(Korea)	Feb. '03
Dr. Joachim Diener*7	Technical Univ. of Muenchen	(Germany)	Feb. '03
Prof. Walter de Heer*7	Georgia Inst. of Tech.	(U.S.A.)	Feb. '03
Prof. Michael A. Duncan*7	Univ. of Georgia	(U.S.A.)	Feb. '03
Dr. Dmitri Kovalev*7	Technical Univ. of Muenchen	(U.S.A.)	Feb. '03
Prof. Fernando Palacio*7	CSIC-Univ. de Saragoza	(Spain)	Feb. '03
Prof. Jos De Jongh*7	Leiden Univ.	(Holland)	Feb. '03
Prof. Coronado Eugenio*7	Univ. de Valencia	(Spain)	Feb. '03
Prof. Hou Xue-Long*2	Shanghai Inst.of Organic Chemistry	(China)	Feb. '03
Prof. Jorn Manz*7	Free Univ. of Berlin	(Germany)	Feb. '03
Prof. Felius Maseras*7	Univ. Autonoma de Barcelona	(Spain)	Feb. '03

Prof. Alejandro Vila[*7]	Univ. of Rosario	(Argentina)	Mar. ’03
Prof. Matthias Ullmann[*7]	Univ. of Hidelberg	(Germany)	Mar. ’03
Prof. Marcellus Ubbink[*7]	Leiden Univ.	(Holland)	Mar. ’03
Prof. S. Mazumdar[*7]	Tata Inst. of Fundamental Res.	(India)	Mar. ’03
Prof. Christin Choma[*7]	Rensselaer Polytechnic Inst.	(U.S.A.)	Mar. ’03
Prof. Andrew J. Thomson[*7]	Univ. of East Anglia	(England)	Mar. ’03
Prof. Gerard W. Canters[*7]	Leiden Univ.	(Holland)	Mar. ’03
Prof. Lucia Banci[*7]	Univ. of Florence	(Italy)	Mar. ’03
Dr. Jaehong Han[*7]	Virginia Tech.	(U.S.A.)	Mar. ’03
Mr. Rafael Fernandez[*7]	Univ. of Edinburgh	(England)	Mar. ’03
Mr. R Murgan[*7]	Tata Inst. of Fundamental Res.	(India)	Mar. ’03
Mr. Nithianantham Stanley[*7]	Bharathidasan Univ.	(India)	Mar. ’03
Mr. Chivukula V.Sastri[*7]	Hyderabad Univ.	(India)	Mar. ’03
Prof. Nenad M. Kostic[*7]	Iowa State Univ.	(U.S.A.)	Mar. ’03
Prof. Prasat Kittakoop[*7]	Natl. Cent. for Genetic Engineering Biotech	(Thai Land)	Mar. ’03
Prof. N.Jayaraman[*7]	Indian Inst. of Sci.	(India)	Mar. ’03
Prof. Zijian Guo[*7]	Nanjing Univ.	(China)	Mar. ’03
Ms. Joo Kim[*7]	Ewha Womans Univ.	(Korea)	Mar. ’03
Mr. Cong Li[*7]	Univ. of Hong Kong	(China)	Mar. ’03
Ms. Kannie Wei-Yan Chan[*7]	Univ. of Hong Kong	(China)	Mar. ’03
Dr. Steve Sheng -Fa Yu[*7]	Acad. Sincia	(China)	Mar. ’03
Ms. Se-Eun Park[*7]	Ewha Womans Univ.	(Korea)	Mar. ’03
Ms. Na Young Ohv	Ewha Womans Univ.	(Korea)	Mar. ’03
Ms. Jun-Hee In[*7]	Ewha Womans Univ.	(Korea)	Mar. ’03
Mr. Masudur Rahmanv	Toyohashi Univ. of Tech.	(Japan)	Mar. ’03
Mr. Jinkyu Kimv	Yonsei Univ.	(Korea)	Mar. ’03
Ms. Soo Hyun Kim[*7]	Sun Moon Univ.	(Korea)	Mar. ’03
Prof. Thomas V. O ’Halloran[*7]	Northeastern Univ.	(U.S.A.)	Mar. ’03
Mr. Rong Chen[*7]	Hong Kong Univ.	(China)	Mar. ’03
Dr. Tapan Kumar Kundu[*7]	Indian Inst. of Tech.	(India)	Mar. ’03
Dr. R.N.Patel[*7]	A. P. S. Univ.	(India)	Mar. ’03
Mr. Pattubala A. N. Reddy[*7]	Indian Inst. of Sci.	(India)	Mar. ’03
Prof. Edmunds Lukevics[*7]	Latvian Inst. of Organic Synthesis	(Latvian)	Mar. ’03
Prof. Myrna S. Mahinay[*7]	MSU-Illigan Inst. of Tech.	(Phillipine)	Mar. ’03
Prof. Bhaskar G. Maiya[*7]	Univ. of Hyderabad	(India)	Mar. ’03
Prof. Siva T. Rao[*7]	Andhra Univ. Assistant	(India)	Mar. ’03
Prof. Wonwoo Nam[*7]	Ewha Womans Univ.	(Korea)	Mar. ’03
Prof. Kenneth D. Karlin[*7]	Johns Hopkins Univ.	(U.S.A.)	Mar. ’03
Prof. Anthony G. Wedd[*7]	Univ. of Melbourne	(Australia)	Mar. ’03
Prof. Jinheung Kim[*7]	Changwon Natl. Univ.	(Korea)	Mar. ’03
Dr. Svitlana Pavlova[*7]	Acad. Sinica	(Taiwan)	Mar. ’03
Mr. Huang-Chou Chen[*7]	Acad. Sinica	(Taiwan)	Mar. ’03
Dr. Rita Song[*7]	Ewha Womans Univ.	(Korea)	Mar. ’03
Mr. Qin Liu[*7]	Nanjing Univ.	(China)	Mar. ’03
Dr. Ping-Yu Chen[*7]	Acad. Sinica	(Taiwan)	Mar. ’03
Dr. Fei Li[*7]	Univ. of Hong Kong	(China)	Mar. ’03
Dr. Yanbing Zu[*7]	Univ. of Hong Kong	(China)	Mar. ’03
Dr. Chang-Li Chen[*7]	Acad. Sinica Ph.D.	(Taiwan)	Mar. ’03
Ms. Pitchumony T. Selvi[*7]	Bharathidasan Univ.	(India)	Mar. ’03
Ms. Miu Fan Kwan[*7]	Univ. of Hong Kong	(China)	Mar. ’03
Prof. Sunney I. Chan[*7]	Acad. Sinica	(Taiwan)	Mar. ’03
Prof. Edward R.T. Tiekink[*7]	Natl. Univ. of Singapore	(Singapore)	Mar. ’03
Prof. Weiyin Sun[*7]	Nanjing Univ.	(China)	Mar. ’03
Prof. Maeng-Joon Jung[*7]	Sangju National Univ.	(Korea)	Mar. ’03
Dr. V.G. Vaidyanathan[*7]	Central Leather Res. Inst.	(India)	Mar. ’03
Prof. Junghee Kim[*7]	Sun Moon Univ.	(Korea)	Mar. ’03
Prof. Fei Gao[*7]	Shanxi Univ.	(China)	Mar. ’03
Prof. Seong K. Kim[*7]	Yeungnam Univ.	(Korea)	Mar. ’03
Prof. Youn Soo Sohn[*7]	Ewha Womans Univ.	(Korea)	Mar. ’03
Prof. Pin Yang[*7]	Shanxi Univ.	(China)	Mar. ’03
Mr. Lei Zhangv	Kanazawa Univ.	(Japan)	Mar. ’03
Mr. Mohd Zulkefeli[*7]	Hiroshima Univ.	(Japan)	Mar. ’03
Prof. Hong-Zhe Sun[*7]	Univ. of Hong Kong	(China)	Mar. ’03
Dr. Ekasith Somsook[*7]	Mahidol Univ.	(Thai Land)	Mar. ’03

Prof. Yuxiang Mo[*6]	Tsinghua Univ.	(China)	Mar. ’03
Dr. Junaid Bushiri[*2]	Univ. of Kerala	(India)	Apr. ’03–Mar. ’04
Dr. Oleksandr Kobryn[*6]	Natl. Ukrainian Acad. of Sci.	(Ukraine)	Apr. ’03–Mar. ’06
Dr. Shiyang Zou[*6]	IMS Dept. of Theoreical Studies	(Japan)	Apr. ’03–Mar. ’05
Mr.Zhongfang Chen[*2]	Erlangen Univ., Inst. of Organic Chemistry	(Germany)	Apr.–Jun. ’03
Prof. Gilbert C. Walker[*3]	Univ. of Pittsuburgh	(U.S.A.)	Apr. ’03–Jan. ’04
Prof. Christpher E. Brion[*7]	Univ. of British Columbia	(Canada)	May ’03
Prof. Myrna, S. Mahinayv	MSU-Illigan Inst. of Tech.	(Phillipine)	Jun. ’03–Jun. ’05
Prof. Puspendu Das[*2]	Indian Inst. of Sci.	(India)	Jun.–Sep. ’03
Prof. Tim Softley[*6]	Univ. of Oxford	(England)	Jun. ’03
Prof. Cheol Min Yoon[*2]	Korea Univ.	(Korea)	Jun.–Aug. ’03
Prof. Artur Ishkhanyan[*2]	Armenian Natl. Acad. of Sci., Engineering Cent.	(Armenia)	Jun.–Dec. ’03
Prof. Giovanni La Penna[*7]	Magnetic Resonance Cent.	(Italy)	Mar. ’03
Prof. Berned A Berg[*7]	Florida State Univ.	(U.S.A.)	Mar. ’03
Prof. Ulrich Hansmann[*7]	Michigan Tech. Univ.	(U.S.A.)	Mar. ’03
Mr. Chirs Saunders[*7]	Washington Univ.	(U.S.A.)	Mar. ’03
Mr. Michael W. Schmidt[*6]	Iowa State Univ.	(U.S.A.)	Jun.–Jul. ’03
Prof. Younkyoo Kim[*2]	Hankkuk Univ. of Foreign Studies	(Korea)	Jun.–Aug. ’03
Prof. Roman Morgunov[*2]	Inst. of Solid State Phisics	(Russia)	Jul. ’03–Mar. ’04
Prof. DaveThirumalai[*7]	Univ. of Maryland	(U.S.A.)	Mar. ’03
Prof. Grenfell N. Patey[*7]	Univ. of British Columbia	(Canada)	Mar. ’03
Dr. Jed Pitera[*7]	IMB Res. Division Almaden Res. Cent.	(U.S.A.)	Apr. ’03
Prof. Cheol Ho Choi[*6]	Kyungpook Natl. Univ.	(Korea)	Jun.–Aug. ’03
Dr. S. Z. Brian[*6]	Georgetown Univ.	(U.S.A.)	Jul. ’03
Prof. Varotsis Constantinos[*6]	Univ. of Crete	(Greece)	Jul.–Oct. ’03
Prof. Pavichev Andrey[*6]	St. Petersburg Univ.	(Russia)	Mar. ’03
Prof. Woell Chirstof[*6]	Ruhr-Univ. Bochum	(Germany)	Jul. ’03
Prof. Bertini Ivano[*2]	Univ. Florence	(Italy)	Jul.–Aug. ’03
Dr. N. Jana[*6]	Inst. of Macromolecular Chemistry Acad. of Sci.	(Czech Republic)	Aug. ’03
Prof. N. Stanislav[*6]	Inst. of Macromolecular Chemistry Acad. of Sci.	(Czech Republic)	Aug. ’03
Prof. Raymond Ziessel[*6]	Univ. Louis Pasteur	(France)	Jun. ’03
Prof. Tarlok Singh Lobana[*6]	Guru Nanak Dev Univ.	(India)	May ’03
Dr. Izabela Rzeznicka[*6]	Hokkaido Univ.	(Japan)	Aug. ’03
Prof. Hobley Jonathan[*6]	Tohoku Postgraduate Sci. Res.	(Japan)	Aug. ’03
Prof. Lupei Voicu[*6]	Inst. of Atomic Physics	(Rumania)	Jul.–Sep. ’03
Prof. Hossain M. Delawar[*6]	Shahjalal Univ. of Sci. and Tech.	(Bangladesh)	Aug. ’03–Mar. ’05
Prof. Hu Chin-Kun[*6]	Inst. of Physics Acad. Sinica	(Taiwan)	Aug. ’03

AWARDS

Emeritus Professor Iwamura's Scientific Achievements

Emeritus Professor Hiizu Iwamura received "The Japan Academy Prize in 2003" for his contribution to the Study of Molecule-based Magnets. The prize was awarded jointly to Profs. Koichi Itoh (Emeritus Professor of Osaka City Univ.) and Minoru Kinoshita (Emeritus Professor of the Univ. of Tokyo).

Iwamura was a faculty member of IMS during1976–1987. It was at IMS in early 80's when he initiated this scientific area by synthesized linear tetrakis(diazo) and pentakis(diazo) compounds in which all the adjacent diazomethylene units were connected by *m*-phenylene units. The polydiazo compounds were photolyzed under cryogenic conditions to show by EPR and magnetic susceptibility measurements that the tetra- and pentacarbenes have nonet (S = 4) and undecet (S = 5) ground states, respectively. Thus, he constructed for the first time paramagnetic hydrocarbons that have ground-state spins and therefore magnetic moments greater than those of d^5 transition metal ions and f^7 lanthanides. Iwamura's scientific achievements of excellence are demonstrated by further extension of this work in three directions: 1) extensive search for ferromagnetic coupling units, 2) synthesis of higher analogues of polycarbenes, and 3) synthesis of stable polyaminoxyl radicals and their use for supramolecular hybrid spin magnets.

1. Iwamura demonstrated that there are two series of diradicals, dicarbenes, and dinitrenes that have high-spin and low-spin ground states depending on the connectivity of the two spin centers through π-electron systems. He determined the energy gap of the ground and higher-energy spin states by analyzing the temperature dependence of their EPR fine structures and/or magnetic susceptibility data. The molecular structures of the high- and low-spin species are correlated by resonance structures to "trimethylenemethane" and "tetramethyleneethane," respectively. These simplest diradicals had been suggested by quantum chemical studies of Wes Borden and others to have triplet and singlet ground states, respectively. Iwamura showed that 1,2-dimethylenecyclohexane-1,2-diyl, a conformationally restricted analogue of the latter does have a singlet ground state, the first conclusive experimental evidence for its ground state.
   Iwamura and coworkers solved a question of how to align electron spins in parallel in the stacking interaction of two π-radical molecules by preparing isomeric [2.2]paracyclophanes in which two diphenylcarbene units are modeled to overlap with the rotation angles of 60, 120 and 180 degrees. The isomers have quintet, singlet, and quintet ground states, respectively (1985), offering the first experimental verification of the theory of Harden McConnell proposed in 1963 and serving as a basis for the crystal design of spin alignment between open-shell molecules.
2. Knowing that the connection of many carbene centers in one dimension is too naïve a prototype for organic magnets, Iwamura synthesized a branched-chain, cyclic and dendritic polydiazo compounds constituting various units of a two-dimensional honey-comb-shaped network structure. A branched chain nonacarbene has a nonadecet (S = 9) ground state, the highest spin ever reported for a well-defined organic molecule. A cyclic hexacarbene derived from a calixarene has a tridecet (S = 6) ground state. However, the expected high spin species were not necessarily obtained upon photolysis of dendritic analogues due to intramolecular dimerization and/or azine formation.
3. In order to overcome these limitations of the polycarbene approach, he turned to stable aminoxyl radicals. A series of bis- and tris(aminoxyl) radicals that have triplet and quartet ground states and are stable under air at room temperature have been synthesized. Again it proved not to be easy to extend the system to higher spin species. Iwamura and Inoue made a major breakthrough by advancing a strategy of making hybrid spin magnets consisting of aminoxyl radials as ligands with magnetic metal ions as linkers. Depending on the disposition of the aminoxyl oxygen atoms in the bis- and tris(aminoxyl) radicals, one-, two- and three-dimensional network structures have been obtained as designed. In many of the resulting mixed ligand complexes with $[Mn(hfac)_2]$, all the 2*p* spins of the aminoxyl ligand and the 3*d* spins of the Mn^{2+} ordered spontaneously to form ferrimagnets at temperatures below 4–60 K.
   Pursuing the first idea of making photomagnetic materials by using polydiazo compounds, Iwamura and Koga developed polydiazo supramolecules by combining various magnetic metal ions with diazodipyridylmethanes. $[Mn(hfac)_2]$ and $[Cu(hfac)_2]$ with diazodi(4-pyridyl)methane, for example, formed well-defined polymer complexes that are dilute paramagnets due to the metal ions. When the diazo groups were photolyzed, the polymer complexes produced ferrimagnetic and ferromagnetic chains, respectively. As a result of the extension of the correlation length, S_{av} in the former approached 300 at 2.0 K. Furthermore the carbene centers formed in the crystal lattice of the complexes were found to be stable up to 240 K.

His important scientific contributions described above are published in about 170 international publications.

Professor Kasai's Scientific Achievements

Prof. Toshio Kasai at Osaka University, a former visiting professor of the institute, received the Scientific Award of the Chemical Society of Japan in 2002 for his contribution to "Studies on Reaction dynamics Using Oriented Molecular Beams: Discovery of Steric (Molecular Orientation) Effects and Its Application to Surface Reactions." Prof. Kasai has studied stereo-dynamics in various gas phase reactions by utilizing the advantage of the oriented molecular beam method. Orientation of reagent molecule can be controlled by an electrostatic field after rotational quantum state selection by hexapole electrostatic field. His scientific achievements related to the award are summarized as follows:

1. *Reaction of excited rare gas atoms with oriented halomethane and related simple molecules:*
   On the basis of experimentally observed steric effect for these reaction systems, Prof. Kasai demonstrated how the molecular orientation affects the reactivity. Experimental observation of steric effect also enabled us to make comparison with theoretical study, and this comparison further allows us to find out direct relationship between the steric effect and the spatial distribution of related molecular orbital.
2. *Reaction dynamics study under collision energy and orientation specified condition:*
   Prof. Kasai has developed a reaction apparatus for time of flight measurement with oriented molecular beam, which made it possible to observe two dimensional reaction cross section. Throughout several studies related to Penning ionization reactions, he has ascribed the origin of the steric effect to the interaction potential of the reagent molecules. He has also pointed out that the observable steric effect depended upon collision energy of the reagent. Furthermore, he has found reaction pathways correlated to Feshbach resonance under both collision energy and orientation specified condition. He successfully characterized these reaction dynamics in gas phase collision in detail.
3. *Hexapole application to molecular clusters:*
   Prof. Kasai has successfully demonstrated that size and structure of molecular clusters could be selected by hexapole field. Furthermore, by combining this method with Doppler time of flight mass spectroscopy, the internal state distribution for the transient species in the photo-dissociation reaction of DCl dimer has been elucidated.
4. *Hexapole application to reactions:*
   Prof. Kasai has developed an ultra-high vacuum oriented molecular beam apparatus for studying surface reactions. The reaction dynamics of oriented CH_3Cl molecule with Si{001}surface was studied and results provided indispensable knowledge for surface reaction control at molecular level.

Associate Professor Tanimura's Scientific Achievements

Associate professor Yoshitaka Tanimura, Department of Theoretical Studies, received the Morino Science Award in 2002 for his contribution to "Studies on Theoretical Bases of Two-dimensional Spectroscopy." With Prof. Mukamel in Rochester University, he proposed two-dimensional optical spectroscopy method for the first time. This method is called "optical version" of two-dimensional nuclear magnetic resonance method. In particular, they showed that the multi-dimensional spectroscopy is realizable in even more complicated systems with the observables such as polarizability and dipole moment than those only with spin angular momenta. This theoretical approach invited the experimental studies on two-dimensional Raman and infrared spectroscopy by Prof. Fleming and Prof. Hochstrasser and can be evaluated as a pioneering work in the field of optical spectroscopy. Prof. Tanimura has been developing analytical methods for studying inhomogeneity in solution, anharmonic oscillators, and non-linear polarizability by using the extended quantum Fockker-Planck equation.

Research Associate Matsuo's Scientific Achievement

Research Associate Dr. Tsukasa Matsuo of Coordination Chemistry Laboratories has been selected to receive the 2002 Chemical Society of Japan Award for Young Chemists for his contribution entitled "Studies on Anion Species of Silyl-Substituted π-Electron System Based on 4- and 5-Membered Rings." One of most remarkable achievements relevant to the award is the investigation of cyclobutadiene dianions. Hückel's rule predicts the cyclobutadiene dianion to be aromatic. However attempts to prepare the planar cyclobutadiene dianion itself and its derivative with D_{4h} symmetry have been failure due to electronic repulsion originating from the large negative charge density per atom. Dr. Matsuo succeeded in synthesizing a dilithio salt of tetrakis(trimethylsiyl)cyclobutadiene dianion by taking advantage of electronic and steric effects of the silyl groups. X-ray crystallographic analysis and NMR spectroscopic studies confirm the aromatic nature of the 6 π-electron cyclobutadine dianion. In addition, since this dianion is a rare example of aromatic organic molecules with degenerate HOπMOs and a nondegenerate LUπMO, he elucidated this type of unusual electronic structure by the simultaneous use of UV-visible absorption and magnetic circular dichroism spectroscopies. This is the first demonstration of a negative Faraday *A* term for an aromatic organic

compound for the first time.

Mr. Kenji Suzuki's Scientific Achievement

Mr. Kenji Suzuki of Yakushi Group, the student of the Graduate University for Advanced Studies, received the Student Award for the Most Impressive Presentation in 83rd Annual Meeting of the Chemical Society of Japan for his contribution "Charge Separation of θ-(BEDT-TTF)$_2$RbZn(SCN)$_4$ under High Pressure." This student award was initiated from 83rd Annual Meeting, and two students were selected in the field of solid state chemistry. His achievement is the drawing of the electronic phase diagram of θ-(BEDT-TTF)$_2$RbZn(SCN)$_4$ in the pressure and temperature space using Raman spectroscopy.

LIST OF PUBLICATIONS

Department of Theoretical Studies

K. KOBAYASHI and S. NAGASE, "A Stable Unconventional Structure of $Sc_2@C_{66}$ found by Density Functional Calculations," *Chem. Phys. Lett.* **362**, 373–379 (2002).
N. TAKAGI and S. NAGASE, "Theoretical Study of an Isolable Compound with a Short Silicon-Silicon Triple Bond, $(t\mathrm{Bu_3Si})_2\mathrm{MeSiSi{\equiv}SiSiMe}(\mathrm{Si}t\mathrm{Bu_3})_2$," *Eur. J. Inorg. Chem.* 2775–2778 (2002).
N. TOKITOH, T. SASAMORI, N. TAKEDA and S. NAGASE, "Systematic Studies on Homo- and Heteronuclear Doubly Bonded Compounds of Heavier Group 15 Elements," *Phosphorus, Sulfur Silicon Relat. Elem.* **177**, 1473–1476 (2002).
K. GOTO, J. KOBAYASHI and T. KAWASHIMA, M. W. SCHMIDT and S. NAGASE, "Bonding Properties of 5-Carbaphosphatranes," *Phosphorus, Sulfur Silicon Relat. Elem.* **177**, 2037–2038 (2002).
N. TOKITOH, K. HATANO, T. SASAKI, T. SASAMORI, N. TAKEDA, N. TAKAGI and S. NAGASE, "Synthesis and Isolation of the First Germacyclopropabenzene: A Study to Elucidate the Intrinsic Factor for the Ring Deformation of Cyclopropabenzene Skeletons," *Organometallics* **21**, 4309–4311 (2002).
S. MATSUKAWA, S. KOJIMA, K. KAJIYAMA, Y. YAMAMOTO, K. -Y. AKIBA, S. RU and S. NAGASE, "Characteristic Reactions and Properties of *C*-Apical *O*-Equatorial (*O*-cis) Spirophosphoranes: Effect of the σ^*_{P-O} Orbital in the Equatorial Plane and Isolation of a Hexacoordinate Oxaphosphetane as an Internediate of the Wittig Type Reaction of 10-P-5 Phosphoranes," *J. Am. Chem. Soc.* **124**, 13154–13170 (2002).
Y. NIINO, T. WAKAHARA, T. AKASAKA, M. T. H. LIU, K. KOBAYASHI and S. NAGASE, "Photochemical Decomposition of Pyrazoline Produced in the Reaction of C_{60} with Diazoadamantane," *ITE Lett. Batt. New Tech. Med.* **3**, 82–84 (2002).
K. KOBAYASHI and S. NAGASE, "Theoretical Calculations of Vibrational Modes in Endohedral Metallofullerenes: $La@C_{82}$ and $Sc_2@C_{84}$," *Mol. Phys.* (a special issue for Prof. YOSHIMINE) **101**, 249–254 (2003).
G. M. A. RAHMAN, Y. MAEDA, T. WAKAHARA, M. KAKO, S. SATO, M. OKAMURA, T. AKASAKA, K. KOBAYASHI and S. NAGASE, "Photochemical Bissilylation of C_{70} with Disilane," *ITE Lett. Batt. New Tech. Med.* **4**, 60–66 (2003).
T. WAKAHARA, G. M. A. RAHMAN, Y. MAEDA, M. KAKO, S. SATO, M. OKAMURA, T. AKASAKA, K. KOBAYASHI and S. NAGASE, "Redox Properties of Carbosilylated and Hydrosilykated Fullerene Derivatives," *ITE Lett. Batt. New Tech. Med.* **4**, 67–73 (2003).
T. WAKAHARA, M. KAKO, Y. MAEDA, T. AKASAKA, K. KOBAYASHI and S. NAGASE, "Synthesis and Characterization of Cyclic Silicon Compounds of Fullerenes," *Curr. Org. Chem.* **7**, 927–943 (2003).
K. NAGAYOSHI, K. KITAURA, S. KOSEKI, S. RE and K. KOBAYASHI, Y. -K. CHOE and S. NAGASE, "Calculation of Packing Structure of Methanol Solid Using Ab Initio Lattice Energy at the MP2 level," *Chem. Phys. Lett.* **369**, 597–604 (2003).
J. LU, S. RE, Y. -K. CHOE, S. NAGASE, Y. ZHOU, R. HAN, L. PENG, X. ZHANG and X. ZHAO, "Theoretical Identification of Carbon Clusters C_{20}: Prevalence of the Monocyclic Isomer and Existences of the Smallest Fullerene and Bowl Isomer," *Phys. Rev. B* **67**, 125415 (7 pages) (2003).
J. LU and S. NAGASE, "Structural and Electronic Properties of Metal-Encapsulated Silicon Clusters in a Large Size Range," *Phys. Rev. Lett.* **90**, 115506 (4 pages) (2003).
J. LU and S. NAGASE, "Metal-Doped Germanium Clusters MGe_n at the Sizes of n = 12 and 10: Divergence of Growth Patterns from the MSi_n Clusters," *Chem. Phys. Lett.* **372**, 394–398 (2003).
Z. SLANINA, K. KOBAYASHI and S. NAGASE, "$Ca@C_{72}$ IPR and Non-IPR Structures; Computed Temperature Development of their Relative Concentrations," *Chem. Phys. Lett.* **372**, 810–814 (2003).
N. TAKAGI, K. YAMAZAKI and S. NAGASE, "Theoretical Investigation of Triple Bonding between Transition Metal and Main Group Elements in $(\eta^5\text{-}C_5H_5)(CO)_2M{\equiv}ER$ (M = Cr, Mo, W; E = Si, Ge, Sn, Pb; R = Terphenyl Groups)," *Bull. Korean Chem. Soc.* (a special issue) **24**, 832–836 (2003).
K. NAGAYOSHI, T. IKEDA, K. KITAURA and S. NAGASE, "Computational Procedure of Lattice Energy Using the Ab Initio MO Method," *J. Theor. Comput. Chem.* **2**, 233–244 (2003).
K. KOBAYASHI, S. NAGASE, Y. MAEDA, T. WAKAHARA and T. AKASAKA, "$La_2@C_{80}$: Is the Circular Motion of Two La Atoms Controllable by Exohedral Addition?" *Chem. Phys. Lett.* **374**, 562–566 (2003).
K. KOBAYASHI, S. NAGASE and K. -P. DINSE, "A Theoretical Study of Spin Density Distributions and Isotropic Hyperfine Couplings of N and P atoms in $N@C_{60}$, $P@C_{60}$, $N@C_{70}$, $N@C_{60}(CH_2)_6$, and $N@C_{60}(SiH_2)_6$," *Chem. Phys. Lett.* **377**, 93–98 (2003).

T. HIROYASU, M. MIKI, M. OGURA and Y. OKAMOTO, "Examination of Parallel Simulated Annealing Using Genetic Crossover," *IPSJ TOM* (in Japanese) **43**, 70–79 (2002).
C. MUGURUMA, Y. OKAMOTO and M. MIKAMI, "An Application of the Multicanonical Monte Carlo Method to the Bulk Water System," *Internet Electro. J Mol. Design* **1**, 583–592 (2002).
T. YOSHIDA, T. HIROYASU, M. MIKI, M. OGURA and Y. OKAMOTO, "Energy Minimization of Protein Tertiary Structure by Parallel Simulated Annealing Using Genetic Crossover," *Proceedings of 2002 Genetic and Evolutionary Computation Conference (GECCO 2002)* 49–51 (2002).
A. MITSUTAKE, Y. SUGITA and Y. OKAMOTO, "Replica-Exchange Multicanonical and Multicanonical

Replica-Exchange Monte Carlo Simulations of Peptides. I. Formulation and Benchmark Test," *J. Chem. Phys.* **11**8, 6664–6675 (2003).
A. MITSUTAKE, Y. SUGITA and Y. OKAMOTO, "Replica-Exchange Multicanonical and Multicanonical Replica-Exchange Monte Carlo Simulations of Peptides. II. Application to a More Complex System," *J. Chem. Phys.* **118**, 6676–6688 (2003).
T. HIROYASU, M. MIKI, S. OGURA, K. AOI, T. YOSHIDA and Y. OKAMOTO, "Atom-Level Simulations of Protein Folding," *Proceedings of the 7th World Multiconference on Systemics, Cybernetics and Informatics (SCI2003)* **Vol. XIV**, 117–122 (2003).

K. NAGAYA, Y. TERANISHI and H. NAKAMURA, "Control of Molecular Processes by a Sequence of Linearly Chirped Pulses," *J. Chem. Phys.* **117**, 9588–9604 (2002).
G. V. MIL'NIKOV and H. NAKAMURA, "Practical Implementation of the Instanton Theory, II. Decay of Metastable State Through Tunneling," *J. Chem. Phys.* **117**, 10081–10087 (2002).
H. FUJISAKI, Y. TERANISHI and H. NAKAMURA, "Control of Photodissociation Branching Using the Complete Reflection Phenomenon: Application to HI Molecule,"
J. Theor. Comput. Chem. **1**, 245–253 (2002).
S. NANBU, M. AOYAGI, H. NAKAMURA, H. KAMISAKA, W. BIAN and K. TANAKA, "Chemical Reactions in the $O(^1D)$ + HCl System, I. Ab Initio Global Potential Energy Surfaces for the $1^1A'$,$2^1A'$, and $1^1A''$ States," *J. Theor. Comput. Chem.* **1**, 263–273 (2002).
S. NANBU, M. AOYAGI, H. NAKAMURA, H. KAMISAKA, W. BIAN and K. TANAKA, "Chemical Reactions in the $O(^1D)$ + HCl System, II. Dynamics on the Ground $1^1A'$ State and Contributions of the Excited ($1^1A''$ and $2^1A'$) states," *J. Theor. Comput. Chem.* **1**, 275–284 (2002).
S. NANBU, M. AOYAGI, H. NAKAMURA, H. KAMISAKA, W. BIAN and K. TANAKA, "Chemical Reactions in the $O(^1D)$ + HCl System, III. Quantum Dynamics on the Excited ($1^1A''$ and $2^1A'$) Potential Energy Surfaces," *J. Theor. Comput. Chem.* **1**, 285–293 (2002).
A. KONDORSKIY and H. NAKAMURA, "Photodissociation of H_2^+ and HD^+ in an Intense Laser Field," *Phys. Rev. A* **66**, 053412 (8 pages) (2002).
G. V. MIL'NIKOV and H. NAKAMURA, "Calculation of Resonances in the $dt\mu$ Molecule by the R-Matrix Method," *Phys. Rev. A* **67**, 034501 (4 pages) (2003).
G. V. MIL'NIKOV, K. YAGI, T. TAKETSUGU, H. NAKAMURA and K. HIRAO, "Tunneling Splitting in Polyatomic Molecules: Application to Malonaldehyde," *J. Chem. Phys.* **119**, 10–13 (2003).
H. NAKAMURA and E. A. SOLOVJEV, "Semiclassical Theory for the Quantum Defect Function of Diatomic Molecules," *J. Phys. B* **36**, 3697–3705 (2003).

Y. SUZUKI and Y. TANIMURA, "Two-Dimensional Spectroscopy for Two-Dimensional Rotator Coupled to a Gaussian-Markovian Noise Bath," *J. Chem. Phys.* **119**, 1650–1660 (2003).
O. KHÜN and Y. TANIMURA, "Two-Dimensional Vibrational Spectroscopy of a Double Minimum System in a Dissipative Environment," *J. Chem. Phys.* **119**, 2155–2164 (2003).

R. DEKA, D. AJITHA and K. HIRAO, "Adsorption of Small Molecules in Zeolite: A Local Hard-Soft Acid-Base Approach," *J. Phys. Chem. B* **107**, 8574–8577 (2003).
T. YANAI, H. NAKANO, T. NAKAJIMA, T. TSUNEDA, S. HIRATA, Y. KAWASHIMA, Y. NAKAO, M. KAMIYA, H. SEKINO and K. HIRAO, "UTChem- A Program for *Ab Initio* Quantum Chemistry," *Computational Science–ICCS 2003, Lecture Notes in Computer Science (Springer)* 84–95 (2003).
T. NAKAJIMA and K. HIRAO, "Douglas-Kroll Transformation to the Relativistic Many-Electron Hamiltonian," *J. Chem. Phys.* **119**, 4105–4111 (2003).
Y. SAKIMOTO, K. HIRAO and D. G. MUSAEV, "Reactivity of Ebtellur Derivatives with the Peroxynitrite Anion: Comparison with their Ebselen Analogues," *J. Phys. Chem. A* **107**, 5631–5639 (2003).
G. V. MIL'NIKOV, K. YAGI, T. TAKETSUGU, H. NAKAMURA and K. HIRAO, "Tunneling Splitting in Polyatomic Molecules: Application to Malonaldehyde," *J. Chem. Phys.* **119**, 10–13 (2003).
J. PAULOVIC, T. NAKAJIMA, K. HIRAO, R. LINDH and P. A. MALMQVIST, "Relativistic and Correlated Calculations on the Ground and Excited States of ThO," *J. Chem. Phys.* **119**, 798–805 (2003).
T. TSUNEDA, M. KAMIYA and K. HIRAO, "Regional Self-Interaction Correction of Density Functional Theory," *J. Comput. Chem.* **24**, 1592–1598 (2003).
D. AJITHA, K. HIRAO and S. PAL, "Energies and Dipole Moments of Excited States of Ozone and Ozone Radical Cation Using Fock Space Multireference Coupled-Cluster Analytical Response Approach," *Collec. Czechoslovak Chem. Commun.* **68**, 47–60 (2003).
H. YUI, T. NAKAJIMA, K. HIRAO and T. SAWADA, "Enhancement of the Stimulated Raman Scattering Derived from Intermolecular Interactions between Aromatic Moieties," *J. Phys. Chem. A* **107**, 968–973 (2003).
D. G. MUSAEV and K. HIRAO, "The Differences and Similarities in the Reactivities of Peroxynitrite Anion and Peroxynitrous Acid with Ebselen. A Theoretical Study," *J. Phys. Chem. A* **107**, 1563–1573 (2003).
D. G. MUSAEV, Y. V. GELETTII, G. L. HILL and K. HIRAO, "Can Ebselen Derivatives Catalyze the Isomerization of Peroxynitrite to Nitrate?" *J. Am. Chem. Soc.* **125**, 3877–3888 (2003).
H. A. WITEK, H. NAKANO and K. HIRAO, "Multireference Perturbation Theory with Optimized Partitioning. I.

Theoretical and Computational Aspects," *J. Chem. Phys.* **118**, 8197–8206 (2003).
H. A. WITEK, H. NAKANO and K. HIRAO, "Multireference Perturbation Theory with Optimized Partitioning. II. Applications to Molecular Systems," *J. Comput. Chem.* **24**, 1390–1400 (2003).
D. G. FEDOROV, T. NAKAJIMA and K. HIRAO, "An Ab Initio Study of Excited States of U and UF," *J. Chem. Phys.* **118**, 4970–4975 (2003).
K. YAGI, C. OYANAGI, T. TAKETSUGU and K. HIRAO, "Ab Initio Potential Energy Surface for Vibrational State of H_2CO," *J. Chem. Phys.* **118**, 1653–1660 (2003).
S. IKEDA, T. NAKAJIMA and K. HIRAO, "A Theoretical Study of Transition Metal Hydroxides: CuOH, AgOH, and AuOH," *Mol. Phys.* (Yoshimine Memorial Issue) **101**, 105–110 (2003).

T. TAKAYANAGI, "A CASPT2 Study of the Doublet Potential Energy Surface for the $CH(X^2\Pi) + N_2(X^1\Sigma_g^+)$ Reaction," *Chem. Phys. Lett.* **368**, 393–398 (2003).
T. TAKAYANAGI, "Ab Initio Calculations of Low-Lying Potential Energy Surfaces of the HHeF System," *Chem. Phys. Lett.* **371**, 675–680 (2003).
T. TAKAYANAGI and M. SHIGA, "Photodissociation of Cl_2 in Helium Clusters: An Application of Hybrid Method of Quantum Wavepacket Dynamics and Path Integral Centroid Molecular Dynamics," *Chem. Phys. Lett.* **372**, 90–96 (2003).
A. WADA, T. TAKAYANAGI and M. SHIGA, "Theoretical Simulations on Photoexcitation Dynamics of the Silver Atom Embedded in Helium Clusters," *J. Chem. Phys*. **119**, 5478–5486 (2003).

H. TORII, "The Role of Atomic Quadrupoles in Intermolecular Electrostatic Interactions of Polar and Nonpolar Molecules," *J. Chem. Phys.* **119**, 2192–2198 (2003).

T. KIMURA, N. MATSUBAYASHI, H. SATO, F. HIRATA and M. NAKAHARA, "Enthalpy and Entropy Decomposition of Free-Energy Changes for Side-Chain Conformations of Asparatic Acid and Asparagine in Acidic, Neutral, and Basic Aqueous Solutions," *J. Phys. Chem. B* **106**, 12336 (2002).
A. KOVALENKO and F. HIRATA, "Toward a Molecular Theory for the van der Waals-Maxwell Description of Fluid Phase Transitions," *J. Theor. Comput. Chem.* (Review article) **2**, 381 (2002).
T. SUMI and F. HIRATA, "A Density-Functional Theory for Polymer Liquids Based on Interaction Site Model," *J. Chem. Phys.* **118**, 2431 (2003).
K. NISHIYAMA, F. HIRATA and T. OKADA, "Solute-Structure Dependence of Solvation Dynamics Studied by Reference Interaction-Site Model Theory," *J. Chem. Phys.* **118**, 2279 (2003).
T. YAMAGUCHI, S-H. CHONG and F. HIRATA, "Dielectric Relaxation Spectrum of Water Studied by the Site-Site Generalized Langevin/modified Mode-Coupling Theory," *Mol. Phys.* **101**, 1211 (2003).
T. YAMAGUCHI, S. -H. CHONG and F. HIRATA, "Theoretical Study on the Molecular Motion of Liquid Water under High Pressure," *J. Chem. Phys.* **119**, 1021(2003).
H. SATO, Y. KOBORI, S. TERO-KUBOTA and F. HIRATA, "Theoretical Study on Electronic and Solvent Reorganization Processes Associated with a Charging Process of Organic Compounds: I. Molecular and Atomic Level Description of Solvent Reorganization," *J. Chem. Phys.* **119**, 2753 (2003).
I. OMELYAN, A. KOVALENKO and F. HIRATA, "Compressibility of Tert-Butyl Alcohol-Water Mixture: the RISM Theory," *J. Theor. Comput. Chem.* **2**, 193 (2003).
A. SETHIA, E. R. BITTNER and F. HIRATA, " Interplay between the Repulsive and Attractive Interaction and the Spacial Dimesionality of an Excess Electron in a Simple Fluid," *J. Theor. Comput. Chem.* **2**, 129 (2003).

M. MORI and K. YONEMITSU, "Charge Ordering Patterns and Their Excitation Spectra in Two-Dimensional Charge-Transfer Compounds," *Mol. Cryst. Liq. Cryst.* **380**, 209–213 (2002).
M. KUWABARA and K. YONEMITSU, "Strong Commensurability Effect on Metal-Insulator Transition in $(DCNQI)_2Cu$," *Mol. Cryst. Liq. Cryst.* **380**, 257–261 (2002).
K. YONEMITSU, "Variation of Excitation Spectra in Mixed-Stack Charge-Transfer Complexes," *Phase Transitions* **75**, 759–767 (2002).
N. MIYASHITA, M. KUWABARA and K. YONEMITSU, "Domain-Wall Dynamics after Photoexcitations near Neutral-Ionic Phase Transitions," *Phase Transitions* **75**, 887–893 (2002).
K. YONEMITSU, "Correlation-Induced Dimensional Crossovers of Charge-Transfer Excitations in Quasi-One-Dimensional Organic Conductors," *Synth. Met.* **133-134**, 7–9 (2003).
M. KUWABARA, K. YONEMITSU and H. OHTA, "Self-Doping Effect on the Mott Transition Accompanied With Three-Fold Charge Ordering in $(DCNQI)_2Cu$," *Synth. Met.* **133-134**, 295–297 (2003).
K. YONEMITSU, "Dynamic Spin Correlations near Neutral-Ionic Phase Transitions," *Physica B* **329-333**, 1219–1220 (2003).
K. YONEMITSU, N. MIYASHITA and M. KUWABARA, "Photoexcited States and Photoinduced Dynamics in Electronic Phases of MMX-Chain Systems," *Synth. Met.* **135-136**, 521–522 (2003).
N. MIYASHITA, M. KUWABARA and K. YONEMITSU, "Photoinduced Dynamics of Ionicity near the Neutral-Ionic Phase Boundary in a One-Dimensional Extended Peierls-Hubbard Model," *Synth. Met.* **135-136**, 645–646 (2003).
K. YONEMITSU and N. MIYASHITA, "Coherence Recovery and Photoinduced Phase Transitions in One-

Dimensional Halogen-Bridged Binuclear Platinum Complexes," *Phys. Rev. B* **68**, 075113 (9 pages) (2003).
Y. OTSUKA, Y. MORITA and Y. HATSUGAI, "Anisotropic Fermi Surface in the Two-Dimensional Hubbard Model," *Phys. Rev. B* **66**, 073109 (4 pages) (2002).
Y. OTSUKA, Y. MORITA and Y. HATSUGAI, "Correlation Effects on the Fermi Surface of the Two-Dimensional Hubbard Model," *J. Phys. Chem. Solids* **63**, 1389–1391 (2002).
Y. OTSUKA and Y. HATSUGAI, "Fermi Surface of the Periodic Anderson Model Detected by Momentum-Resolved Charge Compressibility," *Physica B* **329-333**, 580–581 (2003).

Department of Molecular Structure

E. HARADA, J. KUMAGAI, K. OZAWA, S. IMABAYASHI, A. S. TSAPIN, K. H. NEALSON, T. E. MEYER, M. A. CUSANOVICH and H. AKUTSU, "A Directional Electron Transfer Regulator Based on Heme-Chain Architecture in the Small Tetraheme Cytochrome *c* from *Shewanella oneidensis*," *FEBS Lett.* **532**, 333–337 (2002).
Y. KYOGOKU, Y. FUJIYOSHI, I. SHIMADA, H. NAKAMURA, T. TSUKIHARA, H. AKUTSU, T. ODAHARA, T. OKADA and N. NOMURA, "Structural Genomics of Membrane Proteins," *Acc. Chem. Res.* **36**, 199–206 (2003).
A. K. KHITRIN, T. FUJIWARA and H. AKUTSU, "Phase-Modulated Heteronuclear Decoupling in NMR of Solids," *J. Magn. Reson.* **162**, 46–53 (2003).
Y. MATSUKI, H. AKUTSU and T. FUJIWARA, "Band-Selective Recoupling of Homonuclear Double-Quantum Dipolar Interaction with a Generalized Composite 0degrees Pulse: Application to ^{13}C Aliphatic Region-Selective Magnetization Transfer in Solids," *J. Magn. Reson.* **162**, 54–66 (2003).
A. Y. NOSAKA, T. FUJIWARA, H. YAGI, H. AKUTSU and Y. NOSAKA, "Photocatalytic Reaction Sites at the TiO_2 Surface as Studied by Solid-State ^1H-NMR Spectroscopy," *Langmuir* **19**, 1935–1937 (2003).

T. NAKAMURA, R. KIMURA, H. SAKAI, M. ABE, H. KONDOH, T. OHTA and M. MATSUMOTO, "Nano-Dot Formation Using Self-Assembled 3-Mercaptopropionic Acid Thin Films Prepared by Facile Atmospheric-Vapor-Adsorption Method on Al(111)," *Appl. Surf. Sci.* **202**, 241–251 (2002).
K. TONO, A. TERASAKI, T. OHTA and T. KONDOW, "Electronic and Geometric Structures of $Co_2C_n^-$ and $V_2C_n^-$: Initial Growth Mechanisms of Late and Early 3*d* Transition Metal Carbide Clusters," *J. Chem. Phys.* **117**, 7010–7016 (2002).
Y. OGI, T. ENDO, K. TSUKIYAMA, H. KONDOH, K. TONO, Y. OGAWA, Y. HAMADA, T. OHTA and H. KURODA, "Detection of Vibrationally Hot NO and CO Excited by Infrared Free Electron Laser," *Jpn. J. Appl. Phys.* **41**, 108–112 (2002).
Y. HAMADA, H. KONDOH, Y. OGAWA, K. TONO, T. OHTA, Y. OGI, T. ENDO, K. TSUKIYAMA and H. KURODA, "Infrared Multiphoton-Absorption-Induced Iron Desorption from Solid State C_{60} Fullerene and Anthracene," *Jpn. J. Appl. Phys.* **41**, 113–117 (2002).
T. YOKOYAMA, H. TOKORO, S. OHKOSHI, K. HASHIMOTO, K. OKAMOTO and T.OHTA, "Photoinduced Phase Transition of $RbMnFe(CN)_6$ Studied by X-Ray Absorption Fine Structure Spectroscopy," *Phys. Rev. B* **66**, 184111 (10 pages) (2002).
Y. OGI, T. ENDO, K. TSUKIYAMA, H. KONDOH, K. TONO, Y. OGAWA, Y. HAMADA, T. OHTA and H. KURODA, "Vibrational Excitation of CO Molecules by Infrared Free Electron Laser," *J. Electron Spectrosc.* **128**, 167–173 (2003).
T. YOKOYAMA, D. MATSUMURA, K. AMEMIYA, S. KITAGAWA, N. SUZUKI and T. OHTA, "Spin Reorientation Transitions of Ultrathin Co/Pd(111) Films Induced by Chemisorption: X-Ray Magnetic Circular Dichroism Study," *J. Phys.: Condens. Matter* **15**, S537–S546 (2003).
K. AMEMIYA, S. KITAGAWA, D. MATSUMURA, T. YOKOYAMA and T. OHTA, "Development of a Depth-Resolved X-Ray Magnetic Circular Dichroism: Application to Fe/Cu(100) Ultrathin Films," *J. Phys.: Condens. Matter* **15**, S561–S571 (2003).
H. KONDOH, M. IWASAKI, T. SHIMADA, K. AMEMIYA, T. YOKOYAMA, T. OHTA, M. SHIMOMURA and S. KONO, "Adsorption of Thiolate to Singly Coordinated Sites on Au(111) Evidenced by Photoelectron Diffraction," *Phys. Rev. Lett.* **90**, 66102 (4 pages) (2003).
A. NAMBU, H. KONDOH, I. NAKAI, K. AMEMIYA and T. OHTA, "Film Growth and X-Ray Induced Chemical Reactions of Thiophene Adsorbed on Au(111)," *Surf. Sci.* **530**, 101–110 (2003).
K. TONO, A. TERASAKI, T. OHTA and T. KONDOW, "Chemical Control of Magnetism: Oxidation Induced Ferromagnetism in the Chromium Dimer Evidenced by Photoelectron Spectroscopy," *Phys. Rev. Lett.* **90**, 133402 (4 pages) (2003).
K. OKAMOTO, K. KOHDATE, K. NAGAI, J. MIYAWAKI, H. KONDOH, T. YOKOYAMA, A. NOJIMA and T. OHTA, "Development of Light-Modulated XAFS Spectroscopy," *J. Synchrotron Radiat.* **10**, 242–247 (2003).
K. OKAMOTO, K. NAGAI, J. MIYAWAKI, H. KONDOH and T. OHTA, "XAFS Study on the Photoinduced Spin Transition of $[Fe(2\text{-pic})_3]Cl_2 \cdot C_2H_5OH$," *Chem. Phys. Lett.* **371**, 707–712 (2003).
M. NAGASAKA, I. NAKAI, H. KONDOH, T. OHTA and V. CARAVETTA, "Oxygen *K*-Shell Near Edge X-

Ray Absorption Fine Structure Study of O and OH Overlayers on Pt(111)," *Chem. Phys. Lett.* **375**, 419–424 (2003).

R. MIZOGUCHI, K. ONDA, S. S. KANO and A. WADA, "Thinning-Out in Optimized Pulse Shaping Method Using Genetic Algorithm," *Rev. Sci. Instrum.* **74**, 2670–2674 (2003).
K. ONDA, Y. IWASAWA and A. WADA, "Vibrational Relaxation of Adsorbate and Adsorbent in the CO-Adsorbed DM-20 Zeolite System," *Chem. Phys. Lett.* **370**, 437–442 (2003).
H. ISHIDA, R. MIZOGUCHI, K. ONDA, C, HIROSE, S. S. KANO and A. WADA, "Second Harmonic Observation of Cu(111) Surface: *In Situ* Measurements during Molecular Adsorption," *Surf. Sci.* **526**, 201–207 (2003).
H. NOGUCHI, T. OKADA, K. ONDA, S. S. KANO, A. WADA and K. DOMEN, "Time-Resolved SFG Study of Formate on Ni(111) Surface under Irradiation of Picosecond Laser Pulses," *Surf. Sci.* **528**, 183–188 (2003).
J. KUBOTA, A. WADA, K. DOMEN and S. S. KANO, "Transient Responses of SFG Spectra of D_2 Ice/CO/Pt(111) Interface with Irradiation of Ultra-Short NIR Pump Pulses," *Chem. Phys. Lett.* **362**, 476–482 (2002).

T. YOKOYAMA, H. TOKORO, S. OHKOSHI, K. HASHIMOTO, K. OKAMOTO and T. OHTA, "Photoinduced Phase Transition of $RbMnFe(CN)_6$ Studied by X-Ray-Absorption Fine Structure Spectroscopy," *Phys. Rev. B* **66**, 184111 (10 pages) (2002).
T. YOKOYAMA, D. MATSUMURA, K. AMEMIYA, S. KITAGAWA, N. SUZUKI and T. OHTA, "Spin Reorientation Transitions of Ultrathin Co/Pd(111) Films Induced by Chemisorption: X-Ray Magnetic Circular Dichroism Study," *J. Phys.: Condens. Matter* **15**, S537–S546 (2003).
K. AMEMIYA, S. KITAGAWA, D. MATSUMURA, T. YOKOYAMA and T. OHTA, "Development of a Depth-Resolved X-Ray Magnetic Circular Dichroism: Application to Fe/Cu(100) Ultrathin Films," *J. Phys.: Condens. Matter* **15**, S561–S572 (2003).
H. KONDOH, M. IWASAKI, T. SHIMADA, K. AMEMIYA, T. YOKOYAMA and T. OHTA, "Adsorption of Thiolates to Strongly Coordinated Sites on Au(111) Evidenced by Photoelectron Diffraction," *Phys. Rev. Lett.* **90**, 066102 (4 pages) (2003).
K. OKAMOTO, K. KOHDATE, K. NAGAI, J. MIYAWAKI, H. KONDOH, T. YOKOYAMA, A. NOJIMA and T. OHTA, "Development of Light-Modulated XAFS Spectroscopy," *J. Synchrotron Radiat.* **10**, 242–247 (2003).
T. YOKOYAMA, K. TAKAHASHI and O. SATO, "Metastable Photoinduced Phase of Cu(II) Ethylenediamine Complexes Studied by X-Ray-Absorption Fine-Structure Spectroscopy," *Phys. Rev. B* **67**, 172104 (4 pages) (2003).

K. TANAKA, A. TENGEIJI, T. KATO, N. TOYAMA, M. SHIRO and M. SHIONOYA, "Efficient Incorporation of a Copper Hydroxypyridone Base Pair in DNA," *J. Am. Chem. Soc.* **124**, 12494–12498 (2002).
N. HAYASHI, T. KATO, T. AOKI, T. ANDO and A. FUKUDA, "Orientational Distributions in Smectic Liquid Crystals Showing V-Shaped Switching Investigated by Polarized Raman Scattering," *Phys. Rev. E* **65**, 041714 (2002).
N. HAYASHI, T. KATO, T. ANDO and A. FUKUDA, "Molecular Ordering Deformation Induced by Externally Applied Electronic Field in an Antiferroelectric Liquid Crystal," *Jpn. J. Appl. Phys.* **41**, 5292–5297 (2002).
T. WAKAHARA, S. OKUBO, M. KONDOU, Y. MAEDA, T. AKASAKA, M. WAELCHLI, M. KAKO, K. KOBAYASHI, S. NAGASE, T. KATO, K. YAMAMOTO, X. GAO, E. VAN CAEMELBECKE and K. M. KADISH, "Ionization and Structural Determination of the Major Isomer of $Pr@C_{82}$," *Chem. Phys. Lett.* **360**, 235–239 (2002).
M. KAMO, A. TSUDA, Y. NAKAMURA, N. ARATANI, K. FURUKAWA, T. KATO and A. OSUKA, "Metal-Dependent Regioselective Oxidative Coupling of 5,10,15-Triarylporphyrins with DDQ-$Sc(OTf)_3$ and Formation of an Oxo-Quinoidal Pophyrin," *Org. Lett.* **5**, 2079–2082 (2003).
K. KOBAYASHI, H. OHTSU, T. WADA, T. KATO and K. TANAKA, "Characterization of a Stable Ruthenium Complex with an Oxyl Radical," *J. Am. Chem. Soc.* **125**, 6729–6739 (2003).
K. TANAKA, A. TENGEIJI, T. KATO, N. TOYAMA and M. SHIONOYA, "A Discrete Self-Assembled Metal Array in Artificial DNA," *Science* **299**, 1212–1213 (2003).
M. HIRAOKA, H. SAKAMOTO, K. MIZOGUCHI, T. KATO and R. KATO, "Charge Transport in the Insulating State of $(DMe\text{-}DCNQI)_2Li$ above T_{SP}: A Possible Fractional Charge Soliton Conduction with $\pm 1/2e$," *Phys. Rev. Lett.* **91**, 056604 (2003).
N. HAYASHI, T. KATO, T. ANDO and A. FUKUDA, "Intrinsic Aspect of V-Shaped Switching in Ferroelectric Liquid Crystals: Biaxial Anchoring Arising from Peculiar Short Axis Biasing in the Molecular Rotation around the Long Axis," *Phys. Rev. E* **68**, 011702 (2003).
S. OKUBO and T. KATO, "ESR Parameters of Series of $La@C_n$ Isomers," *Appl. Magn. Reson.* **23**, 481–493 (2003).
T. IKOMA, S. OKADA, S. TERO-KUBOTA, H. NAKANISHI, T. KATO, P. HOEFER, A. KAMLOWSKI and K. AKIYAMA, "Angle-Selective Measurements of Spin Soliton in Ladder Polydiacetylene by Pulsed 94GHz EPR," *Appl. Magn. Reson.* **23**, 445–453 (2003).

Department of Electronic Structure

Y. INOKUCHI, K. OHASHI, H. SEKIYA and N. NISHI, "Positive Charge Distribution in $(benzene)_1(toluene)_2^+$ and $(benzene)_2(toluene)_1^+$ Studied by Photodissociation Spectroscopy," *J. Chem. Phys.* **117**, 10648 (2002).
N. NISHI, K. KOSUGI, K. HINO, T. YOKOYAMA and E. OKUNISHI, "Formation and Magnetic Characteristics of Cobalt-Carbon Nanocluster Magnets Embedded in Amorphous Carbon Matrices," *Chem. Phys. Lett.* **369**, 198 (2003).
T. MICHI, K. OHASHI, Y. INOKUCHI, N. NISHI and H. SEKIYA, "Infrared Spectra and Structures of $(CH_3NH_2)_nH^+(n = 1–4)$," *Chem. Phys. Lett.* **371**, 111 (2003).
Y. INOKUCHI, K. OHASHI, Y. HONKAWA, H. SEKIYA and N. NISHI, "Fermi Resonance Interaction in Hetero-Dimer and Trimer Ions Containing Aniline," *Chem. Phys. Lett.* **373**, 568 (2003).
Y. INOKUCHI, K. OHASHI, Y. HONKAWA, H. SEKIYA and N. NISHI, "Infrared Photodissociation Spectroscopy of $[Aniline\text{-}(Water)_n]^+$ (n = 1–8): Structural Change from Branched and Cyclic to Proton-Transferred Forms," *J. Phys. Chem.* **107**, 4230 (2003).
T. TAKAMUKU, D. MATSUO, M. TABATA, T. YAMAGUCHI and N. NISHI, "Structure of Aqueous Mixtures of N,N-Dimethylacetamide Studied by Infrared Spectroscopy, X-Ray Diffraction, and Mass Spectrometry," *J. Phys. Chem. A* **107**, 6070 (2003).
Y. HONKAWA, Y. INOKUCHI, K. OHASHI, N. NISHI and H. SEKIYA, "Infrared Spectra and Structures of $aniline^+$–furan and $aniline^+$–phenol. Preference between *p*-Type and *s*-Type Hydrogen-Bonded Strucutures," *Chem. Phys. Lett.* **376**, 244–250 (2003).
N. NISHI, K. KOSUGI, K. HINO and T. YOKOYAMA, "Matrix Embedded Cobalt-Carbon Nano-Cluster Magnets: Behavior as Room Temperature Single Domain Magnets," *Eur. J. Phys. D* **24**, 97 (2003).

M. SAKAI, S. ISHIUCHI and M. FUJII, "Picosecond Time-Resolved Nonresonant Ionization Detected IR Spectroscopy on 7-Azaindole Dimer," *Eur. J. Phys. D* **20**, 399–402 (2002).
S. ISHIUCHI, K. DAIGOKU, M. SAEKI, M. SAKAI, K. HASHIMOTO and M. FUJII, "Hydrogen Transfer in Photo-Excited Phenol/ammonia Clusters by UV-IR-UV Ion Dip Spectroscopy and Ab Initio MO Calculations I: Electronic Transitions," *J. Chem. Phys.* **117**, 7077–7082 (2002).
S. ISHIUCHI, K. DAIGOKU, M. SAEKI, M. SAKAI, K. HASHIMOTO and M. FUJII, "Hydrogen Transfer in Photo-Excited Phenol/ammonia Clusters by UV-IR-UV Ion Dip Spectroscopy and Ab Initio MO Calculations II: Vibrational Transitions," *J. Chem. Phys.* **117**, 7083–7093 (2002).
M. SAKAI, T. UEDA, T. YAMANAKA and M. FUJII, "Construction of a Picosecond Time-Resolved IR Dip Spectrometer for Hydrogen-Bond Clusters," *Bull. Chem. Soc. Jpn.* **76**, 509–514 (2003).
T. WATANABE, Y. IKETAKI, T. OMATSU, K. YAMAMOTO, S. ISHIUCHI, M. SAKAI and M. FUJII, "Two-Color Far-Field Super-Resolution Microscope Using a Doughnut Beam," *Chem. Phys. Lett.* **371**, 634–639 (2003).
Y. IKETAKI, T. WATANABE, S. ISHIUCHI, M. SAKAI, T. OMATSU, K. YAMAMOTO, M. FUJII and T. WATANABE, "Investigation of the Fluorescence Depletion Process in Condensed Phase," *Chem. Phys. Lett.* **372**, 773–778 (2003).

K. MISAWA, I. MATSUDA and R. LANG, "Femtosecond Wave Packet Engineering in a Cyanine Dye Molecule," *Proc. SPIE Int. Soc. Opt. Eng.* **4798**, 11–20 (2002).
N. T. HASHIMOTO, K. MISAWA and R. LANG, "Three-Level Picture for Chirp-Dependent Fluorescence Yields under Femtosecond Optical Pulse Irradiation," *Appl. Phys. Lett.* **82**, 2749–2751 (2003).

Department of Molecular Assemblies

O. DROZDOVA, K. YAKUSHI, Y. MISAKI and K. TANAKA, "Optical Study of Two-Dimensional Organic Metal $(EO\text{-}TTP)_2AsF_6$ (EO-TTP = 2-(4,5-ethylenedioxy-1,3- dithiol-2-ylidene)-5-(1,3-dithiol-2-ylidene)-1,3,4,6-tetrathiapentalene)," *J. Solid State Chem.* **168**, 497–502 (2002).
M. MENEGHETTI, C. PECILE, K. YAKUSHI, K. YAMAMOTO, K. KANODA and K. HIRAKI, "Study of the Phase Transitions of $(DI\text{-}DCNQI)_2M$ (M = Ag, Li, Cu) through the Analysis of the Temperature Dependent Vibronic and Vibrational Infrared Absorptions," *J. Solid State Chem.* **168**, 632–638 (2002).
K. YAKUSHI, K. YAMAMOTO, M. SIMONYAN, J. OUYANG, C. NAKANO, Y. MISAKI and K. TANAKA, "Charge-Ordering and Magnetic Phase Transitions in $\theta\text{-}(BDT\text{-}TTP)_2Cu(NCS)_2$," *Phys. Rev. B* **66**, 235102 (5 pages) (2002).
P. TOMAN, S. NESPUREK and K. YAKUSHI, "Electronic States and Infrared Spectroscopy of Nickel and Cobalt Phthalocyanines: *Ab Initio* Calculations for the Neutral and Cation State," *J. Porphyrin Phthalocyanines* **6**, 556–562 (2002).
O. DROZDOVA, K. YAKUSHI, H. YAMOCHI, G. SAITO and D. B. TANNER, "Infrared Study of the Properties of the Normal (metallic) Phase of $\kappa\text{-}(ET\text{-}^{13}C_4)_2\ Cu(CN)[N(CN)_2]$," *Synth. Met.* **133-134**, 119–121 (2003).
T. MIZUTANI, M. TOKUMOTO, T. KINOSHITA, J. S. BROOKS, Y. UWATOKO, O. DROZDOVA, K. YAKUSHI, I. TAMURA, H. KOBAYASHI, T. MANGETSU, J. YAMADA and K. ISHIDA, "Effect of

Uniaxial Strain in Organic Superconductor κ-(BEDT-TTF)$_2$Cu(NCS)$_2$," *Synth. Met.* **133-134**, 229–231 (2003).
K. YAMAMOTO, K. YAKUSHI, K. MIYAGAWA, K. KANODA, A. KAWAMOTO, J. YAMAURA and T. ENOKI, "Vibrational Spectra of BEDT-TTF Based 2D Charge Ordering Systems," *Synth. Met.* **133-134**, 269–272 (2003).
O. DROZDOVA, K. YAKUSHI, A. OTA, H. YAMOCHI and G. SAITO, "Spectroscopic Study of the [0110] Charge Ordering in (EDO-TTF)$_2$PF$_6$," *Synth. Met.* **133-134**, 277–279 (2003).
K. YAKUSHI, K. YAMOMOTO, J. OUYANG, M. SIMONYAN, C. NAKANO, Y. MISAKI and K. TANAKA, "Charge Ordering and Phase Transition in θ-(BDT-TTP)$_2$Cu(NCS)$_2$," *Synth. Met.* **133-134**, 287–289 (2003).
T. YAMAMOTO, H. TAJIMA, R. KATO, M. URUICHI and K. YAKUSHI, "Thermoelectric Power and Raman Spectra of (Me$_2$DCNQI)$_2$Cu$_x$Li$_{1-x}$," *Synth. Met.* **133-134**, 291–292 (2003).
M. URUICHI, K. YAKUSHI, T. SHIRAHATA, K. TAKAHASHI, T. MORI and T. NAKAMURA, "Characterization of Quasi-1D Conductors, (BDTFP)$_2$X(PhCl)$_{0.5}$ (X = PF$_6$, AsF$_6$)," *Synth. Met.* **133-134**, 407–409 (2003).
K. TAKEDA, I. SHIROTANI and K. YAKUSHI, "Insulator to Metal Transition and Electronic Spectra of Bis(1,2-benzoquinonedioximato)-Platinum(II), Pt(bqd)$_2$ at High Pressure," *Synth. Met.* **133-134**, 415–416 (2003).
K. SUZUKI, K. YAMAMOTO and K. YAKUSHI, "Charge Ordering in θ-(BEDT-TTF)$_2$ TlM(SCN)$_4$ (M = Co and Zn) Studied by Vibrational Spectroscopy," *Synth. Met.* **135-136**, 525–526 (2003).
K. YAMAMOTO, K. YAKUSHI, K. HIRAKI, T. TAKAHASHI, K. KANODA, M. MENEGHETTI and C. PECILE, "Charge Distribution and Molecular Arrangement in (DI-DCNQI)$_2$Ag Studied by High-Pressure Vibrational Spectroscopy," *Synth. Met.* **135-136**, 563–564 (2003).
K. YAKUSHI, R. SWIETLIK, K. YAMAMOTO, T. KAWAMOTO, T. MORI, Y. MISAKI and K. TANAKA, "Charge Disproportionation in the Charge-Transfer Salts of TTP," *Synth. Met.* **135-136**, 583–585 (2003).
R. WOJCIECHOWSKI, K. YAMAMOTO, K. YAKUSHI and A. KAWAMOTO, "Raman Study of Charge Disproportionation in α-(BEDT-TTF)$_2$I$_3$," *Synth. Met.* **135-136**, 587–588 (2003).
R. WOJCIECHOWSKI, K. YAMAMOTO, K. YAKUSHI, M. INOKUCHI and A. KAWAMOTO, "High-Pressure Raman Study of the Charge Ordering in α-(BEDT-TTF)$_2$I$_3$," *Phys. Rev. B* **67**, 224105 (11 pages) (2003).
R. SWIETLIK, A. LAPINSKI, L. OUAHAB and K. YAKUSHI, "Charge Ordering in the κ-Phase BEDT-TTF Salts with Co(CN)$_6$ and Fe(CN)$_6$ Anions Studied by Infrared and Raman Spectroscopy," *C. R. Acad. Sci. (Paris) Chimie* **3/6**, 395–403 (2003).

T. NAKAMURA, "Low-Temperature Electronic Phases of EDT-TTF Based Molecular Conductors," *Mol. Cryst. Liq. Cryst.* **380**, 233–237 (2002).
T. NAKAMURA, M. TANIGUCHI, Y. MISAKI, K. TANAKA and Y. NOGAMI, "Microscopic Investigation of a New Two-Component Organic Conductor with Itinerant and Localized Spins: (CHTM-TTP)$_2$TCNQ," *J. Phys. Soc. Jpn.* **71**, 2208–2215 (2002).
T. NAKAMURA, T. TAKAHASHI, S. AONUMA and R. KATO, "*g*-Tensor Analyses of β'-Type Pd(dmit)$_2$ Metal Complexes," *Mol. Cryst. Liq. Cryst.* **379**, 53–58 (2002).
T. SAKURAI, Y. INAGAKI, S. OKUBO, H. OHTA, R. KATO and T. NAKAMURA, "Frequency Dependence Millimeter Wave ESR Measurements of Et$_2$Me$_2$P[Pd(dmit)$_2$]$_2$," *Mol. Cryst. Liq. Cryst.* **379**, 59–64 (2002).
M. URUICHI, K. YAKUSHI, T. SHIRAHATA, K. TAKAHASHI, T. MORI and T. NAKAMURA, "Structural Phase Transition in Quasi-One-Dimensional Conductors (BDTFP)$_2$*X*(PhCl)$_{0.5}$ (*X* = PF$_6$ and AsF$_6$) [BDTFP = 5,7-bis(1,3-dithiol-2-ylidene)-5,7-dihydrofuro [3,4-b] pyrazine; PhCl= chlorbenzene]," *J. Mater. Chem.* **12**, 2696–2700 (2002).
Y. NOGAMI and T. NAKAMURA, "X-Ray Observation of 2k_F and 4k_F Charge Orderings in (TMTTF)$_2$ReO$_4$ and (TMTTF)$_2$SCN Associated with Anion Orderings," *J. Phys. IV France* **12** (PR9), 145–148 (2002).
S. NISHIHARA, T. AKUTAGAWA, T. HASEGAWA S. FUJIYAMA, T. NAKAMURA and T. NAKAMURA, "Two Polymorphs of (Anilinium)(18-crown-6)[Ni(dmit)$_2$]: Structure and Magnetic Properties," *J. Solid State Chem.* **168**, 661–667 (2002).
T. NAKAMURA, "Possible Charge Ordering Patterns of the Paramagnetic Insulating States in (TMTTF)$_2$*X*," *J. Phys. Soc. Jpn.* **72**, 213–216 (2003).
A. ISHIKAWA, N. MATSUNAGA, K. NOMURA, T. NAKAMURA, T. TAKAHASHI and G. SAITO, "Magnetic Field Dependence of Incommensurate SDW Transition in (TMTTF)$_2$Br," *Synth. Met.* **133-134**, 65–66 (2003).
S. FUJIYAMA and T. NAKAMURA, "NMR Investigation of (TMTTF)$_2$*X*: Charge Configurations and Spin Dynamics," *Synth. Met.* **133-134**, 67–68 (2003).
R. CHIBA, K. HIRAKI, T. TAKAHASHI, H.M. YAMAMOTO and T. NAKAMURA, "Charge Ordering in θ-(BEDT-TTF)$_2$*M*Zn(SCN)$_4$ [*M* = Rb, Cs]," *Synth. Met.* **133-134**, 305–306 (2003).
Y. KUBO, Y. TAKANO, K. HIRAKI, T. TAKAHASHI, H.M. YAMAMOTO and T. NAKAMURA, "The Electronic State of α-(BEDT-TTF)$_2$I$_3$ under Hydrostatic Pressure," *Synth. Met.* **133-134**, 307–308 (2003).
M. URUICHHI K. YAKUSHI, T. SHIRAHATA, K. TAKAHASHI and T. NAKAMURA, "Characterization of Quasi-1D Conductors, (BDTFP)$_2$*X*(PhCl)$_{0.5}$ (*X* = PF$_6$, AsF$_6$)," *Synth. Met.* **133-134**, 407–409 (2003).
T. SAKURAI, H. OHTA, S. OKUBO, R. KATO and T. NAKAMURA, "Temperature Dependence Millimeter

Wave ESR Measurements of $Et_2Me_2P[Pd(dmit)_2]_2$," *Synth. Met.* **133-134**, 421–422 (2003).
T. NAKAMURA, M. TANIGUCHI, Y. MISAKI, K. TANAKA and Y. NOGAMI, "Magnetic Investigation of Itinerant and Local Hybrid Spins System, $(CHTM\text{-}TTP)_2TCNQ$," *Synth. Met.* **133-134**, 441–442 (2003).
Y. KUBO, Y. TAKANO, K. HIRAKI, T. TAKAHASHI, H.M. YAMAMOTO and T. NAKAMURA, "^{13}C-NMR Studies of the 'Narrow Gap Semiconducting' State of α-$(BEDT\text{-}TTF)_2I_3$ under Pressure," *Synth. Met.* **135-136**, 591–592 (2003).
R. CHIBA, K. HIRAKI, T. TAKAHASHI, H.M. YAMAMOTO and T. NAKAMURA, "Pressure Effect on the Charge Ordering in θ-$(BEDT\text{-}TTF)_2MZn(SCN)_4$ (M = Rb, Cs)," *Synth. Met.* **135-136**, 595–596 (2003).
T. IMAKUBO, N. TAJIMA, T. SHIRAHATA, A. MIYAKE, H. SAWA, T. NAKAMURA, H. OHNUKI, M. TAMURA, R. KATO, M. IZUMI, Y. NISHIO and K. KAJITA, "Crystal Design of Organic Conductors Using the Iodine Bond," *Synth. Met.* **135-136**, 601–602 (2003).
T. NAKAMURA, "ESR Investigation of Charge Localized States in $(TMTTF)_2X$," *Synth. Met.* **135-136**, 1181–1182 (2003).
S. NISHIHARA, T. AKUTAGAWA, T. HASEGAWA, T. NAKAMURA, S. FUJIYAMA and T. NAKAMURA, "Magnetic and ^{1}H-NMR of $[Ph(NH_3)](18\text{-crown-}6)[Ni(dmit)_2]$ Having Molecular Spin Ladder Structure," *Synth. Met.* **135-136**, 1279–1280 (2003).
T. NAKAMURA, "ESR Study of the Charge Ordering in $(TMTTF)_2X$," *Physica B* **329-333**, 1148–1149 (2003).
A. ISHIKAWA, N. MATSUNAGA, K. NOMURA, T. SASAKI, T. NAKAMURA, T. TAKAHASHI and G. SAITO, "Electron Correlation and Two Dimensionality in the Spin-Density-Wave Phase of $(TMTTF)_2Br$ under Pressure," *Phys. Rev. B* **67**, 212404 (4pages) (2003).

E. FUJIWARA, H. FUJIWARA, H. KOBAYASHI, T. OTSDUKA and A. KOBAYASHI, "A Series of Organic Conductors κ-$(BETS)_2FeBr_xCl_{4-x}$ ($0 < x < 4$) Exhibiting Successive Antiferropmagnetic and Superconducting Transitions [BETS = Bis(ethylenedithio)tetraselenafulvalene]," *Adv. Mater.* **14**, 1376–1379 (2002).
V.GRITSENKO, E. FUJIWARA, H. FUJIWARA and H. KOBAYASHI, "Stable Molecular Metals Based on Bis(ethylenedithio)tetraselenafulvalene and Halogen Ions: κ-$(BETS)_2X\cdot C_2H_4(OH)_2$ (X = Br, Cl)," *Synth. Met.* **128**, 273–278 (2002).
E. FUJIWARA, H. FUJIWARA and H. KOBAYASHI, "Novel π-Electron Donor for Magnetic Conductors Containing a PROXYL Radical," *Chem. Lett.* 1048–1049 (2002).
M. A. TANATAR, T. ISHIGURO, H. TANAKA and H. KOBAYASHI, "Magnetic Field-Temperature Phase Diagram of the Quasi-Two-Dimensional Organic Superconductor, λ-$(BETS)_2GaCl_4$ Studied *via* Thermal Conductivity," *Phys. Rev. B* **66**, 134503 (8 pages) (2002).
A. BHATTACHARJEE, Y. NAKAZAWA, H. KOBAYASHI and M. SORAI, "AC Magnetic Susceptibility of the Assembled-Metal Complex, $\{NBu_4[Fe^{II}Fe^{III}(ox)^3]\}_\infty$ (Bu = n-C_4H_9, ox = oxalato)," *J. Phys. Soc. Jpn.* **71**, 2263–2267 (2002).
H. KOBAYASHI, E. FUJIWARA, F. FUJIWARA, H. TANAKA, H. AKUTSU, I. TAMURA, T. OTSUKA, A. KOBAYASHI, M. TOKUMOTO and P. CASSOUX, "Development and Physical Properties of Magnetic Organic Superconductors Based on BETS Molecules [BETS = bis(ethylenedithio)tetraselenafulvalene]," *J. Phys. Chem. Solids* **63**, 1235–1238 (2002).
I. TAMURA, H. KOBAYASHI and A. KOBAYASHI, "X-Ray Diffraction Study of α-$(BEDT\text{-}TTF)_2I_3$ Single Crystal under High Pressure," *J. Phys. Chem. Solids* **63**, 1255–1257 (2002).
H. KOBAYASHI, E. FUJIWARA, H. FUJIWARA, H. TANAKA, I. TAMURA, B. ZHANG, V. GRITSENKO, T. OTSUKA, A. KOBAYASHI, M. TOKUMOTO and P. CASSOUX, "Magnetic Organic Superconductors—Interplay of Conductivity and Magnetism," *Mol. Cryst. Liq. Cryst.* **379**, 9–18 (2002).
A. KOBAYASHI, W. SUZUKI, E. FUJIWARA, T. OTSUKA, H. TANAKA, Y. OKANO and H. KOBAYASHI, "Molecular Design and Development of Single-Component Molecular Metals with Extended TTF Ligands," *Mol. Cryst. Liq. Cryst.* **379**, 19–28 (2002).
A. KOBAYASHI, W. SUZUKI, H. TANAKA, Y. OKANO and H. KOBAYASHI, "Molecular Metals and Superconductors Based on Transition Metal Complexes with dmit or Extended-TTF Ligands," *Mol. Cryst. Liq. Cryst.* **380**, 37–43 (2002).
H. KOBAYASHI, E. FUJIWARA, H. FUJIWARA, H. TANAKA T. OTSUKA, A. KOBAYASHI, M. TOKUMOTO and P. CASSOUX, "Antiferromagnetic Organic Superconductors, $BETS_2FeX_4$ (X = Br, Cl)," *Mol. Cryst. Liq. Cryst.* **380**,139–144 (2002).
E. OJIMA, H. FUJIWARA, H. KOBAYASHI, M. TOKUMOTO and A. KOBAYASHI, "New Organic Conductors Based on Tellurium-Containing Donor Molecules," *Mol. Cryst. Liq. Cryst.* **380**,175–181 (2002).
M. TOKUMOTO, T. MIZUTANI T. KINOSHITA, J. S. BROOKS, Y. UWATOKO, O. DROZDOVA, K. YAKUSHI, I. TAMURA H. KOBAYASHI, T. MANGETSU, J. YAMADA and K. ISHIDA, "Effect of Uniaxial Pressure in Organic Superconductor κ-$(BEDT\text{-}TTF)_2Cu(NCS)_2$," *Mol. Cryst. Liq. Cryst.* **380**, 227–232 (2002).
H, FUJIWARA, E, FUIWARA and H. KOBAYASHI, "Synthesis, Structures and Physical Properties of the Cation Radical Salts Based on Tempo Radical Containing Electron Donors," *Mol. Cryst. Liq. Cryst.* **380**, 269–275 (2002).
W. SUZUKI, E. FUJIWARA, A. KOBAYASHI, Y. FUJISHIRO, E. NISHIBORI, M. TAKATA, M. SAKATA, H. FUJIWARA and H. KOBAYASHI, "Highly Conducting Crystals Based on Single-Component

Gold Complexes with Extended-TTF Dithiolate Ligands," *J. Am. Chem. Soc.* **125**, 1486–1487 (2003).
S. UJI, T. TERASHIMA, C. TERAKURA, T. YAKABE, Y. TERAI, S. YASUZUKA Y. IMANAKA, M. TOKUMOTO, A. KOBAYASHI, F. SAKAI, H. TANAKA, H. KOBAYASHI, L. BALICAS and J. BROOKS, "Global Phase Diagram of the Magnetic Field-Induced Organic Superconductors λ-$(BETS)_2Fe_xGa_{1-x}Cl_4$," *J. Phys. Soc. Jpn.* **72**, 369–373 (2003).
H. FUJIWARA, H. -J. LEE, H. KOBAYASHI, E FUJIWARA and A. KOBAYASHI, "A Novel TTP Donor Containing a PROXYL Radical for Magnetic Molecular Conductors," *Chem. Lett.* **32**, 482–483 (2003).
H. CUI, T, OTSUKA, E. FUJIWARA, A. KOBAYASHI, Y. MISAKI, and H. KOBAYASHI, "Syntheses and Physical Properties of New Organic Conductors with Lanthanoid Chloride Complex Anions," *Synth. Met.* **135-136**, 641–642 (2003).
E. FUJIWARA, A. KOBAYASHI and H. KOBAYASHI, "Structures and Physical Properties of Nickel Complexes with TTF-Type Ligands," *Synth. Met.* **135-136**, 535–536 (2003).
A. KOBAYASHI, W. SUZUKI, E. FUJIWARA, H. TANAKA, Y. OKANO and H. KOBAYAHSI, "Molecular Design and Development of Single-Component Molecular Metal," *Synth. Met.* **133-134**, 393–395 (2003).
T. MIZUTANI, M. TOKUMOTO, T. KINOSHITA, J. S. BROOKS, Y. UWATOKO, O. DROZDOVA, K. YAKUSHI, I. TAMURA, H. KOBAYASHI, T. MANGETSU, J. YAMADA and K. ISHIDA, "Effect of Uniaxial Strain in Organic Superconductor κ-$(BEDT\text{-}TTF)_2Cu(NCS)_2$," *Synth. Met.* **133-134**, 229–231 (2003).
S. UJI, C. TERAKURA, T. TERASHIMA, T. YAKABE, Y. IMANAKA, T. TERAI, S. YASUZUKA, M. TOKUMOTO, F. SAKAI, A. KOBAYASHI, H. TANAKA, H. KOBAYASHI, L. BALICAS and J. S. BROOKS, "Novel Electronic Properties under Magnetic Fields in Organic Conductors λ-$(BETS)_2Fe_xGa_{1-x}Cl_4$," *Synth. Met.* **133-134**, 481–483 (2003).
S. UJI, C. TERAKURA T. TERASHIMA, T. YAKABE, Y. IMANAKA, T. TERAI, S. YASUZUKA, M. TOKUMOTO, F. SAKAI, A. KOBAYASHI, H. TANAKA, H. KOBAYASHI, L. BALICAS and J. S. BROOKS, "Superconductivity in Organic Alloys λ-$(BETS)_2Fe_xGa_{1-x}Cl_4$," *Synth. Met.* **137**, 1183–1185 (2003).
H. KOBAYASHI, B. ZHANAG, H. TANAKA, H. FUJIWARA, T. OTSUKA, E. FUJIWARA and A. KOBAYASHI, "Interplay of Magnetism and Superconductivity in BETS Conductors (BETS = bis(ethylenedithio)-tetraselenafulvalene)," *Synth. Met.* **137**, 1157–1162 (2003).
H. KOBAYASHI, H. TANAKA, H. FUJIWARA, I. TAMURA, V. GRITSENKO, T. OTSUKA, E. FUJIWARA, A. KOBAYASHI, M. TOKUMOTO and P. CASSOUX, "Electronic Properties of BETS Superconductors with Magnetic Anions," *Synth. Met.* **133-134**, 447–479 (2003).
B. ZHANG, H. TANAKA, A. KOBAYASHI and H. KOBAYASHI, "Magnetoresistance experiment of λ-$BETS_2Fe_{0.40}Ga_{0.60}Cl_4$," *Synth. Met.* **135-136**, 529–530 (2003).
A. KOBAYASHI, W. SUZUKI, E. FUJIWARA, H. TANAKA, Y. FUJISHIRO, E. NISHIBORI, M. TAKATA, M. SAKATA, Y. OKANO and H. KOBAYASHI, "Development of Single-Component Molecular Metals Based on Extended-TTF Dithiolate Ligands," *Synth. Met.* **135-136**, 511–513 (2003).
M. A. TANATAR, M. SUZUKI, T. ISHIGURO, H. TANAKA, H. FUJIWARA, H. KOBAYASHI, T. TOITO and J. YAMADA, "Thermal Conductivity of Organic Superconductors in Oriented Magnetic Field," *Synth. Met.* **137**, 1291–1293 (2003).
H. FUJIWARA, E. FUJIWARA and H. KOBAYASHI, "Synthesis, Structures and Properties of New Organic Donors Connecting to TEMPO Radical through a Pyrrolidine Ring," *Synth. Met.* **133-134**, 359–360 (2003).
H. FUJIWARA, E. FUJIWARA and H. KOBAYASHI, "Synthesis, Structures and Physical Properties of Donors Containing a PROXYL Radical," *Synth. Met.* **135-136**, 533–534 (2003).
H. TANAKA, H. KOBAYASHI and A. KOBAYASHI, "Structural and Physical Properties of Single-Component Molecular Conductors Based on Magnetic Metal Complexes," *Synth. Met.* **135-136**, 549–550 (2003).
S. UJI, C. TERAKURA, T. TERASHIMA, T. YAKABE, Y. TERAI, Y. IMANAKA, S. YASUZUKA, M. TOKUMOTO, F. SAKAI, A. KOBAYASHI, H. TANAKA, H. KOBAYASHI, L. BALICAS and J. S. BROOKS, "Large Anisotropy in Magnetic Field Induced Superconductors λ-$(BETS)_2Fe_xGa_{1-x}Cl_4$," *Physica C* **388-389**, 611–612 (2003).

R. KATO, N. TAJIMA, M. TAMURA and J. -I. YAMAURA, "Uniaxial Strain Effect in a Strongly Correlated Two-Dimensional System β'-$(CH_3)_4As[Pd(dmit)_2]_2$," *Phys. Rev. B* **66**, 020508 (4 pages) (2002).
R. KATO, T. IMAKUBO, H. YAMAMOTO, R. MAEDA, M. FUJIWARA, J. -I. YAMAURA and H. SAWA, "An Application of Supramolecular Chemistry to Molecular Conductors," *Mol. Cryst. Liq. Cryst.* **380**, 61–68 (2002).
T. SAKURAI, Y. INAGAKI, S. OKUBO, H. OHTA, R. KATO and T. NAKAMURA, "Frequency Dependence Millimeter Wave ESR Measurements of $Et_2Me_2P[Pd(dmit)_2]_2$," *Mol. Cryst. Liq. Cryst.* **379**, 59–64 (2002).
S. TARUTANI, J. -I. YAMAURA, K. TAKAHASHI and R. KATO, "High Pressure Properties of Extremely One-Dimensional Electronic Conductors $Me_4X(CPDT\text{-}TCNQ)_2$ (X = N, P and As)," *Solid State Commun.* **123**, 251–255 (2002).
T. YAMAMOTO, H. TAJIMA, R. KATO, M. URUICHI and K. YAKUSHI, "Raman Spectra of $(Me_2\text{-}DCNQI)_2Cu_xLi_{1-x}$($0 \le x \le 1$): The Evidence for Charge Separation at Room Temperature in a One-Dimensional Conductor Having a Quarter-Filled Band," *J. Phys. Soc. Jpn.* **71**, 1956–1964 (2002).
M. FUJIWARA and R. KATO, "Unique Structural and Physical Properties of $Ni(dmit)_2$ Anion Radical Salts Characterized by Short Te···S Contacts (dmit = 1,3-dithiole-2-thione-4,5-dithiolate)," *J. Chem. Soc., Dalton Trans.*

3763–3770 (2002).
M. TAMURA and R. KATO, "Magnetic Susceptibility of β'-[Pd(dmit)$_2$] Salts (dmit = 1,3-dithiol-2-thione-4,5-dithiolate, C_3S_5): Evidence for Frustration in Spin-1/2 Heisenberg Antiferromagnets on a Triangular Lattice," *J. Phys.: Condens. Matter* **14**, L729–L734 (2002).
M. FUJIWARA, N. TAJIMA, T. IMAKUBO, M. TAMURA and R. KATO, "Structural and Physical Properties of New Conducting Cation Radical Salts with Te-Based Counteranions, Tetraiodotellurate(II) and Hexaiododitellurate(II)," *J. Solid State Chem.* **168**, 396–407 (2002).
S. YASUZUKA, C. TERAKURA, T. TERASHIMA, T. YAKABE, Y. TERAI, H. M. YAMAMOTO, J. YAMAURA, R. MAEDA, R. KATO and S. UJI, "Fermi Surface in New Layered Organic Conductors (BEDT-TTF)$_3$Br(pBIB) and (BEDT-TTF)$_3$Cl(DFBIB)," *Synth. Met.* **133-134**, 169–171 (2003).
T. IMAKUBO, N. TAJIMA, M. TAMURA, R. KATO, Y. NISHIO and K. KAJITA, "Supramolecular Organic Conductor θ-(DIETS)$_2$[Au(CN)$_4$]: Unique Crystal Structure and Superconductivity under Uniaxial Strain (DIETS = diiodo(ethylenedithio)diselenadithiafulvalene)," *Synth. Met.* **133-134**, 181–183 (2003).
Y. SHIMOJO, M. A. TANATAR, T. ISHIGURO and R. KATO, "Upper Critical Field of Quasi One-Dimensional Superconductor (DMET-TSeF)$_2$AuI$_2$ under Oriented Magnetic Fields," *Synth. Met.* **133-134**, 247–249 (2003).
T. YAMAMOTO, H. TAJIMA, R. KATO, M. URUICHI and K. YAKUSHI, "Thermoelectric Power and Raman Spectra of (Me$_2$DCNQI)$_2$Cu$_x$Li$_{1-x}$," *Synth. Met.* **133-134**, 291–292 (2003).
T. SHIRAHATA, T. MORI, R. KATO and K. TAKAHASHI, "Synthesis, Crystal Structures and Electrical Properties of Cation Radical Salts of Selenium-Containing π-Extended Donors, BEDT-HBDST and BEDT-HSTT," *Synth. Met.* **133-134**, 321–324 (2003).
J. YAMAURA, R. KATO, S. TARUTANI and K. TAKAHASHI, "High Pressure X-Ray Study on CPDT-TCNQ Anion Radical Salts," *Synth. Met.* **133-134**, 411–413 (2003).
M. HIRAOKA, H. SAKAMOTO, K. MIZOGUCHI and R. KATO, "Spin Soliton Dynamics and Magnetic Susceptibility of (DMe-DCNQI)$_2$Li by ESR under Pressure," *Synth. Met.* **133-134**, 417–418 (2003).
T. SAKURAI, H. OHTA, S. OKUBO, R. KATO and T. NAKAMURA, "Temperature Dependence Millimeter Wave ESR Measurements of Et$_2$Me$_2$P[Pd(dmit)$_2$]$_2$," *Synth. Met.* **133-134**, 421–422 (2003).
Y. TAKANO, K. HIRAKI, T. TAKAHASHI and R. KATO, "Electronic Properties of Two Band System, β'-Pd(dmit)$_2$ Salts," *Synth. Met.* **133-134**, 423–424 (2003).
H. M. YAMAMOTO, M. HAGIWARA and R. KATO, "New Phase of (BEDT-TTF)(TCNQ)," *Synth. Met.* **133-134**, 449–451 (2003).
Y. OSHIMA, H. OHTA, H. M. YAMAMOTO, R. KATO, K. KOYAMA and M. MOTOKAWA, "Magnetooptical Measurements of BEDT-TTF Salts Containing Supramolecular Assemblies," *Synth. Met.* **133-134**, 453–454 (2003).
M. FUJIWARA, N. TAJIMA, T. IMAKUBO, M. TAMURA and R. KATO, "New Te-Based Counter Anions for Conducting Cation Radical Salts: Tetraiodotellurate(II) and Hexaiododitellurate(II)," *Synth. Met.* **133-134**, 459–461 (2003).
Y. NISHIO, S. SASAKI, Y. MORI, K. KAJITA, S. AONUMA, H. SAWA, M. TAMURA and R. KATO, "Deuterium Freedom and M-I Transition in (DMe-DCNQI)$_2$Cu System," *Synth. Met.* **133-134**, 569–571 (2003).
Y. OSHIMA, H. OHTA, K. KOYAMA, M. MOTOKAWA, H. M. YAMAMOTO, R. KATO, M. TAMURA, Y. NISHIO and K. KAJITA, "Fermi Surface Study of Quasi-Two-Dimensional Organic Conductors by Magnetooptical Measurements," *J. Phys. Soc. Jpn.* **72**, 143–148 (2003).
N. TAJIMA, T. IMAKUBO, R. KATO, Y. NISHIO and K. KAJITA, "Effects of Uniaxial Strain on Transport Property of a Supramolecular Organic Conductor θ-(DIETS)$_2$[Au(CN)$_4$]," *J. Phys. Soc. Jpn.* **72**, 1014–1017 (2003).
M. HIRAOKA, H. SAKAMOTO, K. MIZOGUCHI, T. KATO and R. KATO, "Charge Transport in the Insulating State of (DMe-DCNQI)$_2$Li above T_{SP}: A Possible Fractional Charge Soliton Conduction with ±1/2*e*," *Phys. Rev. Lett.* **91**, 056604 (4 pages) (2003).

H. SATO, N. KAWATSU, T. ENOKI, M. ENDO, R. KOBORI, S. MARUYAMA and K. KANEKO, "Drastic Effect of Water-Adsorption on the Magnetism of Nanomagnets," *Solid State Commun.* **125**, 641–645 (2003).
K. ENOMOTO, A. MIYAZAKI and T. ENOKI, "Novel Important Role of π-d Interaction in (DMET)$_2$FeCl$_4$," *Synth. Met.* **135-136**, 561–562 (2003).
J. NISHIJO, E. OGURA, J. YAMAURA, A. MIYAZAKI, T. ENOKI, T. TAKANO, Y. KUWATANI and M. IYODA, "Ferromagnetic Interaction and Metallic Conductivity of Radical Ion Salts (DIEDO)$_2$M(mnt)$_2$ (M = Ni, Pt)," *Synth. Met.* **133-134**, 539–541 (2003).
A. MIYAZAKI and T. ENOKI, "Crystal Structure and Physical Properties of (EDS-TTF)$_2$FeBr$_4$," *Synth. Met.* **133-134**, 543–545 (2003).
K. YAMAMOTO, K. YAKUSHI, K. MIYAGAWA, K. KANODA, A. KAWAMOTO, J. YAMAURA and T. ENOKI, "Vibrational Spectra of BEDT-TTF Based 2D Charge Ordering Systems," *Synth. Met.* **133-134**, 269–272 (2003).
T. ENOKI, H. YAMAZAKI, K. OKABE, K. ENOMOTO, T. KATO, A. MIYAZAKI, E. OGURA, Y. KUWATANI and M. IYODA, "Unconventional TTF-Based Molecular Magnets," *Synth. Met.* **133-134**, 151–153 (2003).
K. ENOMOTO, A. MIYAZAKI and T. ENOKI, "Novel π-d Interaction System (DMET)$_2$FeCl$_4$," *Synth. Met.*

135-136, 561–562 (2003).
T. ENOKI, H. YAMAZAKI, J. NISHIJO, K. UGAWA, E. OGURA, Y. KUWATANI, M. IYODA and Y. V. SUSHKO, "Novel Magnetism of EDO-TTFX_2 Salts (X = Br, I)," *Synth. Met.* **137**, 1173–1174 (2003).
S. OKUBO, K. KURITA, Y. INAGAKI, H. OHTA, K. ENOMOTO, A. MIYAZAKI and T. ENOKI, "Submillimater and Millimeter Wave ESR Measurements of $(DMET)_2FeBr_4$ below T_N," *Synth. Met.* **135-136**, 589–590 (2003).
K. ENOMOTO, A. MIYAZAKI and T. ENOKI, "Electronic and Magnetic Properties of Organic Conductors $(DMET)_2MBr_4$ (M = Fe, Ga)," *Bull. Chem. Soc. Jpn.* **76**, 945–959 (2003).
F. SETIFI, L. OUAHAB, J. GUILLEVIC, A. MIYAZAKI, T. ENOKI, T. TOMITA and J. YAMADA, "New Organic-Inorganic Hybrid Materials Based on DTDH-TTP and Paramagnetic Isothiocyanato Complex Anion: $(DTDH\text{-}TTP)_2[Cr(phen)(NCS)_4]\cdot CH_2Cl_2$," *Synth. Met.* **137**, 1177–1178 (2003).
A. MIYAZAKI, K. OKABE, T. ENOKI, F. SETIFI, S. GOLHEN, L. OUAHAB, T. TOITA and J. YAMADA, "Weak Ferromagnetism of (BDH-TTP)$[M(isoq)_2(NCS)_4]$ (M = Cr, Fe; isoq = isoquinoline)," *Synth. Met.* **137**, 1195–1196 (2003).
K. OKABE, A. MIYAZAKI and T. ENOKI, "Transport Property of π-d Interaction System $(EDTDM)_2FeBr_4$ under Pressure and Magnetic Field," *Synth. Met.* **135-136**, 693–694 (2003).
A. MIYAZAKI, K. OKABE, K. ENOMOTO, J. NISHIJO, T. ENOKI, F. SETIFI, S. GOLHEN, L. OUAHAB, T. TOITA and J. YAMAURA, "π-d Interaction-Based Molecular Magnets," *Polyhedron* **22**, 2227–2234 (2003).
J. NISHIJO, A. MIYAZAKI and T. ENOKI, "Weak-Ferromagnetism in Molecular Magnets Based on Transition Metal Complexes of Crown Thioether," *Polyhedron* **22**, 1755–1758 (2003).
F. SETIFI, L. OUAHAB, S. GOLHEN, A. MIYAZAKI, T. ENOKI, T. TOITA and J. YAMADA, "New Bulk Weak Ferromagnet in Ferrimagnetic Chains of Molecular Material Based on DTDH-TTP and Paramagnetic Thiocyanato Complex Anion: (DTDH-TTP)$[Cr(isoq)_2(NCS)_4]$," *C. R. Chimie* **6**, 309–316 (2003).
M. INAKUMA, A. TANINAKA, H. KATO, H. SHINOHARA and T. ENOKI, "Magnetic Anisotropy of Cerium Endhedral Metallofullerene," *J. Phys. Chem. B* **107**, 6965–6973 (2003).
A. MIYAZAKI, T. KATO, H. YAMAZAKI, T. ENOKI, E. OGURA, Y. KWATANI and M. IYODA, "Anomalous Metallic State of One-Dimensional Molecular Conductor $(EDO\text{-}TTFBr_2)_3I_3$," *Phys. Rev. B* **68**, 085108 (6 pages) (2003).
K. TAKAI, M. OGA, H. SATO, T. ENOKI, Y. OHKI, M. TAO, W. SUENAGEA and S. IIJIMA, "Structure and Electroic Properties of Nongraphitic Disordered Carbon System and Its Heat-Treatment Effect," *Phys. Rev. B* **67**, 214202 (11 pages) (2003).

Department of Applied Molecular Science

H. IMAI, K. INOUE, M. OHBA, H. OKAWA and K. KIKUCHI, "A Novel Two-Dimensional Chiral Complex; $[Cu\text{-}II(R)\text{-}pn]_2[Ni\text{-}II(CN)_4]_2\cdot H_2O$ ((*R*)-pn = (*R*)-1,2-diaminopropane)," *Synth. Met.* **137**, 919–920 (2003).
F. IWAHORI, AS. MARKOSYAN and K. INOUE, "Structures and Magnetic Properties of the Complexes Made up by $Cu(hfac)_2$ and Bisnitroxide Radical Derivatives," *Mol. Cryst. Liq. Cryst.* **376**, 449–454 (2002).
AS. OVCHINNIKOV, IG. BOSTREM, VE. SINITSYN, AS. BOYARCHENKOV, NV. BARANOV and K. INOUE, "Low-Energy Excitations and Thermodynamical Properties of the Quantum (5/2,1/2,1/2) Ferrimagnetic Chain," *J. Phys.: Condens. Matter* **14**, 8067–8078 (2002).
CD. SMITH, SE. BOTTLE, PC. JUNK, K. INOUE and AS. MARKOSYAN, "Synthesis and Properties of $Mn(hfac)_2$ Complexes of Isoindoline Nitroxide Radicals," *Synth Met.* **138**, 501–506 (2003).
H. KUMAGAI, Y. OKA, K. INOUE and M. KURMOO, "Hydrothermal Synthesis, Structure and Magnetism of Square-Grid Cobalt(II)-Carboxylate Layered Compounds with and without Pillars," *J. Chem. Soc., Dalton Trans.* 3442–3446 (2002).
H. KUMAGAI, M. OHBA, K. INOUE and H. OKAWA, "Synthesis and Characterization of a Tetrahedral and Octahedral Cobalt(II) Alternate Chain Complex," *Chem. Lett.* 1006–1007 (2002).
H. KUMAGAI, Y. OKA, S. KAWATA, M. OHBA, K. INOUE, M. KURMOO and H. OKAWA, "Hydrothermal Synthesis, Crystal Structure and Characterization of a New Hexanuclear Cobalt(II) Complex Comprised of Octahedral and Tetrahedral Cobalt Ions," *Polyhedron* **22**, 1917–1920 (2003).
S. HAYAMI, R. KAWAJIRI, G. JUHASZ, T. KAWAHARA, K. HASHIGUCHI, O. SATO, K. INOUE and Y. MAEDA, "Study of Intermolecular Interaction for the Spin-Crossover Iron(II) Compounds," *Bull. Chem. Soc. Jpn.* **76**, 1207–1213 (2003).
Y. HOSOKOSHI, K. KATOH and K. INOUE, "Magnetic Properties on an Organic Ferrimagnetic Compound and Related Materials," *Synth. Met.* **133**, 527–530 (2003).
H. OHTA, K. KIRITA, T. KUNIMOTO, S. OKUBO, Y. HOSOKOSHI, K. KATOH, K. INOUE, A. OGASAHARA and S. MIYASHITA, "Low Dimensionality Observed by ESR Measurements in $S = 1$ Spin Ladder Substance BIP-TENO (3,3',5,5'-Tetrakis(N-Tert-Butylaminoxyl)biphenyl)," *J. Phys. Soc. Jpn.* **71**, 2640–2643 (2002).
T. GOTO, NV. MUSHNIKOV, Y. HOSOKOSHI, K. KATOH and K. INOUE, "High Field Magnetization Processes of BIPNNBNO and PIMBNO at Low Temperature," *Physica B* **329**, 1160–1161 (2003).
Y. YOSHIDA, K. YURUE, M. MITOH, T. KAWAE, Y. HOSOKOSHI, K. INOUE, M. KINOSHITA and K.

TAKEDA, "Field-Induced Magnetic Ordering in an Alternating Heisenberg Chain F5PNN," *Physica B* **329**, 979–980 (2003).
T. SAKAI, N. OKAZAKI, K. OKAMOTO, K. KINDO, Y. NARUMI, Y. HOSOKOSHI, K. KATO, K. INOUE and T. GOTO, "Magnetization Plateau in S = 1 Organic Spin Ladder BIP-TENO," *Physica B* **329**, 1203–1204 (2003).
T. SAKAI, N. OKAZAKI, K. OKAMOTO, K. KINDO, Y. NARUMI, Y. HOSOKOSHI, K. KATO, K. INOUE and T. GOTO, "Magnetization Plateaux in S = 1 Spin Ladder," *Phys. Status Solidi B* **236**, 429–432 (2003).
S. AONUMA, H. CASELLAS, B. GARREAU DE BONNEVAL, I. MALFANT, C. FAULMANN, P. CASSOUX, Y. HOSOKOSHI and K. INOUE, "Structure and Property of M(dmit)$_2$ Salt with Trimethylammonio-TEMPO and Related Magnetic Organic Cations," *Mol. Cryst. Liq. Cryst.* **380**, 263–268 (2002).
K. MUKAI, M. MATSUBARA, H. HISATOU, Y. HOSOKOSHI, K. INOUE and N. AZUMA, "Anomalous Magnetic Behavior in Three Kinds of 3-(Aryl-substituted)-1,5-diphenylverdazyl Radical Crystals (*p*-FPDV, *p*-PyDV and *m*-PyDV) Induced by Frustrated Spin Interaction," *J. Phys. Chem. B* **106**, 8632–8638 (2002).
IS. DUBENKO, I.YU. GAIDUKOVA, E. GRATZ, K. INOUE, AS. MARKOSYAN and VE. RODIMIN, "Magnetic Instability of the Co Sublattice in the $Ho_{(1-x)}Y_xCo_3$ System," *Physica B* **319**, 21–27 (2002).
K. NAGAYOSHI, MD. K. KABIR, H. TOBITA, K. HONDA, M. KAWAHARA, M. KATADA, K. ADACHI, H. NISHIKAWA, I. IKEMOTO, H. KUMAGAI, Y. HOSOKOSHI, K. INOUE, S. KITAGAWA and S. KAWATA, "Design of Novel Inorganic-Organic Hybrid Materials Based on Iron-Chloranilate Mononuclear Complexes: Characteristics of Hydrogen-Bond-Supported Layers toward the Intercalation of Guests," *J. Am. Chem. Soc.* **125**, 221–232 (2002).
K. ADACHI, Y. SUGIYAMA, H. KUMAGAI, K. INOUE, S. KITAGAWA and S. KAWATA, "Synthesis and Crystal Structure of One-Dimensional Copper(II) Coordination Polymer Bridged by Pyrazine Derivative," *Mol. Cryst. Liq. Cryst.* **376**, 71–76 (2002).
NV. BARANOV, K. INOUE, H. MICHOR, G. HILSCHER and AA. YERMAKOV, "Spin Fluctuations in Gd_3Rh Induced by *f–d* Exchange: the Influence on the *T*-linear Specific Heat," *J. Phys.: Condens. Matter* **15**, 531–538 (2003).
T. NAITO, T. INABE, T. AKUTAGAWA, T. HASEGAWA, T. NAKAMURA, Y. HOSOKOSHI and K. INOUE, "Physical Properties of $(ET)_3(MnCl_4)$(TCE) and the Related Salts," *Synth. Met.* **135-136**, 613–614 (2003).
K. MUKAI, S. JINNO, Y. SHIMOBE, N. AZUMA, M. TANIGUCHI, Y. MISAKI, K. TANAKA, K. INOUE and Y. HOSOKOSHI, "Genuine Organic Magnetic Semiconductors: Electrical and Magnetic Properties of the TCNQ and Iodide Salts of Methylpyridinium-Substituted Verdazyl Radicals," *J. Mater. Chem.* **13**, 1614–1621 (2003).
Y. TAKAZAKI, Z. YANG, M. EBIHARA, K. INOUE and T. KAWAMURA, "A Honeycomb Network of a Paddlewheel-Type Dirhodium Complex in Two Oxidation States and Pinningof the Oxidation States," *Chem. Lett.* 120–121 (2003).
IS. DUBENKO, IY. GAIDUKOVA, SA. GRANOVSKY, K. INOUE, AS. MARKOSYAN, S. ROY and N. ALI, "Magnetic Phase Transitions in $(Tb,Y)Mn_2M_2$ (M = Ge and Si) Systems," *J. Appl. Phys.* **93**, 8185–8187 (2003).
M. DOERR, M. ROTTER, M. ELLERBY, AS. MARKOSYAN, SS. SAXENA, Y. HOSOKOSHI, K. INOUE and M. LOEWENHAUPT, "Pressure Dependent Magnetization of $DyCu_2$ Single Crystals," *Physica B*, **329**, 633–634 (2003).

N. ASAKUMA, H. HIRASHIMA, T. FUKUI, M. TOKI, K. AWAZU and H. IMAI, "Photo-Reduction of Amorphous and Crystalline ZnO Films," *Jpn. J. Appl. Phys.* **41**, 3909–3915 (2002).
S. YAMABI, H. IMAI and K. AWAZU, "Biomimetic Approach for Exact Control of TiO_2 Periodic Microstructure," *Chem. Lett.* **7**, 714–715 (2002).
N. ASAKUMA, H. HIRASHIMA, T. FUKUI, M. TOKI, K. AWAZU and H. IMAI, "Photocrystallization of Amorphous ZnO," *J. Appl. Phys.* **92**, 5707–5710 (2002).
K. AWAZU, S. ROORDA, J. L. BREBNER, S. ISHII and K. SHIMA, "Structure of Latent Tracks Created by Swift Heavy Ions in Amorphous SiO_2 and Zinc Phosphate Glass," *Jpn. J. Appl. Phys.* **42**, 3950–3957 (2003).
K. NOMURA, T. NAKANISHI, Y. NAGASAWA, Y. OHKI, K. AWAZU, M. FUJIMAKI, N. KOBAYASHI, S. ISHII and K. SHIMA, "Structural Change Induced in TiO_2 by Swift Heavy Ions and Its Application to Three Dimensional Lithography," *Phys. Rev. B* **68**, 64106 (7 pages) (2003).

K. KIKUCHI, H. NISHIKAWA, I. IKEMOTO, T. TOITA, H. AKUTSU, S. NAKATSUJI and J. YAMADA, "Tetrachloroferrate(III) Salts of BDH-TTP [2,5-Bis(1,3-dithiolan-2-ylidene)-1,3,4,6-tetrathiapentalene] and BDA-TTP [2,5-Bis(1,3-dithian-2-ylidene)-1,3,4,6-tetrathiapentalene]: Crystal Structures and Physical Properties," *J. Solid State Chem.* **168**, 503 (2002).
M. IYODA, K. HARA, E. OGURA, T. TAKANO, M. HASEGAWA, M. YOSHIDA, Y. KUWATANI, H. NISHIKAWA, K. KIKUCHI, I. IKEMOTO and T. MORI, "Synthesis and Electroconductive Properties of Radical Salts Derived from Tetrathiafulvalene Dimmers," *J. Solid State Chem.* **168**, 597 (2002).
M. CHIKAMATSU, S. KAZAOUI, N. MINAMI, K. YASE, T. KODAMA, H. NISHIKAWA, I. IKEMOTO and K. KIKUCHI, " Electrical and Optical Properties of a Potassium-Doped Film of a Long Alkyl Chain-Linked C_{60}," *Mol. Cryst. Liq. Cryst.* **377**, 353 (2002).

H. YOSHINO, K. MURATA, Y. YAMAMURA, T. TSUJI, J. YAMADA, S. NAKATSUJI, H. ANZAI, H. NISHIKAWA, K. KIKUCHI, I. IKEMOTO and K. SAITO, "Electrical Properties of Organic Conductors at High Temperature," *Mol. Cryst. Liq. Cryst.* **380**, 239 (2002).
T. KODAMA, R. FUJII, Y. MIYAKE, K. SAKAGUCHI, H. NISHIKAWA, I. IKEMOTO, K. KIKUCHI and Y. ACHIBA, "Structural Study of Four $Ca@_{82}$ Isomers by ^{13}C NMR Spectroscopy," *Chem. Phys. Lett*. **377**, 197 (2003).
H. NISHIKAWA, A. MACHIDA, T. MORIMOTO, K. KIKUCHI, T. KODAMA, I. IKEMOTO, J. YAMADA, H. YOSHINO and K. MURATA, "A New Organic Superconductor, $(DODHT)_2BF_4 \cdot H_2O$," *Chem. Commun.* 494 (2003).
J. YAMADA, T. TOITA, H. AKUTSU, S. NAKATSUJI, H. NISHIKAWA, I. IKEMOTO, K. KIKUCHI, E. S. CHOI, D. GRAF and J. S. BROOKS, "A New Organic Superconductor, β-$(BDA\text{-}TTP)_2GaCl_4$ [BDA-TTP = 2,5-(1,3-Dithian-2-Ylidene)-1,3,4,6-Tetrathiapentalene]," *Chem. Commun.* 2230 (2003).
J. YAMADA, M. WATANABE, T. TOITA, H. AKUTSU, S. NAKATSUJI, H. NISHIKAWA, I. IKEMOTO and K. KIKUCHI, "Development of New Organic Metals and Superconductors from a Non-TTF Donor System," *Mol. Cryst. Liq. Cryst.* **390**, 121 (2003).
Y. OSHIMA, H. OHTA, K. KOYAMA, M. MOTOKAWA, H. NISHIKAWA, K. KIKUCHI and I. IKEMOTO, "Magnetooptical Measurements of Quasi-One-Dimensional Conductor $(DMET)_2I_3$," *Synth. Met.* **135-136**, 531 (2003).
J. YAMADA, T. TOITA, H. AKUTSU, S. NAKATSUJI, H. NISHIKAWA, I. IKEMOTO and K. KIKUCHI, "Organic Conductors Based on Unsymmetrical BDY Donors," *Synth. Met.* **135-136**, 539 (2003).
K. YOKOYAMA, H. NISHIKAWA, T. KODAMA, I. IKEMOTO, K. KIKUCHI and J. YAMADA, "Crystal Structures and Physical Properties of New Ni Complexes with Dihydro-TTF Dithiolato," *Synth. Met.* **135-136**, 659 (2003).
S. KOJIMA, H. NISHIKAWA, T. KODAMA, I. IKEMOTO and K. KIKUCHI, "Synthesis and Physical Properties of New C_{60} Derivatives Linked with TTF," *Synth. Met.* **135-136**, 775 (2003).
K. KIKUCHI, H. NISHIKAWA, T. MORIMOTO, T. KODAMA, I. IKEMOTO and J. YAMADA, "Structural Studies of DODHT Superconductor and Related Salts," *Synth. Met.* **137**, 1159 (2003).
H. NISHIKAWA, T. MORIMOTO, A. MACHIDA, T. KODAMA, I. IKEMOTO, K. KIKUCHI, J. YAMADA, H. YOSHINO and K. MURATA, "Structure and Properties of Radical Salts of DODHT Derivatives," *Synth. Met.* **137**, 1253 (2003).

Department of Vacuum UV Photoscience

T. GEJO, Y. TAKATA, T. HATSUI, M. NAGASONO, H. OJI, N. KOSUGI and E. SHIGEMASA, "Angle-Resolved Photoion Spectroscopy of NO_2 and SO_2," *Chem. Phys.* **289**, 15 (2003).
N. KOSUGI, "Exchange Interaction in Core Excitation of Diatomic Systems," *Chem. Phys.* **289**, 117 (2003).
A. Y. MATSUURA, T. OBAYASHI, H. KONDOH, T. OHTA, H. OJI, N. KOSUGI, K. SAYAMA and H. ARAKAWA, "Adsorption of Merocyanine Dye on Rutile TiO_2(110)," *Chem. Phys. Lett.* **360**, 133 (2002).
E. SHIGEMASA, T. GEJO, M. NAGASONO, T. HATSUI and N. KOSUGI, "Double and Triple Excitations Near the K-Shell Ionization Threshold of N_2 Revealed by Symmetry-Resolved Spectroscopy," *Phys. Rev. A* **66**, 022508 (2002).

Y. J. LI, O. TAKEUCHI, D. N. FUTBA, K. MIYAKE, H. SHIGEKAWA and Y. KUK, "Characteristic Intra- and Interunit Interactions of the Kr Atoms Adsorbed on Si(111)-7×7 Surface," *Phys. Rev. B* **68**, 033301 (4 pages) (2003).
R. TERO, K. FUKUI, and Y. IWASAWA, "Atom-Resolved Surface Structures and Molecular Adsorption on TiO_2(001) Investigated by Scanning Tunneling Microscopy," *J. Phys. Chem. B* **107**, 3207–3214 (2003).
S. TAKAKUSAGI, K. FUKUI, R. TERO, F. NARIYUKI and Y. IWASAWA, "Self-Limiting Growth of Pt Nanoparticles from MeCpPtMe3 Adsorbed on TiO_2(110) Studied by Scanning Tunneling Microscopy," *Phys. Rev. Lett.* **91**, 066102 (4 pages) (2003).
A. KOIZUMI, H. MORIYA, N. WATANABE, Y. NONOGAKI, Y. FUJIWARA and Y. TAKEDA, "Er-Related Luminescence in Er, O-Codoped InGaAs/GaAs Multiple-Quantum-Well Structures Grown by Organometallic Vapor Phase Epitaxy," *Appl. Phys. Lett.* **80**, 1559–1561 (2002).
Y. FUJIWARA, Y. NONOGAKI, R. OGA, A. KOIZUMI and Y. TAKEDA, "Reactor Structure Dependence of Interface Abruptness in GaInAs/InP and GaInP/GaAs Grown by Organometallic Vapor Phase Epitaxy," *Appl. Surf. Sci.* **216**, 564–568, (2003).
S. D. MORE, J. HUDECECK, and T. URISU, "Hydrophobic/Hydrophilic Interactions of Cytochrome *c* with Functionalized Self-Assembled Monolayers on Silicon," *Surf. Sci.* **532-535**, 993–998 (2003).
C. WANG, S. D. MORE, Z. WANG, S. YAMAMURA, Y. NONOGAKI and T. URISU, "Patterning SiO_2 Thin Films Using Synchrotron Radiation Stimulated Etching with a Co Contact Mask," *J. Vac. Sci. Technol. B* **21**, 818–822 (2003).
S. YAMAMURA, S. YAMAUCHI, S. WATANABE, M. TABE, T. KASAI, Y. NONOGAKI and T. URISU, "Infrared Reflection Absorption Spectroscopy Using $CoSi_2$ Buried Metal Layer Substrates Made by Wafer-Bonding," *Jpn. J. Appl. Phys.* **42**, 3942–3943 (2003).

C. WANG and T. URISU, "Synchrotron Radiation Stimulated Etching SiO_2 Thin Films with a Co Contact Mask for the Area-Selective Deposition of Self-Assenbled Monolayer," *Jpn. J. Appl. Phys.* **42**, 4016–4019 (2003).

K. MITSUKE, "Ultraviolet and Visible Dispersed Spectroscopy for the Photofragments Produced from H_2O in the Extreme Ultraviolet," *J. Chem. Phys.* **117**, 8334–8340 (2002).
M. ONO and K. MITSUKE, "Anisotropy of Fragment Ions from SF_6 by Photoexcitation between 23 and 210 eV," *Chem. Phys. Lett.* **366**, 595–600 (2002).
Y. MAKINO, T. MORI, H. EGUCHI, H. SAITO, B. KYOH and S. MIYAKE, "Preferentially Oriented Anatase Nano-Powder Densified by Pulsed High Current Heating," *J. Mater. Sci. Lett.* **22**, 403–405 (2003).
T. MORI, M. FUJIWARA, R. MANORY, I. SHIMIZU, T. TANAKA and S. MIYAKE, "HfO_2 Thin Films Prepared by Ion Beam Assisted Deposition," *J. Vac. Sci. Technol.* **169-170**, 528–531 (2003).
J. KOU, T. MORI, M. ONO, Y. HARUYAMA, Y. KUBOZONO and K. MITSUKE, "Molecular- and Atomic-Like Photoionization of C_{60} in the Extreme Ultraviolet," *Chem. Phys. Lett.* **374**, 1–6 (2003).
T. MORI, J. KOU, M. ONO, Y. HARUYAMA, Y. KUBOZONO and K. MITSUKE, "Development of a Photoionization Spectrometer for Accurate Ion Yield Measurements from Gaseous Fullerenes," *Rev. Sci. Instrum.* **74**, 3769–3773 (2003).
A. MITSUO, T. MORI, Y. SETSUHARA, S. MIYAKE and T. AIZAWA, "Mechanical Properties of Zirconium Films Prepared by Ion-Beam Assisted Deposition," *Nucl. Instrum. Meth. Phys. Res., Sect. B* **206**, 366–370 (2003).

Coordination Chemistry Laboratories

H. MIYASAKA, R. CLERAC, T. ISHII, H. CHANG, S. KITAGAWA and M.YAMASHITA, "Out-of-Plane Dimers of Mn(III) Quadridentate Schiff-Base Complexes with Saltmen^{2-} and Naphtmen^{2-} Ligands: Structure Analysis and Ferromagnetic Exchange," *J. Chem. Soc., Dalton Trans.* **7**, 1528–1534 (2002).
H. TANAKA, K. MARUMOTO, S. KURODA, T. ISHII, R. KANEHAMA, N. AIZAWA, H. MATSUZAKA, K. SUGIURA, H. MIYASAKA, T. KODAMA, K. KIKUCHI, I. IKEMOTO and M. YAMASHITA, "Electron Spin Resonance Studies of Co(tbp)·C_{60} Single Crystal," *J. Phys.: Condens. Matter* **14**, 3993–4000 (2002).
K. NAKATA, Y. YOSHINO, H. HARA, T. MANABE, T. ISHII, H. MIYASAKA, M. YAMASHITA, H. MATSUZAKA and M. KATADA, "Structure, Magnetic and Electronic Properties of Charge Transfer Complex Containing Hexacyanoferrate Chain and BEDT-TTF Column," *Mol. Cryst. Liq. Cryst.* **380**, 117–122 (2002).
H. ASO, T. MANABE, T. KAWASHIMA, T. ISHII, H. MIYASAKA, H. MATSUZAKA, M. YAMASHITA, N. KURODA and M. SHIRO, "Creations of Solitons and Polarons in MX-Chain Compounds, $\{[Pt(en)_2][PtX_2(en)_2]\}_3(CuX_4)_4$ (X = Cl and Br)," *Mol. Cryst. Liq. Cryst.* **376**, 7–12 (2002).
N. AIZAWA, H. HARA, T. ISHII, M. YAMASHITA, H. MIYASAKA, H. MATSUZAKA, T. KODAMA, K. KIKUCHI and I. IKEMOTO, "Syntheses and Physical Properties of Complexes of Fullerene with Magnetic Metal Porphyrins," *Mol. Cryst. Liq. Cryst.* **376**, 13–18 (2002).
K. TAKIZAWA, T. ISHII, H. MIYASAKA, H. MATSUZAKA, M. YAMASHITA, T. KAWASHIMA, H. MATSUZAKI, H. KISHIDA and H. OKAMOTO, "Crystal and Electronic Structures of Quasi-One-Dimensional Halogen-Bridged Binuclear Platinum Complexes, $\{(C_nH_{2n+1})_2NH_2\}_4[Pt_2(pop)_4I]$ (n = 2–6)," *Mol. Cryst. Liq. Cryst.* **376**, 159–164 (2002).
T. MANABE, K. YOKOYAMA, T. ISHII, H. MIYASAKA, H. MATSUZAKA, M. YAMASHITA, T. KAWASHIMA, H. MATSUZAKI, H. KISHIDA, H. OKAMOTO, K. MARUMOTO, H. TANAKA, H. ITOH and S. KURODA, "Physical Properties of Quasi-One-Dimensional Mixed-Metal and Mixed-Halogen Complexes, $Ni_{1-x}Pd_x(chxn)_2Cl_yBr_{1-y}Y_2$," *Mol. Cryst. Liq. Cryst.* **376**, 165–170 (2002).
H. MIYASAKA, Y. YOSHINO, T. ISHII, R. KANEHAMA, T. MANABE, M. YAMASHITA, H. NISHIKAWA, I. IKEMOTO, H. KISHIDA, H. MATSUZAKI and H. OKAMOTO, "Magnetic/Conducting Hybrid Compound Composed of 1-D Chain $[Mn^{II}_2Cl_5(EtOH)]_\infty^-$ and BEDT-TTF Stacking Layer," *J. Solid State Chem.* **168**, 418–426 (2002).
C. KACHI-TERAJIMA, H. MIYASAKA, T. ISHII, K. SUGIURA and M. YAMASHITA, "Structure and Electrochemistry of the Bridging-Ligand Mono-Substituted Diruthenium Compound, $[Ru_2(II,III)(O_2CCH_3)_3(admpym)(Cl)(MeOH)]$ (Hadmpym = 2-amino-4,6-dimethylpyrimidine)," *Inorg. Chim. Acta* **332**, 210–215 (2002).
H. ITO, M. SUNATA, S. KURODA, T. MANABE and M. YAMASHITA, "Electrical Conduction of Halogen-Bridged Metal Complexes $Ni_{1-x}Pd_x(chxn)_2Br_3$," *Mol. Cryst. Liq. Cryst.* **379**, 285–290 (2002).
H. MIYASAKA, K. SUGIMOTO, K. SUGIURA, T. ISHII and M. YAMASHITA, "Reactions of Mn(III) Quadridentate Schiff Base Compounds with TCNQ Anion to Form Unusual TCNQ Derivatives by Alcoholysis," *Mol. Cryst. Liq. Cryst.* **379**, 197–204 (2002).
H. MIYASAKA, K. MIZUSHIMA, S. FURUKAWA, K. SUGIURA, T. ISHII and M. YAMASHITA, "Out-of-Plane Dimer Structures and Magnetic Properties of Mn(III) Quadridentate Schiff Base Compounds with N,N'-(1,1,2,2-tetramethylethylene)bis(5-chlorosalicylideneiminato)," *Mol. Cryst. Liq. Cryst.* **379**, 171–178 (2002).
K. NAKATA, H. MIYASAKA, T. ISHII, M. YAMASHITA and K. AWAGA, "Synthesis, Structure and Magnetic Properties of the Antiferromagnetic Hexamanganese Cluster $[Mn_6(\mu_4\text{–}O)_2(O_2CC_6HF_4)_{10}(HO_2CCH_3)_4]\cdot(C_7H_8)$," *Mol. Cryst. Liq. Cryst.* **379**, 211–216 (2002).
R. CLERAC, H. MIYASAKA, M. YAMASHITA and C. COULON, "Evidence for Single-Chain Magnet Behavior in a Mn^{III}-Ni^{II} Chain Designed with High Spin Magnetic Units: A Route to High Temperature Metastable

Magnets," *J. Am. Chem. Soc.* **124**, 12837–12844 (2002).
T. MANABE, K. YOKOYAMA, S. FURUKAWA, C. KACHI-TERAJIMA, K. NAKATA, F. IWAHORI, H. MIYASAKA, K. SUGIURA, M. YAMASHITA, H. KISHIDA and H. OKAMOTO, "Tuning of Spin Density Wave Strengths in Quasi-One-Dimensional Mixed-Halogen-Bridged Ni(III) Complexes with Strong-Electron Correlation, $[Ni^{III}(chxn)_2Cl_{1-x}Br_x](NO_3)_2$," *Inorg. Chem.* **41**, 4993–4995 (2002).
R. KANEHAMA, Y. YOSHINO, T. ISHII, T. MANABE, H. HARA, H. MIYASAKA, H. MATSUZAKA, M. YAMASHITA, M. KATADA, H. NISHIKAWA and I. IKEMOTO, "Syntheses and Physical Properties of New Charge-Transfer Salts Consisting of a Conducting BEDT-TTF Column and Magnetic 1D or 2D Fe(III) Networks," *Synth. Met.* **133-134**, 553–554 (2003).
H. MATSUZAKI, T. MATSUOKA, H. KISHIDA, K. TAKIZAWA, H. MIYASAKA, K. SUGIURA, M. YAMASHITA and H. OKAMOTO, "Novel Optical and Magnetic Bistability and Photoinduced Transition in a One-Dimensional Halogen-Bridged Binuclear Pt Complex," *Phys. Rev. Lett.* **90**, 046401 (4 pages) (2003).
M. YAMASHITA, H. ASO, S. MATSUNAGA, K. TAKIZAWA, K. NAKATA, C. KACHI-TERAJIMA, F. IWAHORI, T. ISHII, H. MIYASAKA, K. SUGIURA, T. KAWASHIMA, K. TAKAI, N. KURODA, M. SHIRO, H. KISHIDA, H. OKAMOTO, H. TAKAHASHI, H. TANAKA, K. MARUMOTO and S. KURODA, "Unprecedented Soliton Formation Mechanism in Quasi-One-Dimensional Chloro-Bridged Pt^{II}-Pt^{IV} Mixed-Valence Compound, $\{[Pt(en)_2][PtCl_2(en)_2]\}_3(CuCl_4)_4 \cdot 12H_2O$," *Chem. Lett.* **32**, 278–279 (2003).
H. MIYASAKA, K. MIZUSHIMA, K. SUGIURA and M. YAMASHITA, "A Series of Ni(II) Pyridyloximato (pao^-) Compounds $[Ni(pao)_2(L)_2]$ (L = Unidentate Ligand): As a Coordination Donor Building Block in the Assembly with Mn(III) Salen Analogues," *Synth. Met.* **137**, 1245–1246 (2003).
M. MITO, H. AKAMA, H. DEGUCHI, S. TAKAGI, T. KAWAE, K. TAKEDA, T. ISHII, M. YAMASHITA, H. NAKAO, Y. MURAKAMI and S. YAMAMOTO, "Pressure Effects on an S = 1 Haldane Compound $Ni(C_5H_{14}N_2)_2N_3(PF_6)$," *J. Phys. Soc. Jpn.* **72**, 399–404 (2003).
F. IWAHORI, H. MIYASAKA, T. ISHII, K. SUGIURA and M. YAMASHITA, "Platinum(II) Complex with S = 1/2 Organic Radical Ligand," *Synth. Met.* **135-136**, 355–356 (2003).
T. ONO, M. YAMASHITA, K. YOKOYAMA, S. FURUKAWA, T. MANABE, K. SUGIURA, T. ISHII, H. MIYASAKA, H. MATSUZAKI, H. KISHIDA, H. OKAMOTO, K. MARUMOTO, H. TANAKA, Y. HASEGAWA, S. KURODA and H. ITOU, "Tuning of Spin Density Wave Strength of Ni(III) Complexes with Strong Electron-Correlation," *Synth. Met.* **135-136**, 257–258 (2003).
R. KANEHAMA, H. MIYASAKA, K. SUGIURA, M. YAMASHITA, H. ITOU, S. KURODA, H. KISHIDA and H. OKAMOTO, "New Charge-Transfer Salts $(ET)_8(Mn^{II}Br_4)_2(DCE)_2$ and $(ET)_3Mn^{II}Br_4$: Preparations, Structures and Physical Properties (ET = BEDT-TTF, DCE = 1,2-Dichloroethane)," *Synth. Met.* **135-136**, 633–634 (2003).
H. KISHIDA, M. ONO, H. MATSUZAKI, M. YAMASHITA, Y. TAGUCHI, Y. TOKURA and H. OKAMOTO, "Gigantic Third-Order Optical Nonlinearity in One-Dimensional Mott Insulators," *Synth. Met.* **135-136**, 315–316 (2003).
H. MIYASAKA, H. IEDA, N. MATSUMOTO, K. SUGIURA and M. YAMASHITA, "Structure and Magnetic Properties of the Two-Dimensional Ferrimagnet $(NEt_4)[\{Mn(salen)\}_2Fe(CN)_6]$: Investigation of Magnetic Anisotropy on a Single Crystal," *Inorg. Chem.* **42**, 3509–3515 (2003).
H. TANAKA, K. MARUMOTO, S. KURODA and M. YAMASHITA, "LESR Studies of Long-Lived Photogenerated Spins in the MX-Chain Complex, $Pd(chxn)_2Br_3$," *Synth. Met.* **135-136**, 317–318 (2003).
H. MIYASAKA, T. NEZU, F. IWAHORI, S. FURUKAWA, K. SUGIMOTO, R. CLERAC, K. SUGIURA and M. YAMASHITA, "Heterometallic Hexanuclear Cluster with an S = 8 Spin Ground State: $Mn^{II}\{Mn^{II}(hfac)_2\}_3$-$\{Ni^{II}(pao)_3\}_2$ ($hfac^-$ = Hexafluoroacetylacetonate, pao^- = Pyridine-2-aldoximate)," *Inorg. Chem.* **42**, 4501–4503 (2003).

Y. FUKUMOTO, T. DOHI, H. MASAOKA, N. CHATANI and S. MURAI, "Reaction of Terminal Alkynes with Hydrazines to Give Nitriles Catalyzed by $TpRuCl(PPh_3)_2$: Novel Catalytic Transformation Involving a Vinylidene Ruthenium Intermediate," *Organometallics* **21**, 3845–3847 (2002).
N. CHATANI, A. KAMITANI and S. MURAI, "Ruthenium-Catalyzed Reaction of α,β-Unsaturated Imines with Carbon Monoxide and Alkenes Leading to β,γ-Unsaturated γ-Butyrolactams: Involvement of Direct Carbonylation of Olefinic C–H Bonds as a Key Step," *J. Org. Chem.* **67**, 7014–7018 (2002).
N. CHATANI, S. YORIMITSU, T. ASAUMI, F. KAKIUCHI and S. MURAI, "$Ru_3(CO)_{12}$-Catalyzed C–H/CO/Olefin Coupling of *N*-Pyridylindolines. Direct Carbonylation at a C–H Bond δ to the Pyridine Nitrogen," *J. Org. Chem.* **67**, 7557–7560 (2002).
N. CHATANI, K. AMAKO, M. TOBISU, T. ASAUMI, Y. FUKUMOTO and S. MURAI, "Ruthenium-Catalyzed Carbonylative Cycloaddition of α-Keto Lactones with Alkenes or Alkynes: The Participation of an Ester-Carbonyl group in Cycloaddition Reactions as the Two-Atom Assembling Unit," *J. Org. Chem.* **68**, 1591–1593 (2003).
F. KAKIUCHI, S. KAN, K. IGI, N. CHATANI and S. MURAI, "A Ruthenium-Catalyzed Reaction of Aromatic Ketones with Arylboronates: A New Method for the Arylation of Aromatic Compounds *via* C–H Bond Cleavage," *J. Am. Chem. Soc.* **125**, 1698–1699 (2003).
A. KAMITANI, N. CHATANI and S. MURAI, "Palladium-Catalyzed Carbonylation of 2-(Propargyl)allyl Phosphates Leading to Highly Unsaturated γ-Lactones," *Angew. Chem., Int. Ed.* **42**, 1397–1399 (2003).

N. CHATANI, M. OSHITA, M. TOBISU, Y. ISHII and S. MURAI, "A $GaCl_3$-Catalyzed [4+1] Cycloaddition of α,β-Unsaturated Carbonyl Compounds and Isocyanides Leading to Unsaturated γ-Lactone Derivatives," *J. Am. Chem. Soc.* **125**, 7812–7813 (2003).

T. FUJIWARA, R. OKAMURA, T. WADA and K. TANAKA, "Coordination Ability of 1,10-Phenanthroline-5,6-Dione: Syntheses and Redox Behavior of a Ru(II) Complex with an *o*-Quinoid Moiety and of Bridged Ru(II)-M(II) Complexes (M = Pd, Pt)," *Dalton Trans.* 3221–3226 (2003).
K. KOBAYASHI, H. OHTSU, T. WADA, T. KATO and K. TANAKA, "Characterizationof a Stable Ruthenium Complex with Oxyl Radical", *J. Am. Chem. Soc.* **125**, 6729–6739 (2003).
H. SUGIMOTO, K. SIRE K., H. TSUKUBE and K. TANAKA, "Mono-Dithiolene Molybdenum(IV) Complexes of cis-1,2-Dicyno-1.2-ethylenedithiolate (mnt^{2-}): New Models for Molybdenum Enzymes," *Eur. J. Inorg. Chem.* 2633–2638 (2003).
T. KOIZUMI, T. TOMON and K. TANAKA, "Terpyridine-Analogous (N,N,C)-Tridentate Ligands: Synthesis, Structures and Electrochemical Properties of Ruthenium(II) Complexes Bearing Tridentate Pyridinium and Pyridinylidene Ligands," *Organometallics* **22**, 970–975 (2003).
D. OOYAMA, T. KOBAYASHI, K. SHIREN and K. TANAKA, "Regulation of Electron Donating Ability to Metal Center: Isolation and Characterization of Ruthenium Carbonyl Complexes with *N*,*N*- and/or *N*,*O*-Donor Polypyridyl Ligands," *J. Organomet. Chem.* **665**, 107–113 (2003).
K. SHIREN and K. TANAKA, "Acid-Base Equilibrium of Aqua-Chromium-Dioxolene Complexes Aimed at Formation of Oxo-Chromium Complexes," *Inorg. Chem.* **41**, 5912 (2002).
K. KOBAYASHI, H. OHTSU, T. WADA and K. TANAKA, "Ruthenium Pxyl Radical Complex Containing o-Oquinone Ligand Detected by ESR Measurements of Spin Trapping Technique," *Chem. Lett.* 23–24 (2002).
T. NAGATA and K. TANAKA, "Synthesis of a 6-(2-Pyrrolyl)-2,2'-Bipyridine Derivative and Its Ruthenium Complex," *Bull. Chem. Soc. Jpn.* **75**, 2469 (2002).
H. SUGIMOTO, H. WADA, Y. WAKATSUKI, T. WADA and K. TANAKA, "Novel Diruthenium Disulfinate Complex Formed through Oxygen Capture on Deprotonated Form of Ruthenium-Aqua-Dithiolene: Four Oxygens from O_2 and Four Oxygens from H_2O," *Chem. Lett.* 634–635 (2002).

T. KOMURO, T. MATSUO, H. KAWAGUCHI and K. TATSUMI, "Copper and Silver Complexes Containing the $S(SiMe_2S)_2^{2-}$ Ligand: Efficient Entries into Heterometallic Sulfido Clusters," *Angew. Chem., Int. Ed.* **42**, 465–468 (2003).
T. KOMURO, T. MATSUO, H. KAWAGUCHI and K. TATSUMI, "Unusual Coordination Modes of Arylthiolates in $Mo\{\eta^5\text{-}SC_6H_3\text{-}2,6\text{-}(SiMe_3)_2\}\{\eta^7\text{-}SC_6H_3\text{-}2,6\text{-}(SiMe_3)_2\}$," *J. Am. Chem. Soc.* **125**, 2070–2071 (2003).
S. E. D'ARBELOFF-WILSON, P. HITCHCOCK, J. F. NIXON, H. KAWAGUCHI and K. TATSUMI, "[2+2] Cyclo-addition Reactions of Bis-pentamethylcyclopentadienyl Zirconium Metal Complexes Containing Terminal Chalcogenide Ligands with the Phospha-alkyne PC^tBu. Synthesis, Crystal and Molecular Structures of the Four Complexes $[Zr(\eta^5\text{-}(C_5Me_5)_2(SC(^t Bu)=P))]$, $[Zr(\eta^5\text{-}(C_5Me_5)_2(SeC(^t Bu)=P))]$, $[Zr(\eta^5\text{-}(C_5Me_5)_2(SC(^t Bu)=PSe))]$, and $[Zr(\eta^5\text{-}(C_5Me_5)_2(SC(^t Bu)=PC(Ph)=N))]$," *J. Organomet. Chem.* **672**, 1–10 (2003).
Y. OHKI, N. MATSUURA, T. MARUMOTO, H. KAWAGUCHI and K. TATSUMI, "Heterolytic Cleavage of Dihydrogen Promoted by Sulfido-Bridged Tungsten-Ruthenium Dinuclear Complexes," *J. Am. Chem. Soc.* **125**, 7978 (2003).
H. AIHARA, T. MATSUO and H. KAWAGUCHI, "Titanium N-Hetrocyclic Carbene Complexes Incorporating an Imidazolium-linked Bis(phenol)," *Chem. Commun.* 2204–2205 (2003).
J. FANG, L. GAN, H. KAWAGUCHI, W. -Y. SUN, K. -B. YU and W. -X. TANG, "Reversible Anion Exchanges between the Layered Organic-Inorganic Hybridized Architectures and Structures of Manganese(II) and Copper(II) Complexes Novel Tripodal Ligands," *Chem. Eur. J.* **9**, 3965–3973 (2003).
K. MATSUZAKI, H. KAWAGUCHI, P. VOTH, K. NODA, S. ITOH, H. D. TAKAGI, K. KASHIWABARA and K. TATSUMI, "Syntheses and Characterization of Titanium(IV) and Titanium(III) Complexes with (2-Dimethylphosphino)ethane-1-thiolate and (3- T. Dimethylphosphino)propane-1-thiolate as Ligands," *Inorg. Chem.* **42**, 5320–5329 (2003).
KOMURO, T. MATSUO, H. KAWAGUCHI and K. TATSUMI, "Coordination Chemistry of Silanedithiolato Ligands Derived from Cyclotrisilathiane: Synthesis and Structures of Complexes of Iron(II), Cobalt(II), Palladium(II), Copper(I), and Silver(I)," *Inorg. Chem.* **42**, 5340–5347 (2003).

Y. KAWAI, M. HAYASHI and N. TOKITOH, "Propanone 2-Chloro-4,6-Dinitrophenylhydrazone," *Acta Crystallogr., Sect. E* **58**, o1098–o1099 (2002).
N. TAKEDA, A. SHINOHARA and N. TOKITOH, "Synthesis and Properties of the First 1-Silanaphthalene," *Organometallics* **21**, 4024–4026 (2002).
N. TOKITOH, K. HATANO, T. SASAKI, T. SASAMORI, N. TAKEDA, N. TAKAGI and S. NAGASE, "Synthesis and Isolation of the First Germacyclopropabenzene: A Study to Elucidate the Intrinsic Factor for the Ring Deformation of Cyclopropabenzene Skeletons," *Organometallics* **21**, 4309–4311 (2002).
N. NAKATA, N. TAKEDA and N. TOKITOH, "η^6-Germabenzene Complexes of Chromium and Molybdenum," *Angew. Chem., Int. Ed.* **42**, 115–117 (2003).

N. NAKATA, N. TAKEDA and N. TOKITOH, "Synthesis and Properties of the First Stable Neutral Germaaromatic Compound, 2-{2,4,6-Tris[bis(trimethylsilyl)methyl]phenyl}-2-germanaphthalene," *Organometallics* **22**, 481–489 (2003).
K. NAGATA, N. TAKEDA and N. TOKITOH, "Unusual Oxidation of Dichalcogenido Complexes of Platinum," *Chem. Lett.* **32**, 170–171 (2003).
T. TAJIMA, K. HATANO, T. SASAKI, T. SASAMORI, N. TAKEDA and N. TOKITOH, "The First Examples of Stable Benzenes Fused with Two Three-membered Rings: Synthesis and Structures of the Two Stereoisomers of Bis(silacyclopropa)benzenes," *Chem. Lett.* **32**, 220–221 (2003).
N. NAKATA, N. TAKEDA and N. TOKITOH, "Reaction of Stable Germabenzene with Chalcogens: Synthesis and Structure of a Novel Germanium Analog of Pentathiepane, 1,2,3,4,5,6-Pentathiagermepane," *J. Organomet. Chem.* **672**, 66–71 (2003).
T. SASAMORI, N. TAKEDA and N. TOKITOH, "Synthesis and Reactions of New Diphosphenes Bearing Extremely Bulky Substituents," *J. Phys. Org. Chem.* **16**, 450–462 (2003).
N. TAKEDA, T. KAJIWARA, H. SUZUKI, R. OKAZAKI and N. TOKITOH, "Synthesis and Properties of the First Stable Silylene-Isocyanide Complexes," *Chem. Eur. J.* **9**, 3530–3543 (2003).
K. NAGATA, N. TAKEDA and N. TOKITOH, "Synthesis, Structure, and Properties of the First Disulfur and Diselenium Complexes of Platinum," *Bull. Chem. Soc. Jpn.* **76**, 1577–1587 (2003).

S. NORO, R. KITAURA, M. KONDO, S. KITAGAWA, T. ISHII, H. MATSUZAKA and M. YAMASHITA, "Framework Engineering by Anions and Prous Functionalities of Cu(II)/4,4'-bpy Coordination Polymers," *J. Am. Chem. Soc.* **124**, 2568–2583 (2002).
H. ASO, T. MANABE, T. KWASHIMA, T. ISHII, H. MIYASAKA, H. MATSUZAKA, M. YAMASHITA, M. HASSANUDDIN, N. KURODA and M. SHIRO, " Creations of Solitons and Polarons in MX-Chain Compounds, $\{[Pt(en)_2][PtX_2(en)_2]\}_3(CuX_4)_4$ (X = Cl and Br)," *Synth. Met.* **376**, 7–12 (2002).
N. AIZAWA, H. HARA, T. ISHII, M. YAMASHITA, H. MIYASAKA, H. MATSUZAKA, T. KODAMA, K. KIKUCHI and I. IKEMOTO, "Synthesis and Physical Properties of Complexes of Fullerene with Magnetic Metal Porphyrins," *Synth. Met.* **376**, 13–18 (2002).
K. TAKIZAWA, T. ISHII, H. MIYASAKA, H. MATSUZAKA, M. YSMASHITA, T. KAWASHIMA, H. MATSUZAKI, H. KISHIDA and H. OKAMOTO, "Crystal and Electronic Structures of Quasi-One-Dimensional Halogen-Bridged Binuclear Platinum Complexes, $\{[C_nH_{2n+1})_2NH_2\}_4[Pt_2(pop)_4I]$ (n = 2–6)," *Synth. Met.* **376**, 159–164 (2002).
T. MANABE, K. YOKOYAMA, T. ISHII, H. MIYASAKA, H. MATSUZAKA, M. YAMASHITA, T. KAWASHIMA, H. MATSUZAKI, H. KISHIDA, H. OKAMOTO, K. MARUMOTO, H. TANAKA, H. ITOH and S. KURODA, "Physical Properties of Quasi-One-Dimensional Mixed-Metal and Mixed-Halogen Complexes $Ni_{1-x}Pd_x(chxn)_2Cl_yBr_{1-y}Y_2$," *Synth. Met.* **376**, 165–170 (2002).
H. TANAKA, K. MARUMOTO, S. KRODA, T. ISHII, R. KANEHAMA, N. AIZAWA, H. MATSUZAKA, K. SUGIURA, H. MIYASAKA, T. KODAMA, K. KIKUCHI, I. IKEMOTO and M. YAMASHITA, "Electron Spin Resonance Studies of Co(tbp)·C_{60} Single Crystal," *J. Phys.: Condens. Matter* **14**, 3993–4000 (2002).

K. ONITSUKA, M. YAMAMOTO, S. SUZUKI and S. TAKAHASHI, "Structure and Reactivity of (η^3-Indolylmethyl)palladium Complexes Generated by the Reaction of Organopalladium Complexes with *o*-Alkenylphenyl Isocyanide," *Organometallics* **21**, 581–583 (2002).
M. YAMAMOTO, K. ONITSUKA, M. UNO, and S. TAKAHASHI, "Synthesis of Enantiopure Planar-Chiral Cyclopentadienyl-Ruthenium Binuclear Complexes Bridged by Aromatic Systems," *J. Chem. Soc., Dalton Trans.* 1473–1478 (2002).
K. ONITSUKA, S. SUZUKI and S. TAKAHASHI, "A Novel Route to 2,3-Disubstituted Indoles *via* Palladium-Catalyzed Three-Component Coupling of Aryl Iodide, *o*-Alkenylphenyl Isocyanide and Amine," *Tetrahedron Lett.* **43**, 6197–6199 (2002).
K. ONITSUKA, H. KITAJIMA, M. FUJIMOTO, A. IUCHI, F. TAKEI and S. TAKAHASHI, "Platinum-Acetylide Dendrimers Possessing a Porphyrin Core," *Chem. Commun.* 2576–2577 (2002).
D. -Y. ZHOU, E. YONEDA, K. ONITSUKA and S. TAKAHASHI, "Ruthenium-Catalyzed Carbonylation of Allene: Direct Synthesis of Methacrylates and Methacrylamides," *Chem. Commun.* 2868–2869 (2002).
K. ONITSUKA, A. SHIMIZU and S. TAKAHASHI, "A Divergent Approach to the Precise Synthesis of Giant Organometallic Dendrimers Using Platinum-Acetylides as Building Blocks," *Chem. Commun.* 280–281 (2003).
F. TAKEI, S. NAKAMURA, K. ONITSUKA, N. KOBAYASHI and S. TAKAHASHI, "Preparation and Photochemical Properties of Polyisocyanides with Regularly Arranged Porphyrin Pendants," *Chem. Lett.* **32**, 506–507 (2003).

K. UENO, N. WATANABE, S. ASAMI, M. SAKAI and H. OGINO, "Synthesis of Sefl-Stabilized and Donor-Free Silyl(silylene)tungsten Complexes," *Organometallics* **21**, 1326–1328 (2002).
K. UENO, T. YAMAGUCHI, K. UCHIYAMA and H. OGINO, "Synthesis of the First Gallane-Coordinated Transition Metal Complex," *Organometallics* **21**, 2347–2349 (2002).
M. OKAZAKI, K. SATOH, T. AKAGI, M. IWATA, K. A. JUNG, R. SHIOZAWA, K. UENO, H. TOBITA and H. OGINO, "Convenient Preparation of Li[(η^5-C_5Me_5)M(CO)$_2$] (M = Ru, Fe) by the Reaction of (η^5-

$C_5Me_5)M(CO)_2H$ with *n*-BuLi," *J. Organomet. Chem.* **645**, 201–205 (2002).

Laser Research Center for Molecular Science

S. ONO, Y. SUZUKI, T. KOZEKI, H. MURAKAMI, H. OHTAKE, N. SARUKURA, H. SATO, S. MACHIDA, K. SHIMAMURA and T. FUKUDA, "High-Energy, All-Solid-State, Ultraviolet Laser Power-Amplifier Module Design and Its Output-Energy Scaling Principle," *Appl. Opt.* **41**, 7556–7560 (2002).
Z. LIU, S. ONO, T. KOZEKI, Y. SUZUKI, N. SARUKURA and H. HOSONO, "Generation of Intense 25-fs Pulses at 290 nm by a Hollow Fiber Filled with High-Pressure Argon Gas," *Jpn. J. Appl. Phys.* **41**, L986–L988 (2002).
H. OHTAKE, H. MURAKAMI, T. YANO, S. ONO, N. SARUKURA, H. TAKAHASHI, Y. SUZUKI,G. NISHIJIMA and K. WATANABE, "Anomalous Power and Spectrum Dependence of Terahertz Radiation from Femtosecond-Laser-Irradiated Indium Arsenide in High Magnetic Fields up to 14 T," *Appl. Phys. Lett.* **82**, 1164–1166 (2003).
H. TAKAHASHI, Y. SUZUKI, M. SAKAI, S. ONO, N. SARUKURA, T. SUGIURA, T. HIROSUMI and M. YOSHIDA, "Significant Enhancement of Terahertz Radiation from InSb by Use of a Compact Fiber Laser and an External Magnetic Field," *Appl. Phys. Lett.* **82**, 2005–2007 (2003).
M. TAKESADA, E. VANAGAS, D. TUZHILIN, I. KUDRYASHOV, S. SURUGA, H. MURAKAMI, N. SARUKURA,K. MATSUDA, S. MONONOBE, T. SAIKI, M. YOSHIMOTO and S. KOSHIHARA, "Micro-Character Printing on a Diamond Plate by Femtosecond Infrared Optical Pulses," *Jpn. J. Appl. Phys.* **42**, 4613–4616 (2003).
H. TAKAHASHI, Y. SUZUKI, S. ONO, H. MURAKAMI, N. SARUKURA and T. NAKAMURA, "Mode-Locking Stability Adjustment of a Kerr-Lens Mode-Locked Ti:sapphire Laser, Analyzed by a Recently Developed Real-Time Spectrum Analyzer," *Jpn. J. Appl. Phys.* **42**, 4330–4333 (2003).
H. TAKAHASHI, Y. SUZUKI, A. QUEMA, M.SAKAI, T. YANO, S. ONO, N. SARUKURA, M. HOSOMIZU, T. TSUKAMOTO, G. NISHIJIMA and K. WATANABE, "Magnetic-Field-Induced Enhancement of THz-Radiation Power from Femtosecond-Laser-Iradiated InAs up to 27 T," *Jpn. J. Appl. Phys.* **42**, L532–L534 (2003).
H. TAKAHASHI, M. SAKAI, S. ONO, N. SARUKURA, H. SARO and T. FUKUDA, "Optical Property of Ce^{3+}-Ion-Doped $LiCaAlF_6$ Crystal in Vacuum Ultraviolet Region," *Jpn. J. Appl. Phys.* **42**, L660–L662 (2003).
A. QUEMA, H. TAKAHASHI, M. SAKAI, M. GOTO, S. ONO, N. SARUKURA, N. YAMADA and R. SHIODA, "Identification of Potential Estrogenic Environmental Pollutants by Terahertz Transmission Spectroscopy," *Jpn. J. Appl. Phys.* **42**, L932–L934 (2003).
H. TAKAHASHI, A. QUEMA, R. YOSHIOKA, S. ONO and N. SARUKURA, "Excitation Fluence Dependence of Megahertz Radiation Mechanism from Femtosecond-Laser-Irradiated InAs under Magnetic Field," *Appl. Phys. Lett.* **83**, 1068–1070 (2003).

I. SHOJI and T. TAIRA, "Drastic Reduction of Depolarization Resulting from Thermally Induced Birefringence by Use of a (110)-Cut YAG Crystal," *OSA Trends in Optics and Photonics.* **68**, 521–525 (2002).
V. LUPEI, N. PAVEL and T. TAIRA, "Highly Efficient Continuous-Wave 946-nm Nd:YAG Laser Emission under Direct 885-nm Pumping," *Appl. Phys. Lett.* **81**, 2677–2679 (2002).
Y. SATO and T. TAIRA, "Spectroscopic Properties of Neodymium-Doped Yttrium Orthovanadate Single Crystals with High-Resolution Measurement," *Jpn. J. Appl. Phys.* **41**, 5999–6002 (2002).
T. DASCALU, T. TAIRA and N. PAVEL, "100-W Quasi-Continuously-Wave Diode Radial Pumped Microchip Composite Yb:YAG Laser," *Opt. Lett.* **27**, 1791–1793 (2002).
Y. SATO, T. TAIRA, N. PAVEL and V. LUPEI, "Laser Operation with Near Quantum-Defect Slope Efficiency in Nd:YVO_4 under Direct Pumping into the Emitting Level," *Appl. Phys. Lett.* **82**, 844–846 (2003).
H. ISHIZUKI, T. TAIRA, S. KURIMURA, J.H. RO and M. CHA, "Periodic Poling in 3-mm-thick MgO:$LiNbO_3$ Crystals," *Jpn. J. Appl. Phys.* **42**, 108–110 (2003).
N. E. YU, S. KURIMURA, K. KITAMURA, J. H. RO, M. CHA, S. ASHIHARA, T. SHIMURA, K. KURODA and T. TAIRA, "Efficient Frequency Doubling of a Femtosecond Pulse with Simultaneous Group-Velocity Matching and Quasi Phase Matching in Periodically Poled, MgO-Doped Lithium Niobate," *Appl. Phys. Lett.* **82**, 3388–3390 (2003).
A. LUPEI, V. LUPEI, T. TAIRA, Y. SATO, A. IKESUE and C. GHEORGHE, "Energy Transfer Processes of Nd^{3+} in Y_2O_3 Ceramic," *J. Lumin.* **102-103**, 72–76 (2003).
J. SAIKAWA and T. TAIRA, "Second-Harmonic Nonlinear Mirror CW Mode Locking in Yb:YAG Microchip Lasers," *Jpn. J. Appl. Phys.* **42**, 649–651 (2003).
H. ISHIZUKI, I. SHOJI and T. TAIRA, "Periodical Poling Characteristics of Congruent MgO:$LiNbO_3$ Crystals at Elevated Temperature," *Appl. Phys. Lett.* **82**, 4062–4064 (2003).
Y. SATO, N. PAVEL and T. TAIRA, "Laser Oscillation with More Than 80% Slope Efficiency in Nd:YVO_4 under Direct Pumping into the Emitting Level," *OSA Trends in Optics and Photonics.* **83**, 46–50 (2003).
T. DASCALU, T. TAIRA and N. PAVEL, "Diode Edge-Pumped High Power Microchip Composite Yb:YAG Laser," *OSA Trends in Optics and Photonics.* **83**, 231–234 (2003).
H. ISHIZUKI, I. SHOJI, T. TAIRA and S.KURIMURA, "Periodical Poling Characteristics of 5mol% MgO-

Doped Congruent $LiNbO_3$ Crystals at Elevated Temperature," *OSA Trends in Optics and Photonics.* **83**, 248–253 (2003).
N. PAVEL, I. SHOJI, T. TAIRA, M. IWAI, T. YOSHINO, S. YAMAGUCHI and M. IMAEDA, "High-Power Blie Generation in a Periodically Poled MgO:$LiNbO_3$ Ridge-Type Waveguide by Frequency Doubling of a Diode End-Pumped Nd:YAG Laser," *OSA Trends in Optics and Photonics.* **83**, 388–392 (2003).
Y. SATO, I. SHOJI, T. TAIRA and A. IKESUE, "The Spectroscopic Properties and Laser Characteristics of Polycrystalline Nd:$Y_3Sc_xAl_{(5-x)}O_{12}$ Laser Media," *OSA Trends in Optics and Photonics.* **83**, 444–450 (2003).
S. ASHIHARA, T. SHIMURA, K. KURODA, N. E. YU, S. KURIMURA, K. KITAMURA, J. H. RO, M. CHA and T. TAIRA, "Group-Velocity-Matched Cascaded Quadratic Nonlinearities of Femtosecond Pulses in Periodically Poled MgO:$LiNbO_3$," *Opt. Lett.* **28**, 1442–1444 (2003).
Y. SATO, T. TAIRA and A. IKESUE, "Spectral Parameters of Nd^{3+}-Ion in the Polycrystalline Solid-Solution Composed of $Y_3Al_5O_{12}$ and $Y_3Sc_2Al_3O_{12}$," *Jpn. J. Appl. Phys.* **42**, 5071–5074 (2003).

Research Center for Molecular-scale Nanoscience

K. ITO, T. SUZUKI, Y. SAKAMOTO, D. KUBOTA, Y. INOUE, F. SATO and S. TOKITO, "Oligo(2,6-Anthrylene)s: Acene-Oligomer Approach for Organic Field-Effect Transistors," *Angew. Chem., Int. Ed.* **42**, 1159–1162 (2003).
T. TSUZUKI, N. SHIRASAWA, T. SUZUKI and S. TOKITO, "Color Tunable Organic Light-Emitting Diodes Using Pentafluorophenyl-Substituted Iridium Complexes," *Adv. Mater.* **15**, 1455–1458 (2003).

T. ISHIBASHI, M. ARA, H. TADA and H. ONISHI, "Conformation of *n*-Alkyl Monolayers Covalently Bonded to Si(111) Probed by Infrared-Visible Sum-Frequency Spectroscopy," *Chem. Phys. Lett.* **367**, 376–381 (2003).
M. ARA and H. TADA, "Friction Force Microscopy Using Silicon Cantilevers Covered with Organic Monolayers *via* Silicon-Carbon Covalent Bonds," *Appl. Phys. Lett.* **83**, 578–580 (2003).
H. TADA, M. ARA and S. TANAKA, "Wet Process Molecular Planting in A Specific Site on Siliocn with Si–C Covalent Bonds," *Proceedings of MRS Meeting* **739**, H7. 37. 1–5 (2003).

K. ONO, S. YAMADA, M. OHKITA, K. SAITO, S. TANAKA and T. HANAICHI, " Electrochemical Synthesis and Properties of Poly[1,4-bis(*N*-pyrrolylalkoxy)benzene]s with a Three-dimentional Crosslinked Structure," *Chem. Lett.* 516–517 (2003).
Y. YAMASHITA, M. TOMURA and K. IMAEDA, "Non-Planar BEDT-TTF Derivatives Fused with Tetrahydrofuran Rings Affording Cation Radical Salts with Unusual Crystal Structures," *Mol. Cryst. Liq. Cryst.* **380**, 203–207 (2002).
M. AKHTARUZZAMAN, M. TOMURA, M. B. ZAMAN, J. NISHIDA and Y. YAMASHITA, "Synthesis and Characterization of New π-Conjugated Molecules Containing Bis(ethynylpyridine) Units with a Benzothiadiazole Spacer," *J. Org. Chem.* **67**, 7813–7818 (2002).
Y. YAMASHITA and M. TOMURA, "Preparation and Structures of Dication Salts of Phenyl Substituted TTF Vinylogues," *J. Solid State Chem.* **168**, 427–432 (2002).
M. TOMURA and Y. YAMASHITA, "Unsymmetrical Tetrathiafulvalene with a Fused 1,2,5-Thiadiazole Ring and an Ethylenedioxy Group," *Acta Crystallogr., Sect. E* **59**, o145–o147 (2003).
Y. YAMASHITA, K. SUZUKI and M. TOMURA, "Novel Electron Acceptors Containing Nitrogen, Sulfur-Heterocyclic Units," *Synth. Met.* **133-134**, 341–343 (2003).
M. AKHTARUZZAMAN, M. TOMURA, J. NISHIDA and Y. YAMASHITA, "Linear Molecules with Ethynylpyridine and Bisbenzothiadiazole Units," *Synth. Met.* **137**, 873–874 (2003).
M. AKHTARUZZAMAN, M. TOMURA, K. TAKAHASHI, J. NISHIDA and Y. YAMASHITA, "Hydrogen Bonding Networks Consisted of Conjugation-Extended 4,4'-Bipyridines and Chloranilic Acid," *Supramol. Chem.* **15**, 239–243 (2003).

H. HOCKE and Y. UOZUMI, "A Simple Synthetic Approach to Homochiral 6- and 6'-Sybstituted 1,1'-Binaphthyl Derivatives," *Tetrahedron* **59**, 619–630 (2003).
Y. UOZUMI and R. NAKAO, "Catalytic Oxidation of Alcohols in Water under Atmospheric Oxygen by Use of an Amphiphilic Resin-Dispersion of Nano-Palladium Catalyst," *Angew. Chem., Int. Ed.* **42**, 194–197 (2003).
Y. UOZUMI and Y. KOBAYASHI, "The Sonogashira Reaction in Water via An Amphiphilic Resin-Supported Palladium-Phosphine Complex Under Copper-Free Conditions," *Heterocycles* **59**, 71–74 (2003).
H. HOCKE and Y. UOZUMI, "Polymer-Supported 2,2'-Bis(oxazol-2-yl)-1,1'-Binaphthyls (boxax): Immobilized Chiral Ligands for Asymmetric Wacker-Type Cyclization," *Synlett* 2049–2053 (2002).
Y. UOZUMI and T. KIMURA, "Heck Reaction in Water with Amphiphilic Resin-Supported Palladium-Phosphine Complexes," *Synlett* 2045–2048 (2002).
K. SHIBATOMI and Y. UOZUMI, "New Homochiral Phosphine Ligands Having a Hexahydro-1H-pyrrolo[1,2-c]imidazolone Backbone: Preparation and Use for Pd-Catalyzed Asymmetric Allylic Alkylation of Cycloalkenyl Carbonates," *Tetrahedron: Asymmetry* **13**, 1769–1772 (2002).

T. NAGATA and K. TANAKA, "Syntheses of a 6-(2-Pyrrolyl)-2,2'-Bipyridine Derivative and Its Ruthenium

Complex," *Bull. Chem. Soc. Jpn.* **75**, 2469–2470 (2002).
T. NAGATA, Y. KIKUZAWA and A. OSUKA, "Synthesis and Photoreaction of a Porphyrin/cobalt(III)-Complex Linked Molecule," *Inorg. Chim. Acta* **342**, 139–144 (2003).

O. NAKAGOE, N. TAKAGI and Y. MATSUMOTO, "Thermal Decomposition of Acetylene on Pt(111) Studied by Scanning Tunneling Microscopy," *Surf. Sci.* **514**, 414–419 (2002).
I. KINOSHITA, D. INO, K. NAGATA, K. WATANABE, N. TAKAGI and Y. MATSUMOTO, "Anomalous Quenching of Electronic States of Nanographene on Pt(111) by Deuterium Edge Termination," *Phys. Rev. B* **65**, 241402R (4 pages) (2002).
K. WATANABE, D.T. DIMITROV, N. TAKAGI and Y. MATSUMOTO, "Coherent Surface Phonon at a GaAs(100)-c(8×2) Surface," *Phys. Rev. B* **65**, 235328 (7 pages) (2002).
K. WATANABE, N. TAKAGI and Y. MATSUMOTO, "Impulsive Excitation of a Vibrational Mode of Cs on Pt(111)," *Chem. Phys. Lett.* **366**, 606–610 (2002).
O. NAKAGOE, M. OHTA, K. WATANABE, N. TAKAGI and Y. MATSUMOTO, "Structural Changes of AgO Chains on Ag(110) by Photo- and CO-Induced Oxygen Elimination," S*urf. Sci.* **528**, 144–150 (2003) .
Z. LIU, T. SAWADA, N. TAKAGE, K. WATANABE and Y. MATSUMOTO, "Reaction Intermediates in the Oxidation of Methanol on a Pt(111)-(2×2)O Surface," *J. Chem. Phys.* **119**, 4879–4886 (2003).
O. NAKAGOE, K. WATANABE, N. TAKAGI and Y. MATSUMOTO, "Role of Structural Fluctuation in a Surface Reaction Studied by Scanning Tunneling Microscopy: The CO + O → CO_2 Clean-Off Reaction on Ag(110)(2×1)-O," *Phys. Rev. Lett.* **90**, 226105 (4 pages) (2003).

Y. NEGISHI, T. NAGATA and T. TSUKUDA, "Structural Evolution in $(CO_2)_n$ Clusters ($n < 10^3$) as Studied by Mass Spectrometry," *Chem. Phys. Lett.* **364**, 127–132 (2002).
Y. NEGISHI, H. MURAYAMA and T. TSUKUDA, "Formation of $Pd_n(SR)_m$ Clusters ($n < 60$) in the Reactions of $PdCl_2$ and RSH (R = *n*-$C_{18}H_{37}$, *n*-$C_{12}H_{25}$)," *Chem. Phys. Lett.* **366**, 561–566 (2002).
Y. NEGISHI and T. TSUKUDA, "One-Pot Preparation of Subnanometer-Sized Gold Clusters *via* Reduction and Stabilization by meso-2,3-Dimercaptosuccinic Acid," *J. Am. Chem. Soc.* **125**, 4046–4047 (2003).
H. MURAYAMA, N. ICHIKUNI, Y. NEGISHI, T. NAGATA and T. TSUKUDA, "EXAFS Study on Interfacial Structures of Pd Clusters and *n*-Octadecanethiolate Monolayers: Formation of PdS Interlayer," *Chem. Phys. Lett.* **376**, 26–32 (2003).
S. SATO, N. YAMAMOTO, K. NAKANISHI, H. YAO, K. KIMURA, T. NARUSHIMA, Y. NEGISHI and T. TSUKUDA, "Self-Assembly of Si Clusters into Single Crystal Arrangements: Formation of Si_{10} Cluster Crystals," *Jpn. J. Appl. Phys.* **42**, L616–618 (2003).

Y. YOKOI, G. YELKEN, Y. OUMI, Y. KOBAYASHI, M. KUBO, A. MIYAMOTO and M. KOMIYAMA, "Monte Carlo Simulation of Pyridine Base Adsorption on Heulandite (010)," *Appl. Surf. Sci.* **188**, 377–380 (2002).
M. KOMIYAMA, Y. -J. LI and D. YIN, "Apparent Local Structural Change Caused by Ultraviolet Light on a TiO_2 Surface Observed by Scanning Tunneling Microscopy," *Jpn. J. Appl. Phys.* **41**, 4936–4938 (2002).
M. KOMIYAMA, D. YIN and Y. -J. LI, "Electronic Structure Change on TiO_2 Surface due to UV Light Irradiation," *Stud. Surf. Sci. Catal.* **145**, 153–156 (2003).

M. NAKANO, J. KOMATSU, S. MATSUURA, K. TAKASHIMA, S. KATSURA and A. MIZUNO, "Single-Molecule PCR Using Water-In-Oil Emulsion," *J. Biotechnology* **102**, 117–124 (2003).
Y. MATSUI, S. SATO, K. TAKASHIMA, S. KATSURA and A. MIZUNO, "Simultaneous Removal NO_x and DEP from Diesel Engine Exhaust Using Plasma and Oxidative Catalyst," *SAE Technical paper* **SP1759**, 111–119 (2003).
Z. SU, J. SAWADA, Y. MATSUI, K. TAKASHIMA and A. MIZUNO, "NO_x Removal Using Discharge Plasma and Electrophoresis," *SAE Technical paper* **SP1759**, 139–143 (2003).
A. HASHEM, M. ABDEL-SALAM, A. MIZUNO, A. YEHIA, A. TURKY and A. GABR, "Optimum Operating Conditions for Ozone Generation in AC Corona and AC Silent-Discharge Reactors," *J. Inst. Electrostatics Jpn.* **27**, 129–134 (2003).
G. LI, K. TAKASHIMA, S. KATSURA and A. MIZUNO, "Formation of Pearl-Chain Adhesion of Dielectric Particles in Electrostatic Field," *J. Inst. Electrostatics Jpn.* **27**, 135–139 (2003).
Z. Z. SU, K. ITO, K. TAKASHIMA, S. KATSURA and A. MIZUNO, "OH Radical Generation by Atmospheric Pressure Pulsed Discharge Plasma and its Quantitative Analysis by Monitoring CO Oxidation," *J. Phys. D: Applied Phys.* **35**, 3192–3198 (2002).

K. K. OKUDAIRA, H. YAMANE, K. ITO, M. IMAMURA, S. HASEGAWA and N. UENO, "Photodegradation of Poly(Tetrafluoroethylene) and Poly(Vinylidene Fluoride) Thin Films by Inner Shell Excitation," *Surf. Rev. Lett.* **9**, 335–340 (2002).
K. K. OKUDAIRA, K. OHARA, H. SETOYAMA, T. SUZUKI, Y. SAKAMOTO M. IMAMURA, S. HASEGAWA, K. MASE and N. UENO, "Excited States of Perfluorinated Oligo(*p*-Phenylene) by Inner-Shell Excitation," *Nucl. Instrum. Methods Phys. Res., Sect. B* **199**, 265–269 (2003).
H. YAMANE, K. ITO, S. KERA, K. K. OKUDAIRA and N. UENO, "Low-Energy Electron Transmission

through Organic Monolyers: An Estimation of the Effective Monolayer Potential by an Excess Electron Inteface," *J. Appl. Phys.* **92**, 5203–5207 (2002).

N. WATANABE, K. YAMAUCHI, Y. KAMATA, Y. UDAGAWA and T. MÜLLER, "Electron Correlation Effects in N_2 and CO Studied by X-Ray Scattering and CISD Calculations," *Mol. Phys.* **100**, 2839–2847 (2002).
M. TAKAHASHI, T. SAITO, M. MATSUO and Y. UDAGAWA, "A High Sensitivity Electron Momentum Spectrometer with Simultaneous Detection in Energy and Momentum," *Rev. Sci. Instrum.* **73**, 2242–2248 (2002).
T. HATANO, Y. KONDO, K. SAITO, T. EJIMA, M. WATANABE and M. TAKAHASHI, "Multilayer Polarizers for the Use of He-I and He-II Resonance Lines," *Surf. Rev. Lett.* **9**, 587–591 (2002).
N. SAITO, A. De FANIS, K. KUBOZUKA, M. MACHIDA, M. TAKAHASHI, H. YOSHIDA, I. H. SUZUKI, A. CASSIMI, A. CZASCH, R. DÖRNER, K. WANG, B. ZIMMERMANN, V. MCKOY, I. KOYANO and K. UEDA, "Carbon K-Shell Photoelectron Angular Distribution from Fixed-in-Space CO_2 Molecules," *J. Phys. B: At., Mol. Opt. Phys.* **36**, L25–L30 (2003).
M. TAKAHASHI, T. HATANO, T. EJIMA, Y. KONDO, K. SAITO, M. WATANABE, T. KINUGAWA and J. H. D. ELAND, "Polarization Measurements of Laboratory VUV Light: a First Comparison between Multilayer Polarizers and Photoelectron Angular Distributions," *J. Electron Spectrosc.* **130**, 79–84 (2003).
M. TAKAHASHI, T. SAITO, J. HIRAKA and Y. UDAGAWA, "The Impact Energy Dependence of Momentum Profiles of Glyoxal and Biacetyl and Comparison with Theory at Their High-Energy Limits," *J. Phys. B: At., Mol. Opt. Phys.* **36**, 2539–2251 (2003).

Y. KUBOZONO, Y. TAKABAYASHI, K. SHIBATA, T. KANBARA, S. FUJIKI, S. KASHINO, A. FUJIWARA and S. EMURA, "Crystal Structure and Electronic Transport of Dy@C_{82}," *Phys. Rev. B* **67**, 115410 (8 pages) (2003).
T. TAKENOBU, DAM HIEU CHI, S. MARGADONNA, K. PRASSIDES, Y. KUBOZONO, A. N. FITCH, K. KATO and Y. IWASA, "Synthesis, Structure, and Magnetic Properties of the Fullerene-Based Ferromagnets, Eu_3C_{70} and Eu_9C_{70}," *J. Am. Chem. Soc*. **125**, 1897–1904 (2003).
D. H. CHI, Y. IWASA, K. UEHARA, T. TAKENOBU, T. ITO, T. MITANI, E. NISHIBORI, M. TAKATA, M. SAKATA, Y. OHISHI, K. KATO and Y. KUBOZONO, "Pressure-Induced Structural Phase Transition in Fullerides Doped with Rare Earth Metals," *Phys. Rev. B* **67**, 094101 (7 pages) (2003).
J. KOU, T. MORI, M. ONO, Y. HARUYAMA, Y. KUBOZONO and K. MITSUKE, "Molecular- and Atomic-Like Photoionization of C_{60} in the Extreme Ultraviolet," *Chem. Phys. Lett.* **374**, 1–6 (2003).
J. B. CLARIDGE, Y. KUBOZONO and M. J. ROSSEINSKY, "A Complex Fulleride Superstructure-Decoupling Cation Vacancy and Anion Orientational Ordering in $Ca_{3+x}C_{60}$ with Maximum Entropy Methods," *Chem. Mater.* **15**, 1830–1839 (2003).
T. MORI, J. KOU, M. ONO, Y. HARUYAMA, Y. KUBOZOZN and K. MITSUKE, "Development of a Photoionizaion Spectrometer for Gaseous Fullerenes in the Extreme Ultraviolet," *Rev. Sci. Instrum.* **74**, 3769–3773 (2003).
K. SHIBATA, Y. RIKIISHI, T. HOSOKAWA, Y. HARUYAMA, Y. KUBOZONO, S. KASHINO, T. URUGA, A. FUJIWARA, H. KITAGAWA, T. TAKANO and Y. IWASA, "Structural and Electronic Properties of Ce@C_{82}," *Phys. Rev. B* **68**, 094104 (7 pages) (2003).
T. KANBARA, K. SHIBATA, S. FUJIKI, Y. KUBOZONO, S. KASHINO, T. URISU, M. SAKAI, A. FUJIWARA, R. KUMASHIRO and K. TANIGAKI, "N-Channel Field Effect Transistors with Fullerene Thin Films and Their Application to a Logic Gate Circuit," *Chem. Phys. Lett.* **379**, 223–229 (2003).

H. YAMANE, K. ITO, S. KERA, K. K. OKUDAIRA and N. UENO, "Low Energy Electron Transmission Study of Indium/(perylenel-3,4,9,10-tetracarboxylic dianhydride) System," *Jpn. J. Appl. Phys.* **41** 6591–6594 (2002).
S. KERA, H.YAMANE, I. SAKURAGI, K. K. OKUDAIRA and N. UENO, "Very Narrow Photoemission Bandwidth of the Highest Occupied State in a Copper-Phthalocyanine Monolayer," *Chem. Phys. Lett.* **364**, 93–98 (2002).
H.YAMANE, D. YOSHIMURA, K. K. OKUDAIRA, K. SEKI and N.UENO, "Intermolecular Energy-Band Dispersion in PTCDA Multilayers," *Phys. Rev. B* **68**, 33102 (3 pages) (2003).

I. UECHI, M. FUJIWARA, Y. FUJIWARA, Y. YAMAMOTO and Y. TANIMTOTO, "Magnetic Field Effects on Anodic Oxidation of Potassium Iodide," *Bull. Chem. Soc. Jpn.* **75**, 2379–2382 (2002).
Y. TANIMOTO, S. IZUMI, K. FURUTA, T. SUZUKI, Y. FUJIWARA, M. FUJIWARA, T. HIRATA and S. YAMADA, "Effects of High Magnetic Field on *Euglena gracilis*," *Int. J. Appl. Electromag. Mechanics* **14**, 311–316 (2001/2002).
T. HAINO, H. ARAKI, Y. FUJIWARA, Y. TANIMOTO and Y. FUKAZAWA, "Fullerene Sensors Based on Calix[5]arene," *Chem. Commun.* 2148–2149 (2002).
A. KATSUKI, I. UECHI, M. FUJIWARA and Y. TANIMOTO, "High Magnetic Field Effect on the Growth of 3-Dimentional Silver Dendrites," *Chem. Lett.* 1186–1187 (2002).
M. G. SUNG, K. SASSA, H. OGAWA, Y. TANIMOTO and S. ASAI, "Strengthening of Carbon Fibers by Imposition of a High Magnetic Field in a Carbonization Process," *Mater. Trans.* **43**, 2087–2091 (2002).

T. ISHIDA, M. MURAKAMI, G. WATANABE, H. YOSHIKAWA and S. NISHIKIORI, "Theoretical Study on Photoinduced Color Change and Charge Transfer of Methylviologen," *Internet Electronic J. Mol. Design* **2**, 14–23 (2003).
T. ISHIDA and G. C. SCHATZ, "A Local Interpolation Scheme Using No Derivatives in Potential Sampling: Application to $O(^1D) + H_2$ System," *J. Comput. Chem.* **24**, 1077–1086 (2003).
M. HIRAMA, T. ISHIDA and J. AIHARA, "Possible Molecular Hydrogen Formation Mediated by the Radical Cations of Anthracene and Pyrene," *J. Comput. Chem*. **24**, 1378–1382 (2003).
K. H. KIM, Y. S. LEE, G. -H. JEUNG and T. ISHIDA, "Potential Energy Surface Generation Using Ab Initio Calculations and IMLS/Shepard Interpolation for the LiH + H $\leftrightarrows$ Li + H_2 Reactions," *J. Chem. Phys.* **119**, 4689–4694 (2003).
H. YOSHIKAWA, S. NISHIKIORI and T. ISHIDA, "Crystal Structure and Spectroscopic Properties of the CT Complex of Methyl Viologen Dication and *o*-Dimethoxybenzene Included in a Polycyano-Polycadmate Host, and Theoretical Study on Its Red Shifted CT Absorption," *J. Phys. Chem. B* **107**, 9261–9267 (2003).

T. OBA and H. TAMIAKI, "Which Side of the π-Macrocycle Plane of (Bacterio)chlorophylls Is Favored for Binding of the Fifth Ligand?" *Photosynth. Res.* **74**, 1–10 (2002).
T. OBA and H. TAMIAKI, "Coordination Chemistry of Chlorophylls: Which Side of the Chlorin Macrocycle Is Favored for the Ligand Coordination?" *J. Photosci.* **9**, 362–363 (2002).

UVSOR (Ultraviolet Synchrotron Orbital Radiation) Facility

K. TAKAHASHI, T. NAKAYAMA, Y. MATSUMI, S. SOLOMON, T. GEJO, E. SHIGEMASA and T. J. WALLINGTON, "Atmospheric Lifetime of SF_5CF_3," *Geophys. Res. Lett.* **29**, 1–4 (2002).
T. GEJO, Y. TAKATA, T. HATSUI, M. NAGASONO, H. OJI, N. KOSUGI and E. SHIGEMASA, "Angle-Resolved Photoion Spectroscopy of NO_2 and SO_2," *Chem. Phys.* **289**, 15–29 (2003).

M. HOSAKA, M. KATOH, A. MOCHIHASHI, J. YAMAZAKI, K. HAYASHI, K. TAKASHIMA and H. HAMA, "Q-Switching Operation of the UVSOR-FEL," *Nucl. Instrum. Methods Phys. Res., Sect. A* **507**, 289–293 (2003).

K. G. NATH, Y. UFUKTEPE, S. KIMURA, Y. HARUYAMA, T. KINOSHITA, T.MATSUMURA, T. SUZUKI, H. OGASAWARA and A. KOTANI, "Photoemission Study of Mixed-Valent Tm-Monochalcogenides: Evidence of Electron-Correlation Effect in Different Tm-Core Levels," *J. Phys. Soc. Jpn.* **72**, 1792–1799 (2003).
S. KIMURA, T. NISHI, T. TAKAHASHI, T. HIRONO, Y. IKEMOTO, T. MORIWAKI and H. KIMURA, "Infrared Spectroscopy under Extreme Conditions," *Physica B* **329-333**, 162–1626 (2003).
S. KIMURA, H. IWATA, K. KANAI, S. SHIN, G. SCHMERBER, J. P. KAPPLER and J. C. PARLEBAS, "Collapse of Kondo Lattice in $Ce_{1-x}La_xPd_3$ (x = 0, 0.03)," *Acta Physica Polonica B* **34**, 975–978 (2003).
J. SICHELSCHMIDT, V. VOEVODIN, S. PASCHEN, W. CARRILLO-CABRERA, YU. GRIN, F. STEGLICH and S. KIMURA, "Optical Reflectivity of the Clathrate Compound Ba_6Ge_{25}," *Acta Physica Polonica B* **34**, 613–616 (2003).

Computer Center

T. MIKAMI and S. OKAZAKI, "An Analysis of Molecular Origin of Vibrational Energy Transfer from Solute to Solvent based upon Path Integral Influence Functional Theory," *J. Chem. Phys.* **119**, 4790–4797 (2003).

S. NANBU, M. AOYAGI, H. KAMISAKA, H. NAKAMURA, W. BIAN and K. TANAKA, "Chemical Reactions in the $O(^1D)$ + HCl System I. Ab Initio Global Potential Energy Surfaces for the $1^1A'$, $2^1A'$, and $1^1A''$ States," *J. Theor. Comput. Chem.* **1**, 263–273 (2002).
H. KAMISAKA, H. NAKAMURA, S. NANBU, M. AOYAGI, W. BIAN and K. TANAKA, "Chemical Reactions in the $O(^1D)$ + HCl System II. Dynamics on the Ground $1^1A'$ State and Contributions of the Excited ($1^1A''$, and $2^1A'$) States," *J. Theor. Comput. Chem.* **1**, 275–284, (2002).
H. KAMISAKA, H. NAKAMURA, S. NANBU, M. AOYAGI, W. BIAN and K. TANAKA, "Chemical Reactions in the $O(^1D)$ + HCl System III. Quantum Dynamics on the Excited ($1^1A''$, and $2^1A'$) Potential Energy Surfaces," *J. Theor. Comput. Chem.* **1**, 285–293 (2002).
I. TOKUE, H. TANAKA, K. YAMASAKI and S. NANBU, "Formation of HCl^+ ($A^2\Sigma^+$) and HBr^+ ($A^2\Sigma^+$) Resulting from He (2^3S) Penning Ionization of HCl and HBr," *J. Phys. Chem. A* **106**, 6068–6074 (2002).
K. HARADA, K TANAKA, T. TANAKA, S.NANBU and M. AOYAGI, "Millimeter-Wave Spectroscopy of the Internal Rotation Band of the He-HCN Cluster and Determination of the Empirical Intermolecular Potential Energy Surface," *J. Chem. Phys.* **117**, 7041–7050 (2002).
J. -I. CHOE, S. -K. CHANG, S. MINAMINO and S. NANBU, "Ab Initio Study of Complexation Behavior of Calix[5]arene Derivative toward Alkyl Ammonium Cations," *Bull. Korean Chem. Soc.* **24**, 75–80 (2003).
S. MINAMINO, J. -I. CHOE, S. -K. CHANG, F. MIZUTANI and S. NANBU, "Theoretical Study of Vibrational Spectra of p-Tert-Butylcalix[4]crown-6-Ether Complexed with Ethyl Ammonium Cation," *Chem. Phys. Lett.* **374**,

572–576 (2003).

Center for Integrative Bioscience

R. YASUDA , T. MASAIKE , K. ADACHI, H. NOJI, H. ITOH and K. KINOSITA, Jr., "The ATP-Waiting Conformation of Rotating F_1-ATPase Revealed by Single-Pair Fluorescence Resonance Energy Transfer," *Proc. Natl. Acad. Sci. U.S.A.* **100**, 9314–9318 (2003).
K. ADACHI, H. NOJI and K. KINOSITA, Jr., "Single Molecule Imaging of the Rotation of F_1-ATPase," *Methods in ENZYMOLOGY.* **361**, 211–227 (2003).

H. SAWAI, N. KAWADA, K. YOSHIZATO, H. NAKAJIMA, S. AONO and Y. SHIRO, "Characterization of the Heme Environmental Structure of Cytoglobin, a Fourth Globin in Humans," *Biochemistry* **42**, 5133–5142 (2003).

H. FUJII and Y. FUNAHASHI, "Trigonal Bipyramidal Ferric Aqua Complex with Sterically Hindered Salen Ligand as a Model for Active Site of Protocatechuate 3,4-Dioxygenase," *Angew. Chem., Int. Ed.* **41**, 3638–3641 (2002).
X. ZHANG, H. FUJII, K. MANSFIELD MATERA, C. T. MIGITA, D. SUN, M. SATO, M. IKEDA-SAITO and T. YOSHIDA, "Regiospecificity of Each of the Three Steps of Heme Oxygenase Reaction from Hemin to *meso*-Hydroxyhemin, from *meso*-Hydroxyhemin to Verdoheme, and from Verdoheme to Biliverdin," *Biochemistry* **42**, 7418–7426 (2003).
M. OHASHI, T. KOSHIYAMA, TAKAFUMIUENO, M. YANASE, H. FUJII and Y. WATANABE, "Preparation of Artificial Metalloenzymes by Insertion of Chromium(III) Schiff Base Complexes into Apomyoglobin Mutants," *Angew. Chem., Int. Ed.* **42**, 1005–1008 (2003).

Y. MIZUTANI and T. KITAGAWA, "Vibrational Energy Relaxation of Metalloporphyrins in a Condensed Phase Probed by Time-Resolved Resonance Raman Spectroscopy," *Bull. Chem. Soc. Jpn.* **75**, 623–639 (2002).
K. SATO, S. NAGATOMO, C. DENNISON, T. NIIZEKI, T. KITAGAWA and T. KOHZUMA, "UV Resonance Raman and NMR Spectroscopic Studies on the pH Dependent Metal Ion Release from Pseudoazurin," *Inorg. Chim. Acta* **339**, 383–392 (2002).
S. OGO, R. YAMAHARA, M. ROACH, T. SUENOBU, M. AKI, T. OGURA, T. KITAGAWA, H. MASUDA, S. FUKUZUMI and Y. WATANABE, "Structural and Spectroscopic Features of a *cis* (Hydroxo)-Fe^{III}-(Carboxylato) Configuration as an Active Site Model for Lipoxygenases," *Inorg. Chem.* **41**, 5513–5520 (2002).
T. OSAKO, S. NAGATOMO, Y. TACHI, T. KITAGAWA and S. ITOH, "Low-Temperature Stopped-Flow Studies on the Reactions of Copper(II) Complexes and H_2O_2: The First Detection of a Mononuclear Copper(II)-Peroxo Intermediate," *Angew. Chem., Int. Ed.* **41**, 4325–4328 (2002).
N. C. MAITI, T. TOMITA, T. KITAGAWA, K. OKAMOTO and T. NISHINO, "Resonance Raman Studies on Xanthine Oxiase: Observation of the Mo^{VI}-Ligand Vibration," *J. Biol. Inorg. Chem.* **8**, 327–333 (2003).
H. ARII, Y. SAITO, S. NAGATOMO, T. KITAGAWA, Y. FUNAHASHI, K. JITSUKAWA and H. MASUDA, "C–H Activation by $Cu(III)_2$–O_2 Intermediate with Secondary Amino Ligand," *Chem. Lett.* **32**, 156–157 (2003).
D. OKUNO, T. IWASE, K. SHINZAWA-ITOH, S. YOSHIKAWA and T. KITAGAWA, "FTIR Detection of Protonation/Deprotonation of Key Carboxyl Side Chains Caused by Redox Change of the Cu_A-Heme *a* Moiety and Ligand Dissociation from the Heme a_3-Cu_B Center of Bovine Heart Cytochrome *c* Oxidase," *J. Am. Chem. Soc.* **125**, 7209–7218 (2003).
T. UCHIDA, Q. HE, C. Y. RALSTON, M. BRENOWITZ and M. R. CHANCE, "Linkage of Monovalent and Divalent Ion Binding in the Folding of the P4-P6 Domain of the *Tetrahymena* Ribozyme," *Biochemistry* **41**, 5799–5806 (2002).
T. UCHIDA, K. TAKAMOTO, Q. HE, M. R. CHANCE and M. BRENOWITZ, "Multiple Monovalent Ion-Dependent Pathways for the Folding of the L-21 *Tetrahymena Thermophila* Ribozyme," *J. Mol. Biol.* **328**, 463–478 (2003).

A. YAMADA, T. KAKITANI, S. YAMAMOTO and T. YAMATO, "A Computational Study on the Stability of the Protonated Schiff Base of Retinal in Rhodopsin," *Chem. Phys. Lett.* **366**, 670–675 (2002).
T. KAWATSU, T. KAKITANI and T. YAMATO, "Destructive Interference in the Electron Tunneling through Protein Media," *J. Phys. Chem. B* **106**, 11356–11366 (2002).
A. YAMADA, T. YAMATO, T. KAKITANI and S. YAMAMOTO, "Analysis of *cis-trans* Photoisomerization Mechanism of Rhodopsin Based on the Tertiary Structure of Rhodopsin," *J. Photosci.* **9**, 51–54 (2002).
T. KAKITANI, T. KAWATSU, A. KIMURA, A. YAMADA, T. YAMATO and S. YAMAMOTO, "Unique Mechanism of Excitation Energy Transfer and Photoisomerization in Biological Systems," *J. Biol. Phys.* **28**, 367–381 (2002).

REVIEW ARTICLES AND TEXTBOOKS

Department of Theoretical Studies

T. AKASAKA and S. NAGASE, *Endofullerenes: A New Family of Carbon Clusters*, Kluwer Academic Publishers; Dordrecht (2002).
Z. SLANINA, F. UHLIK, K. KOBAYASHI and S. NAGASE, "Excited Electronic States and Stabilities of Isomeric Fullerenes," in *The Exciting World of Nanocages and Nanotubues*, P. Kamat, D. Guldi and K. M. Kadish, Eds., The Electrochemical Society, Inc.; Pennington, **12**, pp. 739–747 (2002).
K. KOBAYASHI and S. NAGASE, "Structures and Electronic Properties of Endohedral Metallofullerenes," in *Endofullerenes: A New Family of Carbon Clusters*, T. Akasaka and S. Nagase, Eds., Kluwer Academic Publishers; Dordrecht, pp. 99–120 (2002).
T. WAKAHARA, T. AKASAKA, K. KOBAYASHI and S. NAGASE, "Chemical Properties of Endohedral Metallofullerenes," in *Endofullerenes: A New Family of Carbon Clusters*, T. Akasaka and S. Nagase, Eds., Kluwer Academic Publishers; Dordrecht, pp. 231–251 (2002).
T. WAKAHARA, Y. MAEDA, S. OHKUBO, J. KOBAYASHI, M. KONDO, T. AKASAKA, K. KOBAYASHI, S. NAGASE, T. KATO, K. YAMAMOTO and K. M. KADISH, "Endohedral Fullerene Ions: Synthesis, Structure and Reaction," in *Structural and Electronic Properties of Molecular Nanostructures*, H. Kuzmany, J. Fink, M. Mehring and S. Roth, Eds., Am. Inst. Phys.; pp. 43–46 (2002).
S. NAGASE, "Molecular Design by Theory and Computation," in *the Advance Chemistry Series IV* (in Japanese), Chem. Soc. Jpn., Ed., Maruzen; Tokyo, pp. 16–20 (2003).
S. NAGASE, "General Features of Main Group Element Chemistry," in *Handbook of Organometallic Reagents* (in Japanese), K. Tamao, Ed., Kagaku Doujin; Kyoto, pp. 4–10 (2003).

S. OKAZAKI and Y. OKAMOTO, "Computer Simulations of Biological Systems," in *Frontiers of Chemistry* (in Japanese), S. OKAZAKI and Y. OKAMOTO, Eds., Kagaku Dojin; Kyoto, **No.8**, 1–262 (2002).
Y. OKAMOTO, "Recent Developments in Protein Tertiary Structure Predictions," in *special issue: This Year in Physical Science, Parity* (in Japanese) **18**, 54–56 (2003).
H. OKUMURA and F. YONEZAWA, "Theory for the Anomaly of the Bulk Viscosity due to the Metal-Nonmetal Transition in Liquid Mercury," *Solid State Physics* (in Japanese) **38**, 57–64 (2003).
Y. OKAMOTO, "How Much Can Computational Chemistry Say about Biological Phenomena," in *The Advance Chemistry Series IV* (in Japanese), Chem. Soc. Jpn., Ed., Maruzen; Tokyo, pp. 63–67 (2003).

H. NAKAMURA, "Nonadiabatic Transition and Laser Control of Molecular Processes," in *Science of Superstrong Field Interactions*, K. Nakajima and M. Deguchi, Eds., Am. Inst. Phys. pp.355–361(2002).
H. NAKAMURA, "Current Developments in Atomic, Molecular, and Chemical Physics with Applications," in *Nonadiabatic Transitions and Chemical Dynamics*, Man Mohan, Ed., Kluwer Academic/Plenum; New York, pp.71–77 (2002).

M. KUWABARA, K. YONEMITSU and H. OHTA, "Spin Solitons in the Alternate Charge Polarization Background of MMX Chains," in *EPR in the 21st Century*, A. Kawamori, J. Yamauchi and H. Ohta, Eds., Elsevier Science; Amsterdam, 59–62 (2002).
K. YONEMITSU, "Origins of Various Electronic Properties in Low-Dimensional Assembled Metal Complexes," in *Science of Assembled Metal Complexes* (in Japanese), H. Okawa and T. Ito, Eds., Kagaku-Dojin, 251–259 (2003).

Department of Molecular Structure

T. KATO, "Electron Spin Resonance Spectroscopy for Metallofullerenes," in *Endofullerenes A New Family of Carbon Clusters*, Takeshi Akasaka and Shigeru Nagase, Eds., Kluwer Academic Publishers, 153–168 (2002).
T. KATO, K. FURUKAWA, N. TOYAMA, S. OKUBO, T. AKASAKA, H. KATO and H. SHINOHARA, "High-Field/High-Frequency ESR Study of Metallofullerenes," in *Proceedings of the International Symposium on Fullerenes, Nanotubes, and Carbon Nanoclusters*, P. V. Kamat, D. M. Guldi and K. M. Kadish, Eds., The Electrochemical Society, Inc.; Pennington, **12**, 372–376 (2002).
H. MATSUOKA, T. YOSHIDA, K. KUBONO, K. SATO, D. SHIOMI, K. FURUKAWA, T. KATO, K. YOKOI and T. TAKUI, "Pseudo-Octahedral High-Spin Co(II) Complexes with Orbitally Degenerate Ground States as Studied by SQUID and ESR Spectroscopy," *Synth. Met.* **137**, 1213–1214 (2003).

Department of Electronic Structure

N. NISHI, K. KOSUGI and K. HINO,"Metal-Molecule-Hybrid NanoCluster Magnets," *Nano Gakkai Kaiho* **1**, 73 (2003).

Department of Applied Molecular Science

K. AWAZU and M. FUJIMAKI, "Nano/Microstructure in Metal Oxides Prepared by MeV Ions, Laser and Synchrotron Radiation," in *Handbook of Organic-Inorganic Hybrid Materials and Nanocomposites*, American Scientific Publishers, Chapter K, 1–29 (2002).

H. NISHIKAWA, S. KOJIMA, T. KODAMA, K. KIKUCHI, I. IKEMOTO, M. FUJITSUKA and O. ITO, "Synthesis and Properties of New Fullerene-Tetrathiafulvalene Dyads," in *Fullerenes—Volume 12: The Exciting World of Nanocages and Nanotubes*, Proceedings—Electrochemical Society, **2002–12**, 115 (2002).

Department of Vacuum UV Photoscience

N. KOSUGI, "Molecular Inner-Shell Spectroscopy: Polarization Dependence and Characterization of Unoccupied States," in *Chemical Applications of Synchrotron Radiation: Dynamics and VUV spectroscopy*, T. -K. Sham, Ed., World Scientific, Chapter 5, 228–284 (2002).

Coordination Chemistry Laboratories

K. TANAKA and D. OOYAMA, "Multi-Electron Reduction of CO_2 *via* Ru–CO_2, –C(O)OH, –CO, –CHO and –CH_2OH Species," *Coord. Chem. Rev.* **226**, 211–218 (2002).

N. TOKITOH and R. OKAZAKI, "Multiply Bonded Germanium, Tin and Lead Compounds," in *The Chemistry of Organic Germanium, Tin and Lead Compounds Vol. 2*, Z. Rappoport, Ed., John Wiley & Sons; New York, 843–901 (2002).
N. TAKEDA, N. TOKITOH and R. OKAZAKI, "Digermenes and Digermanes," "Metalated Germanium Compounds," "Germanium Oxides, Sulfides, Selenides, and Tellurides (Double Bonded)," "Iminogermanes," "Germenes," "Germylenes," "Tin Oxides, Sulfides, Slenides, and Tellurides (Double Bonded)," "Iminostannanes," "Stannenes," "Stannylenes," "Diplumbenes and Diplumbanes," "Metalated Lead Compounds," "Organoplumbyl Oxides, Sulfides, Selenides, and Tellurides (Double Bonded)," "Plumbylenes," in *Scienece of Synthesis, Category 1: Organometallics, Volume 5: Compounds of Group 14 (Ge, Sn, Pb)*, M. G. Moloney, Ed., Georg Thieme Verlag; Stuttgart, New York, 27–54, 299–314, 637–651 (2003).

K. ONITSUKA, Y. MATSUSHIMA and S. TAKAHASHI, "Synthesis and Stereochemistry of Planar-Chiral Cyclopentadienyl Complexes of Late Transition Metal," *Yuki Gosei Kagaku Kyokaishi (J. Synth. Org. Chem. Jpn.)* (in Japanese) **60**, 752–761 (2002).
K. ONITSUKA and S. TAKAHASHI, "Metallodendrimers Composed of Organometallic Building Blocks," *Top. Curr. Chem.* **228**, 39–63 (2003).

Laser Research Center for Molecular Science

T. TAIRA, J. SAIKAWA, T. KOBAYASHI and R. BYER, "Diode-Pumped Tunable Yb:YAG Miniature Lasers at Room Temperature: Modeling and Experiment," in *Tunable Solid-State Lasers, SPIE Milestone Series*, **MS173**, pp. 375–379 (2002).

Research Center for Molecular-scale Nanoscience

T. TSUKUDA and K. KAYA, "Nano-Clusters," in *Kagaku Souchi* (in Japanese) 74–76 (2003).

M. KOMIYAMA, "Observation of Catalyst Surfaces by Probe Microscopy," *Surface Technol.* **53**, 906–908 (2002).

A. MIZUNO and S. KATSURA, "Manipulation of a Large DNA Molecules Using the Phase Transition," *J. Bio. Phys.* **28**, 587–603 (2002).
A. MIZUNO, "Manipulation of Single DNA Molecules," in *Micromachines As Tools for Nanotechnology (Microtechnology and Mems)*, H. FUJITA, Ed., Springer Verlag, 45–81 (2003).
S. KATSURA, "Manipulation of DNA Molecules," *Seimitsukougakukai-shi* (in Japanese) **68**, 1415–1418 (2002).

N. WATANABE, S. TEN-NO, S. IWATA and Y. UDAGAWA, "Electron Correlation and Coulomb Hole Deduced from X-Ray Scattering Intensities: Experimental and Theoretical Studies," in *Review of Modern Quantum Chemistry*, K. D. Sen, Ed., World Scientific; Singapore, pp. 553–576 (2002).
M. TAKAHASHI, Y. KHAJURIA, T. SAITO and Y. UDAGAWA, "Probing Electron Momentum Densities of Molecular Orbitals Using a New Multichannel (*e*,2*e*) Spectrometer," in *Electron and Photon Impact Ionization and Related Topics 2002*, L. U. Ancarani Ed., Inst. Phys. Publishing; Bristol and Philadelphia, IOP series **172**, pp. 131–140 (2003).

Y. TANIMOTO, "Current Status of Magneto-Science," "Magnetic Field Effects on Electroless Deposition of Silver and Copper Deposition," and "Magnetic Field Effects on the Behavior of *Euglena gracilis*," in *Magneto-Science* (in Japanese), K. Kitazawa (General Ed.), S. Ozeki, Y. Tanimoto and M. Yamaguchi, Eds., IPC; Tokyo (2002).
M. FUJIWAWA, "Magnetic Orientation of Carbon Nanotubes," and "Magnetic Separation of Paramagnetic Metal Ions," in *Magneto-Science* (in Japanese), K. Kitazawa (General Ed.), S. Ozeki, Y. Tanimoto, and M. Yamaguchi, Eds., IPC; Tokyo (2002).

Computer Center

S. OKAZAKI and Y. OKAMOTO, *Computer Simulation of Biosystems* (in Japanese), Kagaku Dojin; Kyoto (2002).

Center for Integrative Bioscience

S. AONO, "Structural and Functional Properties of the CO Sensing Transcriptional Activator CooA," in *Oxygen and Life—Oxygenases, oxidases and lipid mediators—*, Y. Ishimura, M. Nozaki, S. Yamamoto, T. Shimizu, S. Narumiya and F. Mitani, Eds., International Congress Series 1233, Elsevier Science; Tokyo, pp.243–249 (2002).
S. AONO, "Structure and Function of Heme-Based Sensor Proteins," *Seibutsu Butsuri* (in Japanese) **42**, 230–235 (2002).
S. AONO, "Structure and Function of the CO-Sensing Transcriptional Regulator CooA," *Molecular Medicine* (in Japanese) **40**, 160–164 (2003).
S. AONO, "Regulation of Gene Expression by CO," *Bioscience and Industry* (in Japanese) **61**, 37–38 (2003).

M. IKEDA-SAITO and H. FUJII, "EPR Characterzation of the Heme Oxygenase Reaction Intermediates and Its Implication for the Catalytic Mechanism," in *Paramagnetic Resonance of Metallobiomolecules*, J. Telser, Ed., ACS Book Series 858; Washington, pp. 97–112 (2003).

T. KITAGAWA, "Overview ICPP-2: Resoance Raman Spectroscopy," *J. Porphyrins Phthalocyanines* **6**, 301–302 (2002).
Y. IWASAWA, T. KITAGAWA and H. HAMAGUCHI, ED., *Physical Chemistry* (translation), Tokyo Kagaku Dozin; Tokyo (2003).

AUTHOR INDEX

to "Research Activities" and "Special Research Projects"

L

M

N

O

U

V

W

Y

Z